

Falko Mecklenbrauck

Still Dwelling in the Rich Club? –

The Role of Structural Hubs and Cortical Chronoarchitecture

in the Processing of Hierarchically Nested Stimuli

– 2026 –

Fach Psychologie

Still Dwelling in the Rich Club? –
The Role of Structural Hubs and Cortical Chronoarchitecture
in the Processing of Hierarchically Nested Stimuli

Inaugural-Dissertation

Zur Erlangung des Doktorgrades

Im Fachbereich Psychologie und

Sportwissenschaft der Universität Münster

Vorgelegt von

Falko Mecklenbrauck

aus Hamm (Westfalen)

– 2026 –

Dekanin:	Prof. Dr. Ricarda I. Schubotz
Erste Gutachterin:	Prof. Dr. Ricarda I. Schubotz
Zweiter Gutachter:	Prof. Dr. Joachim Groß
Tag der mündlichen Prüfung:	13.04.2026
Tag der Promotion:	13.04.2026
ORCID (Falko Mecklenbrauck)	0000-0002-8187-6826

Acknowledgements

I am not sure how far back I have to begin with this, but I would like to thank everyone who accompanied me on my journey through PhD life.

First and foremost, I want to thank my supervisor, Prof. Dr. Ricarda Schubotz, for her support, trust, and the freedom to let me develop in the way I wanted. Thank you as well for still reading my far-too-long manuscripts. My thanks also extend to my two other committee members, Prof. Dr. Joachim Groß and Prof. Dr. Moritz Wurm, for their willingness to serve on my committee and for contributing their time and expertise to the evaluation of this thesis.

Secondly, I owe my thanks my parents, Birgit and Jörg, for enduring the brunt of all my frustration about everything that did not go as planned. I am sorry that you mostly got to hear the downsides, the venting sessions that did not need constructive feedback and the stressed phone calls during my bike rides home. But please know that I truly enjoyed my time as a PhD student. It is the best job in the world (if things work out).

Furthermore, I am especially thankful to Rabea, who is not only my sister by birth but also my sister in scientific struggles. Thank you for always understanding and empathizing, and for being my role model throughout my life.

I am also fortunate to have my PhD family. Thank you, Sophie, for being there through all the highs and lows and for being a true north star for PhD survival. Thank you, Nina, Marius, and Anoush – only after you three joined, the feeling of a real PhD *family* crept in. I probably would not have pulled through without you there. My thanks also go to Monika, for being the good soul of the work group and for bringing some normality into the chaos that is science.

Last but not least, I would like to thank all the current and former PhD students, student assistants and group members who crossed my path in the Bipsy group (I hope I am not forgetting anyone across the eternity I spent at the University of Münster): Anas, Amelie, Alea, Anna, Benjamin, Basti, Britt, Christin, Ima, Isabelle, Jennifer, Juliane, Jutta, Katharina, Kinan, Kristin,

Lana, Lars, Laura, Lena I., Lena L., Lena P., Leon, Marlen, Marc, Maike, Maria, Nihan, Niklas, Pia, Rosari, Simon, Tabea, Thea, Viviana, and Yannah.

Outside of this university, I owe a great deal all the kind people I bothered with questions regarding analyses and methods, namley Jorge Sepulcre, Sam Nastase, Gang Chen, Siemon de Lange, Dan Lurie, and Takuya Ito. I always received thoughtful and genuinely helpful responses. People like you are the giants of science on whose shoulders we can stand.

Beyond work, I am deeply thankful for my friends – Philipp, Robin, Lisa, Melina, Justin, Gianni, and Johanna – who kept me grounded, sane, and reminded me that there is more to life than academia. Whether through fantastical heroes, unnecessarily over-the-top birthday presents, chaotic vacations, late-night deep talks in the car, or simply being kindred spirits over many, many years; thank you for sticking with me.

Reaching back a bit further, I am grateful to Nadiya El-Sourani for trusting me during my bachelor's and especially my master's theses. Through the freedom in my work, I was able to develop my own interests and the drive that ultimately led me into science. Also (he will probably never read this, but still), I want to thank my high school math teacher, Mr. Georg Kussel, for showing me that being good in school is something you can be proud of, no matter what others say.

Last but not least, I want to thank you, whoever is reading this, for taking the time to read what I have produced over the last more than five years of my life.

It has been a pleasure,



Table of Contents

Summary 1

List of Original Publications 4

1 General Introduction 5

1.1 Environmental hierarchies 6

1.1.1 Features of hierarchically nested stimuli. 6

1.2 Cortical hierarchies 10

1.2.1 Hierarchy as a gradient of features. 11

1.2.2 Hierarchy as a progression of scales. 17

1.3 The time of the brain 28

1.3.1. The time of the brain – in theory. 29

1.3.2. The time of the brain – in practice. 32

1.4 Summary & Research Questions 36

2 Research Articles 39

2.1 Study 1: The significance of structural rich club hubs for the processing of hierarchical stimuli 39

2.2 Study 2: Decoding cortical chronotopy – Comparing the influence of different cortical organizational schemes 68

2.3 Study 3: Time Points or Plot Points – Are movies processed according to their temporal duration or their underlying content structure? 93

3 General Discussion 162

3.1 Summary of the presented studies 162

3.2 The functional processing hierarchy along the uni-to-multimodal gradient 167

3.2.1 The timescales of integration. 172

3.2.2 Considerations regarding the stimulus design..... 175

3.3 Missing link between the rich club hubs and the multimodal association cortices 178

3.3.1 Differences in rich club identification. 178

3.3.2 Structural-functional misalignment. 181

3.3.3 Validity of in vivo diffusion-weighted connectomes. 182

3.3.4 Limitations of the structural networks in Studies 1 & 2..... 186

3.4 Future investigation of the structural and functional hierarchy 190

3.4.1 The structural network underlying the functional processing gradient. 190

3.4.2 Looking beyond the network horizon. 197

4 Conclusion 200

5 References..... 202

Appendix A – Selected Supplemental Material for Study 1 244

Appendix B – Selected Supplemental Material for Study 2..... 278

Appendix C – Supplemental Material for Study 3..... 288

Appendix D – Supplemental Analysis: Testing the uni-to-multimodal gradient in Study 1 328

Abbreviations..... 333

List of Figures 334

Curriculum Vitae..... 335

Declerations 339

Summary

Our environment presents us with a multitude of stimuli, including language, actions, movies, or music that can all be described as hierarchically nested, in that lower levels are contained within higher levels. One crucial feature of these hierarchical stimuli is that the individual levels differ in respect to their temporal persistency, as hierarchically lower levels require less time than the higher levels they are nested within.

Interestingly, also the brain can be examined through the lens of hierarchy. On the one hand, a range of microstructural, chemoarchitectural as well as functional gradients have been described that culminate in a dynamic, functional hierarchy from low-level unimodal regions to high-level multimodal association cortices. On the other hand, the macrostructural connectivity reflects a hierarchically nested network architecture that enables both functional specification as well as an effective integration of different cortical areas. Especially fundamental to this network structure is the so-called *rich club,* a conglomerate of densely connected network hubs that has been suggested to function as a nexus for long-distance, brain-wide communication thereby shaping the functional uni-to-multimodal gradient. In this context, the connective rich club of hubs in interaction with the micro- and chemoarchitectural gradients were indicated to support a hierarchy of cortical dynamics – forming the *chronoarchitecture*. This hierarchical organization can be observed in both the intrinsic cortical timescales at rest as well as the area-specific temporal receptive windows (TRWs) during stimulus presentation, demonstrating that high-level cortical hub areas generate slower temporal dynamics and can integrate signals over longer periods of time, which might enable more complex levels of cortical processing.

Time thus seems to play an essential role both in the environment and within our brain activity. This thesis will therefore investigate the coherence between the functional processing hierarchy and the brain's chronoarchitecture. The focus thereby lays particularly on the significance of the structural rich club in orchestrating the cortical dynamics and the functional processing of hierarchically higher levels of the stimuli.

Study 1 presented participants with hierarchically nested sequences of numbers that varied in respect to their regularity and temporal persistency in a functional magnetic resonance imaging (fMRI) experiment. In the same sample, diffusion-weighted images were acquired to estimate individual structural networks and identify the rich club hubs in a group-wise binary connectome. In this context, **Study 1** developed a novel identification procedure for rich club hubs that – closer to its original definition – validates if the selected hubs actually form a club structure. These rich club hubs then served as regions of interest (ROIs) in the functional analysis examining whether the structural hub regions were especially involved in the processing of high-level, temporally more persistent stimuli. The results indicated that higher levels of the number sequence stimulus activated areas that were more central to the structural network. However, the rich club hubs compared to other nodes were not specifically more engaged by hierarchically higher stimuli. The topography of activity rather depicted a posterior-lateral-to-anterior-medial gradient in the frontal lobe with increasing temporal persistency of the stimulus.

To further inspect the rich club's role in shaping the cortical dynamics, **Study 2**, which was based on the same data as **Study 1**, comprehensively compared this structural network architecture against alternative organizational schemes. These alternatives included (1) the diverse club, a hub definition based on the modular network structure, (2) the functional uni-to-multimodal gradient, and (3) the spatial posterior-lateral-to-anterior-medial gradient identified in **Study 1**. Additionally, we examined the relevance of (4) various other graph theoretical nodal centrality measures and (5) a gradient describing the cortical thickness across the cortex. Using Bayesian modal comparison, **Study 2** identified the functional uni-to-multimodal gradient rather than the structural rich club architecture as the best organizational scheme for explaining the distribution of intrinsic cortical timescales at rest as well as TRWs estimated using the hierarchically nested number sequence of **Study 1**.

Finally, **Study 3** investigated the central assumption that differences in temporal persistency across hierarchically nested level underlie the cortical processing of naturalistic

stimuli – in **Study 3's** case a movie. In an fMRI experiment participants therefore watched a manipulated version of a movie, which disentangled the dependency between the complexity of the depicted content and the temporal duration through careful, frame-wise manipulation. Leveraging inter-subject correlation of cortical activity during the movie paradigm, **Study 3** identified a distinction between the anterior and posterior scene network for longer and more complex stimuli, respectively, thereby underlining the significance of both the content and duration of a stimulus for its processing. Importantly, the results further highlighted that temporal persistency might be especially crucial for higher levels of cognition, for instance the integration with previous memories.

In conclusion however, the studies only partially corroborated the overall assumptions of the thesis. While the temporal persistency of the different levels of a hierarchically nested stimulus indeed played a systematic part in its cortical processing, the specific role of the structural rich club in this processing remains elusive. Although some results indicated a possible functional significance, other organizational schemes, particularly the uni-to-multimodal gradient, were demonstrated to be more meaningful to the brain's temporal processing hierarchy. The combined work thus provided comprehensive evidence for a gradient of increasing intrinsic cortical timescales as well as TRWs along the uni-to-multimodal cortical hierarchy. Most notably, especially longer stimuli displaying rich, complex content engaged areas related to more intricate levels of processing, understanding, and prediction that are shared between people watching the same stimulus material. Finally, the inconsistency of the theoretically proposed function of the rich club and outlined empirical findings emphasises the need for methodological advancements and improved cortical hub definitions, which will aid in future investigations of the relationship between the functional hierarchy and the underlying structural architecture. In this context, the results suggest that the structural rich club hubs may primarily provide the infrastructure that facilitates integration across different functional modules without serving a fixed functional role in integrative processes.

List of Original Publications

This thesis is based on the following original research articles:

Study 1 Mecklenbrauck, F., Gruber, M., Siestrup, S., Zahedi, A., Grotegerd, D., Mauritz, M., Trempler, I., Dannlowski, U., & Schubotz, R. I. (2024). The significance of structural rich club hubs for the processing of hierarchical stimuli. *Human brain mapping*, *45*(4), Article e26543. https://doi.org/10.1002/hbm.26543

Study 2 Mecklenbrauck, F., Sepulcre, J., Fehring, J., & Schubotz, R. I. (2024). Decoding cortical chronotopy—Comparing the influence of different cortical organizational schemes. *NeuroImage*, *303*, Article 120914. https://doi.org/10.1016/j.neuroimage.2024.120914

Study 3 Mecklenbrauck, F. & Schubotz, R. I. (2026). Time Points or Plot Points – Are movies processed according to their temporal duration or their underlying content structure? *Manuscript under review*

1 General Introduction

"Every situation – nay, every moment – is of infinite worth;

for it is the representative of a whole eternity."

— Johann Wolfgang von Goethe, *Conversations of Goethe with Eckermann and Soret*

When engaging with our surroundings, we are often confronted with complex stimuli that can be described as hierarchical: Language consists of sentences, words, and phonemes (Jeon, 2014). Actions involve goals, sub-goals and movements (Grafton & Hamilton, 2007; Hamilton & Grafton, 1993). Music includes sections, phrases, and motifs (Lerdahl & Jackendoff, 1996). Movies depict scenes, shots and frames (Cutting, Brunick, & DeLong, 2011; Hasson, Yang, et al., 2008).

Similarly, hierarchy is also a commonly used concept within our brain, as the cortex for example can be subdivided into lobes and further parcelled into areas, columns, and single neurons (for a review see Hilgetag & Goulas, 2020). Consequently, it has been previously theorized that the cortical hierarchy is underlying the processing and representation of the environmental hierarchies (Botvinick, 2008; Golesorkhi, Gomez-Pilar, Zilio, et al., 2021; Soltani et al., 2021). For instance, early investigations on action processing and selection illustrated a progression from more posterior regions of the frontal lobe (e.g., the dorsal premotor cortex) to the frontopolar cortex that supposedly represented the action hierarchy from individual movements located more posteriorly to overarching goals in the frontal apex (Badre & D'Esposito, 2007; Botvinick, 2007; Fuster, 2001; Grafton & Hamilton, 2007; Koechlin et al., 1999, 2003; Koechlin & Summerfield, 2007). These studies provided initial evidence for the interrelationship of the cortical and environmental hierarchies that this thesis will spotlight.

But what exactly is *hierarchy*? Before diving into a detailed introduction of the theoretical and evidential background, the "buzzword" hierarchy needs to be defined and clearly differentiated in both the environment and the brain (cf. Hilgetag & Goulas, 2020)

1.1 Environmental hierarchies

As introduced above, many stimuli that we come across in our daily lives, can be seen through the lens of hierarchy (Fitch & Martins, 2014; Jeon, 2014). It was thereby hypothesized that the dominance of hierarchical thinking in humans originates from symbolic language, as the representation of different examples of the increasingly specific concepts naturally lends itself to a hierarchical organization (Ludwigs, 2020). According to the *hierarchy theory*, a hierarchy describes a comprehensive way to organize a complex system into more manageable sub-elements that are arranged in layers or levels (Simon, 1977; J. Wu, 2013). Thus, hierarchization offers a compelling strategy to bring structure to complex systems, like our environment or our brain (Reed, 2020).

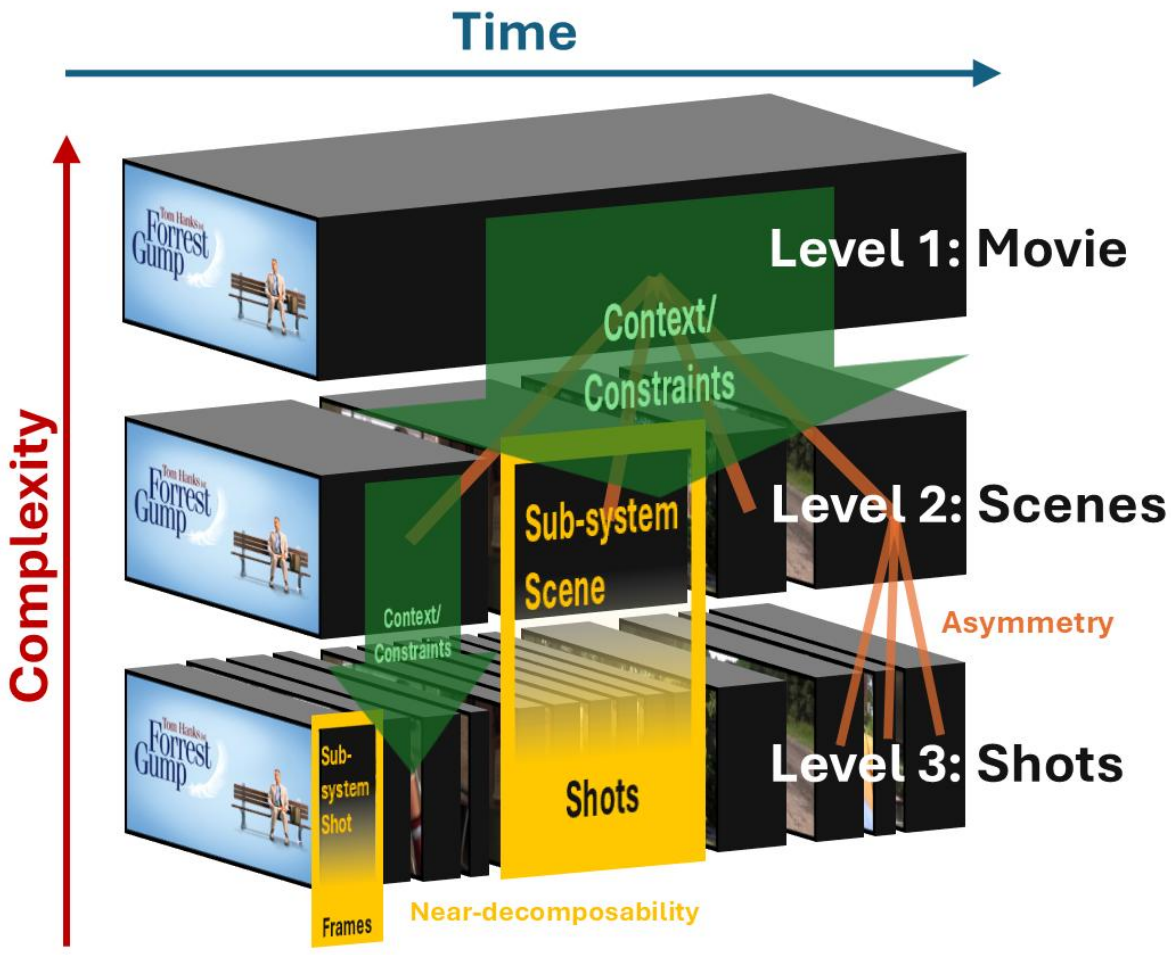
1.1.1 Features of hierarchically nested stimuli. In this context, hierarchies are attributed five specific features (Valentine & May, 1996; J. Wu, 2013), which I would like to illustrate using the hierarchically nested structure of movies. For this example, I will consider two levels of the movie hierarchy, namely movie *scenes* and *shots* (Figure 1; Haq et al., 2019; Mecklenbrauck & Schubotz, in review; Zacks et al., 2010).

A scene of a movie is thereby technically defined by a specific place and time as described by the screenplay (Field, 2005). The definition is sometimes extended to include specific characters (Cutting, 2014) or an overarching action goal (Magliano & Zacks, 2011). Nevertheless, a scene always describes a confined chunk of the movie's plot (Cutting, 2019a; Smith et al., 2012). A shot on the other hand is clearly defined as a continuous run of frames (i.e., images taken by the camera), which is bordered on both sides by cuts, so abrupt visual shifts often accompanied by a change in camera perspective (Cutting, 2014; Cutting et al., 2012). The visual transitions are so noticeable that they can also be used to automatically annotate shots throughout the movie (Chakraborty et al., 2021; Mas & Fernandez, 2003; Rui et al., 1998; Zhu et al., 2023).

1.1.1.1 Time. The first feature attributed to hierarchies is, that higher levels, in this case scenes, are temporally longer than the lower levels (Valentine & May, 1996; J. Wu, 2013). Looking at the distribution of scene and shot length across the last 100 years of film making, shots usually lay in the range of 10 to 20 seconds, while scenes can take 20 seconds to over a minute (Cutting et al., 2012), underlining this feature (Figure 1).

Figure 1

The definition of hierarchically nested stimuli using the example of a movie



Note. Like other hierarchically nested, natural stimuli, movies can be structured into multiple levels: whole movie (level 1), movie scenes (level 2), shots (level 3). These levels are distinguished (1) by their temporal duration and (2) by their complexity of the content. (3) Higher levels provide context and constraints to the lower levels. (4) Nested, hierarchical stimuli are created though asymmetric, mono-hierarchical relationships. Multiple lower levels elements construct one higher level element. (5) The structure can be described as near-decomposable, which means it can be divided into sub-systems that rarely interact with each other and aggregate the contained lower levels.

1.1.1.2 Complexity. Secondly, higher levels are described to be more complex (J. Wu, 2013). This feature refers to the literal meaning of the word *complex*, that is, made up of multiple

parts (Cutting, 2019b). In the example, a movie scene – by definition – is a sequence of the shots that take place at a given location and time (Figure 1; Cutting, 2014; Cutting et al., 2012). Furthermore, a scene is also more visually complex than a shot, as it is composed of multiple visually distinct camera angles (Cutting, 2016). Additionally, this complexity can also be seen in the narrative structure, as shots describe the smallest narrative element (Cutting, 2016) while scenes usually describe broader, more overarching events in the movie (Cutting, 2014).

1.1.1.3 Context and constraints. The third characteristic defines that higher levels of the hierarchy constrain and provide context to lower levels (Figure 1; Valentine & May, 1996; J. Wu, 2013). As scenes are confined to a specific place and time (Cutting, 2014; Magliano & Zacks, 2011), they restrict shots that belong to that scene also to the same spatiotemporal confines while simultaneously contextualizing them within the plot structure of the movie (Cutting, 2019b).

1.1.1.4 Asymmetry. Fourthly, hierarchies are said to describe asymmetric relationships between the levels, which means that one higher, more abstract level influences multiple more concrete lower levels (Figure 1). Hence, a scene is not only a more abstract narrative element (Cutting, 2016, 2019b), it also provides context to the multiple shots on the level below. In this sense, the relationship is mono-hierarchical, as multiple lower levels only relate to a single parent on the higher level (Cornet & Chute, 2016).

This asymmetric relationship moreover implies a feature of the movie hierarchy, which is, however, not necessarily part of every hierarchical system: It is nested (J. Wu, 2013), sometimes also called compositional (Salthe, 2012) or constitutive (Valentine & May, 1996), which means that the lower levels, in this case the shots, combine to form higher levels (i.e., the scene). Like a "Russian doll", the elements of one level are enclosed within the next higher layer (Salthe, 2012; Valentine & May, 1996; J. Wu, 2013). Non-nested hierarchies on the other hand can describe an ordered sequence (Valentine & May, 1996) or different developmental steps, from more general to more specific levels (Salthe, 2012). An example for this hierarchy in the movie contrxt could for instance be a ranking of movies based on rating of critics' reviews. While also describing a specific

order, features like temporal persistency or complexity cannot be used to distinguish between levels.

1.1.1.5 Near-decomposability. The fifth and last feature that is proclaimed in the hierarchy theory is called near-decomposability (Figure 1; Simon, 1977). This characteristic is two-fold: Firstly, it means that a hierarchy can be seen as a system of subsystems. In the example, a movie is a combination of scenes, and each scene is a system of multiple shots. Further, interactions between subsystems tend to be weaker than interactions within each subsystem. Thus, a scene as an individual event can stand more on its own than a single shot (Cutting, 2014, 2019b). Secondly, near-decomposability also describes that when focussing on one specific level of a hierarchy, the lower and higher levels can be neglected, as lower levels are too transient to have an impact, while higher levels are too persistent to provide more than a constant context (Simon, 1977). To illustrate this feature in the movie example, the entire movie will act as the overarching higher level, the scenes as the focus level and the shots as the transient lower level. When following the plot and focusing on scene structure, the movie as a whole only provides a constant, unchanging context. On the lower level, the shots are too brief to be noticed and are blending together (Simon, 1977; J. Wu, 2013). This aggregation can even be noticed during the viewing experience, as cuts and therefore shot transitions are designed to go unnoticed to create the illusion of a continuous environment (Magliano & Zacks, 2011). Only when focusing on the cuts, which shifts the focus to a lower level, the shot transitions are noticed.

Thus, in this work I define nested hierarchies in environmental stimuli as asymmetric, mono-hierarchical relationships between a higher level and a lower level. The higher level is thereby more abstract, complex and importantly more temporally persistent, while also providing context to lower-level elements. These lower-level elements in turn are shorter, more concrete and combine to form the higher-level elements (Figure 1).

1.2 Cortical hierarchies

The features that make up hierarchical stimuli can not only be applied in the environment but also to the structural and functional system of the brain. Like in the environment, hierarchies in the brain are useful to organize the complex cortical system into more interpretable subunits (Huntenburg et al., 2018). However, throughout the years of neuroscientific research, many different structural and functional cortical hierarchies and organizational schemes have been described: ranging from microstructural differences (R. Gao et al., 2020) to macroscale connectivity patterns (Goulas et al., 2014; Margulies et al., 2016), including individual as well as evolutionary developments (Sydnor et al., 2021), and detailing gradients of genetic expression patterns (Burt et al., 2018), neurotransmitter concentrations (Hansen, Shafiei, Markello, et al., 2022) or differences in dendritic spine density (Froudist-Walsh et al., 2023).

Historically, the investigation of the brain's structural and functional hierarchy can be traced back to mappings of (micro-)structural differences in post-mortem brains (Brodmann, 1909; Vogt & Vogt, 1928; von Economo & Koskinas, 1926). Particularly influential was the parcellation by Brodmann (1909), which was based on cytoarchitectural differences defined by the distribution of cell types, shapes and sizes in the layers of the cortical surface (for more recent reviews see Amunts & Zilles, 2015; Zilles & Amunts, 2010). As Brodmann (1909) already hypothesized however, this cytoarchitectural delineation is not only structurally but also functionally significant (Amunts & Zilles, 2015; Damiani et al., 2020), as the differences in cytoarchitecture and the emerging connectivity patterns map onto the functional processing hierarchy (Chanes & Feldman Barrett, 2016; Hilgetag et al., 2016, 2022; Mesulam, 1998): Primary sensory areas show distinguished granular layers while multimodal areas higher in the processing hierarchy exhibit simpler architectures, sometimes missing the granular layer entirely (Chanes & Feldman Barrett, 2016). Additionally, the connectivity patterns amongst the laminar layers clearly depict feedforward and feedback connections that support the functional hierarchy (Felleman &

Van Essen, 1991; Huntenburg et al., 2018; Markov et al., 2014; Markov & Kennedy, 2013; Reid et al., 2009; Vezoli et al., 2021).

Yet, considering Brodmann's (1909) organization from the perspective of hierarchy theory (e.g., J. Wu, 2013), both nested (e.g., the functional integration from unimodal to multimodal association cortices) and non-nested hierarchies (e.g., gradual changes in cytoarchitecture) are intermingled under the umbrella term "cortical hierarchy". Based on the definitions proposed by Hilgetag and Goulas (2020), the following sections will aim to distinguish different cortical schemes to specify and distil an overarching organizational principle of the cortical hierarchy.

1.2.1 Hierarchy as a gradient of features. The first set of structural principles that falls under the term cortical hierarchy can be described as a gradient of cortical features, which, among others, include the previously mentioned historical cyto- and myeloarchitectural mappings (Brodmann, 1909; Huntenburg et al., 2018; Mesulam, 1998). From the perspective of hierarchy theory, these gradients describe non-nested hierarchies or positional structures, as the cortical areas can only be sorted by the investigated features but do not satisfy the criteria outlined for nested hierarchies (see section 1.1.1; Valentine & May, 1996; J. Wu, 2013). However, despite being predominantly descriptive, these non-nested gradients can still offer various insights into the organization and processes of the brain since they relate to the functional processing hierarchy, as demonstrated by the cytoarchitectural differences (e.g., Felleman & Van Essen, 1991).

1.2.1.1 Microstructure. More recent investigations of microstructural variations established approximation methods to determine cyto- and myeloarchitectural differences using magnetic resonance imaging (MRI) instead of the classic post-mortem approaches (e.g., Brodmann, 1909). Cytoarchitecture thereby is estimated through the cortical thickness determined by the difference between pial and white matter surfaces (Goto et al., 2022; Wagstyl et al., 2015) while differences in the myelinization can be visualized by the ratio of T1- and T2-weighted MRI images (Glasser & van Essen, 2011). These *in vivo* techniques allow for a wider

availability and facilitate the acquisition of microstructural gradients in large samples (e.g., Van Essen et al., 2013). Crucially, like the post-mortem findings, the resulting approximate gradients were shown to relate to the cortical processing hierarchy as well, since unimodal sensory cortices were characterized by lower cortical thickness and higher levels of myelinization, while the opposite pattern was demonstrated for the high-level, multimodal association cortices (R. Gao et al., 2020; Huntenburg et al., 2017, 2018; Paquola et al., 2019, 2020; Rowley et al., 2015; Saberi et al., 2023; Wagstyl et al., 2015, 2020).

1.2.1.2 Gene expression. Closely related to the microarchitectural differences are the gradients of gene expression which also correlate with the functional processing hierarchy (Burt et al., 2018; R. Gao et al., 2020; G. Shafiei et al., 2020). Based on individual gene expression profiles or combined transcriptomes, previous investigations found an overlap between genetic gradients and the uni-to-multimodal axis (Burt et al., 2018; A. Chen et al., 2023; Hansen, Markello, et al., 2022; Hawrylycz et al., 2012). Further research was also able to distinguish cortical as well as subcortical functional networks based on transcriptional differences (Anderson et al., 2018; Krienen et al., 2016; Richiardi et al., 2015; Vértes et al., 2016). These gradients allow for a closer look into possible molecular processes shaping the cortical hierarchy. For example, long-range connections that may enable integration across distant brain areas are supported by genes that promote oxidative metabolism (Vértes et al., 2016). Further, as some genetic profiles were distinct for higher cognitive processes and neurological diseases that are unique to humans and non-human primates, genetic expressions gradients can also provide information on the evolutionary history of cortical hierarchy (Anderson et al., 2018; Burt et al., 2018; A. Chen et al., 2023).

1.2.1.3 Chemoarchitecture. Since many of the investigated genes encode for neurotransmitters and receptors (Anderson et al., 2018; Burt et al., 2018; A. Chen et al., 2023), it seems reasonable to also examine the chemoarchitectural gradients. Surprisingly, however, the relationship between neurotransmitter and gene expression is less straightforward than expected (Beliveau et al., 2017; Hansen, Markello, et al., 2022). Nevertheless, the transmitter and receptor

distributions also vary across the cortex and can similarly be used to distinguish between unimodal sensory and multimodal association cortices (Froudist-Walsh et al., 2021, 2023; Goulas et al., 2021; Hansen, Shafiei, Markello, et al., 2022; Kantonen et al., 2020; Naganawa et al., 2021; Savli et al., 2012) as well as different functional networks (Froudist-Walsh et al., 2023; Hansen, Shafiei, Markello, et al., 2022). Thereby, especially a relatively higher ratio of excitatory compared to inhibitory receptors characterizes higher-level areas, complementing findings that excitatory long-range connections support the integrative functions of the multimodal, associative cortices (Burt et al., 2018; Chaudhuri et al., 2015; Goulas et al., 2021; Turk et al., 2016). Additionally, these chemoarchitectural investigations revealed that multimodal integration areas contain so-called metabotropic or metabotropic-like transmitter receptors which allow for a delayed signal transmission (Goulas et al., 2021). This might shape the temporal dynamics of the cortex and help maintain the continuous activity necessary for high-level cognition and integration (Froudist-Walsh et al., 2021; R. Gao et al., 2020; Hansen, Shafiei, Markello, et al., 2022; M. Wang et al., 2013; X.-J. Wang, 2020).

1.2.1.4 Functional processing hierarchy. Evidently, these microscale features play a major role in shaping the cortical processing hierarchy by enabling localized, fast-paced signals in unimodal sensory areas, while the high-level, multimodal association cortices are characterized by slower dynamics and long-range connections that allow for integration of information over longer periods of time (cf. X.-J. Wang, 2020). On the macroscale, these micro-feature differences materialize into gradients of functional connectivity (e.g., Golesorkhi, Gomez-Pilar, Zilio, et al., 2021; Krienen et al., 2016) as well as different intrinsic and processing timescales across the cortex (e.g., Cavanagh et al., 2020; R. Gao et al., 2020). Consequently, both the gradients of functional connectivity (cf. Margulies et al., 2016) and timescales (cf. Raut et al., 2020) were shown to follow the cortical processing hierarchy like their underlying microarchitectural substructures (e.g., R. Gao et al., 2020).

Especially, the gradient of functional connectivity offers a widely applicable estimation method for the uni-to-multimodal gradient through correlation patterns in human resting-state functional magnetic resonance imaging (fMRI) data, circumventing the need for invasive tract-tracing studies (e.g., Felleman & Van Essen, 1991) and thus facilitating relating other cortical feature gradients to the processing hierarchy (e.g., Markello et al., 2022). In their influential paper Margulies et al. (2016) extracted principal components explaining the majority of variance in the functional connectivity. They found that the first component mapped onto the uni-to-multimodal-axis while the second component distinguished between the different sensory modalities. Further, these functional gradients were able to distinguish the previously described functional network architecture (Yeo et al., 2011), placing for instance the multimodal default-mode network (DMN) – involved in complex cognitive processes like emotional processing, memory and introspection (for a review see Raichle, 2015) – at the upper end of this hierarchy. This gradient from unimodal to multimodal areas within the functional connectivity network was further replicated using different methodologies (Sepulcre et al., 2012; J. Zhang et al., 2019), therefore describing a robust organizational principle of human as well as non-human brains (Margulies et al., 2016). Accordingly, it was suggested that especially similarities in the structural cyto- and myeloarchitecture play a major role in shaping which areas exhibit correlations in their functional time courses (Huntenburg et al., 2017, 2018; Paquola et al., 2019).

1.2.1.5 Cortical timescales. Others have argued that the functional connectivity between regions is grounded in the intrinsic cortical timescales, linking similarly slow dynamics of areas to a higher functional connection strength (Baria et al., 2013; Chaudhuri et al., 2015; Lurie et al., 2024; Manea et al., 2022; Salvador et al., 2005). In this context, previous studies revealed a gradient from faster to slower intrinsic time scales that also maps on the axis from unimodal to multimodal cortices (Golesorkhi, Gomez-Pilar, Tumati, et al., 2021; Ito et al., 2020; Murray et al., 2014; Ogawa & Komatsu, 2010; Raut et al., 2020). This gradient further extends to subcortical and cerebellar regions (Raut et al., 2020) and can distinguish between different functional networks

(Golesorkhi, Gomez-Pilar, Tumati, et al., 2021; Ito et al., 2020; Raut et al., 2020). In addition, these temporal differences were importantly directly related to stimulus processing and various cognitive tasks: Examining the cortical dynamics during tasks demonstrated that the intrinsic timescales adapt to the environmental demands and cognitive load (Cavanagh et al., 2020; Golesorkhi, Gomez-Pilar, Tumati, et al., 2021; Ito et al., 2020; Song et al., 2024; H. Zhang et al., 2022). Moreover, using hierarchically nested naturalistic stimuli, such as movies (see 1.1.1), previous studies demonstrated that additional multimodal areas were engaged when participants were presented with a persistent, intact section of the stimulus belonging to a higher hierarchical level (e.g., a movie scene) while shuffled, low-level stimuli (e.g., shots) only consistently activated the modality-specific primary sensory areas (Aberbach-Goodman & Mukamel, 2023; Farbood et al., 2015; Hasson, Yang, et al., 2008; Lerner et al., 2011). These findings indicated a gradient of so-called *temporal receptive windows* (TRWs) that – in analogy to their spatial namesake – describe the area-specific time frame over which the incoming sensory information can be integrated. Different TRWs therefore segregate or integrate information depending on the temporal structure of the stimulus and intrinsic dynamics of the area (Cavanagh et al., 2020; Golesorkhi, Gomez-Pilar, Zilio, et al., 2021; Hasson et al., 2015; Himberger et al., 2018; Soltani et al., 2021; Wolff et al., 2022).

The foundations of this temporal processing gradient were suggested to lay within the connective and chemoarchitectural profile of the areas, as demonstrated in a seminal computational model of the macaque cortex: Chaudhuri et al. (2015) constructed a network architecture of local excitatory connections combined with systematic long, inter-regional connections that was able to reproduce the range of intrinsic timescales, unfolding along the cortical hierarchy. Extended by more realistic synaptic properties, this model even allowed for more continuous activity in high-order areas that is necessary for complex cognition (Chaudhuri et al., 2015; M. Wang et al., 2013; X.-J. Wang, 2020). The authors further underlined the necessity of regional heterogeneity in microscale features for the emergence of timescale diversity, which

has been expanded to intra-area differences (Cavanagh et al., 2020; Rossi-Pool et al., 2021; Song et al., 2024). Only on the level of neuronal populations, the constant regional timescales and therefore the dynamic gradient along uni-to-multimodal axis is revealed (Runyan et al., 2017). This intra-regional, neuronal diversity might in turn explain the adaptation of cortical timescales to task demands (Rossi-Pool et al., 2021; Runyan et al., 2017; Song et al., 2024).

To summarize, the gradient of cortical timescales is instrumental for the functional processing hierarchy by facilitating the precise processing of individual sensory inputs in the unimodal cortices and offering a mechanism that can explain the integrative processes necessary for complex cognition in high-level, multimodal cortical areas (Golesorkhi, Gomez-Pilar, Zilio, et al., 2021; X.-J. Wang, 2020; Wolff et al., 2022). Consequently, it was suggested that the neural dynamics underlie the functional specification of cortical networks and areas (Chaudhuri et al., 2015; R. Gao et al., 2020; Kiebel et al., 2008) and play an especially pivotal role in the processing of hierarchically nested stimuli that I defined above (see 1.1.1; e.g., Hasson et al., 2015).

1.2.1.6 Overarching gradients. This review of various gradients of features in the brain not only illustrates the multitude of cortical characteristics but more importantly demonstrates the interrelationships between many of the gradients. These relationships can be utilized to combine multiple gradients to construct multimodal cortical maps that can more precisely distinguish between different cortical areas (Amunts & Zilles, 2015; Glasser et al., 2016; Hilgetag & Goulas, 2020). Thus, while feature gradients are primarily descriptive, their mechanistic relationship especially to the cortical processing hierarchy highlights their functional significance (Hansen, Shafiei, Voigt, et al., 2022; Huntenburg et al., 2018; Markello et al., 2022; Sydnor et al., 2023). In respect to the processing of environmental stimuli, the different cortical features can therefore be aggregated into a gradient ranging from the sensory-bound unimodal cortices to the integrative, more interoceptive multimodal association cortices (e.g., Chaudhuri et al., 2015; J. Zhang et al., 2019). The areas along this gradient are not only functionally distinct, belonging to different functional networks (e.g., Margulies et al., 2016), but – crucially for the processing of

hierarchically nested stimuli – also vary in regards to their preferred hierarchical level of integration. Based on area-specific temporal dynamics, these variations allow the brain to segregate or integrate different levels of hierarchal stimuli based on their temporal duration (for a review see Hasson et al., 2015).

As highlighted, the spatiotemporal functional gradient is supported by a specific structural and chemical architecture (Chaudhuri et al., 2015). The cortical layout thereby systematically combines excitatory local, recurrent interconnections and long-range, cross-regional connections with inhibitory input-control at the high-level, multimodal and output-control at the low-level, unimodal areas. This structure forms a scaffolding that can quickly adapt but is also able to maintain signals for extended periods of time (X.-J. Wang, 2020). The framework is further supplemented by a range of neurotransmitter receptors that allow for fast and precise forwarding of neural signals in the unimodal end, while the multimodal areas are characterized by slow-acting receptors, like N-methyl-D-aspartate (NMDA), that enable long-lasting postsynaptic depolarization, opening the time window for integration and high-level cognitive processes (Chaudhuri et al., 2015; X.-J. Wang, 2020).

1.2.2 Hierarchy as a progression of scales. The structural network architecture that underlies the cortical gradients implies an asymmetrical connectivity between areas, as multiple low-level communities feed into a smaller number of high-level, multimodal integration areas (Cavanagh et al., 2020; Chaudhuri et al., 2015; X.-J. Wang & Kennedy, 2016). Additionally, the theoretical formulations (Hasson et al., 2015; Wolff et al., 2022) as well as the empirical findings on TRWs (e.g. Aberbach-Goodman & Mukamel, 2023; Farbood et al., 2015; Hasson, Yang, et al., 2008; Honey et al., 2012; Lerner et al., 2011) suggest a nested organization of temporal integration that matches the defined environmental hierarchies (see 1.1.1). Both these definitions go beyond cortical hierarchies in the sense of a simple gradient of features. These organizations rather resemble a different understanding of cortical hierarchies – a *progression of scales* (Hilgetag & Goulas, 2020). In this sense, the cortical hierarchy is not constituted of an ordering of features but

is defined by a hierarchically nested organization of neurons, areas and networks, comparable to how different levels in environmental stimuli can be structured (see 1.1.1; e.g., Grafton & Hamilton, 2007).

From this network perspective, the brain is often described based on either tangible, structural connections or based on correlating functional activity patterns (Betzel & Bassett, 2017; Bullmore & Sporns, 2009; Sporns, 2013). On the functional side, Margulies et al. (2016), for instance, utilized the correlation between resting-state brain activity to identify the aforementioned gradient of functional connectivity (see 1.2.1.4). Beyond this gradient, the brain can also be divided into a hierarchical set of sub-networks nested within the global functional network (Meunier et al., 2009; van den Heuvel & Hulshoff Pol, 2010; Yeo et al., 2011). Most notable are the macroscale functional network differentiations that categorize groups of functionally associated areas into collectives that are engaged at specific states of task or rest (Ji et al., 2019; Power et al., 2011; Yeo et al., 2011).

On the structural side, early invasive tract-tracing methods mapped the structural connections down to the microscale level in macaques, cats, or nematodes (Felleman & Van Essen, 1991; Hubel & Wiesel, 1962; Stephan et al., 2001; J. H. Thomas, 1986). The development of diffusion-weighted imaging (DWI) then enabled the non-invasive, in vivo reconstruction and investigation of the physical connections between different cortical areas also in the human brain (Hagmann et al., 2007; Le Bihan, 2003; Le Bihan et al., 1986). DWI thereby visualizes movement of diffusing water molecules that is restricted both within the axons as well as by hydrophobic myelin along them, thus mapping the white matter streamlines (Jones et al., 2013; Le Bihan et al., 2001). Using this method, it was possible to demonstrate that also the structural cortical network of humans exhibits a hierarchically nested architecture (Bassett et al., 2010; Hagmann et al., 2008).

To examine both these nested structural and functional network hierarchies, the brain has to be represented as a set of areas that are either connected by white matter streamlines or

associated by functional correlations (Yao et al., 2015). This representation allows for an entirely new methodological avenue to investigate the cortical organization – *graph theoretical analyses* (for a review see Sporns, 2018), which the next sections will illuminate in detail, highlighting the hierarchical organization discovered within cortical graphs.

1.2.2.1 Graph theoretical architecture. In the context of graph theory, a *graph* is a construct of *nodes*, in the case of the brain often predefined cortical macroscale areas, connected through a network of *edges*, which are physical white matter stream lines or correlations between functional activity (Sporns, 2011, 2018; Sporns et al., 2005). However, neuroscientific graphs can also describe the individual microscale connections of neurons if the data is available through animal tract-tracing studies (e.g., Hubel & Wiesel, 1962; Stephan et al., 2001; J. H. Thomas, 1986). Additionally, this graph-structure is not limited to the context of neuroscience. Graphs can be used to describe the internet, airplane routes or even social networks (Colizza et al., 2006; McAuley et al., 2007; Milgram, 1967). Regardless of the context, the developed methods and calculations are applicable to any graph (e.g., Colizza et al., 2006; Watts & Strogatz, 1998). Thus, when investigating a network, graph theory offers an ever-growing plethora of methods to examine the properties of the global network as well as individual nodes like cortical areas (Farahani et al., 2019; Oldham et al., 2019; Rubinov & Sporns, 2010).

The nested, hierarchical cortical structure of the brain can thereby be quantified by the network's capacity for integration and segregation (Sporns, 2013). Integration on the one hand is commonly defined by the average path length between pairs of nodes, since short paths between remote areas allow for an effective global communication (Latora & Marchiori, 2001; Watts & Strogatz, 1998). Segregation on the other hand describes the presence of spatially confined clusters of nodes (i.e., sub-networks) nested within the global network structure that are more densely connected with each other than to other nodes outside this cluster (Newman, 2004; Watts & Strogatz, 1998). Interestingly, despite superficially describing opposed concepts, both

integration and segregation co-exist within the human brain network (Farahani et al., 2019; Tononi et al., 1994).

Crucially, it was proposed that only this nested, hierarchical system that combines specialized but also integrated clusters, enables the intricate parallel processing necessary for high-level cognition (Sporns et al., 2004; Tononi et al., 1994; Zamora-López et al., 2009). This balance between integration and segregation within a network was termed *small-worldness* (Watts & Strogatz, 1998). Originally based on social communities (Milgram, 1967), small-world networks, like our brain, are characterized by segregated, specialized communities – also called modules – that are interconnected by a few inter-modular nodes, that allow for a shorter path length and therefore global integration across the entire network (Bassett & Bullmore, 2006; Fornito et al., 2016; Sporns & Zwi, 2004; Watts & Strogatz, 1998).

This definition however also exposes two additional features of small-world networks: Firstly, the network can be sub-divided into a nested modular structure, which was demonstrated for both structural and functional cortical networks (Bassett et al., 2010; Hagmann et al., 2008; Harriger et al., 2012; Meunier et al., 2009; Sporns & Zwi, 2004; van den Heuvel et al., 2008). As a hierarchical system, this module structure is not only nested within the global network but can also be described as near-decomposable since the segregated communities have more intra-modular than inter-modular edges (Bassett et al., 2010; Meunier et al., 2009). Small-world networks thus fulfill the criteria for nested hierarchies (Simon, 1977; see 1.1.1).

Secondly, small-world networks feature a set of connector nodes with long-range edges linking between modules, while other nodes only connect within their own module (Guimerà & Nunes Amaral, 2005; Hagmann et al., 2008). This shows that nodes can occupy different positions within the hierarchy of the network based on their local connectivity profile (Sporns, 2018). These roles can not only be defined based on the modular structure of the graph but also other nodal measures, which classify a node's centrality for the network (Oldham et al., 2019; Oldham & Fornito, 2023; Sporns et al., 2007; van den Heuvel et al., 2010). One of the most commonly

employed measure of nodal centrality in this context is *degree*, which simply counts the number of edges that are connected to a node (Rubinov & Sporns, 2010). Despite its simplicity, especially the degree distribution can be highly informative of the network's organization (Rubinov & Sporns, 2010; Sporns et al., 2004).

Complex graphs like the brain and other small-world networks for instance were shown to approximately depict a so-called power law distribution of degrees, which classifies the existence of only a small number of well-connected, high-degree nodes – the so-called *hubs* of the network (Achard et al., 2006; Barabási & Albert, 1999; Watts & Strogatz, 1998). Interestingly, in the human brain, these hubs often represent the nodes of long-range connection and integration, which are commonly located in multimodal association areas (Achard et al., 2006; Sporns et al., 2004; Zamora-López et al., 2010). Hence, hubs are crucial for the network's integrity, hosting the majority of its information flow and even are suggested to play a role in the maintenance of information over longer periods of time (Sporns et al., 2007; van den Heuvel et al., 2010). Further, these high-degree nodes were shown to form their own densely connected "meta-network" coordinating across multiple sub-systems nested within the global network, as it contains the majority inter-module connections (Gómez-Gardeñes et al., 2010; Hagmann et al., 2008; Harriger et al., 2012; Zamora-López et al., 2009, 2010).

Therefore, it was suggested that the complex connectivity of cortical networks that supports the brain's manifold functionality is not only characterized by a small-world architecture but more importantly also by this richly interconnected set of central regions (Achard et al., 2012; Gómez-Gardeñes et al., 2010; Mišić et al., 2014; Zamora-López et al., 2016). This conglomerate of regions was termed the *rich club*, based on the high-degree (i.e., rich) regions that are constituting it. Moreover, true to the motto "the rich get richer", these well-connected nodes also share the tendency to accumulate even more connections during network development (Albert & Barabási, 2002; Zhou & Mondragón, 2004). Due to its importance for the network's integrity and

nested hierarchical structure (e.g., Gómez-Gardeñes et al., 2010; Mišić et al., 2014), the next paragraphs will review the rich club in detail.

1.2.2.2 The rich club. The rich club was first described by Zhou and Mondragón (2004) not in the context of neuroscience but for the links between websites. It describes a set of nodes in the graph that have many connections to other nodes but, more importantly, are over-proportionately connected to each other, forming a club structure (Colizza et al., 2006). The presence of a rich club architecture can therefore be determined by the rich club coefficient

$$\phi(k) = \frac{2E_{>k}}{N_{>k}(N_{>k}-1)} \quad (1),$$

with k representing a specific nodal degree, $E_{>k}$ the number of connections between nodes of a degree higher than k and $\frac{N_{>k}(N_{>k}-1)}{2}$ the maximal number of connection possible between all nodes $N_{>k}$ that have more than k connections. Thus, a rich club coefficient $\phi(k) = 1$ would mean that all nodes that share a degree higher than k also mutually connect to each other while $\phi(k) = 0$ indicates that none of the nodes share any edges gaining their degree only from connections to lower-degree nodes and not forming an interconnected club. However, an increase in the rich club coefficient $\phi(k)$ with the degree k alone is not sufficient for the presence of rich club architecture as this increase can also occur in randomly assorted networks (Colizza et al., 2006). Therefore, a crucial extension was made to normalize the rich club coefficient $\phi(k)$ using values calculated from appropriate null models or random graphs that have the same degree distribution as the empirical network (Colizza et al., 2006; McAuley et al., 2007):

$$\phi_{norm}(k) = \frac{\phi(k)}{\phi_{random}(k)} \quad (2).$$

The presence of the rich club phenomenon can thus also be verified and statically compared against the distribution of random coefficients using permutation tests to identify a significant range of degrees k – the so-called rich club regime – for which high-degree hubs of the empirical network are more inter-connected than in the random networks (van den Heuvel & Sporns, 2011).

After describing the rich club phenomenon in complex, environmental networks like air traffic connections (e.g., Colizza et al., 2006), the presence of highly connected hubs within the brain strongly suggested existence of a cortical rich club as well (Hagmann et al., 2008; Sporns et al., 2007). Consequently, van den Heuvel and Sporns (2011) were able to demonstrate the rich club also within the human structural connectome. In their groundbreaking paper the authors showed a network of high-degree nodes located in areas around the cortical midline – namely, the superior frontal cortex, the superior parietal lobe (SPL), and the precuneus – as well as subcortically extending to the hippocampus, putamen and thalamus. These hubs were not only densely connected with each other but also linked different structural modules, hence possibly representing areas of multimodal integration that are central for functional integration as well (Sporns, 2013; Zamora-López et al., 2009, 2010).

In the years since its discovery, the rich club was established as a consistent network feature of the cortex (for reviews see Griffa & van den Heuvel, 2018; D. J. Kim & Min, 2020). Multiple studies were able to replicate the locations of the rich club hubs across different populations and cortical parcellation schemes signifying the robustness of the phenomenon (Ball et al., 2014; Grayson et al., 2014; Khalilian et al., 2021; Kocher et al., 2015; Liang et al., 2019; Mišić et al., 2014; Riedel et al., 2022; van den Heuvel et al., 2012). While mainly concerning structural networks (Z. Wang et al., 2015), the rich club architecture was also uncovered in functional networks (M. Cao et al., 2014; Grayson et al., 2014; Liang et al., 2018; Schroeter et al., 2015). As the structural network was shown to predict the functional topography (Hermundstad et al., 2013; Honey et al., 2009; Z. Wang et al., 2015), the functional rich club hubs even showed considerable overlap with the structurally identified regions as functional hubs were located for instance in superior frontal cortex, precuneus, hippocampus or putamen (Grayson et al., 2014; Jiao et al., 2020; F. Li et al., 2022; Peng et al., 2023). However, due to the variability of functional networks, the activity between structural rich club hubs was only moderately correlated indicating that they could participate across different task domains (Collin, Sporns, et al., 2014; Griffa & van den Heuvel,

2018). Beyond that, rich club hub locations were even largely similar across species, particularly in those areas not undergoing substantial evolutionary development, suggesting that the rich club phenomenon is part of the general blueprint for cortex construction (de Reus & van den Heuvel, 2013b; Fulcher & Fornito, 2016; Griffa & van den Heuvel, 2018; Harriger et al., 2012; D. J. Kim & Min, 2020; Nigam et al., 2016; Scholtens et al., 2014; Zamora-López et al., 2010).

Yet, despite being such a fundamental network feature, the rich club and its long-range connections were found to be very costly and energy-intensive for the brain, as they make up a large part of the metabolic consumption (Collin, Sporns, et al., 2014; Fulcher & Fornito, 2016; Hansen, Shafiei, Voigt, et al., 2022) and account for the majority of the network's wiring (Harriger et al., 2012; Rubinov et al., 2015; van den Heuvel et al., 2012). At first glance, this appears to be contradictory to the previously largely assumed principle of wiring cost minimization in the brain (Kaiser & Hilgetag, 2006). Therefore, tolerating the high costs suggests an irreplaceable role that the rich club fulfils that justifies the upkeep of such a high-maintenance network structure.

This important role becomes especially apparent when examining the consequences of pathological variations in the rich club architecture: Studies across multiple, different neurological and psychiatric diseases could demonstrate abnormalities related to the rich club hubs in the clinical samples (R. Cao et al., 2020; Collin et al., 2017; Crossley et al., 2014; Griffa et al., 2013; W. J. Lee et al., 2018; O'Donoghue et al., 2017; Ray et al., 2014; Reavis et al., 2020; van den Heuvel et al., 2013; Y. Wang et al., 2019; Yan et al., 2018). However, the issues do not necessarily affect the entire rich club, but rather individual hubs that can be related to the specific deficit of the disorder at hand (Crossley et al., 2014). Taking Alzheimer's disease as an example, the structural hub abnormalities were mainly located in the middle temporal lobe, the hippocampus and the frontal lobe (R. Cao et al., 2020; Crossley et al., 2014; W. J. Lee et al., 2018; Yan et al., 2018), which might be linked to the characteristic issues in memory and executive functioning associated with this disease (Pini et al., 2021; Tang et al., 2024). Additionally, variations in the rich club organization also prominently explain differences in healthy aging

(Baggio et al., 2015) or individuals with outstanding cortical abilities (Bathelt et al., 2018; D. J. Kim et al., 2016; Ma et al., 2017; Solé-Casals et al., 2019).

All these findings, however, still raise the question of what exactly makes this organizational pattern so indispensable for unimpaired brain functionality, justifying the high wiring and metabolic costs.

Based on clinical studies, the alterations in rich club architecture were often linked with increases in segregation and decreases in integration of the network, leading to a difference in small-wordless and reduction in communication efficiency (for reviews see Crossley et al., 2014; Griffa et al., 2013). These changes can also be computationally investigated by simulating the loss of the rich club through specifically targeted attacks on network hubs or connecting edges compared with randomly selected nodes (e.g., Albert et al., 2011). In this context, studies identified that specifically targeting the densely connected nodes of a network caused significant reductions in the global efficiency of the network (Alstott et al., 2009; Crossley et al., 2014; Oldham & Fornito, 2023). Similarly, removing edges between rich club hubs also had detrimental impact on the efficiency of the network as the majority of shortest paths through the network involved the rich club connections (de Reus & van den Heuvel, 2013b; Liang et al., 2019; van den Heuvel et al., 2012; van den Heuvel & Sporns, 2011). Lesions of network hubs could even lead to a collapse of the network (Alstott et al., 2009; Joyce et al., 2013; Newman, 2002; Tian & Sun, 2022).

Beyond the pure structural impact, these simulations also highlighted that an unharmed rich club architecture is instrumental for an effective functional connectivity (Honey & Sporns, 2008; Lopes et al., 2017; van den Heuvel & Sporns, 2013a; Váša et al., 2015) as the rich club connects and integrates information across the different functional modules (Aerts et al., 2016; Gómez-Gardeñes et al., 2010; van den Heuvel & Sporns, 2013a). The relatively few energy-intensive, long-range intermodular connections of the rich club thereby allow for a short path length across the network comparable to that of random networks (Harriger et al., 2012; van den Heuvel et al., 2008; van den Heuvel & Sporns, 2011). Thus, having this connective backbone is

globally more energy-efficient than replacing it with a fragmented path of multiple short-range links (Bassett & Bullmore, 2006; Bullmore & Sporns, 2009; Sporns, 2013). Despite being biologically costly, the rich club therefore represents the optimal organization for the balance between integration and segregation (Bullmore & Sporns, 2012; Zamora-López et al., 2010) that allows for specialized and parallel-working modules as well as their aggregation within the rich core (de Reus & van den Heuvel, 2013b; van den Heuvel & Sporns, 2013a).

In addition, this coexistence of integration and segregation that is supported by the rich club also allows for a higher network complexity, which is reflected in the functional dynamics (Váša et al., 2015). The rich club hubs were thereby shown to be integral for complex and flexible activity patterns that shape the dynamics of the entire cortex (Bullmore & Sporns, 2009; Gollo et al., 2015; Gómez-Gardeñes et al., 2010; Griffa & van den Heuvel, 2018; Harriger et al., 2012; Mišić et al., 2014; Oldham & Fornito, 2023; Schmidt et al., 2015; Senden et al., 2014, 2017, 2018; Sporns, 2013, 2018; Sporns & Zwi, 2004; Watanabe, 2013).

In their seminal paper, Gollo et al. (2015) simulated the temporal dynamics within the macaque's neuronal network and demonstrated that the structural rich club architecture, defined by a densely connected core linking the sparsely connected periphery, allowed for complex and hierarchically organized functional dynamics. They found that the rich club hubs sat at the apex of so-called resonant connective motifs. These connective profiles are perfectly suited for slower, more stable dynamics and can synchronize neighbouring regions (also see Csermely et al., 2013). The authors therefore proposed a c*hronoarchitecture*[1] formed from the slow, persistent rich core and the fast, transient periphery which they respectively related to the processing of rather persistent introspective and more fluctuating exteroceptive perception (Gollo et al., 2015).

Further computational modelling studies were able to replicate the rich club's role in the efficient synchronization and integration across functionally segregated modules (Schmidt et al.,

[1] The term chronoarchitecture was adapted from the spatiotemporal cortical topography during the perception of naturalistic stimuli (Bartels & Zeki, 2004, 2005).

2015; Watanabe, 2013). The presence of the structural rich club phenomenon thus enabled functional complexity and diversity of the cortex (Gu et al., 2019; Senden et al., 2014, 2017, 2018). In this context, it was suggested that the rich club core is especially important for the execution of tasks (compared to resting-state) as it gates the integration across specialized modules in the periphery, acting as a global workspace (Senden et al., 2017, 2018). The structural rich club is therefore instrumental for guiding and integrating the cortical dynamics through its slow, stable rhythms, sitting in the centre of the cortical chronoarchitecture (Bassett et al., 2013; Gollo et al., 2015).

Ultimately, this hypothesis of a more persistent, slower core network nested within and connecting a segregated and specialized global network circles back to the idea of Chaudhuri et al. (2015), who similarly proposed heterogenous cortical dynamics based on the combination of interconnected local and few long-range connections. Thus, approaching the concept of cortical hierarchies from either the perspective of a gradient of feature (see 1.2.1) or from the perspective of a nested progression of network scales (see 1.2.2), both converged on one central element in the end – *time*.

1.3 The time of the brain

Throughout the last chapters, I have illustrated that the cortical hierarchy, as defined by gradients of features or as a nested network of connected, specialized modules, is keenly suited for producing and processing signals at different temporal scales (e.g., Chaudhuri et al., 2015; Gollo et al., 2015). But why is specifically time so central to the brain? What role does the chronoarchitecture play in the context of the hierarchically nested stimulus structures in our environment?

The cortical network as well as the microstructural and chemoarchitectural gradients that shape the dynamic hierarchy of the brain were suggested to have evolved in adaptation to environmental demands, including the need to process a wide range of durations and rhythms in natural stimuli (Soltani et al., 2021). The world that we – and therefore also our brains – inhabit, unceasingly changes on a multitude of different timescales (e.g., Golesorkhi, Gomez-Pilar, Zilio, et al., 2021). On an environmental scale, a flash might light up the sky only the for fraction of a second, while the tides turn about every six hours and climate changes (usually) slowly unfold over more than a single human's lifetime (cf. Lohmann et al., 2020). Similarly, on a more tangible, individual scale, these dynamics can be illustrated once again using the movie example introduced above (see 1.1.1): A movie is about two hours long. During its runtime we watch movements and gestures that might only take seconds, we listen to dialogues that can last minutes and ultimately, we assimilate the plot structure that makes up the entire length of the movie (cf. Cutting, 2014).

Like in the brain, where the intrinsic timescales were put forth as an organizing principle (e.g., Gollo et al., 2015), the environment can therefore also be structured according to its depicted rhythms. As defined for hierarchically nested stimuli (see 1.1.1), one important feature that distinguishes the different hierarchical levels is their temporal duration (Valentine & May, 1996; J. Wu, 2013). Higher levels, like the movie scene or weather trends are more persistent than lower levels like a single frame if the movie or flash in the night sky. Since many different

environmental stimuli can be represented as nested hierarchies (e.g., Fitch & Martins, 2014; Jeon, 2014), it was proposed that the temporal persistency could also be the overarching, organizational principal in the world around us: Uithol and colleagues (2012) fundamentally compared different possible organizations in the context of the action hierarchy, which describes the arrangement of individual movements and actions that fall under one overarching goal (e.g., Hamilton & Grafton, 1993). They concluded that an arrangement of the individual levels based on their temporal persistency represents the self-organizing, flexible structure that is necessary to adequately model the hierarchical architecture of actions, while still accommodating for clear distinction between elements, multiple parallel goals and a mutual bottom-up and top-down influences. Beyond actions, time as an organizational principal was furthermore also applied to other nested hierarchical stimuli like movies (e.g., Hasson, Yang, et al., 2008; also see Figure 1), language (e.g., Poeppel, 2003), music (e.g., Farbood et al., 2015), or even autobiographical memories (e.g., Conway, 2005). Moreover, based on the variations of neural dynamics, temporal stability may offer a specific mechanism for implementing and representing environmental hierarchies within the brain (e.g., Golesorkhi, Gomez-Pilar, Zilio, et al., 2021). Thus, the concept of time is not only essential to the neural architecture but also for the stimulus structures in the world that the brain is adapted to (e.g., Soltani et al., 2021).

1.3.1. The time of the brain – in theory. Consequently, various neuroscientific theories and models already proposed that the temporal organization forms the intersection between the external and internal world:

Originally, Fuster (2001) suggested a hierarchical *perception-action cycle* that was anchored on the upper end by the multimodal association cortices on the sensory side and by the prefrontal cortex (PFC) in the motor hierarchy. Both these high-level regions were indicated to interact with each other and integrate information over longer periods of time, even across sensory discontinuities, with the purpose of controlling and performing actions. This proposal was later incorporated into computational models, which further highlighted the importance of

integrating as well as maintaining information across time (Botvinick, 2007, 2008). More recent investigations could then empirically demonstrate the proposed slower intrinsic timescales within the multimodal cortices (Golesorkhi, Gomez-Pilar, Tumati, et al., 2021; Hasson et al., 2015; Raut et al., 2020). The integrative role Fuster (2001) affiliated with the multimodal areas was also supported by the convergence of structural (e.g., Felleman & Van Essen, 1991) as well as functional cortical pathways (Sepulcre et al., 2012) within the multimodal areas. In this context, Fuster's (2001) cortical hierarchy was also translated into a network neuroscience perspective, as the frontal and parietal aspects of the perception-action cycle were mapped onto the functional fronto-parietal control network (FPN) that orchestrates the integration across more modality-specific subnetworks (E. Y. Choi et al., 2018; Nee, 2021). Also in the structural network, dynamically stable, integrative hub regions (e.g., the rich club hubs) were suggested to overlap with the multimodal association cortices (e.g., Zamora-López et al., 2010). In accordance, the temporally persistent, higher levels of the action selection gradient were specifically associated with structural network hubs in the dorsal-lateral PFC (Nee & D'Esposito, 2016).

In a similar vein, Koechlin and Summerfield (2007) introduced a rostro-caudal gradient of executive control, starting in the premotor cortex and culminating in the frontopolar regions, along which temporal integration progressively increases. The so-called *cascade model* proposed that the more caudal regions only utilize the immediate sensory information for action section and control while the more rostral areas incorporate information over longer periods of time, allowing for more differentiated consideration of a longer episodic context and therefore hierarchically higher, more temporally persistent, complex action goals (Koechlin & Summerfield, 2007). In accompanying fMRI studies, Koechlin et al. (1999, 2003) could also demonstrate initial neurofunctional evidence for their proposed temporal processing gradient. Nevertheless, this one-dimensional gradient along the lateral frontal lobe was soon deemed as too simplistic (Reynolds et al., 2012). The concept was therefore supplemented by a medial-lateral aspect, distinguishing between laterally located representation and medially calculated predictions (W.

H. Alexander & Brown, 2011, 2018) as well as subcortical loops, which gate the updating of higher-level context information (Badre & Frank, 2012; Chatham et al., 2014; Nee & Brown, 2013). Nonetheless, the aspect of increasing temporal integration persisted across the revisions (Badre & Nee, 2018; Fuster & Bressler, 2015).

Beyond the action hierarchy, early models of visual perception similarly indicated that the signal processing steps along the sensory path were specifically adapted to increasingly longer spatiotemporal frequencies of the environment arguing for the coherence of environmental and sensory hierarchies (Simoncelli & Olshausen, 2001). Against this backdrop, a prominent computational study by Kiebel and colleagues (2008) expanded on the relationship of environmental and sensory dynamics as they differentiated between long-term environmental causes or contexts encoded within high-level cortical areas and the more transient percepts processed in lower cortical regions. The authors linked the distinction between high and low cortical areas firstly to differences in neurotransmitters, specifically mentioning the slow-operating NMDA receptors, and secondly to the connective architecture of forward and backward trajectories, mirroring the concepts later included in Chaudhuri et al.'s (2015) network model. Moreover, Kiebel et al. (2008) placed the temporal specialization of different cortical regions into the larger context of prediction, as they argued that the brain learned a predictive model of the environmental rhythms across multiple temporal scales in parallel, minimizing the prediction error along the way. The more persistent rhythms can thus exert control by providing context to the more transient predictions. In the movie example, the temporally more stable scenes for instance can offer the context for the transient environmental sounds that are occurring. Thus, having access to multiple temporal levels allows a more flexible model for predicting and adapting to the sensory environment (e.g., Lawson et al., 2017).

Recently, a more overarching perceptive processing model was introduced as an extension of Kiebel et al.'s (2008) idea. Based on a moving stimulus input, the *dynamic predictive coding model* by L. P. Jiang and Rao (2024) autonomously learned a hierarchy of spatiotemporal

receptive windows that mirrored the receptive fields and intrinsic timescales of empiric findings (e.g., Murray et al., 2014). The higher hierarchical levels thereby represent increasingly more abstract states that directly influence the transition dynamics of the lower levels, while higher level state shifts occur only when the prediction error at a lower level becomes too large, indicating that the higher-level model no longer fits and needs to be adjusted (L. P. Jiang & Rao, 2024). To illustrate these state transitions, I will use three levels from the hierarchical movie structure introduced above (see 1.1.1): frame, shot and scene.

According to the model, when our brain watches the frames of a movie, it infers a higher-level representation (i.e., a shot) that predicts the dynamics of the frames. So, within each shot, the subsequent frames can be predicted. Simultaneously, a predictive model of the shot transition dynamics is generated, as the brain learns about the scene level. If the prediction error evoked by a frame becomes too large (i.e., the visual differences too striking), the shot level transitions to its next state, which is still predicted by the overarching scene model. However, when prediction error of the frame is so large that it can no longer be accommodated by a shot transition, the next highest level needs to change its state, thus the next scene state begins. This model therefore works comparably to automatic shots and scene annotation systems that use transitions in low-level and more abstract visual and auditory information to automatically identify cuts and narrative shifts in a movie (e.g., Zhu et al., 2023).

1.3.2. The time of the brain – in practice. Even more intriguingly, this exact transition between dynamic cognitive states that represent the different nested hierarchical levels of the movie structure was also shown empirically. Using hidden Markov models (Baldassano et al., 2017; Sava-Segal et al., 2023; E. Yang et al., 2023) or a greedy state boundary search (Geerligs et al., 2022; Oetringer et al., 2025), previous studies did not only show that the brain indeed transitions between representative states on multiple temporal scales at once, but also localized these different states in specific cortical areas and networks. Specifically, states associated with hierarchically more persistent, higher levels of the stimulus (e.g., specific scenes) were

represented in areas higher in the visual processing hierarchy that demonstrated less frequent shifts in cortical activation patterns (e.g., medial parietal cortex; Baldassano et al., 2017), while more transient, low-level visual features were associated with frequent state changes in the primary visual cortices (Oetringer et al., 2025).

Particularly the course state transition in high-level, multimodal association cortices thereby aligned with behaviourally acquired narrative scene boundaries in the movie (Baldassano et al., 2017), suggesting that these cortical transitions represent consciously perceived stimulus features (cf. Sava-Segal et al., 2023; van der Meer et al., 2020). This is further supported by E. Yang et al. (2023) who showed that the brain state transitions coincided with the occurrence of certain semantical concepts. In this context, they place special emphasis on DMN, which also demonstrated the temporally most persistent brain states and the least frequent state transitions (E. Yang et al., 2023). The involvement of the DMN, which sits on the upper end of the cortical uni-to-multimodal hierarchy (Margulies et al., 2016) and is characterized by slow intrinsic timescales (Golesorkhi, Gomez-Pilar, Tumati, et al., 2021; Ito et al., 2020), was further implied to support a high-level understanding of a presented stimulus that is shared between people even when the stimulus is presented in different modalities (J. Chen et al., 2017; Sava-Segal et al., 2023; Yeshurun et al., 2021; Zadbood et al., 2017). Overall, these studies suggest, that the processing of the temporal structure of complex, nested-hierarchical stimuli, like movies, is directly related to the timeframes of brain states across the cortical hierarchy.

Furthermore, the identified network state dwell times across the cortex (e.g., E. Yang et al., 2023) also line up with the previously introduced gradient of TRWs (see 1.2.1.5) that also indicated the specific attunement of hierarchically higher cortical areas to more temporally persistent and content-rich stimuli while less complex, more transient stimuli are only engaging the primary sensory areas (for a review see Hasson et al., 2015). According to the hierarchy of process memory framework, TRWs are defined as “the window of time in which prior information from an ongoing stimulus can affect the processing of newly arriving information.” (Hasson et al.,

2015, p.307) and were therefore closely linked to the prediction of future input based on the previously experienced stimuli (Aberbach-Goodman & Mukamel, 2023; Mattar et al., 2016; Wolff et al., 2022).

The study of TRWs goes back to the work of Hasson, Yang and colleagues (2008) who established this hierarchy of temporal integration in an fMRI experiment. In their seminal study, they parcellated a naturalistic, hierarchically nested stimulus – in their case a silent movie – into segments of different duration (around 4 s, 12 s and 36 s, respectively). These movies segments were then shuffled and reassembled to create movie clips that varied in respect to the duration of continuous presentation (Hasson, Yang, et al., 2008). Using *inter-subject correlation* (ISC), the authors found consistent engagement across participants only in the early visual areas like the V1 and area MT+ when the stimulus was shuffled at the shortest time window (~4 s). Increasing the temporal persistency of presented segments (~12 s) in turn additionally engaged hierarchically higher areas like the parahippocampal place area, the fusiform face area or the precuneus. Finally, presenting the longest segments (~36 s) or the entire movie specifically identified the frontal eye fields and the temporo-parietal junction (TPJ; Hasson, Yang, et al., 2008).

Since then, the results have been replicated multiple times using different stimulus modalities: Lerner et al. (2011) used an auditory narration and located short TRWs in the early auditory areas, while the long TRWs were demonstrated similarly in the TPJ and precuneus but also the superior temporal sulcus (STS). These findings were partially reproduced when presenting participants with a piece of music as also an increase of TRWs was found from early to higher auditory areas along the STS (Farbood et al., 2015). Mirroring Uithol et al.'s (2012) time-based action hierarchy, Aberbach-Goodman and Mukamel (2023) as well as R. M. Thomas et al. (2018) showed longer TRWs in areas related to the overarching action goals like the SPL.

Beyond these findings in fMRI, the variation of TRWs has also been identified in extra- and intracranial electrophysiological signals, extending the temporal range also to faster frequencies (Honey et al., 2012; Norman-Haignere et al., 2022). This generalizability was further supported by

Stephens et al. (2013) showing that the distribution of TRWs was also reflected in the signal's overall power spectra of the engaged cortical areas, mirroring the intrinsic timescales at rest (cf. Golesorkhi, Gomez-Pilar, Zilio, et al., 2021). In addition, similar to findings regarding intrinsic cortical dynamics (e.g., Cavanagh et al., 2020), TRWs were also suggested to be adaptive to the dynamic features of the stimulus to accommodate natural event boundaries changing on varying timescales (Geerligs et al., 2022). Accordingly, it was shown that the timeframe of integration was – at least to a certain degree – able to adjust to the frequency of stimulus presentation (Baumgarten et al., 2021; Lerner et al., 2014). Thus, although TRWs – like intrinsic cortical timescales – are thought to be grounded in the microstructural and chemoarchitectural cortical framework (e.g., Chaudhuri et al., 2015) and reflect naturally occurring temporal coherencies (Baumgarten et al., 2021; Golesorkhi, Gomez-Pilar, Zilio, et al., 2021), these results nevertheless indicate a range of adaptability for environmental demands.

Overall, the study of TRWs therefore underlined a functional principle that already showcased in Fuster's (2001) perception-action cycle: Processing the temporally short, hierarchically low-level elements of a stimulus only engages the modality specific early sensory areas, while longer, hierarchically higher stimulus events are integrated within multimodal hubs that include for instance the medial PFC, precuneus, angular gyrus, or TPJ (Aberbach-Goodman & Mukamel, 2023; Farbood et al., 2015; Hasson, Yang, et al., 2008; Lerner et al., 2011). These consistently engaged high-level areas interestingly overlapped remarkedly with the DMN (Yeshurun et al., 2021), linking long TRWs to brain states related to high-level understanding and memory encoding of the presented stimulus (Baldassano et al., 2017; J. Chen et al., 2016; E. Yang et al., 2023; Zadbood et al., 2017).

1.4 Summary & Research Questions

The last paragraphs have illuminated the relationship between environmental and cortical hierarchies. Ultimately, the temporal structure – or chronoarchitecture – emerged as the central principle for both the outside world and the cortical organization. More precisely, environmental stimuli, like movies or actions, can be represented as nested, hierarchical structures, in that lower, less abstract and temporally shorter levels mono-hierarchically combine to form higher levels that, in contrast, are more abstract and persist for longer periods (e.g., J. Wu, 2013). In this context, especially the temporal duration was indicated as a generalizable and flexible organizational principle across different kinds of stimuli (e.g., Uithol et al., 2012).

More importantly, time also offers a promising mechanism for representing the different hierarchical levels in the brain through the persistency of cortical dynamics, since these dynamics were shown to vary systematically across the cortical hierarchy (e.g., Golesorkhi, Gomez-Pilar, Zilio, et al., 2021). The outlined evidence therefore suggests that areas with slower temporal dynamics integrate incoming stimulus signals over longer periods of time. This allows the synthesis of information across multiple transient, low-level stimuli into more persistent, high-level representations. These long-lasting stimulus representations can in turn also influence and predict the incoming lower-level stimuli (e.g., L. P. Jiang & Rao, 2024; Wolff et al., 2022).

The analysis of cortical hierarchies revealed, that these variations in cortical functional dynamics can be ascribed to the interplay of the macro-level structural connectivity and the microstructural as well as chemoarchitectural properties of the cortical areas (e.g., Chaudhuri et al., 2015; Gollo et al., 2015). Although theoretically suggested and demonstrated in computational models, the direct relation between the processing of hierarchically nested stimuli and the structural cortical hierarchy, particularly the rich club architecture has not been tested empirically. This thesis set out to close this gap in research. For this purpose, I investigated three Research Questions within the scope of this PhD project:

1. Is the rich club architecture and the rich-core-periphery axis a possible spatial layout on which the levels of the environmental hierarchy unfold? (Study 1)
2. How is this temporal persistency reflected within the brain's structural and functional layout? (Study 2)
3. Are the hierarchically nested stimuli processed based on the temporal persistency of their hierarchical levels? (Study 3)

Since the theoretical background provided clear evidence for the significance of the structural rich club for the processing of hierarchically nested stimuli, **Study 1** tested this central assumption of Research Question 1. We therefore predicted that areas that are part of the cortical structural rich club that we specified through a group-wise connectome within the study's sample would be more involved in the processing of hierarchically higher levels of a nested stimulus structure. Based on previous investigations, these regions of interest might include the superior frontal gyrus (SFG), the SPL as well as the precuneus (cf. van den Heuvel & Sporns, 2011). Approaching the question from the opposite side, we additionally analysed the specific spatial layout and structural network centrality of the areas engaged by the hierarchically nested stimulus to investigate if the gradient of functional processing maps onto the axis from more peripheral nodes to highly central network hubs, which would accordingly be more involved in the integration of temporally persistent stimulus material.

In line with Research Question 2, **Study 2** further examined the role the structural rich club plays in shaping the temporal layout of the cortex. For this we directly compared the rich club architecture's ability to explain the distribution of intrinsic resting-state timescales as well as TRWs identified using the experimental data of **Study 1** across the cortex against other spatial layouts. These competing organizational schemes included the diverse club, proposed as a direct alternative to the rich club (Bertolero et al., 2017), the functional uni-to-multimodal gradient (Ji et al., 2019; Sepulcre et al., 2012), and the spatially defined posterior-lateral-to-anterior-medial

axis. Further we explored the influence of various other centrality measures as well as cortical thickness as an approximation of cytoarchitectural differences (Wagstyl et al., 2015). In line with the presented theoretical background (e.g., Gollo et al., 2015), we hypothesized that primarily the structural rich club orchestrates the temporal layout of the cortex. Accordingly, we expected that the rich club model would emerge victorious in a Bayesian model comparison between the considered functional and structural organizations. In this context, we also inspected the similarity amongst cortical organizations, as for instance previous rich club findings suggested a substantial overlap between the hub regions and the multimodal association cortices (cf. Zamora-López et al., 2010).

Finally, **Study 3** delved deeper into the processing of environmental stimuli and investigated how the persistency compared with the complexity of the depicted stimulus content affects the cortical processing (cf. Research Question 3). Since both temporal duration as well as the complexity increase in unison from lower or higher hierarchical levels (e.g., J. Wu, 2013), the effects demonstrated for TRWs using naturalistic stimuli (cf. Hasson et al., 2015) cannot be attributed unequivocally to either duration or content complexity. Using a frame-wise manipulation of a naturalistic movie, **Study 3** aimed to disentangle the influences that these two aspects of hierarchically nested stimuli have on cortical processing. Based on previous research regarding natural stimulus processing (e.g., Baldassano et al., 2017; Baumgarten et al., 2021; Geerligs et al., 2022; Hasson et al., 2015), we hypothesised that duration and content complexity interact but also engage distinct cortical processes.

Together, these studies investigate the cortical organization underlining the processing of hierarchically nested stimuli. The main focus lies on the chronoarchitectrue shaped by the structural rich club network and on how the temporal composition of the stimuli relate to their cortical processing. The combined results provide evidence on the theorized significance of the rich club for the cortical dynamics and the structural basis of cortical integration and complex cognition.

2 Research Articles

2.1 Study 1: The significance of structural rich club hubs for the processing of hierarchical stimuli

Running title: 2.1 The significance of structural rich club hubs

Falko Mecklenbrauck, Marius Gruber, Sophie Siestrup, Anoushiravan Zahedi, Dominik Grotegerd, Marco Mauritz, Ima Trempler, Udo Dannlowski, & Ricarda I. Schubotz (2024)

Human Brain Mapping, *45*(4), Article e26543

https://doi.org/10.1002/hbm.26543

Check for updates

Received: 9 June 2023 | Revised: 17 October 2023 | Accepted: 9 November 2023
DOI: 10.1002/hbm.26543

RESEARCH ARTICLE

WILEY

The significance of structural rich club hubs for the processing of hierarchical stimuli

Falko Mecklenbrauck[1,2] | Marius Gruber[3,4] | Sophie Siestrup[1,2] | Anoushiravan Zahedi[1,2] | Dominik Grotegerd[3] | Marco Mauritz[3,5] | Ima Trempler[1,2] | Udo Dannlowski[2,3] | Ricarda I. Schubotz[1,2]

[1]Department of Psychology, Biological Psychology, University of Münster, Münster, Germany
[2]Otto Creutzfeldt Center for Cognitive and Behavioral Neuroscience, University of Münster, Münster, Germany
[3]Institute for Translational Psychiatry, University of Münster, Münster, Germany
[4]Department for Psychiatry, Psychosomatic Medicine and Psychotherapy, University Hospital Frankfurt, Goethe University, Frankfurt, Germany
[5]Institute for Computational and Applied Mathematics, University of Münster, Münster, Germany

Correspondence
Falko Mecklenbrauck, Department of Psychology, Biological Psychology, University of Münster, Münster, Germany.
Email: f_meck01@uni-muenster.de

Abstract

The brain's structural network follows a hierarchy that is described as rich club (RC) organization, with RC hubs forming the well-interconnected top of this hierarchy. In this study, we tested whether RC hubs are involved in the processing of hierarchically higher structures in stimulus sequences. Moreover, we explored the role of previously suggested cortical gradients along anterior-posterior and medial-lateral axes throughout the frontal cortex. To this end, we conducted a functional magnetic resonance imaging (fMRI) experiment and presented participants with blocks of digit sequences that were structured on different hierarchically nested levels. We additionally collected diffusion weighted imaging data of the same subjects to identify RC hubs. This classification then served as the basis for a region of interest analysis of the fMRI data. Moreover, we determined structural network centrality measures in areas that were found as activation clusters in the whole-brain fMRI analysis. Our findings support the previously found anterior and medial shift for processing hierarchically higher structures of stimuli. Additionally, we found that the processing of hierarchically higher structures of the stimulus structure engages RC hubs more than for lower levels. Areas involved in the functional processing of hierarchically higher structures were also more likely to be part of the structural RC and were furthermore more central to the structural network. In summary, our results highlight the potential role of the structural RC organization in shaping the cortical processing hierarchy.

KEYWORDS
cortical hierarchies, DWI, fMRI, nested hierarchies, rich club, structural connectivity

1 | INTRODUCTION

One of the most intriguing properties of the brain's connectome is the *rich club* (RC) phenomenon (van den Heuvel et al., 2012; van den Heuvel & Sporns, 2011). The RC consists of highly connected areas or nodes, that is, *hubs*, which are also particularly well-connected with each other (Colizza et al., 2006), remarkably at the expense of high energetic costs (Collin, Sporns, et al., 2014; Harriger et al., 2012; van den Heuvel et al., 2012). Following its first discovery in the human connectome, the RC organization was consistently found as a

This is an open access article under the terms of the Creative Commons Attribution-NonCommercial-NoDerivs License, which permits use and distribution in any medium, provided the original work is properly cited, the use is non-commercial and no modifications or adaptations are made.
© 2023 The Authors. *Human Brain Mapping* published by Wiley Periodicals LLC.

10970193, 2024, 4, Downloaded from https://onlinelibrary.wiley.com/doi/10.1002/hbm.26543 by Universitäts- und Landesbibliothek Münster, Wiley Online Library on [25/01/2026]. See the Terms and Conditions (https://onlinelibrary.wiley.com/terms-and-conditions) on Wiley Online Library for rules of use; OA articles are governed by the applicable Creative Commons License

structural network property across different individuals and age groups (Ball et al., 2014; Grayson et al., 2014; Kocher et al., 2015; Riedel et al., 2022; Sporns, 2013). Van den Heuvel and Sporns (2013) theorized that the RC serves as a *global workspace* that integrates information from many different areas with unparalleled efficiency (Crossley et al., 2013; Harriger et al., 2012; Hermundstad et al., 2013; Zamora-López et al., 2010). However, since the RC organization as a graph theoretical property is foremost a mathematical construct (Griffa & van den Heuvel, 2018; Sporns, 2011), its functional role has yet to be clarified.

A strong argument in favor of the functional significance of the structural RC comes from clinical observations (for a review, see Griffa et al., 2013). Thus, changes in structural RC organization were found for autism and attention–deficit/hyperactivity disorder (Ray et al., 2014), Alzheimer's disease (R. Cao et al., 2020; Lee et al., 2018; Yan et al., 2018), bipolar disorder (Collin et al., 2017; O'Donoghue et al., 2017; Reavis et al., 2020; Wang, Deng, et al., 2019), and schizophrenia (Bassett et al., 2008; Collin et al., 2017; Collin, Kahn, et al., 2014; Reavis et al., 2020; van den Heuvel et al., 2013). Also, studies in nonclinical populations support a link between the structural RC organization and individual cognitive abilities (Baggio et al., 2015; Bathelt et al., 2018; Kim et al., 2016; Ma et al., 2017; Solé-Casals et al., 2019). Together, these observations point toward a very important function of the structural RC without specifying it in detail.

To understand the underlying function of the RC, Gollo et al. (2015) proposed that the RC organization enables the brain to produce slower and more stable dynamics in the rich and densely interconnected core while peripheral nodes of the network showed faster fluctuations. This multiscale temporal organization is crucial for the ability to process incoming stimuli by segregating or integrating hierarchically nested stimulus structures (Golesorkhi, Gomez-Pilar, Zilio, et al., 2021). These stimulus structures are omnipresent in our environment: Every action sequence toward a goal (Fitch & Martins, 2014; Grafton & Hamilton, 2007; Hamilton & Grafton, 1993; Wakita, 2014), every piece of music (Farbood et al., 2015) or paragraph of text (Lerner et al., 2011) requires hierarchical processing (for a review, see Jeon, 2014). A prominent hypothesis is that the brain's intrinsic hierarchical structure enables it to encode, decode, and process hierarchical structures in our environment (Botvinick, 2008; Hamilton & Grafton, 1993). Evidence in favor of this correspondence has been established by anatomical gradients in the frontal brain. Thus, a temporally organized processing gradient was suggested that follows an anterior–posterior axis (Badre & Nee, 2018; Chanes & Feldman Barrett, 2016; Dixon et al., 2017; Fuster, 2001; Hilgetag et al., 2016; Kiebel et al., 2008; Koechlin & Summerfield, 2007; Sanides, 1964), and a lateral to medial/midline gradient through the frontal cortex for the processing of hierarchically higher levels (W. H. Alexander & Brown, 2018; Badre & Nee, 2018).

Excitingly, it is unclear and remains to be investigated whether the RC architecture discussed above may underlie or correspond to these anatomical gradients. For instance, medial structures processing hierarchically higher structures in the stimulus (J. Chen et al., 2017; Hasson et al., 2015) were reliably demonstrated to be RC hub areas (Q. Cao et al., 2013; Z. Chen et al., 2013; Huang et al., 2015; Riedel et al., 2022; Wang, Zhan, et al., 2019). However, the concept of a hierarchal processing gradient has not yet been empirically tested with relation to the RC architecture of the brain.

Against this background, in the present study we investigated whether the processing of hierarchically organized stimuli corresponds to the structural RC architecture and anatomical gradients of cortical processing hierarchies.

To this end, we collected diffusion weighted imaging (DWI) data of participants and used a combined diffusion tensor imaging (DTI) and generalized Q-sampling imaging (GQI; Yeh et al., 2010) approach (de Lange et al., 2023) to identify the RC hubs in a group average connectome. During a functional magnetic resonance imaging (fMRI) session, the same group of participants saw nested, hierarchically structured digit sequences. Finally, we integrated the structural and functional results using two different approaches: First, by using the structurally defined network nodes and hubs as regions of interest (ROIs) for the analysis of the subject-level fMRI data. Secondly, we analyzed the structural network centrality in areas that were identified as significant clusters in the functional whole-brain analysis to further investigate the relationship between cortical function and the underlying network structure. Both of these methods of integration define their group-wise independent variables (structural ROIs and functionally identified clusters) and subject-level dependent variables (fMRI data and structural network centrality) crossmodally, thus avoiding the problem of circularity (Kriegeskorte et al., 2009).

We had two hypotheses: processing hierarchically higher structures of the stimulus (I) involves RC hubs more than other nodes and (II) anterior and/or medial regions more than posterior and/or lateral areas of the frontal cortex.

2 | MATERIALS AND METHODS

2.1 | Participants

Data of 48 right-handed participants (32 females, $M = 21.75$, $SD = 2.74$ years; range = 18–28 years) were collected in this study. Four participants had to be excluded due to technical difficulties. Additional participants had to be excluded due to an inadequate performance in the experiment (one participant) or movement during the experiment that exceeded 1.5 times the voxel size (3.3 mm) in one direction within a run (three participants). Consequently, $N = 40$ (29 females, $M = 21.73$, $SD = 2.75$ years; range = 18–28 years) subjects were included in the analysis. All subjects gave informed written consent approved by the University of Münster Research Ethics Committee in accordance with the declaration of Helsinki. None of the participants reported any history of neurological or psychiatric diseases or any ferromagnetic material inside their bodies. Participants had (corrected-to-) normal vision and were right-handed ($M = 84.85$, $SD = 16.07$, range = 30–100) as assessed by the Edinburgh Handedness Inventory (Oldfield, 1971). They received money or course credit as remuneration for participating in the experiment.

10970193, 2024, 4, Downloaded from https://onlinelibrary.wiley.com/doi/10.1002/hbm.26543 by Universitäts- und Landesbibliothek Münster, Wiley Online Library on [25/01/2026]. See the Terms and Conditions (https://onlinelibrary.wiley.com/terms-and-conditions) on Wiley Online Library for rules of use; OA articles are governed by the applicable Creative Commons License

2.2 | Stimuli

Subjects were presented with sequences of digits made up of the numbers 4, 5, 6, 7, 8, 9, and 0 (for task instructions, see Section 2.3). Digits 1–3 were excluded due to evidence for different neural processing of these numbers in humans (Goffin, 2019). Importantly, only one digit was presented on screen at a time. The nested digit sequences were constructed from chunks of subsequently presented digits of varying length depending on the experimental condition (see below). Additionally, digit sequences were pseudorandomly interrupted by targets which required a response (button press) by the participants to ensure their constant attention. Target trials were characterized by the presentation of the number zero due to this digit's special role on the number scale (Brysbaert, 1995; Nieder, 2016; Pinhas & Tzelgov, 2012).

The experimental design comprised four conditions: (1) *Single*, where the transition probability between all digits was equal (i.e., no digit allowed an above-chance prediction of the subsequent one); (2) *Triplet*, in which the digits appeared in predefined chunks of 3 (4-5-6, 6-5-4, 7-8-9, and 9-8-7); (3) *Nonet*, with predefined chunks of nine digits created by repeating a triplet three times each (4-5-6–4-5-6–4-5-6, 6-5-4–6-5-4–6-5-4, 7-8-9–7-8-9–7-8-9 and 9-8-7–9-8-7–9-8-7); and finally (4) *Complete*, where subjects were presented with the complete sequence of 36 numbers the other conditions were nested in (4-5-6–4-5-6–4-5-6—6-5-4–6-5-4–6-5-4—9-8-7–9-8-7–9-8-7—7-8-9–7-8-9–7-8-9) (Figure 1a). The nested hierarchy of this sequence was chosen to resemble the structure and subsequent division of the natural stimuli used previously to analyze temporal receptive windows (TRW; Farbood et al., 2015; Hasson et al., 2008, 2010; Lerner et al., 2011). Each condition was presented five times during the main experiment (divided into 20 experimental blocks with one condition presented per block) and once each during a preceding training session.

Transition probabilities of Single digits, Triplet, and Nonet chunks were balanced using concatenated de Bruijn sequences of the order of two (de Bruijn, 1946), creating ideal pseudorandom sequences (Aguirre et al., 2011) of 144 digits. Each sequence was completed by 18 pseudorandomly inserted zeros (targets), which occurred at 12.5% of transitions on a chunk level, and neither in the first three trials of each block nor in direct succession. For each condition, six different digit sequences were created. Then, these unique sequences were randomly assigned to each training and experimental block to avoid the repetition of sequences within the same condition. The creation of all digit sequences and balancing of transition probabilities was done using MATLAB (Version 9.6.0 [R2019a]; The MathWorks Inc., 2019). For the creation of the de Bruijn sequences, we used the MATLAB-based de Bruijn sequence generator (Brimijoin & O'Neill, 2010).

Stimuli were presented using Neurobs Presentation software (Version 20.3, Neurobehavioral Systems, Inc., Berkeley, CA, www.neurobs.com). "Microsoft JhengHei Light" was chosen as the font as it represented the best balance between readability and minimization of relative pixel overlap (Wong & Szücs, 2013). Digits were presented at a visual angle of approximately 1.29° in very light gray, RGB = (230, 230, 230), on a dark gray background, RGB = (40, 40, 40).

2.3 | Procedure

The experiment was divided into two sessions in the MRI scanner that were completed on two separate days: the fMRI-task day and the

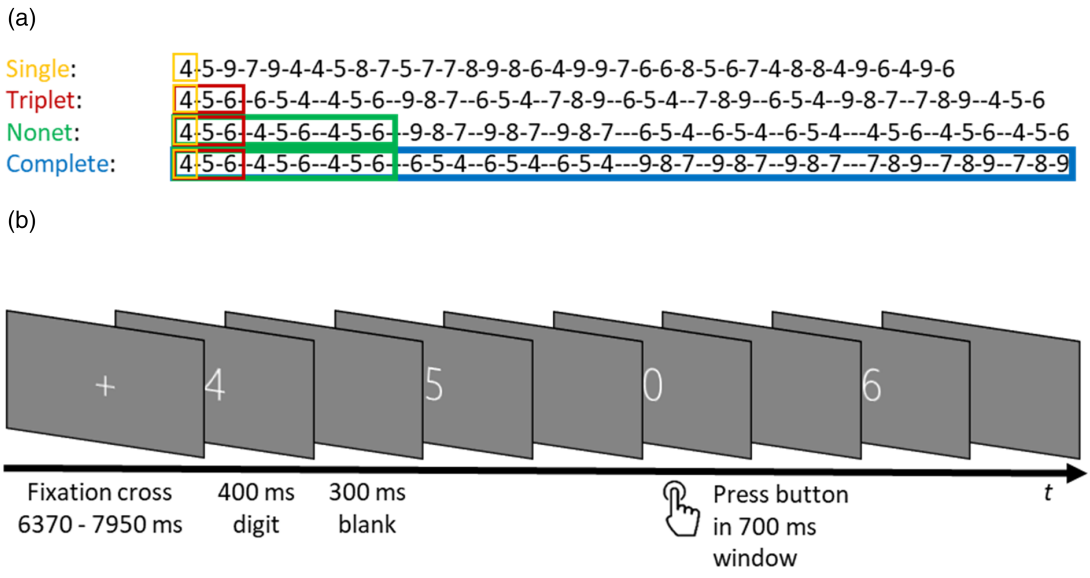


FIGURE 1 Experimental paradigm on the functional magnetic resonance imaging (fMRI)-experiment day. Example sequences for the four conditions. (a) Colors show nested hierarchical structure. (b) Presentation of digit sequence. Participants had to press a button when a zero was presented.

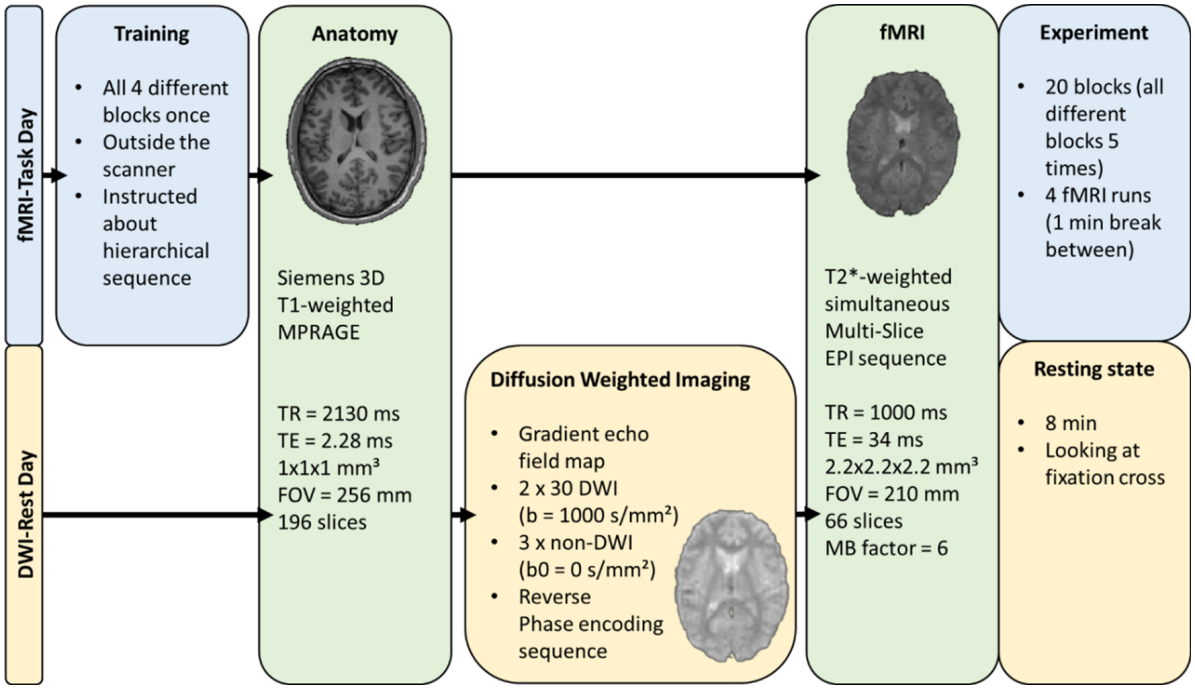


FIGURE 2 Diagram of the experimental procedure. DWI, diffusion weighted imaging; EPI, echo planar imaging; FOV, field of view; MB, multiband; MPRAGE, magnetization prepared rapid acquisition gradient echo; TE, echo time; TR, time of repetition. Note that the order of the two sessions (functional magnetic resonance imaging [fMRI]-task and DWI-rest) were counterbalanced across participants.

DWI-rest day (Figure 2). The order of sessions was counterbalanced across the group. On average 7.58 days ($SD = 6.05$ days) passed between sessions.

On the fMRI-task day, participants saw 24 blocks of the digit task, four blocks in the training outside the scanner, and then 20 blocks during the experiment in the MR scanner. Every participant was assigned a different order of blocks, with the first blocks in training and the main experiment counterbalanced across participants between the four conditions. The training (including all four conditions) and the main experiment started with the same condition. The block order was pseudorandomized using adjusted de Bruijn sequences to control that the transition probabilities between each condition were the same, but two blocks of the same condition could never be presented directly after each other. Each of the four blocks of the training and the 20 blocks of the main experiment consisted of 162 trials in total. At the start of each block, a fixation cross was presented for a block-specific jittered duration of 6370–7950 ms. The fixation cross blinked three times in the rhythm of number presentation signaling the approaching start of the next block. Each trial took 700 ms, consisting of a 400 ms digit presentation followed by 300 ms of a blank screen. If a zero was presented, the participant had the whole 700 ms to press the response button with the right index finger (Figure 1b). The experiment continued regardless of the response without feedback. Additionally, the main experiment contained a break of 1 after every five blocks, where the participants were informed about their progress in the experiment. To motivate participants, they could earn extra money/course credit when they responded to the zeros. At the end of the experiment, they were notified about the amount of additional reward they won. In total, the participants spend approximately 60 min in the scanner during the fMRI-task day.

For the DWI-rest day, measurements included an anatomical T1-weighted image (approx. 5 min), multiple diffusion-weighted (DW) images and non-DW images (approx. 15 min; see Section 2.4) and a resting-state fMRI scan (approx. 8 min). Participants were asked to remain as still as possible for the duration of the measurements. We presented the participants with a fixation cross during the resting-state fMRI scans, which is recommended for resting-state measurement (Agcaoglu et al., 2019; Patriat et al., 2013; van Dijk et al., 2010). The total scanner time on the DWI-rest day was about 30 min.

All stimuli were projected on a screen that was positioned behind the scanner bore. Participants viewed the screen via an adjustable 45° mirror. Movements were minimized with form-fitting cushions. To reduce scanner noise, ear plugs and noise-cancelling headphones were provided.

2.4 | MRI data acquisition

Brain images were recorded with a 3 T Siemens Magnetom scanner (Siemens, Erlangen) using a 20-channel head coil. Functional blood-

10970193, 2024, 4, Downloaded from https://onlinelibrary.wiley.com/doi/10.1002/hbm.26543 by Universitäts- und Landesbibliothek Münster, Wiley Online Library on [25/01/2026]. See the Terms and Conditions (https://onlinelibrary.wiley.com/terms-and-conditions) on Wiley Online Library for rules of use; OA articles are governed by the applicable Creative Commons License

10970193, 2024, 4, Downloaded from https://onlinelibrary.wiley.com/doi/10.1002/hbm.26543 by Universitäts- und Landesbibliothek Münster, Wiley Online Library on [25/01/2026]. See the Terms and Conditions (https://onlinelibrary.wiley.com/terms-and-conditions) on Wiley Online Library for rules of use; OA articles are governed by the applicable Creative Commons License

oxygen-level-dependent (BOLD) images on both days were acquired parallel to the anterior commissure/posterior commissure line. We used a T2*-weighted simultaneous multi-slice echo-planar imaging (SMS-EPI; 94 × 94 data acquisition matrix; 210 mm field of view [FOV]; 57° flip angle; time of repetition [TR] = 1000 ms; echo time [TE] = 34 ms). Each volume consisted of 66 adjacent axial slices with a slice thickness of 2.2 mm, a gap of 0.11 mm (5%), and a voxel size of 2.2 × 2.2 × 2.2 mm^3. Slice acquisition and multislice mode were interleaved. The acceleration factor was 6. The functional acquisition on the fMRI-task day was completed in four runs between which the participants had a 1-min break.

Structural reference images during both days were acquired for each participant using a standard Siemens 3D T1-weighted MPRAGE sequence for a detailed reconstruction of anatomy with isotropic voxel size (1 × 1 × 1 mm) in a 256-mm FOV (256 × 256 matrix; 192 slices; 8° flip angle; TR = 2130 ms; TE = 2.28 ms).

For DWI, we applied the parameters of the imaging sequences used in the Marburg-Münster Affective Disorders Cohort Study (Vogelbacher et al., 2018). Imaging started with a gradient echo field map (320 mm FOV; 60° flip angle; TR = 616 ms; TE1 = 5.19 ms; TE2 = 7.65 ms; 56 slices, slice thickness = 2.5 mm; 0 mm gap; voxel size 2.5 × 2.5 × 2.5 mm^3; interleaved slice acquisition). This was followed by two times 30 DW images with a *b*-value of 1000 s/mm^2 and in total five non-DW images (b = 0 s/mm^2), that had the same parameters except for their *b*-value (320 mm FOV; initial rotation −90°; TR = 7300 ms; TE = 90 ms; 56 slices, slice thickness = 2.5 mm; 0 mm gap; voxel size = 2.5 × 2.5 × 2.5 mm^3; interleaved slice acquisition; GRAPPA acceleration factor = 2). DWI was completed by a reverse phase encoding sequence (320 mm FOV; initial rotation −90°; TR = 7300 ms; TE = 90 ms; 56 slices, slice thickness = 2.5 mm; 0 mm gap; voxel size = 2.5 × 2.5 × 2.5 mm^3; interleaved slice acquisition; GRAPPA acceleration factor = 2).

2.5 | fMRI preprocessing

Preprocessing of functional and anatomical data was performed using the Statistical Parametric Mapping software (SPM12; The Wellcome Centre for Human Neuroimaging, London, UK) implemented in MATLAB (Version 9.10.0 [R2021a]; The MathWorks Inc., 2021). Preprocessing included manual reorientation to MNI space (Montreal Neurological Institute, Montreal, QC, Canada), slice time correction to the temporal and spatial middle slice (slice 34), realignment to the mean EPI image, and co-registration of the functional images to the individual structural scans. The subjects' co-registered anatomical (T1) scans were then segmented into native space tissue components. To this end, we used DARTEL (Ashburner, 2007) implemented in SPM12 with the default settings to create a group-specific template. Individually created flow fields were then used to normalize the functional images to MNI space. Finally, a Gaussian kernel of 8 mm^3 full-width at half-maximum was applied by DARTEL to smooth the data. A 160 s temporal high-pass filter was applied to remove low-frequency noise from the functional images' timeseries. To pre-whiten the data and correct for temporal autocorrelations, we applied the FAST model as recommended for TR ≤ 1400 ms (Corbin et al., 2018).

2.6 | Network reconstruction

To be able to analyze the structural network of the brain, the white matter network has to be reconstructed from the DW images to then determine the structural connectivity matrix describing this network. This reconstruction of the DWI-based structural connectivity matrices was done with the Connectivity Analysis TOolbox (CATO, v3.1.2.; de Lange et al., 2023). To this end, additional (preprocessing) steps had to be performed on the anatomical (T1) and DW images.

First, cortical surface reconstruction from the T1 images was performed using recon-all from FreeSurfer (v7.2.0; Fischl, 2012). This processing step was necessary as the T1 images are captured in voxels that do not directly contain the information of the brain's location and surface structure. It also included the automatic parcellation of the brain's surface according to the Desikan–Killiany atlas (Desikan et al., 2006). To ensure the quality of the anatomical reconstruction and parcellation, we applied the quality control protocol used by the ENIGMA consortium (https://enigma.ini.usc.edu/). Thus, we extracted the cortical thickness (in mm) and the surface area (in mm^2) of every parcel according to the Desikan–Killiany atlas of each participant to identify outliers, which might indicate issues in the parcellation but could also just reflect anatomical variability. Then, the parceled cortical surfaces of every subject were visually inspected internally, for accurate segmentation between gray and white matter and tracing of sulci, and externally, for successful differentiation of areas, and for general parcellation errors by one of the authors (FM) and three student assistants. No participants had to be excluded based on the results of this quality control. Thus, we ended up with parcellated cortical surfaces of all 40 participants.

Second, to merge the 60 DW and five b0 images per participant, we used fslmerge from FSL 6.0 (Jenkinson et al., 2012; CATO uses FSL to prepare the DWI data). The pipeline included a susceptibility correction using FSL topup (Andersson et al., 2003; Smith et al., 2004) based on the recorded Reverse Phase Encoding images and an eddy current as well as movement correction using FSL's eddy (Andersson & Sotiropoulos, 2016). For the reconstruction of the anatomical network, CATO allowed us to use a combined method of DTI and GQI (Yeh et al., 2010). Thus, in cases of multiple diffusion peaks because of more complex fiber configurations (e.g., kissing or crossing fibers), the voxel-wise diffusion profiles were determined using GQI. Otherwise, the informed RESTORE algorithm (Chang et al., 2005, 2012) was applied to model the tensor and remove outliers during the fitting, which helps with reducing the influence of physiological noise on the DTI modeling. Following the reconstruction of the diffusion signal, white matter tracts were reconstructed using deterministic tractography. For the reconstruction of the fibers following the diffusion peaks in each voxel, the FACT algorithm (Mori et al., 1999) was applied, extended for multiple peaks. This step resulted in the estimation of every participant's white matter streamlines.

Third, for the reconstruction of the DWI-based connectivity matrices (Figure 3), we used the default settings of CATO based on van den Heuvel et al. (2013). The algorithm started with eight seeds from each voxel in the brain mask, following the main direction of the diffusion to the next voxel and stopped in one of five cases: (1) the reconstructed white matter streamline reached a voxel with a fractional anisotropy (FA) value of 0.1, which often corresponds to gray matter; (2) the streamline tried to exit the brain mask; (3) it made a sharp turn larger than 45°; (4) it revisited a previous voxel; or (5) it entered a region defined as a *forbidden region*, which describes the cerebellum. Only streamlines that fully connected two brain regions were considered. The connectivity matrices for each participant were constructed based on a parcellation of their T1 anatomy. The parcellation of the individual anatomy in accordance with the same atlas or parcellation scheme is necessary to have an equal definition of parcels that form the nodes of the network and can be compared or combined across subjects. CATO extents on the classical Desikan–Killiany (Desikan et al., 2006) parcellation and includes the *Lausanne sub-parcellations*, which represent an approach to achieve the optimal scaling for connectivity matrices (Cammoun et al., 2012). We considered both

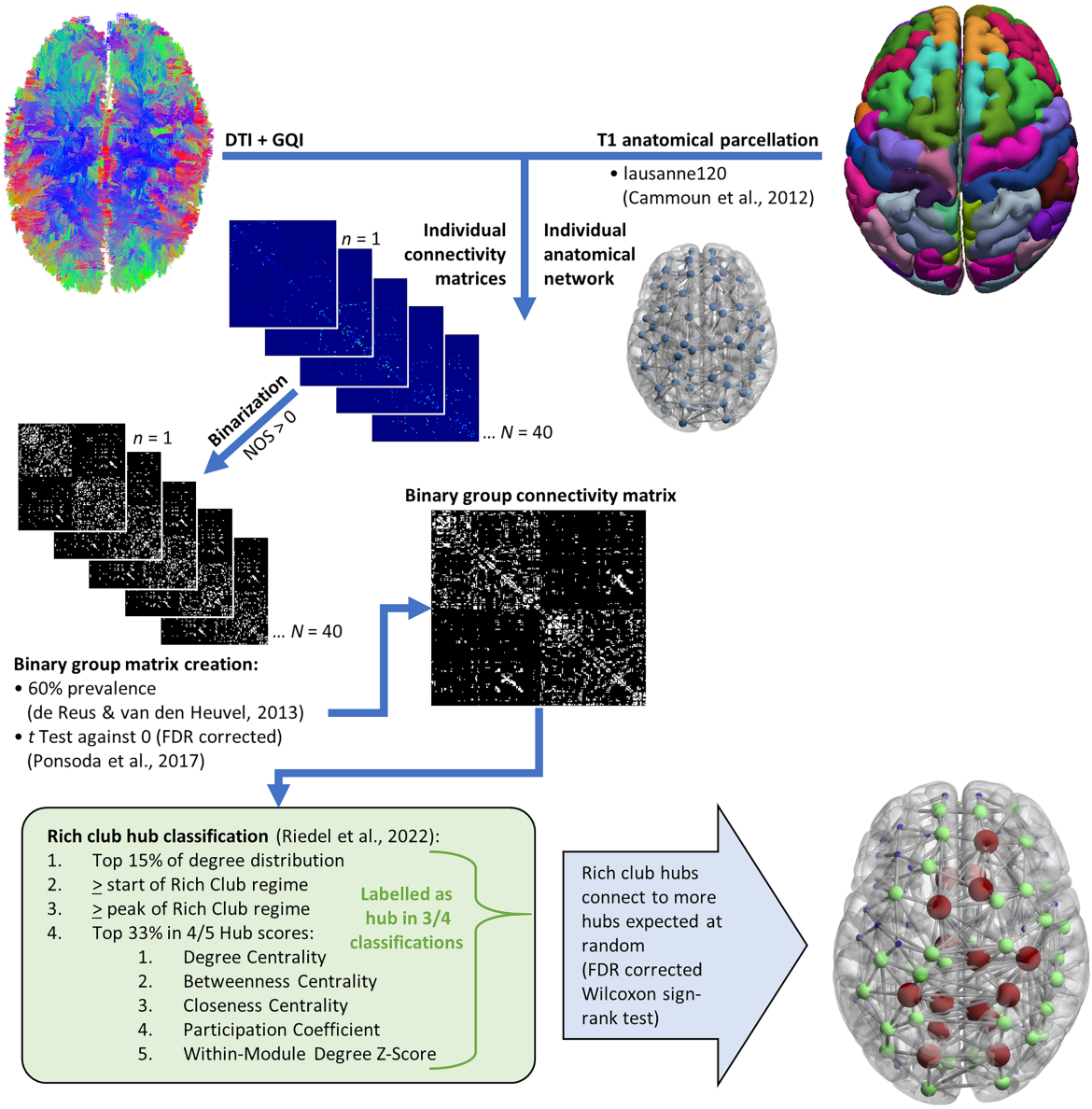


FIGURE 3 Flowchart from diffusion weighted images to rich club hubs. DTI, diffusion tensor imaging; FDR, false discovery rate; GQI, generalized Q-sampling imaging; NOS, number of streamlines.

10970193, 2024, 4, Downloaded from https://onlinelibrary.wiley.com/doi/10.1002/hbm.26543 by Universitäts- und Landesbibliothek Münster, Wiley Online Library on [25/01/2026]. See the Terms and Conditions (https://onlinelibrary.wiley.com/terms-and-conditions) on Wiley Online Library for rules of use; OA articles are governed by the applicable Creative Commons License

10970193, 2024, 4, Downloaded from https://onlinelibrary.wiley.com/doi/10.1002/hbm.26543 by Universitäts- und Landesbibliothek Münster, Wiley Online Library on [25/01/2026]. See the Terms and Conditions (https://onlinelibrary.wiley.com/terms-and-conditions) on Wiley Online Library for rules of use; OA articles are governed by the applicable Creative Commons License

the *lausanne120* and *lausanne250* parcellation schemes, as they showed the best reliability (Cammoun et al., 2012) and represent a meaningful meso-level parcellation of the cortex (Amunts & Zilles, 2015). The main manuscript is focused on the lausanne120 parcellation scheme (Figure 3) while all analyses using the lausanne250 parcellation are contained in the Supplemental Material.[1] The results according to both parcellation schemes are discussed together. The application of the lausanne120 parcellation resulted in the construction of 114 × 114 connectivity matrices for each subject. Note we did not include subcortical regions, as our functional hypotheses focused on cortical areas.

Finally, as connectivity matrices tend to be sensitive to outliers (Chung et al., 2017), we controlled the quality of the connectivity matrices based on the guidelines described in van den Heuvel et al. (2019). We determined outliers based on the following matrix measures: average number of streamlines (NOS), average FA, average mean diffusivity, average length, average streamline density controlled for the volume of the connected regions (in number of voxels), and distance to group prevalence map. Outliers were identified as values either below Q1 − 2 × IQR or above Q3 + 2 × IQR (Q1 = first quartile, Q3 = third quartile, IQR = Q3 − Q1 = interquartile range). Only connectivity matrices of participants that showed no outlier in any of the measures were used for further analysis. No subjects had to be excluded due to this quality check of matrix norms. Consequently, the network construction resulted in an individual DTI-GQI-based weighted connectivity matrix according to the lausanne120 parcellation scheme for all 40 participants.

2.7 | From connectivity matrices to ROIs

To investigate hypothesized relationships between hierarchies in function and structure, we identified the RC hubs of the group network and used these hubs as ROIs for the analysis of task-based BOLD data. First, we created a binary connectivity matrix for each participant (Figure 3) to reduce the bias from inaccuracies caused by the applied DWI sequence (Fornito et al., 2016). We binarized the individual DTI-GQI-based connectivity matrices by setting every edge that had at least one streamline (NOS > 0) to one while others were given a value of zero. These binarized matrices were then summed and thresholded in two different ways (Figure 3) that are both used to avoid false positive streamlines. The first way was based on the results of de Reus and van den Heuvel (2013a), who found that keeping connections that are present in at least 60% of the participants produces a good balance between false negative and false positive connections. The second method applied used one-tailed one-sample *t* tests to examine whether an edge's *relative NOS* (NOS/total NOS of a given participant) was larger than zero (Ponsoda et al., 2017). *T* tests were then corrected for multiple comparisons using the Benjamini and Hochberg (1995) method to control the false discovery rate (FDR) and adjust the *p* value accordingly. These two methods resulted in two different group-wise connectomes for the lausanne120 parcellation scheme with 463 and 455 edges, respectively (Figure S5.1).

The following identification of hubs was based on the methods described in Riedel et al. (2022). In deviation from their approach, we used binarized group matrices instead of individual weighted matrices. This deviation was implemented since the individual differences in RC organization were not relevant for our purposes. Also, major structural connectivity patterns are more apparent in group-wise connectomes (Hagmann et al., 2008). The Brain Connectivity Toolbox (BCT) for MATLAB (Rubinov & Sporns, 2010) was applied to determine the RC coefficient

$$\phi(k) = \frac{2E_{>k}}{N_{>k}(N_{<k} - 1)} \quad (1)$$

(rich_club_bu.m from the BCT) for each node degree *k*. The node degree *k*, also called degree centrality, describes the number of edges an individual node has with other network nodes (Rubinov & Sporns, 2010). The undirected and binary RC coefficient $\phi(k)$ was then calculated as the proportion of the links between nodes with a degree higher than *k* divided by the total possible number of links between all nodes of this subset (van den Heuvel & Sporns, 2011). These RC coefficients were normalized by dividing them by the mean RC coefficient of 2500 random networks. The randomization was achieved by applying the randmio_und.m function from the BCT 2500 times to the group network, rewiring each connection ten times.

As the RC coefficient $\phi(k)$ is calculated for every node degree *k*, it is possible to identify a range of degrees for which the empirical RC coefficient $\phi(k)$ is significantly higher than in the random networks. This range of degrees is called the RC regime (van den Heuvel & Sporns, 2011). We used the same rules as Riedel et al. (2022) to identify the RC regime as the largest range of consecutive degrees *k*, for which the empirical RC coefficient was significantly larger ($\alpha = .05$) than the random coefficients. Therefore, we calculated the *p* values using the formula described in van den Heuvel and Sporns (2011). We adjusted for multiple comparisons by controlling the FDR.

Based on this range of *k* with significantly larger empirical RC coefficients $\phi(k)$, we identified individual hubs by following the criteria used in Riedel et al. (2022) (Figure 3): (a) The regions belonged to the top 15% of the degree distribution (also applied in, e.g., Liu et al., 2020; Repple et al., 2020; Yan et al., 2018). (b) The region's degree was at least as large as the start degree of the RC regime, so the first node degree *k* for which the empirical RC coefficient $\phi(k)$ is significantly larger than in the random networks. (c) The region's degree was at least as large as the degree *k* with the largest normalized RC coefficient within the RC regime. (d) The region was within the top 33% in four of the following five *hub scores*: node degree, betweenness centrality, nodal path length or closeness centrality, between-module participation coefficient, and within-module degree *z*-score. The calculation of modularity was done exactly as in Riedel et al. (2022) using the Louvain algorithm. Thus, we determined 100 partitions of the group network ($\gamma = 1$) with the

[1]Note the ROI and centrality analyses results of both parcellation schemes were very similar. The decision to feature the lausanne120 parcellation in the manuscript was made for the sake of clarity of the connectome depictions.

community_louvain.m function, found an agreement matrix of all partitions (agreement.m) and arrived at the final partition by applying consensus_und.m to threshold the agreement matrix ($\tau = .6$) applying the Louvain algorithm 100 times resulting in a single ideal community structure. In the end, we defined hubs using four different approaches.

Since the four hub definitions (a–d) produced inconsistent results, we applied additional criteria to reach a conclusive hub definition. First, we only looked at regions identified as hubs in at least three of the four hub criteria introduced above. Of these regions, only those were considered that were connected to other identified hub regions more likely than in random networks, as this is in line with the definition of the RC in general (Colizza et al., 2006). Therefore, for each identified region, we calculated the proportion of edges connecting to other identified hub regions in relation to the total degree *k* of that region (Figure 3). Only those regions with edge proportions significantly larger than the average edge proportions calculated from the 2500 random networks were finally labeled as *RC hubs*. To test the difference between empirical and random networks, we applied a Wilcoxon sign-rank test FDR corrected for multiple comparisons. This step resulted in the final set of RC hubs (Tables S6.1–S6.2).

To use the hub classification in the analysis of the task-based data, we subsequently created binary ROI maps for each parcel to extract the functional BOLD neural responses from the parcels. To create these binary ROI maps of the lausanne120 parcels, we used the *Multi-Scale Brain Parcellator* (Tourbier et al., 2019) to parcellate the MNI-152 standard template according to the lausanne120 atlas. This parcellated template was implemented as an atlas in the WFU pick atlas toolbox for SPM (Maldjian et al., 2003). In the WFU pick atlas toolbox we could make use of the *DILATE* option to dilate the only surface-level defined ROIs by one voxel size three-dimensionally as it is commonly applied when combining fMRI and diffusion-based tractography (Jarret et al., 2022). So, each of the 114 cortical areas could be extracted as an ROI. We categorized each network node and thereby ROI as RC, which is an area identified as an RC hub, or *Feeder*, which is an area that is not itself an RC hub but shares a direct edge with a RC hub in the binary group network underlying this classification, or *Local*, an area that neither belongs to nor is connected to the RC (Figure 4 and Tables S6.5–S6.6). This classification was later used for the ROI and centrality analyses (see Sections 2.8.3 and 2.8.4).

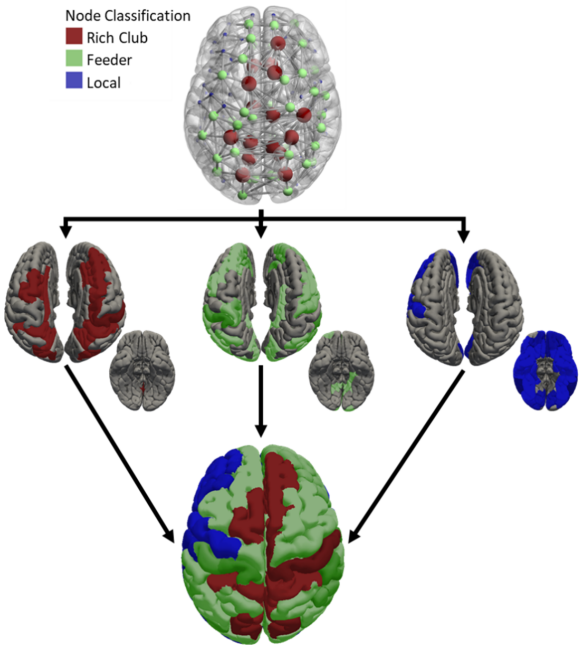


FIGURE 4 Transition from network node classification to regions of interest in MNI space. Rich Club = area is an identified rich club hub, Feeder = area directly connect to a rich club hub, Local = areas neither part of, nor connection to a rich club hub. MNI, Montreal Neurological Institute.

2.8 | Statistical data analysis

2.8.1 | Behavioral analysis

The behavioral and all other data analyses were performed using R (Version 4.2.2.; R Core Team, 2022) and RStudio (Version 2022.7.2.576; RStudio Team, 2022).

Reaction time

We expected a main effect of the different conditions on reaction times (RTs). Specifically, RTs in the Single condition were expected to be shorter than in the structured conditions because expectation violations were found to lengthen RTs (Badre & Wagner, 2004; Kühn & Schubotz, 2012; Nattkemper & Prinz, 1997). Accordingly, it was also to be expected that zeros appearing within a sequential structure would lead to longer RTs than those appearing between sequence transitions. To investigate this assumption, we applied Bayesian hierarchical generalized linear modeling implemented via the brms library in R (Bürkner, 2017) to model the influence of the different blocked conditions and the level of structure disruption. HIERARCHY, a four-level within-subject factor, was comprised of the different conditions of hierarchy: Single, Triplet, Nonet, and Complete. The second factor, LEVEL OF VIOLATION, referred to where in the sequential structure a zero occurred; this factor also had four levels: *Between Single*, *Between Triplet*, *Between Nonet*, and *Between Complete*. However, the levels of the two factors were not fully crossed, as not all levels of violation could occur at each level of HIERARCHY. Thus, we used two different models (Equations 2 and 3) to investigate the influence of sequential structure on the RT. Both models included a random intercept and random slopes for the trial number, the trial number in the block, the times the participant saw this condition already to control for learning and tiredness as well as the distance of a zero to the last recorded reaction and the Shannon surprise (Shannon, 1948) of that zero in the sequence up to this point. The second model also included a random slope for the factor HIERARCHY. The surprise of a stimulus was calculated using the formula derived from the infinite time scale model (Harrison

10970193, 2024, 4, Downloaded from https://onlinelibrary.wiley.com/doi/10.1002/hbm.26543 by Universitäts- und Landesbibliothek Münster, Wiley Online Library on [25/01/2026]. See the Terms and Conditions (https://onlinelibrary.wiley.com/terms-and-conditions) on Wiley Online Library for rules of use; OA articles are governed by the applicable Creative Commons License

TABLE 1 Average hit rates and false alarm rates of reacting to zeros in the digit sequences.

Hit rate	Hierarchy			
Level of Violation	Single	Triplet	Nonet	Complete
Between Single	97.61 (3.30)	97.54 (3.81)	97.47 (4.97)	97.57 (3.29)
Between Triplet		97.91 (3.25)	97.53 (4.44)	97.25 (4.76)
Between Nonet			98.00 (4.64)	97.46 (7.36)
Between Complete				100.00 (0.00)
False alarm rate	0.07 (0.16)	0.07 (0.10)	0.10 (0.15)	0.12 (0.20)

Note: Reported is *M*(*SD*) in %, $N = 40$.

et al., 2006). This variable was used as part of the random structure in our models. See Supplemental Material for details on the calculation of surprise.

For the first model, we combined Hierarchy and Level of Violation to the factor Combination to model the mean RT for each possible combination of the two factors.

$$\text{RT} \sim \text{Combination} + (1 + \text{Trial Number Total} + \text{Trial Number Block} + \text{Times Block} + \text{Last Zero} + \text{Surprise}|\text{Subject}) \quad (2)$$

The data for the second model than excluded the Single condition and added the factor Position, which was labeled *Between* for a violation during the transition of the condition-specific highest chunk (e.g., insertion between triplets in the Triplet condition) while *Within* described all other positions in the sequence. Thus, we could model an interaction effect between Hierarchy and Position.

$$\text{RT} \sim \text{Hierarchy} \times \text{Position} + (1 + \text{Hierarchy} + \text{Trial Number Total} + \text{Trial Number Block} + \text{Times Block} + \text{Last Zero} + \text{Surprise}|\text{Subject}) \quad (3)$$

We used uninformative priors for both models as recommended for multilevel modeling (Bürkner, 2017). For β coefficients we used $N(0, 5)$; for the standard deviation a Student's $t(3, 0, 5)$ distribution was applied; and finally for the correlation in Equation 3, a Lewandowski–Kurowicka–Joe (LKJ(2)) distribution was used. For both models, we used the shifted lognormal family. The RT models were calculated with ten chains, each with 4000 iterations from which the first 1000 were warmups.

Hit rate

Due to the apparent ceiling effect (Table 1) and its effect on the statistical analysis (Cramer & Howitt, 2011; Rhodes et al., 2019), we only descriptively report the hit and false alarm rates of Hierarchy and Level of Violation and refrain from further analyses.

2.8.2 | fMRI design specifications

The whole brain analysis and extraction of data for the ROI analysis were conducted in the SPM12. A general linear model (GLM) was used to model the fMRI timeseries on the first level. The GLM included four regressors for each of the different blocked conditions: Single, Triplet, Nonet, and Complete. These regressors were modeled as epochs with a duration of 162 trials (entire block duration). The onsets were time-locked to the start of the blocks, resulting in five onsets per condition. We further included the fixation epochs, the 360 events of a zero interrupting the digit sequence, and six rigid-body transformations (regressors of nuisance). Regressors were convolved with the canonical hemodynamic response function.

To identify areas that process hierarchically lower or higher structures in the digits sequence, we built contrasts between the four levels of Hierarchy: Triplet > Single, Nonet > Triplet, and Complete > Nonet. On the second level, we applied one-sample *t* tests across the participants. For the particular contrasts of interest, we employed a cluster-forming threshold of $p < .001$ and a cluster extend threshold of 47 voxels. This cluster threshold was determined by 10,000 Monte Carlo simulations and represents a cluster-wise $p < .05$ corrected for multiple comparisons (Slotnick, 2017; Slotnick et al., 2003; for simulation results, see Supplemental Material).

Finally, to specifically test for the predicted anterior-medial trend in the frontal lobe for the processing of hierarchically higher stimulus structures, we computed the correlations between the Euclidian distance to an anterior-medial reference point, $X_{MNI} = 0$, $Y_{MNI} = 72$, and the extracted beta values of the step-wise contrasts from the frontal lobe. Using the Hittner et al. (2003) modification of the *z* test by Dunn and Clark (1969) within the cocor framework (Diedenhofen & Musch, 2015), we then compared the contrast-specific correlations to see if the beta values increase or decrease differently with distance from the anterior-medial reference point (for more details see Supplemental Material). For higher-level contrasts, we expected larger beta values to be located closer to the anterior-medial reference point while for lower-level contrasts the beta values should increase with the distance. Consequently, the correlations of higher-level contrasts should be smaller than in lower levels.

2.8.3 | ROI analysis

In preparation for the ROI analyses, we used the same GLM to estimate the mean activations per condition by calculating the contrast of the respective condition against the implicit baseline, which is the predicted BOLD activation when all predictors are set to zero. Then we

10970193, 2024, 4, Downloaded from https://onlinelibrary.wiley.com/doi/10.1002/hbm.26543 by Universitäts- und Landesbibliothek Münster, Wiley Online Library on [25/01/2026]. See the Terms and Conditions (https://onlinelibrary.wiley.com/terms-and-conditions) on Wiley Online Library for rules of use; OA articles are governed by the applicable Creative Commons License

10970193, 2024, 4, Downloaded from https://onlinelibrary.wiley.com/doi/10.1002/hbm.26543 by Universitäts- und Landesbibliothek Münster, Wiley Online Library on [25/01/2026]. See the Terms and Conditions (https://onlinelibrary.wiley.com/terms-and-conditions) on Wiley Online Library for rules of use; OA articles are governed by the applicable Creative Commons License

extracted the unthresholded, estimated beta values from the contrast images for each ROI per level of HIERARCHY in each participant, using the spm_get_data.m function from the SPM12. We subsequently averaged the beta values from all voxels of an ROI for every level of HIERARCHY and participant. ROIs were grouped into RC hubs, Feeder nodes, and Local nodes, depending on their RC membership and connectivity. The extraction and classification were done for both group network construction methods. After inspection of the Cullen–Frey plots, to judge the skewness and kurtosis of the data (Cullen & Frey, 1999), extreme averaged beta values (below $Q1 - 3 \times IQR$ or above $Q3 + 3 \times IQR$) were excluded from the analysis.

The statistical ROI analysis was performed using Bayesian hierarchical generalized linear models via the brms package (Bürkner, 2017). In the model, HIERARCHY, NODE CLASSIFICATION, and the HIERARCHY by NODE CLASSIFICATION interaction were included as predictors. The model also incorporated random intercepts for the individual ROIs, subjects, and a random HIERARCHY effect for each subject (Equation 4).

$$\text{Beta} \sim \text{Hierarchy} \times \text{Node Classification} + (1 + \text{Hierarchy} \,|\, \text{Subject}) + (1 \,|\, \text{ROI}) \quad (4)$$

As the model was multilevel, we used the same priors as for the behavioral data (see "Reaction Time" section). The skewed normal family was utilized for modeling the data. All models were calculated with ten chains, each having 4000 iterations, 1000 warmups, and a maximal treedepth of 15.

We hypothesized that the RC hubs would be more activated in conditions that involve the processing of hierarchically higher stimulus structures. Thus, the interaction between HIERARCHY and NODE CLASSIFICATION was of particular interest, as beta values should increase significantly with hierarchically higher structures. This was especially expected in areas identified as RC hub regions, and possibly also in Feeder nodes which are (by definition) directly connected to the RC.

2.8.4 | Centrality analysis

We then examined the graph theoretical node properties of the areas with hierarchal level-specific BOLD responses. Again, we assumed that areas that process hierarchically higher structures of the stimulus also occupy hierarchically higher levels in the structural graph, which are more central to the network.

First, we started with using the already established individual DTI-GQI-based connectivity matrices referenced to the lausanne120 parcellation scheme before the merging to group-wise matrices (see Section 2.6). To be able to use the binarized matrices on a subject-level, we applied a different binarization method than on the group-level. At the individual level we fixed the threshold for keeping an edge at three or more streamlines to correct for false positives (Brown et al., 2011), setting edges clearing this threshold to one and all others to zero. Based on these individual binary connectivity matrices, we calculated the five centrality measures that make up the hub score in the RC identification (Riedel et al., 2022) for each individual network: nodal degree/degree centrality, betweenness centrality, closeness centrality, within module degree *z*-score, and participation coefficient.

Second, we used the resulting clusters of the group-averaged BOLD contrasts Triplet > Single, Nonet > Triplet, and Complete > Nonet that were significant at the cluster threshold of 47 voxels (Table 3 and Figure S5.2) as functional ROIs and extracted them binarized maps.

Third, based on these maps, we assigned the functionally defined *Rhat* activation clusters to parcels of the lausanne120 atlas (see Supplemental Material for lausanne250). Therefore, we calculated the proportion of each binarized functional cluster that was contained in the parcels of the lausanne120 parcellation scheme. As a result, we determined the lausanne120 parcels that comprised activations of the Triplet > Single, Nonet > Triplet, and Complete > Nonet contrasts as well as a percentage of the contrasts contained in each of these parcels.

Fourth, for each of the three BOLD contrasts, we then determined the weighted average for all five node centralities, weighted by the percentage of overlap between contrasts and parcel.

We repeated this step for each subject to receive individual structural centrality measures based on the subject's binary network for all clusters of the functional analysis. These individual measures were also controlled for the total amount of activated voxels of a contrast covered by any parcel. This culminated in five controlled centrality measures for each of the stepwise contrasts for all 40 participants. Finally, we *z*-scaled every centrality measure to obtain comparable values for all five measures.

To analyze the difference between the mean centrality of the stepwise contrasts we applied a multivariate multilevel model via brms (Bürkner, 2017) with the factor HIERARCHY CONTRAST describing the influence of the different levels of contrasts (Equation 5).

$$\begin{aligned}&(\text{Degree Centrality}, \text{Betweenness Centrality}, \text{Closeness Centrality},\\ &\text{Within Module Degree } z\text{–Score}, \text{Participation Coefficient}) \sim\\ &\text{Hierarchy Contrast} + (1|\text{Subject})\end{aligned} \quad (5)$$

We expected that the average centrality of the areas activated by hierarchically higher structures of the stimulus would increase with the levels of hierarchy.

2.8.5 | Validation using the human connectome project dataset

As this article is the first to apply the additional step of using the connections between hub regions as a criterium for RC hub definition, we sought to validate the results of the node classification as well as the subsequent ROI and the centrality analyses on an independent dataset. For this purpose, we made use of the publicly available data from the Human Connectome Project (HCP; Van Essen et al., 2013; for details see Supplemental Material). We applied the exact same methods described in Sections 2.6–2.8.4 to the structural and DW data of 100 unrelated subjects from the HCP database. The resulting node classification was compared to the results of our own data.

Subsequently, the HCP-based classifications and structural centrality measures were utilized to replicate the ROI and centrality analyses.

2.8.6 | Bayesian hypothesis testing

The hypotheses for the Bayesian multilevel models were tested using the hypothesis function from the brms library (Bürkner, 2017). A Bayes factors (BF) > 3 indicates significant evidence in favor of the tested hypothesis (van Doorn et al., 2021). Bayes factors for one-sided hypotheses (BF_{+0}) are defined as the division of the posterior probability of the hypothesis by the posterior probability of the alternative, that is, the evidence ratio (Bürkner, 2018).

3 | RESULTS

3.1 | Behavioral results

3.1.1 | Hit and false alarm rates

Table 1 reports hit rates and false alarms rate in detecting the zero broken down by HIERARCHY and LEVEL OF VIOLATION only for hit rates.

3.1.2 | Reaction times

The RT model (Equation 2) tested the influence of all combinations of HIERARCHY and LEVEL OF VIOLATION on the RT for detecting a zero, controlled for participant-specific effects of learning, tiredness, and surprise. The model had no divergent transitions, all *Rhat* < 1.05, and all variables had bulk- and tail-effective samples ≥ 1373 and ≥ 2665, respectively. Posterior checks showed that the cumulative count model simulations reasonably capture the means and distributions of the observed data (Figure S7.1). Posteriors drawn from the estimated model (Equation 2) were used to compare the RT between the levels of HIERARCHY per LEVEL OF VIOLATION. As aforementioned, we expected that a zero inserted within the sequence would be slower than a zero presented between chunks of the sequence. It was found that the RT for a zero occurring Between Single was increased for Nonet condition in comparison to the Single condition (H_+: *Nonet:Between Single > Single:Between Single*; $M = 0.02$ [0.01, 0.04], $SD = 0.01$, p.p. $= 1$, $BF_{+0} = 217.98$; Figure 5a).

The second RT model (Equation 3) focused on the structured conditions to test the influence of HIERARCHY, POSITION (i.e., if the zero was inserted within or between the sequences), and their interaction on the RT. This model also had no divergent transitions, all *Rhat* = 1.00, and all variables had bulk- and tail-effective samples ≥ 2133 and ≥ 4822, respectively. Posterior checks again showed that the cumulative count model simulations reasonably capture the means and distributions of the observed data (Figure S7.2). Posteriors drawn from the estimated model (Equation 3) revealed a larger RT in the Within position compared to the Between position in the Nonet condition (H_+: *Nonet:Between* − *Nonet:Within* < 0; $M = -0.04$ [−0.07, −0.02], $SD = 0.02$, p.p. $= 1$, $BF_{+0} = 308.28$; Figure 5b). This difference was also larger than in the Triplet condition (H_+: *Triplet:(Within > Between)* − *Nonet:(Within > Between)* < 0; $M = -0.04$ [−0.07, −0.01], $SD = 0.02$, p.p. $= 0.98$, $BF_{+0} = 58.06$; Figure 5b). These results show a tendency for a larger influence of the interruption and position of insertion on the RT with stimuli containing hierarchically higher structures. The results of the Complete condition break this pattern (H_+: *Nonet:(Within > Between)* − *Complete:(Within > Between)* < 0; $M = 0.07$ [0.01, 0.12], $SD = 0.03$, p.p. $= 0.02$, $BF_{+0} = 0.02$; Figure 5b). However, it must be noted, that the participants saw far fewer Between Complete insertions (3 per participant) than Between Nonet insertions (18 per participant).

3.2 | fMRI results

According to the hypothesis of a stepwise increase of the activation with the nested levels of hierarchy in the stimulus structure, we

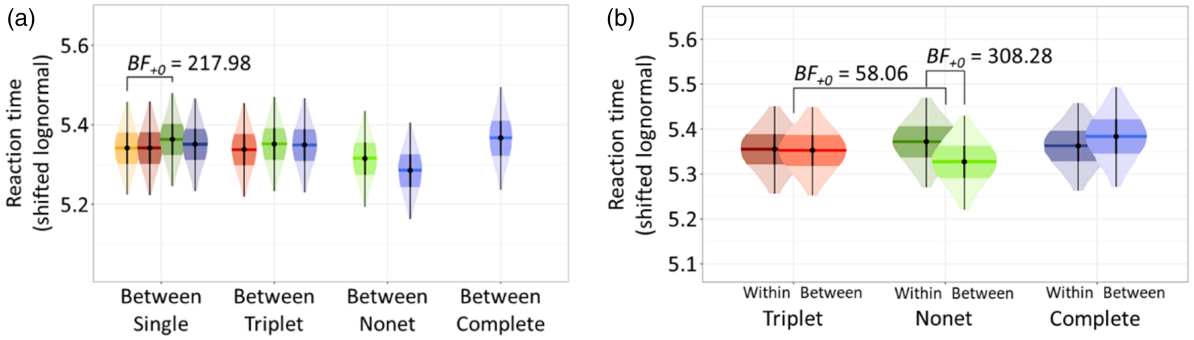


FIGURE 5 Results of reaction time analysis. Density plots of posterior distributions with mean point estimate, 50 and 95% highest probability density areas marked. BF, Bayes factor. (a) Estimates of all conditions of the HIERARCHY × LEVEL OF VIOLATION interaction. Yellow, Single; Red, Triplet; Green, Nonet; Blue, Complete. (b) Interaction of HIERARCHY × POSITION in structured conditions. Red, Triplet; Green, Nonet; Blue, Complete; Dark, Within; Light, Between.

10970193, 2024, 4, Downloaded from https://onlinelibrary.wiley.com/doi/10.1002/hbm.26543 by Universitäts- und Landesbibliothek Münster, Wiley Online Library on [25/01/2026]. See the Terms and Conditions (https://onlinelibrary.wiley.com/terms-and-conditions) on Wiley Online Library for rules of use; OA articles are governed by the applicable Creative Commons License

examined the significant clusters at a cluster threshold of 47 voxels that was determined using the simulation introduced by Slotnick et al. (2003); Slotnick (2017). This approach revealed activation clusters for the contrasts Triplet > Single and Nonet > Triplet (Table 2 and Figure 6, for a graphic depicting all clusters see Figure S5.2). Because of their stepwise nature, we will also refer to these contrasts as Triplet-specific and Nonet-specific, respectively. The Triplet > Single contrast comprised a single cluster in the left inferior frontal junction (IFJ). The Nonet > Triplet contrast showed additional frontal clusters in right middle frontal gyrus (MFG) and two separate clusters in the right superior frontal gyrus (SFG). In the temporal lobe, we found clusters in the left inferior temporal sulcus and a cluster in the right middle temporal gyrus. Finally, we also found bilateral clusters in the inferior parietal lobule (IPL) and a cluster in the right posterior cingulate gyrus (PCG). No significant clusters were revealed in the Complete > Nonet contrast. Activation clusters resulting from the stepwise comparison of the increasing hierarchical structure were later used as the basis for the analysis of the centrality measures (see Section 3.5).

To test for the predicted anterior-medial trend in the frontal lobe, we compared the correlations between the Euclidian distance to the anterior-frontal reference point, $X_{MNI} = 0$, $Y_{MNI} = 72$, and the extracted beta values of the Triplet > Single and Nonet > Triplet contrasts. We found that the correlations for the Nonet-specific betas, $r_{EdN} = -.07$, $t(2020557) = -97.81$, $p < .001$, as well as the Triplet-specific betas with the Euclidian distance were significantly different from zero, $r_{EdT} = .09$, $t(2020557) = 122.88$, $p < .001$. Additionally, the Nonet-specific correlation was significantly smaller than the Triplet-specific correlation, $z = -126.60$, $p < .001$. Accordingly,

TABLE 2 Activation clusters from second-level whole-brain block contrasts with cluster threshold = 47 voxels.

Localization	H	Cluster extent (in voxel)	MNI coordinates			t Value	p Value
			x	y	z		
Nonet > Triplet							
Superior frontal gyrus	R	73	22	60	14	3.80	<.001
Superior frontal gyrus	R	401	22	18	58	4.32	<.001
Medial superior frontal gyrus	R	l.m.	12	36	42	4.01	<.001
Superior frontal gyrus	R	l.m.	22	32	56	3.96	<.001
Middle frontal gyrus	R	108	38	24	40	4.08	<.001
Inferior temporal sulcus	L	144	−56	−24	−26	5.51	<.001
Middle temporal gyrus	R	123	64	−30	−16	3.95	<.001
Posterior cingulate gyrus	R	101	4	−40	28	4.04	<.001
Inferior parietal lobule	L	118	−54	−58	44	4.14	<.001
	R	190	44	−62	36	4.10	<.001
Triplet > Single							
Inferior frontal junction	L	77	−36	0	28	3.91	<.001

Abbreviations: H, hemisphere; L, left; l.m., local maximum; MNI, Montreal Neurological Institute; R, right.

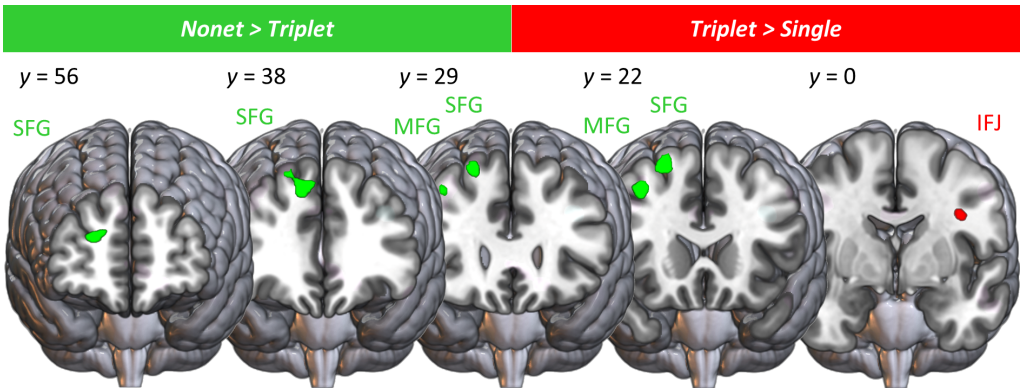


FIGURE 6 BOLD activation clusters in the frontal cortex for the contrasts Triplet > Single and Nonet > Triplet. Significant clusters at the cluster threshold of 47 voxels, depicted on MNI template. BOLD, blood-oxygen-level-dependent; IFJ, Inferior frontal junction; MFG, Middle frontal gyrus; MNI, Montreal Neurological Institute; SFG, Superior frontal gyrus; *y*, y coordinate.

10970193, 2024, 4, Downloaded from https://onlinelibrary.wiley.com/doi/10.1002/hbm.26543 by Universitäts- und Landesbibliothek Münster, Wiley Online Library on [25/01/2026]. See the Terms and Conditions (https://onlinelibrary.wiley.com/terms-and-conditions) on Wiley Online Library for rules of use; OA articles are governed by the applicable Creative Commons License

Nonet-specific beta values are higher in anterior and medial areas, while Triplet specific betas are higher in lateral and more posterior portions of the frontal lobe.

3.3 | RC results

The final set of RC hubs identified with the lausanne120 parcellation (Figure 7c,d) and the group-based connectivity matrix based on 60% prevalence (de Reus & van den Heuvel, 2013a; Figure 7a,b) are depicted in Figure 6. The RC hubs of the remaining identification methods and a summary of all hub measures can be found in the supplemental material (Figures S5.1 and S5.3 and Tables S6.5–S6.8). The comparison with the HCP-based RC definition is also described in the supplemental material (Table S9.1).

3.4 | ROI analysis results—The function of different structural nodes

The ROI analysis model (Equation 4) tested the influence of HIERARCHY and the NODE CLASSIFICATION (Local, Feeder, RC) as well as their

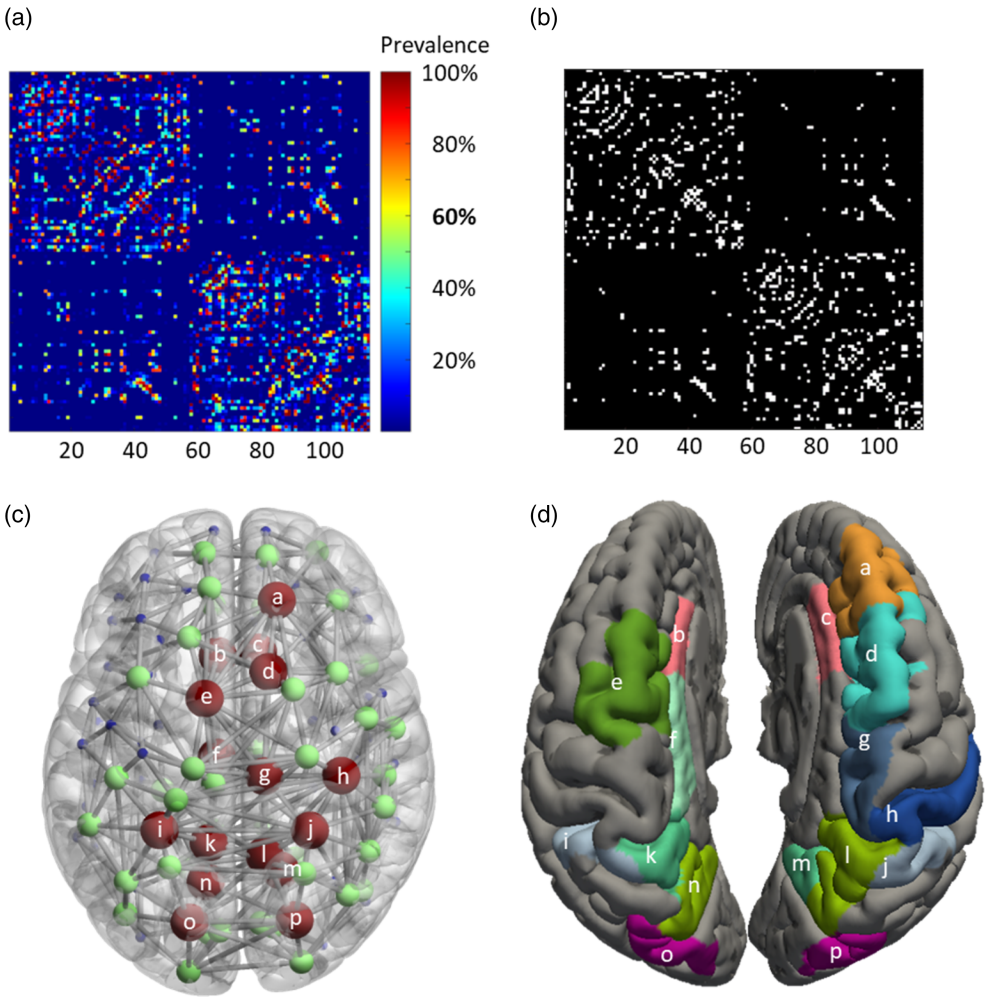


FIGURE 7 Connectivity matrices and rich club network combining lausanne120 parcellation scheme and 60% prevalence-based group matrix. (a) Group matrix depicting prevalence of connection in percent. For further analyses, the matrix was binarized by thresholding at 60% prevalence (Figure 3). (b) Binarized group network based on 60% prevalence threshold. (c) Node classification and identified RC network for the lausanne120 parcellation scheme and a 60% prevalence-based group matrix. Red, RC nodes; green, Feeder nodes; Blue, Local nodes. (d) Surface render of the RC hubs; colors code different parcels of the lausanne120 atlas (lausanne120 labels: (a) right superiorfrontal_2, (b) left caudalanteriorcingulate_1, (c) right caudalanteriorcingulate_1, (d) right superiorfrontal_3, (e) left superiorfrontal_4, (f) left posteriorcingulate_1, (g) right paracentral_1, (h) right postcentral_2, (i) left superiorparietal_1, (j) right superiorparietal_1, (k) left precuneus_1, (l) right precuneus_2, (m) right precuneus_1, (n) left precuneus_2, (o) left superiorparietal_3, and (p) right superiorparietal_3).

10970193, 2024, 4, Downloaded from https://onlinelibrary.wiley.com/doi/10.1002/hbm.26543 by Universitäts- und Landesbibliothek Münster, Wiley Online Library on [25/01/2026]. See the Terms and Conditions (https://onlinelibrary.wiley.com/terms-and-conditions) on Wiley Online Library for rules of use; OA articles are governed by the applicable Creative Commons License

interaction on the beta values extracted from the ROIs. We calculated the same model for both group matrix methods (prevalence and *t* test, see Supplemental Material for lausanne250). All beta values were derived from a GLM that estimated the mean activations per condition compared to the implicit baseline. The models differed in the classification of the nodes, corresponding to different group networks (Figures 7c and S5.3). None of the models had divergent transitions and all *Rhat* < 1.05. The bulk- and tail-effective samples of each model are given in Table 3 and S4.1–S4.3, respectively. Posterior checks showed that the cumulative count model simulations reasonably capture the means and distributions of the observed data (Figures S7.3–S7.6). We were especially interested in the interaction of HIERARCHY and NODE CLASSIFICATION. Since the tendencies were the same for both approaches, Table 3 reports the results for the variant lausanne120 parcellation and 60% prevalence-based group matrix (see Tables S4.1–S4.3 for remaining results).

Regarding the expected interaction, we found an increase in the beta values between the conditions Triplet and Nonet for all levels of NODE CLASSIFICATION, and this increase showed a nonsignificant tendency to be stronger for RC hubs and Feeder nodes than for Local nodes. In general, the beta values decreased for the RC hubs and Feeder nodes compared to local nodes (Figure 8 for lausanne120

TABLE 3 Results of the hypothesis test of model Equation 4 for the data from parcellation scheme lausanne120 and 60% prevalence-based group matrix.

Hypothesis	*M*	*SD*	CI lower	CI upper	Evidence ratio (BF)	Posterior probability
Increase of beta values with level of Hierarchy separated by node classification						
Local						
Triplet > Single	−0.08	0.12	−0.28	0.12	0.34	0.26
Nonet > Triplet	**0.38**	**0.20**	**0.06**	**0.71**	**33.97**	**0.97**
Complete > Nonet	−0.07	0.16	−0.33	0.19	0.50	0.33
Feeder						
Triplet > Single	−0.04	0.13	−0.25	0.16	0.60	0.37
Nonet > Triplet	**0.48**	**0.20**	**0.15**	**0.80**	**106.91**	**0.99**
Complete > Nonet	−0.12	0.16	−0.38	0.15	0.30	0.23
RC						
Triplet > Single	0.02	0.14	−0.21	0.26	1.33	0.57
Nonet > Triplet	**0.43**	**0.21**	**0.09**	**0.77**	**48.10**	**0.98**
Complete > Nonet	−0.14	0.17	−0.42	0.14	0.26	0.21
Increase of beta values with level of Hierarchy compared between node classifications						
Triplet > Single						
Feeder > Local	0.04	0.07	−0.07	0.15	2.63	0.72
RC > Local	0.10	0.09	−0.04	0.25	7.17	0.88
RC > Feeder	0.06	0.09	−0.09	0.22	3.08	0.76
Nonet > Triplet						
Feeder > Local	0.09	0.07	−0.01	0.20	12.25	0.92
RC > Local	0.05	0.09	−0.10	0.20	2.32	0.70
RC > Feeder	−0.05	0.09	−0.20	0.11	0.44	0.31
Complete > Nonet						
Feeder > Local	−0.05	0.07	−0.16	0.06	0.30	0.23
RC > Local	−0.07	0.09	−0.22	0.08	0.27	0.21
RC > Feeder	−0.02	0.10	−0.18	0.13	0.67	0.40
No difference of beta values between node classifications						
Local = Feeder	**−1.04**	**0.28**	**−1.59**	**−0.48**	**0.01**	**0.01**
Local = RC	**−1.39**	**0.39**	**−2.14**	**−0.63**	**0.04**	**0.03**
Feeder = RC	−0.35	0.4	−1.14	0.47	11.57	0.92

Note: The evidence ratio of one-sided hypothesis tests is equal to the Bayes factor. All Rhat = 1.00, Bulk_ESS ≥ 3634, Tail_ESS ≥ 5167, $N = 17{,}905$.
Bold values: Evidence ratio/Bayes factor of > 3 (see Section 2.8.6 for more detail) or more precisely from a posterior probability > 0.95. The posterior probabiltiy can be intepreted similar to a p-value in frequentist statistics. For results in favor of the tested hypothesis the posterior probability must be > 0.95 and for results in favor of the alternative hypothesis posterior probabilty must by < 0.05. So significance is already given and highlighted. I am not sure, what might be missing.
Abbreviations: BF, Bayes factor; CI, credible interval; RC, rich club.

10970193, 2024, 4, Downloaded from https://onlinelibrary.wiley.com/doi/10.1002/hbm.26543 by Universitäts- und Landesbibliothek Münster, Wiley Online Library on [25/01/2026]. See the Terms and Conditions (https://onlinelibrary.wiley.com/terms-and-conditions) on Wiley Online Library for rules of use; OA articles are governed by the applicable Creative Commons License

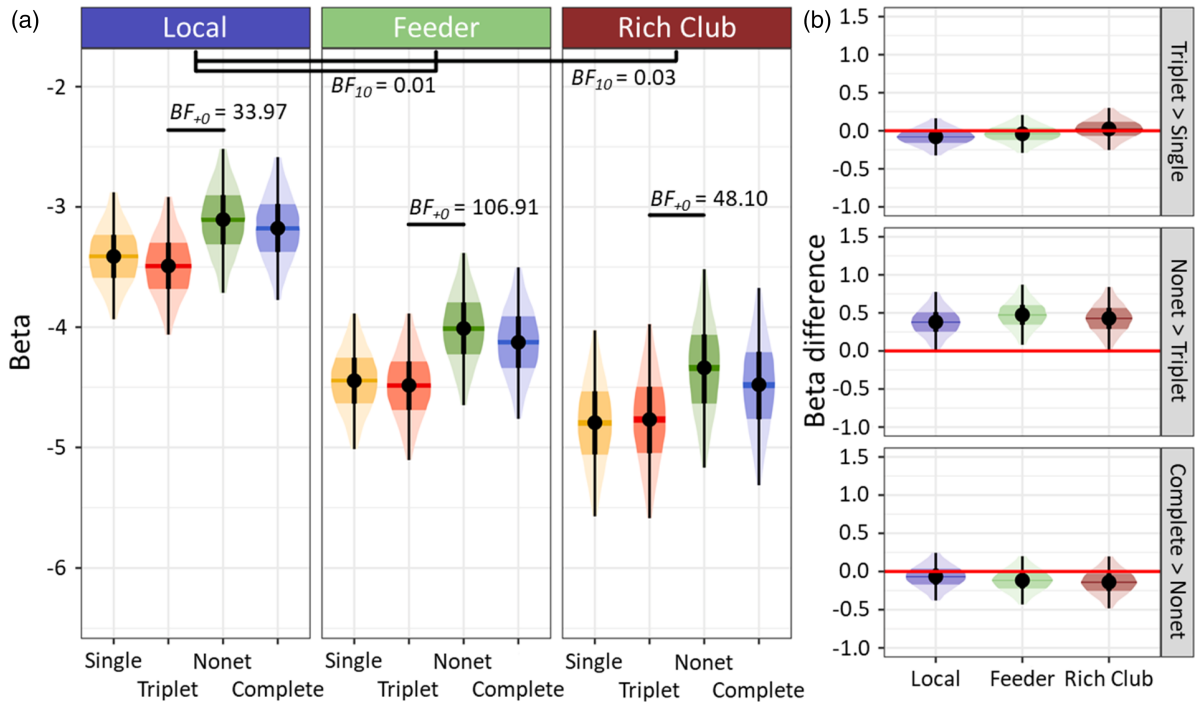


FIGURE 8 Results of region of interest analysis based on lausanne120 parcellation scheme and 60% prevalence-based group matrix. Beta values represent mean activations per condition compared to the implicit baseline. Density plots of posterior distributions with mean point estimate, 50 and 95% highest probability density areas marked. Local, no connection rich club; Feeder, connection to rich club; rich club, rich club hubs. Yellow, Single; Red, Triplet; Green, Nonet; Blue, Complete; Dark blue, Local; Light green, Feeder, Dark red, Rich Club. (A) Level of HIERARCHY estimates in different NODE CLASSIFICATIONS. (B) HIERARCHY differences in different NODE CLASSIFICATIONS. Red line marks no difference.

parcellation and 60% prevalence-based group matrix, Supplemental Material for remaining results).

3.5 | Centrality analysis results—Network centrality of the functional clusters

On a descriptive level, we looked at the regions that were covered by the functional clusters identified in the whole brain analysis (see Section 3.2). Specifically, we examined if the clusters were classified as RC hub, Feeder or Local node and focused on the differences in classification between the Triplet- and Nonet-specific clusters (Figure 9, Supplemental Material for remaining results).

On the model side, we used a MANOVA-like approach within the brms (Bürkner, 2017) framework to compare the centrality measures calculated for each subject between the identified clusters. No model had any divergent transitions, all *Rhat* = 1.00, and all variables had bulk- and tail-effective samples ≥ 4173 and ≥ 4061, respectively. Posterior checks showed that the cumulative count model simulations reasonably capture the means and distributions of the observed data (Figure S7.7).

First, we compared the model (Equation 5) including the factor HIERARCHY CONTRAST with a null model, to see if the factor explained any variance of the centrality measures. The leave-one-out-cross-validation (loo) comparison revealed a significant increase in the expected log pointwise predictive density (elpd) with the inclusion of the factor HIERARCHY CONTRAST (Table 4).

Next, we specifically tested whether the centrality measures of the areas derived from the Nonet > Triplet contrast were higher than those for the Triplet > Single contrast. Only the within-module degree *z*-score, which describes the module-specific degree of a node (Rubinov & Sporns, 2010), failed to show the predicted effect. For degree centrality, closeness centrality, betweenness centrality, and the participation coefficient the Nonet > Triplet clusters demonstrated the expected effect displaying significantly higher scores (Table 5 and Figure 10). This pattern shows that functional activation clusters for hierarchically higher structures of the stimulus coincide with areas of higher structural network centrality.

4 | DISCUSSION

Humans show a preference for exploring higher-order structures in the presence of complex, hierarchically nested, eventful stimuli such as actions (Williams et al., 2022) or language (Yedetore et al., 2023). In the current study, we used DWI and fMRI to investigate the

10970193, 2024, 4, Downloaded from https://onlinelibrary.wiley.com/doi/10.1002/hbm.26543 by Universitäts- und Landesbibliothek Münster, Wiley Online Library on [25/01/2026]. See the Terms and Conditions (https://onlinelibrary.wiley.com/terms-and-conditions) on Wiley Online Library for rules of use; OA articles are governed by the applicable Creative Commons License

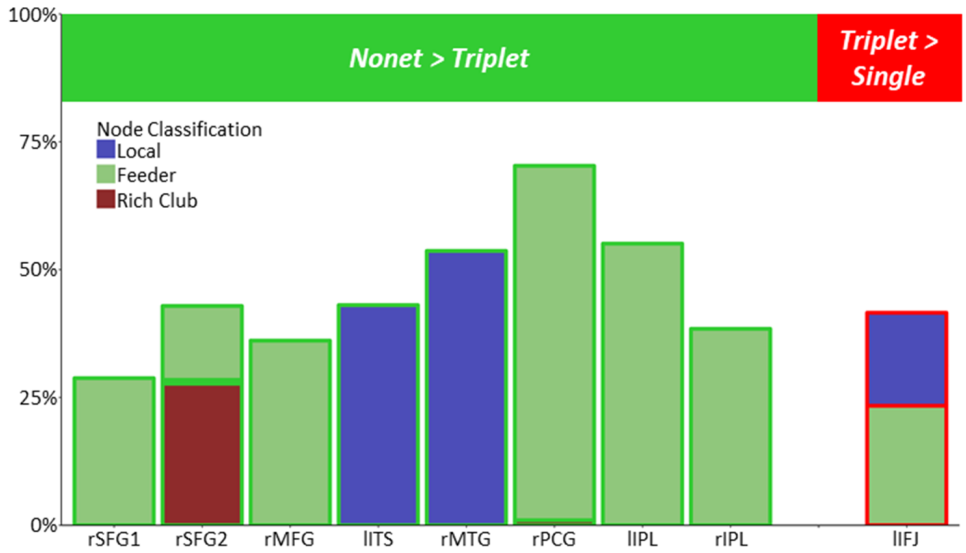


FIGURE 9 Percentage of overlap of activation clusters of the whole brain analysis with the parcellation. Colored according to lausanne120 and 60% prevalence-based NODE CLASSIFICATION. IFJ, inferior frontal junction; IPL, inferior parietal lobule; ITS, inferior temporal sulcus; l, left; MFG, middle frontal gyrus; MTG, middle temporal sulcus; PCG, posterior cingulate gyrus; r, right; rSFG1, rSFG (22, 60, 14); rSFG2, rSFG (22, 18, 58); SFG, superior frontal gyrus.

TABLE 4 Fit indices of the HIERARCHY contrast model (Equation 5) compared to the null model for lausanne120 parcellation scheme.

Model	$\widehat{elpd}_{diff}$	$se\left(\widehat{elpd}_{diff}\right)$	$\widehat{elpd}_{loo}$	$se\left(\widehat{elpd}_{loo}\right)$
Hierarchy contrast + (1 | Subject)	0.0	0.0	−1817.70	42.36
1 + (1 | Subject)	−12.7	3.6	−1830.40	42.19

Note: Models are considered to be better if the absolute difference is larger than the standard error (Mohor et al., 2021); $\widehat{elpd}_{loo}$, expected log pointwise predictive density for a new dataset using PSIS leave-one-out-cross-validation (loo) criterion. The closer to zero the better the model; $\widehat{elpd}_{diff}$, difference between the $\widehat{elpd}_{loo}$ of the two compared models; *se*, standard error of the variable.
Abbreviation: PSIS, Pareto smoothed importance sampling.

TABLE 5 Results of testing (Nonet > Triplet) > (Triplet > Single) for model Equation 5 for all five centrality measures extracted from individual connectivity matrices following lasuanne120 parcellation scheme.

Centrality measure	*M*	*SD*	CI lower	CI upper	Evidence ratio (BF)	Posterior probability
Degree centrality	**0.59**	**0.16**	**0.32**	**0.85**	**>999**	**1**
Closeness centrality	**0.28**	**0.16**	**0.02**	**0.54**	**26.73**	**0.96**
Betweenness centrality	**0.54**	**0.16**	**0.27**	**0.81**	**>999**	**1**
Within-module degree z-score	−0.21	0.17	−0.49	0.06	0.12	0.10
Participation coefficient	**0.46**	**0.17**	**0.19**	**0.73**	**>999**	**1**

Note: The evidence ratio of one-sided hypothesis tests is equal to the Bayes factor.
Abbreviations: BF, CI, credible interval; RC, rich club.

importance of the brain's intrinsic hierarchical structure for processing nested hierarchical stimuli. To identify brain structures that process hierarchically higher stimulus structures, we presented subjects with different levels of hierarchically nested digit sequences. We collected DWI data from the same participants to determine the global hierarchical node structure of the brain expressed in Local and, Feeder nodes, and RC hubs. We tested two separate hypotheses: (I) We hypothesized that the processing of hierarchically higher stimulus structures would involve network hubs that are part of the RC. (II) We also expected a trend toward more anterior and medial regions of the frontal cortex for processing hierarchically higher stimulus structures.

10970193, 2024, 4, Downloaded from https://onlinelibrary.wiley.com/doi/10.1002/hbm.26543 by Universitäts- und Landesbibliothek Münster, Wiley Online Library on [25/01/2026]. See the Terms and Conditions (https://onlinelibrary.wiley.com/terms-and-conditions) on Wiley Online Library for rules of use; OA articles are governed by the applicable Creative Commons License

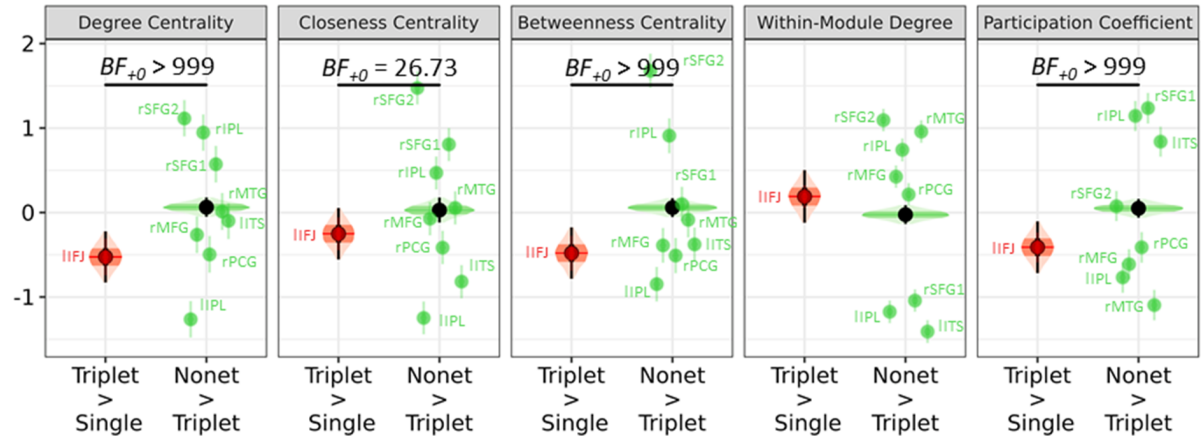


FIGURE 10 Results of the centrality analysis for lausanne120 parcellation scheme. Density distributions with mean point estimate, 50 and 95% highest probability density areas marked. Centrality measures are controlled for cluster size and *z*-standardized for comparability. Eye plots describe distribution of contrast on average, colorful point-interval plots describe each individual cluster. BF, Bayes factor; IFJ, inferior frontal junction; IPL, inferior parietal lobule; ITS, inferior temporal sulcus; l, left; MFG, middle frontal gyrus; MTG, middle temporal sulcus; PCG, posterior cingulate gyrus; r, right; rSFG1, rSFG (22, 60, 14); rSFG2, rSFG (22, 18, 58); SFG, superior frontal gyrus.

4.1 | fMRI results—The anterior–posterior and medial-lateral gradient

BOLD activation results confirmed the expected shift toward more anterior and medial regions for processing hierarchically higher structures. Visually inspecting the frontal activation clusters of the stepwise contrasts of the Nonet > Triplet blocks and the Triplet > Single blocks, we can describe the clusters in the Nonet-specific activations were located in more anterior and medial areas of the SFG and MFG. The only Triplet-specific cluster, however, was found in the more posterior and lateral IFJ. Additionally, we examined the correlations between contrast-specific beta values and the distance from the anterior-medial section of the frontal lobe. The comparison between Nonet- and Triplet-specific correlations revealed that the Nonet-specific activations increased closer to the anterior-medial frontal cortex. The Triplet-specific beta values in contrast significantly increased with distance. Thus, the correlations provide evidence for the anterior-medial shift for processing hierarchically higher stimulus structures beyond the visual inspection of the identified clusters.

The concept of a posterior-to-anterior processing gradient throughout the frontal lobe has been discussed even before the dawn of brain imaging (Ingvar, 1985). This gradient was proposed to be organized according to the temporal persistency of the processed levels (Fuster, 2001; Golesorkhi, Gomez-Pilar, Zilio, et al., 2021; Kiebel et al., 2008; Koechlin & Summerfield, 2007; Uithol et al., 2012). Also, it was found not only in fMRI BOLD responses (Badre & D'Esposito, 2007; Koechlin et al., 1999) but also in cytoarchitecture (Chanes & Feldman Barrett, 2016; Hilgetag et al., 2016; Sanides, 1964) and recently also in patterns of cortical frequencies (Mahjoory et al., 2020; Raut et al., 2020). Notably, this progression of time scales might also characterize the association cortices in the parietal and temporal lobes as well, which were found to integrate information across time (Badre & Wagner, 2004; Bussey & Saksida, 2005; Cui, 2014; Golesorkhi, Gomez-Pilar, Zilio, et al., 2021; Jeon, 2014; Kravitz et al., 2013; Naya et al., 2003). Yet, theoretical and empirical work sees the frontal lobe at the top of the entire cortical processing hierarchy (Brunia, 1999; Fuster & Bressler, 2015; Gómez et al., 2004; Koechlin et al., 1999; E. K. Miller & Cohen, 2001). However, the initial notion of the frontal pole being the apex of the hierarchy has been challenged by several findings (Badre & Nee, 2018; Crittenden & Duncan, 2014; Goulas et al., 2014; Nee & D'Esposito, 2016; Ramnani & Owen, 2004; Reynolds et al., 2012). More recent studies included the structure of cortical layers in the gradient and argued for more medial aspects of the PFC and the limbic system to be superordinate to the frontal pole (W. H. Alexander & Brown, 2018; Chanes & Feldman Barrett, 2016; Nee & D'Esposito, 2016). This progression from posterior-lateral toward anterior-medial frontal lobes for processing hierarchically higher structures of stimuli was also reflected in our results (Figure 6, also Supplemental Material).

Beyond the frontal effects our hypotheses focused on, the Nonet > Triplet contrast also revealed significant activation clusters in posterior parietal cortex. The lateral fronto-parietal network has been related to the processing of numbers (Dormal et al., 2012; Goffin, 2019; Sokolowski et al., 2017) and numerical magnitude (Ansari et al., 2006; Molko et al., 2003; Piazza et al., 2004, 2007), including the so-called mental number line in the angular gyrus (Dehaene et al., 2003). More generally, the parietal cortex is proposed to provide frontal areas with information about spatial and temporal relational metrics such as order, number, duration, length, distance, and proportion (Genovesio et al., 2014). Because digits were presented and processed in all conditions in our study, one might suggest that the hierarchically higher structure of the digit sequences (Nonet > Triplet) required greater temporally extended integration that is also associated

10970193, 2024, 4, Downloaded from https://onlinelibrary.wiley.com/doi/10.1002/hbm.26543 by Universitäts- und Landesbibliothek Münster, Wiley Online Library on [25/01/2026]. See the Terms and Conditions (https://onlinelibrary.wiley.com/terms-and-conditions) on Wiley Online Library for rules of use; OA articles are governed by the applicable Creative Commons License

with the fronto-parietal network (Bor & Seth, 2012; Golde et al., 2010; Hasson et al., 2015; Noonan et al., 2013).

4.2 | RC analysis—A largely consistent structure emerges

Based on the DWI data, we identified the structural graph including Local, Feeder, and RC areas, for the RC analysis. The RC hubs we identified closely resemble those hub regions identified by previous studies, including those in the bilateral precuneus and bilateral superior parietal lobe (Q. Cao et al., 2013; Z. Chen et al., 2013; Hagmann et al., 2010; Riedel et al., 2022; Wang, Zhan, et al., 2019), in the bilateral superior frontal gyri (Q. Cao et al., 2013; Z. Chen et al., 2013; Riedel et al., 2022; Wang, Zhan, et al., 2019), the anterior and posterior cortex cingulate (Huang et al., 2015) as well as the paracentral lobe (Z. Chen et al., 2013) and the superior and middle occipital lobe (Q. Cao et al., 2013; Z. Chen et al., 2013; Huang et al., 2015).

Although the results of network measures are sufficiently reliable even with the use of different methods, there is still no gold standard for identifying RC hubs or graph-theoretical measures in general (Braun et al., 2012; H. Cao et al., 2014; Welton et al., 2015). Most studies use only nodal degree-relative thresholds to determine RCs (Keown et al., 2017; O'Donoghue et al., 2017; Ray et al., 2014; van den Heuvel et al., 2013; Yan et al., 2018). In contrast, we decided to implement additional criteria for a node to qualify as an RC hub. In particular, we followed the definition of Colizza et al. according to which RC hubs are more densely connected to other high-degree nodes than expected in a random network (Colizza et al., 2006). As far as we can see, we are the first to apply this additional, theory-based step in the identification process, although as early as van den Heuvel and Sporns (2013) it was recommended to use more than just the degree as an identifier for the RC membership. A degree-based definition of hubs may generally be inadequate for identifying network structures that are important for global network communication. For instance, structures characterized by specific nodal properties such as an exceptionally high participation coefficient, making up a *diverse club*, might be more critical for efficient global integration than the RC hubs' outstanding connection strength (Bertolero et al., 2017).

However, as a result of using not just the degree to identify hubs, we did not find all RC hubs that are typically reported when more liberal criteria are applied. For instance, while we identified the insula as a highly connected node when following the criteria for RC qualification introduced by Riedel et al. (2022), this node failed to be more connected to other high-degree nodes than expected at random (Tables S6.1–S6.4). The insula, though commonly reported as a hub (Q. Cao et al., 2013; Z. Chen et al., 2013; Riedel et al., 2022), was even labeled as a Local node, according to our definition, as it was not directly connecting to any other RC hub. Especially because of these discrepancies between our results using additional constraints in the RC hub identification and the hubs found in the related literature, the performed validation analysis using the HCP data was a crucial step. According to the conventions for inter-rater reliability by Landis and Koch (1977), the results showed only a slight agreement (Table S9.1) in hub identification. Thus, sticking with the insula as an example, the parcels of the insula in the HCP dataset were mostly identified as Feeder nodes. Occasionally across the different parcellation schemes and group matrix creation methods some insula parcels were even classified as RC hubs. But importantly, areas that were found to be crucial for the processing of hierarchically higher stimulus structures (J. Chen et al., 2017; Hasson et al., 2015) and were consistently found as RC hubs in previous studies (e.g., Riedel et al., 2022) like parcels in the superior frontal cortex or the precuneus were identified in both our own and the HCP dataset (Tables S6.1–S6.4 and Table S9.8). Thus, the consistent findings between both datasets for the ROI and centrality analyses might be especially influenced by these coherently identified RC hubs.

To summarize, the applied RC hub identification in this article adheres more closely to the original definition of the RC by Colizza et al. (2006). Therefore, the identified hubs can be more likely considered as RC hubs, while other identification methods that, for example, only use the node degree might rather identify general hubs, not necessarily RC hubs. Nevertheless, this method is still dependent on acquisition parameters and processing of the connectivity matrices (some decision will be discussed in Section 4.4). Hence, more research is necessary to determine if the proposed extra step of comparing the hub connections to the connectivity in random networks is a valuable improvement to the RC identification methodology.

4.3 | Combining the results—The significance of RC hubs for the processing of nested hierarchical stimuli

To our knowledge, our study was the first to attempt to relate task-based fMRI activity to the structurally determined RC in the same group of subjects. Therefore, we developed the described procedures specifically for this analysis. We applied two complementary approaches, the ROI analysis, and the centrality analysis, to tackle the question of the functional significance of the structural hubs from different sides, which will be discussed separately in the following paragraphs. As mentioned before, these methods of combining structure and function both prevent any notion of circularity by identifying their areas of interest and outcome variables drawn from them crossmodally based on the fMRI and structural connectivity data, respectively (Kriegeskorte et al., 2009).

On the one hand, we modeled the beta values extracted from each parcel by their condition (HIERARCHY) and network relevance (NODE CLASSIFICATION). Especially looking at the activations within the RC hubs, Feeder nodes, and Local nodes revealed that all three kinds of nodes were depicting the same pattern of activity: Beta values were higher for the Nonet condition in comparison to the Triplet condition, while the Single and Triplet conditions as well as the Nonet and Complete did not differ significantly. Using the node classifications from the HCP validation dataset we were able to replicate the same pattern (Figure S9.1 and Tables S9.2–S9.5). We found a

10970193, 2024, 4, Downloaded from https://onlinelibrary.wiley.com/doi/10.1002/hbm.26543 by Universitäts- und Landesbibliothek Münster, Wiley Online Library on [25/01/2026]. See the Terms and Conditions (https://onlinelibrary.wiley.com/terms-and-conditions) on Wiley Online Library for rules of use; OA articles are governed by the applicable Creative Commons License

10970193, 2024, 4, Downloaded from https://onlinelibrary.wiley.com/doi/10.1002/hbm.26543 by Universitäts- und Landesbibliothek Münster, Wiley Online Library on [25/01/2026]. See the Terms and Conditions (https://onlinelibrary.wiley.com/terms-and-conditions) on Wiley Online Library for rules of use; OA articles are governed by the applicable Creative Commons License

nonsignificant trend that the Nonet > Triplet difference was slightly larger for RC and Feeder nodes than for Local nodes. When using the HCP dataset-based classification of nodes and the *t* test-based group matrices the difference between the Nonet and Triplet was significantly larger in RC hubs for both parcellation schemes (Tables S9.3 and S9.5 and Figures S9.1B and S9.1D).

Nevertheless, due to the inconsistent results, the hypothesis that RC hubs are specifically more involved in the processing of hierarchically higher structures of stimuli could neither be confirmed nor disproven with our analysis. However, this very similar activation pattern in Local, Feeder, and RC nodes could be a direct result of a core function of the RC, namely network synchronization (Gómez-Gardeñes et al., 2010; Senden et al., 2017; Watanabe, 2013). Specifically, Gollo et al. (2015) found that the RC hubs sit on top of so-called resonant network motifs, each consisting of three non-fully connected nodes with edges facing away from the central node. These network motifs are particularly efficient at synchronizing the activity of their neighboring nodes. Thus, finding very similar activation patterns all across the brain regardless of the type of node might indicate that the activation is synchronized throughout the network. The well-connected RC could be the prime candidate to achieve this synchronization. In order to assess the influence of the RC on the overall neural network, other methods may be more informative than those that average neural activity over the entire time span of the experiment. The synchronization effect imposed by the RC can be tested using the autocorrelation of the network nodes (Aguilar-Velázquez & Guzmán-Vargas, 2019). For instance, the autocorrelation decay method was recently used to show different intrinsic timescales across the cortex (Ito et al., 2020; Raut et al., 2020). Using this approach could reveal additional information on the dynamic influence of the RC hubs on the rest of the network and its modulation depending on the task at hand.

On the other hand, we analyzed the centrality measures obtained from the structural nodes at the location of significant functional clusters to assess the cluster's network importance. To this end, we first inspected the network-based classification of each of the functionally identified clusters. As a result, the clusters in the frontal and parietal lobes and the PCG cluster were contained in parcels that were classified as RC hubs or Feeder nodes. In contrast, the temporal lobe activity identified in the Nonet > Triplet contrast belonged to parcels that were classified as Local nodes. Also, the cluster in the left IFJ identified in the Triplet > Single contrast did not overlap with any parcels that were labeled as RC hubs. While a little less distinct, using the node classification from the HCP dataset, we could again show a tendency of the Nonet-specific clusters to share more overlap with parcels that were classified as RC hub (see Supplemental Material). So, compared with Triplet-specific activation cluster, Nonet-specific clusters showed greater overlap with the locations of RC hubs and Feeder nodes in frontal and parietal cortices. This observation is consistent with the hypothesis that hierarchically higher stimulus structures were processed in, or closer to, the structurally identified RC hubs.

Based on this overlap between the functionally found clusters and the network nodes, we extracted the following five centrality measures from the structural network nodes underlying the functional clusters: degree centrality, closeness centrality, betweenness centrality, within-module degree z-score, and participation coefficient. We expected that the centrality measures of nodes underlying the Nonet-specific clusters would be higher than for the Triplet-specific cluster. We indeed found a general significant influence of the HIERARCHY CONTRAST, an effect depending on whether the cluster was Nonet- or Triplet-specific, on the examined centrality measures. This general effect was replicated also using structural centrality measures extracted from the HCP data. Looking at the individual measures, the predicted effect was identified for degree centrality, betweenness centrality and the participation coefficient for both parcellation schemes and additionally for closeness centrality using the lausanne120 parcellation. Similarly, the individual measures from the HCP data also differed significantly between the Nonet-specific and Triplet-specific clusters extracted from functional data presented in this article. Significant differences were found for degree centrality and participation coefficient for both parcellation schemes, and additionally for betweenness centrality for the lausanne120 parcellation (Table S9.7 and Figure S9.3). Thus, the results of the centrality analysis largely met our expectations and were also very similar across the two parcellation schemes and datasets. The found differences for degree centrality, betweenness centrality and closeness centrality suggest that the structural nodes underlying Nonet-specific activations are more important for the integration and resilience of the connectome than the Triplet-specific cluster (Rubinov & Sporns, 2010). The consistent finding of an increased participation coefficient for Nonet-specific clusters further indicates that these nodes are also more structurally connected to different modules. The participation coefficient is usually interpreted and investigated alongside the within-module degree z-score (e.g., Fukushima et al., 2018; Jao et al., 2020; Pedersen et al., 2020). Only nodes with a high within-module degree and high participation coefficient are described connector nodes, which encourage global integration (Guimerà & Nunes Amaral, 2005; Rubinov & Sporns, 2010) and are crucial for communication across the cortical network (Crossley et al., 2014; Wu et al., 2011).Yet, the previously mentioned diverse club is just characterized by high participation coefficient nodes and their connectivity (Bertolero et al., 2017) showing that nodes with a high participation coefficient alone could indicate importance for the network's communication. More research on centrality measures is necessary to settle if there are meaningful and systematic relations between individual graph centrality measures of nodes and their function. This could be especially intriguing as the dynamic association between structural and functional networks was found to be dependent on the segregation or integration of the functional network (Fukushima et al., 2018).

In summary, the results of the centrality analysis demonstrate that areas that are functionally activated by hierarchically higher stimulus structures are more important for the integration and integrity of the structural network. In combination with the larger overlap of these functional clusters with RC hub regions, these results provide potential evidence for the hypothesis that the RC hubs are more involved in the processing of hierarchically higher structures of incoming stimuli.

10970193, 2024, 4, Downloaded from https://onlinelibrary.wiley.com/doi/10.1002/hbm.26543 by Universitäts- und Landesbibliothek Münster, Wiley Online Library on [25/01/2026]. See the Terms and Conditions (https://onlinelibrary.wiley.com/terms-and-conditions) on Wiley Online Library for rules of use; OA articles are governed by the applicable Creative Commons License

Taken together, both the ROI and centrality analysis allude to the involvement of RC hubs in the processing of hierarchically higher stimulus structures. In this context, it has to be pointed out that the results were very consistent across methods of parcellation and group-matrix creation and were even replicated using a large independent structural dataset. Thus, even though, the methods for combining structure and function in this article were specifically developed for the investigated question and consequently applied for the first time, the displayed consistency of the found results demonstrates their suitability.

4.4 | Limitations and open questions

Some limitations of the study have to be considered. The paradigm and stimulus structure we applied was based on the TRW approach (Hasson et al., 2008, 2010). As previous findings using this approach could demonstrate a distinction of specific areas activated for certain hierarchical structures in the stimulus levels and that the additionally engaged areas per hierarchical level also extend along an anterior–posterior gradient (Farbood et al., 2015; Lerner et al., 2011), we as well expected to find a distinction between the four levels implemented in our stimulus sequences. However, neither the behavioral, neurofunctional, nor ROI analysis results could consistently distinguish between the four implied hierarchical levels. The ROI results rather showed a distinction between a hierarchically low (Single and Triplet) and hierarchically high (Nonet and Complete) level. Especially the Complete condition behaved unexpectedly across all analyses, as it did not differ from the Nonet condition in any applied contrast. It can be speculated that the 36-digit sequence of the Complete condition was too long for subjects to notice the repeating pattern of digits. If the stimuli are processed one by one as they are presented, studies on working memory capacity would predict a maximum capacity of nine items depending on the modality (Bick & Rabinovich, 2009; G. A. Miller, 1956). This would include the ranges for the Single, Triplet, and Nonet conditions and might also explain the similarity of the Nonet and Complete conditions as they are practically the same when only looking at the last nine digits.

A second limitation relates to the method of structural network reconstruction and RC hub identification. In constructing the connectivity matrices used for the RC analysis, we decided on the one hand to binarize the matrices and on the other hand to use group-averaged matrices. The binarization was implemented as a necessary compromise (Calamante, 2019). Since the acquisition parameters of our DWI sequence did not fully comply with current recommendation (Jones et al., 2013), we binarized the structural connectivity matrices to mitigate biases that can occur when using weighted graphs with subpar DW data (Fornito et al., 2016). The decision to use a group-wise connectivity matrix was made because we employed group-level statistics for the combination of functional and structural data. Additionally, it has been already shown that large structural connectivity patterns, such as the RC, are more detectable in group-connectomes (Hagmann et al., 2008). Still, it should be considered that both steps reduce the information included in the analysis, which affects the interpretability and generalizability of the results (Calamante, 2019). However, the consistency of results across parcellation schemes, group matrix creation methods and datasets demonstrated in this article nonetheless supports the credibility of our findings.

Furthermore, for the parcellation schemes, we opted for the extensions of the FreeSurfer inherent Desikan–Killiany atlas introduced in Cammoun et al. (2012) that are included in CATO (de Lange et al., 2023). More precisely, we used the lausanne120 and lausanne250 options with 114 and 219 cortical areas, respectively, as this resolution might come closer to meso-level parcellations related to multimodal differences between the areas (Amunts & Zilles, 2015). However, while the Desikan–Killiany atlas is based on the borders of gyri and sulci (Desikan et al., 2006), thus having an anatomical justification, the extensions aimed for a near voxel-level parcellation and are not particularly based on any natural borders in the cortex (Cammoun et al., 2012). Parcellation on the levels of voxel size is referred to as random (Qi et al., 2015) as the resolution becomes arbitrary (de Reus & van den Heuvel, 2013b). An increase in parcellation resolution would also require an improvement in DWI quality (Yeh et al., 2018). It can, however, be argued that the level of detail of the chosen parcellation might be dependent on the purpose of the investigation, as a "correct" parcellation is unlikely to be accomplished (Schaefer et al., 2018). Nevertheless, in trying to bridge the gap between structural connectivity and cortical function, it might be more interesting to utilize a parcellation scheme that uses functional information as the basis for boundaries (Craddock et al., 2012; Schaefer et al., 2018; Shen et al., 2013), or even an approach using multiple sources of information (Glasser et al., 2016). This is especially relevant since the parcellation scheme has been shown to largely influence the appearance of the network (Bassett et al., 2011; Bryce et al., 2021; Cammoun et al., 2012; Qi et al., 2015; Seguin et al., 2020; Sporns, 2011), which can also be seen in this study when comparing the networks between the lausanne120 and lausanne250 parcellations (Figure S5.3).

Also, we varied the method that constructed the group connectivity matrix. The prevalence method was based on the false-positive and false-negative balance calculation (de Reus & van den Heuvel, 2013a), while the *t* test method was based on the analyses in Ponsoda et al. (2017). Since the results differed especially for the lausanne250 parcellation scheme between the two methods (Figure S5.3), it might be necessary to investigate the false-positive rates, like de Reus and van den Heuvel (2013a) did before, depending on the parcellation scheme used. Previously it could be shown that graph theoretical measures are only more reliable with lower resolution parcellations (Welton et al., 2015) which in turn might be less representative for a functionally viable parcellation of the cortex (Amunts & Zilles, 2015).

Finally, we did not include the subcortex since the focus of the functional analysis was on cortical activations. Hence, our approach was not designed to identify subcortical hubs as others did, for instance in the thalamus, putamen, and caudate nucleus (Riedel et al., 2022). The DTI algorithms used to reconstruct the white matter

10970193, 2024, 4, Downloaded from https://onlinelibrary.wiley.com/doi/10.1002/hbm.26543 by Universitäts- und Landesbibliothek Münster, Wiley Online Library on [25/01/2026]. See the Terms and Conditions (https://onlinelibrary.wiley.com/terms-and-conditions) on Wiley Online Library for rules of use; OA articles are governed by the applicable Creative Commons License

streamlines for structural connectivity analyses are less reliable in the subcortex due to kissing and crossing fibers (Prčkovska et al., 2016). Even though, we used a combined DTI and GQI algorithm, which showed good performance in the benchmarking test (de Lange et al., 2023), additional methodical considerations regarding DWI sequence and tract algorithm are necessary to accurately identify the streamlines and model the connectivity of the subcortex (Kai et al., 2022). Nevertheless, via basal ganglia-thalamocortical loops, the subcortical areas play a major role in shaping the cortical hierarchy (G. E. Alexander et al., 1986; Badre & Nee, 2018). Thus, given a reliable acquisition and tract-detection, investigating the relationship between structural connectivity in the subcortex and the processing hierarchically structured stimuli could be a compelling next step. Especially, as the striatum is commonly found as an RC hub (Riedel et al., 2022) and also is a key structure for the chunking of sequences, it could be vital for the processing of nested hierarchical structures (Graybiel, 2008).

This article considered both graph-theoretical and anatomical gradients but did not intend to determine which one is better suited to describe our brain's organization. In fact, either gradient may explain distinct portions of variance (Golesorkhi, Gomez-Pilar, Tumati, et al., 2021). Recent studies on cortical gradients explored methods to combine and compare different gradient definitions (Hansen et al., 2022; Suárez et al., 2020). For instance, approaches using resting-state fMRI could already demonstrate the relationship between the intrinsic timescales and structurally determined measures of centrality (Fallon et al., 2020; Lurie et al., 2023; Sethi et al., 2017) as well as cytoarchitectonic (Gao et al., 2020) and functional unimodal to transmodal gradients (Shafiei et al., 2020; Wolff et al., 2022). Future studies should compare gradients defined by various modalities not only in respect to the brain's resting state but also with regard to their task-relevance.

5 | CONCLUSION

To summarize, we could observe a shift of activation clusters for processing hierarchically higher stimulus structures toward more anterior and medial areas in the frontal cortex. The evidence for the importance of structural RC hubs for processing of hierarchically higher structures in nested stimuli, however, remains inconclusive. On the one hand, we determined a set of hub structures that match previously found compositions of the RC. We also are the first to demonstrate that areas in the frontal and parietal regions of the brain that are related to the processing of hierarchically higher structures of stimuli share more overlap with areas that were identified as RC hubs or directly connected Feeder nodes. Also, these areas identified for the functional processing of higher levels were found to be more central to the structural network. On the other hand, while the ROI analysis did determine the involvement of RC hubs in the processing of hierarchically higher stimulus structures, the found activity pattern was not specific to the RC and was instead found across all node classifications. This alludes to a more complex relationship between the functional processing of hierarchically structured stimuli and the levels of nodes in the structural network. We suggest alternative analysis methods that focus more on the temporal structure of the neurofunctional signal as well as possible refinements of the hub identification methods to further assess the relationship between the hierarchy of our cortical network and the hierarchical structures in the world around us.

AUTHOR CONTRIBUTIONS

Falko Mecklenbrauck contributed project conceptualization, experimental design and setup, data acquisition and analysis, data interpretation, writing and revising the manuscript. Sophie Siestrup contributed data analysis, writing and revising the manuscript. Marius Gruber and Ima Trempler contributed data analysis and writing the manuscript. Anoushiravan Zahedi contributed supervision of the project, data analysis, data interpretation, and writing the manuscript. Dominik Grotegerd and Marco Mauritz contributed data analysis. Udo Dannlowski contributed resources and writing the manuscript. Ricarda I. Schubotz contributed project conceptualization, experimental design and setup, supervision of the project, data analysis, resources, writing and revising the manuscript.

ACKNOWLEDGMENTS

Data were provided in part by the Human Connectome Project, WU-Minn Consortium (Principal Investigators: David Van Essen and Kamil Ugurbil; 1U54MH091657) funded by the 16 NIH Institutes and Centers that support the NIH Blueprint for Neuroscience Research; and by the McDonnell Center for Systems Neuroscience at Washington University. The authors thank Monika Mertens and Lena M. Puder for their help during data collection; Lena M. Puder, Simon Wieczorek, and Maria L. Hofmann for help in the quality control process; Kristin Stroop and Simon Wieczorek for help in testing the paradigm; Alea M. Bexten and Leon G. Exeler for their help in extracting the regions of interest maps; and Maria L. Hofmann and Juliane Diefenthal for their help in revising the manuscript. Open Access funding enabled and organized by Projekt DEAL.

FUNDING INFORMATION

The authors received no specific funding for this work.

CONFLICT OF INTEREST STATEMENT

The authors have declared that no competing interests exist.

DATA AVAILABILITY STATEMENT

The data that support the findings of this study are available from the corresponding author (Falko Mecklenbrauck, f_meck01@uni-muenster.de) upon request. The authors can confirm that all relevant data are included in the article.

ORCID

Falko Mecklenbrauck https://orcid.org/0000-0002-8187-6826
Marius Gruber https://orcid.org/0000-0002-6094-9950
Sophie Siestrup https://orcid.org/0000-0002-6365-3055

Anoushiravan Zahedi https://orcid.org/0000-0002-5532-3910
Dominik Grotegerd https://orcid.org/0000-0001-8718-0128
Ima Trempler https://orcid.org/0000-0003-2968-4795
Udo Dannlowski https://orcid.org/0000-0002-0623-3759
Ricarda I. Schubotz https://orcid.org/0000-0001-5802-6869

REFERENCES

Agcaoglu, O., Wilson, T. W., Wang, Y. P., Stephen, J., & Calhoun, V. D. (2019). Resting state connectivity differences in eyes open versus eyes closed conditions. *Human Brain Mapping*, *40*(8), 2488–2498. https://doi.org/10.1002/hbm.24539

Aguilar-Velázquez, D., & Guzmán-Vargas, L. (2019). Critical synchronization and 1/f noise in inhibitory/excitatory rich-club neural networks. *Scientific Reports*, *9*(1), 1–13. https://doi.org/10.1038/s41598-018-37920-w

Aguirre, G. K., Mattar, M. G., & Magis-Weinberg, L. (2011). De Bruijn cycles for neural decoding. *NeuroImage*, *56*(3), 1293–1300. https://doi.org/10.1016/j.neuroimage.2011.02.005

Alexander, G. E., DeLong, M. R., & Strick, P. L. (1986). Parallel organization of functionally segregated circuits linking basal ganglia and cortex. *Annual Review of Neuroscience*, *9*, 357–381. https://doi.org/10.1146/annurev.ne.09.030186.002041

Alexander, W. H., & Brown, J. W. (2018). Frontal cortex function as derived from hierarchical predictive coding. *Scientific Reports*, *8*(1), 1–11. https://doi.org/10.1038/s41598-018-21407-9

Amunts, K., & Zilles, K. (2015). Architectonic mapping of the human brain beyond Brodmann. *Neuron*, *88*(6), 1086–1107. https://doi.org/10.1016/j.neuron.2015.12.001

Andersson, J. L. R., Skare, S., & Ashburner, J. (2003). How to correct susceptibility distortions in spin-echo echo-planar images: Application to diffusion tensor imaging. *NeuroImage*, *20*(2), 870–888. https://doi.org/10.1016/S1053-8119(03)00336-7

Andersson, J. L. R., & Sotiropoulos, S. N. (2016). An integrated approach to correction for off-resonance effects and subject movement in diffusion MR imaging. *NeuroImage*, *125*, 1063–1078. https://doi.org/10.1016/j.neuroimage.2015.10.019

Ansari, D., Dhital, B., & Siong, S. C. (2006). Parametric effects of numerical distance on the intraparietal sulcus during passive viewing of rapid numerosity changes. *Brain Research*, *1067*(1), 181–188. https://doi.org/10.1016/j.brainres.2005.10.083

Ashburner, J. (2007). A fast diffeomorphic image registration algorithm. *NeuroImage*, *38*(1), 95–113. https://doi.org/10.1016/j.neuroimage.2007.07.007

Badre, D., & D'Esposito, M. (2007). Functional magnetic resonance imaging evidence for a hierarchical organization of the prefrontal cortex. *Journal of Cognitive Neuroscience*, *19*(12), 2082–2099. https://doi.org/10.1162/jocn.2007.19.12.2082

Badre, D., & Nee, D. E. (2018). Frontal cortex and the hierarchical control of behavior. *Trends in Cognitive Sciences*, *22*(2), 170–188. https://doi.org/10.1016/j.tics.2017.11.005

Badre, D., & Wagner, A. D. (2004). Selection, integration, and conflict monitoring. *Neuron*, *41*(3), 473–487. https://doi.org/10.1016/s0896-6273(03)00851-1

Baggio, H. C., Segura, B., Junque, C., de Reus, M. A., Sala-Llonch, R., & Van den Heuvel, M. P. (2015). Rich club organization and cognitive performance in healthy older participants. *Journal of Cognitive Neuroscience*, *27*(9), 1801–1810. https://doi.org/10.1162/jocn_a_00821

Ball, G., Aljabar, P., Zebari, S., Tusor, N., Arichi, T., Merchant, N., Robinson, E. C., Ogundipe, E., Rueckert, D., Edwards, A. D., & Counsell, S. J. (2014). Rich-club organization of the newborn human brain. *Proceedings of the National Academy of Sciences of the United States of America*, *111*(20), 7456–7461. https://doi.org/10.1073/pnas.1324118111

Bassett, D. S., Brown, J. A., Deshpande, V., Carlson, J. M., & Grafton, S. T. (2011). Conserved and variable architecture of human white matter connectivity. *NeuroImage*, *54*(2), 1262–1279. https://doi.org/10.1016/j.neuroimage.2010.09.006

Bassett, D. S., Bullmore, E., Verchinski, B. A., Mattay, V. S., Weinberger, D. R., & Meyer-Lindenberg, A. (2008). Hierarchical organization of human cortical networks in health and schizophrenia. *Journal of Neuroscience*, *28*(37), 9239–9248. https://doi.org/10.1523/JNEUROSCI.1929-08.2008

Bathelt, J., Gathercole, S. E., Butterfield, S., & Astle, D. E. (2018). Children's academic attainment is linked to the global organization of the white matter connectome. *Developmental Science*, *21*(5), 1–14. https://doi.org/10.1111/desc.12662

Benjamini, Y., & Hochberg, Y. (1995). Controlling the false discovery rate: A practical and powerful approach to multiple testing. *Journal of the Royal Statistical Society*, *57*(1), 289–300.

Bertolero, M. A., Yeo, B. T. T., & D'Esposito, M. (2017). The diverse club. *Nature Communications*, *8*(1), 1–10. https://doi.org/10.1038/s41467-017-01189-w

Bick, C., & Rabinovich, M. I. (2009). Dynamical origin of the effective storage capacity in the brain's working memory. *Physical Review Letters*, *103*(21), 1–4. https://doi.org/10.1103/PhysRevLett.103.218101

Bor, D., & Seth, A. K. (2012). Consciousness and the prefrontal parietal network: Insights from attention, working memory, and chunking. *Frontiers in Psychology*, *3*(MAR), 1–14. https://doi.org/10.3389/fpsyg.2012.00063

Botvinick, M. M. (2008). Hierarchical models of behavior and prefrontal function. *Trends in Cognitive Sciences*, *12*(5), 201–208. https://doi.org/10.1016/j.tics.2008.02.009

Braun, U., Plichta, M. M., Esslinger, C., Sauer, C., Haddad, L., Grimm, O., Mier, D., Mohnke, S., Heinz, A., Erk, S., Walter, H., Seiferth, N., Kirsch, P., & Meyer-Lindenberg, A. (2012). Test-retest reliability of resting-state connectivity network characteristics using fMRI and graph theoretical measures. *NeuroImage*, *59*(2), 1404–1412. https://doi.org/10.1016/j.neuroimage.2011.08.044

Brimijoin, W. O., & O'Neill, W. E. (2010). Patterned tone sequences reveal non-linear interactions in auditory spectrotemporal receptive fields in the inferior colliculus. *Hearing Research*, *267*(1–2), 96–110. https://doi.org/10.1016/j.heares.2010.04.005

Brown, J. A., Terashima, K. H., Burggren, A. C., Ercoli, L. M., Miller, K. J., Small, G. W., & Bookheimer, S. Y. (2011). Brain network local interconnectivity loss in aging APOE-4 allele carriers. *Proceedings of the National Academy of Sciences of the United States of America*, *108*(51), 20760–20765. https://doi.org/10.1073/pnas.1109038108

Brunia, C. H. M. (1999). Neural aspects of anticipatory behavior. *Acta Psychologica*, *101*(2–3), 213–242. https://doi.org/10.1016/s0001-6918(99)00006-2

Brysbaert, M. (1995). Arabic number reading: On the nature of the numerical scale and the origin of phonological recoding. *Journal of Experimental Psychology: General*, *124*(4), 434–452. https://doi.org/10.1037/0096-3445.124.4.434

Bryce, N. V., Flournoy, J. C., Guassi Moreira, J. F., Rosen, M. L., Sambook, K. A., Mair, P., & McLaughlin, K. A. (2021). Brain parcellation selection: An overlooked decision point with meaningful effects on individual differences in resting-state functional connectivity. *NeuroImage*, *243*(March), 118487. https://doi.org/10.1016/j.neuroimage.2021.118487

Bürkner, P. C. (2017). Brms: An R package for Bayesian multilevel models using Stan. *Journal of Statistical Software*, *80*(1), 1–28. https://doi.org/10.18637/jss.v080.i01

Bürkner, P. C. (2018). Is the evidence ratio for a one sided hypothesis equivalent to a one sided Bayes factor? Retrieved from https://github.com/paul-buerkner/brms/issues/311

Bussey, T. J., & Saksida, L. M. (2005). Object memory and perception in the medial temporal lobe: An alternative approach. *Current Opinion in Neurobiology*, *15*(6), 730–737. https://doi.org/10.1016/j.conb.2005.10.014

Calamante, F. (2019). The seven deadly sins of measuring brain structural connectivity using diffusion MRI streamlines fibre-tracking. *Diagnostics*, *9*(3), 1–17. https://doi.org/10.3390/diagnostics9030115

10970193, 2024, 4, Downloaded from https://onlinelibrary.wiley.com/doi/10.1002/hbm.26543 by Universitäts- und Landesbibliothek Münster, Wiley Online Library on [25/01/2026]. See the Terms and Conditions (https://onlinelibrary.wiley.com/terms-and-conditions) on Wiley Online Library for rules of use; OA articles are governed by the applicable Creative Commons License

Cammoun, L., Gigandet, X., Meskaldji, D., Thiran, J. P., Sporns, O., Do, K. Q., Maeder, P., Meuli, R., & Hagmann, P. (2012). Mapping the human connectome at multiple scales with diffusion spectrum MRI. *Journal of Neuroscience Methods*, *203*(2), 386–397. https://doi.org/10.1016/j.jneumeth.2011.09.031

Cao, H., Plichta, M. M., Schäfer, A., Haddad, L., Grimm, O., Schneider, M., Esslinger, C., Kirsch, P., Meyer-Lindenberg, A., & Tost, H. (2014). Test-retest reliability of fMRI-based graph theoretical properties during working memory, emotion processing, and resting state. *NeuroImage*, *84*, 888–900. https://doi.org/10.1016/j.neuroimage.2013.09.013

Cao, Q., Shu, N., An, L., Wang, P., Sun, L., Xia, M. R., Wang, J. H., Gong, G. L., Zang, Y. F., Wang, Y. F., & He, Y. (2013). Probabilistic diffusion tractography and graph theory analysis reveal abnormal white matter structural connectivity networks in drug-naive boys with attention deficit/hyperactivity disorder. *Journal of Neuroscience*, *33*(26), 10676–10687. https://doi.org/10.1523/JNEUROSCI.4793-12.2013

Cao, R., Wang, X., Gao, Y., Li, T., Zhang, H., Hussain, W., Xie, Y., Wang, J., Wang, B., & Xiang, J. (2020). Abnormal anatomical rich-club organization and structural–functional coupling in mild cognitive impairment and Alzheimer's disease. *Frontiers in Neurology*, *11*(February), 1–17. https://doi.org/10.3389/fneur.2020.00053

Chanes, L., & Feldman Barrett, L. (2016). Redefining the role of limbic areas in cortical processing. *Trends in Cognitive Sciences*, *20*(2), 96–106. https://doi.org/10.1016/j.tics.2015.11.005

Chang, L.-C., Jones, D. K., & Pierpaoli, C. (2005). RESTORE: Robust estimation of tensors by outlier rejection. *Magnetic Resonance in Medicine*, *53*(5), 1088–1095. https://doi.org/10.1002/mrm.20426

Chang, L.-C., Walker, L., & Pierpaoli, C. (2012). Informed RESTORE: A method for robust estimation of diffusion tensor from low redundancy datasets in the presence of physiological noise artifacts. *Magnetic Resonance in Medicine*, *68*(5), 1654–1663. https://doi.org/10.1002/mrm.24173

Chen, J., Leong, Y. C., Honey, C. J., Yong, C. H., Norman, K. A., & Hasson, U. (2017). Shared memories reveal shared structure in neural activity across individuals. *Nature Neuroscience*, *20*(1), 115–125. https://doi.org/10.1038/nn.4450

Chen, Z., Liu, M., Gross, D. W., & Beaulieu, C. (2013). Graph theoretical analysis of developmental patterns of the white matter network. *Frontiers in Human Neuroscience*, *7*(NOV), 1–13. https://doi.org/10.3389/fnhum.2013.00716

Chung, M. K., Lee, H., Solo, V., Davidson, R. J., & Pollak, S. D. (2017). Topological distances between brain networks. *Lecture Notes in Computer Science*, *10511*, 161–170. https://doi.org/10.1007/978-3-319-67159-8_19

Colizza, V., Flammini, A., Serrano, M. A., & Vespignani, A. (2006). Detecting rich-club ordering in complex networks. *Nature Physics*, *2*(2), 110–115. https://doi.org/10.1038/nphys209

Collin, G., Kahn, R. S., De Reus, M. A., Cahn, W., & van den Heuvel, M. P. (2014). Impaired rich club connectivity in unaffected siblings of schizophrenia patients. *Schizophrenia Bulletin*, *40*(2), 438–448. https://doi.org/10.1093/schbul/sbt162

Collin, G., Scholtens, L. H., Kahn, R. S., Hillegers, M. H. J., & van den Heuvel, M. P. (2017). Affected anatomical rich club and structural–functional coupling in young offspring of schizophrenia and bipolar disorder patients. *Biological Psychiatry*, *82*(10), 746–755. https://doi.org/10.1016/j.biopsych.2017.06.013

Collin, G., Sporns, O., Mandl, R. C. W., & Van Den Heuvel, M. P. (2014). Structural and functional aspects relating to cost and benefit of rich club organization in the human cerebral cortex. *Cerebral Cortex*, *24*(9), 2258–2267. https://doi.org/10.1093/cercor/bht064

Corbin, N., Todd, N., Friston, K. J., & Callaghan, M. F. (2018). Accurate modeling of temporal correlations in rapidly sampled fMRI time series. *Human Brain Mapping*, *39*(10), 3884–3897. https://doi.org/10.1002/hbm.24218

Craddock, R. C., James, G. A., Holtzheimer, P. E., Hu, X. P., & Mayberg, H. S. (2012). A whole brain fMRI atlas generated via spatially constrained spectral clustering. *Human Brain Mapping*, *33*(8), 1914–1928. https://doi.org/10.1002/hbm.21333

Cramer, D., & Howitt, D. (2011). *The SAGE dictionary of statistics*. SAGE Publications. https://doi.org/10.4135/9780857020123

Crittenden, B. M., & Duncan, J. (2014). Task difficulty manipulation reveals multiple demand activity but no frontal lobe hierarchy. *Cerebral Cortex*, *24*(2), 532–540. https://doi.org/10.1093/cercor/bhs333

Crossley, N. A., Mechelli, A., Scott, J., Carletti, F., Fox, P. T., Mcguire, P., & Bullmore, E. T. (2014). The hubs of the human connectome are generally implicated in the anatomy of brain disorders. *Brain*, *137*(8), 2382–2395. https://doi.org/10.1093/brain/awu132

Crossley, N. A., Mechelli, A., Vértes, P. E., Winton-Brown, T. T., Patel, A. X., Ginestet, C. E., McGuire, P., & Bullmore, E. T. (2013). Cognitive relevance of the community structure of the human brain functional coactivation network. *Proceedings of the National Academy of Sciences of the United States of America*, *110*(28), 11583–11588. https://doi.org/10.1073/pnas.1220826110

Cui, H. (2014). From intention to action: Hierarchical sensorimotor transformation in the posterior parietal cortex. *ENeuro*, *1*(1), 1–6. https://doi.org/10.1523/ENEURO.0017-14.2014

Cullen, A. C., & Frey, H. C. (1999). *Probabilistic techniques in exposure assessment: A handbook for dealing with variability and uncertainty in models and inputs*. Springer Science+Business Media.

de Bruijn, G. N. (1946). A combinatorial problem. *Proceedings of the Koninklijke Nederlandse Akademie van Wetenschappen*, *49*, 758–764. Retrieved from http://ci.nii.ac.jp/naid/10019660672/en/

de Lange, S. C., Helwegen, K., & van den Heuvel, M. P. (2023). Structural and functional connectivity reconstruction with CATO—A connectivity analysis TOolbox. *NeuroImage*, *273*(April), 120108. https://doi.org/10.1016/j.neuroimage.2023.120108

de Reus, M. A., & van den Heuvel, M. P. (2013a). Estimating false positives and negatives in brain networks. *NeuroImage*, *70*, 402–409. https://doi.org/10.1016/j.neuroimage.2012.12.066

de Reus, M. A., & van den Heuvel, M. P. (2013b). The parcellation-based connectome: Limitations and extensions. *NeuroImage*, *80*, 397–404. https://doi.org/10.1016/j.neuroimage.2013.03.053

Dehaene, S., Piazza, M., Pinel, P., & Cohen, L. (2003). Three parietal circuits for number processing. *Cognitive Neuropsychology*, *20*(3–6), 487–506. https://doi.org/10.1080/02643290244000239

Desikan, R. S., Ségonne, F., Fischl, B., Quinn, B. T., Dickerson, B. C., Blacker, D., Buckner, R. L., Dale, A. M., Maguire, R. P., Hyman, B. T., Albert, M. S., & Killiany, R. J. (2006). An automated labeling system for subdividing the human cerebral cortex on MRI scans into gyral based regions of interest. *NeuroImage*, *31*(3), 968–980. https://doi.org/10.1016/j.neuroimage.2006.01.021

Diedenhofen, B., & Musch, J. (2015). Cocor: A comprehensive solution for the statistical comparison of correlations. *PLoS One*, *10*(4), 1–12. https://doi.org/10.1371/journal.pone.0121945

Dixon, M. L., Girn, M., & Christoff, K. (2017). Hierarchical organization of frontoparietal control networks underlying goal-directed behavior. In *The prefrontal cortex as an executive, emotional, and social brain* (pp. 133–148). Springer Japan. https://doi.org/10.1007/978-4-431-56508-6_7

Dormal, V., Dormal, G., Joassin, F., & Pesenti, M. (2012). A common right fronto-parietal network for numerosity and duration processing: An fMRI study. *Human Brain Mapping*, *33*(6), 1490–1501. https://doi.org/10.1002/hbm.21300

Dunn, O. J., & Clark, V. (1969). Correlation coefficients measured on the same individuals. *Journal of the American Statistical Association*, *64*(325), 366–377. https://doi.org/10.1080/01621459.1969.10500981

Fallon, J., Ward, P. G. D., Parkes, L., Oldham, S., Arnatkevičiūtė, A., Fornito, A., & Fulcher, B. D. (2020). Timescales of spontaneous fMRI

10970193, 2024, 4, Downloaded from https://onlinelibrary.wiley.com/doi/10.1002/hbm.26543 by Universitäts- und Landesbibliothek Münster, Wiley Online Library on [25/01/2026]. See the Terms and Conditions (https://onlinelibrary.wiley.com/terms-and-conditions) on Wiley Online Library for rules of use; OA articles are governed by the applicable Creative Commons License

fluctuations relate to structural connectivity in the brain. *Network Neuroscience*, *4*(3), 788–806. https://doi.org/10.1162/netn_a_00151
Farbood, M. M., Heeger, D. J., Marcus, G., Hasson, U., & Lerner, Y. (2015). The neural processing of hierarchical structure in music and speech at different timescales. *Frontiers in Neuroscience*, *9*(APR), 1–13. https://doi.org/10.3389/fnins.2015.00157
Fischl, B. (2012). FreeSurfer. *NeuroImage*, *62*(2), 774–781. https://doi.org/10.1016/j.neuroimage.2012.01.021
Fitch, W. T., & Martins, M. D. (2014). Hierarchical processing in music, language, and action: Lashley revisited. *Annals of the New York Academy of Sciences*, *1316*(1), 87–104. https://doi.org/10.1111/nyas.12406
Fornito, A., Zalesky, A., & Bullmore, E. (2016). *Fundamentals of brain network analysis*. Elsevier. https://doi.org/10.1016/C2012-0-06036-X
Fukushima, M., Betzel, R. F., He, Y., van den Heuvel, M. P., Zuo, X. N., & Sporns, O. (2018). Structure–function relationships during segregated and integrated network states of human brain functional connectivity. *Brain Structure and Function*, *223*(3), 1091–1106. https://doi.org/10.1007/s00429-017-1539-3
Fuster, J. M. (2001). The prefrontal cortex—An update: Time is of the essence. *Neuron*, *30*(2), 319–333. https://doi.org/10.1016/S0896-6273(01)00285-9
Fuster, J. M., & Bressler, S. L. (2015). Past makes future: Role of pFC in prediction. *Journal of Cognitive Neuroscience*, *27*(4), 639–654. https://doi.org/10.1162/jocn_a_00746
Gao, R., van den Brink, R. L., Pfeffer, T., & Voytek, B. (2020). Neuronal timescales are functionally dynamic and shaped by cortical microarchitecture. *eLife*, *9*, 1–26. https://doi.org/10.7554/eLife.61277
Genovesio, A., Wise, S. P., & Passingham, R. E. (2014). Prefrontal–parietal function: from foraging to foresight. *Trends in Cognitive Sciences*, *18*(2), 72–81. https://doi.org/10.1016/j.tics.2013.11.007
Glasser, M. F., Coalson, T. S., Robinson, E. C., Hacker, C. D., Harwell, J., Yacoub, E., Ugurbil, K., Andersson, J., Beckmann, C. F., Jenkinson, M., Smith, S. M., & Van Essen, D. C. (2016). A multi-modal parcellation of human cerebral cortex. *Nature*, *536*(7615), 171–178. https://doi.org/10.1038/nature18933
Goffin, C. (2019). How does the brain represent digits? Investigating the neural correlates of symbolic number representation using fMRI—Adaptation [The University of Western Ontario]. Retrieved from https://ir.lib.uwo.ca/etd/6613
Golde, M., von Cramon, D. Y., & Schubotz, R. I. (2010). Differential role of anterior prefrontal and premotor cortex in the processing of relational information. *NeuroImage*, *49*(3), 2890–2900. https://doi.org/10.1016/j.neuroimage.2009.09.009
Golesorkhi, M., Gomez-Pilar, J., Tumati, S., Northoff, G., Fraser, M., & Northoff, G. (2021). Temporal hierarchy of intrinsic neural timescales converges with spatial core-periphery organization. *Communications Biology*, *4*(1), 1–14. https://doi.org/10.1038/s42003-021-01785-z
Golesorkhi, M., Gomez-Pilar, J., Zilio, F., Berberian, N., Wolff, A., Yagoub, M. C. E., & Northoff, G. (2021). The brain and its time: Intrinsic neural timescales are key for input processing. *Communications Biology*, *4*(1), 1–16. https://doi.org/10.1038/s42003-021-02483-6
Gollo, L. L., Zalesky, A., Matthew Hutchison, R., van den Heuvel, M. P., & Breakspear, M. (2015). Dwelling quietly in the rich club: Brain network determinants of slow cortical fluctuations. *Philosophical Transactions of the Royal Society B: Biological Sciences*, *370*(1668), 20140165. https://doi.org/10.1098/rstb.2014.0165
Gómez, C. M., Vaquero, E., & Vázquez-Marrufo, M. (2004). A neurocognitive model for short-term sensory and motor preparatory activity in humans. *Psicológica*, *25*(2), 217–229. https://www.redalyc.org/articulo.oa?id=16925206
Gómez-Gardeñes, J., Zamora-López, G., Moreno, Y., & Arenas, A. (2010). From modular to centralized organization of synchronization in functional areas of the cat cerebral cortex. *PLoS One*, *5*(8), e12313. https://doi.org/10.1371/journal.pone.0012313
Goulas, A., Uylings, H. B. M., & Stiers, P. (2014). Mapping the hierarchical layout of the structural network of the macaque prefrontal cortex. *Cerebral Cortex*, *24*(5), 1178–1194. https://doi.org/10.1093/cercor/bhs399
Grafton, S. T., & Hamilton, A. F. D. C. (2007). Evidence for a distributed hierarchy of action representation in the brain. *Human Movement Science*, *26*(4), 590–616. https://doi.org/10.1016/j.humov.2007.05.009
Graybiel, A. M. (2008). Habits, rituals, and the evaluative brain. *Annual Review of Neuroscience*, *31*, 359–387. https://doi.org/10.1146/annurev.neuro.29.051605.112851
Grayson, D. S., Ray, S., Carpenter, S., Iyer, S., Dias, T. G. C., Stevens, C., Nigg, J. T., & Fair, D. A. (2014). Structural and functional rich club organization of the brain in children and adults. *PLoS One*, *9*(2), 1–13. https://doi.org/10.1371/journal.pone.0088297
Griffa, A., Baumann, P. S., Thiran, J. P., & Hagmann, P. (2013). Structural connectomics in brain diseases. *NeuroImage*, *80*, 515–526. https://doi.org/10.1016/j.neuroimage.2013.04.056
Griffa, A., & van den Heuvel, M. P. (2018). Rich-club neurocircuitry: Function, evolution, and vulnerability. *Dialogues in Clinical Neuroscience*, *20*(2), 121–132. https://doi.org/10.31887/dcns.2018.20.2/agriffa
Guimerà, R., & Nunes Amaral, L. A. (2005). Functional cartography of complex metabolic networks. *Nature*, *433*(7028), 895–900. https://doi.org/10.1038/nature03288
Hagmann, P., Cammoun, L., Gigandet, X., Meuli, R., Honey, C. J., Van Wedeen, J., & Sporns, O. (2008). Mapping the structural core of human cerebral cortex. *PLoS Biology*, *6*(7), 1479–1493. https://doi.org/10.1371/journal.pbio.0060159
Hagmann, P., Sporns, O., Madan, N., Cammoun, L., Pienaar, R., Wedeen, V. J., Meuli, R., Thiran, J. P., & Grant, P. E. (2010). White matter maturation reshapes structural connectivity in the late developing human brain. *Proceedings of the National Academy of Sciences of the United States of America*, *107*(44), 19067–19072. https://doi.org/10.1073/pnas.1009073107
Hamilton, A. F. D. C., & Grafton, S. T. (1993). The motor hierarchy: from kinematics to goals and intentions. In *Sensorimotor foundations of higher cognition* (pp. 381–407). Oxford University Press. https://doi.org/10.1093/acprof:oso/9780199231447.003.0018
Hansen, J. Y., Shafiei, G., Voigt, K., Liang, E. X., Cox, S. M. L., Leyton, M., Jamadar, S. D., & Misic, B. (2022). Multimodal, multiscale connectivity blueprints of the cerebral cortex. BioRxiv, 2022.12.02.518906. Retrieved from https://www.biorxiv.org/content/10.1101/2022.12.02.518906v1.abstract
Harriger, L., van den Heuvel, M. P., & Sporns, O. (2012). Rich club organization of macaque cerebral cortex and its role in network communication. *PLoS One*, *7*(9), e46497. https://doi.org/10.1371/journal.pone.0046497
Harrison, L. M., Duggins, A., & Friston, K. J. (2006). Encoding uncertainty in the hippocampus. *Neural Networks*, *19*(5), 535–546. https://doi.org/10.1016/j.neunet.2005.11.002
Hasson, U., Chen, J., & Honey, C. J. (2015). Hierarchical process memory: Memory as an integral component of information processing. *Trends in Cognitive Sciences*, *19*(6), 304–313. https://doi.org/10.1016/j.tics.2015.04.006
Hasson, U., Malach, R., & Heeger, D. J. (2010). Reliability of cortical activity during natural stimulation. *Trends in Cognitive Sciences*, *14*(1), 40–48. https://doi.org/10.1016/j.tics.2009.10.011
Hasson, U., Yang, E., Vallines, I., Heeger, D. J., & Rubin, N. (2008). A hierarchy of temporal receptive windows in human cortex. *Journal of Neuroscience*, *28*(10), 2539–2550. https://doi.org/10.1523/JNEUROSCI.5487-07.2008
Hermundstad, A. M., Bassett, D. S., Brown, K. S., Aminoff, E. M., Clewett, D., Freeman, S., Frithsen, A., Johnson, A., Tipper, C. M., Miller, M. B., Grafton, S. T., & Carlson, J. M. (2013). Structural foundations of resting-state and task-based functional connectivity in the human brain. *Proceedings of the National Academy of Sciences of*

10970193, 2024, 4, Downloaded from https://onlinelibrary.wiley.com/doi/10.1002/hbm.26543 by Universitäts- und Landesbibliothek Münster, Wiley Online Library on [25/01/2026]. See the Terms and Conditions (https://onlinelibrary.wiley.com/terms-and-conditions) on Wiley Online Library for rules of use; OA articles are governed by the applicable Creative Commons License

the United States of America, *110*(15), 6169–6174. https://doi.org/10.1073/pnas.1219562110

Hilgetag, C. C., Medalla, M., Beul, S. F., & Barbas, H. (2016). The primate connectome in context: Principles of connections of the cortical visual system. *NeuroImage*, *134*, 685–702. https://doi.org/10.1016/j.neuroimage.2016.04.017

Hittner, J. B., May, K., & Silver, N. C. (2003). A Monte Carlo evaluation of tests for comparing dependent correlations. *Journal of General Psychology*, *130*(2), 149–168. https://doi.org/10.1080/00221300309601282

Huang, H., Shu, N., Mishra, V., Jeon, T., Chalak, L., Wang, Z. J., Rollins, N., Gong, G., Cheng, H., Peng, Y., Dong, Q., & He, Y. (2015). Development of human brain structural networks through infancy and childhood. *Cerebral Cortex*, *25*(5), 1389–1404. https://doi.org/10.1093/cercor/bht335

Ingvar, D. H. (1985). "Memory of the future": An essay on the temporal organization of conscious awareness. *Human Neurobiology*, *4*(3), 127–136.

Ito, T., Hearne, L. J., & Cole, M. W. (2020). A cortical hierarchy of localized and distributed processes revealed via dissociation of task activations, connectivity changes, and intrinsic timescales. *NeuroImage*, *221*(July), 117141. https://doi.org/10.1016/j.neuroimage.2020.117141

Jao, C.-W., Yeh, J.-H., Wu, Y.-T., Lien, L.-M., Tsai, Y.-F., Chu, K.-E., Hsiao, C.-Y., Wang, P.-S., & Lau, C. I. (2020). Alteration of the intra- and inter-lobe connectivity of the brain structural network in normal aging. *Entropy*, *22*(8), 826. https://doi.org/10.3390/e22080826

Jarret, J., Boré, A., Bedetti, C., Descoteaux, M., & Brambati, S. M. (2022). A methodological scoping review of the integration of fMRI to guide dMRI tractography. What has been done and what can be improved: A 20-year perspective. *Journal of Neuroscience Methods*, *367*, 109435. https://doi.org/10.1016/j.jneumeth.2021.109435

Jenkinson, M., Beckmann, C. F., Behrens, T. E. J., Woolrich, M. W., & Smith, S. M. (2012). Fsl. *NeuroImage*, *62*, 782–790. https://doi.org/10.1016/j.neuroimage.2011.09.015

Jeon, H. A. (2014). Hierarchical processing in the prefrontal cortex in a variety of cognitive domains. *Frontiers in Systems Neuroscience*, *8*(NOV), 1–8. https://doi.org/10.3389/fnsys.2014.00223

Jones, D. K., Knösche, T. R., & Turner, R. (2013). White matter integrity, fiber count, and other fallacies: The do's and don'ts of diffusion MRI. *NeuroImage*, *73*, 239–254. https://doi.org/10.1016/j.neuroimage.2012.06.081

Kai, J., Khan, A. R., Haast, R. A., & Lau, J. C. (2022). Mapping the subcortical connectome using in vivo diffusion MRI: Feasibility and reliability. *NeuroImage*, *262*(March), 119553. https://doi.org/10.1016/j.neuroimage.2022.119553

Keown, C. L., Datko, M. C., Chen, C. P., Maximo, J. O., Jahedi, A., & Müller, R.-A. (2017). Network organization is globally atypical in autism: A graph theory study of intrinsic functional connectivity. *Biological Psychiatry: Cognitive Neuroscience and Neuroimaging*, *2*(1), 66–75. https://doi.org/10.1016/j.bpsc.2016.07.008

Kiebel, S. J., Daunizeau, J., & Friston, K. J. (2008). A hierarchy of timescales and the brain. *PLoS Computational Biology*, *4*(11), e1000209. https://doi.org/10.1371/journal.pcbi.1000209

Kim, D. J., Davis, E. P., Sandman, C. A., Sporns, O., O'Donnell, B. F., Buss, C., & Hetrick, W. P. (2016). Children's intellectual ability is associated with structural network integrity. *NeuroImage*, *124*, 550–556. https://doi.org/10.1016/j.neuroimage.2015.09.012

Kocher, M., Gleichgerrcht, E., Nesland, T., Rorden, C., Fridriksson, J., Spampinato, M. v., & Bonilha, L. (2015). Individual variability in the anatomical distribution of nodes participating in rich club structural networks. *Frontiers in Neural Circuits*, *9*(APR), 1–7. https://doi.org/10.3389/fncir.2015.00016

Koechlin, E., Basso, G., Pietrini, P., Panzer, S., & Grafman, J. (1999). The role of the anterior prefrontal cortex in human cognition. *Nature*, *399*(6732), 148–151. https://doi.org/10.1038/20178

Koechlin, E., & Summerfield, C. (2007). An information theoretical approach to prefrontal executive function. *Trends in Cognitive Sciences*, *11*(6), 229–235. https://doi.org/10.1016/j.tics.2007.04.005

Kravitz, D. J., Saleem, K. S., Baker, C. I., Ungerleider, L. G., & Mishkin, M. (2013). The ventral visual pathway: An expanded neural framework for the processing of object quality. *Trends in Cognitive Sciences*, *17*(1), 26–49. https://doi.org/10.1016/j.tics.2012.10.011

Kriegeskorte, N., Simmons, W. K., Bellgowan, P. S., & Baker, C. I. (2009). Circular analysis in systems neuroscience: The dangers of double dipping. *Nature Neuroscience*, *12*(5), 535–540. https://doi.org/10.1038/nn.2303

Kühn, A. B., & Schubotz, R. I. (2012). Temporally remote destabilization of prediction after rare breaches of expectancy. *Human Brain Mapping*, *33*(8), 1812–1820. https://doi.org/10.1002/hbm.21325

Landis, J. R., & Koch, G. G. (1977). The measurement of observer agreement for categorical data. *Biometrics*, *33*(1), 159. https://doi.org/10.2307/2529310

Lee, W. J., Han, C. E., Aganj, I., Seo, S. W., & Seong, J. K. (2018). Distinct patterns of rich club organization in Alzheimer's disease and subcortical vascular dementia: A white matter network study. *Journal of Alzheimer's Disease*, *63*(3), 977–987. https://doi.org/10.3233/JAD-180027

Lerner, Y., Honey, C. J., Silbert, L. J., & Hasson, U. (2011). Topographic mapping of a hierarchy of temporal receptive windows using a narrated story. *Journal of Neuroscience*, *31*(8), 2906–2915. https://doi.org/10.1523/JNEUROSCI.3684-10.2011

Liu, Y., Yang, K., Hu, X., Xiao, C., Rao, J., Li, Z., Liu, D., Zou, Y., Chen, J., & Liu, H. (2020). Altered rich-club organization and regional topology are associated with cognitive decline in patients with frontal and temporal gliomas. *Frontiers in Human Neuroscience*, *14*(February), 1–13. https://doi.org/10.3389/fnhum.2020.00023

Lurie, D. J., Pappas, I., Esposito, M. D., Lurie, D. J., & D'Esposito, M. (2023). Cortical timescales and the modular organization of structural and functional brain networks. BioRxiv. https://doi.org/10.1101/2023.07.12.548751

Ma, J., Kang, H. J., Kim, J. Y., Jeong, H. S., Im, J. J., Namgung, E., Kim, M. J., Lee, S., Kim, T. D., Oh, J. K., Chung, Y. A., Lyoo, I. K., Lim, S. M., & Yoon, S. (2017). Network attributes underlying intellectual giftedness in the developing brain. *Scientific Reports*, *7*(1), 1–9. https://doi.org/10.1038/s41598-017-11593-3

Mahjoory, K., Schoffelen, J. M., Keitel, A., & Gross, J. (2020). The frequency gradient of human resting-state brain oscillations follows cortical hierarchies. *eLife*, *9*, 1–18. https://doi.org/10.7554/ELIFE.53715

Maldjian, J. A., Laurienti, P. J., Kraft, R. A., & Burdette, J. H. (2003). An automated method for neuroanatomic and cytoarchitectonic atlas-based interrogation of fMRI data sets. *NeuroImage*, *19*(3), 1233–1239. https://doi.org/10.1016/S1053-8119(03)00169-1

Miller, E. K., & Cohen, J. D. (2001). An integrative theory of prefrontal cortex function. *Annual Review of Neuroscience*, *24*(1), 167–202. https://doi.org/10.1146/annurev.neuro.24.1.167

Miller, G. A. (1956). The magical number seven, plus or minus two: Some limits on our capacity for processing information. *Psychological Review*, *63*(2), 81–97. https://doi.org/10.1037/h0043158

Mohor, G. S., Thieken, A. H., & Korup, O. (2021). Residential flood loss estimated from Bayesian multilevel models. *Natural Hazards and Earth System Sciences*, *21*(5), 1599–1614. https://doi.org/10.5194/nhess-21-1599-2021

Molko, N., Cachia, A., Rivière, D., Mangin, J. F., Bruandet, M., Le Bihan, D., Cohen, L., & Dehaene, S. (2003). Functional and structural alterations of the intraparietal sulcus in a developmental dyscalculia of genetic origin. *Neuron*, *40*(4), 847–858. https://doi.org/10.1016/S0896-6273(03)00670-6

Mori, S., Crain, B. J., Chacko, V. P., & van Zilj, P. C. M. (1999). Three-dimensional tracking of axonal projections in the brain by magnetic resonance imaging. *Annals of Neurology*, *45*(2), 265–269. https://doi.org/10.1002/1531-8249(199902)45:2<247::AID-ANA16>3.0.CO;2-U

Nattkemper, D., & Prinz, W. (1997). Stimulus and response anticipation in a serial reaction task. *Psychological Research*, *60*(1–2), 98–112. https://doi.org/10.1007/BF00419683

10970193, 2024, 4, Downloaded from https://onlinelibrary.wiley.com/doi/10.1002/hbm.26543 by Universitäts- und Landesbibliothek Münster, Wiley Online Library on [25/01/2026]. See the Terms and Conditions (https://onlinelibrary.wiley.com/terms-and-conditions) on Wiley Online Library for rules of use; OA articles are governed by the applicable Creative Commons License

Naya, Y., Yoshida, M., & Miyashita, Y. (2003). Forward processing of long-term associative memory in monkey inferotemporal cortex. *Journal of Neuroscience*, *23*(7), 2861–2871. https://doi.org/10.1523/jneurosci.23-07-02861.2003

Nee, D. E., & D'Esposito, M. (2016). The hierarchical organization of the lateral prefrontal cortex. *eLife*, *5*(MARCH2016), 1–26. https://doi.org/10.7554/eLife.12112

Nieder, A. (2016). Representing Something Out of Nothing: The Dawning of Zero. *Trends in Cognitive Sciences*, *20*(11), 830–842. https://doi.org/10.1016/j.tics.2016.08.008

Noonan, K. A., Jefferies, E., Visser, M., & Lambon Ralph, M. A. (2013). Going beyond inferior prefrontal involvement in semantic control: Evidence for the additional contribution of dorsal angular gyrus and posterior middle temporal cortex. *Journal of Cognitive Neuroscience*, *25*(11), 1824–1850. https://doi.org/10.1162/jocn_a_00442

O'Donoghue, S., Kilmartin, L., O'Hora, D., Emsell, L., Langan, C., McInerney, S., Forde, N. J., Leemans, A., Jeurissen, B., Barker, G. J., McCarthy, P., Cannon, D. M., & McDonald, C. (2017). Anatomical integration and rich-club connectivity in euthymic bipolar disorder. *Psychological Medicine*, *47*(9), 1609–1623. https://doi.org/10.1017/S0033291717000058

Oldfield, R. C. (1971). The assessment and analysis of handedness: The Edinburgh inventory. *Neuropsychologial*, *9*(9), 97–113. https://doi.org/10.1007/978-3-319-55065-7_301010

Patriat, R., Molloy, E. K., Meier, T. B., Kirk, G. R., Nair, V. A., Meyerand, M. E., Prabhakaran, V., & Birn, R. M. (2013). The effect of resting condition on resting-state fMRI reliability and consistency: A comparison between resting with eyes open, closed, and fixated. *NeuroImage*, *78*, 463–473. https://doi.org/10.1016/j.neuroimage.2013.04.013

Pedersen, M., Omidvarnia, A., Shine, J. M., Jackson, G. D., & Zalesky, A. (2020). Reducing the influence of intramodular connectivity in participation coefficient. *Network Neuroscience*, *4*(2), 416–431. https://doi.org/10.1162/netn_a_00127

Piazza, M., Izard, V., Pinel, P., Le Bihan, D., & Dehaene, S. (2004). Tuning curves for approximate numerosity in the human intraparietal sulcus. *Neuron*, *44*(3), 547–555. https://doi.org/10.1016/j.neuron.2004.10.014

Piazza, M., Pinel, P., Le Bihan, D., & Dehaene, S. (2007). A magnitude code common to numerosities and number symbols in human intraparietal cortex. *Neuron*, *53*(2), 293–305. https://doi.org/10.1016/j.neuron.2006.11.022

Pinhas, M., & Tzelgov, J. (2012). Expanding on the mental number line: zero is perceived as the "smallest". *Journal of Experimental Psychology: Learning, Memory, and Cognition*, *38*(5), 1187–1205. https://doi.org/10.1037/a0027390

Ponsoda, V., Martínez, K., Pineda-Pardo, J. A., Abad, F. J., Olea, J., Román, F. J., Barbey, A. K., & Colom, R. (2017). Structural brain connectivity and cognitive ability differences: A multivariate distance matrix regression analysis. *Human Brain Mapping*, *38*(2), 803–816. https://doi.org/10.1002/hbm.23419

Prčkovska, V., Rodrigues, P., Puigdellivol Sanchez, A., Ramos, M., Andorra, M., Martinez-Heras, E., Falcon, C., Prats-Galino, A., & Villoslada, P. (2016). Reproducibility of the structural connectome reconstruction across diffusion methods. *Journal of Neuroimaging*, *26*(1), 46–57. https://doi.org/10.1111/jon.12298

Qi, S., Meesters, S., Nicolay, K., ter Haar Romeny, B. M., & Ossenblok, P. (2015). The influence of construction methodology on structural brain network measures: A review. *Journal of Neuroscience Methods*, *253*(500), 170–182. https://doi.org/10.1016/j.jneumeth.2015.06.016

R Core Team. (2022). *R: A language and environment for statistical computing*. R Core Team Retrieved from https://www.r-project.org/

Ramnani, N., & Owen, A. M. (2004). Anterior prefrontal cortex: Insights into function from anatomy and neuroimaging. *Nature Reviews Neuroscience*, *5*(3), 184–194. https://doi.org/10.1038/nrn1343

Raut, R. V., Snyder, A. Z., & Raichle, M. E. (2020). Hierarchical dynamics as a macroscopic organizing principle of the human brain. *Proceedings of the National Academy of Sciences of the United States of America*, *117*(34), 20890–20897. https://doi.org/10.1073/pnas.2003383117

Ray, S., Miller, M., Karalunas, S., Robertson, C., Grayson, D. S., Cary, R. P., Hawkey, E., Painter, J. G., Kriz, D., Fombonne, E., Nigg, J. T., & Fair, D. A. (2014). Structural and functional connectivity of the human brain in autism spectrum disorders and attention-deficit/hyperactivity disorder: A rich club-organization study. *Human Brain Mapping*, *35*(12), 6032–6048. https://doi.org/10.1002/hbm.22603

Reavis, E. A., Lee, J., Altshuler, L. L., Cohen, M. S., Engel, S. A., Glahn, D. C., Jimenez, A. M., Narr, K. L., Nuechterlein, K. H., Riedel, P., Wynn, J. K., & Green, M. F. (2020). Structural and functional connectivity of visual cortex in schizophrenia and bipolar disorder: A graph-theoretic analysis. *Schizophrenia Bulletin Open*, *1*(1), 1–11. https://doi.org/10.1093/schizbullopen/sgaa056

Repple, J., Mauritz, M., Meinert, S., de Lange, S. C., Grotegerd, D., Opel, N., Redlich, R., Hahn, T., Förster, K., Leehr, E. J., Winter, N., Goltermann, J., Enneking, V., Fingas, S. M., Lemke, H., Waltemate, L., Nenadic, I., Krug, A., Brosch, K., … van den Heuvel, M. P. (2020). Severity of current depression and remission status are associated with structural connectome alterations in major depressive disorder. *Molecular Psychiatry*, *25*(7), 1550–1558. https://doi.org/10.1038/s41380-019-0603-1

Reynolds, J. R., O'Reilly, R. C., Cohen, J. D., & Braver, T. S. (2012). The function and organization of lateral prefrontal cortex: A test of competing hypotheses. *PLoS One*, *7*(2), e30284. https://doi.org/10.1371/journal.pone.0030284

Rhodes, S., Cowan, N., Parra, M. A., & Logie, R. H. (2019). Interaction effects on common measures of sensitivity: Choice of measure, type I error, and power. *Behavior Research Methods*, *51*(5), 2209–2227. https://doi.org/10.3758/s13428-018-1081-0

Riedel, L., van den Heuvel, M. P., & Markett, S. (2022). Trajectory of rich club properties in structural brain networks. *Human Brain Mapping*, *43*(14), 4239–4253. https://doi.org/10.1002/hbm.25950

RStudio Team. (2022). *RStudio: Integrated development environment for R*. RStudio Team Retrieved from http://www.rstudio.com/

Rubinov, M., & Sporns, O. (2010). Complex network measures of brain connectivity: Uses and interpretations. *NeuroImage*, *52*(3), 1059–1069. https://doi.org/10.1016/j.neuroimage.2009.10.003

Sanides, F. (1964). Structure and function of the human frontal lobe. *Neuropsychologia*, *2*(3), 209–219. https://doi.org/10.1016/0028-3932(64)90005-3

Schaefer, A., Kong, R., Gordon, E. M., Laumann, T. O., Zuo, X.-N., Holmes, A. J., Eickhoff, S. B., & Yeo, B. T. T. (2018). Local-global parcellation of the human cerebral cortex from intrinsic functional connectivity MRI. *Cerebral Cortex*, *28*(9), 3095–3114. https://doi.org/10.1093/cercor/bhx179

Seguin, C., Tian, Y., & Zalesky, A. (2020). Network communication models improve the behavioral and functional predictive utility of the human structural connectome. *Network Neuroscience*, *4*(4), 980–1006. https://doi.org/10.1162/netn_a_00161

Senden, M., Reuter, N., van den Heuvel, M. P., Goebel, R., & Deco, G. (2017). Cortical rich club regions can organize state-dependent functional network formation by engaging in oscillatory behavior. *NeuroImage*, *146*, 561–574. https://doi.org/10.1016/j.neuroimage.2016.10.044

Sethi, S. S., Zerbi, V., Wenderoth, N., Fornito, A., & Fulcher, B. D. (2017). Structural connectome topology relates to regional BOLD signal dynamics in the mouse brain. *Chaos*, *27*(4), 047405. https://doi.org/10.1063/1.4979281

Shafiei, G., Markello, R. D., De Wael, R. V., Bernhardt, B. C., Fulcher, B. D., & Misic, B. (2020). Topographic gradients of intrinsic dynamics across neocortex. *eLife*, *9*, 1–24. https://doi.org/10.7554/eLife.62116

10970193, 2024, 4, Downloaded from https://onlinelibrary.wiley.com/doi/10.1002/hbm.26543 by Universitäts- und Landesbibliothek Münster, Wiley Online Library on [25/01/2026]. See the Terms and Conditions (https://onlinelibrary.wiley.com/terms-and-conditions) on Wiley Online Library for rules of use; OA articles are governed by the applicable Creative Commons License

Shannon, C. E. (1948). A mathematical theory of communication. *Bell System Technical Journal*, *27*(3), 379–423. https://doi.org/10.1002/j.1538-7305.1948.tb01338.x

Shen, X., Tokoglu, F., Papademetris, X., & Constable, R. T. (2013). Groupwise whole-brain parcellation from resting-state fMRI data for network node identification. *NeuroImage*, *82*, 403–415. https://doi.org/10.1016/j.neuroimage.2013.05.081

Slotnick, S. D. (2017). Cluster success: fMRI inferences for spatial extent have acceptable false-positive rates. *Cognitive Neuroscience*, *8*(3), 150–155. https://doi.org/10.1080/17588928.2017.1319350

Slotnick, S. D., Moo, L. R., Segal, J. B., & Hart, J. (2003). Distinct prefrontal cortex activity associated with item memory and source memory for visual shapes. *Cognitive Brain Research*, *17*(1), 75–82. https://doi.org/10.1016/S0926-6410(03)00082-X

Smith, S. M., Jenkinson, M., Woolrich, M. W., Beckmann, C. F., Behrens, T. E. J., Johansen-Berg, H., Bannister, P. R., de Luca, M., Drobnjak, I., Flitney, D. E., Niazy, R. K., Saunders, J., Vickers, J., Zhang, Y., de Stefano, N., Brady, J. M., & Matthews, P. M. (2004). Advances in functional and structural MR image analysis and implementation as FSL. *NeuroImage*, *23*(SUPPL. 1), 208–219. https://doi.org/10.1016/j.neuroimage.2004.07.051

Sokolowski, H. M., Fias, W., Mousa, A., & Ansari, D. (2017). Common and distinct brain regions in both parietal and frontal cortex support symbolic and nonsymbolic number processing in humans: A functional neuroimaging meta-analysis. *NeuroImage*, *146*, 376–394. https://doi.org/10.1016/j.neuroimage.2016.10.028

Solé-Casals, J., Serra-Grabulosa, J. M., Romero-Garcia, R., Vilaseca, G., Adan, A., Vilaró, N., Bargalló, N., & Bullmore, E. T. (2019). Structural brain network of gifted children has a more integrated and versatile topology. *Brain Structure and Function*, *224*(7), 2373–2383. https://doi.org/10.1007/s00429-019-01914-9

Sporns, O. (2011). The human connectome: A complex network. *Annals of the New York Academy of Sciences*, *1224*(1), 109–125. https://doi.org/10.1111/j.1749-6632.2010.05888.x

Sporns, O. (2013). Structure and function of complex brain networks. *Dialogues in Clinical Neuroscience*, *15*(3), 247–262. https://doi.org/10.31887/dcns.2013.15.3/osporns

Suárez, L. E., Markello, R. D., Betzel, R. F., & Misic, B. (2020). Linking structure and function in macroscale brain networks. *Trends in Cognitive Sciences*, *24*(4), 302–315. https://doi.org/10.1016/j.tics.2020.01.008

The MathWorks Inc. (2019). *MATLAB version: 9.6.0 (R2019a)*. The MathWorks Inc Retrieved from https://www.mathworks.com

The MathWorks Inc. (2021). *MATLAB version: 9.10.0 (R2021a)*. The MathWorks Inc Retrieved from https://www.mathworks.com

Tourbier, S., Aleman-Gomez, Y., Griffa, A., Bach Cuadra, M., & Hagmann, P. (2019). sebastientourbier/multiscalebrainparcellator: Multi-scale brain parcellator v1.1.1. https://doi.org/10.5281/ZENODO.3627097

Uithol, S., van Rooij, I., Bekkering, H., & Haselager, P. (2012). Hierarchies in action and motor control. *Journal of Cognitive Neuroscience*, *24*(5), 1077–1086. https://doi.org/10.1162/jocn_a_00204

van den Heuvel, M. P., Kahn, R. S., Goñi, J., & Sporns, O. (2012). High-cost, high-capacity backbone for global brain communication. *Proceedings of the National Academy of Sciences of the United States of America*, *109*(28), 11372–11377. https://doi.org/10.1073/pnas.1203593109

van den Heuvel, M. P., Scholtens, L. H., van der Burgh, H. K., Agosta, F., Alloza, C., Arango, C., Auyeung, B., Baron-Cohen, S., Basaia, S., Benders, M. J. N. L., Beyer, F., Booij, L., Braun, K. P. J., Filho, G. B., Cahn, W., Cannon, D. M., Chaim-Avancini, T. M., Chan, S. S. M., Chen, E. Y. H., … de Lange, S. C. (2019). 10kin1day: A bottom-up neuroimaging initiative. *Frontiers in Neurology*, *10*(MAY), 1–7. https://doi.org/10.3389/fneur.2019.00425

van den Heuvel, M. P., & Sporns, O. (2011). Rich-club organization of the human connectome. *Journal of Neuroscience*, *31*(44), 15775–15786. https://doi.org/10.1523/JNEUROSCI.3539-11.2011

van den Heuvel, M. P., & Sporns, O. (2013). Network hubs in the human brain. *Trends in Cognitive Sciences*, *17*(12), 683–696. https://doi.org/10.1016/j.tics.2013.09.012

van den Heuvel, M. P., Sporns, O., Collin, G., Scheewe, T., Mandl, R. C. W., Cahn, W., Goni, J., Pol, H. E. H., & Kahn, R. S. (2013). Abnormal rich club organization and functional brain dynamics in schizophrenia. *JAMA Psychiatry*, *70*(8), 783–792. https://doi.org/10.1001/jamapsychiatry.2013.1328

van Dijk, K. R. A., Hedden, T., Venkataraman, A., Evans, K. C., Lazar, S. W., & Buckner, R. L. (2010). Intrinsic functional connectivity as a tool for human connectomics: Theory, properties, and optimization. *Journal of Neurophysiology*, *103*(1), 297–321. https://doi.org/10.1152/jn.00783.2009

van Doorn, J., van den Bergh, D., Böhm, U., Dablander, F., Derks, K., Draws, T., Etz, A., Evans, N. J., Gronau, Q. F., Haaf, J. M., Hinne, M., Kucharský, Š., Ly, A., Marsman, M., Matzke, D., Gupta, A. R. K. N., Sarafoglou, A., Stefan, A., Voelkel, J. G., & Wagenmakers, E. J. (2021). The JASP guidelines for conducting and reporting a Bayesian analysis. *Psychonomic Bulletin and Review*, *28*(3), 813–826. https://doi.org/10.3758/s13423-020-01798-5

Van Essen, D. C., Smith, S. M., Barch, D. M., Behrens, T. E. J., Yacoub, E., & Ugurbil, K. (2013). The WU-Minn human connectome project: An overview. *NeuroImage*, *80*, 62–79. https://doi.org/10.1016/j.neuroimage.2013.05.041

Vogelbacher, C., Möbius, T. W. D., Sommer, J., Schuster, V., Dannlowski, U., Kircher, T., Dempfle, A., Jansen, A., & Bopp, M. H. A. (2018). The Marburg-Münster affective disorders cohort study (MACS): A quality assurance protocol for MR neuroimaging data. *NeuroImage*, *172*(December 2017), 450–460. https://doi.org/10.1016/j.neuroimage.2018.01.079

Wakita, M. (2014). Broca's area processes the hierarchical organization of observed action. *Frontiers in Human Neuroscience*, *7*(JAN), 1–7. https://doi.org/10.3389/fnhum.2013.00937

Wang, B., Zhan, Q., Yan, T., Imtiaz, S., Xiang, J., Niu, Y., Liu, M., Wang, G., Cao, R., & Li, D. (2019). Hemisphere and gender differences in the rich-club organization of structural networks. *Cerebral Cortex*, *29*(11), 4889–4901. https://doi.org/10.1093/cercor/bhz027

Wang, Y., Deng, F., Jia, Y., Wang, J., Zhong, S., Huang, H., Chen, L., Chen, G., Hu, H., Huang, L., & Huang, R. (2019). Disrupted rich club organization and structural brain connectome in unmedicated bipolar disorder. *Psychological Medicine*, *49*(3), 510–518. https://doi.org/10.1017/S0033291718001150

Watanabe, T. (2013). Rich-club network topology to minimize synchronization cost due to phase difference among frequency-synchronized oscillators. *Physica A: Statistical Mechanics and its Applications*, *392*(5), 1246–1255. https://doi.org/10.1016/j.physa.2012.11.041

Welton, T., Kent, D. A., Auer, D. P., & Dineen, R. A. (2015). Reproducibility of graph-theoretic brain network metrics: A systematic review. *Brain Connectivity*, *5*(4), 193–202. https://doi.org/10.1089/brain.2014.0313

Williams, G., Palminteri, S., & Haggard, P. (2022, February 1). Assembling hierarchies of action using sequencing and abstraction: Studies and models of zero-shot learning assembling hierarchies of action using sequencing and abstraction: Studies and models of zero-shot learning. https://doi.org/10.31234/osf.io/gzjur

Wolff, A., Berberian, N., Golesorkhi, M., Gomez-Pilar, J., Zilio, F., & Northoff, G. (2022). Intrinsic neural timescales: Temporal integration and segregation. *Trends in Cognitive Sciences*, *26*(2), 159–173. https://doi.org/10.1016/j.tics.2021.11.007

Wong, B., & Szücs, D. (2013). Single-digit Arabic numbers do not automatically activate magnitude representations in adults or in children: Evidence from the symbolic same-different task. *Acta Psychologica*, *144*(3), 488–498. https://doi.org/10.1016/j.actpsy.2013.08.006

10970193, 2024, 4, Downloaded from https://onlinelibrary.wiley.com/doi/10.1002/hbm.26543 by Universitäts- und Landesbibliothek Münster, Wiley Online Library on [25/01/2026]. See the Terms and Conditions (https://onlinelibrary.wiley.com/terms-and-conditions) on Wiley Online Library for rules of use; OA articles are governed by the applicable Creative Commons License

Wu, K., Taki, Y., Sato, K., Sassa, Y., Inoue, K., Goto, R., Okada, K., Kawashima, R., He, Y., Evans, A. C., & Fukuda, H. (2011). The overlapping community structure of structural brain network in young healthy individuals. *PLoS One*, *6*(5), 1–14. https://doi.org/10.1371/journal.pone.0019608

Yan, T., Wang, W., Yang, L., Chen, K., Chen, R., & Han, Y. (2018). Rich club disturbances of the human connectome from subjective cognitive decline to Alzheimer's disease. *Theranostics*, *8*(12), 3237–3255. https://doi.org/10.7150/thno.23772

Yedetore, A., Linzen, T., Frank, R., & McCoy, R. T. (2023). How poor is the stimulus? Evaluating hierarchical generalization in neural networks trained on child-directed speech. Retrieved from http://arxiv.org/abs/2301.11462

Yeh, C.-H., Smith, R. E., Liang, X., Calamante, F., & Connelly, A. (2018). Investigating the streamline count required for reproducible structural connectome construction across a range of brain parcellation resolutions. *Proceedings of ISMRM*, *1558*, 1–4. http://cds.ismrm.org/protected/18MPresentations/abstracts/1558.html

Yeh, F. C., Wedeen, V. J., & Tseng, W. Y. I. (2010). Generalized q-sampling imaging. *IEEE Transactions on Medical Imaging*, *29*(9), 1626–1635. https://doi.org/10.1109/TMI.2010.2045126

Zamora-López, G., Zhou, C., & Kurths, J. (2010). Cortical hubs form a module for multisensory integration on top of the hierarchy of cortical networks. *Frontiers in Neuroinformatics*, *4*(MAR), 1–13. https://doi.org/10.3389/neuro.11.001.2010

SUPPORTING INFORMATION

Additional supporting information can be found online in the Supporting Information section at the end of this article.

How to cite this article: Mecklenbrauck, F., Gruber, M., Siestrup, S., Zahedi, A., Grotegerd, D., Mauritz, M., Trempler, I., Dannlowski, U., & Schubotz, R. I. (2024). The significance of structural rich club hubs for the processing of hierarchical stimuli. *Human Brain Mapping*, *45*(4), e26543. https://doi.org/10.1002/hbm.26543

10970193, 2024, 4, Downloaded from https://onlinelibrary.wiley.com/doi/10.1002/hbm.26543 by Universitäts- und Landesbibliothek Münster, Wiley Online Library on [25/01/2026]. See the Terms and Conditions (https://onlinelibrary.wiley.com/terms-and-conditions) on Wiley Online Library for rules of use; OA articles are governed by the applicable Creative Commons License

2.2 Study 2: Decoding cortical chronotopy – Comparing the influence of different cortical organizational schemes

Running title: 2.2 Decoding cortical chronotopy

Falko Mecklenbrauck, Jorge Sepulcre, Jana Fehring, & Ricarda I. Schubotz (2024)

NeuroImage, *303*, Article 120914

https://doi.org/10.1016/j.neuroimage.2024.120914

Associated online data:

Code repository: https://github.com/FalkMeck/Decoding_Cortical_Chronotopy.git

Minimally processed subject data: https://osf.io/ubfyt/overview?view_only=edb44902e884424c9b3e4cb86648ad3e

NeuroImage 303 (2024) 120914

Contents lists available at ScienceDirect

NeuroImage

journal homepage: www.elsevier.com/locate/ynimg

Decoding cortical chronotopy—Comparing the influence of different cortical organizational schemes

Falko Mecklenbrauck [a,b,*], Jorge Sepulcre [c], Jana Fehring [b,d], Ricarda I. Schubotz [a,b]

[a] Department of Psychology, Biological Psychology, University of Münster, Germany
[b] Otto Creutzfeldt Center for Cognitive and Behavioral Neuroscience, University of Münster, Germany
[c] Department of Radiology and Biomedical Imaging, Yale PET Center, Yale School of Medicine, Yale University, New Haven, CT, USA
[d] Institute for Biomagnetism and Biosignal Analysis, Münster, Germany

ARTICLE INFO

Keywords:
Bayesian model comparison
Cortical timescales
DWI
fMRI
Nested hierarchies
Inter-subject correlation
Cortical hierarchies

ABSTRACT

The brain's diverse intrinsic timescales enable us to perceive stimuli with varying temporal persistency. This study aimed to uncover the cortical organizational schemes underlying these variations, revealing the neural architecture for processing a wide range of sensory experiences. We collected resting-state fMRI, task-fMRI, and diffusion-weighted imaging data from 47 individuals. Based on this data, we extracted six organizational schemes: (1) the structural Rich Club (RC) architecture, shown to synchronize the connectome; (2) the structural Diverse Club architecture, as an alternative to the RC based on the network's module structure; (3) the functional uni-to-multimodal gradient, reflected in a wide range of structural and functional features; and (4) the spatial posterior/lateral-to-anterior/medial gradient, established for hierarchical levels of cognitive control. Also, we explored the effects of (5) structural graph theoretical measures of centrality and (6) cytoarchitectural differences. Using Bayesian model comparison, we contrasted the impact of these organizational schemes on (1) intrinsic resting-state timescales and (2) inter-subject correlation (ISC) from a task involving hierarchically nested digit sequences. As expected, resting-state timescales were slower in structural network hubs, hierarchically higher areas defined by the functional and spatial gradients, and thicker cortical regions. ISC analysis demonstrated hints for the engagement of higher cortical areas with more temporally persistent stimuli. Finally, the model comparison identified the uni-to-multimodal gradient as the best organizational scheme for explaining the chronotopy in both task and rest. Future research should explore the microarchitectural features that shape this gradient, elucidating how our brain adapts and evolves across different modes of processing.

1. Introduction

The discovery that different brain regions vary in terms of their processing rhythms or *intrinsic timescales* (Murray et al., 2014; Ogawa and Komatsu, 2010; Raut et al., 2020) sparked the investigation of the possible function of these timescales (for reviews see Cavanagh et al., 2020; Soltani et al., 2021). One exciting idea is that cortical processes are organized according to a hierarchy of timescales (Chen et al., 2015; Hasson et al., 2015; Jeon, 2014; Manea et al., 2022). The different intrinsic timescales make our brain perfectly adapted for the processing and representation of the different external nested rhythms in nature (Golesorkhi et al., 2021b; Wolff et al., 2022). Thus, different areas of the brain can segregate and integrate incoming stimuli depending on their own intrinsic timescale and the temporal structure of the stimulus (Baldassano et al., 2017; Cavanagh et al., 2020; Golesorkhi et al., 2021b).

Using hierarchically nested stimuli, previous studies were able to distinguish cortical areas according to their specific response to hierarchical levels of temporally persistency of the stimulus (Aberbach-Goodman and Mukamel, 2023; Farbood et al., 2015; Hasson et al., 2008; Lerner et al., 2011). For each region, a so-called *temporal receptive window* (TRW) was determined (Hasson et al., 2008). Analogical to spatial receptive windows, TRWs describe the specific time frame of an area in which information of the ongoing stimulus is integrated (Hasson et al., 2015). Appropriately, areas with longer TRWs were also found to have slower intrinsic timescales (Chaudhuri et al., 2015; Gao

* Corresponding author at: University of Münster, Institute of Psychology, Fliednerstr. 21, D-48149 Münster, Germany.
E-mail addresses: f_meck01@uni-muenster.de (F. Mecklenbrauck), jorge.sepulcre@yale.edu (J. Sepulcre), fehringj@uni-muenster.de (J. Fehring), rschubotz@uni-muenster.de (R.I. Schubotz).

https://doi.org/10.1016/j.neuroimage.2024.120914
Received 15 July 2024; Received in revised form 22 October 2024; Accepted 1 November 2024
Available online 2 November 2024
1053-8119/© 2024 The Authors. Published by Elsevier Inc. This is an open access article under the CC BY license (http://creativecommons.org/licenses/by/4.0/).

et al., 2020; Honey et al., 2012; Moraczewski et al., 2020; Stephens et al., 2013).

The origin of different intrinsic cortical timescales and TRWs however has yet to be determined. The current paper aims to explore and evaluate multiple alternative cortical foundations of this *chronotopy*. To this end, we compared the congruity of different, established cortical organizational schemes with the chronotopy of the cortex at rest and during a task.

For the chronotopy at rest, we collected resting-state functional magnetic resonance imaging (rs-fMRI) and applied a model-free approach (Raut et al., 2020) to calculate the autocorrelation decay of each area, which is a valid and direct measure to estimate the intrinsic cortical timescales (Zilio et al., 2021). The variance of timescales contains meaningful information to distinguish between different cortical areas (Murray et al., 2014; Ogawa and Komatsu, 2010).

To investigate the chronotopy in a task-setting, we used hierarchically nested stimuli to ascertain the distribution of TRWs across the cortex. Based on previous TRW studies (Farbood et al., 2015; Hasson et al., 2008; Lerner et al., 2011), we designed digit sequences of four different, nested levels of temporal persistency. We used inter-subject correlation (ISC; Hasson et al., 2004, 2010) to determine the reliability of the cortical signal for the four hierarchically structured levels of the stimulus and thus identified areas that integrate information over shorter or longer periods of time.

Regarding potential cortical foundations of the chronotopy, we considered in total six commonly reported organizational schemes and features:

(1) The structural Rich Club (RC) is a set of highly interconnected network nodes (Colizza et al., 2006), topologically organized in resonant network motifs that are particularly efficient in synchronizing neighbouring nodes via their slow intrinsic timescales (Aguilar-Velázquez and Guzmán-Vargas, 2019; Gollo et al., 2015; Gómez-Gardeñes et al., 2010; Senden et al., 2017; Watanabe, 2013). This finding was recently supported by studies showing that the intrinsic cortical timescales correlate with the connectivity of a node (Fallon et al., 2020; Lurie et al., 2024; Sethi et al., 2017). Due to its particular architecture of connections, the RC organization was previously proclaimed as the prime candidate to shape the brain's diverse temporal dynamics (Gollo et al., 2015; Zamora-López et al., 2016).
(2) The structural Diverse Club (DC) was discussed as a competing topological concept to the RC and possibly might be even more meaningful for the communication of the network (Bertolero et al., 2017). Instead of the nodal degree the DC is based on the structural participation coefficient which describes the membership of a node to multiple network modules (Guimerà and Nunes Amaral, 2005) and recently was found to relate to the cortical timescales as well (Lurie et al., 2024).
(3) Prior studies on the temporal organization of the brain made a distinction between unimodal and multimodal cortices, finding timescales to be faster in unimodal as compared to multimodal cortical areas (Golesorkhi et al., 2021a; Ito et al., 2020; Shafiei et al., 2020; Wolff et al., 2022). This gradient of cortical hierarchy was also reflected in functional connectivity (Margulies et al., 2016), electrophysiological responses (Gao et al., 2020; Honey et al., 2012), cortical thickness (Burt et al., 2018; Wagstyl et al., 2015), neural development (Sydnor et al., 2021, 2023), and brain evolution (Xu et al., 2020). Also, the topological distribution of TRWs follows a progression from sensory to higher order areas, with the longest TRWs in frontal and parietal association cortices (Hasson et al., 2015; Jääskeläinen et al., 2021). We defined this gradient in two different ways: data-driven, based on the stepwise functional connectivity (Sepulcre et al., 2012) and atlas-based using the previously introduced functional differentiation (Ito et al., 2020) in the atlas by Ji et al. (2019).
(4) Cortical frequencies were furthermore found to progress along a posterior-to-anterior gradient, with the slowest frequencies being detected towards the frontal cortex (Mahjoory et al., 2020). This gradient is part of many classical theories of cognitive control (Fuster, 2001; Kiebel et al., 2008; Koechlin and Summerfield, 2007). Moreover, it was reflected in the expression of genes (Hansen et al., 2021; Hawrylycz et al., 2012) as well as the covariance of cortical thickness (Valk et al., 2020) and correlated with the degree of myelinisation, the brain's metabolism and certain frequencies of the electrophysiological power spectrum (Markello et al., 2022). Lately, the posterior-to-anterior trend was extended by a lateral-to-medial aspect (Alexander and Brown, 2018) forming a posterior/lateral-to-anterior/medial gradient that is also mirrored in the intrinsic cortical dynamics (Mahjoory et al., 2020).
(5) Additionally, we explored how of measures of structural network centrality relate to the cortical chronotopy. These graph theoretical measures classify nodes that are important for an intact communication throughout the network (Hagmann et al., 2008) and were recently found to relate the cortical timescales as well (Fallon et al., 2020; Lurie et al., 2024; Sethi et al., 2017).
(6) Lastly, studies have suggested that an interaction between microstructural and macro-level connectivity patterns affect the temporal layout of the cortex (Huntenburg et al., 2018). More specifically, cytoarchitectonic differences between areas may shape intrinsic timescales at the microscale (Gao et al., 2020), reflecting a relationship between myelinisation and timescales (Ito et al., 2020). Consequently, we also considered cortical thickness, which can approximate microstructural differences (Wagstyl et al., 2015).

We modelled the distribution of intrinsic timescales as well as ISC values across these different, commonly found organizational schemes and comprehensively contrasted their significance using Bayesian model comparison (Vehtari et al., 2017). It has to be noted, that the aforementioned organizational schemes and features of the cortex are not independent of each other (Burt et al., 2018; van den Heuvel et al., 2015; van den Heuvel and Sporns, 2013b). By directly comparing the organizational schemes, this paper seeks to find the model that best explains the emergence of different intrinsic timescales and TRWs across the brain and thus resembles the true cortical organization the closest.

2. Materials & methods

The following method section is divided into five segments: firstly, general information on the data acquisition and first processing steps; secondly, a section on the resting-state data, including preprocessing and the estimation of the intrinsic timescales using autocorrelation decay; thirdly, an explanation of the preprocessing of the task data and calculation of the ISC values; fourthly, we describe the identification of the six organizational schemes of interest, whose influence on the cortical chronotropy we compared; and lastly, we outline all conducted statistical analyses and tests.

2.1. General methods

2.1.1. Participants

Data of 47 participants was collected for this study. One participant was excluded due to movement during the rs-fMRI measurement that exceeded 1.5 times the voxel size. The remaining $N_{RS} = 46$ (32 female, $M = 21.76$, $SD = 2.75$ years, range = 18–28 years) were all right-handed ($M = 85.15$, SD = 16.46; range = 30–100) as assessed by the Edinburgh Handedness Inventory (Oldfield, 1971) and had (corrected-to-) normal vision. Additionally to the analysis of rs-fMRI data and their intrinsic timescales, we also collected task data of the same participants. The task-data was analyzed before using a classic contrast-based fMRI

analysis (Mecklenbrauck et al., 2024). The present paper reanalyzed the data using ISC (Hasson et al., 2004, 2010). From the task-fMRI data we had to exclude a further seven participants because of movement during the task session (three participants), sub-par attention to the task (one) and technical difficulties (three). So, the data of $N_{ISC} = 39$ participants (29 female, $M = 21.67$, $SD = 2.77$ years, range = 18–28) entered the ISC analysis. None reported any history of neurological or psychiatric diseases or any ferromagnetic material inside their bodies. The participants received money or course credit as renumeration on completion of the experiment.

2.1.2. Procedure and stimuli

The task-fMRI and the rs-fMRI together with the diffusion-weighted imaging (DWI) data were acquired in two sessions on separate days (Fig. 1). The order of the two session was counterbalanced across participants with $M_{RS} = 7.02$ days ($SD_{RS} = 5.93$ days) or $M_{ISC} = 6.73$ days ($SD_{ISC} = 4.70$ days) passing between sessions, respectively.

Starting with the DWI-Rest Day, the MRI measurements included an anatomical T1-weighted image (5 min), multiple sequences for DWI (15 min) and rs-fMRI (8 min). The participants were instructed to lie as still as possible during the anatomical and DW imaging but could leave their eyes opened or closed. The experimenters informed the participants via an intercom system about the start of the rs-fMRI measurement during which participants looked at a fixation cross (Agcaoglu et al., 2019; Patriat et al., 2013; Van Dijk et al., 2010). In total 480 rs-fMRI volumes were acquired.

In the scanning session on the fMRI-Task Day participants completed a task presenting them with sequences of digits. A detailed description of the stimuli and their creation was reported before (Mecklenbrauck et al., 2024). To summarize, we created abstract stimuli (hierarchically nested sequences of digits) that were inspired by the structure of the hierarchically nested natural stimuli previously used to identify TRW (e.g., Lerner et al., 2011). The sequences were made up from the digits 4 through 9. Digits 1 to 3 were excluded due to their representation as quantities (Dehaene, 2001). The sequences were presented one digit at a time. The hierarchically nested structure of the sequences created four experimental conditions: (1) *Single*, where the digits appeared pseudo-randomly (equal transition probabilities between all digits. (2) In the *Triplet* condition the digits were presented in predefined chunks of three (4-5-6, 6-5-4, 7-8-9 and 9-8-7). (3) The *Nonet* condition then contained chunks of nine digits with each chunk consisting of three repeating Triplet chucks (4-5-6–4-5-6–4-5-6, 6-5-4–6-5-4–6-5-4, 7-8-9–7-8-9–7-8-9 and 9-8-7–9-8-7–9-8-7). (4) Finally, the *Complete* condition displayed the entire sequence of 36 digits in which all other conditions were nested in (4-5-6–4-5-6–4-5-6–-6-5-4–6-5-4–6-5-4–-9-8-7–9-8-7–9-8-7—7-8-9–7-8-9–7-8-9) (Fig. 2A). We generated de Bruijn sequences (Brimijoin and O'Neill, 2010; de Bruijn, 1946) to ideally pseudo-randomize (Aguirre et al., 2011) not only the transition between single digits and chunks but also the occurrence of the different blocks in the blocked presentation of the experimental conditions. In deviation to the passive watching paradigms usually applied in the context of TRW (e.g., Hasson et al., 2008), we included a task during the watching of the digit sequences. All sequences were pseudo-randomly interrupted by inserted zeros. The zeros acted as targets for the participants, who had to press a button upon seeing a zero, to keep their attention on the digits. The zero was chosen specifically due to its particular role among other numbers (Brysbaert, 1995; Nieder, 2016; Pinhas and Tzelgov, 2012). We included 18 targets per block of each experimental condition, so 360 zeros were presented during the entire fMRI experiment. The zeros were inserted in a way that we could control how often they interrupted a transition within and between chucks of the sequence.

The task consisted of 24 blocks, so that the subjects completed each experimental condition six times. Four blocks (each condition once) were presented outside the scanner as a training, while the remaining 20 blocks were then part of the main fMRI experiment in the scanner. We counterbalanced the first condition participants saw. Before each block subjects were presented with a fixation cross for a jittered duration of 6370–7950 ms. The fixation cross flashed three times to signal the start of the next block. The blocks themselves were then made up from sequences of 162 digits including the 18 targets. The sequences were presented in trials, one digit at a time. Each trial was 700 ms long. Digits

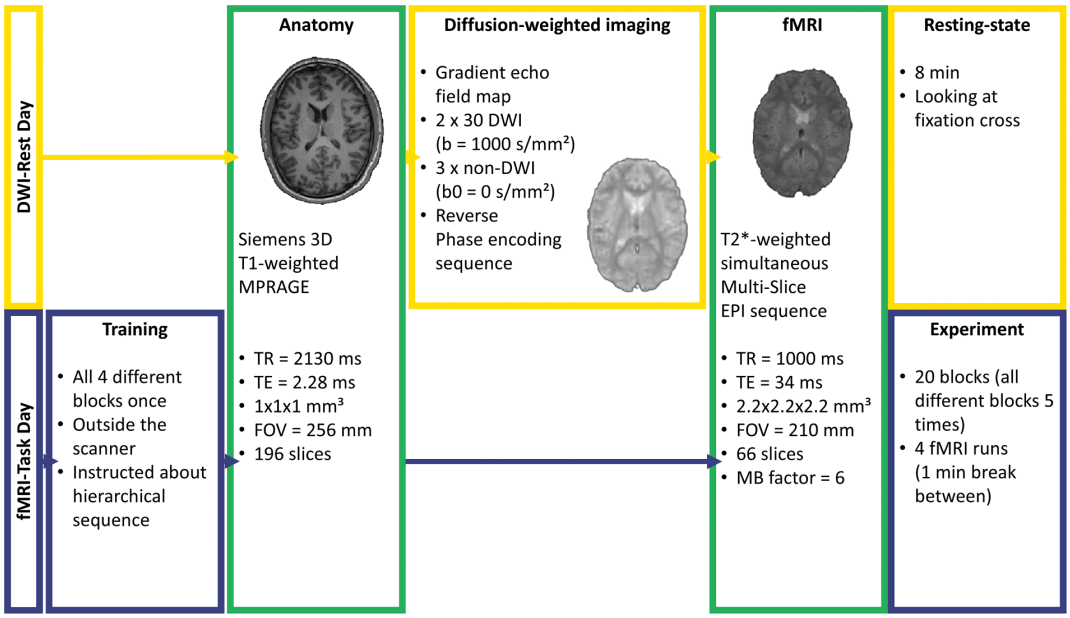


Fig. 1. Diagram of procedure during the scanning sessions DWI-Rest- and fMRI-Task-Day.
Note. MPRAGE = Magnetization prepared rapid acquisition gradient echo, TR = Time of repetition, TE = Echo time, FOV = Field of view, DWI = Diffusion-weighted imaging, EPI = Echo planar imaging, MB = Multiband. Note that the order of the two sessions was counterbalanced across participants.

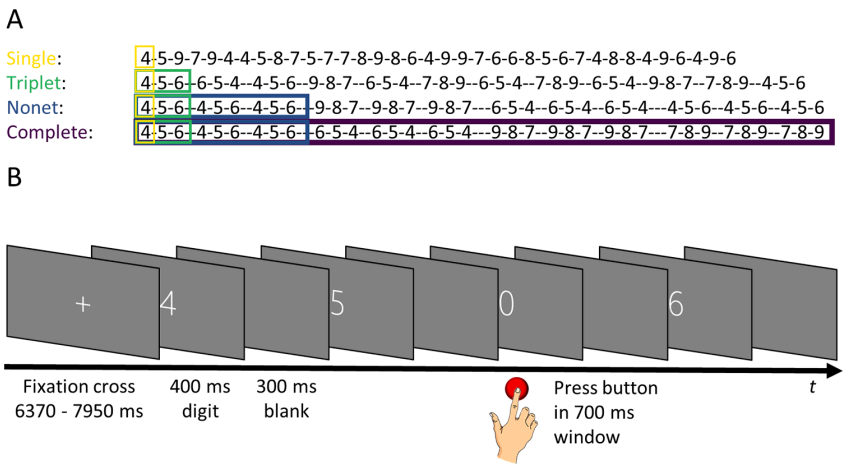


Fig. 2. Experimental paradigm on the fMRI-Task Day.
Note. (A) Example sequences for the four experimental conditions. Colors show nested hierarchical structure. (B) Presentation of digit sequence. Participants had to press a button when a 0 was presented.

were presented for 400 ms and followed by 300 ms of blank screen. The participants had the entire 700 ms to react if they saw a zero by pressing a button with their right index finger (Fig. 2B). As further motivation, the participants could win additional course credit or money on top of their standard renumeration based on their performance in the task. Lastly, we included a one-minute break after five blocks in the scanner in which the participants were informed about their progress in the experiment. In total, participants spent approximately 60 min in the scanner on the fMRI-Task-Day.

All digits and fixation crosses in both scanning sessions were displayed on a screen positioned behind the scanner bore and were viewed by the subjects through an adjustable 45° mirror at a visual angle of approximately 1.29°. Movements were minimized with form-fitting cushions. Subjects wore ear plugs and noise-cancelling headphones to reduce scanner noise.

2.1.3. MRI data acquisition

Brain images were recorded with a 3T Siemens Magnetom scanner (Siemens, Erlangen) using a 20-channel head coil. Functional blood-oxygen-level-dependent (BOLD) images during rs-fMRI and task-fMRI were acquired parallel to the anterior commissure/posterior commissure line. We used a T2*-weighted simultaneous multislice echo-planar imaging (SMS-EPI; 94 × 94 data acquisition matrix; 210 mm field of view (FOV); 57° flip angle; time of repetition (TR) = 1000 ms; echo time (TE) = 34 ms). Each volume consisted of 66 adjacent axial slices with a slice thickness of 2.2 mm, a gap of 0.11 mm (5 %), and a voxel size of 2.2 × 2.2 × 2.2 mm^3. Slice acquisition and multislice mode were interleaved. The acceleration factor was 6.

T1-weigthed anatomical images were acquired using a standard Siemens 3D MPRAGE sequence for a detailed reconstruction of anatomy with isotropic voxel size (1 × 1 × 1 mm) in a 256-mm FOV (256 × 256 matrix; 192 slices; 8° flip angle; TR = 2130 ms; TE = 2.28 ms).

For DWI, we applied the parameters of the imaging sequences used in the Marburg-Münster Affective Disorders Cohort Study (Vogelbacher et al., 2018). Imaging started with a gradient echo field map (320 mm FOV; 60° flip angle; TR = 616 ms; TE1 = 5.19 ms; TE2 = 7.65 ms; 56 slices, slice thickness = 2.5 mm; 0 mm gap; voxel size 2.5 × 2.5 × 2.5 mm^3; interleaved slice acquisition). This was followed by two times 30 DW images with a b-value of 1000 s/mm^2 and in total five non-DW images (b = 0 s/mm^2), that had the same parameters except for their b-value (320 mm FOV; initial rotation −90°; TR = 7300 ms; TE = 90 ms; 56 slices, slice thickness = 2.5 mm; 0 mm gap; voxel size = 2.5 × 2.5 × 2.5 mm^3; interleaved slice acquisition; GRAPPA acceleration factor = 2). DWI was completed by a Reverse Phase Encoding sequence (320 mm FOV; initial rotation −90°; TR = 7300 ms; TE = 90 ms; 56 slices, slice thickness = 2.5 mm; 0 mm gap; voxel size = 2.5 × 2.5 × 2.5 mm^3; interleaved slice acquisition; GRAPPA acceleration factor = 2).

2.1.4. Cortical parcellation

Parcellating the cortex allowed us to investigate and compare the cortical organizational schemes across different modalities in a common reference frame (Eickhoff et al., 2018; Glasser et al., 2016; Tzourio-Mazoyer et al., 2002). We applied recon-all from FreeSurfer (v7.2.0; Fischl, 2012) as well as functions from the Connectivity Analysis Toolbox (CATO, v3.1.2.; de Lange et al., 2023) on the individual T1-weigthed anatomical images to reconstruct and parcel the brain's surface. The quality of the individually parcellated cortical surfaces was controlled according to the ENIGMA protocols (https://enigma.ini.usc.edu/) by one of the authors (FM) and three student assistants. No data had to be excluded based on the quality control. CATO extends on the classical Desikan-Killiany parcellation (Desikan et al., 2006) that is included in FreeSurfer by the *Lausanne sub-parcellations* (Cammoun et al., 2012) which divide the larger parcel from the Desikan–Killiany atlas into equally sized smaller parcels for a higher resolution. For our analyses we specifically chose the *lausanne250* parcellation scheme as it showed exceptional reliability (Cammoun et al., 2012) and portrays a meaningful meso-level parcellation of the cortex (Amunts and Zilles, 2015). The application of the lausanne250 parcellation divided the brain into 219 cortical regions. Note that we did not include subcortical regions in the analysis as the DWI resolution would not have allowed for reliable estimation of streamlines (Kai et al., 2022).

2.2. Resting-state fMRI and intrinsic timescales

2.2.1. Preprocessing

For preprocessing the rs-fMRI data we made use of FSL (v6.0; Jenkinson et al., 2012) tools also within CATO (de Lange et al., 2023). For this we discarded the first five volumes as recommended for signal stabilization (Buxton, 2009; Caballero-Gaudes and Reynolds, 2017). The functional preprocessing in CATO included slice timing correction using FSL's sliceTimer and the application of FSL's MCFLIRT (Jenkinson et al., 2002) for the motion correction. The six estimated rigid motion correction parameters were used to calculate the framewise displacement and change in signal intensity between frames. The calculation of

both motion metrics was based on Power et al. (2012). Additionally, an average of all motion corrected volumes was calculated and aligned with the individual T1-weigthed anatomical image. This alignment enables the registration of the functional data with the anatomical parcellation based on the structural data.

The slice time and motion corrected rs-fMRI data was then passed through a nuisance regression model (Ciric et al., 2017) to remove any unwanted influences on the data. To this end, we first extracted three masks from the individual anatomical images using the cortex parcellation from CATO: a whole brain, a white matter and a ventricle mask. For the regressors of nuisance we extracted the average time series from the white matter and the ventricles for each subject using these masks. Also, we calculated the first derivative of the six rigid motion correction parameters. Lastly, the rs-fMRI time series of each participant was de-meaned and de-trended. The nuisance regression model then removed the influence of the six rigid motion correction parameters and their six first derivatives as well as the quadratics of all variables. For noise reduction, a component-based method (CompCor; Behzadi et al., 2007) was applied on the extracted white matter and ventricle time series. The top five components of both the white matter and ventricle signals as well as their derivatives and quadratics were thus also removed as nuisance from the rs-fMRI data. Lastly, as recommended (Ciric et al., 2017), we included a spike regression according to Satterthwaite et al. (2013) in the model, removing every spike based on its framewise displacement.

Returning to CATO, we used the whole brain mask to extract the nuisance-corrected signal from cortical voxels. This signal was then bandpass filtered between 0.01 Hz and 0.1 Hz using a standard zero-phase Butterworth bandpass filter.

2.2.2. Calculation of intrinsic timescales

To analyze the distribution of intrinsic timescales across the cortex we first needed to extract the time series. Using CATO, we could obtain the individual, averaged time series from of the 219 cortical parcels from the lausanne250 parcellation (see Section 2.1.4). Based on these time series, we estimated the intrinsic timescale of each parcel via the decay of the autocorrelation function (ACF). We applied a model-free procedure (Raut et al., 2020) to determine the decay of the ACF. Applying the published code from Raut et al. (2020) we first de-meaned the nuisance-corrected rs-fMRI signal of every participant. We then determined the ACF by first calculating the lagged covariance in 24-s window for all lag $\Delta \in [-12,12]$,

$$c_x(\Delta) = \frac{1}{T-|\Delta|}\sum_{t=1}^{T-|\Delta|} x(t+\Delta) * x(t) \quad (1)$$

before normalizing the results by the covariance at lag 0, so that $r_x(0) = 1$,

$$r_x(\Delta) = \frac{c_x(\Delta)}{c_x(0)} \quad (2)$$

The resulting $r_x(\Delta)$ can be interpreted as the lagged autocorrelation rather than covariance. The intrinsic timescale for each individual parcel was then determined as the precise abscissa of the ACF at $r_x(\Delta) = 0.5$, which describes the half of the full width at half maximum of the function. This calculation was achieved with the fnzeros function in MATLAB which computes the zeros of a spline fit of a function.

2.3. Task-fMRI

2.3.1. Preprocessing

Processing of the task data for the ISC analysis was based on the procedure described in Nastase et al. (2019). Preprocessing was completed using Statistical Parametric Mapping software (SPM12; FIL Methods Group, 2017) implemented in MATLAB (Version 9.10.0 [R2021a]; The MathWorks Inc., 2021) and included slice time correction to the spatially and temporally middle slice, realignment, co-registration to anatomical data, normalization to MNI space and smoothing using a $6 \times 6 \times 6$ mm^3 Gaussian smoothing kernel. The signal was further high-pass filtered at 1/160 s based on previous results (Mecklenbrauck et al., 2024). The nuisance regression in accordance with the recommendation (Nastase et al., 2019) included the six motion parameters estimated during realignment as well as the averaged white matter and cerebral-spinal-fluid signal. Additionally, we included all button presses of the subjects as a regressor of nuisance which was convolved with the canonical hemodynamic response function. For modelling, we applied the FAST algorithm to correct for autocorrelation as recommended for TR $\leq$ 1.4 s (Corbin et al., 2018). The following ISC analysis was performed on the residuals of the nuisance regression. In preparation of the ISC analysis, the residuals were z-scaled and masked with an average grey matter mask before concatenating the blocks of each experimental condition in the same order into a single four-dimensional file for each condition, synchronizing the digit presentation across subjects.

2.3.2. Inter-subject correlation

ISC is a measure of neural synchrony or reliability (Redcay and Moraczewski, 2020). The method requires a synchronized presentation of the same stimuli across subjects (Nastase et al., 2019). A high ISC value in a voxel then suggests that this voxel holds information about the presented stimulus as the synchronized stimulus is the only commonality between all participants which creates this correlation (Nastase et al., 2019). In the context of hierarchically structured stimuli, participants are presented with different hierarchically nested levels of the stimuli (e.g., Lerner et al., 2011). These levels differ by their temporal persistency, with hierarchically higher levels of the stimulus being more persistent (Uithol et al., 2012). Voxels that only depict higher ISC values in conditions that present more temporally persistent levels of the stimulus, have longer TRWs to process the longer persistence in the stimulus. Voxels with shorter TRWs on the other hand already have higher ISC values for more transient levels of the stimulus, but also show increased values for hierarchically higher levels, as the more transient levels are nested within the more persistent levels of the stimulus structure.

For the calculation of the ISC, we opted for the leave-one-out-method of ISC calculation to allow us later to apply classical statistical methods (Nastase et al., 2019; Thomas et al., 2018). Therefore, we adjusted available code (Nastase et al., 2019) to calculate individual ISC maps for each experimental condition. Finally, the ISC values were Fisher z-transformed to help with the normal distribution of the correlation values (Bond and Richardson, 2004). Based on these maps we extracted the average ISC value for each cortical parcel in the lausanne250 parcellation scheme. Therefore, we parcellated the individual normalized brains of each subject using the Multi-Scale Brain Parcellator (Tourbier et al., 2019), extracted the parcels as binary maps and dilated these maps three-dimensionally by one voxel size using functions from the WFU pick atlas toolbox (Maldjian et al., 2003) to accommodate for the smoothing of the data. These individual averaged ISC values for each parcel in each experimental condition were the basis of the following analyses.

2.4. The six organizational schemes of interest

As outlined in the introduction, our goal was to find a cortical organizational principle that best explains the distribution of intrinsic timescales and ISC values. We considered the following six candidate organizational schemes: (1) the RC architecture, (2) the DC architecture, (3) the uni-to-multimodal gradient, and (4) the posterior/lateral-to-anterior/medial gradient. Additionally, we explored the relationship of the chrontopy with (5) different graph theoretical measures of the individual structural networks as well as (6) cortical thickness as an approximation of cytoarchitectural differences (Wagstyl et al., 2015).

The extraction all organizational schemes will be described in the following sections.

2.4.1. Rich Club architecture

For the individual RC architecture (as well as the DC architecture (see Section 2.4.2) and graph theoretical measures of network centrality (see Section 2.4.5)), we first had to reconstruct the structural network from the estimated white matter streamlines.

2.4.1.1. Structural network reconstruction. To reconstruct the structural white matter network, we used the same pipeline as in Mecklenbrauck et al. (2024). Thus, we applied the structural pipeline from CATO (de Lange et al., 2023) which calls upon FreeSurfer (Fischl, 2012) and FSL (Jenkinson et al., 2012) for the structural (pre-)processing steps. Building on the reconstruction and parcellation of the cortical surface (see Section 2.1.4), the structural pipeline started by applying fslmerge, topup (Andersson et al., 2003; Smith et al., 2004) and eddy (Andersson and Sotiropoulos, 2016) of the FSL package to merge the DWI data and correct susceptibly as well as movement and eddy current artefacts. We then continued using CATO to reconstruct the white matter network using a combined diffusion tensor imaging (DTI) and generalized Q-sampling imaging (GQI; Yeh et al., 2010) model. This model showed the best benchmark results in respect to false positive and false negative streamlines (de Lange et al., 2023). GQI helps with solving the issue of multiple diffusion peaks in the case of crossing or kissing fibers. Thus, the combined method applied the classical informed RESTORE algorithm (Chang et al., 2005, 2012) for DTI modelling in cases of single diffusion peaks and opted for the GQI algorithm in more complex cases. The white matter tracts were then reconstructed deterministically using the FACT algorithm (Mori et al., 1999) adjusted for multiple diffusion peaks. The creation of connectivity matrices used the standard settings of CATO which are derived from van den Heuvel et al. (2013). Therefore, the algorithm started with eight seeds from each voxel included in the whole brain mask and followed the main diffusion direction to the next voxel until one of five stop cases occurred: (1) The algorithm reached a voxel with a low fractional anisotropy value (FA < 0.1), which often represents a grey matter voxel. (2) The reconstructed streamline exited the brain mask. (3) The streamline turned at an angle larger than 45°. (4) The reconstruction reentered a previously visited voxel. (5) The streamline reached the cerebellum. Only streamlines that fully connected two brain regions were considered for the connectivity matrices. The connectivity matrix of each subject was subsequently generated by combining these estimated streamlines with individual parcellated anatomical images. In accordance with the lausanne250 parcellation scheme we ended up with 219 $\times$ 219 connectivity matrices for each subject. Lastly, we controlled the individual structural connectivity matrices for outliers (van den Heuvel et al., 2019). No connectivity matrix showed any outliers, so all matrices were suitable for graph theoretical analysis.

2.4.1.2. Rich Club hub classification. The general procedure of the RC identification (Fig. 4A) was reported in Mecklenbrauck et al. (2024) and was inspired by Riedel et al. (2022). To summarize, we calculated the RC coefficient $\phi(k)$ in binarized structural connectivity matrices. The RC coefficient was then normalized based on the mean of 2500 random networks. The random networks were created by rewiring each connection of the empirical network ten times. Using the formula reported by van den Heuvel and Sporns (2011) we identified a range of degrees k, for which the empirical RC coefficient was significantly ($\alpha = 0.05$) larger than in the random networks. Significant evidence for this so-called RC regime (van den Heuvel and Sporns, 2011) indicated the presence of RC organization in the network. Based on this RC regime we used the previously described criteria (Mecklenbrauck et al., 2024; Riedel et al., 2022) to identify nodes of the network as possible hubs: (a) A node was in the top 15 % of highest degrees. (b) The degree of a node was at least as large as the start degree of the RC regime. (c) A node's degree was at least as large as the degree k with the largest normalized RC coefficient within the RC regime. (d) The node was within the top 33 % in four of five measures of node centrality: nodal degree/degree centrality, betweenness centrality, closeness centrality, between-module participation coefficient, and within-module degree z-score. The calculation of the participation coefficients and within-module degree z-degree requires the determination the module partition. Like Riedel et al. (2022), we identified this partition in a 60 % prevalence-based group-average network using the Louvain algorithm (Blondel et al., 2008). For this purpose, we first determined the optimal module resolution γ (Lurie et al., 2024). A higher resolution, so a larger value of γ, leads to a more nuanced module differentiation. We varied γ between the values of 0.5 and 3.5 (in increments of 0.1) using the Louvain algorithm (community_louvain.m) for module identification 1000 times per value of resolution γ. We then found the agreement between these 1000 partitions at each resolution γ (agreement.m). Using consensus-based clustering 100 times (consensus_und.m; $\tau = 0.6$), we identified a stable module partition at every level of resolution. To find the best resolution as describes by Lurie et al. (2024) we calculated the variation of information (Meilă, 2003), i.e., the similarity between the partition across all levels of resolution. The most representative module partition then was determined by the lowest median variation of information thus identifying the optimal module resolution γ. This most representative module partition was ultimately used for the calculation of the between-module participation coefficient and the within-module degree z-score. For the group-wise matrix in this case we determined the optimal $\gamma = 2.3$ (10 communities).

Importantly, the four hub definition criteria (a–d) introduced above do not necessarily result in a single consistent hub definition. To achieve this congruent definition, we applied additional criteria. Firstly, we only considered nodes that were labelled as hubs in at least three of the four criteria. Secondly and most vitally, we compared the proportions of edges between the identified hubs in the empirical structural with the inter-hub connections in the 2500 random networks. As the RC is defined by a particularly high connectivity between hub regions (Colizza et al., 2006), we used false discovery rate (FDR)-corrected Wilcoxon signed-rank test to test whether the possible hubs were more likely to connect to each other in the empirical network than in the 2500 random networks. The final set of *RC hubs* only contained nodes that were significantly more interconnected in the empirical network. We then classified nodes as *Feeder* nodes if they were directly connected to an RC hub but not part of the RC, and as *Local* nodes all nodes that were neither part of the RC nor connected to it.

In deviation to the previously applied identification (Mecklenbrauck et al., 2024), we classified the parcels as RC hub, Feeder node or Local node not in a group-averaged network but individual binarized connectivity matrices. Therefore, we binarized the individual matrices by setting every edge with at least three streamlines (Number of Streamlines ≥ 3) to one and all others to zero, as recommended for individual binarized connectivity matrices to correct for false positive edges (Brown et al., 2011). As described, following previous practice (Lurie et al., 2024; Riedel et al., 2022) only the module partition was based on the group-averaged binary connectivity matrix. This resulted in individual classifications of RC hubs, Feeder nodes and Local nodes. At this point, we had to exclude two participants from further analyses, as they did not depict RC architecture, reducing the sample size for the timescale analysis to $N_{RS} = 44$ and the ISC analysis to $N_{ISC} = 37$.

2.4.2. Diverse Club architecture

The procedure to identify DC hubs was in large parts similar to the RC hub identification (Fig. 5A). To determine if a DC architecture was present, we applied the modified clubness coefficient, that can calculate clubness not just on basis of the degree centrality but based on any nodal measure (Bertolero et al., 2017). Here we used the between-module participation coefficient as the nodal measure to identify a club of

nodes which are particularly well connected with the modules of the network. As the module structure is central to the participation coefficient, we determined the optimal modularity not in a group-average network, like in the RC identification, but in each subject's network individually. As for the RC, we then normalized the DC coefficient on the basis of 2500 random networks using the same individual module classification for all random networks. We validated the presence of DC architecture in each subject by identifying a range of participation coefficients for which the empirical DC coefficient was significantly ($\alpha = 0.05$) larger than on average in the random networks; thus, mirroring the procedure for RC coefficients (van den Heuvel and Sporns, 2011). Furthermore, only one criterion was used to determine possible hubs: Following Bertolero et al. (2017) the top 20 % of the participation coefficient distribution was considered as a hub. Finally, to identify the DC hubs, we compared the proportions of inter-hub connections between the empirical and random networks, as we did for RC hubs. We only classified hubs as *DC hubs* if they connected to significantly more other hubs in the empirical network than in the random networks. Again, we used an FDR-corrected Wilcoxon signed-rank test to validate this comparison. Further, we also classified Feeder nodes and Local nodes based on the connections to the identified DC.

2.4.3. Uni-to-multimodal gradient

To identify parcels that are functionally classified as multimodal we used two different strategies: a data-driven approach using SFC (Fig. 6A1; Sepulcre et al., 2012) and an atlas-based approach employing the classification of functional modules introduced in Ji et al. (2019) (Fig. 6A2; Golesorkhi, Gomez-Pilar, Tumati, et al., 2021; Ito et al., 2020). Both approaches were validated by correlating the resulting uni-to-multimodal gradient maps with other previously established uni-to-multimodal gradients (Margulies et al., 2016; Sydnor et al., 2021; see Supplemental Material 1).

2.4.3.1. Stepwise functional connectivity. The SFC analysis calculates paths through the functional network starting at a seed region. It then maps the connectivity pattern of that seed region or multiple seed regions at different so-called link-step distances, so progressions of the connectivity along the calculated paths. In their seminal paper Sepulcre et al. (2012) demonstrated that when starting the paths in the primary visual, auditory and somatosensory cortices the paths reach a steady state after seven link-steps. The stable pattern of SFC converged in regions of the brain that can be described as cortical hubs or multimodal areas (e.g., Sepulcre et al., 2010). To capture the full spectrum of the uni-to-multimodal gradient from the SFC maps, we extracted the normalized SFC pattern at link-step one, which specifies the unimodal areas (Sepulcre et al., 2012), as well as the normalized SFC map at link-step seven to locate the multimodal hubs. Subtracting the SFC maps at the first step from the maps at link-step seven combines the topographies to portray the extent of the uni-to-multimodal gradient in one single map. The resulting values are higher for multimodal and lower for unimodal areas.

Therefore, we first aligned the individual, preprocessed and nuisance-regressed rs-fMRI data (see Section 2.2.1) to the MNI standard space using SPM12. In doing so, images were downsampled to a voxel resolution of $8 \times 8 \times 8$ mm^3. This downsampling rendered the voxel-wise connectivity matrices computationally manageable (Pretus et al., 2019; Sepulcre et al., 2012). We again used functions from CATO (de Lange et al., 2023) to extract the time course signal of 475 resting-state acquisition timepoints. The signal was extracted on the voxel level from a whole brain mask, which included 4575 $8 \times 8 \times 8$ mm^3 voxels. This signal was then filtered between 0.01 Hz and 0.1 Hz using a standard zero-phase Butterworth bandpass filter. For the SFC analysis we firstly calculated the individual 4575×4575 connectivity matrices using product-moment correlation. Only positive correlations were considered. Additionally, the correlations were Fisher z-transformed and then normalized between 0 and 1. To correct the adjacency matrix for false positive connections, we applied a conservative Bonferroni-correction at a significance level of $\alpha = 0.001$. Coherent with recent publications using SFC (Bueichekú et al., 2020; Diez and Sepulcre, 2018; Ortiz-Terán et al., 2017), we used these filtered weighted adjacency matrices for the analysis instead of binarizing them. We determined the normalized SFC at each link-step distance up to seven steps for each individual subject. As seed regions, we used the following MNI coordinates (x, y, z), identified based on the coordinated reported in Sepulcre et al. (2012) and further consultation of the SPM Anatomy Toolbox (Eickhoff et al., 2005): left visual (−8, −85, 4), right visual (8, −83, 4), left auditory (−47, −19, 8), right auditory (43, −32, 11), left somatosensory (−42, −29, 65) and right somatosensory (38, −29, 65). Each of these seeds was comprised of a single $8 \times 8 \times 8$ mm^3 voxel. To have a single SFC map per subject at each link-step we averaged the stepwise maps of all six seeds. We then subtracted the averaged, individual SFC maps at the first step from the maps at the seventh link-step to estimate the topography of the uni-to-multimodal gradient for each subject. Finally, we extracted the individual, averaged results from of uni-to-multimodal gradient maps for each parcel of the lausanne250 parcellation to arrive at a continuous representation of multimodality that can be related to the cortical chronotopy.

2.4.3.2. Ji atlas-based multimodality. The functional atlas introduced by Ji et al. (2019) is based on the Glasser atlas (Glasser et al., 2016). Each parcel in the surface-based Glasser atlas is assigned to one of twelve functional networks: Auditory, Visual1, Visual2, Somatomotor, Cingulo-Opercular, Default, Dorsal-Attention, Frontoparietal, Language, Orbito-Affective, Posterior-Multimodal, Ventral-Multimodal. In the distinction of unimodal and multimodal areas, previous papers labeled all parcels belonging to Auditory, Visual1, Visual2 and Somatomotor networks as unimodal or "periphery", and all others as multimodal or "core" (Golesorkhi et al., 2021a; Ito et al., 2020). To also assign the parcels of the lausanne250 parcellation to these categories, we determined the overlap between a parcellation of the MNI standard brain according to the Lausanne atlas (Cammoun et al., 2012) and a voxel-wise version of the Glasser atlas published by Horn (2016) and adjusted by Gorgolewski (2016). The comparison gave us a percentage for each parcel of the Lausanne atlas describing how much of its volume belonged to a multimodal area according to the definition by Ito et al. (2020). These percentages also described a continuous way of operationalizing multimodality to be related to the cortical timescales and ISC values.

2.4.4. Posterior/lateral-to-anterior/medial gradient

For the approximation of the posterior-to-anterior and lateral-to-medial gradients which are part of many theories on cortical organization (e.g., Alexander and Brown, 2018), we considered the average MNI coordinates of each parcel of a subject's cortex (Fig. 7A). Thus, we averaged the x-, y- and z- coordinates in FreeSurfer reference space (MNI305/fsaverage space; Fischl, 2012) of each parcel for each individual parcellation. We used the absolute values of the x-coordinate to model the lateral-to-medial trend, while an effect of the y-coordinate on the cortical chronotopy might signal a posterior-to-anterior trend, as was indicated previously (Mahjoory et al., 2020). The z-coordinates were used as control variables in all models.

2.4.5. Graph theoretical measures of network centrality

Furthermore, we considered graph theoretical measures of centrality of the parcels as explanatory variables. Therefore, we included the five nodal measures that were used in the identification of the RC (Mecklenbrauck et al., 2024; Riedel et al., 2022): degree centrality, betweenness centrality, closeness centrality, participation coefficient, and within-module degree z-score (Fig. 8A). For participation coefficient and within-module degree z-score we however used the individual

optimal module distribution that was calculated for the DC identification.

2.4.6. Cortical thickness

The surface-based morphometry measures were calculated based on the surface tessellation using FreeSurfer (Dale et al., 1999). The cortical thickness can be calculated from the distance of the white matter surface and the pial surface, while the surface is described by the area of the vertices spanning the cortex (Fig. 9A; Goto et al., 2022). As a possible organizational scheme, we only explored the average cortical thickness (in mm) as it can be seen as an approximation for cytoarchitectural differences between the areas (Wagstyl et al., 2015) which were previously suggested to shape the cortical dynamics (Gao et al., 2020). The surface area (in mm^2) on the other hand was used as a control variable in all models of both the timescale and ISC analyses.

2.5. Statistical data analysis

2.5.1. Spin test analysis

To identify similarities between the six organizational schemes as well as the intrinsic timescales cortical and ISC values per experimental condition prior to the formal analysis we calculated Pearson correlation between all variables averaged over all subjects. As the RC and DC classifications are categorial variables we used the mode for each parcel instead of the mean. Also, we did not determine a correlation but used the Kruskal–Wallis-test and the χ^2-test of independence, respectively, to assess their relationship with the other continuous variables and between each other. Finally, we calculated the effect sizes of the test statistics (η^2 and Cramer's V; Tomczak and Tomczak, 2014) to compare them with the correlations. We tested the significance of these correlations and effect sizes via 100,000 spin test permutations (Alexander-Bloch et al., 2018) implemented in the neuromaps toolbox (Markello et al., 2022). The spin test accounts for the spatial autocorrelation of the cortical maps by rotating their spherical surface projection and thus creating a null distribution of the maps whilst keeping spatial features of the original map intact. The p-values of the test are then calculated by comparing how many of the permutated correlations, based on rotated maps, are equal or larger than the original correlation coefficient based on the initial orientation (Alexander-Bloch et al., 2018). Finally, we applied FDR correction (Benjamini and Hochberg, 1995) to correct the spin test results for multiple testing.

2.5.2. Resting-state timescale analysis

Data analyses were performed using R (Version 4.2.2.; R Core Team, 2022) and RStudio (Version 2022.7.2.576; RStudio Team, 2022). Bayesian hierarchical generalized linear modelling was executed using the brms library in R (Bürkner, 2017). All model equations were constructed from the same base formula:

$$\text{Resting-state timescales} \sim 1 + \text{Organizational Scheme} + \text{Surface area} + z\text{-Coordinate} + \text{ICV} + (1|\text{Subject}) \quad (3)$$

For the Organizational Scheme we were first interested in (1) the individual RC architecture of each subject. Second, the timescales were modelled by (2) the individual DC classification. The next set of models concerned in the effect of (3) the uni-to-multimodal gradient on the timescales. One model looked at the individually determined gradient calculated from SFC and the other uni-to-multimodal model included the percentage of each area that was part of a multimodal area according to the Ji atlas-based classification by (Golesorkhi et al., 2021a; Ito et al., 2020). Fourth, one model included the average x- and y-coordinates of each parcel, as well as their interaction to model (4) the posterior/lateral-to-anterior/medial gradient. Note that the absolute values of the x-coordinates were calculated to model a lateral-to-medial rather than a left-to-right gradient. Fifth, we built a model that included (5) all five centrality measures we considered. Finally, a model used (6) the areas' average cortical thickness as organization of interest. Additionally, all models controlled for the surface area and average z-coordinate of an area as well as the intracranial volume (ICV) of each participant and included a random intercept for each subject. All continuous independent variables were z-scaled for better interpretability of the intercepts.

We prepared the data by taking the natural logarithm of the timescales and excluded outliers (below $Q1 - 1.5 \times IQR$ or above $Q3 + 1.5 \times IQR$). The following inspection of the Cullen-Frey plots to judge the skewness and kurtosis of the data revealed that we could assume a distribution from the gaussian family for all models (Cullen and Frey, 1999). For estimating the models in brms we used uninformative priors as it is recommended for multilevel modelling (Bürkner, 2017). For β coefficients we used a flat prior and for the standard deviation a Student's $t(3, 0, 2.5)$ distribution was applied. All models were then calculated with ten chains, each with 4000 iterations, from which the first 1000 were warmups, setting the target average proposal acceptance probability (adapt_delta) to 0.99. Convergence within and between chains was examined through the improved convergence diagnostic $\widehat{R}$, with values under 1.05 indicating successful convergence (Vehtari et al., 2021). Further, we used posterior predictive checks to evaluate whether the models captured the observed data (Kruschke, 2011). We tested the effects of the different organizational schemes of interest on the intrinsic timescales using the hypothesis function from the brms library (Bürkner, 2017). Bayes factors for one-sided hypotheses are defined by the evidence ratio (Bürkner, 2018). Generally, evidence ratios >10 are considered strong evidence for the tested hypothesis (van Doorn et al., 2021).

(1) For the RC architecture, we expected that the areas classified as RC would show slower timescales than the areas classified as Feeder and Local nodes, while Feeder nodes also have slower timescales than in Local nodes (Gollo et al., 2015). (2) Likewise, for the DC architecture, we would envision the areas classified as DC to be the slowest, followed by Feeder nodes and then Local nodes. (3) Based on previous results (e.g., Ito et al., 2020), we assumed slower timescales with increasing multimodality for both uni-to-multimodal gradient approaches. (4) In the posterior/lateral-to-anterior/medial gradient model, we predicted the slowest timescales to be located to the medial frontal lobe (Mahjoory et al., 2020). So, we expected a positive trend for y-coordinates and negative trend for x-coordinates as well as negative interaction effect on the timescales. Based on prior findings related, a positive relationship between (5) the centrality measures (Fallon et al., 2020; Lurie et al., 2024) as well as (6) thicker cortical areas (Gao et al., 2020) and slower intrinsic cortical timescales could be suggested.

As it was the purpose of this study to find the best fitting organizational schemes, we did not specify a preferred model in advance, to not bias the analysis. However, judging from previous studies we expected the RC architecture to play a major role in shaping the intrinsic timescales of the cortex (e.g., Gollo et al., 2015).

2.5.3. Inter-subject correlation analysis

After inspection of the Cullen–Frey plots, we excluded outlier values (below $Q1 - 1.5 \times IQR$ or above $Q3 + 1.5 \times IQR$) to reduce kurtosis of the distribution (Cullen and Frey, 1999). In the same way as with the intrinsic timescales we modelled the distribution of ISC values by the different organization schemes of interest. Now we additionally included the Condition in interaction with the Organizational Scheme as an independent variable:

$$\text{ISC}_{\text{Fisher } z} \sim 1 + \text{Condition} \times \text{Organizational Scheme} + \text{Surface area} + z\text{-Coordinate} + \text{ICV} + (1|\text{Subject}) \quad (4)$$

The factor Condition included four levels: Single, Triplet, Nonet, and Complete. For the Organizational Scheme we focused on the same six organizational schemes of interest as for the resting-state timescales (see Section 2.5.2). The models further again included the surface area of

each parcel in mm^2, the area's *z*-coordinates in MNI space, the intercranial volume of each participant in liters and a random intercept on the level of subjects as control. The continuous independent variables were again *z*-scaled.

The estimation of all models in brms used uninformative priors as it is recommended for multilevel modelling (Bürkner, 2017). For β coefficients we used a $N(0, 5)$ distributed priors while Student's $t(3, 0, 5)$ distribution was applied as prior for the standard deviations. We made use of the skewed normal family for the models. All models were then calculated with ten chains, each with 4000 iterations, with 1000 warmups. We left the target average proposal acceptance probability (adapt_delta) at the default of 0.8 but increased the maximal treedepth to 15. Convergence of the chains was monitored using the improved convergence diagnostic $\widehat{R}$ (Vehtari et al., 2021). Applying posterior predictive checks, we assessed the coherence between the modelled and observed data (Kruschke, 2011). We tested the effects of the different organizational schemes of interest on the ISC values across experimental conditions using the hypothesis function from the brms library (Bürkner, 2017).

Based on previous investigations on TRWs (Farbood et al., 2015; Hasson et al., 2015; Lerner et al., 2011), we generally expected that higher order structures in the organizational schemes are more involved in the processing of hierarchically higher structures in the stimuli, i.e., in the conditions Nonet and Complete. Specifically, we thus expected for the (1) RC and (2) DC classification that the ISC values in Local nodes do not differ across the experimental conditions, as the Local nodes handle the processing of more transient stimuli which are included in all hierarchically nested levels (Gollo et al., 2015). Further we assumed that the hubs in both classifications then show increased ISC values for hierarchically higher stimulus structures as hubs of the structural core are engaged by more persistent stimuli (Gollo et al., 2015). If the tested gradients better explained the processing of hierarchically structured stimuli we would expect (3) the uni-to-multimodal and (4) posterior/lateral-to-anterior/medial trends to be more pronounced for the processing of hierarchically higher stimuli structures, as the higher order regions only show an increase in ISC values with these more persistent stimuli (Wolff et al., 2022). In line with the timescale hypotheses, we would also expect that the effects of (5) the graph theoretical measures of centrality as well as (6) cortical thickness on the ISC values would be more pronounced for hierarchically higher conditions.

2.5.4. Bayesian model comparison

Finally, we compared the models using Bayesian statistics to find out which cortical organizational scheme best explains the respective distributions of resting-state timescales and ISC values across the cortex. Bayesian model comparison, in contrast to its frequentist counterpart, does not require the compared models to be nested and thus is ideal to evaluate different competing theories (Geweke, 2007; Hollenbach and Montgomery, 2020; Rouder et al., 2018). We ran leave-one-out-cross validations (LOO-CV) and used the results to estimate the *expected log pointwise predictive density* ($elpd_{loo}$) for each model. The $elpd_{loo}$ describes a model's accuracy in predicting future, out-of-sample data and thus captures the goodness of fit of the model while also controlling for overfitting (Gelman et al., 2014). The $elpd_{loo}$ value can be both positive or negative, with higher values (meaning closer to zero in the case of negative values) indicating a better predictive performance (Vehtari, 2024). To mitigate the high computational demands of cross-validations, LOO-CV can be approximated using Pareto smoothed importance sampling (Vehtari et al., 2017). When comparing models using $elpd_{loo}$, a model is considered better when the absolute difference in $elpd_{loo}$ between the compared models is larger than one standard error ($se(elpd_{loo})$; Mohor et al., 2021).

3. Results

3.1. Spin test

The spin test results reporting the similarity between organizational schemes as well as the chronotopy are depicted in Fig. 3. A Kruskal–Wallis-test revealed that the intrinsic resting-state timescales differed significantly between the classifications as Local, Feeder or DC hub according to the DC architecture, $H(2) = 31.99$, $\eta_H^2 = 0.14$, $p_{spin} = 0.018$. Appropriately, also the participation coefficient correlated significantly with the resting-state-timescales, $r = 0.27$, $p_{spin} = 0.039$. Moreover, a χ^2-test showed that the DC classification and the RC classification in Local, Feeder and RC hub were significantly dependent, $\chi^2(2, N = 219) = 195.97$, $V = 0.67$, $p_{spin} = 0.003$. We also found that the SFC-based uni-to-multimodal gradient correlated significantly with the resting-state timescales, $r = 0.48$, $p_{spin} = 0.003$, and the Ji atlas-based estimation of the uni-to-multimodal gradient, $r = 0.52$, $p_{spin} = 0.002$. Additionally, the uni-to-multimodal-gradient based on SFC correlated negatively with the ISC values in the Single condition, $r = -0.31$, $p_{spin} = 0.027$, Triplet condition, $r = -0.31$, $p_{spin} = 0.006$, Nonet condition, $r = -0.31$, $p_{spin} = 0.012$, and Complete condition, $r = -0.43$, $p_{spin} = 0.003$. Furthermore, the spin test revealed that the percentage of overlap with a multimodal area in the Ji atlas (Ji et al., 2019) correlated significantly negatively with the ISC values in the Complete conditions, $r = -0.43$, $p_{spin} = 0.006$.

Beyond that, we found several significant correlations between the graph theoretical measures of centrality. The degree centrality correlated significantly with closeness centrality, $r = 0.72$, $p_{spin} = 0.001$, betweenness centrality, $r = 0.79$, $p_{spin} = 0.001$, participation coefficient, $r = 0.59$, $p_{spin} = 0.002$, and within-module degree *z*-score, $r = 0.79$, $p_{spin} = 0.001$. Closeness centrality correlated also with betweenness centrality, $r = 0.79$, $p_{spin} = 0.001$, the participation coefficient, $r = 0.76$, $p_{spin} = 0.002$, and the within-module degree *z*-score, $r = 0.33$, $p_{spin} = 0.001$. Lastly, the correlations of betweenness centrality with the participation coefficient, $r = 0.76$, $p_{spin} = 0.002$, and the within-module degree *z*-score, $r = 0.46$, $p_{spin} = 0.001$, were also significant.

Finally, all the ISC values of the different experimental conditions were significantly correlated with each other. The ISC values of the Single condition shared correlations with the Triplet, $r = 0.76$, $p_{spin} = 0.002$, Nonet, $r = 0.83$, $p_{spin} = 0.002$, and Complete conditions, $r = 0.79$, $p_{spin} = 0.002$. The values of the Triplet condition correlated with the values in the Nonet, $r = 0.82$, $p_{spin} = 0.002$, and Complete conditions, $r = 0.81$, $p_{spin} = 0.003$. Also, the ISC values of the Nonet and Complete conditions were significantly correlated, $r = 0.84$, $p_{spin} = 0.002$. Note, reported *p*-values of the spin tests are FDR-corrected.

3.2. Results of the six organizational schemes

All models successfully converged as evaluated by the convergence diagnostic $\widehat{R}$ (Vehtari et al., 2021; for more details see Supplemental Tables S2.1 & S2.2). Graphical assessment affirmed that the predictive posterior distributions reasonably replicated the distributions as well as the means of the observed data (Supplemental Figs. S3.1–S4.8). Examining the multicollinearity resulted in no variance inflation factors over the threshold of ten (Wooldridge, 2013; Supplemental Figs. S3.1–S3.8). To test our hypotheses about the different organizational schemes we drew posteriors from the estimated models (Supplemental Tables S2.1 & S2.2).

3.2.1. Rich Club architecture

Beginning with the resting-state timescales, for the RC architecture the hypothesis tests revealed a significance increase in timescales between Local nodes and Feeder nodes as well as a significantly slower timescales in RC hubs than Local nodes, while RC hubs did not differ from Feeder nodes (Fig. 4B).

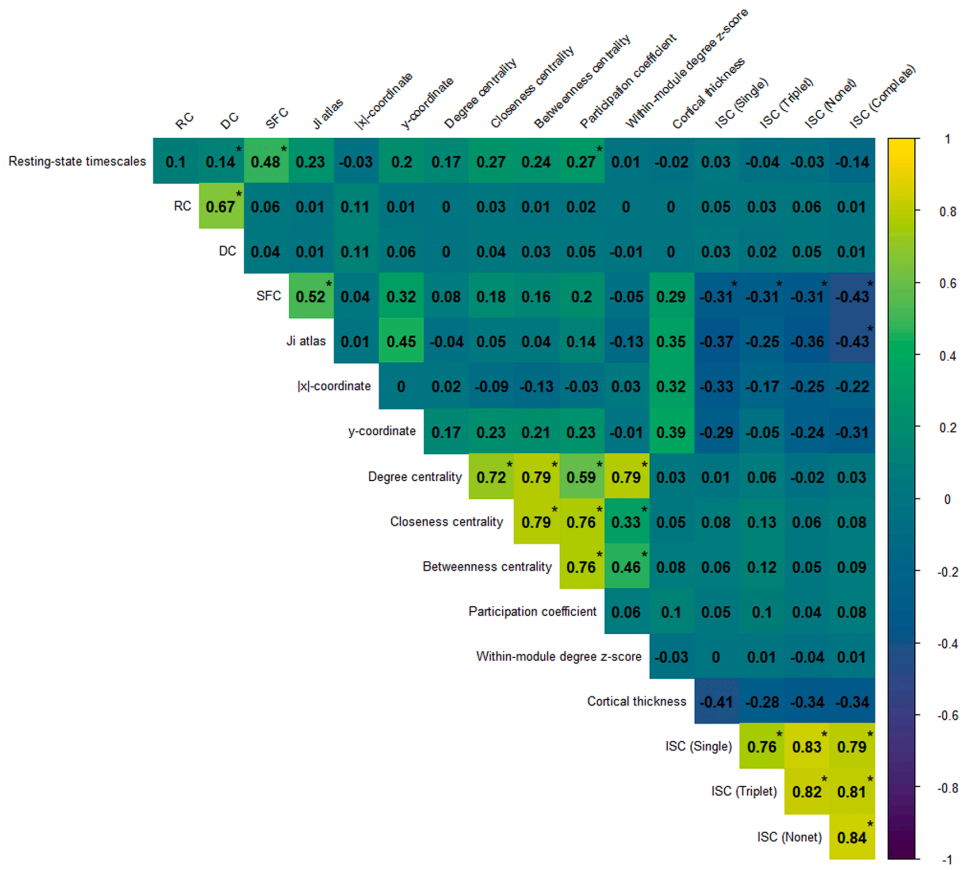


Fig. 3. Results of the exploratory spin tests.
Note. For Rich Club and Diverse Club effect sizes (η^2 and Cramer's *V*) are reported instead of Pearson correlation coefficient. RC = Rich Club, DC = Diverse Club, SFC = Stepwise functional connectivity, ISC = Inter-subject correlation, * $p_{FDR} < 0.05$.

Looking at the results for the ISC values, the tests revealed no significant differences between RC hubs, Feeder nodes and Local nodes in any experimental condition. Only testing for equal ISC values between conditions showed significant results, which suggests that we could not find an increase of ISC values of the temporal persistency of hierarchically structured stimulus in neither RC hubs nor Feeder nodes (Fig. 4C).

3.2.2. *Diverse Club architecture*

Regarding the resting-state timescales, we found a significant increase in the estimated mean timescale between Local nodes and DC hubs and between Feeder nodes and DC hub, while Local nodes did not differ from Feeder nodes (Fig. 5B).

The task data revealed a very similar pattern to the RC architecture. The Local nodes, Feeder nodes and DC hubs did not differ in their ISC values. Also, no significant increase of ISC values was found between the experimental conditions for any of the node classification (Fig. 5C).

3.2.3. *Uni-to-multimodal gradient*

For the resting-state timescales both approaches at modelling this gradient revealed a significant increase of intrinsic timescales with a higher value of multimodality (Fig. 6B).

Also, in the analysis of ISC values the two approaches at modelling multimodality produced largely similar results. The hypothesis test for both models revealed significantly negative effects of multimodality on the ISC values, in the Single, Triplet and Complete conditions, while the effect in the Nonet condition was only significantly negative for the model using the Ji atlas (Ji et al., 2019). So, an increase in multimodality predicted a decrease in the ISC value. When comparing the effects between the conditions, both approaches identified an increase in the influence of multimodality on the ISC value between the Single and Triplet conditions. Additionally, only for the SFC model the test also showed a significantly larger effect of multimodality in the Nonet compared to the Triplet condition (Fig. 6C).

3.2.4. *Posterior/lateral-to-anterior/medial gradient*

The resting-state timescales model for the posterior/lateral-to-anterior/medial gradient did not reveal an effect of the absolute *x*-coordinate but displayed significantly longer timescales with an increase in the *y*-coordinate as well as significant negative interaction between the absolute *x*-coordinate and the *y*-coordinate (Fig. 7B).

Looking at the task data, the results depicted a significantly negative effect of the absolute *x*-coordinate in all experimental conditions but the Triplet condition. Also, the effect of the *y*-coordinate was significantly negative in all conditions except for Triplet while the interaction effect on the ISC values was only significantly negative in the Single and Complete conditions. When comparing the effects between the experimental conditions, we found a significant decrease of the effect of the absolute *x*-coordinate on the ISC value between the Triplet and Nonet conditions. Also, the interaction effect decreased significantly between these two experimental conditions. The effect of the *y*-coordinate however increased between the Single and Triplet conditions (Fig. 7C).

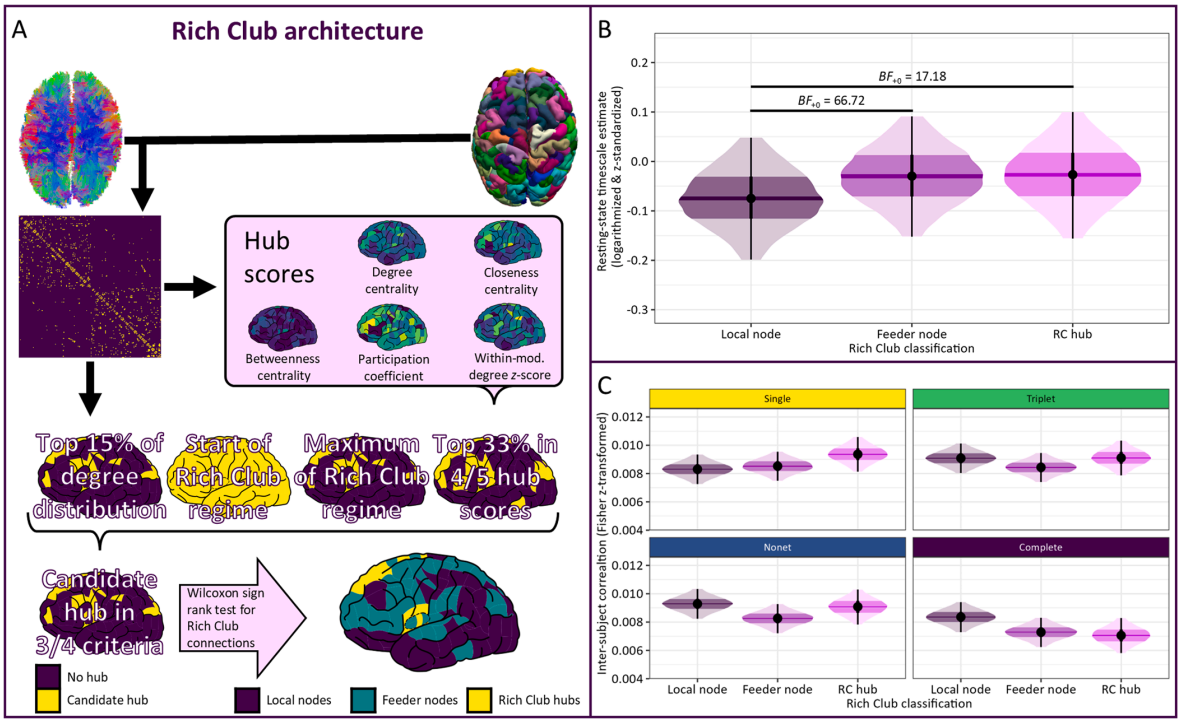


Fig. 4. Methods for extraction and results of intrinsic resting-state timescale and inter-subject correlation analyses for Rich Club architecture.
Note. (A) Rich Club (RC) identification was performed on individual binarized structural connectivity matrices with 219 cortical nodes according to the lausanne250 parcellation scheme (Cammoun et al., 2012). A combination of four different nodal cutoffs (top 15 % of degree distribution, start of RC regime, maximum of RC regime, top 33 % in at least four of five hubscores/nodal measures of centrality) resulted in a set of candidate hub. The final RC hubs were determined by testing if hub connections were more likely than expected at random in compliance with the RC definition (Colizza et al., 2006). (B) Density plots of the posterior distributions of node classifications according to Rich Club architecture with mean point estimate, 50 % and 95 % highest probability density areas marked. (C) Plots are arranged according to Condition. Density plots of the posterior distributions of node classifications according to Rich Club architecture with mean point estimate, 50 % and 95 % highest probability density areas marked. RC = Rich Club, BF = Bayes factor.

3.2.5. *Graph theoretical measures of network centrality*

In the resting-state model including all considered graph theoretical measures of centrality we detected a significantly positive effect of betweenness centrality as well as closeness centrality on the length of the timescales (Fig. 8B).

For the task-data, none of the effects of any graph measure in any experimental condition differed from zero. Comparing the conditions on the other hand revealed a significant increase of the effect of degree centrality on the ISC value between the Single and Triplet as well as an increase of the effect of the participation coefficient between the Nonet and Complete conditions (Fig. 8C).

3.2.6. *Cortical thickness*

Finally, modelling the effect of cortical thickness on the resting-state timescales revealed a significant increase of intrinsic cortical timescales with the average cortical thickness of an area (Fig. 9B).

Analyzing the ISC values, the two-sided hypothesis tests for the model using cortical thickness as the explanatory variable unveiled significant decreases of ISC values with the area's average cortical thickness in all conditions. In the comparison of the experimental conditions however we could not identify any increase in the influence of the cortical thickness on the ISC values between any of the tested conditions (Fig. 9C).

3.3. *Model comparison*

Additionally to the hypothesis tests, we compared the estimated models to find the organizational schemes that best explain the distribution of intrinsic timescales as well as ISC values across the cortex.

3.3.1. *Resting-state timescales*

Comparing the $elpd_{loo}$ (Vehtari et al., 2017) of the intrinsic cortical timescale models identified that modelling the uni-to-multimodal gradient using the overlap of each parcel with a multimodal area according to the Ji atlas (Ji et al., 2019) as an estimation of multimodality as the best fitting model (Table 1). Inspecting the differences in $elpd_{loo}$ showed that this model performed significantly better than the null model only containing the control variables as well as the models for the RC and DC architectures, as the difference was larger than one standard error (Mohor et al., 2021). All other models however did not perform significantly worse than the Ji atlas model (Fig. 10A).

3.3.2. *Inter-subject correlation values from task-fMRI data*

We also examined the $elpd_{loo}$ to compare the models of the ISC values across the four experimental conditions. The results revealed that modelling the uni-to-multimodal gradient using the Ji atlas (Ji et al., 2019) approach most accurately predicted the distribution of ISC values (Table 2). The $elpd_{loo}$ of this model was significantly larger compared with all other models. The second-best model was the posterior/lateral-to-anterior/medial gradient modelled via the MNI space coordinates which still fitted the data significantly better than the other organizational schemes. The model using the cortical thickness as an approximation for cytoarchitectural differences came in third and fitted the ISC values also significantly better than the models

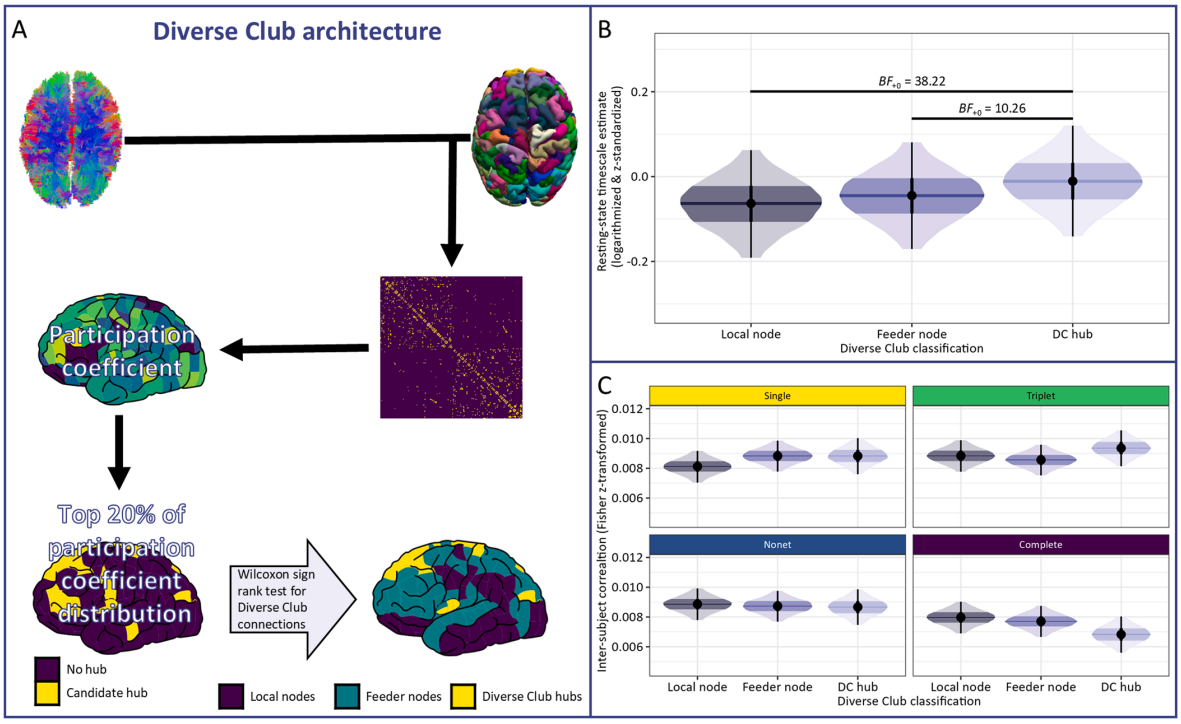


Fig. 5. Methods for extraction and results of intrinsic resting-state timescale and inter-subject correlation analyses for Diverse Club architecture.
Note. (A) Diverse Club (DC) identification was performed on individual binarized structural connectivity matrices with 219 cortical nodes according to the lausanne250 parcellation scheme (Cammoun et al., 2012). Using the top 20 % of the participation coefficient distribution resulted in a set of candidate hubs. The final DC hubs were determined by testing if hub connections were more likely than expected at random like in the Rich Club identification. (B) Density plots of the posterior distributions of node classifications according to Diverse Club architecture with mean point estimate, 50 % and 95 % highest probability density areas marked. (C) Plots are arranged according to Condition. Density plots of the posterior distributions of node classifications according to Diverse Club architecture with mean point estimate, 50 % and 95 % highest probability density areas marked. DC = Diverse Club, BF = Bayes factor.

representing the RC and DC architectures, the model including the graph theoretical measures of centrality as well as the null model. All other models did not significantly differ from the null model that contained no explanatory organizational scheme (Fig. 10B).

4. Discussion

Intrinsic timescales of the human brain may underly our capacity to process the complex temporal structure of our environment (Golesorkhi et al., 2021b; Wolff et al., 2022), but we do not know how they actually arise. In this paper we examined six different cortical organizational schemes and features of the cortical areas to investigate their role in shaping the cortical timescales at rest as well as during a task presenting stimuli of varying temporal persistence. The following discussion will highlight the key findings while also discussing the individual organization schemes more in depth.

4.1. The uni-to-multimodal gradient best explains the cortical chronotopy

The aim of this paper was to find the organizational scheme that best explains the chronotopy of the cortex. The Bayesian model comparison of all considered organizational schemes identified the uni-to-multimodal gradient modelled by the Ji atlas-based classification to be the best fitting model for both the resting-state timescales and the distribution of ISC values in the task-based fMRI data. This corroborates previous results finding the uni-to-multimodal gradient for the distribution of timescales (Gao et al., 2020; Golesorkhi et al., 2021a; Ito et al., 2020; Raut et al., 2020) as well as for TRWs (Farbood et al., 2015; Hasson et al., 2004, 2008; Lerner et al., 2011). A gradient from the primary sensory cortices to multimodal association cortices is a well-established concept in neuroscience (Huntenburg et al., 2018; Margulies et al., 2016; Mesulam, 1998; Sepulcre et al., 2012). Traversing from unimodal over supramodal to multimodal cortices (Zamora-López et al., 2011), the gradient's apex is assumed to be located within the limbic system (Chanes and Feldman Barrett, 2016; Margulies et al., 2016; Mesulam, 1998). In functional terms, the multimodal cortices are considered particularly important for the integration of information and for the retention and retrieval of past information (Murphy et al., 2019; Wang, 2020). Moreover, the activity of areas higher on the gradient is less stimulus-determined and relates more to abstract and domain-general processes (Taylor et al., 2015; Yeo et al., 2015), while it was proposed that these areas perform similar tasks among various domains (Goldman-Rakic, 1988). Besides the cortical timescales (e.g., Raut et al., 2020), many other, especially microarchitectural features like cortical thickness, neuron density (Burt et al., 2018; Wagstyl et al., 2015) and myelinization (Demirtaş et al., 2019; Huntenburg et al., 2017; Ito et al., 2020) as well as gene expression gradients (Burt et al., 2018; Hansen et al., 2021; Shafiei et al., 2020) were found to follow an uni-to-multimodal axis (for more information see Huntenburg et al., 2018; Markello et al., 2022; Sydnor et al., 2021).

Despite the consistency and comprehensiveness of previous findings, the question remains how exactly timescales are shaped along this gradient. Previous modelling work was able to establish, that timescales are driven by both local excitatory connections as well as by long-range connections of an area (Chaudhuri et al., 2015; Schmidt et al., 2016; for reviews see Cavanagh et al., 2020; Duarte et al., 2017). On the local

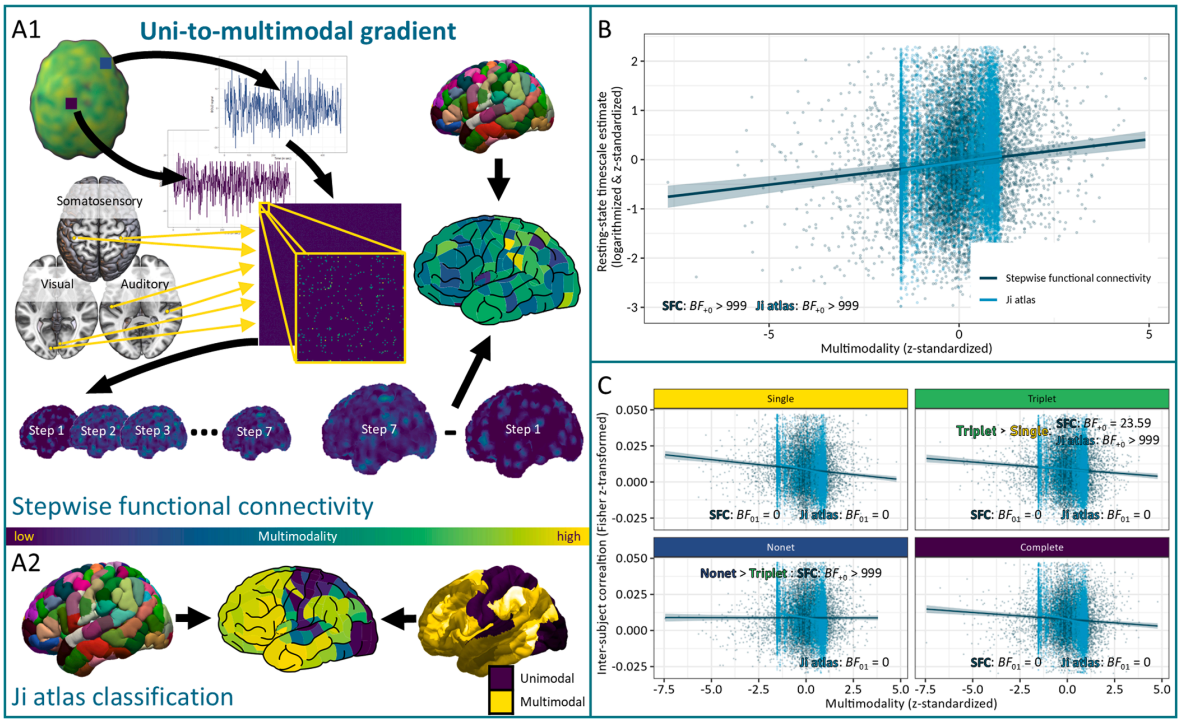


Fig. 6. Methods for extraction and results of intrinsic resting-state timescale and inter-subject correlation analyses for uni-to-multimodal gradient.
Note. Two approaches at modelling the uni-to-multimodal gradient as a constant measure of multimodality: (A1) First, stepwise functional connectivity follows network path through individual voxel-wise functional connectivity networks starting in seeds in the primary auditory, somatosensory and visual cortices. Paths converge in multimodal areas after seven link-steps. Individual uni-to-multimodal gradients were estimated by subtracting the stepwise functional connectivity values at first link-step from the values at the seventh link-step. Results were extracted using the lausanne250 parcellation scheme to model multimodality. (A2) Second, we considered the Ji atlas (Ji et al., 2019) based classification assorting cortex into uni- and multimodal areas. The overlap of classification in the Ji atlas and lausanne250 parcellation scheme was used as the second approach at modelling multimodality. (B) Fixed effect predictions of stepwise functional connectivity and Ji atlas approaches to model uni-to-multimodal gradient with 95 % credibility interval marked. (C) Plots are arranged according to Condition. Fixed effect predictions of stepwise functional connectivity and Ji atlas approaches to model uni-to-multimodal gradient with 95 % credibility interval marked. SFC = Stepwise functional connectivity, BF = Bayes factor.

scale, the ratio of excitatory pyramidal interneurons was found to increase with the cortical hierarchy (Torres-Gomez et al., 2020). These interconnected excitatory pyramidal cells in granular level III were also proposed to possess different ratios of neuronal receptors across the cortex (Cavanagh et al., 2020; Wang, 2001). Thereby, especially the density of glutaminergic NMDA receptors plays a crucial role for slower and maintained cortical dynamics of these pyramidal cells (Wang, 2001). Interestingly, the distribution of NMDA receptors was suggested to increase along the uni-to-multimodal gradient as well (Burt et al., 2018; Wang et al., 2012). Based on these findings, Wang (2020) concisely illustrated that the association cortices have more excitatory inter-neuronal connections as well as more input controlling inhibitory connections, while sensory cortices have more output-controlling connections. Similar to Gollo et al.'s (2015) proposal for RC architecture, this connectivity pattern enables the association cortices to produce slower intrinsic timescales while also having the ability of integrate information over longer periods of time. As these results clearly indicate the importance of the dynamics on the neuronal level, investigating the timescales on the microscale promises fruitful results to aid in the deeper understanding of the biological and connective mechanisms behind the temporal hierarchy of the cortex.

While we identified the Ji atlas approach as the best fitting model, we also examined the SFC approach to the uni-to-multimodal gradient. Using SFC, previous studies could show that paths starting from unimodal seed regions converge in multimodal areas after seven steps (Diez and Sepulcre, 2018; Pretus et al., 2019; Sepulcre, 2014; Sepulcre et al., 2012). To determine a gradient from the unimodal seeds to the multimodal cortices, we subtracted the initial SFC pattern at link-step one, which determines the unimodal areas, from the pattern at link-steps seven, which localizes the multimodal cortices. In contrast, the Ji atlas describes the classification of twelve functional networks based on neurobiological data, defining multimodality by these networks (Ji et al., 2019). Despite these considerable differences in approaching the concept of the uni-to-multimodal gradient, we were able to confirm the validity of both these methods by comparing the resulting uni-to-multimodal gradients with previously discovered gradients (see Supplemental Material 1; Margulies et al., 2016; Sydnor et al., 2021). Moreover, we also find largely coherent results between the two approaches. Both models predicted an increase of the intrinsic resting-state timescales with a higher multimodality and generally showed a decrease of ISC values with an increase in multimodality across the experimental conditions. Also, when exploring the relationship between the organizational schemes using the spin test approach (Alexander-Bloch et al., 2018) we found a significant correlation between the group average patterns of the two multimodality approaches. Therefore, the question remains as to why the SFC model did not perform as well as the Ji atlas approach in the model comparison. Based on the presented results, we speculate that there are still some methodological differences between the two approaches that could explain remaining divergences between the gradients. Firstly, for the SFC approach we determined

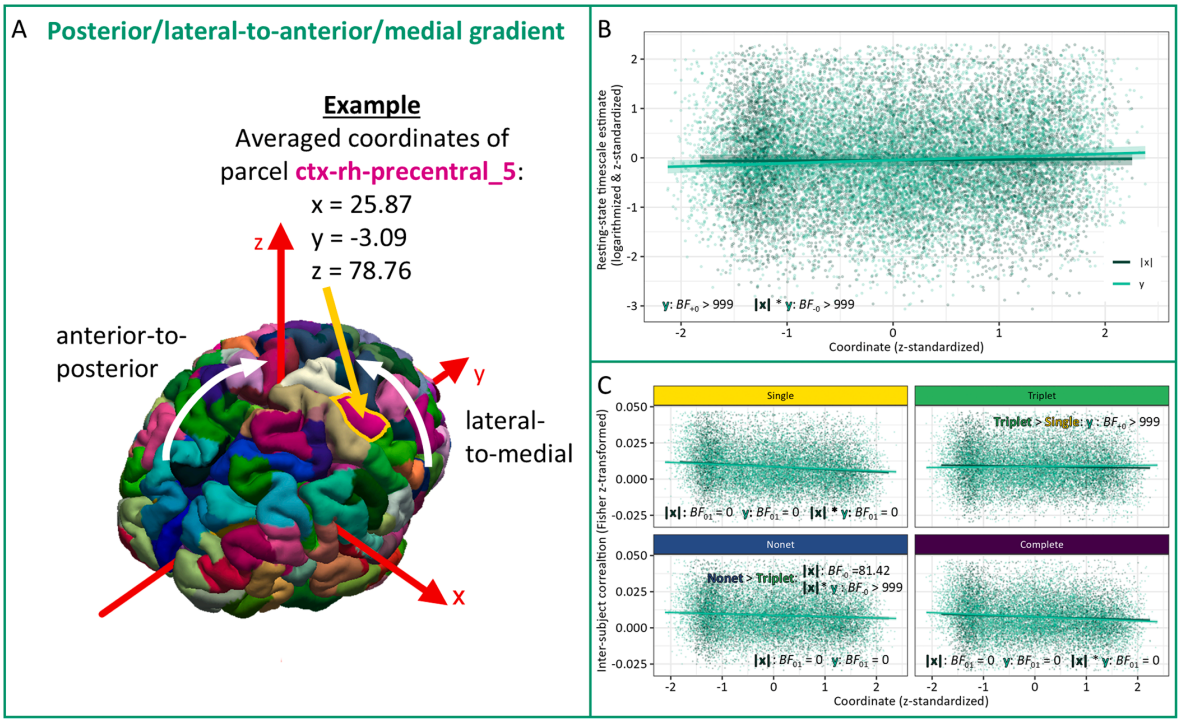


Fig. 7. Methods for extraction and results of intrinsic resting-state timescale and inter-subject correlation analyses for posterior/lateral-to-anterior/medial gradient. *Note*. (A) The lateral-to-medial and posterior-to-anterior gradients were modelled by using the averaged, individual *x*- and *y*-coordinates of each parcel, respectively. Absolute *x*-coordinates were used to model a lateral-to-medial rather than a left-to-right trend. (B) Fixed effect predictions of |*x*|- and *y*-coordinates to model lateral-to-medial and posterior-to-anterior gradients with 95 % credibility interval marked. (C) Plots are arranged according to Condition. Fixed effect predictions of |*x*|- and *y*-coordinates to model lateral-to-medial and posterior-to-anterior gradients with 95 % credibility interval marked. BF = Bayes factor.

multimodality values for each individual subject while the Ji atlas-based multimodality scores were the same for the entire group. The group-wise approach might have the advantage that global patterns of cortical organization are better revealed in group average networks (Hagmann et al., 2008). Secondly, the different spatial resolution of the two modelling approaches can be critical. The SFC approach requires the creation of downsampled voxel-wise connectivity matrices, which is a significant but computationally necessary limitation (Pretus et al., 2019). The Ji atlas on the other hand was originally based on state-of-the art parcellation of the data (Glasser et al., 2016). Thirdly, the definition of multimodality differs between the two approaches: Multimodal areas in the SFC approach describe the final step in the functional hierarchy (Sepulcre et al., 2012), while the Ji atlas-based classification defines all but the purely sensory networks as multimodal (Golesorkhi et al., 2021a; Ito et al., 2020). As the deployed task may not have been able to engage the apex of the processing hierarchy (as discussed in more detail in Section 4.3), the broader classification of multimodality in the Ji atlas-based gradient might have been more fitting especially to the distribution of ISC values.

On a different note, we only investigated two of many possible ways to define the uni-to-multimodal gradient. In validating the two here applied approaches we performed an additional analysis comparing the group-average uni-to-multimodal maps from the described analysis with two previously established gradients (see Supplemental Material S1). For this we used the gradients from Margulies et al. (2016), that are based on the decomposition of functional connectivity data into principal gradients, and Sydnor et al. (2021), who integrated multiple measures defining the gradient into one converging uni-to-multimodal map. We found that both our approaches to the uni-to-multimodal gradient significantly correlated with these two established gradients, that were previously also related to the chronotopy of the cortex (Fehring et al., 2024; Huntenburg et al., 2018). Therefore, the results not only validate the chosen approaches but further highlight the importance of the uni-to-multimodal gradient as a cortical organizational scheme. Beyond these four different approaches there is still a multitude of other functional and structural features can be used to define the uni-to-multimodal gradient (Sydnor et al., 2021). Thus, also the selection of six organizational schemes we investigated in this study only makes up a fraction of possible organizations. Moreover, we used Bayesian model comparison to find the best organizational scheme. While Bayesian model comparison in general allows for the comparison of non-nested models and thus is perfectly suited for comparing different theories or competing organizational schemes like in this paper (Geweke, 2007; Hollenbach and Montgomery, 2020; Rouder et al., 2018), model comparison is not able to detect the "true" model for the data. It is bound to the model space and will only identify the best fitting among the evaluated models (Alston et al., 2004). There could be a plethora of other organizational patterns and structures that could explain cortical timescales at various spatial scales (Betzel and Bassett, 2017; Hansen et al., 2022; Keller et al., 2023; Markello et al., 2022; Sydnor et al., 2021). Nevertheless, the consistency of our findings with previous investigations gives us confidence in the assessment that the uni-to-multimodal gradient best explains the chronotopy across the cortex at rest and during task.

4.2. *Resting-state timescales relate to all organizational schemes*

Our second major finding concerns the resting-state timescales. We

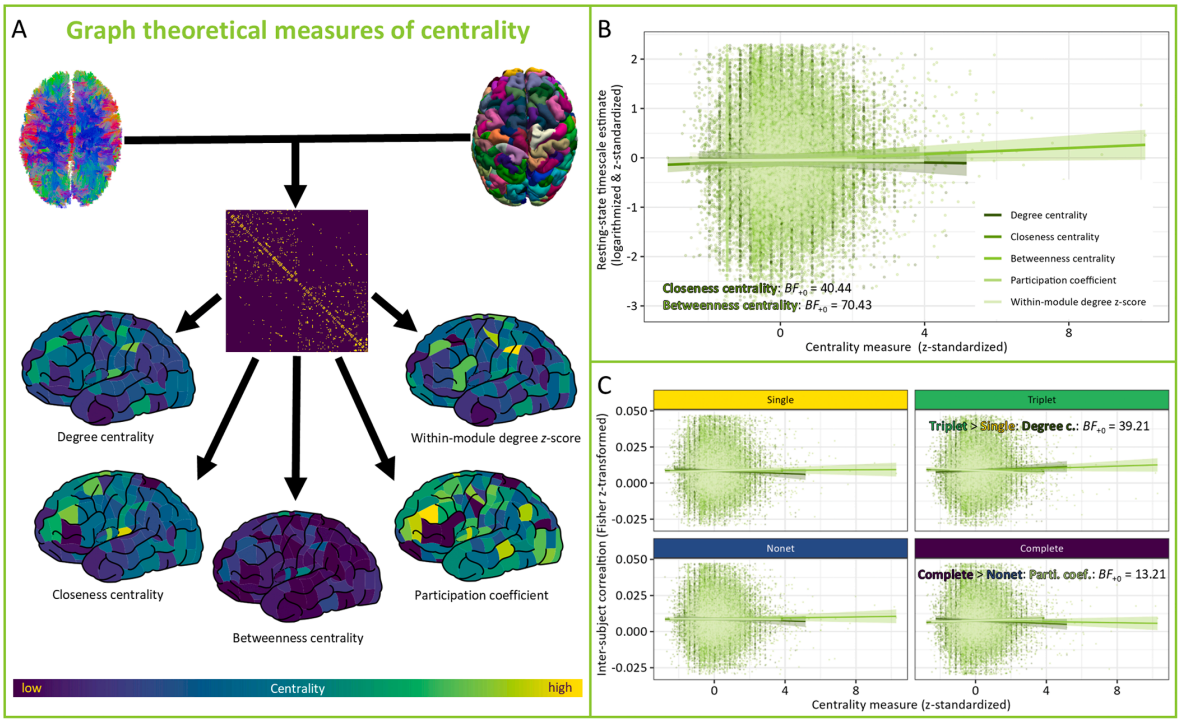


Fig. 8. Methods for extraction and results of intrinsic resting-state timescale and inter-subject correlation analyses for the graph theoretical measures of network centrality.
Note. (A) Individual nodal measures of centrality were calculated for each of the 219 nodes. We considered degree centrality, closeness centrality, betweenness centrality, participation coefficient and within-module degree *z*-score. (B) Fixed effect predictions of all investigated graph measures of centrality with 95 % credibility interval marked. (C) Plots are arranged according to Condition. Fixed effect predictions of all investigated graph measures of centrality with 95 % credibility interval marked. Degree c. = Degree centrality, Parti. coef. = Participation coefficient, BF = Bayes factor.

hypothesized for each organizational scheme that the resting-state timescales as estimated by the decay of the ACF (Raut et al., 2020) would increase, thus being slower, in hierarchically higher areas. Before discussing the individual organizational schemes, we can summarize that by and large we found this trend for all organizational schemes.

4.2.1. Rich Club architecture

Starting with the RC architecture, we discovered the resting-state timescales increase from Local nodes to Feeder nodes and RC hubs, while the timescales in Feeder nodes and RC hubs did not differ significantly. Thus, we could in large parts corroborate our hypothesis and replicate previous findings (Gollo et al., 2015; Senden et al., 2017). The non-significant differences between hubs and Feeder nodes could be caused by the synchronization of neighbouring nodes by the RC. As Gollo et al. (2015) described, the resonant network motifs that connect RC hubs with their direct neighbours are perfectly suited to accommodate such synchronization. Thus, our findings can be seen as further indication of this previously suggested synchronization (Aguilar-Velázquez and Guzmán-Vargas, 2019; Senden et al., 2014, 2017; Watanabe, 2013) .

4.2.2. Diverse Club architecture

For the DC architecture, our findings resembled those for the RC architecture and largely followed the predicted trends. DC hubs in comparison to both Local and Feeder nodes had slower intrinsic timescales. Additionally, we could find a non-significant trend for slower timescales in Feeder nodes compared with Local nodes. Thus, the results rather depict a slow increase in timescales from one level of node classification to the next. The synchronization between directly neighbouring nodes that was shown for the RC (Gollo et al., 2015) is not as prevalent in DC nodes. This finding corresponds to previous studies suggesting that the DC might be more involved in tasks rather than in synchronization (Bertolero et al., 2017; Keller et al., 2023). Thus, our resting-state results also slightly favor the RC architecture in explaining the cortical timescales in absence of a task, hinting at the importance of the RC for complex resting-state dynamics (Zamora-López et al., 2016).

4.2.3. Rich or Diverse Club?

The reported similarities between DC and RC architectures are likely caused by the similarity of the architectures in their classification of nodes. As our spin χ^2-test between the group-wise classifications indicated, the two architectures are highly dependent (Lee, 2016). Thus, naturally the question remains, what distinguishes RC and DC. In its initial proposal the DC was directly compared with the RC, but, in contrast to our results, no substantial overlap between DC and RC hubs was reported (Bertolero et al., 2017). Beyond that, it was suggested that the DC lays at a lower level in the cortical hierarchy than the RC (Keller et al., 2023). However, we used a refined identification of the RC hubs (Mecklenbrauck et al., 2024; Riedel et al., 2022) in this study that not only adheres closer to the original definition of RC (Colizza et al., 2006) but also uses multiple combined measures of the RC regime and centrality as previously recommended (van den Heuvel and Sporns, 2013a). This differed from the definition in Bertolero et al. (2017) that used a nodal strength cutoff. The overlap between DC and RC thereby will certainly also be influenced by the inclusion of the participation coefficient as well as other centrality measures that focus more on efficiency and communication (Hagmann et al., 2008; Jung et al., 2017) in our definition of RC. Furthermore, we also adjusted the classification of the

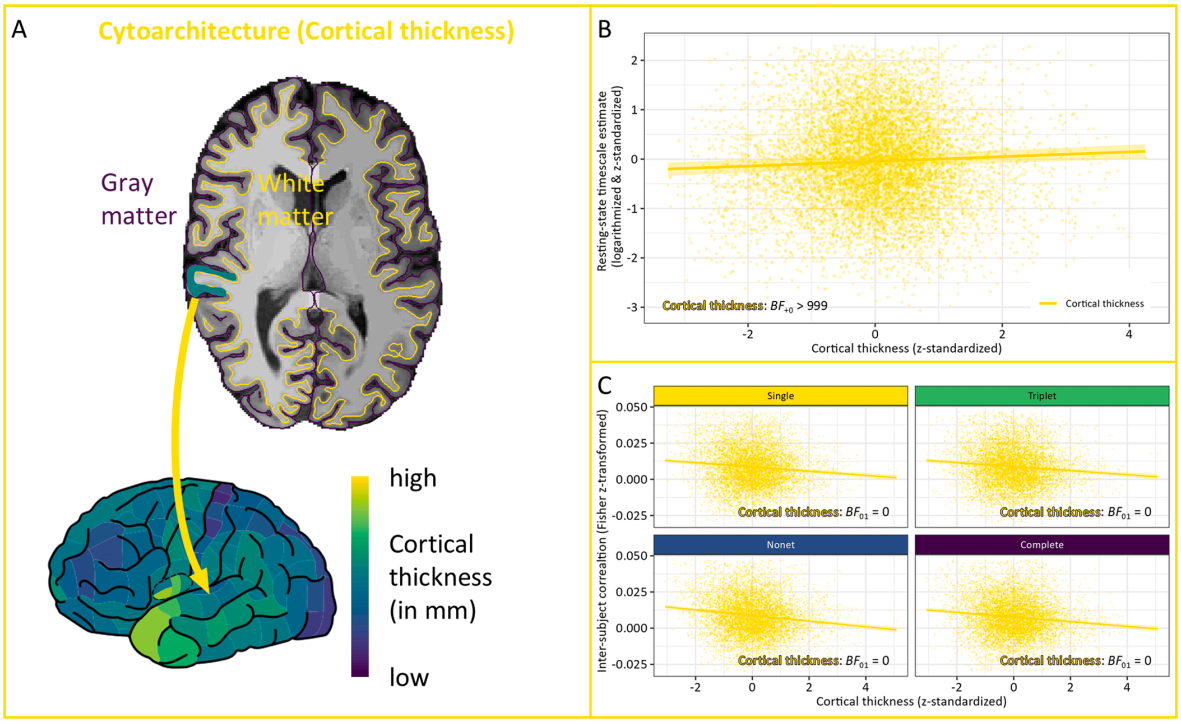


Fig. 9. Methods for extraction and results of intrinsic resting-state timescale and inter-subject correlation analyses for cortical thickness as an approximation of cytoarchitectural differences.
Note. (A) Cortical thickness can be used as an approximation for cytoarchitectural differences (Wagstyl et al., 2015). It was calculated as the average distance between the gray matter and white matter for each parcel (Goto et al., 2022). (B) Fixed effect prediction of cortical thickness as approximation of cytoarchitectural differences with 95 % credibility interval marked. (C) Plots are arranged according to Condition. Fixed effect prediction of cortical thickness as approximation of cytoarchitectural differences with 95 % credibility interval marked. BF = Bayes factor.

Table 1
Comparison of $\widehat{\text{elpd}}_{\text{loo}}$ of the models for the investigated organizational schemes in the intrinsic resting-state timescale analysis.

Organizational scheme	$\widehat{\text{elpd}}_{\text{loo}}$	$se(\widehat{\text{elpd}}_{\text{loo}})$	$\widehat{\text{elpd}}_{\text{diff}}$	$se\left(\widehat{\text{elpd}}_{\text{diff}}\right)$
Uni-to-multimodal gradient (Ji atlas)	−11789.63	69.01	0.00	0.00
Posterior/lateral-to-anterior/medial gradient	−11808.58	68.92	−18.95	10.77
Uni-to-multimodal gradient (SFC)	−11843.28	68.89	−53.65	13.93
Graph measures of centrality	−11852.35	68.84	−62.71	13.16
Cytoarchitecture (Cortical thickness)	−11854.55	68.84	−64.92	10.99
Rich Club architecture	−11866.26	68.82	−76.63	12.33
Null model/No scheme	−11866.79	68.79	−77.16	12.38
Diverse Club architecture	−11866.89	68.80	−77.26	12.36

Note. Models are considered to be better if the absolute elpd_{loo} difference is larger than one standard error (Mohor et al., 2021). $\widehat{\text{elpd}}_{\text{loo}}$ = expected log pointwise predictive density for a new dataset calculated using Pareto smoothed importance sampling leave-one-out-cross-validation (PSIS-LOO-CV), $\widehat{\text{elpd}}_{\text{diff}}$ = difference between the $\widehat{\text{elpd}}_{\text{loo}}$ of a model and the best performing model, *se* = standard error of the variable, SFC = Stepwise functional connectivity.

DC hubs according to the original definition of clubness (Colizza et al., 2006) but still based the identification of candidate hubs just on the participation coefficient, as proposed by Bertolero et al. (2017). However, the exclusive usage of the participation coefficient to identify hubs has recently been questioned as it could lead to misleading results if not carefully controlled (Oldham and Fornito, 2023). Nevertheless, the participation coefficient in general captures additional information about the centrality of a node other measures do not contain (Oldham et al., 2019). Recent results have even shown that RC and DC can capture complementary properties of the network (Lohia et al., 2024; Xue et al., 2020). Ultimately, more research and a revised and standardized definition of RC and especially DC are necessary to settle the debate between the RC and DC architectures.

4.2.4. *Uni-to-multimodal gradient*

As discussed in detail in Section 4.1, we used two approaches that

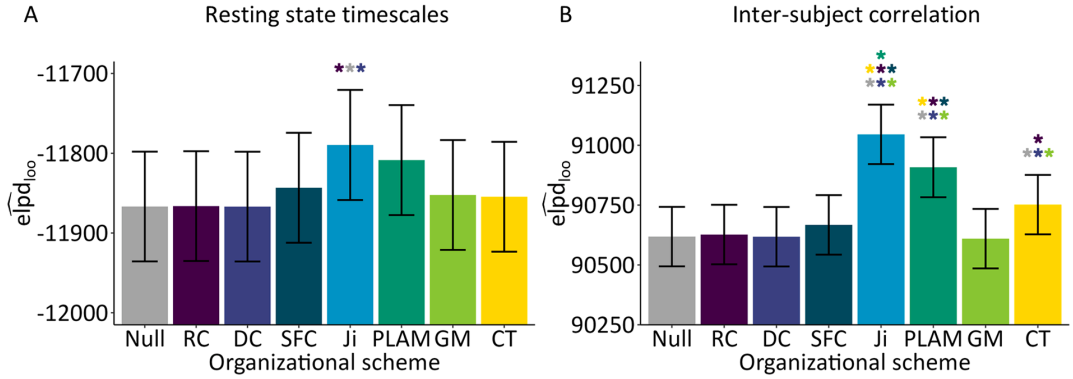


Fig. 10. Results of Bayesian model comparison.

Note. (A) Model comparison for resting-state timescale analysis. (B) Model comparison for Inter-subject correlation analysis. $\widehat{elpd}_{loo}$ = expected log pointwise predictive density for new dataset using Pareto smoothed importance sampling leave-one-out-cross-validation criterion; Null = Null model (no organizational scheme); RC = Rich Club architecture; DC = Diverse Club architecture; SFC = Uni-to-multimodal gradient (stepwise functional connectivity); Ji = Uni-to-multimodal gradient (Ji atlas classification); PLAM = Posterior/lateral-to-anterior/medial gradient; GM = Graph measures of centrality; CT = Cytoarchitecture (cortical thickness); * model has significantly higher $\widehat{elpd}_{loo}$ than models coded in respective color.

Table 2

Comparison of $\widehat{elpd}_{loo}$ of the models for the investigated organizational schemes in the inter-subject correlation analysis.

Organizational scheme	$\widehat{elpd}_{loo}$	$se(\widehat{elpd}_{loo})$	$\widehat{elpd}_{diff}$	$se(\widehat{elpd}_{diff})$
Uni-to-multimodal gradient (Ji atlas)	91045.48	124.18	0.00	0.00
Posterior/lateral-to-anterior/medial gradient	90908.07	125.30	−137.41	28.04
Cytoarchitecture (Cortical thickness)	90752.00	124.14	−293.48	25.85
Uni-to-multimodal gradient (SFC)	90667.29	124.37	−378.19	30.19
Rich Club architecture	90626.95	124.32	−418.53	30.00
Null model/No scheme	90618.35	124.25	−427.13	29.58
Diverse Club architecture	90617.87	124.27	−427.61	29.93
Graph measures of centrality	90609.78	124.28	−435.70	30.31

Note. Models are considered to be better if the absolute $elpd_{loo}$ difference is larger than one standard error (Mohor et al., 2021). $\widehat{elpd}_{loo}$ = expected log pointwise predictive density for a new dataset calculated using Pareto smoothed importance sampling leave-one-out-cross-validation (PSIS-LOO-CV), $\widehat{elpd}_{diff}$ = difference between the $\widehat{elpd}_{loo}$ of a model and the best performing model, *se* = standard error of the variable, SFC = Stepwise functional connectivity.

address the multimodality as a continuous measure very differently. The uni-to-multimodal gradient was firstly determined by the difference between the SFC pattern at the seventh and the first link-step and secondly by the multimodality percentage based on the overlap between the Ji atlas (Ji et al., 2019) and the applied lausanne250 parcellation (Cammoun et al., 2012). Even though we used two different continuous approaches in modelling multimodality we were able to replicate findings that used dichotomous classification of uni- and multimodal cortices (Golesorkhi et al., 2021a; Ito et al., 2020). Both modelling approaches produced the expected, similar results, predicting an increase of the resting-state timescales with the multimodality of an area.

4.2.5. *Posterior/lateral-to-anterior/medial gradient*

We found an increase of the resting-state timescales from posterior to anterior areas, mirroring the results observed for cortical peak frequencies (Mahjoory et al., 2020). Against our prediction, we were not able to find a general increase of timescales towards more medial regions. However, we did find the predicted significant interaction between the poster-to-anterior and lateral-to-medial trends, suggesting that the lateral-to-medial trend is specifically focused to the frontal lobe. Indeed, we included the posterior/lateral-to-anterior/medial gradient because it is a part of many classic theories of cortical control which mainly concern the frontal lobe (Badre and D'Esposito, 2009; Badre and Nee, 2018; Fuster, 2001; Ingvar, 1985; Koechlin and Summerfield, 2007). Notably, in their proposal of an additional medial trend Alexander and Brown (2018) also focused on the frontal lobe. Thus, it seems plausible that we found an interaction effect identifying slower timescales not more medial in general but especially when moving towards frontal areas of the brain. Based on these theoretical, but also structural and functional findings, there is considerable evidence that medial-frontal areas are involved in higher levels of cognitive processing (Alexander and Brown, 2018; Badre and Nee, 2018; Chanes and Feldman Barrett, 2016; Jobson et al., 2021).

4.2.6. *Graph measures of centrality*

Since previous studies reported the relationship between nodal measures of centrality and the chronotopy (Fallon et al., 2020; Lurie et al., 2024; Sethi et al., 2017) we also explored how the graph measures we used as hub scores in the RC identification (also see Mecklenbrauck et al., 2024; Riedel et al., 2022) faired in explaining the differences in resting-state timescales. We found significantly slower resting-state timescales with an increasing betweenness centrality and increasing closeness centrality as well as a non-significant positive trend between timescales and the participation coefficient of a node. Our results thus extend upon previous findings which reported on relationships for degree centrality (Fallon et al., 2020; Lurie et al., 2024; Sethi et al., 2017) as well as the participation coefficient and within module degree z-score (Lurie et al., 2024) but did not consider the betweenness and closeness centralities. Modelling all five measures together, we could however not replicate all these previous findings. One possible explanation for this is the high correlation between the measures of centrality (Oldham et al., 2019) we also showed in the spin test using the group average scores. Since we combined all fives measures into a single model, overlap in the proportions of explained variance could be a reason for replicating previous results. However, we examined all models for issues with multicollinearity and did not identify any violations (Wooldridge, 2013). Still, especially betweenness and closeness centrality describe similar concepts as both indicate nodes that are important for short paths in the network (Rubinov and Sporns, 2010) and characterize

important integrative hubs (Bassett et al., 2008; de Reus and van den Heuvel, 2013; Hagmann et al., 2008; Harriger et al., 2012; Jung et al., 2017; Sepulcre et al., 2010; Whitaker et al., 2016). Moreover, a recent study showed that both betweenness and closeness centrality negatively related to the complexity of the signal in task and at rest, which can be interpreted as a less diverse activity in these nodes (Neudorf et al., 2020), thus is comparable to the higher autocorrelation, i.e., slower timescales we found for both centrality measures. Hence, our results could also imply that highly integrative nodes display slower rhythms. Beyond that, there are many more centrality measures (Oldham et al., 2019) indicative of important nodes (i.e., Katz centrality; Fletcher and Wennekers, 2018). Thus, based on our and other previous results, future research might be inclined to explore more relationships between timescales and different centrality measures, especially since it was already shown for betweenness centrality that variation in centrality measures can be used as a biomarker (Bassett et al., 2008).

4.2.7. Cortical thickness

Lastly, we also explored the relationship between cytoarchitecture approximated by cortical thickness and the intrinsic timescales. Previous studies revealed that areas higher up the cortical hierarchy have a less laminar pattern but a higher cortical thickness (Chanes and Feldman Barrett, 2016; Saberi et al., 2023; Wagstyl et al., 2015). Accordingly, we found that the resting-state timescales increased with a higher cortical thickness, replicating previous findings (Gao et al., 2020). It should be noted that the detected relation of the cortical thickness and the cortical chronotopy strongly depends on the selected parcellation scheme of the cortex, as the cytoarchitectural differences do not follow gyral and sulcal boarders (Amunts et al., 2007). This is critical since the applied parcellation scheme, lausanne250, is based on the structural margins of the Desikan-Killiany atlas (Cammoun et al., 2012; Desikan et al., 2006). Thus, a future deeper investigation of the relation between cytoarchitecture and the temporal scales of the cortex will require a parcellation based on the cortical microstructure (e.g., Amunts et al., 2020).

4.2.8. Summary of resting-state timescale results

To summarize, we found evidence for the relationship of different organizational schemes and structural features with the intrinsic cortical timescales as estimated by the decay of the ACF (Raut et al., 2020). Since we could corroborate nearly all our hypotheses for the resting-state analysis and replicated many previous findings, the question remains how distinct the investigated organizational schemes are. While we explored the relationships amongst the organizational schemes using spin tests (Alexander-Bloch et al., 2018) and found significant relationships between the RC and DC architectures and expectedly between the two approaches to the uni-to-multimodal gradient and the different centrality measures, previous studies revealed additional, significant coherence between several of the here examined features. For instance, a higher cortical thickness was previously related to multimodal cortices (Burt et al., 2018; Wagstyl et al., 2015) and RC hubs (Scholtens et al., 2014; van den Heuvel et al., 2015). Just based on their definitions, multimodal cortices and RC hubs describe largely overlapping concepts (van den Heuvel and Sporns, 2013b; Zamora-López et al., 2011) as both organizational patters are proposed to integrate information across different functional networks (Chaudhuri et al., 2015; van den Heuvel and Sporns, 2013b, 2013a; Yeo et al., 2015; Zamora-López et al., 2009, 2010). Therefore, it comes to no surprise that the uni-to-multimodality gradient and the RC architecture are used rather synonymously (e.g., Golesorkhi et al., 2021a; Ji et al., 2019; Murphy et al., 2019). These two patterns thus could describe a functional and a structural view on the same question. Possible remaining differences between them could relate to the decoupling of functional and structural features in higher cortical areas (Liu et al., 2023; Preti and Van De Ville, 2019; Vázquez-Rodríguez et al., 2019). Furthermore, the RC also is mainly found within midline areas (van den Heuvel and Sporns, 2011) which could explain an overlap with the spatial posterior/lateral-to-anterior/medial gradient, even though RC hubs are usually found in both frontal and parietal areas (e.g., Mecklenbrauck et al., 2024; Riedel et al., 2022).

To conclude, while we did not find a complete overlap between the investigated organizational schemes, they are certainly not independent of each other. Thus, a promising future avenue could focus on the integration of multiple descriptions of cortical hierarchy into a single gradient or classification index across imaging modalities and methods. Recent studies provide positive preliminary evidence for this approach (Hansen et al., 2022; Shafiei et al., 2023; Sydnor et al., 2021).

4.3. Task effects

We hypothesized that areas higher in the cortical hierarchy should demonstrate larger ISC values in conditions that contain hierarchically higher, temporally more persistent structures in the stimuli, as these areas with longer TRWs should be engaged specifically by more persistent stimuli (e.g., Hasson et al., 2004). We found that the ISC values in all four experimental conditions (Single, Triplet, Nonet and Complete) reduced with higher multimodality in the Ji atlas-based model and in all but the Nonet condition in the SFC-based model. Also, for thicker areas in the cortical thickness model the ISC values decreased, which is further indication for the relationship between these two organizational schemes (Burt et al., 2018; Wagstyl et al., 2015). This decrease of ISC towards hierarchically higher areas can be explained by the less stimulus-determined processes (Ren et al., 2017; Schmälzle et al., 2017) and more diverse functions in these regions (Cui et al., 2020). When comparing the effects between experimental conditions we found the predicted increase in the effect of multimodality on the ISC values between the Single and Triplet condition for both approaches of the uni-to-multimodal gradient as well as between the Nonet and Triplet conditions for just the SFC model. Similarly, the posterior-to-anterior gradient was significantly more pronounced in the Triplet condition compared to the Single condition. The lateral-to-medial gradient as well as the interaction of the posterior-to-anterior and lateral-to-medial gradients however were more pronounced in the Nonet as compared to the Triplet condition. This could imply the additional engagement of higher order areas in in medial and especially anterior-medial cortex, thus providing evidence for the tuning of higher order areas being to temporally more persistent structures in the stimulus (e.g., Aberbach-Goodman and Mukamel, 2023; Farbood et al., 2015; Hasson et al., 2015; Lerner et al., 2011). These results also match our previous findings of a posterior-to-anterior trend for processing hierarchically higher levels of the stimulus (Mecklenbrauck et al., 2024). Additionally, the Triplet compared to the Single condition exhibited a larger effect of degree centrality on the ISC values. Further, the effect of the participation coefficient was larger in the Complete compared to the Nonet condition. These two findings might conform to previous findings showing that highly connected nodes are essential for integrating stimuli (Fallon et al., 2020) while especially diverse nodes that connect between different modules of the network are more involved in integrative tasks (Bertolero et al., 2017; Keller et al., 2023; Lurie et al., 2024). However, looking at the credibility intervals of the effects across models revealed that specifically the Triplet condition behaved distinctly from all the other experimental conditions, even though the four conditions were incrementally nested. This inconsistency demands caution with the presented interpretations.

Beyond that, the applied paradigm might have restrained our ability to identify consistent task results across the organizational schemes: Firstly, the ISC values that were calculated based on task data using the hierarchically nested but abstract digit sequences were much lower than in paradigms using more complex, naturalistic stimuli (e.g., Schmälzle et al., 2017). Controllable, abstract stimuli are the standard in neuroscience (Rust and Movshon, 2005). However, the choice of control over ecological validity might have limited a reliable and widespread activation in multimodal areas (Hasson et al., 2010; Sonkusare et al., 2019).

Secondly, in deviation to other ISC studies (e.g., Lerner et al., 2011) we included a task in our paradigm. Hierarchically nested sequences of stimuli can be chunked into bigger units to make full use of working memory capacity (Mathy and Feldman, 2012). Chunking however requires attention to the stimulus to provoke a global activation of hierarchically higher cortical areas (Dehaene et al., 2015; Mashour et al., 2020). The addition of a visual task might have prevented the necessary attention to the sequence, thus impeding the ignition of higher order areas (Bekinschtein et al., 2009). Finding correlations across participants could then have been further restricted by the more diverse activity in these higher order areas (Cui et al., 2020; Ren et al., 2017; Schmälzle et al., 2017).

4.4. Limitations

In addition to the task paradigm, there are a few other limitations to consider. As stated above, the relation between the chronotopy of the cortex and its features is dependent of the applied parcellation scheme (Amunts et al., 2007). Previous studies further found that the choice of parcellation scheme has a large effect on the appearance of cortical network as a whole (Bassett et al., 2011; Bryce et al., 2021; Cammoun et al., 2012; Qi et al., 2015; Seguin et al., 2020; Sporns, 2011). As most of the investigated organizational schemes were derived from structural and functional networks, our choice for the Lausanne parcellation scheme with 219 cortical parcels certainly had an impact on the results. We specifically selected this parcellation scheme since it was the most reliable (Cammoun et al., 2012) and neuroanatomically valid (Amunts and Zilles, 2015) parcellation scheme of the ones available in the CATO toolbox (de Lange et al., 2023) we applied for network reconstruction. However, the Lausanne parcellation scheme is not without its limitations. Firstly, as a sub-parcellation of the Desikan-Killiany atlas (Desikan et al., 2006) it follows gyral and sulcal boundaries, which not all features adhere to (Amunts et al., 2007). Secondly, the sub-parcellation was done by dividing each original parcel in a set of equally sized smaller parcels to achieve a voxel-level resolution. This procedure is rather arbitrary, and its anatomical validity is questionable (Qi et al., 2015). There is a multitude of possible parcellations of the human brain (Eickhoff et al., 2018) making use of only anatomical (Desikan et al., 2006; Destrieux et al., 2010; Tzourio-Mazoyer et al., 2002) or only functional guidelines (Craddock et al., 2012; Gordon et al., 2016; Schaefer et al., 2018; Shen et al., 2013) or also combining multiple sources of data (Fan et al., 2016; Glasser et al., 2016). Finding the appropriate parcellation scheme might be more dependent on the research question (Schaefer et al., 2018). Faced with this arbitrariness, it can be a common approach to compare the results across different parcellation schemes (e.g., Riedel et al., 2022). We have not included this option in the scope of this paper, which is a limitation. However, the consistency of our main finding that the uni-to-multimodal gradient shapes the cortical chronotopy with previous studies using various other parcellation schemes (Gao et al., 2020; Golesorkhi et al., 2021a; Ito et al., 2020; Raut et al., 2020) gives us sufficient confidence in this result.

We also have to mention the data quality of the DWI data, that did not follow current recommendations (Jones et al., 2013). Consequently, we had to exclude subcortical areas from the analysis, even though the cortical hierarchy was found to extend also to the subcortex (Alexander et al., 1986; Badre and Nee, 2018; Siegle et al., 2021). Recent studies even found a variation of timescales in subcortical areas that mirror that of the cortex (Raut et al., 2020) and indicated that the thalamus plays a crucial role in shaping functional dynamics (Harris et al., 2019; Müller et al., 2020; Shine et al., 2019). However, despite using a combined DTI and GQI algorithm that performed the best in distinguishing crossing and kissing fibres (de Lange et al., 2023), the available data would have limited the interpretability of results from the subcortex (Kai et al., 2022). The limited data quality also led to our decision to binarize the structural connectivity matrices since weighted connectivity measure might be biased (Calamante, 2019; Fornito et al., 2016). Given an improved data quality, future research could therefore make use of the entire variability of weighted network measures (Fornito et al., 2016) and also consider the previously found role of the subcortex in processing hierarchically nested stimuli (Graybiel, 2008).

5. Conclusion

To conclude, we investigated the effect of six cortical organizational schemes and features on the intrinsic resting-state timescales and the ISC values from a task that presented participants with a hierarchically nested stimulus sequence of increasing temporal persistency. In both cases, the uni-to-multimodal gradient, as determined by an atlas classification, proved to be the best fitting model. In addition, we provide further evidence for the relationship between the intrinsic timescales and the functional hierarchy of the cortex, the network structure of the human connectome as well as cytoarchitectural properties of an area, corroborating previous results. Future studies investigating the brain's microstructural organization are needed to gain deeper insights into how exactly the uni-to-multimodal gradient shapes the cortex's chronotopy and how different organizational schemes interrelate.

Ethics statement

This study was conducted in accordance with the Declaration of Helsinki and approved by the Local Ethics Committee of the University of Münster. Participants signed an informed consent before participation.

Funding

The authors received no specific funding for this work.

CRediT authorship contribution statement

Falko Mecklenbrauck: Writing – review & editing, Writing – original draft, Visualization, Software, Project administration, Methodology, Investigation, Formal analysis, Data curation, Conceptualization. **Jorge Sepulcre:** Software, Methodology. **Jana Fehring:** Writing – review & editing, Software, Methodology. **Ricarda I. Schubotz:** Writing – review & editing, Writing – original draft, Supervision, Resources, Project administration, Methodology, Funding acquisition.

Declaration of competing interest

The authors declare that they have no conflict of interest.

Acknowledgement

The authors thank Monika Mertens and Lena M. Puder for their help during data collection, Lena M. Puder, Simon Wieczorek, and Maria L. Hofmann for help in the quality control process, Kristin Stroop and Simon Wieczorek for help in testing the paradigm, and Sophie Siestrup for helpful comments on the manuscript.

Supplementary materials

Supplementary material associated with this article can be found, in the online version, at doi:10.1016/j.neuroimage.2024.120914.

Data availability

All code, one exemplary, minimally processed participant and data sets to replicate the main analyses are available at https://github.com/FalkMeck/Decoding_Cortical_Chronotopy.git

References

Aberbach-Goodman, S., Mukamel, R., 2023. Temporal hierarchy of observed goal-directed actions. Sci. Rep. 13 (1), 1–13. https://doi.org/10.1038/s41598-023-46917-z.

Agcaoglu, O., Wilson, T.W., Wang, Y.P., Stephen, J., Calhoun, V.D., 2019. Resting state connectivity differences in eyes open versus eyes closed conditions. Hum. Brain Mapp. 40 (8), 2488–2498. https://doi.org/10.1002/hbm.24539.

Aguilar-Velázquez, D., Guzmán-Vargas, L., 2019. Critical synchronization and 1/f noise in inhibitory/excitatory rich-club neural networks. Sci. Rep. 9 (1), 1–13. https://doi.org/10.1038/s41598-018-37920-w.

Aguirre, G.K., Mattar, M.G., Magis-Weinberg, L., 2011. De Bruijn cycles for neural decoding. Neuroimage 56 (3), 1293–1300. https://doi.org/10.1016/j.neuroimage.2011.02.005.

Alexander, G.E., DeLong, M.R., Strick, P.L., 1986. Parallel organization of functionally segregated circuits linking basal ganglia and cortex. Annu. Rev. Neurosci. 9, 357–381. https://doi.org/10.1146/annurev.ne.09.030186.002041.

Alexander, W.H., Brown, J.W., 2018. Frontal cortex function as derived from hierarchical predictive coding. Sci. Rep. 8 (1), 1–11. https://doi.org/10.1038/s41598-018-21407-9.

Alexander-Bloch, A.F., Shou, H., Liu, S., Satterthwaite, T.D., Glahn, D.C., Shinohara, R.T., Vandekar, S.N., Raznahan, A., 2018. On testing for spatial correspondence between maps of human brain structure and function. Neuroimage 178 (February), 540–551. https://doi.org/10.1016/j.neuroimage.2018.05.070.

Alston, C., Kuhnert, P., Low Choy, S., Mcvinish, R., Mengersen, K., Choy, S.L., Mcvinish, R., Mengersen, K., 2004. Bayesian model comparison: review and discussion. In: ISI 2005: the 55th Session of the International Statistical Institute, Sydney, 2005, pp. 1–4. http://iase-web.org/documents/papers/isi55/Alston-Kuhnert-Low_Choy-McVinish-Mengersen.pdf.

Amunts, K., Mohlberg, H., Bludau, S., Zilles, K., 2020. Julich-brain: a 3D probabilistic atlas of the human brain's cytoarchitecture. Science 369 (6506), 988–992. https://doi.org/10.1126/science.abb4588.

Amunts, K., Schleicher, A., Zilles, K., 2007. Cytoarchitecture of the cerebral cortex-more than localization. Neuroimage 37 (4), 1061–1065. https://doi.org/10.1016/j.neuroimage.2007.02.037.

Amunts, K., Zilles, K., 2015. Architectonic mapping of the human brain beyond brodmann. Neuron 88 (6), 1086–1107. https://doi.org/10.1016/j.neuron.2015.12.001.

Andersson, J.L.R., Skare, S., Ashburner, J., 2003. How to correct susceptibility distortions in spin-echo echo-planar images: application to diffusion tensor imaging. Neuroimage 20 (2), 870–888. https://doi.org/10.1016/S1053-8119(03)00336-7.

Andersson, J.L.R., Sotiropoulos, S.N., 2016. An integrated approach to correction for off-resonance effects and subject movement in diffusion MR imaging. Neuroimage 125, 1063–1078. https://doi.org/10.1016/j.neuroimage.2015.10.019.

Badre, D., D'Esposito, M., 2009. Is the rostro-caudal axis of the frontal lobe hierarchical? Nat. Rev. Neurosci. 10 (9), 659–669. https://doi.org/10.1038/nrn2667.

Badre, D., Nee, D.E., 2018. Frontal cortex and the hierarchical control of behavior. Trends Cogn. Sci. 22 (2), 170–188. https://doi.org/10.1016/j.tics.2017.11.005. Elsevier Ltd.

Baldassano, C., Chen, J., Zadbood, A., Pillow, J.W., Hasson, U., Norman, K.A., 2017. Discovering event structure in continuous narrative perception and memory. Neuron 95 (3), 709–721.e5. https://doi.org/10.1016/j.neuron.2017.06.041.

Bassett, D.S., Brown, J.A., Deshpande, V., Carlson, J.M., Grafton, S.T., 2011. Conserved and variable architecture of human white matter connectivity. Neuroimage 54 (2), 1262–1279. https://doi.org/10.1016/j.neuroimage.2010.09.006.

Bassett, D.S., Bullmore, E., Verchinski, B.A., Mattay, V.S., Weinberger, D.R., Meyer-Lindenberg, A., 2008. Hierarchical organization of human cortical networks in health and schizophrenia. J. Neurosci. 28 (37), 9239–9248. https://doi.org/10.1523/JNEUROSCI.1929-08.2008.

Behzadi, Y., Restom, K., Liau, J., Liu, T.T., 2007. A component based noise correction method (CompCor) for BOLD and perfusion based fMRI. Neuroimage 37 (1), 90–101. https://doi.org/10.1016/j.neuroimage.2007.04.042.

Bekinschtein, T.A., Dehaene, S., Rohaut, B., Tadel, F., Cohen, L., Naccache, L., 2009. Neural signature of the conscious processing of auditory regularities. Proc. Natl. Acad. Sci. USA 106 (5), 1672–1677. https://doi.org/10.1073/pnas.0809667106.

Benjamini, Y., Hochberg, Y., 1995. Controlling the false discovery rate : a practical and powerful approach to multiple testing. *J. R. Stat. Soc.* Ser. B (Methodological) 57 (1), 289–300.

Bertolero, M.A., Yeo, B.T.T., D'Esposito, M., 2017. The diverse club. Nat. Commun. 8 (1), 1–10. https://doi.org/10.1038/s41467-017-01189-w.

Betzel, R.F., Bassett, D.S., 2017. Multi-scale brain networks. Neuroimage 160 (November 2016), 73–83. https://doi.org/10.1016/j.neuroimage.2016.11.006.

Blondel, V.D., Guillaume, J.L., Lambiotte, R., Lefebvre, E., 2008. Fast unfolding of communities in large networks. J. Stat. Mech. 2008 (10), 1–12. https://doi.org/10.1088/1742-5468/2008/10/P10008.

Bond, C.F., Richardson, K., 2004. Seeing the Fisher Z-transformation. Psychometrika 69 (2), 291–303. https://doi.org/10.1007/BF02295945.

Brimijoin, W.O., O'Neill, W.E., 2010. Patterned tone sequences reveal non-linear interactions in auditory spectrotemporal receptive fields in the inferior colliculus. Hear. Res. 267 (1–2), 96–110. https://doi.org/10.1016/j.heares.2010.04.005.

Brown, J.A., Terashima, K.H., Burggren, A.C., Ercoli, L.M., Miller, K.J., Small, G.W., Bookheimer, S.Y., 2011. Brain network local interconnectivity loss in aging APOE-4 allele carriers. Proc. Natl. Acad. Sci. USA 108 (51), 20760–20765. https://doi.org/10.1073/pnas.1109038108.

Bryce, N.V., Flournoy, J.C., Guassi Moreira, J.F., Rosen, M.L., Sambook, K.A., Mair, P., McLaughlin, K.A., 2021. Brain parcellation selection: an overlooked decision point with meaningful effects on individual differences in resting-state functional connectivity. Neuroimage 243 (March), 118487. https://doi.org/10.1016/j.neuroimage.2021.118487.

Brysbaert, M., 1995. Arabic number reading: on the nature of the numerical scale and the origin of phonological recoding. J. Exp. Psychol. 124 (4), 434–452. https://doi.org/10.1037/0096-3445.124.4.434.

Bueichekú, E., Aznárez-Sanado, M., Diez, I., Uquillas, F.d.O., Ortiz-Terán, L., Qureshi, A. Y., Suñol, M., Basaia, S., Ortiz-Terán, E., Pastor, M.A., Sepulcre, J., 2020. Central neurogenetic signatures of the visuomotor integration system. Proc. Natl. Acad. Sci. USA 117 (12), 6836–6843. https://doi.org/10.1073/pnas.1912429117.

Bürkner, P.C., 2017. brms: An R package for Bayesian multilevel models using Stan. J. Stat. Softw. 80 (1). https://doi.org/10.18637/jss.v080.i01.

Bürkner, P.C. (2018). *Is the evidence ratio for a one sided hypothesis equivalent to a one sided bayes factor?* https://github.com/paul-buerkner/brms/issues/311.

Burt, J.B., Demirtaş, M., Eckner, W.J., Navejar, N.M., Ji, J.L., Martin, W.J., Bernacchia, A., Anticevic, A., Murray, J.D., 2018. Hierarchy of transcriptomic specialization across human cortex captured by structural neuroimaging topography. Nat. Neurosci. 21 (9), 1251–1259. https://doi.org/10.1038/s41593-018-0195-0.

Buxton, R.B., 2009. Introduction to Functional Magnetic Resonance Imaging. Cambridge University Press. https://doi.org/10.1017/CBO9780511605505.

Caballero-Gaudes, C., Reynolds, R.C., 2017. Methods for cleaning the BOLD fMRI signal. Neuroimage 154 (December 2016), 128–149. https://doi.org/10.1016/j.neuroimage.2016.12.018.

Calamante, F., 2019. The seven deadly sins of measuring brain structural connectivity using diffusion MRI streamlines fibre-tracking. Diagnostics 9 (3). https://doi.org/10.3390/diagnostics9030115.

Cammoun, L., Gigandet, X., Meskaldji, D., Thiran, J.P., Sporns, O., Do, K.Q., Maeder, P., Meuli, R., Hagmann, P., 2012. Mapping the human connectome at multiple scales with diffusion spectrum MRI. J. Neurosci. Methods 203 (2), 386–397. https://doi.org/10.1016/j.jneumeth.2011.09.031.

Cavanagh, S.E., Hunt, L.T., Kennerley, S.W., 2020. A diversity of intrinsic timescales underlie neural computations. Front. Neural Circuits 14 (December), 1–18. https://doi.org/10.3389/fncir.2020.615626.

Chanes, L., Feldman Barrett, L., 2016. Redefining the role of limbic areas in cortical processing. Trends Cogn. Sci. 20 (2), 96–106. https://doi.org/10.1016/j.tics.2015.11.005.

Chang, L.-C., Jones, D.K., Pierpaoli, C., 2005. RESTORE: robust estimation of tensors by outlier rejection. Magn. Reson. Med. 53 (5), 1088–1095. https://doi.org/10.1002/mrm.20426.

Chang, L.-C., Walker, L., Pierpaoli, C., 2012. Informed RESTORE: a method for robust estimation of diffusion tensor from low redundancy datasets in the presence of physiological noise artifacts. Magn. Reson. Med. 68 (5), 1654–1663. https://doi.org/10.1002/mrm.24173.

Chaudhuri, R., Knoblauch, K., Gariel, M.A., Kennedy, H., Wang, X.J., 2015. A large-scale circuit mechanism for hierarchical dynamical processing in the primate cortex. Neuron 88 (2), 419–431. https://doi.org/10.1016/j.neuron.2015.09.008.

Chen, J., Hasson, U., Honey, C.J., 2015. Processing timescales as an organizing principle for primate cortex. Neuron 88 (2), 244–246. https://doi.org/10.1016/j.neuron.2015.10.010.

Ciric, R., Wolf, D.H., Power, J.D., Roalf, D.R., Baum, G.L., Ruparel, K., Shinohara, R.T., Elliott, M.A., Eickhoff, S.B., Davatzikos, C., Gur, R.C., Gur, R.E., Bassett, D.S., Satterthwaite, T.D., 2017. Benchmarking of participant-level confound regression strategies for the control of motion artifact in studies of functional connectivity. Neuroimage 154 (March), 174–187. https://doi.org/10.1016/j.neuroimage.2017.03.020.

Colizza, V., Flammini, A., Serrano, M.A., Vespignani, A., 2006. Detecting rich-club ordering in complex networks. Nat. Phys. 2 (2), 110–115. https://doi.org/10.1038/nphys209.

Corbin, N., Todd, N., Friston, K.J., Callaghan, M.F., 2018. Accurate modeling of temporal correlations in rapidly sampled fMRI time series. Hum. Brain Mapp. 39 (10), 3884–3897. https://doi.org/10.1002/hbm.24218.

Craddock, R.C., James, G.A., Holtzheimer, P.E., Hu, X.P., Mayberg, H.S., 2012. A whole brain fMRI atlas generated via spatially constrained spectral clustering. Hum. Brain Mapp. 33 (8), 1914–1928. https://doi.org/10.1002/hbm.21333.

Cui, Z., Li, H., Xia, C.H., Larsen, B., Adebimpe, A., Baum, G.L., Cieslak, M., Gur, R.E., Gur, R.C., Moore, T.M., Oathes, D.J., Alexander-Bloch, A.F., Raznahan, A., Roalf, D. R., Shinohara, R.T., Wolf, D.H., Davatzikos, C., Bassett, D.S., Fair, D.A., Satterthwaite, T.D., 2020. Individual variation in functional topography of association networks in youth. Neuron 106 (2), 340–353.e8. https://doi.org/10.1016/j.neuron.2020.01.029.

Cullen, A.C., Frey, H.C., 1999. Probabilistic Techniques in Exposure Assessment: A Handbook for Dealing with Variability and Uncertainty in Models and Inputs. Springer Science & Business.

Dale, A.M., Fischl, B., Sereno, M.I., 1999. Cortical surface-based analysis. Neuroimage 9 (2), 179–194. https://doi.org/10.1006/nimg.1998.0395.

de Bruijn, G.N., 1946. A combinatorial problem. Proc. Koninklijke Nederlandse Acad. van Wetenschappen 49, 758–764. http://ci.nii.ac.jp/naid/10019660672/en/.

de Lange, S.C., Helwegen, K., van den Heuvel, M.P., 2023. Structural and functional connectivity reconstruction with CATO—A connectivity analysis TOolbox. Neuroimage 273 (April), 120108. https://doi.org/10.1016/j.neuroimage.2023.120108.

de Reus, M.A., van den Heuvel, M.P., 2013. Rich club organization and intermodule communication in the cat connectome. J. Neurosci. 33 (32), 12929–12939. https://doi.org/10.1523/jneurosci.1448-13.2013.

Dehaene, S., 2001. Précis of the number sense. Mind Lang. 16 (1), 16–36. https://doi.org/10.1111/1468-0017.00154.

Dehaene, S., Meyniel, F., Wacongne, C., Wang, L., Pallier, C., 2015. The neural representation of sequences: from transition probabilities to algebraic patterns and linguistic trees. Neuron 88 (1), 2–19. https://doi.org/10.1016/j.neuron.2015.09.019.

Demirtaş, M., Burt, J.B., Helmer, M., Ji, J.L., Adkinson, B.D., Glasser, M.F., Van Essen, D. C., Sotiropoulos, S.N., Anticevic, A., Murray, J.D., 2019. Hierarchical heterogeneity across human cortex shapes large-scale neural dynamics. Neuron 101 (6), 1181–1194.e13. https://doi.org/10.1016/j.neuron.2019.01.017.

Desikan, R.S., Ségonne, F., Fischl, B., Quinn, B.T., Dickerson, B.C., Blacker, D., Buckner, R.L., Dale, A.M., Maguire, R.P., Hyman, B.T., Albert, M.S., Killiany, R.J., 2006. An automated labeling system for subdividing the human cerebral cortex on MRI scans into gyral based regions of interest. Neuroimage 31 (3), 968–980. https://doi.org/10.1016/j.neuroimage.2006.01.021.

Destrieux, C., Fischl, B., Dale, A., Halgren, E., 2010. Automatic parcellation of human cortical gyri and sulci using standard anatomical nomenclature. Neuroimage 53 (1), 1–15. https://doi.org/10.1016/j.neuroimage.2010.06.010.

Diez, I., Sepulcre, J., 2018. Neurogenetic profiles delineate large-scale connectivity dynamics of the human brain. Nat. Commun. 9 (1), 1–10. https://doi.org/10.1038/s41467-018-06346-3.

Duarte, R., Seeholzer, A., Zilles, K., Morrison, A., 2017. Synaptic patterning and the timescales of cortical dynamics. Curr. Opin. Neurobiol. 43 (April), 156–165. https://doi.org/10.1016/j.conb.2017.02.007.

Eickhoff, S.B., Stephan, K.E., Mohlberg, H., Grefkes, C., Fink, G.R., Amunts, K., Zilles, K., 2005. A new SPM toolbox for combining probabilistic cytoarchitectonic maps and functional imaging data. Neuroimage 25 (4), 1325–1335. https://doi.org/10.1016/j.neuroimage.2004.12.034.

Eickhoff, S.B., Yeo, B.T.T., Genon, S., 2018. Imaging-based parcellations of the human brain. Nat. Rev. Neurosci. 19 (11), 672–686. https://doi.org/10.1002/jmri.27188.

Fallon, J., Ward, P.G.D., Parkes, L., Oldham, S., Arnatkevičiūtė, A., Fornito, A., Fulcher, B.D., 2020. Timescales of spontaneous fMRI fluctuations relate to structural connectivity in the brain. Netw. Neurosci. 4 (3), 788–806. https://doi.org/10.1162/netn_a_00151.

Fan, L., Li, H., Zhuo, J., Zhang, Y., Wang, J., Chen, L., Yang, Z., Chu, C., Xie, S., Laird, A. R., Fox, P.T., Eickhoff, S.B., Yu, C., Jiang, T., 2016. The human brainnetome atlas: a new brain atlas based on connectional architecture. Cereb. Cortex 26 (8), 3508–3526. https://doi.org/10.1093/cercor/bhw157.

Farbood, M.M., Heeger, D.J., Marcus, G., Hasson, U., Lerner, Y., 2015. The neural processing of hierarchical structure in music and speech at different timescales. Front. Neurosci. 9 (APR), 1–13. https://doi.org/10.3389/fnins.2015.00157.

Fehring, J., Balestrieri, E., Focke, N.K., Dannlowski, U., Stier, C., Gross, J., 2024. Neurophysiological correlates of cortical hierarchy across the lifespan. BioRxiv Neurosci. 1–28. https://www.biorxiv.org/content/10.1101/2024.07.15.602693v1?rss=1&utm_source=researcher_app&utm_medium=referral&utm_campaign=RESR_MRKT_Researcher_inbound.

FIL Methods Group. (2017). *SPM12 Manual*. 15(3), 1–508. https://www.fil.ion.ucl.ac.uk/spm/doc/manual.pdf%0Ahttp://www.fil.ion.ucl.ac.uk/spm/.

Fischl, B., 2012. FreeSurfer. Neuroimage 62 (2), 774–781. https://doi.org/10.1016/j.neuroimage.2012.01.021.

Fletcher, J.M.K., Wennekers, T., 2018. From structure to activity: using centrality measures to predict neuronal activity. Int. J. Neural Syst. 28 (2). https://doi.org/10.1142/S0129065717500137.

Fornito, A., Zalesky, A., Bullmore, E., 2016. Fundamentals of Brain Network Analysis. Elsevier. https://doi.org/10.1016/C2012-0-06036-X.

Fuster, J.M., 2001. The prefrontal cortex—An update: time is of the essence. Neuron 30 (2), 319–333. https://doi.org/10.1016/S0896-6273(01)00285-9.

Gao, R., van den Brink, R.L., Pfeffer, T., Voytek, B., 2020. Neuronal timescales are functionally dynamic and shaped by cortical microarchitecture. Elife 9, 1–26. https://doi.org/10.7554/eLife.61277.

Gelman, A., Hwang, J., Vehtari, A., 2014. Understanding predictive information criteria for Bayesian models. Stat. Comput. 24 (6), 997–1016. https://doi.org/10.1007/s11222-013-9416-2.

Geweke, J., 2007. Bayesian model comparison and validation. Am. Econ. Rev. 97 (2), 60–64. https://doi.org/10.1257/aer.97.2.60.

Glasser, M.F., Coalson, T.S., Robinson, E.C., Hacker, C.D., Harwell, J., Yacoub, E., Ugurbil, K., Andersson, J., Beckmann, C.F., Jenkinson, M., Smith, S.M., Van Essen, D. C., 2016. A multi-modal parcellation of human cerebral cortex. Nature 536 (7615), 171–178. https://doi.org/10.1038/nature18933.

Goldman-Rakic, P.S., 1988. Topography of cognition: parallel distributed networks in primate association cortex. Annu Rev. Neurosci. 11, 137–156. https://doi.org/10.1146/annurev.ne.11.030188.001033.

Golesorkhi, M., Gomez-Pilar, J., Tumati, S., Fraser, M., Northoff, G., 2021a. Temporal hierarchy of intrinsic neural timescales converges with spatial core-periphery organization. Commun. Biol. 4 (1), 1–14. https://doi.org/10.1038/s42003-021-01785-z.

Golesorkhi, M., Gomez-Pilar, J., Zilio, F., Berberian, N., Wolff, A., Yagoub, M.C.E., Northoff, G., 2021b. The brain and its time: intrinsic neural timescales are key for input processing. Commun. Biol. 4 (1), 1–16. https://doi.org/10.1038/s42003-021-02483-6.

Gollo, L.L., Zalesky, A., Matthew Hutchison, R., van den Heuvel, M.P., Breakspear, M., 2015. Dwelling quietly in the rich club: brain network determinants of slow cortical fluctuations. Philos. Trans. R. Soc. B 370 (1668). https://doi.org/10.1098/rstb.2014.0165.

Gómez-Gardeñes, J., Zamora-López, G., Moreno, Y., Arenas, A., 2010. From modular to centralized organization of synchronization in functional areas of the cat cerebral cortex. PLoS One 5 (8). https://doi.org/10.1371/journal.pone.0012313.

Gordon, E.M., Laumann, T.O., Adeyemo, B., Huckins, J.F., Kelley, W.M., Petersen, S.E., 2016. Generation and evaluation of a cortical area parcellation from resting-state correlations. Cereb. Cortex 26 (1), 288–303. https://doi.org/10.1093/cercor/bhu239.

Gorgolewski, K.J. (2016). *MPM 1.0 asymetrical (improved reconstruction)*. https://identifiers.org/neurovault.image:29489.

Goto, M., Abe, O., Hagiwara, A., Fujita, S., Kamagata, K., Hori, M., Aoki, S., Osada, T., Konishi, S., Masutani, Y., Sakamoto, H., Sakano, Y., Kyogoku, S., Daida, H., 2022. Advantages of using both voxel-and surface-based morphometry in cortical morphology analysis: a review of various applications. Magn. Reson. Med. Sci. 21 (1), 41–57. https://doi.org/10.2463/mrms.rev.2021-0096.

Graybiel, A.M., 2008. Habits, rituals, and the evaluative brain. Annu Rev. Neurosci. 31, 359–387. https://doi.org/10.1146/annurev.neuro.29.051605.112851.

Guimerà, R., Nunes Amaral, L.A., 2005. Functional cartography of complex metabolic networks. Nature 433 (7028), 895–900. https://doi.org/10.1038/nature03288.

Hagmann, P., Cammoun, L., Gigandet, X., Meuli, R., Honey, C.J., Van Wedeen, J., Sporns, O., 2008. Mapping the structural core of human cerebral cortex. PLoS Biol. 6 (7), 1479–1493. https://doi.org/10.1371/journal.pbio.0060159.

Hansen, J.Y., Markello, R.D., Vogel, J.W., Seidlitz, J., Bzdok, D., Misic, B., 2021. Mapping gene transcription and neurocognition across human neocortex. Nat. Hum. Behav. 5 (9), 1240–1250. https://doi.org/10.1038/s41562-021-01082-z.

Hansen, J.Y., Shafiei, G., Voigt, K., Liang, E.X., Cox, S.M.L., Leyton, M., Jamadar, S.D., & Misic, B. (2022). Multimodal, multiscale connectivity blueprints of the cerebral cortex. bioRxiv, 2022.12.02.518906. https://www.biorxiv.org/content/10.1101/2022.12.02.518906v1%0Ahttps://www.biorxiv.org/content/10.1101/2022.12.02.518906v1.abstract.

Harriger, L., van den Heuvel, M.P., Sporns, O., 2012. Rich club organization of macaque cerebral cortex and its role in network communication. PLoS One 7 (9). https://doi.org/10.1371/journal.pone.0046497.

Harris, J.A., Mihalas, S., Hirokawa, K.E., Whitesell, J.D., Choi, H., Bernard, A., Bohn, P., Caldejon, S., Casal, L., Cho, A., Feiner, A., Feng, D., Gaudreault, N., Gerfen, C.R., Graddis, N., Groblewski, P.A., Henry, A.M., Ho, A., Howard, R., Zeng, H., 2019. Hierarchical organization of cortical and thalamic connectivity. Nature 575 (7781), 195–202. https://doi.org/10.1038/s41586-019-1716-z.

Hasson, U., Chen, J., Honey, C.J., 2015. Hierarchical process memory: memory as an integral component of information processing. Trends Cogn. Sci. 19 (6), 304–313. https://doi.org/10.1016/j.tics.2015.04.006.

Hasson, U., Malach, R., Heeger, D.J., 2010. Reliability of cortical activity during natural stimulation. Trends Cogn. Sci. 14 (1), 40–48. https://doi.org/10.1016/j.tics.2009.10.011.

Hasson, U., Nir, Y., Levy, I., Fuhrmann, G., Malach, R., 2004. Intersubject synchronization of cortical activity during natural vision. Science 303 (5664), 1634–1640. https://doi.org/10.1126/science.1089506.

Hasson, U., Yang, E., Vallines, I., Heeger, D.J., Rubin, N., 2008. A hierarchy of temporal receptive windows in human cortex. J. Neurosci. 28 (10), 2539–2550. https://doi.org/10.1523/JNEUROSCI.5487-07.2008.

Hawrylycz, M.J., Lein, E.S., Guillozet-Bongaarts, A.L., Shen, E.H., Ng, L., Miller, J.A., van de Lagemaat, L.N., Smith, K.A., Ebbert, A., Riley, Z.L., Abajian, C., Beckmann, C.F., Bernard, A., Bertagnolli, D., Boe, A.F., Cartagena, P.M., Chakravarty, M.M., Chapin, M., Chong, J., Jones, A.R., 2012. An anatomically comprehensive atlas of the adult human brain transcriptome. Nature 489 (7416), 391–399. https://doi.org/10.1038/nature11405.

Hollenbach, F.M., Montgomery, J.M., 2020. Bayesian Model Selection, Model Comparison, and Model Averaging. The SAGE Handbook of Research Methods in Political Science and International Relations, pp. 937–960. https://doi.org/10.4135/9781526486387.n52.

Honey, C.J., Thesen, T., Donner, T.H., Silbert, L.J., Carlson, C.E., Devinsky, O., Doyle, W. K., Rubin, N., Heeger, D.J., Hasson, U., 2012. Slow cortical dynamics and the accumulation of information over long timescales. Neuron 76 (2), 423–434. https://doi.org/10.1016/j.neuron.2012.08.011.

Horn, A. (2016). *HCP-MMP1.0 projected on MNI2009a GM (volumetric) in NIfTI format*. https://doi.org/10.6084/m9.figshare.3501911.v5.

Huntenburg, J.M., Bazin, P.L., Goulas, A., Tardif, C.L., Villringer, A., Margulies, D.S., 2017. A systematic relationship between functional connectivity and intracortical myelin in the human cerebral cortex. Cereb. Cortex (New York, NY: 1991) 27 (2), 981–997. https://doi.org/10.1093/cercor/bhx030.

Huntenburg, J.M., Bazin, P.L., Margulies, D.S., 2018. Large-scale gradients in human cortical organization. Trends. Cogn. Sci. 22 (1), 21–31. https://doi.org/10.1016/j.tics.2017.11.002.

Ingvar, D.H., 1985. ``Memory of the future'': an essay on the temporal organization of conscious awareness. Hum. Neurobiol. 4 (3), 127–136.

Ito, T., Hearne, L.J., Cole, M.W., 2020. A cortical hierarchy of localized and distributed processes revealed via dissociation of task activations, connectivity changes, and intrinsic timescales. Neuroimage 221 (February), 117141. https://doi.org/10.1016/j.neuroimage.2020.117141.

Jääskeläinen, I.P., Sams, M., Glerean, E., Ahveninen, J., 2021. Movies and narratives as naturalistic stimuli in neuroimaging. Neuroimage 224 (June 2020), 117445. https://doi.org/10.1016/j.neuroimage.2020.117445.

Jenkinson, M., Bannister, P., Brady, M., Smith, S., 2002. Improved optimization for the robust and accurate linear registration and motion correction of brain images. Neuroimage 17 (2), 825–841. https://doi.org/10.1006/nimg.2002.1132.

Jenkinson, M., Beckmann, C.F., Behrens, T.E.J., Woolrich, M.W., Smith, S.M., 2012. FSL. Neuroimage 62 (2), 782–790. https://doi.org/10.1016/j.neuroimage.2011.09.015.

Jeon, H.A., 2014. Hierarchical processing in the prefrontal cortex in a variety of cognitive domains. Front. Syst. Neurosci. 8 (NOV), 1–8. https://doi.org/10.3389/fnsys.2014.00223. Frontiers Research Foundation.

Ji, J.L., Spronk, M., Kulkarni, K., Repovš, G., Anticevic, A., Cole, M.W., 2019. Mapping the human brain's cortical-subcortical functional network organization. Neuroimage 185 (October 2018), 35–57. https://doi.org/10.1016/j.neuroimage.2018.10.006.

Jobson, D.D., Hase, Y., Clarkson, A.N., Kalaria, R.N., 2021. The role of the medial prefrontal cortex in cognition, ageing and dementia. Brain Commun. 3 (3). https://doi.org/10.1093/braincomms/fcab125.

Jones, D.K., Knösche, T.R., Turner, R., 2013. White matter integrity, fiber count, and other fallacies: the do's and don'ts of diffusion MRI. Neuroimage 73, 239–254. https://doi.org/10.1016/j.neuroimage.2012.06.081.

Jung, J.Y., Cloutman, L.L., Binney, R.J., Lambon Ralph, M.A., 2017. The structural connectivity of higher order association cortices reflects human functional brain networks. Cortex 97, 221–239. https://doi.org/10.1016/j.cortex.2016.08.011.

Kai, J., Khan, A.R., Haast, R.A., Lau, J.C., 2022. Mapping the subcortical connectome using in vivo diffusion MRI: feasibility and reliability. Neuroimage 262 (March), 119553. https://doi.org/10.1016/j.neuroimage.2022.119553.

Keller, A.S., Sydnor, V.J., Pines, A., Fair, D.A., Bassett, D.S., Satterthwaite, T.D., 2023. Hierarchical functional system development supports executive function. Trends. Cogn. Sci. 27 (2), 160–174. https://doi.org/10.1016/j.tics.2022.11.005.

Kiebel, S.J., Daunizeau, J., Friston, K.J., 2008. A hierarchy of time-scales and the brain. PLoS Comput. Biol. 4 (11). https://doi.org/10.1371/journal.pcbi.1000209.

Koechlin, E., Summerfield, C., 2007. An information theoretical approach to prefrontal executive function. Trends Cogn. Sci. 11 (6), 229–235. https://doi.org/10.1016/j.tics.2007.04.005.

Kruschke, J.K., 2011. Tutorial: doing Bayesian data analysis with R and BUGS. In: Expanding the Space of Cognitive Science - Proceedings of the 33rd Annual Meeting of the Cognitive Science Society, CogSci 2011, pp. 56–57.

Lee, D.K., 2016. Alternatives to P value: confidence interval and effect size. Korean J. Anesthesiol. 69 (6), 555. https://doi.org/10.4097/kjae.2016.69.6.555.

Lerner, Y., Honey, C.J., Silbert, L.J., Hasson, U., 2011. Topographic mapping of a hierarchy of temporal receptive windows using a narrated story. J. Neurosci. 31 (8), 2906–2915. https://doi.org/10.1523/JNEUROSCI.3684-10.2011.

Liu, Z.Q., Shafiei, G., Baillet, S., Misic, B., 2023. Spatially heterogeneous structure-function coupling in haemodynamic and electromagnetic brain networks. Neuroimage 278 (July), 120276. https://doi.org/10.1016/j.neuroimage.2023.120276.

Lohia, K., Soans, R.S., Saxena, R., Mahajan, K., Gandhi, T.K., 2024. Distinct rich and diverse clubs regulate coarse and fine binocular disparity processing: evidence from stereoscopic task-based fMRI. iScience, 109831. https://doi.org/10.1016/j.isci.2024.109831.

Lurie, D.J., Pappas, I., D'Esposito, M, 2024. Cortical timescales and the modular organization of structural and functional brain networks. Hum. Brain Mapp. 45 (2). https://doi.org/10.1002/hbm.26587.

Mahjoory, K., Schoffelen, J.M., Keitel, A., Gross, J., 2020. The frequency gradient of human resting-state brain oscillations follows cortical hierarchies. Elife 9, 1–18. https://doi.org/10.7554/ELIFE.53715.

Maldjian, J.A., Laurienti, P.J., Kraft, R.A., Burdette, J.H., 2003. An automated method for neuroanatomic and cytoarchitectonic atlas-based interrogation of fMRI data sets. Neuroimage 19 (3), 1233–1239. https://doi.org/10.1016/S1053-8119(03)00169-1.

Manea, A.M.G., Zilverstand, A., Ugurbil, K., Heilbronner, S.R., Zimmermann, J., 2022. Intrinsic timescales as an organizational principle of neural processing across the whole rhesus macaque brain. Elife 11, 1–20. https://doi.org/10.7554/eLife.75540.

Margulies, D.S., Ghosh, S.S., Goulas, A., Falkiewicz, M., Huntenburg, J.M., Langs, G., Bezgin, G., Eickhoff, S.B., Castellanos, F.X., Petrides, M., Jefferies, E., Smallwood, J., 2016. Situating the default-mode network along a principal gradient of macroscale cortical organization. Proc. Natl. Acad. Sci. USA 113 (44), 12574–12579. https://doi.org/10.1073/pnas.1608282113.

Markello, R.D., Hansen, J.Y., Liu, Z.Q., Bazinet, V., Shafiei, G., Suárez, L.E., Blostein, N., Seidlitz, J., Baillet, S., Satterthwaite, T.D., Chakravarty, M.M., Raznahan, A., Misic, B., 2022. Neuromaps: structural and functional interpretation of brain maps. Nat. Methods 19 (11), 1472–1479. https://doi.org/10.1038/s41592-022-01625-w.

Mashour, G.A., Roelfsema, P., Changeux, J.P., Dehaene, S., 2020. Conscious processing and the global neuronal workspace hypothesis. Neuron 105 (5), 776–798. https://doi.org/10.1016/j.neuron.2020.01.026.

Mathy, F., Feldman, J., 2012. What's magic about magic numbers? Chunking and data compression in short-term memory. Cognition 122 (3), 346–362. https://doi.org/10.1016/j.cognition.2011.11.003.

Mecklenbrauck, F., Gruber, M., Siestrup, S., Zahedi, A., Grotegerd, D., Mauritz, M., Trempler, I., Dannlowski, U., Schubotz, R.I., 2024. The significance of structural rich club hubs for the processing of hierarchical stimuli. Hum. Brain Mapp. 45 (4), 1–28. https://doi.org/10.1002/hbm.26543.

Meilă, M., 2003. Comparing clusterings by the variation of information. In: Lecture Notes in Artificial Intelligence (Subseries of Lecture Notes in Computer Science), 2777, pp. 173–187. https://doi.org/10.1007/978-3-540-45167-9_14.

Mesulam, M.M., 1998. From sensation to cognition. Brain 121 (6), 1013–1052. https://doi.org/10.1093/brain/121.6.1013.

Mohor, G.S., Thieken, A.H., Korup, O., 2021. Residential flood loss estimated from Bayesian multilevel models. Nat. Haz. Earth Syst. Sci. 21 (5), 1599–1614. https://doi.org/10.5194/nhess-21-1599-2021.

Moraczewski, D., Nketia, J., Redcay, E., 2020. Cortical temporal hierarchy is immature in middle childhood. Neuroimage 216 (June 2019), 116616. https://doi.org/10.1016/j.neuroimage.2020.116616.

Mori, S., Crain, B.J., Chacko, V.P., van Zilj, P.C.M., 1999. Three-dimensional tracking of axonal projections in the brain by magnetic resonance imaging. Ann. Neurol. 45 (2), 265–269. https://doi.org/10.1002/1531-8249(199902)45:2<247::AID-ANA16>3.0.CO;2-U.

Müller, E.J., Munn, B., Hearne, L.J., Smith, J.B., Fulcher, B., Arnatkevičiūtė, A., Lurie, D. J., Cocchi, L., Shine, J.M., 2020. Core and matrix thalamic sub-populations relate to spatio-temporal cortical connectivity gradients. Neuroimage 222 (August), 117224. https://doi.org/10.1016/j.neuroimage.2020.117224.

Murphy, C., Wang, H.T., Konu, D., Lowndes, R., Margulies, D.S., Jefferies, E., Smallwood, J., 2019. Modes of operation: a topographic neural gradient supporting stimulus dependent and independent cognition. Neuroimage 186 (November 2018), 487–496. https://doi.org/10.1016/j.neuroimage.2018.11.009.

Murray, J.D., Bernacchia, A., Freedman, D.J., Romo, R., Wallis, J.D., Cai, X., Padoa-Schioppa, C., Pasternak, T., Seo, H., Lee, D., Wang, X.J., 2014. A hierarchy of intrinsic timescales across primate cortex. Nat. Neurosci. 17 (12), 1661–1663. https://doi.org/10.1038/nn.3862.

Nastase, S.A., Gazzola, V., Hasson, U., Keysers, C., 2019. Measuring shared responses across subjects using intersubject correlation. Soc. Cogn. Affect. Neurosci. 14 (6), 669–687. https://doi.org/10.1093/scan/nsz037.

Neudorf, J., Ekstrand, C., Kress, S., Borowsky, R., 2020. Brain structural connectivity predicts brain functional complexity: diffusion tensor imaging derived centrality accounts for variance in fractal properties of functional magnetic resonance imaging signal. Neuroscience 438, 1–8. https://doi.org/10.1016/j.neuroscience.2020.04.048.

Nieder, A., 2016. Representing something out of nothing: the dawning of zero. Trends Cogn. Sci. 20 (11), 830–842. https://doi.org/10.1016/j.tics.2016.08.008.

Ogawa, T., Komatsu, H., 2010. Differential temporal storage capacity in the baseline activity of neurons in macaque frontal eye field and area V4. J. Neurophysiol. 103 (5), 2433–2445. https://doi.org/10.1152/jn.01066.2009.

Oldfield, R.C., 1971. The assessment and analysis of handedness: the Edinburgh inventory. Neuropsychologia1 9, 97–113. https://doi.org/10.1007/978-3-319-55065-7_301010.

Oldham, S., Fornito, A., 2023. Hubs and rich clubs. Connectome Analysis: Characterization, Methods, and Analysis. INC. https://doi.org/10.1016/B978-0-323-85280-7.00015-4.

Oldham, S., Fulcher, B., Parkes, L., Arnatkeviciūtė, A., Suo, C., Fornito, A., 2019. Consistency and differences between centrality measures across distinct classes of networks. PLoS One 14 (7), 1–23. https://doi.org/10.1371/journal.pone.0220061.

Ortiz-Terán, L., Diez, I., Ortiz, T., Perez, D.L., Aragón, J.I., Costumero, V., Pascual-Leone, A., El Fakhri, G., Sepulcre, J, 2017. Brain circuit-gene expression relationships and neuroplasticity of multisensory cortices in blind children. Proc. Natl. Acad. Sci. USA 114 (26), 6830–6835. https://doi.org/10.1073/pnas.1619121114.

Patriat, R., Molloy, E.K., Meier, T.B., Kirk, G.R., Nair, V.A., Meyerand, M.E., Prabhakaran, V., Birn, R.M., 2013. The effect of resting condition on resting-state fMRI reliability and consistency: a comparison between resting with eyes open, closed, and fixated. Neuroimage 78, 463–473. https://doi.org/10.1016/j.neuroimage.2013.04.013.

Pinhas, M., Tzelgov, J., 2012. Expanding on the mental number line: zero is perceived as the "smallest''. J. Exp. Psychol. 38 (5), 1187–1205. https://doi.org/10.1037/a0027390.

Power, J.D., Barnes, K.A., Snyder, A.Z., Schlaggar, B.L., Petersen, S.E., 2012. Spurious but systematic correlations in functional connectivity MRI networks arise from subject motion. Neuroimage 59 (3), 2142–2154. https://doi.org/10.1016/j.neuroimage.2011.10.018.

Preti, M.G., Van De Ville, D., 2019. Decoupling of brain function from structure reveals regional behavioral specialization in humans. Nat. Commun. 10 (1), 1–7. https://doi.org/10.1038/s41467-019-12765-7.

Pretus, C., Marcos-Vidal, L., Martínez-García, M., Picado, M., Ramos-Quiroga, J.A., Richarte, V., Castellanos, F.X., Sepulcre, J., Desco, M., Vilarroya, Ó., Carmona, S., 2019. Stepwise functional connectivity reveals altered sensory-multimodal integration in medication-naïve adults with attention deficit hyperactivity disorder. Hum. Brain Mapp. 40 (16), 4645–4656. https://doi.org/10.1002/hbm.24727.

Qi, S., Meesters, S., Nicolay, K., ter Haar Romeny, B.M., Ossenblok, P., 2015. The influence of construction methodology on structural brain network measures: a review. J. Neurosci. Methods 253 (500), 170–182. https://doi.org/10.1016/j.jneumeth.2015.06.016.

R Core Team. (2022). *R: A Language and Environment for Statistical Computing*. https://www.r-project.org/.

Raut, R.V., Snyder, A.Z., Raichle, M.E., 2020. Hierarchical dynamics as a macroscopic organizing principle of the human brain. Proc. Natl. Acad. Sci. USA 117 (34), 20890–20897. https://doi.org/10.1073/pnas.2003383117.

Redcay, E., Moraczewski, D., 2020. Social cognition in context: a naturalistic imaging approach. Neuroimage 216 (October 2019), 116392. https://doi.org/10.1016/j.neuroimage.2019.116392.

Ren, Y., Nguyen, V.T., Guo, L., Guo, C.C., 2017. Inter-subject functional correlation reveal a hierarchical organization of extrinsic and intrinsic systems in the brain. Sci. Rep. 7 (1), 1–12. https://doi.org/10.1038/s41598-017-11324-8.

Riedel, L., van den Heuvel, M.P., Markett, S., 2022. Trajectory of rich club properties in structural brain networks. Hum. Brain Mapp. 43 (14), 4239–4253. https://doi.org/10.1002/hbm.25950.

Rouder, J.N., Haaf, J.M., Aust, F., 2018. From theories to models to predictions: a Bayesian model comparison approach. Commun. Monogr. 85 (1), 41–56. https://doi.org/10.1080/03637751.2017.1394581.

RStudio Team. (2022). *RStudio: Integrated Development Environment for R*. http://www.rstudio.com/.

Rubinov, M., Sporns, O., 2010. Complex network measures of brain connectivity: uses and interpretations. Neuroimage 52 (3), 1059–1069. https://doi.org/10.1016/j.neuroimage.2009.10.003.

Rust, N.C., Movshon, J.A., 2005. In praise of artifice. Nat. Neurosci. 8 (12), 1647–1650. https://doi.org/10.1038/nn1606.

Saberi, A., Paquola, C., Wagstyl, K., Hettwer, M.D., Bernhardt, B.C., Eickhoff, S.B., Valk, S.L., 2023. The regional variation of laminar thickness in the human isocortex is related to cortical hierarchy and interregional connectivity. PLoS Biol. 21 (11 November), 1–29. https://doi.org/10.1371/journal.pbio.3002365.

Satterthwaite, T.D., Elliott, M.A., Gerraty, R.T., Ruparel, K., Loughead, J., Calkins, M.E., Eickhoff, S.B., Hakonarson, H., Gur, R.C., Gur, R.E., Wolf, D.H., 2013. An improved framework for confound regression and filtering for control of motion artifact in the preprocessing of resting-state functional connectivity data. Neuroimage 64 (1), 240–256. https://doi.org/10.1016/j.neuroimage.2012.08.052.

Schaefer, A., Kong, R., Gordon, E.M., Laumann, T.O., Zuo, X.-N., Holmes, A.J., Eickhoff, S.B., Yeo, B.T.T., 2018. Local-global parcellation of the human cerebral cortex from intrinsic functional connectivity MRI. Cereb. Cortex 28 (9), 3095–3114. https://doi.org/10.1093/cercor/bhx179.

Schmälzle, R., Imhof, M.A., Grall, C., Flaisch, T., Schupp, H.T., Schmälzle, R., Imhof, M. A., Grall, C., Flaisch, T., & Schupp, H.T. (2017). Reliability of fMRI time series: similarity of neural processing during movie viewing. bioRxiv, 158188. https://doi.org/10.1101/158188.

Schmidt, M., Bakker, R., Shen, K., Bezgin, G., Diesmann, M., Van Albada, S.J., & Schmidt, M. (2016). *Full-density multi-scale account of structure and dynamics of macaque visual cortex correspondence to:* https://doi.org/10.48550/arXiv.1511.09364.

Scholtens, L.H., Schmidt, R., de Reus, M.A., van den Heuvel, M.P., 2014. Linking macroscale graph analytical organization to microscale neuroarchitectonics in the macaque connectome. J. Neurosci. 34 (36), 12192–12205. https://doi.org/10.1523/JNEUROSCI.0752-14.2014.

Seguin, C., Tian, Y., Zalesky, A., 2020. Network communication models improve the behavioral and functional predictive utility of the human structural connectome. Netw. Neurosci. 4 (4), 980–1006. https://doi.org/10.1162/netn_a_00161.

Senden, M., Deco, G., De Reus, M.A., Goebel, R., van den Heuvel, M.P., 2014. Rich club organization supports a diverse set of functional network configurations. Neuroimage 96, 174–182. https://doi.org/10.1016/j.neuroimage.2014.03.066.

Senden, M., Reuter, N., van den Heuvel, M.P., Goebel, R., Deco, G., 2017. Cortical rich club regions can organize state-dependent functional network formation by engaging in oscillatory behavior. Neuroimage 146, 561–574. https://doi.org/10.1016/j.neuroimage.2016.10.044.

Sepulcre, J., 2014. Integration of visual and motor functional streams in the human brain. Neurosci. Lett. 567, 68–73. https://doi.org/10.1016/j.neulet.2014.03.050.

Sepulcre, J., Liu, H., Talukdar, T., Martincorena, I., Thomas Yeo, B.T., Buckner, R.L., 2010. The organization of local and distant functional connectivity in the human brain. PLoS Comput. Biol. 6 (6), 1–15. https://doi.org/10.1371/journal.pcbi.1000808.

Sepulcre, J., Sabuncu, M.R., Yeo, T.B., Liu, H., Johnson, K.A., 2012. Stepwise connectivity of the modal cortex reveals the multimodal organization of the human brain. J. Neurosci. 32 (31), 10649–10661. https://doi.org/10.1523/JNEUROSCI.0759-12.2012.

Sethi, S.S., Zerbi, V., Wenderoth, N., Fornito, A., Fulcher, B.D., 2017. Structural connectome topology relates to regional BOLD signal dynamics in the mouse brain. Chaos 27 (4). https://doi.org/10.1063/1.4979281.

Shafiei, G., Fulcher, B.D., Voytek, B., Satterthwaite, T.D., Baillet, S., Misic, B., 2023. Neurophysiological signatures of cortical micro-architecture. Nat. Commun. 14 (1). https://doi.org/10.1038/s41467-023-41689-6.

Shafiei, G., Markello, R.D., De Wael, R.V., Bernhardt, B.C., Fulcher, B.D., Misic, B., 2020. Topographic gradients of intrinsic dynamics across neocortex. Elife 9, 1–24. https://doi.org/10.7554/eLife.62116.

Shen, X., Tokoglu, F., Papademetris, X., Constable, R.T., 2013. Groupwise whole-brain parcellation from resting-state fMRI data for network node identification. Neuroimage 82, 403–415. https://doi.org/10.1016/j.neuroimage.2013.05.081.

Shine, J.M., Hearne, L.J., Breakspear, M., Hwang, K., Müller, E.J., Sporns, O., Poldrack, R.A., Mattingley, J.B., Cocchi, L., 2019. The low-dimensional neural architecture of cognitive complexity is related to activity in medial thalamic nuclei. Neuron 104 (5), 849–855.e3. https://doi.org/10.1016/j.neuron.2019.09.002.

Siegle, J.H., Jia, X., Durand, S., Gale, S., Bennett, C., Graddis, N., Heller, G., Ramirez, T. K., Choi, H., Luviano, J.A., Groblewski, P.A., Ahmed, R., Arkhipov, A., Bernard, A., Billeh, Y.N., Brown, D., Buice, M.A., Cain, N., Caldejon, S., Koch, C., 2021. Survey of spiking in the mouse visual system reveals functional hierarchy. Nature 592 (7852), 86–92. https://doi.org/10.1038/s41586-020-03171-x.

Smith, S.M., Jenkinson, M., Woolrich, M.W., Beckmann, C.F., Behrens, T.E.J., Johansen-Berg, H., Bannister, P.R., De Luca, M., Drobnjak, I., Flitney, D.E., Niazy, R.K., Saunders, J., Vickers, J., Zhang, Y., De Stefano, N., Brady, J.M., Matthews, P.M., 2004. Advances in functional and structural MR image analysis and implementation as FSL. Neuroimage 23 (SUPPL. 1), 208–219. https://doi.org/10.1016/j.neuroimage.2004.07.051.

Soltani, A., Murray, J.D., Seo, H., Lee, D., 2021. Timescales of cognition in the brain. Curr. Opin. Behav. Sci. 41, 30–37. https://doi.org/10.1016/j.cobeha.2021.03.003.

Sonkusare, S., Breakspear, M., Guo, C., 2019. Naturalistic stimuli in neuroscience: critically acclaimed. Trends. Cogn. Sci. 23 (8), 699–714. https://doi.org/10.1016/j.tics.2019.05.004.

Sporns, O., 2011. The human connectome: a complex network. Ann. N. Y. Acad. Sci. 1224 (1), 109–125. https://doi.org/10.1111/j.1749-6632.2010.05888.x.

Stephens, G.J., Honey, C.J., Hasson, U., 2013. A place for time: the spatiotemporal structure of neural dynamics during natural audition. J. Neurophysiol. 110 (9), 2019–2026. https://doi.org/10.1152/jn.00268.2013.

Sydnor, V.J., Larsen, B., Bassett, D.S., Alexander-Bloch, A., Fair, D.A., Liston, C., Mackey, A.P., Milham, M.P., Pines, A., Roalf, D.R., Seidlitz, J., Xu, T., Raznahan, A., Satterthwaite, T.D., 2021. Neurodevelopment of the association cortices: patterns, mechanisms, and implications for psychopathology. Neuron 109 (18), 2820–2846. https://doi.org/10.1016/j.neuron.2021.06.016.

Sydnor, V.J., Larsen, B., Seidlitz, J., Adebimpe, A., Alexander-Bloch, A.F., Bassett, D.S., Bertolero, M.A., Cieslak, M., Covitz, S., Fan, Y., Gur, R.E., Gur, R.C., Mackey, A.P., Moore, T.M., Roalf, D.R., Shinohara, R.T., Satterthwaite, T.D., 2023. Intrinsic activity development unfolds along a sensorimotor–association cortical axis in youth. Nat. Neurosci. 26 (4), 638–649. https://doi.org/10.1038/s41593-023-01282-y.

Taylor, P., Hobbs, J.N., Burroni, J., Siegelmann, H.T., 2015. The global landscape of cognition: hierarchical aggregation as an organizational principle of human cortical networks and functions. Sci. Rep. 5 (November), 1–18. https://doi.org/10.1038/srep18112.

The MathWorks Inc., 2021. MATLAB version: 9.10.0 (R2021a). The MathWorks Inc. https://www.mathworks.com.

Thomas, R.M., De Sanctis, T., Gazzola, V., Keysers, C., 2018. Where and how our brain represents the temporal structure of observed action. Neuroimage 183 (November 2017), 677–697. https://doi.org/10.1016/j.neuroimage.2018.08.056.

Tomczak, M., Tomczak, E., 2014. The need to report effect size estimates revisited. An overview of some recommended measures of effect size. Trends Sport Sci. 1 (21), 19–25. http://www.wbc.poznan.pl/Content/325867/5_Trends_Vol21_2014_no1_20.pdf.

Torres-Gomez, S., Blonde, J.D., Mendoza-Halliday, D., Kuebler, E., Everest, M., Wang, X.-J., Inoue, W., Poulter, M.O., Martinez-Trujillo, J., 2020. Changes in the proportion of inhibitory interneuron types from sensory to executive areas of the primate neocortex: implications for the origins of working memory representations. Cereb. Cortex 30 (8), 4544–4562. https://doi.org/10.1093/cercor/bhaa056.

Tourbier, S., Aleman-Gomez, Y., Griffa, A., Bach Cuadra, M., & Hagmann, P. (2019). *Sebastientourbier/multiscalebrainparcellator: Multi-Scale Brain Parcellator v1.1.1.* https://doi.org/10.5281/ZENODO.3627097.

Tzourio-Mazoyer, N., Landeau, B., Papathanassiou, D., Crivello, F., Etard, O., Delcroix, N., Mazoyer, B., Joliot, M., 2002. Automated anatomical labeling of activations in SPM using a macroscopic anatomical parcellation of the MNI MRI single-subject brain. Neuroimage 15 (1), 273–289. https://doi.org/10.1006/nimg.2001.0978.

Uithol, S., van Rooij, I., Bekkering, H., Haselager, P., 2012. Hierarchies in action and motor control. J. Cogn. Neurosci. 24 (5), 1077–1086. https://doi.org/10.1162/jocn_a_00204.

Valk, S.L., Xu, T., Margulies, D.S., Masouleh, S.K., Paquola, C., Goulas, A., Kochunov, P., Smallwood, J., Yeo, B.T.T., Bernhardt, B.C., Eickhoff, S.B., 2020. Shaping brain structure: genetic and phylogenetic axes of macroscale organization of cortical thickness. Sci. Adv. 6 (39), 1–14. https://doi.org/10.1126/sciadv.abb3417.

van den Heuvel, M.P., Scholtens, L.H., Barrett, L.F., Hilgetag, C.C., de Reus, M.A., 2015. Bridging cytoarchitectonics and connectomics in human cerebral cortex. J. Neurosci. 35 (41), 13943–13948. https://doi.org/10.1523/JNEUROSCI.2630-15.2015.

van den Heuvel, M.P., Scholtens, L.H., van der Burgh, H.K., Agosta, F., Alloza, C., Arango, C., Auyeung, B., Baron-Cohen, S., Basaia, S., Benders, M.J.N.L., Beyer, F., Booij, L., Braun, K.P.J., Filho, G.B., Cahn, W., Cannon, D.M., Chaim-Avancini, T.M., Chan, S.S.M., Chen, E.Y.H., de Lange, S.C., 2019. 10kin1day: a bottom-up neuroimaging initiative. Front. Neurol. 10 (MAY). https://doi.org/10.3389/fneur.2019.00425.

van den Heuvel, M.P., Sporns, O., 2011. Rich-club organization of the human connectome. J. Neurosci. 31 (44), 15775–15786. https://doi.org/10.1523/JNEUROSCI.3539-11.2011.

van den Heuvel, M.P., Sporns, O., 2013a. An anatomical substrate for integration among functional networks in human cortex. J. Neurosci. 33 (36), 14489–14500. https://doi.org/10.1523/JNEUROSCI.2128-13.2013.

van den Heuvel, M.P., Sporns, O., 2013b. Network hubs in the human brain. Trends Cogn. Sci. 17 (12), 683–696. https://doi.org/10.1016/j.tics.2013.09.012.

van den Heuvel, M.P., Sporns, O., Collin, G., Scheewe, T., Mandl, R.C.W., Cahn, W., Goni, J., Pol, H.E.H., Kahn, R.S., 2013. Abnormal rich club organization and functional brain dynamics in schizophrenia. JAMA Psychiatry 70 (8), 783–792. https://doi.org/10.1001/jamapsychiatry.2013.1328.

Van Dijk, K.R.A., Hedden, T., Venkataraman, A., Evans, K.C., Lazar, S.W., Buckner, R.L., 2010. Intrinsic functional connectivity as a tool for human connectomics: theory, properties, and optimization. J. Neurophysiol. 103 (1), 297–321. https://doi.org/10.1152/jn.00783.2009.

van Doorn, J., van den Bergh, D., Böhm, U., Dablander, F., Derks, K., Draws, T., Etz, A., Evans, N.J., Gronau, Q.F., Haaf, J.M., Hinne, M., Kucharský, Š., Ly, A., Marsman, M., Matzke, D., Gupta, A.R.K.N., Sarafoglou, A., Stefan, A., Voelkel, J.G., Wagenmakers, E.J., 2021. The JASP guidelines for conducting and reporting a Bayesian analysis. Psychon. Bull. Rev. 28 (3), 813–826. https://doi.org/10.3758/s13423-020-01798-5.

Vázquez-Rodríguez, B., Suárez, L.E., Markello, R.D., Shafiei, G., Paquola, C., Hagmann, P., Van Den Heuvel, M.P., Bernhardt, B.C., Spreng, R.N., Misic, B, 2019. Gradients of structure–function tethering across neocortex. Proc. Natl. Acad. Sci. USA 116 (42), 21219–21227. https://doi.org/10.1073/pnas.1903403116.

Vehtari, A., 2024. Loo Package Glossary - Loo-Glossary. Loo-Glossary • Loo. https://mc-stan.org/loo/reference/loo-glossary.html.

Vehtari, A., Gelman, A., Gabry, J., 2017. Practical Bayesian model evaluation using leave-one-out cross-validation and WAIC. Stat. Comput. 27 (5), 1413–1432. https://doi.org/10.1007/s11222-016-9696-4.

Vehtari, A., Gelman, A., Simpson, D., Carpenter, B., Bürkner, P.-C., 2021. Rank-normalization, folding, and localization: an improved R for assessing convergence of MCMC (with discussion). Bayesian Anal. 16 (2), 667–718. https://doi.org/10.1214/20-BA1221.

Vogelbacher, C., Möbius, T.W.D., Sommer, J., Schuster, V., Dannlowski, U., Kircher, T., Dempfle, A., Jansen, A., Bopp, M.H.A., 2018. The Marburg-Münster affective disorders cohort study (MACS): a quality assurance protocol for MR neuroimaging data. Neuroimage 172 (December 2017), 450–460. https://doi.org/10.1016/j.neuroimage.2018.01.079.

Wagstyl, K., Ronan, L., Goodyer, I.M., Fletcher, P.C., 2015. Cortical thickness gradients in structural hierarchies. Neuroimage 111, 241–250. https://doi.org/10.1016/j.neuroimage.2015.02.036.

Wang, M., Yang, Y., Wang, C., Gamo, N.J., Jin, L.E., Mazer, J.A., Morrison, J.H., Wang, X., Arnsten, A.F.T., 2012. Article NMDA receptors subserve persistent neuronal firing during working memory in dorsolateral prefrontal cortex. Neuron 77 (4), 736–749. https://doi.org/10.1016/j.neuron.2012.12.032.

Wang, X.-J., 2001. Synaptic reverberation underlying mnemonic persistent activity. Trends Neurosci. 24 (8), 455–463. https://doi.org/10.1016/S0166-2236(00)01868-3.

Wang, X.-J., 2020. Macroscopic gradients of synaptic excitation and inhibition in the neocortex. Nat. Rev. Neurosci. 21 (3), 169–178. https://doi.org/10.1038/s41583-020-0262-x.

Watanabe, T., 2013. Rich-club network topology to minimize synchronization cost due to phase difference among frequency-synchronized oscillators. Physica A 392 (5), 1246–1255. https://doi.org/10.1016/j.physa.2012.11.041.

Whitaker, K.J., Vértes, P.E., Romero-Garciaa, R., Váša, F., Moutoussis, M., Prabhu, G., Weiskopf, N., Callaghan, M.F., Wagstyl, K., Rittman, T., Tait, R., Ooi, C., Suckling, J., Inkster, B., Fonagy, P., Dolan, R.J., Jones, P.B., Goodyer, I.M., Bullmore, E.T., 2016. Adolescence is associated with genomically patterned consolidation of the hubs of the human brain connectome. Proc. Natl. Acad. Sci. USA 113 (32), 9105–9110. https://doi.org/10.1073/pnas.1601745113.

Wolff, A., Berberian, N., Golesorkhi, M., Gomez-Pilar, J., Zilio, F., Northoff, G., 2022. Intrinsic neural timescales: temporal integration and segregation. Trends Cogn. Sci. 26 (2), 159–173. https://doi.org/10.1016/j.tics.2021.11.007.

Wooldridge, J.M., 2013. Introductory Econometrics: A Modern Approach, fifth ed. South-Western Cengage Learning.

Xu, T., Nenning, K.H., Schwartz, E., Hong, S.J., Vogelstein, J.T., Goulas, A., Fair, D.A., Schroeder, C.E., Margulies, D.S., Smallwood, J., Milham, M.P., Langs, G., 2020. Cross-species functional alignment reveals evolutionary hierarchy within the connectome. Neuroimage 223 (September), 117346. https://doi.org/10.1016/j.neuroimage.2020.117346.

Xue, C., Sun, H., Hu, G., Qi, W., Yue, Y., Rao, J., Yang, W., Xiao, C., Chen, J., 2020. Disrupted patterns of rich-club and diverse-club organizations in subjective cognitive decline and amnestic mild cognitive impairment. Front. Neurosci. 14 (October), 1–14. https://doi.org/10.3389/fnins.2020.575652.

Yeh, F.C., Wedeen, V.J., Tseng, W.Y.I., 2010. Generalized q-sampling imaging. IEEE Trans. Med. ImAging 29 (9), 1626–1635. https://doi.org/10.1109/TMI.2010.2045126.

Yeo, B.T.T., Krienen, F.M., Eickhoff, S.B., Yaakub, S.N., Fox, P.T., Buckner, R.L., Asplund, C.L., Chee, M.W.L., 2015. Functional specialization and flexibility in human association cortex. Cereb. Cortex 25 (10), 3654–3672. https://doi.org/10.1093/cercor/bhu217.

Zamora-López, G., Chen, Y., Deco, G., Kringelbach, M.L., Zhou, C., 2016. Functional complexity emerging from anatomical constraints in the brain: the significance of network modularity and rich-clubs. Sci. Rep. 6 (November), 1–18. https://doi.org/10.1038/srep38424.

Zamora-López, G., Zhou, C., Kurths, J., 2009. Graph analysis of cortical networks reveals complex anatomical communication substrate. Chaos 19 (1). https://doi.org/10.1063/1.3089559.

Zamora-López, G., Zhou, C., Kurths, J., 2010. Cortical hubs form a module for multisensory integration on top of the hierarchy of cortical networks. Front. Neuroinform. 4 (MAR), 1–13. https://doi.org/10.3389/neuro.11.001.2010.

Zamora-López, G., Zhou, C., Kurths, J., 2011. Exploring brain function from anatomical connectivity. Front. Neurosci. 5 (JUN), 1–11. https://doi.org/10.3389/fnins.2011.00083.

Zilio, F., Gomez-Pilar, J., Cao, S., Zhang, J., Zang, D., Qi, Z., Tan, J., Hiromi, T., Wu, X., Fogel, S., Huang, Z., Hohmann, M.R., Fomina, T., Synofzik, M., Grosse-Wentrup, M., Owen, A.M., Northoff, G., 2021. Are intrinsic neural timescales related to sensory processing? Evidence from abnormal behavioral states. Neuroimage 226 (November 2020), 117579. https://doi.org/10.1016/j.neuroimage.2020.117579.

2.3 Study 3: Time Points or Plot Points – Are movies processed according to their temporal duration or their underlying content structure?

Running title: 2.3 Time Points or Plot Points

Falko Mecklenbrauck & Ricarda I. Schubotz (2026)

Manuscript under review

Associated online data:

Code repository: https://github.com/FalkMeck/Time_Points_or_Plot_Points

Data for replication: https://osf.io/xk6cv/overview?view_only=036a15ee8620401a9b1db5fd6fc25086

Time Points or Plot Points – Are movies processed according to their temporal duration or their underlying content structure?

Falko Mecklenbrauck[1,2] & Ricarda I. Schubotz[1,2]

[1]Department of Psychology, Biological Psychology, University of Münster, Germany,

[2]Otto Creutzfeldt Center for Cognitive and Behavioral Neuroscience, University of Münster, Germany

Data and Code Availability Statement: All code for stimulus creation, running the experiment as well as data preprocessing, analysis and visualization is available at https://github.com/FalkMeck/Time_Points_or_Plot_Points.
Data of one exemplary, minimally processed participant, all pairwise-ISC maps and the ROI analysis data can be downloaded at https://uni-muenster.sciebo.de/s/TLFLHTP4ysQgayr.

Ethics Statement: This study was conducted in accordance with the Declaration of Helsinki and approved by the Local Ethics Committee of the University of Münster. Participants signed an informed consent before participation.

Funding: The authors received no specific funding for this work.

Declaration of Interest Statement: The authors have declared that no competing interests exist.

Correspondence: f_meck01@uni-muenster.de, rschubotz@uni-muenster.de

Corresponding author: Falko Mecklenbrauck, f_meck01@uni-muenster.de, University of Münster, Institute of Psychology, Fliednerstr. 21, D-48149 Münster, Germany

Author Contributions

Falko Mecklenbrauck: Conceptualization, Data curation, Formal analysis, Investigation, Methodology, Project administration, Software, Visualization, Writing – original draft, Writing – review & editing.

Ricarda I. Schubotz: Conceptualization, Funding acquisition, Methodology, Project administration, Resources, Supervision, Writing – original draft, Writing – review & editing.

ORCID

Falko Mecklenbrauck: 0000-0002-8187-6826

Ricarda I. Schubotz: 0000-0001-5802-6869

Acknowledgment

The authors thank Monika Mertens, Anna Sophia Asdonk, Thea Maria Bröring, Maike Denguth, Vanessa Klein, Pia Niedrée, Yannah Loïs Schröder, and Zübeyde Nihan Yildirm for their help during data collection, Sebastian Bias, Laura Sophie Petretto, and Zübeyde Nihan Yildirm for help in testing the paradigm, and Lena Charlotte Innig for helpful comments on the manuscript.

Highlights

- First study to decouple content and duration effects on movie-evoked brain signals.
- Frame-based design reproduces established neural patterns of natural movies.
- Content complexity drives engagement in visually-attuned posterior scene network.
- Temporal duration drives engagement in memory-attuned anterior scene network.
- Content and duration together shift ISC in ROIs along the visual cortical hierarchy.

Abstract

Movie-watching studies have shown that specific cortical areas are tuned to stimulus segments of certain durations. However, increases in stimulus duration naturally co-occur with increases in content complexity. This study aimed to disentangle the effects of stimulus content and duration to determine whether hierarchically nested, complex, naturalistic stimuli, like movies, are processed primarily on the basis of their underlying temporal or content structure. To this end, 48 participants watched six equal-length blocks of movie frames presented at a constant frame rate in an fMRI experiment. Frames were extracted from either movie scenes or movie shots (CONTENT LEVEL) and displayed as continuous segments for 4s, 12s or 36s (DURATION). We applied inter-subject correlation and three-dimensional linear mixed-effects modeling with crossed random effects to identify cortical areas selectively modulated by CONTENT LEVEL and DURATION. Effects along the visual processing hierarchy were additionally assessed in a ROI analysis. Whole-brain results were located predominantly within distinct subnetworks of the scene network: Movie scenes, compared to shots, elicited stronger engagement in the visually-attuned posterior subnetwork containing the occipital and posterior parahippocampal place areas. Longer stimuli whereas additionally engaged the memory-related anterior scene network including the anterior parahippocampal place area, retrosplenial cortex, and caudal inferior parietal lobe. ROI analyses confirmed that temporally extended, content-rich stimuli preferentially engaged hierarchically higher areas. Overall, these findings support a functional differentiation within the scene network while expanding on its relation to temporal receptive windows, demonstrating that CONTENT LEVEL and DURATION interact in shaping the cortical processing of naturalistic movie stimuli.

Keywords: naturalistic movie watching, hierarchically nested stimuli, temporal receptive windows, visual processing hierarchy, fMRI, inter-subject correlation, scene network

1. Introduction

Hierarchically nested stimuli are all around us (Ludwigs, 2020; Wu, 2013): The steps and individual movements of an action (Fitch & Martins, 2014; Grafton & Hamilton, 2007; Hamilton & Grafton, 2006; Uithol et al., 2012; Wakita, 2014), a text, made of paragraphs, sentences and words (Fitch & Martins, 2014; Jeon, 2014; Lerner et al., 2011) or a movie, that contains scenes, shots and individual captured frames (Haq et al., 2019; Hasson, Yang, et al., 2008).

This study focuses on the structure of movies, as movies represent a compelling method to investigate cortical responses in a highly engaging, essentially naturalistic setting (Finn & Bandettini, 2021; Hasson, Landesman, et al., 2008). Additionally, movies not only portray a captivating narrative structure (Cutting, 2016), but can also be organized in a hierarchically nested architecture (e.g., Haq et al., 2019). Here we concentrate on three distinct levels of this hierarchical structure: *frames* (low level), *shots* (intermediate level), and *scenes* (high level).

At the lowest level, a frame refers to a single image captured by the camera (e.g., Yeh et al., 2016). When presented rapidly, frames are perceived as continuous motion rather than individual images (Wilcox et al., 2015).

The intermediate level, a movie shot, is a continuous sequence of frames without a cut, forming the smallest narrative unit (Cutting, 2016). Cuts mark abrupt transitions between shots and are often accompanied by a change in camera angle, thus leading to a jarring visual difference between adjacent frames, that, e.g., automatic annotation programs can use to parcellate different shots (Chakraborty et al., 2021; Mas & Fernandez, 2003; Rui et al., 1998; Zhu et al., 2023). For the observer, however, cuts between shots are often designed to go unnoticed (Magliano & Zacks, 2011), while salient transitions typically announce more narratively significant shifts, i.e., between movie scenes.

Movie scenes represent high-level, visually and narratively complex segments, encompassing multiple shots, i.e., camara perspectives, taking place at a certain location and time, or involving a distinct set of characters (Cutting, 2014). A more technical scene definition

relies on screenplay slug lines, which specify the setting and time the scene will be filmed in (Field, 2005). Since definitions of higher-order units (e.g., sequences or action changes) are less consistent (Cutting, 2019a; Magliano & Zacks, 2011), we restrict our analysis to hierarchical levels of frames, shots, and scenes (Figure 1).

Like all hierarchically nested stimuli, a generalizable way to organize these levels is by their temporal duration (Uithol et al., 2012; Valentine & May, 1996; Wu, 2013), since hierarchically higher levels (i.e., scenes) persist longer than hierarchically lower levels (i.e., shots; Cutting et al., 2012; Cutting & Candan, 2015). For the brain to be able to process stimuli according to their temporal durations, it was proposed that different cortical areas contain a range of so-called *temporal receptive windows* (TRWs; Hasson, Yang, et al., 2008). In analogy to spatial receptive windows, TRWs integrate or separate incoming information by their temporal duration (Golesorkhi, Gomez-Pilar, Zilio, et al., 2021; Wolff et al., 2022). The existence and range of these TRWs in the cortex was shown by previous findings, demonstrating that the different hierarchically nested levels of the stimulus' content consistently engaged additional areas corresponding to their duration (for a review see Hasson et al., 2015). Specifically, activation related to shorter stimuli (~ 4 sec) was found in primary cortices reflecting the presented stimulus modality, while longer stimuli (~ 10 – 40 seconds) were additionally encoded in the precuneus, the temporoparietal junction, the posterior superior temporal sulcus and areas in the medial frontal cortex (Aberbach-Goodman & Mukamel, 2023; Farbood et al., 2015; Hasson, Yang, et al., 2008; Lerner et al., 2011). These results point to an increase in TRWs along the unimodal-to-multimodal gradient (Hasson et al., 2015; Wolff et al., 2022) which also aligns with the distribution of intrinsic cortical time scales observed at rest (Golesorkhi, Gomez-Pilar, Tumati, et al., 2021; Ito et al., 2020; Mecklenbrauck, Sepulcre, et al., 2024). Additionally, the retention and recall of longer, temporally coherent stimuli and event structures have been linked to the hippocampus and parahippocampus (Baldassano et al., 2017; Ben-Yakov & Henson, 2018; J. Chen et al., 2016;

Hasson, Furman, et al., 2008; Zadbood et al., 2017), which are functionally connected to areas of longer TRW (J. Chen et al., 2016; Rugg & Vilberg, 2013; E. Yang et al., 2023; Yeshurun et al., 2021).

Overall, the presented results highlight the importance of the stimulus' duration and persistence for its neuronal processing across different cortical areas and networks. However, these previous studies also underscore the inherent link between the temporal structure of a stimulus and its hierarchical organization (Uithol et al., 2012; Valentine & May, 1996; Wu, 2013). In naturalistic stimuli, like the ones applied in the context of TRWs (e.g., Lerner et al., 2011), the duration of a stimulus and the complexity of its content are implicitly confounded. Staying on the topic of movies, a movie scene presents the viewers with a multitude of shots and therefore visually distinct camera angles of possibly different characters or action (Cutting et al., 2012). Showing only one of the shots contained within that scene, however, will not only be temporally shorter but also less visually and narratively diverse.

In the context of this study, we therefore define two distinct factors – the CONTENT LEVEL and the DURATION. The CONTENT LEVEL characterizes whether a stimulus covers a higher or lower level within the hierarchical content structure, i.e., in the movie example, whether viewers perceive a single scene or shot of that movie. The differences between the two levels are manifold: Movie scenes are inherently more visually diverse than shots as because they encompass multiple camera angles (Cutting et al., 2012; T. J. Smith et al., 2012). Also, movie scenes define specific narrative events within the story and transitions between scenes mark identifiable narrative shifts (Cutting et al., 2012; Magliano & Zacks, 2011). A movie scene is thus not only visually but also more narratively complex, integrating multiple, less complex subunits linked by a stable location or timeframe (Cutting, 2019b; Cutting et al., 2012; Cutting & Iricinschi, 2015; Hammoud & Kouam, 2000; Markhabayeva & Tseng, 2024). Hence, we define the difference between the two CONTENT LEVELS as reflecting increases in both visual and narrative complexity, collectively termed *content complexity*.

The DURATION in turn describes the time a stimulus remains within one narrative unit, so how long a continuous section of the movie is presented for before switching to a different segment. In the context of TRW studies, these stimulus durations have ranged from very brief segments lasting less than one second (e.g., Honey et al., 2012) to longer events of up to about one minute (e.g., Farbood et al., 2015).

So far, no studies have tried to specifically disentangle potentially separate contributions of the CONTENT LEVEL and DURATION. The general procedure of TRW studies is to parcellate a natural stimulus according to its content structure which is naturally confounded with its duration (e.g., Uithol et al., 2012) and then to shuffle the segments before the presentation, so the different conditions vary in temporal as well as content persistency (e.g., Lerner et al., 2011). Areas significantly engaged by only higher levels of stimulus persistency are interpreted to have longer TRW, although through the time-content-confound these regions could also be excited by higher-levels of content. Thus, it remains an open question whether the neural processing of a stimulus is (1) based only on its DURATION, (2) based only on the underlying CONTENT LEVEL, or (3) influenced by both factors. In this study we focused specifically on movie stimuli to address this question within the introduced hierarchically nested framework of scenes, shots and frames.

Earlier movie studies applying the TRW predominantly focused on the DURATION, as they did not divide the stimulus according to narrative structure, but only according to visual or acoustic onsets, creating ever finer segments (Hasson, Yang, et al., 2008; Honey et al., 2012). Intriguingly, they still found specific brain areas encoding these different segments, corroborating a duration-based processing. A more recent investigation, however, demonstrated two separate systems integrating stimuli over time and a certain amount of information, respectively (Baumgarten et al., 2021), outlining the importance of both the presented stimulus content as well as their duration. These two systems were further suggested to be adaptive, adjusting to the frequency of stimulus presentation (Baumgarten et al., 2021; Rubin & Turano, 1992; Vagharchakian et al., 2012), which follows the theory that neural processing is accommodating to

the characteristics of the stimuli and environment (VanRullen & Koch, 2003). This adaptability was also described within the TRW framework, as the TRW of areas were shown to be modulated by the speed of stimulus presentation (Lerner et al., 2014) as well as by the attention to the stimulus (Shahdloo et al., 2019). Crucially in the context of movies, Geerligs et al. (2022) suggested that TRWs also adjust to the narrative event structure of a stimulus. This proposed interaction between stimulus duration and hierarchical content structure was further supported by findings that a movie's structure is detected and represented across multiple timescales (Baldassano et al., 2017; Oetringer et al., 2025). Interestingly, these studies demonstrated that the scale of content representation, similarly to TRW (Hasson et al., 2015; Wolff et al., 2022) also follows the cortical hierarchy, as engagement by high-level content elements was observed higher along the visual processing hierarchy (Baldassano et al., 2017; Geerligs et al., 2022; Oetringer et al., 2025). Appropriately, high-level representations were also shown to be modality-independent and shared amongst subjects (J. Chen et al., 2017; Zadbood et al., 2017). Overall, the evidence points to both the CONTENT LEVEL and the DURATION influencing the processing of naturalistic stimuli across the cortex.

In this study we therefore systematically extracted different number of frames from both shots and scenes. By maintaining a constant frame rate, we could generate three duration conditions – 4, 12 and 36 seconds – for the two structural CONTENT LEVELS of interest. Since this frame-level manipulation strips the movie stimulus of its auditory information, these durations were specifically chosen to mirror the experimental setup of Hasson, Yang, et al. (2008), who comparatively presented silent film stimuli. Thus, replicating the whole-brain engagement presented by Hasson, Yang, et al. (2008) would reinforce the validity of the applied stimulus manipulation. Accordingly, we also used the same analysis method – *inter-subject correlation* (ISC), which allows the localization of areas consistently engaged by the manipulated stimuli of different levels of DURATION and CONTENT LEVEL (Hasson et al., 2004; Kauppi et al., 2010; Nastase et al., 2019; Pajula et al., 2012). Importantly, the ISC approach enables the flexible analysis of

naturalistic stimuli without the need for a specific stimulus model (Nastase et al., 2019; Pajula et al., 2012), which is able to identify processes that remain hidden to classic massed univariate models (Ben-Yakov et al., 2012). It is therefore perfectly suited to answer the question, whether natural, hierarchically nested stimuli like movies are processed by the brain according to their temporal duration, based on the content complexity alone, or based on the combination or interaction of the two. Further, as both TRW (e.g., Wolff et al., 2022) and processing of content structure (e.g., Baldassano et al., 2017), were shown to extend along the cortical hierarchy, we further examined the effects of CONTENT LEVEL and DURATION in established regions of interest representing the visual processing hierarchy (Baldassano et al., 2017). Given the presented theoretical backdrop (e.g., Baldassano et al., 2017; Baumgarten et al., 2021; Geerligs et al., 2022; Hasson, Yang, et al., 2008), we expected to find both DURATION and CONTENT LEVEL to play a role in processing hierarchically nested, naturalistic stimuli like movies.

2. Materials & methods

2.1. Participants

In total, 56 right-handed participants (48 Female, *M* = 22.52, *SD* = 2.44 years; range = 19 - 29 years) were recruited for this study. Six participants were excluded because of excessive (> 2.5 mm (one voxel size)) movement during the experiment. An additional subject refrained from participation before entering the MR scanner and another missed the scanning session. Finally, data of 48 (40 Female, *M* = 22.63, *SD* = 2.45 years; range = 19 - 29 years) subjects entered the analysis. All subjects gave informed written consent approved by the University of Münster Research Ethics Committee in accordance with the declaration of Helsinki. The participants ensured to have no history of neurological or psychiatric diseases or any ferromagnetic material inside their bodies. The Edinburgh Handedness Inventory (Oldfield, 1971) was used to assess right-handedness of the subjects (*M* = 85.88, *SD* = 14.30, range = 40 - 100). All participants had (corrected-to-) normal vision. Upon finishing or aborting the study the participants received course credit or money for their participation.

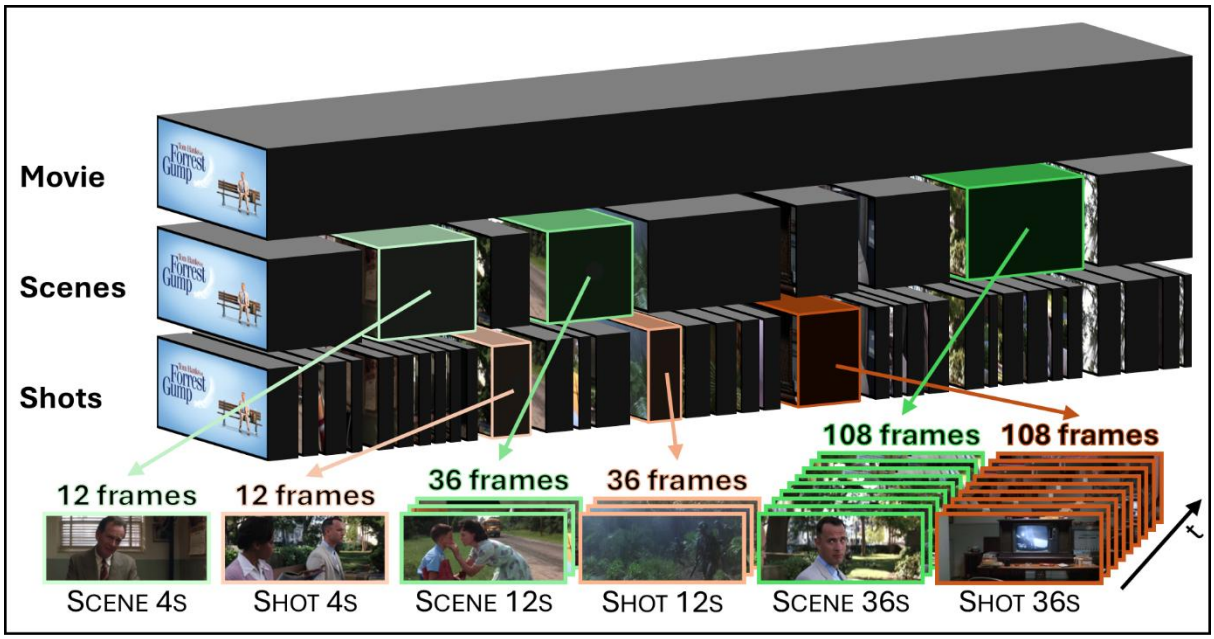
2.2. Stimuli

As stimuli, the participants saw frames that were extracted from movie shots and movie scenes of the Hollywood movie “Forrest Gump” (Zemeckis, 1994). Previous work as part of the StudyForrest project (https://www.studyforrest.org/) meticulously annotated the movie down to the level of perceptual confounds of individual frames (Häusler et al., 2021). We used these publicly available annotations (Häusler & Hanke, 2016) to parcellate the movie into its scenes and shots. This movie and these annotations in particular already served as the basis in multiple other studies investigating the neural processing of naturalistic movie stimuli (e.g., Ben-Yakov & Henson, 2018; Oetringer et al., 2025). In total, the “Forrest Gump” is comprised of 205 scenes containing 848 shots, with an average of 4.12 (*SD* = 7.04, range = 1 – 68) shots per scene. Using the shot-wise rating of emotional arousal of 36 labelled characters, we selected only shots and scenes that contained people with a rated emotional arousal (Hanke et al., 2015). We could thus also determine the number of characters and average emotional arousal within each scene and shot.

In contrast to previous research on TRWs, we did not present the participants with the same stimuli across the conditions (e.g., Hasson, Yang, et al., 2008) but each condition contained non-repetitive content of the movie to mitigate neural attenuation throughout the experiment (Hasson et al., 2006; Larsson & Smith, 2012). For the SCENE conditions we thus selected scenes that depicted at least one character and had at least two shots. Additionally, we excluded scenes that were exceptionally long (> Q3 + 1.5 IQR; > 158.4 seconds) or shorter than four seconds. This selection left us with 80 possible scenes. For the SHOT conditions we also excluded shots without people in them and importantly any shot already included in the selected movie scenes, thus all conditions were created from unique sections of the movie (Figure 1). This resulted in mainly selecting suitable one-shot scenes (66 scenes only comprised of a single shot) as well as shots from the discarded scenes (109) that were longer than four seconds.

Figure 1

Hierarchical movie structure and overview over isochronic frame extraction of all conditions



Note. Movie was annotated into movie scenes and further into movie shots according to (Häusler & Hanke, 2016). We selected specific movie scenes that had at least two shots and movie shots that either were one-shot scenes or shots from longer scenes not selected for the movie scenes before. Selected movie scenes and shots were assorted into six conditions, balancing the segment's duration, emotional arousal, number of characters time and location between conditions (Table 1). Depending on the condition 12, 36 or 108 frames were extracted from each movie SCENE or SHOT, which were presented at a constant frame rate of 3 FPS to manipulate the DURATION (4S, 12S, 36S) of each movie segment in the experiment independently from its CONTENT LEVEL.

For the experiment, the selected shots and scenes were needed to be balanced and assigned to the following across the six experimental conditions: SCENE 4S, with frames extracted from scenes presented for four seconds (12 frames with three frames per second (FPS)), SCENE 12S (36 frames), SCENE 36S (108 frames), SHOT 4S (12 frames), SHOT 12S (36 frames), and SHOT 36S (108 frames; Figure 1). As the conditions were presented in blocks of equal length (648 frames), we needed to distribute the scenes and shots differently amongst the conditions. Fifty-four shots and scenes were needed for 4S conditions, 18 for 12S conditions and six for the 36S conditions, so 78 shots and scenes, respectively, were needed in total. For the final selection, we minimized the Euclidian distance of the number of characters, average arousal and average duration in seconds to match 78 scenes to 78 shots. While this matched movie scenes and shots as closely as possible, natural differences in distributions of arousal and duration between scenes and shots made it impossible to perfectly match the material (Table 1).

Table 1

Summary of emotional arousal, video duration, characters per movie segment and scene features of the selected shots and scenes across the levels of DURATION

Average emotional arousal of depicted characters			
DURATION		CONTENT LEVEL - SHOT	CONTENT LEVEL - SCENE
	4S	-0.35 (0.41)	-0.22 (0.44)
	12S	-0.39 (0.30)	-0.21 (0.33)
	36S	-0.52 (0.25)	-0.21 (0.36)
Video duration (in seconds)			
DURATION		CONTENT LEVEL - SHOT	CONTENT LEVEL - SCENE
	4S	19.94 (17.93)	33.26 (21.92)
	12S	20.81 (9.97)	43.04 (22.96)
	36S	17.53 (23.91)	37.59 (20.43)
Characters per movie segment			
DURATION		CONTENT LEVEL - SHOT	CONTENT LEVEL - SCENE
	4S	1.74 (0.73)	1.87 (0.75)
	12S	1.89 (0.76)	2.17 (0.92)
	36S	1.83 (0.98)	2.17 (0.98)
Scene feature – Time: DAY vs. NIGHT			
DURATION		CONTENT LEVEL - SHOT	CONTENT LEVEL - SCENE
	4S	DAY = 33, NIGHT = 21	DAY = 48, NIGHT = 6
	12S	DAY = 12, NIGHT = 6	DAY = 16, NIGHT = 2
	36S	DAY = 4, NIGHT = 2	DAY = 5, NIGHT = 1
Scene feature – Location: EXT vs. INT			
DURATION		CONTENT LEVEL - SHOT	CONTENT LEVEL - SCENE
	4S	EXT = 34, INT = 20	EXT = 35, INT = 19
	12S	EXT = 10, INT = 8	EXT = 11, INT =7
	36S	EXT = 4, INT = 2	EXT = 4, INT = 2

Note. Values were calculated based on publicly available annotations of "Forrest Gump" (Häusler & Hanke, 2016). EXT = *exterior scene*, INT = *interior scene*.

Subsequently, we assigned the matched shots and scenes to the different conditions while controlling for the average emotional arousal, number of characters, duration and, specifically for scenes, the number of shots. Also, we balanced the number of indoor (INT) or outdoor (EXT) as well as DAY or NIGHT settings amongst the blocks. In this final assignment of conditions, the selected scenes and shots were distributed equally across the movie's runtime, as assessed by comparing the onset timestamp of each segment between conditions, $F_{\text{CONTENT LEVEL}}(1, 150) = 1.20$, $p = .275$, $\eta_p^2 = 0.01$; $F_{\text{DURATION}}(2, 150) = 2.80$, $p = .064$, $\eta_p^2 = 0.04$; $F_{\text{CONTENT LEVEL x DURATION}}(2, 150) = 0.98$, $p = .377$, $\eta_p^2 = 0.01$.

As scenes are generally longer than shots (Cutting & Candan, 2015), compressing them to the same number of frames will shorten scenes disproportionally more than shots, creating

differences in the *duration ratio*, i.e., the perceived tempo. We mitigated this bias by repeating the balancing of scenes and shots between conditions 100 times and selecting the distribution that minimized the difference in this duration-shortening ratio. Thus, the final mean ratios for each condition were as follows: $\overline{\text{Ratio}}_{\text{SCENE 4S}} = 8.32$, $\overline{\text{Ratio}}_{\text{SCENE 12S}} = 3.59$, $\overline{\text{Ratio}}_{\text{SCENE 36S}} = 1.04$, $\overline{\text{Ratio}}_{\text{SHOT 4S}} = 4.98$, $\overline{\text{Ratio}}_{\text{SHOT 12S}} = 1.73$, $\overline{\text{Ratio}}_{\text{SHOT 36S}} = 0.49$. The remaining differences will be discussed later.

As a last step, we pseudo-randomly shuffled the movie segments within each condition. The resulting order thereby balanced the chronological leaps forward and backward through the movie, while not allowing for consecutive sections of the movie or repetitions of the same depicted locations.

Using the timestamps, we cut the movie into short clips of each movie scene and shot with ffmpeg (4.2.7; Tomar, 2006). We then applied an isochronic frame extraction approach to select the necessary number of frames from each clip at regular intervals while keeping the relative temporal structure of the movie segment intact. While this frame extraction allowed us to control the temporal duration of each segment, it unfortunately prevented us from presenting the stimuli with their audio. Therefore, the stimuli that the participants saw consisted of a sequence of images depicting the respective movie scenes or shots for 12, 36, or 108 frames at a time, presented without the associated audio track and thus comparable to the silent film stimuli in Hasson, Yang, et al. (2008)

After extracting all frames for the experiment, we compared the conditions with regard to the visual features of the frames. The analysis revealed that the conditions did not significantly vary with regard to static low-level visual features, including luminance, color contrast, saturation, and overall image complexity. Measures, however, that quantified the variations of one frame to the next, like motion energy and normalized perceptual difference, did vary significantly between CONTENT LEVELS and DURATIONS. Although, this was to be expected, based on the visual and temporal gaps introduced by the frame-wise stimulus manipulation, we will take these

differences into account when interpreting and discussing the results (for all details, see Supplemental Material 1).

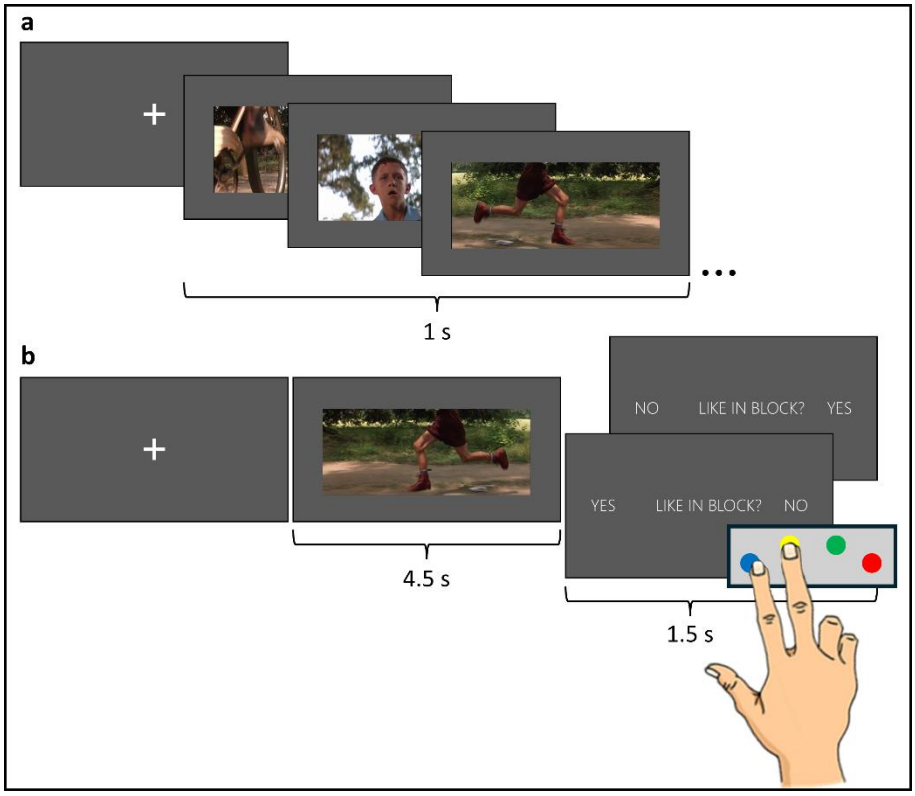
In preparation of the experiment, we created 48 different orders of the six blocked conditions, counterbalancing across participants that each condition appeared at every block position in the experiment as well as each condition transitioning to each other condition equally often. Consequently, every participant viewed a different order of conditions.

As task during the fMRI measurement, participants were instructed to attentively watch the presented frames. After each block, they were then presented with individual frames of the previous block, that could be presented either correctly or mirrored, flipping left to right. The task was to evaluate if the frames stayed the same (answering “YES”) or were mirrored (answering “NO”). For this, we chose six movie segments per block and selected one isochronically extracted frame that resembled the key frame (Katna v0.9.2; Jain et al., 2021) of the respective scene or shot. We made sure that all selected task frames portrayed a person but contained no text. Further, we controlled the overall number of mirrored frames in the experiment and counterbalanced which frames appeared mirrored across participants. For the purpose of this paper, we consider this task as a cover-task, since it just ensured the attention of the participants to the presented frames.

Stimulus selection and balancing was accomplished using RStudio (2024.9.1.394; Posit team, 2024) and MATLAB (9.10.0.1602886 (R2021a); The MathWorks Inc., 2021). Stimuli during the fMRI session were presented using Neurobs Presentation® software (20.3, Neurobehavioral Systems, Inc., Berkeley, CA, www.neurobs.com). Frames were presented at a visual angle of 3.09° on a dark grey background, RGB = (20, 20, 20).

Figure 2

Overview of experimental procedure in fMRI session



Note. (a) Example of frame presentation in a block. Frame rate was set at 3 frames per second. (b) Example of a cover-task trial at the end of each block. Participants saw a frame for 4.5 s and had to determine if it was depicted like in the block before ("YES") or mirrored ("NO"). The assignment of the answers to the response buttons could change randomly between trials.

2.3. Procedure

The experiment was divided into two sessions: one group session where multiple participants watched the movie and the individual experimental fMRI sessions two days later.

For the movie session we invited all participants (three to five at a time) that would partake in the fMRI session two days later to watch the movie. This session was included to familiarize the participants with the material. As some participants had never seen "Forrest Gump" (Zemeckis, 1994) prior to the study while others already had watched it up to five times (62.5% knew the movie, $M_{\text{Times seen}} = 1.83$, $SD_{\text{Times seen}} = 1.03$), we aligned the different levels of experience by showing each participant the movie in advance. The session started with a short questionnaire assessing the subjects' current mood before the movie using the Self-Assessment Manikin (SAM; Bradley & Lang, 1994; Knejzlíková et al., 2021) and the Positive and Negative Affect Schedule (PANAS; Janke & Glöckner-Rist, 2014; Watson et al., 1988), which are used to evaluate the affect of individuals

(e.g., Thorenz et al., 2023). Then the participants watched the movie as if they were at the cinema. After the movie the subjects repeated the SAM and PANAS and answered additional questions on their experience with “Forrest Gump”, their opinion on the movie as well as if they rated certain scenes especially crucial for the plot, particularly memorable and whether specific scenes where personally relevant to them.

Two days later, the participants returned for individual fMRI sessions. These sessions started with capturing a high-resolution T1-weighted anatomical reference image. After that, we collected eight minutes of open-eyed resting-state fMRI from the participants. The subjects had to focus on a fixation cross for the duration, which is recommended for controlled resting-state measurements (Agcaoglu et al., 2019; Patriat et al., 2013; Van Dijk et al., 2010). The following main experiment then consisted of six blocks, presenting each combination of CONTENT LEVELS and DURATIONS once. The order of blocks was counterbalanced across participants. Each block started with a fixation cross (2100 – 2600 ms), that blinked three times in rapid succession signaling the start of the frame presentation. The blocks contained 648 frames, that were presented with a frame rate of 3 FPS (Figure 2a). After this sequence of frames, the participants were noticed about the upcoming task, which had six trials. Each trial stated with a fixation cross (800 – 1300 ms), followed by 4.5 seconds of frame presentation. This frame could be presented correctly or mirrored. The participants then saw the question “LIKE IN BLOCK?”, which they had to answer with “YES” if the frame looked correct or “NO” if it was mirrored. They had 1.5 seconds to give an answer, skipping to the next trial after they pressed a button. The assignment of the two answer buttons to “YES” and “NO” could randomly switch between trials. The current assignment for each trial was always presented with the question (Figure 2b). The random switches were implemented to prevent any preparatory activation in the motor areas during the presentation of the frame (Schubotz & Von Cramon, 2002). After each block the participants had a break of approximately one minute while the frames for the next block were pre-loading. During this break the experimenters would check in with the subjects, asking them if they were ready to continue.

At the end of the experiment, the participants received feedback of how many of the 36 total cover-task trials they answered correctly. The scanning protocol finished with the acquisition of five phase-inverted functional scans that were later used for field map correction. In total the participants spent about 45 minutes in the MR scanner. After the scanning session the participants filled out a final questionnaire, asking for scenes that were crucial for the plot, especially memorable, or personally important as well as assessing their MRI experience.

2.4. MRI data acquisition

MRI images were recorded using a 3 T Siemens Magnetom scanner (Siemens, Erlangen) equipped with a 20-channel head coil. High-resolution structural reference images were acquired using a standard Siemens 3D T1-weighted magnetization-prepared rapid acquisition gradient echo (MPRAGE) sequence (voxel size = 1 x 1 x 1 mm (isotropic); field of view (FOV) = 256 mm; 256 x 256 data acquisition matrix; 192 slices; 8° flip angle; time of repetition (TR) = 2130 ms; echo time (TE) = 2.28 ms). Resting-state as well as task-related functional blood-oxygen-level-dependent (BOLD) images were acquired parallel to the anterior commissure/posterior commissure line. A T2*-weighted simultaneous multi-slice echo-planar imaging (SMS-EPI; 84 x 84 matrix; FOV = 210 mm; 71° flip angle; TR = 1500 ms; TE = 30 ms) was applied. Each acquired volumed was made up of 63 axial slices with a slice thickness of 2.5mm, a distance factor of 5% (0.125 mm) and a voxel size of 2.5 x 2.5 x 2.4 mm^3. Slice acquisition and multi-slice mode were interleaved with an acceleration factor of 3. The functional data was acquired in one 8 min resting state run and six task-blocks sequences were each 5:10 min long. Additionally, we acquired five supplementary volumes at the end using the same acquisition parameters but flipping the phase encoding direction. The volumes were later used to estimate and correct field inhomogeneities using FSL's topup (Andersson et al., 2003; S. M. Smith et al., 2004).

2.5. fMRI preprocessing and nuisance regression

In preparation of the ISC analysis, the preprocessing of the fMRI task-data was in large parts based on the recommendations in Nastase et al. (2019) for data processing in the Statistical

Parametric Mapping software (SPM12; FIL Methods Group, 2017). Additionally, after manual reorientation to MNI space, we applied topup in FSL (6.0.5.1; Andersson et al., 2003; Smith et al., 2004) to correct for magnetic field inhomogeneities. We then returned to SPM12 for the slice time correction of the data to the temporally first slice. Functional images were then realigned to the mean image, co-registered with anatomical data and normalized to MNI standard space, before being smoothed using a 6 x 6 x 6 mm^3 Gaussian smoothing kernel. This smoothing kernel size was chosen based on recommendations for temporal ISC (Nastase et al., 2019). Further, as we planned to correct for multiple comparisons by controlling the familywise error rate (FWE), a smoothing kernel of at least twice the voxel size was necessary to fulfill the smoothness assumptions of Gaussian random field theory underlying FWE (Poldrack et al., 2011). After smoothing, the signal was the high pass filtered at 0.01 Hz in accordance with Nastase et al.'s (2019) ISC tutorial. To filter any unwanted signal out of the data, we then applied a nuisance regression. As an extension to the guidelines, the applied model included the six motion six motion parameters from the realignment as well as the top five components of both the white matter and cerebrospinal fluid signal (Behzadi et al., 2007). This nuisance regression model was shown to offer the best balance between maximizing ISCs and controlling for adverse influences of movement (Nastase & Hasson, 2024).

2.6. Inter-subject correlation

In general, ISC can be used to determine the reliability of neural activity across a group of subjects who viewed a temporally synchronized stimulus. If the ISC is particularly high in a specific area, it can be assumed that this area encodes information about the presented stimulus (Nastase et al., 2019). In the context of the TRW framework, ISC can identify areas that are specifically engaged by different levels of the hierarchically nested stimulus, as shuffling the stimulus according to its structure will only engage areas that are tuned to specific, maintained aspects of the stimulus (e.g., Lerner et al., 2011).

The following ISC analysis was conducted on the residuals resulting from the completed nuisance regression. These residuals were further *z*-scaled per condition and voxel, and masked using a gray matter mask, averaged across all normalized participants. This gray matter mask included a total of 99709 voxels. As recommended (Nastase et al., 2019), we excluded the first five images (7.5 seconds) of each block, which left a time course of 147 images representing 220.5 s of stimulus presentation per condition. ISC was then used to correlate the voxel-wise time courses of all 99709 voxels across participants (Figure 3).

We specifically calculated the correlations using the pairwise-ISC approach which correlates the voxel-wise time course of one subject with the time course in the same voxel of every other subject (Hasson et al., 2004) using Pearson correlation:

$$r_{AB}=r(x_A, x_B)= \frac{\sum_{t=1}^{T}(x_A(t)-\bar{x}_A)(x_B(t)-\bar{x}_B)}{\sqrt{\sum_{t=1}^{T}(x_A(t)-\bar{x}_A)^2}\sqrt{\sum_{t=1}^{T}(x_B(t)-\bar{x}_B)^2}} \quad (1),$$

with $x_A(t)$ and $x_B(t)$ being the time course of the same single voxel of subjects A and B, respectively. Applying Eq. 1 on to all voxel-wise time courses resulted in $\frac{N*(N-1)}{2}=\frac{48*47}{2}=1128$ pairwise-ISC whole-brain maps per condition. Each of the 99709 gray matter voxels in every whole-brain map therefore contained the correlation between time course evoked by a specific condition for a subject pair in this particular voxel. These maps were the basis for the following whole-brain analysis (Figure 3). The goal of the analysis was to identify clusters of voxels in which the conditions differed significantly regarding the evoked ISC correlation.

Statistically ISC data have to be handled carefully. Through the correlation of data between participants, the resulting values violate the independence assumption, preventing the use of conventional analysis methods (G. Chen et al., 2016; Kauppi et al., 2014; Nastase et al., 2019). A recent set of papers established advanced methods to specifically handle the complex covariance structure amongst pairwise-ISC data in a linear mixed-effect modeling framework by using crossed random effects for both subjects involved in the pairwise correlations (G. Chen et al., 2016, 2017, 2020). Thus, 3dISC (G. Chen et al., 2017) in AFNI (25.1.03; Cox, 1996) allowed us

to specifically consider the dependencies between participants when modeling and comparing the ISC values in each single voxel to identify cortical areas specifically engaged by different levels of CONTENT LEVEL and DURATION in the stimuli.

2.6.1. Mean effect calculation. Before contrasting the conditions to identify the effects of CONTENT LEVEL and DURATION, we first calculated the condition-wise average ISC maps. With these ISC maps we wanted to validate the applied manipulation by reproducing the effects detailed for naturalistic movie stimuli before (Hasson, Yang, et al., 2008) using just our frame-wise manipulation. Therefore, we Fisher *z*-transformed every gray matter voxel the individual ISC maps to normally distribute the correlation values (Bond & Richardson, 2004). Then we applied a simple, intercept-only model within the 3dISC framework (G. Chen et al., 2017) that estimated z_{AB}, i.e., the Fisher *z*-transformed correlation in a specific voxel between two subjects, by the grand average of this voxel for the condition and the crossed random effects for the given subject pair (Figure 3):

$$z_{AB} \sim 1 + (1|\,\mathrm{Subj}_A) + (1|\mathrm{Subj}_B) \quad (2).$$

This model therefore determined the average ISC for each condition in every voxel, which were projected to ICBM152 surface space using BrainNet Viewer (1.7; Xia et al., 2013; http://www.nitrc.org/projects/bnv/) and are depicted in Figure 4.

2.6.2. Contrast calculation. To then estimate the differences between conditions, we calculated contrasts between the pairs of ISC whole-brain maps. Specifically, we considered six two-sided comparisons to cover all main effects and interactions of interest: SHOT vs. SCENE for the main effect of CONTENT LEVEL, 4S vs. 12S, 4S vs. 36S, and 12S vs. 36S for the effects of DURATION, and SCENE X 12 S = (SCENE 4S > SHOT 4S) vs. (SCENE 12S > SHOT 12S) and SCENE X 36S = (SCENE 4S > SHOT 4S) vs. (SCENE 36S > SHOT 36S) for the specific effects of the interactions for longer scenes. Additional contrasts that were not part of the main analysis are reported in Supplemental Material 6. All contrasts were determined by applying AFNI's 3dcalc to calculate weighted averages as well as differences between the Fisher's *z* transformed ISC maps (Figure 3). We thus ended up with

1128 whole-brain maps of all pairs for each contrast. Using these contrast maps, we could apply a similar model to Eq. 2 just with the pairwise difference Δz_{AB} and estimated the effects of each contrast in each gray matter voxel across all subject pairs (Figure 3):

$$\Delta z_{AB} \sim 1+(1|\,\mathrm{Subj}_A)+(1|\mathrm{Subj}_B) \quad (3).$$

Using Monte Carlo simulations, we determined the cluster threshold that corresponded to an FWE-corrected $\alpha < .05$ at a cluster forming threshold of $p < .001$ for both the average ISC maps and the contrast maps. Therefore, we first estimated the smoothness of the data from the underlining residuals used in each model (AFNI's 3dFMWHx), before applying AFNI's ClustSim to determine the cluster thresholds (Figure 3). The resulting thresholds included an average of 35.08 voxels (range = 34 – 36 voxels). The specific thresholds are noted in the respective result tables (Tables 2-4) and figures (Figure 4 – 7). Finally, we applied these thresholds to the results of 3dISC using AFNI's 3dCulterize for bisided tests and clusters connected to their neighbors, face-, edge- and cornerwise (*NN* = 3). The procedure was applied to the whole-brain results for both the condition-wise averages as well as the contrasted maps.

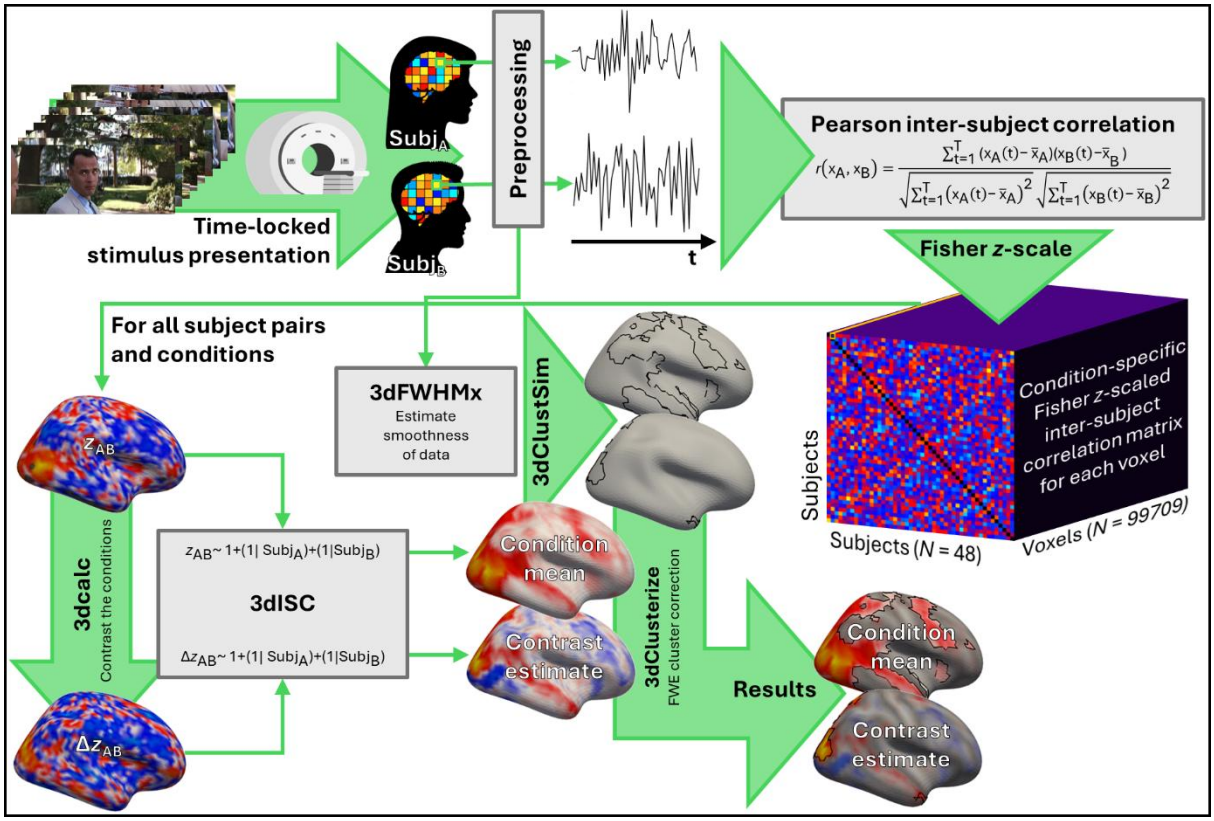
2.6.2.1. Whole-brain figure construction. The resulting thresholded whole-brain contrasts are depicted on the brain's surface, mirroring the result graphics of previous TRW studies for easier comparison (e.g., Hasson, Yang, et al., 2008). Additionally, we followed the "Highlight, don't Hide" principle (Taylor et al., 2023), i.e., the clusters passing the significance threshold are plotted at full opacity with a black outline, while the opacity of all results below the threshold is scaled down to represent their respective level of significance. This method of plotting improves overall objectivity, reliability, and reproducibility of the result reports (Taylor et al., 2023).

To achieve this portrayal, we plotted a combination of three whole-brain maps resulting from the 3dISC analysis described above (Figure 3): the thresholded cluster maps created by 3dClusterize, the unthresholded contrast estimates produced by the 3dISC modeling and the t-values associated with these unthresholded voxel-wise maps. All three images were translated

from MNI volume-space into fsaverage surface space using nilearn.surface.vol_to_surf (0.11.1; https://nilearn.github.io/dev/modules/generated/nilearn.surface.vol_to_surf.html) which is common practice for this conversion (e.g., Pang et al., 2023). This function sampled the voxel values within a 3 mm radius around each pial surface vertex. A 3 mm sampling radius thereby corresponded to the 6 x 6 x 6 mm^3 smoothing kernel that was applied in preprocessing; thus, no additional blurring was introduced. Having obtained a value for each vertex, we plotted the 3D surfaces using pyvista.Plotter(0.45.2; https://docs.pyvista.org/api/plotting/_autosummary/pyvista.plotter). In this context, we scaled the absolute *t*-values to values between 0 and 1 and used them as the opacity parameter for the depiction of the unthresholded contrast estimates. Lastly, the cluster maps were used to overlay the thresholded, significant clusters on top of the unthresholded results, plotted at full opacity and outlined in black, making them more discernible against the surface plots. The full code for figure creation together with all the other code from stimulus selection to analysis as well as a link to data for replication can be found at https://github.com/FalkMeck/Time_Points_or_Plot_Points.

Figure 3

Analysis pipeline of whole-brain inter-subject correlation (ISC) analysis



Note. Frames were presented in a time-locked manner for each condition. Cortical time courses were therefore synchronized between participants. Preprocessing included slice time correction, motion correction, normalization to Montreal Neurological Institute (MNI) standard space, smoothing with a 6mm Gaussian kernel, as well as nuisance regression of the data. The preprocessed gray matter voxel time courses were then Pearson inter-subject correlated between each pair of subjects and Fisher *z*-scaled for normal distribution (Bond & Richardson, 2004). Condition-specific z-scaled voxel-wise inter-subject correlations (ISCs) then either directly modeled for the condition-wise means or further contrasted between conditions for estimating the effects of CONTENT LEVEL and DURATION. Modeling was performed using AFNI's 3dISC (G. Chen et al., 2016) specifically modeling the convoluted covariance structure of ISC data via crossed random effects for each subject pair. Data smoothness was estimated (3dFWHMx) and cluster size was determined (3dClustSim) using a $p < .001$ initial cluster forming threshold and representing an FWE-corrected $\alpha = 5\%$. Thresholds were applied to the modeling results through 3dClusterize to produce the final results for the condition-wise means and estimated effects of CONTENT LEVEL and DURATION.

2.6.3. Region of interest analysis. As previous studies found a distinction for both the duration and content of the stimulus throughout the visual processing hierarchy (Baldassano et al., 2017; Hasson et al., 2015; Jääskeläinen et al., 2021; Wolff et al., 2022), we additionally looked at the effects of CONTENT LEVEL and DURATION not only at whole-brain level but also in specific regions of interest (ROIs) along the cortical hierarchy. For this purpose, we based our selection of ROIs on the areas established by Baldassano et al. (2017), who chose four bilateral ROIs outlining the visual processing hierarchy: the primary visual cortex (V1), an area in the extrastriate visual cortex, namely hV4 (Wade et al., 2002), the angular gyrus (AG) and the posterior medial cluster

from the default mode network (pmDMN; Shirer et al., 2012). As a control ROI Baldassano et al. (2017) included the Heschel's Gyrus which represents the primary auditory cortex (A1). We defined the same ROIs using the same methods described in Baldassano et al. (2017): Thus, hV4 was based on the probabilistic atlas introduced in L. Wang et al. (2015) thresholded at a probability of 25%. AG was obtained from the Anatomy toolbox (Eickhoff et al., 2005) based on the Jülich atlas (Amunts et al., 2020). The cluster pmDMN was extracted from the maps published in accordance with Shirer et al. (2012) and split into a left and right hemispheric cluster. The control area A1/Heschl's Gyrus was pulled from the probabilistic Harvard-Oxford atlas (Desikan et al., 2006; Frazier et al., 2005; Goldstein et al., 2007; Makris et al., 2006) threshold at 25% probability. Lastly, since the definition of V1 was not closer described, we retrieved V1 from the Anatomy toolbox (Eickhoff et al., 2005).

From these five ROIs we extracted the average, Fisher *z*-transformed pairwise-ISC for each condition, separately for both hemispheres using MarsBaR (Brett et al., 2002).

To analyze the effects of CONTENT LEVEL, DURATION and their interaction in the ROIs, we modelled the data in using the lme4 framework (Bates et al., 2015) in RStudio (Posit team, 2024). As the 3dISC tool is also based on lme4, we were able to also model the dependencies in covariance structure using crossed random effects for the involved subjects mirroring the whole-brain model. Hence, we used the same model in all ten ROIs across both hemispheres:

$$\overline{z_{AB_{ROI}}} = 1 + \text{CONTENT LEVEL} * \text{DURATION} + (1|\text{Subj}_A) + (1|\text{Subj}_B) \quad (4),$$

with the CONTENT LEVELS SCENE and SHOT, the DURATIONS 4S, 12S, and 36S and $\overline{z_{AB_{ROI}}}$ being the average Fisher *z*-transformed ISC per ROI. As the dependencies between data points complicate the specification of the degrees of freedom, we employed parametric bootstrapping within lme4 (bootMer, N_{boot} = 500) to determine the estimates, confidence intervals and *p*-values for all fixed effects. Lastly, we adjusted the p-values for multiple comparisons across all contrasts between conditions and ROIs controlling the false discovery rate (FDR) at α =.05 (Benjamini &

Hochberg, 1995; Benjamini & Yekutieli, 2001). Results are reported with the FDR-corrected p-values.

Complementary to the five ROIs related to the visual processing hierarchy, we additionally investigated five more areas that were commonly found in the context of movie watching studies in a supplementary analysis: the parahippocampal gyrus (PHG), the anterior (aHC) and posterior hippocampus (pHC), the temporo-parietal junction (TPJ), and the medial prefrontal cortex (mPFC; for all details see Supplemental Material 4).

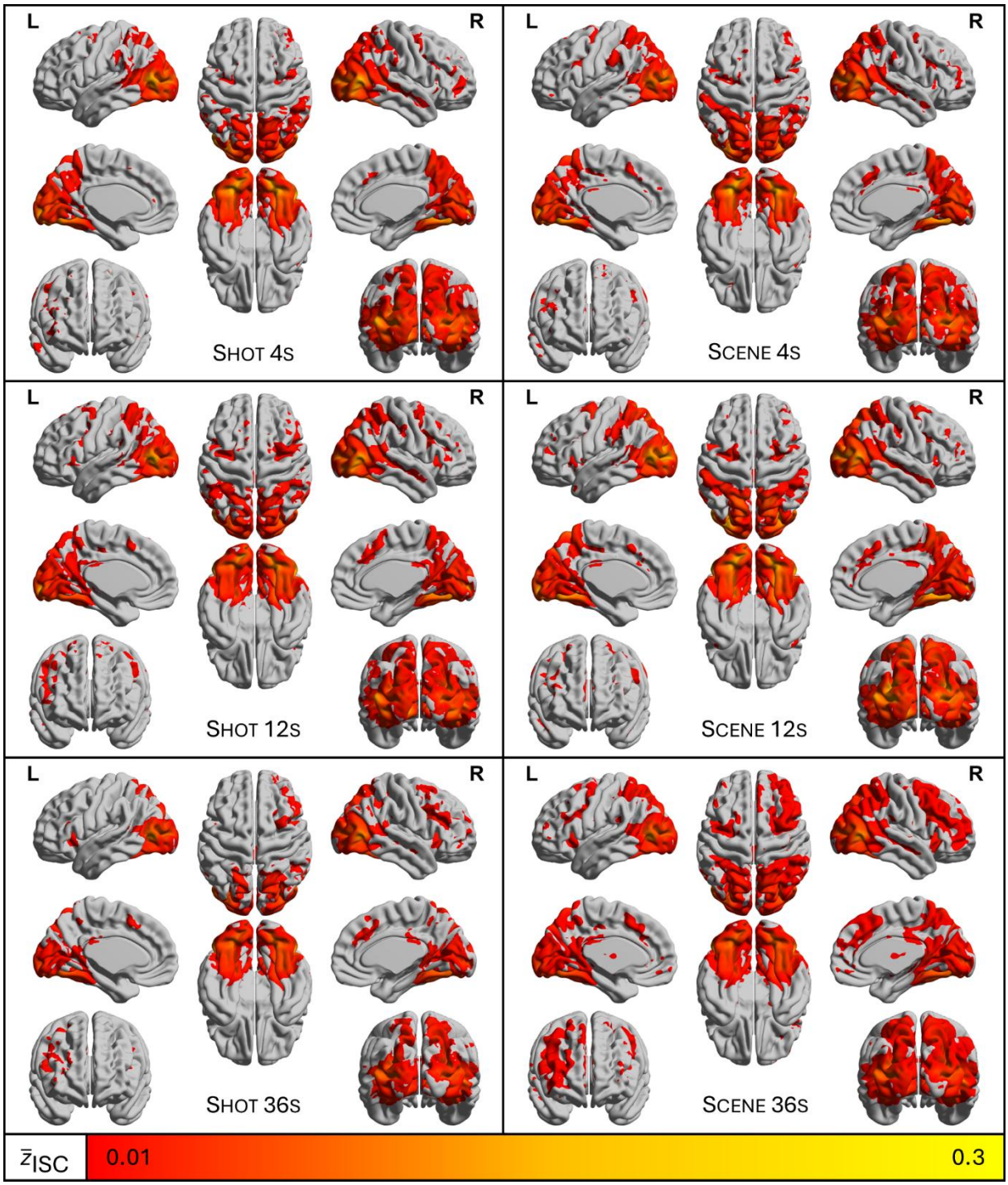
3. Results

Before directly comparing the six conditions of the 2 CONTENT LEVEL x 3 DURATIONS design, we looked at the average ISC within each condition across subjects (Figure 4).

Regardless of the condition, the stimuli consistently engaged the entire occipital lobe, including ventral areas like the fusiform gyrus (FG) or lingual gyrus (LingG). Furthermore, all conditions induced reliable signal in superior parietal lobe (SPL), engaging areas along the intraparietal sulcus (IPS), as well as precuneal areas. In the temporal lobe, the condition-wise average ISC extended along the right superior temporal sulcus (STS), while only in the SCENE 36S condition we found consistent engagement also along the left STS, indicating a difference between the conditions. This difference was also noticeable in the frontal lobe. Although all conditions showed increased ISC values bilaterally along the precentral sulcus as well as the right medial frontal cortex (Brodman area 8), the engagement of additional areas in the lateral portions of the frontal lobe varied between the conditions. For instance, the SCENE conditions engaged areas in both the left and right middle frontal gyrus (MFG), while the SHOT 36S condition in particular depicted a more lateralized effect, only engaging the right MFG. To specifically test these visually identified differences, we conducted direct comparisons between the conditions to identify the main effects of CONTENT LEVEL and DURATION and their interaction.

Figure 4

Average Fisher z-transformed pairwise inter-subject correlation by condition of the CONTENT LEVEL x DURATION design



Note. Maps are FWE-cluster corrected at α = .05 with a cluster forming threshold of p < .001, Monte Carlo simulated cluster extend threshold is are in order top-left to bottom-right 36, 35, 36, 36, 36, and 34 voxels, respectively. Maps are depicted on the ICBM152 template using BrainNet Viewer (1.7; Xia et al., 2013; http://www.nitrc.org/projects/bnv/).

3.1. Effect of CONTENT LEVEL

Bidirectionally comparing the average ISC between the SCENE and SHOT conditions, we only found significant differences for the comparison SCENE > SHOT (Table 2, Figure 5). SCENE stimuli compared to SHOTS significantly engaged a large cluster in the left middle occipital gyrus (MOG) that overlapped with the occipital place area (OPA; Dilks et al., 2013) and early visual cortices like V3A/B, while also extending to the right precuneus and bilaterally to the SPL. Moreover, we found a cluster in the right MOG which included OPA as well and spread to the right IPS. Additionally, more engagement for SCENES was found bilaterally in the collateral sulcus between the FG and LingG, continuing into the posterior parahippocampal place area (PPA; Steel et al., 2025). Finally, we localized significant clusters in the right anterior middle temporal gyrus (MTG), i.e., the temporal pole, as well as the left supramarginal gyrus (SMG) and cingulate sulcus.

3.2. Effect of DURATION

Next, we compared the three levels of DURATION against each other while averaging across the two CONTENT LEVELS. In the bidirectional comparison between the 4S and 12S DURATION (Table 3, Figure 6a) we identified the bilateral collateral sulcus extending into the PHG in the left hemisphere, which overlapped with the anterior PPA (Steel et al., 2025). Further clusters emerged in the bilateral SPL and bilateral superior frontal gyrus (SFG) as well as the right retrosplenial cortex (RSC) and right inferior parietal lobe (IPL), that were significantly more engaged by stimuli of 12S DURATION. In the opposite comparison, we found that the left LingG and left FG to be more reliably engaged by 4S DURATION stimuli.

When comparing the 36S and 4S DURATIONS (Table 3, Figure 6b), we located three clusters in the right hemisphere, namely in the RSC, the IPL and the inferior frontal junction, that were significantly more reliably engaged by stimuli of 36S DURATION. Areas that were more engaged by 4S DURATION stimuli included a large cluster spanning from the left collateral sulcus, representing the posterior PPA, to the left inferior occipital gyrus (IOG), bilateral cuneus and left superior LingG as well as additional clusters in the right LingG, the left SMG and the right STS.

Lastly, contrasting the conditions of 36s and 12s Duration (Table 3, Figure 6c), we did not identify any clusters that were significantly more engaged for 36s Duration stimuli. But the opposite side of this bidirectional contrast yielded a large cluster covering the left IOG, right anterior LingG and bilateral cuneus. An IOG cluster was also found in the right hemisphere. In addition, clusters emerged in the collateral sulcus in both hemispheres, which comprised the entire PPA in the right and the anterior PPA in the left hemisphere. Finally, the contrast revealed clusters in the right inferior postcentral sulcus, the left RSC, left precuneus, left SMG, and left MOG/MTG overlapping with area MT+ (Dumoulin et al., 2000).

3.3. Interaction between Content Level and Duration

To test for an interaction effect between the two factors, we contrasted the respective differences between Scenes and Shots of 12s (Scene 12s > Shot 12s) and Scenes and Shots of 36s (Scene 36s > Shot 36s) with the difference of Scenes and Shots of 4s Duration (Scene 4s > Shot 4s). With these comparisons we could specifically determine areas that were more reliably engaged by Scenes of a longer Duration (Scene x 12s and Scene x 36s, respectively). The contrast between these two interactions is reported in Figure S6.4. For Scene x 12s stimuli the engaged areas included a cluster in the left MOG encompassing OPA and extending to the area MT+ and the IPS as well as a cluster in the left collateral sulcus covering PPA that spread laterally into the left temporo-occipital incision. We further located clusters in the left SPL, left RSC and right precuneus as well as the right PHG, which circumscribed the anterior PPA, engaged in the Scene x 12s condition (Table 4, Figure 7a). Similarly, for the Scene x 36s condition we also found a cluster in precuneus but in the left hemisphere as well as clusters in the right LingG and the left IPS, that both expanded into the left and right MOG, respectively, and contained the OPAs. Additionally, we identified the bilateral IOG as well as the bilateral MOG/MTG representing area MT+. Lastly, we found clusters in the bilateral STG and STS stretching anterior to the temporal pole to be specially engaged for this interaction (Table 4, Figure 7b). The respective opposite contrasts did not yield any significant clusters.

Table 2

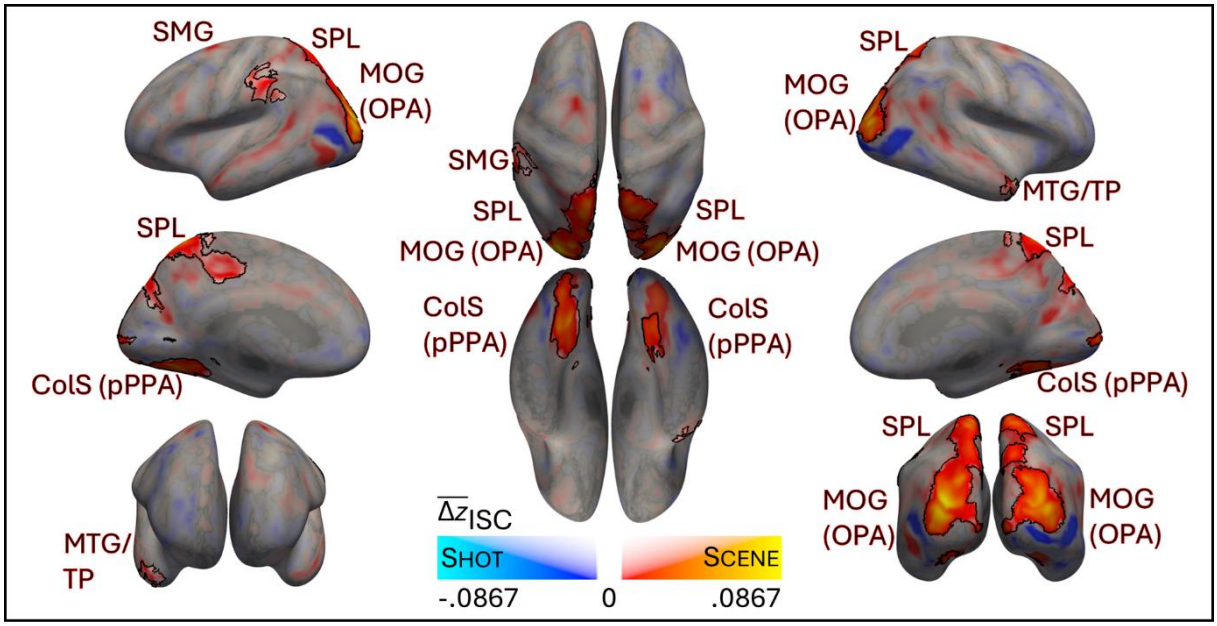
Significant differences in Fisher z-transformed inter-subject correlations between the SCENE and SHOT conditions averaged across DURATIONS

Localization	H	Cluster extent (in voxel)	Peak coordinates (MNI space) x	y	z	*z* value difference
SCENE > SHOT						
Superior partial lobe	R	67	20.5	-74.5	45	0.04
Supramarginal gyrus	L	75	-57	-29.5	40	0.02
Cingulate sulcus	L	69	-12	-27	37.5	0.02
Middle occipital gyrus (OPA)	L	1594	-32	-89.5	12.5	0.09
Superior parietal lobe	L	l.m.	-14.5	-59.5	62.5	0.05
	L	l.m.	-14.5	-74.5	47.5	0.04
Superior parietal lobe	R	l.m.	13	-57	65	0.05
	R	l.m.	25.5	-57	62.5	0.04
Middle occipital gyrus (OPA)	R	588	33	-84.5	10	0.07
Intraparietal sulcus	R	l.m.	30.5	-79.5	20	0.06
Collateral sulcus (posterior PPA)	R	56	30.5	-59.5	-7.5	0.04
Collateral sulcus (posterior PPA)	L	310	-27	-62	-10	0.07
Middle temporal gyrus/ Temporal pole	R	78	55.5	8	-22.5	0.02
SCENE < SHOT						
No significant clusters						

Note. Results are FWE-cluster corrected at α = .05 with a cluster forming threshold of $p < .001$, Monte Carlo simulated cluster extend threshold is 36 voxels. H = *Hemisphere*; L = *left*; R = *right*; MNI = *Montreal Neurological Institute*; l.m. = *local maximum*; OPA =*occipital place area*; PPA = *parahippocampal lace area*.

Figure 5

Whole-brain results of the differences in Fisher z-transformed inter-subject correlations between the SCENE and SHOT conditions averaged across DURATIONS



Note. SCENE > SHOT contrast in warm colors, SHOT > SCENE contrast in cold colors. Results are FWE-cluster corrected at α = .05 with a cluster forming threshold of $p < .001$, Monte Carlo simulated cluster extend threshold was 36 voxels. Significant clusters are depicted with a black border and are labelled accordingly. Red labels describe clusters belonging to the SCENE > SHOT contrast. Results figures applies the "Highlight, don't Hide" principle (Taylor et al., 2023). Thus, clusters with non-significant *p*-values are not omitted but displayed at lower opacity. Whole-brain results are projected on inflated fsaverage pial surface. ColS = *collateral sulcus,* MOG = *middle occipital gyrus*, MTG = *middle temporal gyrus*, OPA = *occipital place area*, pPPA = posterior parahippocampal place area, SMG = supramarginal gyrus, SPL = superior parietal lobe, TP = temporal pole.

Table 3

Significant differences in Fisher z-transformed inter-subject correlations between the levels of DURATION averaged across the CONTENT LEVELS

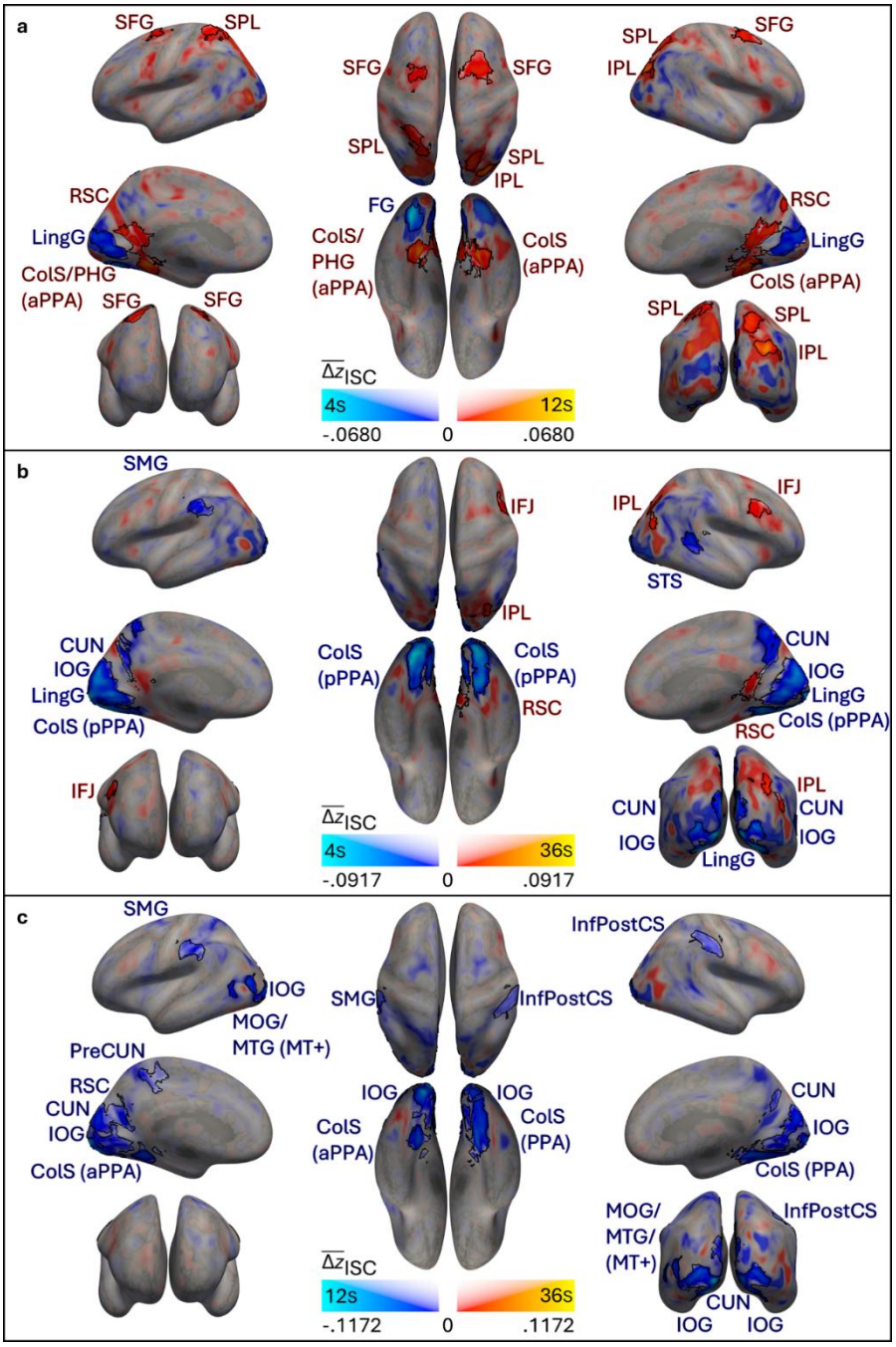
Localization	H	Cluster extent (in voxel)	Peak coordinates (MNI space) x	y	z	*z* value difference
12s > 4s						
Superior parietal lobe	L	67	-22	-59.5	62.5	0.03
Superior frontal gyrus	L	34	-27	-2	60	0.02
Superior frontal gyrus	R	120	23	3	57.5	0.02
Superior parietal lobe	R	129	18	-64.5	52.5	0.03
Inferior parietal lobe	R	84	33	-77	25	0.05
Retrosplenial cortex	R	326	15.5	-52	7.5	0.05
Collateral sulcus (anterior PPA)	R	179	28	-39.5	-10	0.04
Collateral sulcus/ Parahippocampal gyrus (anterior PPA)	L	137	-27	-44.5	-10	0.05
12s < 4s						
Superior lingual gyrus	L	440	-2	-77	7.5	-0.03
Inferior lingual gyrus	L	l.m.	-7	-72	2.5	-0.02
Fusiform gyrus	L	95	-29.5	-77	-12.5	-0.07

36s > 4s						
Inferior frontal junction	R	48	38	8	30	0.03
Inferior parietal lobe	R	58	35.5	-74.5	27.5	0.04
Retrosplenial cortex	R	67	8	-49.5	7.5	0.02
36s < 4s						
Supramarginal gyrus	L	84	-62	-32	32.5	-0.03
Superior temporal sulcus	L	66	50.5	-37	5	-0.03
Lingual Gyrus	R	347	18	-92	-5	-0.09
Collateral sulcus (posterior PPA)	L	2374	-24.5	-82	-15	-0.09
Cuneus	R	l.m.	0.5	-79.5	37.5	-0.03
	L	l.m.	-2	-77	25	-0.04
	L	l.m.	-2	-92	17.5	-0.03
	R	l.m.	0.5	-74.5	12.5	-0.05
	R	l.m.	0.5	-89.5	10	-0.04
Superior lingual gyrus	L	l.m.	-4.5	-69.5	2.5	-0.04
Inferior occipital gyrus	L	l.m.	-14.5	-92	-5	-0.07
36s > 12s						
		No significant clusters				
36s < 12s						
Precuneus	L	35	-7	-44.5	55	-0.02
Supramarginal gyrus	L	73	-59.5	-27	37.5	-0.02
Inferior postcentral sulcus	R	95	60.5	-19.5	37.5	-0.02
Retrosplenial cortex	L	85	-17	-59.5	15	-0.03
Middle occipital gyrus/ Middle temporal gyrus (MT+)	L	54	-49.5	-77	10	-0.05
Inferior occipital gyrus	R	274	18	-92	-2.5	-0.07
Inferior occipital gyrus	L	1197	-14.5	-94.5	-7.5	-0.12
Cuneus	R	l.m.	3	-79.5	32.5	-0.03
	L	l.m.	-4.5	-79.5	25	-0.03
Anterior lingual gyrus	R	l.m.	10.5	-64.5	0	-0.03
Collateral sulcus (anterior PPA)	L	116	-29.5	-47	-7.5	-0.06
Collateral sulcus (anterior and posterior PPA)	R	250	30.5	-44.5	-7.5	-0.07

Note. Results are FWE-cluster corrected at α = .05 with a cluster forming threshold of $p < .001$, Monte Carlo simulated cluster extend threshold is 34 voxels (12s ≠ 4s), 34 voxels (36s ≠ 4s), and 35 voxels (36s ≠ 12s), respectively. H = *Hemisphere*; L = *left*; R = *right*; MNI = *Montreal Neurological Institute*; l.m. = *local maximum*; PPA = *parahippocampal place area*.

Figure 6

Whole-brain results of the differences in Fisher z-transformed inter-subject correlations between the levels of DURATIONS averaged across the CONTENT LEVELS



Note. (a) Results of contrasting 12s and 4s DURATION. (b) Results of contrasting 36s and 4s DURATIONS. (c) Results of contrasting 36s and 12s DURATIONS. Longer DURATION > shorter DURATION contrasts in warm colors, shorter DURATION > longer DURATION contrasts cold colors. Results are FWE-cluster corrected at α = .05 with a cluster forming threshold of $p < .001$, Monte Carlo simulated cluster extend thresholds were 34 (a), 34 (b) and 35 (c) voxels, respectively. Significant clusters are depicted with a black border and are labelled accordingly. Red labels describe clusters belonging to the longer DURATION > shorter DURATION contrast, blue labels describe clusters belonging to the short DURATION > longer DURATION contrast. Results figures applies the "Highlight, don't Hide" principle (Taylor et al., 2023). Thus, clusters with non-significant *p*-values are not omitted but displayed at lower opacity. Whole-brain results are projected on inflated fsaverage pial surface. (a)PPA = (*anterior) parahippocampal place area*, ColS = *collateral sulcus*, CUN = *cuneus*, FG = fusiform gyrus, IFJ = *inferior frontal junction*, InfPostCS = *Inferior postcentral sulcus*, IOG = *inferior occipital gyrus*, IPL = intraparietal lobe, LingG = lingual gyrus, MOG = *middle occipital gyrus*, MTG = middle temporal gyrus, pPPA = *posterior parahippocampal place area*, PreCUN = *precuneus*, PHG = *parahippocampal* gyrus, RSC = retrosplenial cortex, SFG = superior frontal gyrus, SMG = *supramarginal gyrus*, SPL = superior parietal lobe.

Table 4

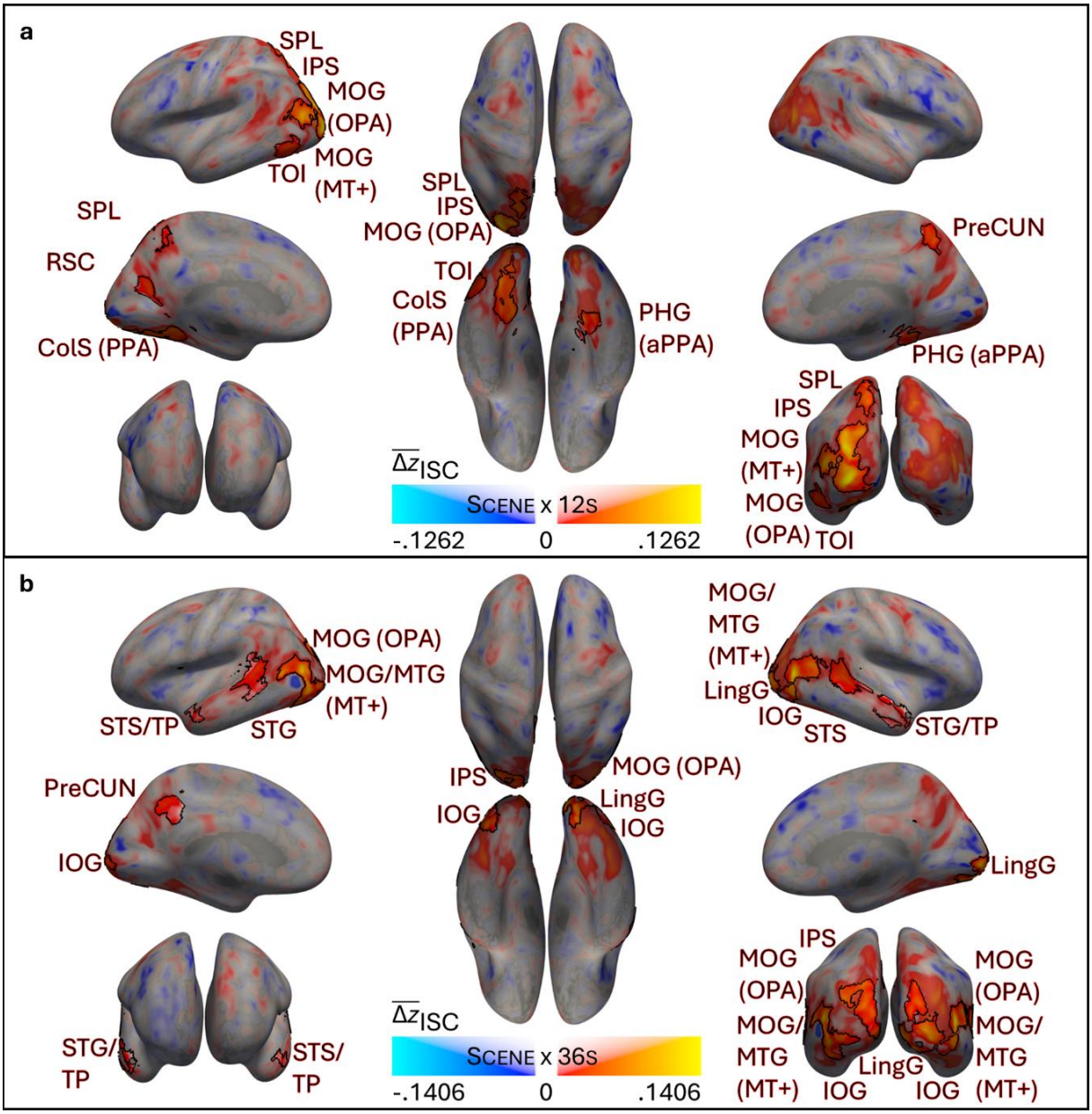
Significant differences in Fisher z-transformed inter-subject correlations from testing the specific interaction effects for Scenes of longer Durations (Scene x 12s and Scene x 36s)

Localization	H	Cluster extent (in voxel)	Peak coordinates (MNI space) x	y	z	*z* value difference
Scene x 12s = (Scene 12s > Shot 12s) > (Scene 4s > Shot 4s)						
Superior parietal lobule	L	91	-17	-72	50	0.08
Precuneus	R	56	3	-54.5	45	0.07
Retrosplenial cortex	L	44	-17	-59.5	15	0.05
Middle occipital gyrus (OPA)	L	462	-29.5	-94.5	0	0.13
Intraparietal sulcus	L	l.m.	-29.5	-84.5	17.5	0.12
Middle occipital gyrus (MT+)	L	l.m.	-47	-74.5	15	0.10
Parahippocampal gyrus (anterior PPA)	R	50	30.5	-42	-7.5	0.08
Collateral sulcus (anterior and posterior PPA)	L	146	-27	-69.5	-12.5	0.09
Temporo-occipital incision	L	l.m.	-47	-67	-10	0.06
Scene x 36s = (Scene 36s > Shot 36s) > (Scene 4s > Shot 4s)						
Precuneus	L	53	-7	-49.5	37.5	0.05
Intraparietal sulcus	L	213	-27	-87	22.5	0.10
Middle occipital gyrus (OPA)	L	l.m.	-17	-97	12.5	0.09
Middle occipital gyrus/ Middle temporal gyrus (MT+)	R	119	50.5	-69.5	10	0.14
Middle occipital gyrus/ Middle temporal gyrus (MT+)	L	87	-49.5	-74.5	10	0.12
Superior temporal gyrus	L	121	-62	-44.5	7.5	0.06
Superior temporal sulcus	R	113	48	-37	5	0.07
Lingual gyrus	R	372	13	-89.5	-2.5	0.14
Middle occipital gyrus (OPA)	R	l.m.	20.5	-92	17.5	0.07
Inferior occipital gyrus	L	182	-42	-82	-5	0.11
Inferior occipital gyrus	R	48	45.5	-77	-5	0.09
Superior temporal gyrus/ Temporal pole	R	77	55.5	5.5	-15	0.04
Superior temporal sulcus/ Temporal pole	L	35	-49.5	3	-22.5	0.03

Note. Results are FWE-cluster corrected at α = .05 with a cluster forming threshold of $p < .001$, Monte Carlo simulated cluster extend threshold is 35 voxels (Scene x 12s) and 34 voxels (Scene x 36s), respectively. H = *Hemisphere*; L = *left*; R = *right*; MNI = *Montreal Neurological Institute*; l.m. = *local maximum*; OPA = *occipital place area*; PPA = *parahippocampal place area*.

Figure 7

Whole-brain results of the differences in Fisher z-transformed correlations from testing the specific interaction effects for SCENES of longer DURATIONS



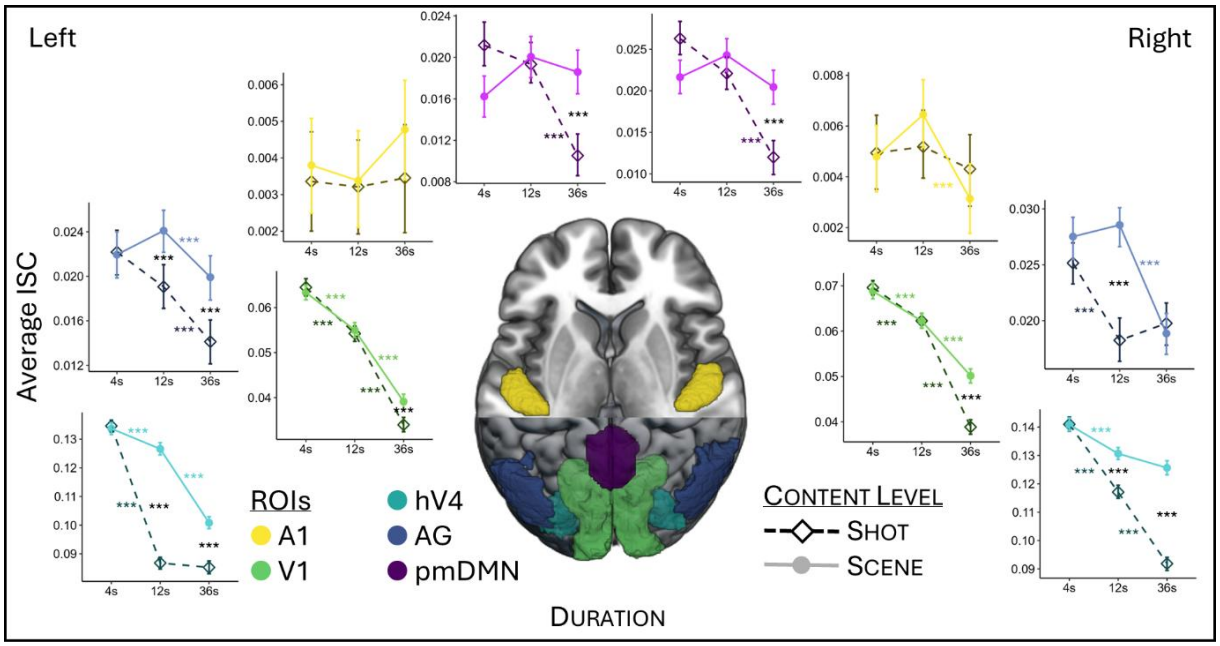
Note. (a) Results for the SCENE x 12S interaction. (b) Results for the SCENE x 36S interaction. SCENE x 12S > 0 and SCENE x 36S > 0 contrasts in warm colors, opposing contrasts in cold colors. Results are FWE-cluster corrected at α = .05 with a cluster forming threshold of $p < .001$, Monte Carlo simulated cluster extend thresholds were 35 (a) and 34 (b) voxels, respectively. Significant clusters are depicted with a black border and are labelled accordingly. Red labels describe clusters belonging to the SCENE x 12S > 0 and SCENE x 36S > 0 contrasts. Results figures applies the "Highlight, don't Hide" principle (Taylor et al., 2023). Thus, clusters with non-significant *p*-values are not omitted but displayed at lower opacity. Whole-brain results are projected on inflated fsaverage pial surface. ColS = *collateral sulcus*, IOG = *inferior occipital gyrus*, IPS = *intraparietal sulcus*, LingG = *lingual gyrus*, MOG = *middle occipital gyrus*, MTG = *middle temporal gyrus*, OPA = *occipital place area*, PHG = *parahippocampal gyrus*, PostCS = postcentral sulcus, (a)PPA = *(anterior) parahippocampal place area*, PreCUN = *precuneus*, RSC = *retrosplenial cortex*, SPL= *superior parietal lobe*, STG = *superior temporal gyrus*, STS = *superior temporal sulcus,* TOI = *temporo-occipital incision,* TP = *temporal pole*.

3.4. Region of interest analysis

To investigate the interaction between CONTENT LEVEL and DURATION in more detail, we conducted a ROI analysis. We modelled the average ISC per ROI by their CONTENT LEVEL and DURATION and then used parametric bootstrapping to test the post-hoc comparisons, FDR-corrected for multiple comparisons, and identified significant differences between the conditions (Figure 6, Table S1.1 in Supplemental Material 1). We analyzed the ISC values from five previously defined bilateral ROIs (see 2.6.3.): A1, V1, hV4, AG, pmDMN describing the visual processing hierarchy (plus A1 as control ROI) according to Baldassano et al. (2017; Figure 8).

Figure 8

Post-hoc test results of region of interest analysis for the visual cortical processing hierarchy



Note. Results for the ROIs based on the visual cortical processing hierarchy (Baldassano et al., 2017). CONTENT LEVEL SHOT in darker shade and dashed line, CONTENT LEVEL SCENE in lighter shade and solid line. ROI = *region of interest*, A1 = *primary auditory cortex*, V1 = *primary visual cortex*, hV4 = *extrastriate visual cortex*, AG = *angular gyrus*, pmDMN = *posterior medial cluster of the default mode network*. * $p_{FDR\text{-}boot} < .05$, ** $p_{FDR\text{-}boot} < .01$, *** $p_{FDR\text{-}boot} < .001$, $N_{boot} = 500$. ROI masks are depicted on the MNI152 standard template. For a depiction of the ROIs on the pial fsaverage surface space see Figure S6.5a.

The results were very similar for the left and right ROIs (Table S2.1). Thus, we will summarize the depicted trends for both hemispheres combined. As expected, we did not see many differences between the conditions in the control ROI A1, as just right A1 showed significantly less ISC in the SCENE 36S than the SCENE 12S condition. In V1 we identified a

significant decrease in ISC with increasing DURATION of the stimuli while only at DURATION 36S we found a significantly higher ISC for SCENES than for SHOTS. This trend of a decreasing ISC with higher levels of DURATION continued for hV4 although now also featuring a definite distinction between the CONTENT LEVELS: SCENES produced significantly higher ISC than SHOTS for the DURATIONS 12S and 36S, but did not differ at 4S, indicating the interaction between CONTENT LEVELS and DURATIONS that was shown at the whole-brain level already in hV4. Following the trend, in AG we still saw a continuous decrease of the ISC values for the CONTENT LEVEL SHOT, whereas for SCENES only between the 12S and 36S DURATIONS a significant decline emerged. This was complemented by significantly higher ISC for SCENES than SHOTS bilaterally for the 12S DURATION and only in the left AG for the 36S DURATION. Also, for the pmDMN ROI, we saw a significant decrease in ISC between SHOTS of 12S and 36S DURATION, while the ISC for the CONTENT LEVEL SCENE remained constant. Accordingly, ISC was significantly higher in the SCENE 36S than the SHOT 36S condition.

Additionally, we considered five more ROIs, which described areas that were previously related the cortical processing of movies (e.g., Jääskeläinen et al., 2021): TPJ, PHG, aHC, pHC, and mPFC. All results of this ROI analysis are reported in the Supplemental Material 4.

4. Discussion

When we watch rich, naturalistic stimuli like movies, our entire brain is involved in processing everything from low-level visual features to the understanding of the plot (Rajimehr et al., 2024; E. Yang et al., 2023). While some aspects of this processing are idiosyncratic and can be used to differentiate between individuals (Eickhoff et al., 2020; Finn & Bandettini, 2021; Nastase et al., 2019), the majority is shared between subjects when synchronously watching a movie, especially for well-structured and -edited Hollywood movies guiding the viewers' attention (Hasson, Landesman, et al., 2008). Previous studies used this shared processing to identify cortical areas that are reliably engaged by naturalistic stimuli (e.g., Hasson, Yang, et al., 2008), resulting in regions that were additionally engaged when longer, more persistent portions of the

movie or other stimuli were presented (Aberbach-Goodman & Mukamel, 2023; Farbood et al., 2015; Hasson, Yang, et al., 2008; Lerner et al., 2011). However, because longer durations of naturalistic stimuli coincide with an increase in the presented content, a longer section of a movie likely includes presenting multiple camera shots or even scenes. This confound is not only part of movies, but is a general feature of all naturally occurring hierarchically nested stimuli from language to action sequences (Fitch & Martins, 2014; Uithol et al., 2012; Valentine & May, 1996; Wu, 2013). Thus, using naturalistic stimuli, it is impossible to answer the question whether the additional areas were engaged simply by a longer stimulus or if the depicted content also played a role in what areas were reliably activated.

To answer this question, the present study was the first to disentangle the dependency between DURATION and CONTENT LEVEL of naturalistic stimuli by applying the ISC approach in a controlled experimental setting and identifying areas specifically and separately engaged by different levels of temporal persistency or content complexity. For this, we presented a fixed number of frames extracted from movie SHOTS or SCENES, thus manipulating the DURATION independently of the CONTENT LEVEL of SHOTS and SCENES. The findings exposed differences in the processing of movie SHOTS and movie SCENES as well as differences based on the DURATION of the content and also areas which were specifically engaged by stimuli of a higher CONTENT LEVEL presented for a longer DURATION, i.e., longer movie scenes. The identified areas predominantly laid within a visual scene-processing network (Epstein & Baker, 2019). More specifically, while the effects of CONTENT LEVEL were found in the posterior portion of the network, the DURATION effects were located in the anterior regions, supporting a functional distinction between the two subnetworks (Baldassano et al., 2016; Steel et al., 2021). Additionally, a ROI analysis was conducted to investigate the differences in ISC along the visual processing hierarchy (Baldassano et al., 2017) and other areas related to the processing of movies (Jääskeläinen et al., 2021; see Supplemental Material 4), highlighting the differences in processing SHOTS and SCENES at various DURATION across the cortex.

4.1. Inter-subject correlation using only frames – a prove of concept

In contrast to the previous studies using the ISC approach with continuous sections of naturalistic stimuli (e.g., Hasson, Yang, et al., 2008), we only presented our participants with isochronally extracted frames at a constant frame rate of 3 FPS – lower than the necessary frame rate for motion perception (Wilcox et al., 2015). Thus, our stimulus material differed from naturalistic, well-structured movies that maximize the synchrony of the viewers' reaction (Hasson, Landesman, et al., 2008; Loschky et al., 2020). Despite the differences, we were able to find significant ISC across our experimental conditions that mirrored the results of Hasson, Yang, et al. (2008), who – comparatively to the individual frames without sound – used clips from silent films. Hence, summarized across all six conditions, we also found significant ISC in the entire occipital lobe, including the primary as well as higher order visual cortices like the lateral occipital complex and PPA that Hasson, Yang, et al. (2008) pointed out specifically. When looking at the ISC especially found for SCENES of longer DURATIONS, we saw the same spread towards parietal, temporal and frontal regions, including the precuneus, SPL and TPJ as well as significant clusters in the mPFC, SFG and STS that Hasson, Yang, et al. (2008) demonstrated to be engaged particularly for longer stimuli. Thus, we could not only replicate the findings shown specifically for the ISC distribution of movies, while only depicting individual frames, but also reproduced a trend found for the ISC using other stimulus modalities (e.g., Farbood et al., 2015; Hasson et al., 2015; Lerner et al., 2011): While temporally shorter and hierarchically lower situated stimuli only reliably engage the cortices processing the respective modality (visual, auditory, etc.), longer stimuli that involve higher CONTENT LEVELS and DURATIONS additionally show significant ISC in multimodal integration areas like the precuneus or the mPFC (e.g., Sepulcre et al., 2012). Replicating these results proves that the manipulation worked and that the stimuli were processed similarly enough to naturalistic stimuli to allow us to generalize the results of the comparison between conditions in this study to the processing of actual naturalistic stimuli.

4.2. Comparing inter-subject correlation between conditions – revealing the scene network

The investigated contrasts between the CONTENT LEVELS and the different DURATIONS resulted in significant clusters all across the cortex, including early visual cortices as well as hierarchically higher integration areas like the precuneus or temporal pole. For the sake of brevity, this discussion will focus primarily on the regions related to the scene-processing network (Epstein & Baker, 2019) as our main, novel finding. All other results will be discussed in detail in Supplemental Material 3.

4.2.1. The effect of Content Level. Contrasting the ISC of the SHOT and SCENE conditions averaged across DURATION revealed, clusters in the bilateral MOG including areas V3A/B, the bilateral collateral sulcus, the bilateral SPL as well as the left SMG and right MTG that were additionally more engaged for SCENES.

The clusters in the MOG overlap with the previously described OPA (Dilks et al., 2013), located around the transverse occipital sulcus. Together with the PPA (Epstein & Kanwisher, 1998) and the RSC (Epstein, 2008) it forms the human *scene network* (Epstein & Baker, 2019). It is pivotal to note that a *scene* in the context of the scene network and movie scenes, are not the same. A scene in the more general definition of the network is a "[...] semantically coherent (and often nameable) view of a real-world environment comprising background elements and multiple discrete objects arranged in a spatially licensed manner." (Henderson & Hollingworth, 1999, p.244). In this sense, every frame in our experiment represented a scene, which could explain the reliable engagement of the scene network areas in all six experimental conditions.

More recent evidence however indicates that these three areas, OPA, PPA and RSC, do not capture the full extent of the network. It was suggested that the scene network is divided into two subnetworks, an anterior and a posterior part (Baldassano et al., 2017; Steel et al., 2021, 2023, 2025). While there is no full agreement of all regions included in each subnetwork, it is evident that the posterior portions are linked more closely to the sensory input as it receives signal from the early visual cortices, while the anterior portions of the network integrate memory into the

process with their connections to, e.g., the hippocampus (Baldassano et al., 2016; Nasr et al., 2013; Silson et al., 2016). According to this division, the posterior scene network is made up of the OPA, the posterior PPA and possibly a more perceptively attuned part of the RSC which is also called medial place area (MPA; Baldassano et al., 2016; Steel et al., 2025). The anterior network consists of an area in the caudal inferior parietal lobe (cIPL) referenced also as the lateral place memory area (LPMA; Steel et al., 2021), the anterior portions of the PPA as well as the RSC or at least the memory-attuned part of the MPA (Baldassano et al., 2016; Steel et al., 2025). This distinction within the scene network is crucial for interpreting our results since – as will be highlighted throughout the discussion – the different contrasts were associated only with specific subnetworks.

Thus, the contrast of the CONTENT LEVELS revealed that specifically the OPA as well as the posterior PPA were more reliably engaged by movie SCENES than movie SHOTS regardless of their DURATION. Both these areas are part of the posterior scene network and thus are more involved with perceptual processing than the integration from memory (Baldassano et al., 2016; Steel et al., 2025). Accordingly, the OPA was previously shown to be activated when distinguishing between different sceneries based on the own, *egocentric* perspective representing the sense of left or right and distance (Epstein & Baker, 2019; Kamps et al., 2016). Further, this area is possibly used for the immediate localization of near boundaries or obstacles (Julian et al., 2018). This egocentric perspective taking is especially essential for movie SCENES, because in contrast to a SHOT which depicts a single camera perspective, movie SCENES per definition often depict multiple SHOTS and thus include changes in the perspective taken by the camera, i.e., the viewer, making SCENES more visually variable (Cutting et al., 2011; Haq et al., 2019; Ji et al., 2019), which a comparison the visual features our SCENE and SHOT stimuli also demonstrated (see Supplemental Material 1). Subsequently, SCENES regardless of the duration have more egocentric views that need to be processed, which could explain the more reliable engagement of the OPA,

as more frequent changes leave less room for idiosyncratic processing, increasing the stimulus-driven ISC (Faber et al., 2018).

Additionally, the SCENE > SHOT contrast also revealed clusters in the collateral sulcus which anchors the PPA (Epstein & Baker, 2019). The identified clusters specifically overlap with the posterior PPA, which is often identified in the context of visually guided spatial perception (Baldassano et al., 2013; Häusler et al., 2022; Steel et al., 2025). This is supported by findings demonstrating that particularly the posterior PPA is functionally related to spatial relationship (Aminoff & Bar, 2003; Aminoff & Tarr, 2015; Bilalić et al., 2019; Van den Stock et al., 2014), the existence of specific retinotopic maps in the posterior PPA (Arcaro et al., 2009; Beyh et al., 2022) and its general preference for simpler stimuli (Arcaro et al., 2009; Nasr et al., 2014; Rajimehr et al., 2011).

To summarize, the SCENE > SHOT contrast revealed engagement in a network of regions that process visual scenery. Intriguingly, only the more perceptively specialized posterior portion of this network consisting of the OPA and the posterior PPA was involved. This subnetwork is related to collecting and processing environmental features necessary for spatial navigation (e.g., Baldassano et al., 2016). Therefore, the results suggest that the necessary integration across multiple SHOTS in a SCENE is processed as the perception of visual scenery from multiple different egocentric perspectives.

4.2.2. The effect of Duration. While clearly engaging the scene network the clusters identified for the effect of CONTENT LEVEL were interestingly only found in the posterior subnetwork. Looking at the effects of DURATION however, we identified clusters overlapping with the anterior scene network (Baldassano et al., 2016; Steel et al., 2025). Thus, the contrast of 12S > 4S revealed significant engagement in the bilateral RSC, the anterior PPA as well as the right cIPL for longer stimuli. Also, in the contrast between the 36S > 4S condition we identified clusters in the right RSC and right cIPL. Only the 12S > 36S contrast did not uncover any more reliably engaged areas for the

longer stimuli. This null finding could however be related to limitations regarding the 36s conditions, that will be discussed later (also see Supplemental Material 3).

The anterior portion of the scene network is suggested to extend on the function of the posterior part by helping with spatial navigation but also integrating information from memory indicated by its close connection to the hippocampus (Baldassano et al., 2016; Silson et al., 2016; D. M. Watson & Andrews, 2024) as well as its activity in imagining scenes without actual input (Boccia et al., 2015). This higher level of visual processing is supported by findings about the individual regions that are part of this subnetwork:

Starting with the anterior PPA, its connectivity to the default mode network (DMN) as well as its relatively lower sensitivity to objects, suggest a focus on more global scene features and possibly a recall of features from memory (Aminoff et al., 2007; Baldassano et al., 2013). Moreover, previous studies showed that the anterior PPA is more concerned with non-visual information about scenery, while the posterior PPA processes visual cues (Häusler et al., 2022). Consequently, the anterior PPA is involved in mental imagery (Boccia et al., 2015) and the recall of spatial scenes (Bainbridge et al., 2021; Srokova et al., 2022). Recently, Steel et al. (2025) defined the spatial distinction between memory and perception related scene processing areas, also splitting the PPA into a posterior, visually-attuned and anterior, memory-attuned area. Our results are further support of this distinction of the posterior PPA and anterior PPA possibly linking the anterior PPA to slower intrinsic signals, longer TRWs and integration over longer periods of time.

Along the same line, we also identified the RSC only for stimuli of longer duration (12s > 4s and 36s > 4s). The RSC as part of the anterior scene subnetwork fulfills the role of orientation and navigation of an individual within a scene (Baldassano et al., 2016). This proposed function matches the rich literature on the RSC indicating that it encodes the heading direction of an individual (for reviews see Julian et al., 2018; Vann et al., 2009). In this context, the RSC processes consistent landmarks of the environment to from both egocentric and allocentric perspectives

while also transitioning between these reference frames (Auger & Maguire, 2018; Balcerek et al., 2021; Julian et al., 2018; Peer et al., 2021; Sulpizio et al., 2020). Additionally, Alexander et al. (2023) proposed that the RSC is not only representing the spatial environment but also the temporal context, playing a role in episodic memory retrieval, which is supported by its involvement in recalling a previously watched movie (Zadbood et al., 2017). Moreover, recent evidence also suggests a functional distinction within the RSC and neighboring scene processing areas along the parieto-occipital fissure (Balcerek et al., 2021; Silson et al., 2019; Steel et al., 2021), dividing this area into a more visually-guided posterior and more memory-attuned anterior MPA (Silson et al., 2019; Steel et al., 2021, 2025). Based on the recently published coordinates for the MPA, the clusters we identified in the DURATION contrasts rather overlap with the memory-attuned anterior part (Steel et al., 2025). This could further indicate that with increasing temporal duration the stimuli are not only visually processed but integrated with information from memory or other high-level processing steps which corresponds to an increase of TRWs along the cortical hierarchy (Golesorkhi, Gomez-Pilar, Zilio, et al., 2021; Hasson et al., 2015; Wolff et al., 2022).

For both the 12S > 4S and 36S > 4S we also identified a third cluster in the right hemisphere which is part of the anterior subnetwork of the scene network, namely the cIPL (Baldassano et al., 2016) or LPMA (Steel et al., 2021). Located anterior and lateral to the OPA this area was previously related to the processing of familiar scenes regardless of the egocentric view point (Epstein et al., 2007) as well as imagery of familiar places (Scrivener et al., 2025) and the egocentric, orientation in larger environmental contexts (Han & Epstein, 2025; Steel et al., 2023). Thus, the cIPL – like the other anterior scene network regions – is also implied to be involved in a memory-based navigation of the own person in space.

Overall, finding these clusters specifically in longer DURATION conditions might suggest that memory integration is only more reliable with longer time. This is supported by recent results, demonstrating that the signal time course in a recall tasks peaks after four to twelve seconds in

all three memory-attuned place areas – cIPL, anterior PPA, and RSC – and therefore later than in their perception-attuned equivalents (Steel et al., 2023).

Interestingly, the contrasts of DURATION also revealed unexpected stronger effects for the 12S than 36S conditions (see Supplemental Material 3 for further discussion). Also, the supplemental ROI analysis in the PHG, that mainly overlapped with the canonical anterior PPA location (Steel et al., 2025), revealed an attunement to the 12S DURATION for both SHOTS and SCENES (see Supplemental Material 4). These results might indicate that specifically the 12S DURATION rather than the 36S DURATION was more relevant to the anterior scene network. In this context, studies investigating the shifts in cortical network states while watching a movie identified the brain state dwell times in networks and regions associated with the anterior scene network (Baldassano et al., 2013, 2016; D. M. Watson & Andrews, 2024) in the range of ten to 16 seconds (E. Yang et al., 2023), while no brain state regularly persisted for as long as 36 seconds (Geerligs et al., 2022; E. Yang et al., 2023). These brain state shifts are thought to coincide with the event boundaries (Baldassano et al., 2017; Geerligs et al., 2022; Sava-Segal et al., 2023) - for example, changes in location - that are specifically processed in the scene network (Rah et al., 2025; Zacks et al., 2010). Complex stimuli with fewer event boundaries, like the 36s condition, have been shown to produce less synchronized behavioral and neural state boundaries (Sava-Segal et al., 2023). Moreover, longer periods without discernible situational changes increase the chance of mind wandering (Faber et al., 2018). Thus, the regular, noticeable spatial boundary shifts in the 12S condition, identified by the scene network, might have enhanced the ISC for this DURATION. Additionally, while the average movie SCENE can take somewhere in the range of 20 seconds to over a minute (Cutting et al., 2012; Zacks et al., 2009, 2010), movie SHOTS usually only last a few seconds (Cutting et al., 2011; Cutting & Candan, 2015; Pearlman, 2019). Hence, especially for the SHOT condition, 12S stimuli could represent a more natural movie watching experience, possibly leading to a more synchronized viewing and thus relatively higher ISCs than in 36S conditions. Since this study used three distinct levels of DURATION, mirroring Hasson, Yang,

et al. (2008), future studies could investigate a broader range of time windows, to more precisely estimate the relevant event durations for the anterior and posterior scene networks (e.g., Aberbach-Goodman & Mukamel, 2023) and further distinguish effects of DURATION and CONTENT LEVEL. This is especially relevant as the anterior scene network, through its connectivity with the hippocampus, may also play a role in encoding events into memory (Baldassano et al., 2016; Ritchey & Cooper, 2020; Torres-Morales & Cansino, 2024). Using other time frames, previous studies have similarly identified the increase of TRW along the cortical hierarchy (Honey et al., 2012; Lerner et al., 2011). Since it was also found that the cortical dynamics can, to a certain degree, adjust to the stimulus (Cavanagh et al., 2020; Lerner et al., 2014; Soltani et al., 2021), it is possible that our findings could be replicated at different scales of annotation or presentation frame rate. In contrast, the structural basis of cortical timescales (Chaudhuri et al., 2015; X.-J. Wang, 2020) might only allow for a limited temporal flexibility.

To conclude, SCENES and SHOTS of longer DURATION compared with 4S stimuli specifically engaged the anterior portion of the scene network that was related to memory integration processes (e.g., Baldassano et al., 2017). Thus, these results could indicate that only longer stimulus durations allow for higher levels of processing, enabling deeper understanding of meaning, retention of the content, or prediction of upcoming events (Alexander et al., 2023; Steel et al., 2023). Short stimuli, on the other side of the spectrum, are too transient for these slower processes, only engaging earlier visual processing levels (Geerligs et al., 2022; Oetringer et al., 2025).

4.2.3. Interaction effect – areas reliably engaged by longer scenes. Since the effects of CONTENT LEVEL and DURATION both revealed significant but also distinct areas, we also looked at regions that were additionally engaged for SCENES of a longer DURATION (SCENE x 12S and SCENE x 36S). Some identified clusters, especially within the scene network, were shared between the main effects and the interactions, which supports that CONTENT LEVEL and DURATION together are relevant for engaging this network. More specifically, across the two interactions of interest we

located areas in both the anterior and posterior subnetworks, like the OPA or the anterior PPA and parts of the RSC. So, we saw the expected conjunction of visually-attuned and memory-attuned areas in the processing of the content-rich and temporally persistent SCENE conditions. Therefore, even more interesting are areas specifically engaged by the interaction. Here we found clusters in the precuneus, the lateral MOG merging into MTG and along the entire STS specifically for the SCENE x 36S contrast.

The precuneus is an area which is commonly found in movie-watching studies (Jääskeläinen et al., 2021; Oren et al., 2016; Zacks et al., 2001). In that context, it was related to the understanding and recalling the temporally consecutive order of events of the movie (Baldassano et al., 2017; Kwok et al., 2012; Lahnakoski et al., 2017; Tylén et al., 2015; Whitney et al., 2009; Yeshurun et al., 2017; Zacks et al., 2010; Zadbood et al., 2017). This level of complex and deeper comprehension could be explained by the precuneus' role as high-level rich and integrative cortical hub (Gollo et al., 2015; Mecklenbrauck, Gruber, et al., 2024; Riedel et al., 2022). Multiple studies have identified the precuneus and its subfields as parts of different functional networks related to memory integration, working memory, as well as the processing of naturalistic stimuli (Cavanna & Trimble, 2006; Dadario & Sughrue, 2023; Deng et al., 2019; Yeo et al., 2011). Accordingly, we also discovered reliable precuneus engagement for longer SCENE stimuli which allow for a more profound understanding of the content.

The other clusters in the lateral MOG/MTG as well as the extension along the STS might be related to a recently described third visual pathway which appropriately involves the human motion selective area MT+ in the lateral MOG/MTG, the posterior STS as well as the anterior STS (Pitcher & Ungerleider, 2021). This network supposedly processes dynamic movements in a social context and aids in the understanding of actions of other individuals (Pitcher & Ungerleider, 2021). This is supported by motion selective regions located along the STS (Allison et al., 2000; Cheng et al., 2025; Grossman et al., 2005; Herrington et al., 2011; McAleer et al., 2014) culminating in a face-focused region in the temporal pole (Duchaine & Yovel, 2015; H. Yang et al., 2016). However,

we see significantly reliable engagement in this pathway mainly in the results for the SCENE x 36S interaction which contains the contrast of SCENES and SHOTS of 36S. Hence, this contrast could have been dominated by the perception of an ever-changing, motion-inducing SCENE 36S conditions compared to a more constant, still-frame-like SHOT 36S condition (see Supplemental Material 3 for further discussion). Yet, in the context of movie watching especially the anterior STS is also a sign for a high-level understanding and retention of the content (AbdulSabur et al., 2014; Akimoto et al., 2014; Hasson, Furman, et al., 2008; Lahnakoski et al., 2017; Speer et al., 2007; Yeshurun et al., 2017; Zacks et al., 2010). To investigate the effects of CONTENT LEVEL and DURATION along the STS in more detail, we conducted an exploratory ROI analysis of three functionally distinct areas along the STS (Zhen et al., 2015). This analysis demonstrated that the anterior portions of the STS are not only more engaged by the longer, content-richer SCENES but also that the engagement increased significantly with DURATION (see Supplemental Material 5), supporting the anterior STS's specific role in higher-level and social aspects of stimulus processing (e.g., J. Chen et al., 2017; Lee Masson & Isik, 2021; Yeshurun et al., 2017).

In this light, the presence of clusters in the anterior STS or the precuneus for longer SCENES is consistent with evidence that extended stimulus segments permit integration with memory content (Steel et al., 2023), thereby supporting higher-level comprehension.

4.3. The effects of CONTENT LEVEL and DURATION along the visual cortical hierarchy

There is evidence for both the processing of the stimulus content (Baldassano et al., 2017; Geerligs et al., 2022; Oetringer et al., 2025) and of the temporal organization (Chaudhuri et al., 2015; Golesorkhi, Gomez-Pilar, Tumati, et al., 2021; Hasson et al., 2015) to align with the cortical hierarchy. As discussed, our whole-brain analysis confirmed the relevance of both factors, as longer, more content-rich movie scenes engaged hierarchically higher areas. To examine the relationship between CONTENT LEVEL, DURATION and the cortical hierarchy in greater detail, we conducted a ROI analysis. Thereby, the ROIs were chosen to reflect the visual processing hierarchy described by Baldassano et al. (2017) as well as region commonly implicated in movie

perception (e.g., Jääskeläinen et al., 2021). The results for the latter are reported and discussed in Supplemental Material 4.

At the earliest stage of hierarchy, we found no major differences between movie SCENES and SHOTS. Instead, ISC decreased with longer DURATION across all conditions. Given that the early visual cortex is primarily engaged by low-level visual features, such as contrasts, edges or motion (Grill-Spector & Malach, 2004; Seidemann & Geisler, 2018; Tong, 2003), stimulus properties that are largely shared between the CONTENT LEVELS (see Supplemental Material 1), no difference in engagement was expected (see Supplemental Material 3 for further discussion).

One step higher, in hV4, we observed the first clear separation between the CONTENT LEVELS. SCENES elicited stronger ISC than SHOTS at 12S and 36S DURATION. This is consistent with hV4's functions not only encompassing color and motion perception (Cohen et al., 2019; Grill-Spector & Malach, 2004; Wade et al., 2002) but also the integration of visual information across larger receptive fields (Grill-Spector & Malach, 2004; Winawer & Witthoft, 2015). Its role as an early integrative hub and first branching point between the dorsal and ventral processing streams (Winawer & Witthoft, 2015) may further explain why differences between SCENES and SHOTS already emerged at this stage in the processing.

At the upper end of the visual processing hierarchy, the angular gyrus and the posterior-medial DMN cluster (precuneus/posterior cingulate cortex) showed robust differences in the ISC between movie SCENES and SHOTS, especially at longer DURATIONS. Both regions are well-established as integrative hubs, associated with memory and narrative comprehension (Ben-Yakov & Henson, 2018; Hasson et al., 2015; Raichle, 2015; Rockland & Graves, 2023; Seghier, 2023). The angular gyrus, as part of the DMN, is functionally linked to the hippocampus (Rockland & Graves, 2023) and involved in semantic processing (Ben-Yakov & Henson, 2018; Seghier, 2023). The posterior-medial DMN cluster (Shirer et al., 2012) whereas forms a core network hub (Fransson & Marrelec, 2008; Hagmann et al., 2008) that is part of the hippocampal-parietal

memory system (Raichle, 2015). Our ROI results support this high-level role in the integration of temporally extended, content-rich information.

Thus, in line with our whole-brain findings, the ROI results also suggest an interaction of CONTENT LEVEL and DURATION. Hierarchically higher areas showed relatively greater ISC for longer SCENES than SHOTS, consistent with the idea that more complex and persistent stimuli engage regions with longer TRWs that integrate information over longer periods of time (Hasson et al., 2015; Wolff et al., 2022). The functional distinction between the anterior and posterior scene subnetworks further supports this account: Clusters specifically engaged by 12S and 36S stimuli overlapped with the memory-related regions identified by Steel et al. (2021, 2025). Crucially, Steel et al. (2025) demonstrated that the visually attuned posterior regions and memory-related anterior regions occupy distinct positions within the cortical hierarchy (e.g., Margulies et al., 2016), with posterior areas closer to unimodal cortices and anterior areas closer to multimodal integration zones. Fittingly, this uni-to-multimodal gradient was shown to explain both internal timescales and ISC distributions across the cortex (Golesorkhi, Gomez-Pilar, Tumati, et al., 2021; Ito et al., 2020; Mecklenbrauck, Sepulcre, et al., 2024; Raut et al., 2020). The anterior portions of the scene network regions are also more strongly connected to the DMN (Baldassano et al., 2013, 2017; D. M. Watson & Andrews, 2024), including the posterior DMN cluster investigated here (Shirer et al., 2012), which has been specifically associated with slow, self-referential, memory-based integration processes (Menon, 2023; Raichle, 2015). Thus, both ROI and whole-brain results suggest that hierarchically higher, more integrative areas are engaged more reliably by longer, more complex stimuli and evidently contain longer TRWs.

However, while our results are broadly consistent with previous TRW findings, the ISC pattern we observed differed in some important respects from previous investigations. Earlier work reported stable ISCs in the primary cortices regardless of the duration and demonstrated an increase in higher-level areas when both duration and content were extended (Aberbach-Goodman & Mukamel, 2023; Farbood et al., 2015; Hasson, Yang, et al., 2008; Lerner et al., 2011).

In contrast, we discovered a general decline in ISC with DURATION, with the only relatively higher values for SCENES reflecting a less steep decrease compared to SHOTS. This overall decline of ISC might however be an artifact of our stimulus design: Instead of well-structured and continuous naturalistic movie clips, participants viewed only sequences of still frames, which may have reduced inter-subject synchrony (Hasson, Landesman, et al., 2008; Loschky et al., 2020).

Moreover, although conditions were carefully balanced, some natural differences remained – particularly at longer DURATIONS, as movie shots are inherently shorter and visually more uniform than movie scenes (Cutting et al., 2011; Cutting & Candan, 2015). We see these differences firstly in the duration-shorting ratio between longer and shorter conditions as well as SHOTS and SCENES (see 2.2.). While neural dynamics were shown to adapt to the environmental and task demands (Cavanagh et al., 2020; Golesorkhi, Gomez-Pilar, Zilio, et al., 2021; Lerner et al., 2014; Soltani et al., 2021; Song et al., 2024), a significant acceleration of a stimulus can result in less reliable neural activity across subjects (Lerner et al., 2014). Yet, SCENES, that were overall more accelerated than SHOTS, still evoked significantly higher ISC, which suggests the effects of CONTENT LEVEL persisted despite this stronger temporal compression.

The other remaining differences concern the higher visual variability within and between movie segments at shorter DURATIONS (see Supplemental Material 1). The fewer, isochronously extracted frames of shorter conditions naturally produced more noticeable visual gaps. Additionally, the shorter the DURATION, the more distinct segments – and thus transitions – were presented. Although these differences are inherent to the naturalistic stimulus material and present in other TRW studies as well (e.g., Hasson, Yang, et al., 2008), these confounds still have to be considered when interpreting the results. Specifically, the effects in the early visual cortex for the contrast between shorter and longer durations might have been affected by these remaining visual differences (see Supplemental Material 3; Lee & Chen, 2024; Lu et al., 2016; Nunez-Elizalde et al., 2019; Oetringer et al., 2025). Nevertheless, the replication of the key

engagement patterns reported by (Hasson, Yang, et al., 2008), despite these methodological differences, still supports the robustness of our findings and interpretation.

4.4. Conclusions and future research

The present study investigated the processing of movie stimuli. We disentangled the effects of the CONTENT LEVEL (SHOTS and SCENES) from DURATION to determine their respective roles in parsing hierarchically nested, complex, naturalistic stimuli. Overall, our results point to the engagement of a network responsive to visual scenery (Epstein & Baker, 2019) during movie viewing. With higher CONTENT LEVEL, we observed additional engagement of a posterior subnetwork more tightly linked to the incoming visual input and integrating across viewpoints. This is complemented, at longer DURATION, by greater engagement of an anterior subnetwork supporting integration – and possible prediction – from memory (Alexander et al., 2023; Baldassano et al., 2016; Steel et al., 2021).

On the one hand, previous studies have suggested processing as a function of the stimulus duration (e.g., Hasson et al., 2015). Based on our results, the DURATION of the stimulus does play a crucial role in enabling more in-depth processing. However, in particular the interaction of CONTENT LEVEL and DURATION indicates that longer as well as more content-rich stimuli engage higher-level cortical areas. On the other hand, two separate systems have been proposed for integrating across content or across time (Baumgarten et al., 2021). While the focus of effects of CONTENT LEVEL and DURATION to the posterior and anterior portions of the scene network, respectively, could suggest a distinction, these two subnetworks are constantly exchanging information supporting the integration of visual and memory content. In doing so, these networks possibly represent the intersection between externally and internally focused processing (Steel et al., 2024), therefore emphasizing two collaborating rather than distinct cortical systems.

Future studies applying eye-tracking or using actual, naturalistic stimuli are required to further demonstrate the interplay of CONTENT LEVEL and DURATION in the scene network when

watching a movie. Furthermore, even though Steel et al. (2025) recently demonstrated that the anterior scene subnetwork represents a higher level in the cortical hierarchy than the posterior portion and our results indicate a possible difference in TRWs between the two subnetworks, the precise mechanisms underlying naturalistic stimulus processing remain unresolved. What makes a movie scene a movie scene? What content is integrated from memory? How is the scene network with its connection to both the DMN and the hippocampus as well as the early visual cortices related to the top-down-bottom-up hierarchy in prediction (Alexander et al., 2023)? Beyond the realm of cinema, it would also be interesting to see whether effects of CONTENT LEVEL and DURATION can be generalized to other hierarchically nested, natural stimuli like language, music, or actions, and whether the anterior and posterior scene networks operate cross-modally or if similar networks can be found for non-visual modalities as well.

Ultimately, this study demonstrates the importance and the interplay of stimulus content complexity as well as its temporal duration during movie watching and reveals that the two subnetworks of the scene network – previously primarily linked to spatial navigation – are key to movie comprehension.

References

AbdulSabur, N. Y., Xu, Y., Liu, S., Chow, H. M., Baxter, M., Carson, J., & Braun, A. R. (2014). Neural correlates and network connectivity underlying narrative production and comprehension: A combined fMRI and PET study. *Cortex*, *57*, 107–127. https://doi.org/10.1016/j.cortex.2014.01.017

Aberbach-Goodman, S., & Mukamel, R. (2023). Temporal hierarchy of observed goal-directed actions. *Scientific Reports*, *13*(1), 1–13. https://doi.org/10.1038/s41598-023-46917-z

Agcaoglu, O., Wilson, T. W., Wang, Y. P., Stephen, J., & Calhoun, V. D. (2019). Resting state connectivity differences in eyes open versus eyes closed conditions. *Human Brain Mapping*, *40*(8), 2488–2498. https://doi.org/10.1002/hbm.24539

Akimoto, Y., Sugiura, M., Yomogida, Y., Miyauchi, C. M., Miyazawa, S., & Kawashima, R. (2014). Irony comprehension: Social conceptual knowledge and emotional response. *Human Brain Mapping*, *35*(4), 1167–1178. https://doi.org/10.1002/hbm.22242

Alexander, A. S., Place, R., Starrett, M. J., Chrastil, E. R., & Nitz, D. A. (2023). Rethinking retrosplenial cortex: Perspectives and predictions. *Neuron*, *111*(2), 150–175. https://doi.org/10.1016/j.neuron.2022.11.006

Allison, T., Puce, A., & McCarthy, G. (2000). Social perception from visual cues: role of the STS region. *Trends in Cognitive Sciences*, *4*(7), 267–278. https://doi.org/10.1016/S1364-6613(00)01501-1

Aminoff, E. M., & Bar, M. (2003). Cortical analysis of visual context. *Neuron*, *38*(2), 347—358.

Aminoff, E. M., Gronau, N., & Bar, M. (2007). The parahippocampal cortex mediates spatial and nonspatial associations. *Cerebral Cortex*, *17*(7), 1493–1503. https://doi.org/10.1093/cercor/bhl078

Aminoff, E. M., & Tarr, M. J. (2015). Associative processing is inherent in scene perception. *PLoS ONE*, *10*(6), 1–19. https://doi.org/10.1371/journal.pone.0128840

Amunts, K., Mohlberg, H., Bludau, S., & Zilles, K. (2020). Julich-Brain: A 3D probabilistic atlas of the human brain's cytoarchitecture. *Science*, *369*(6506), 988–992. https://doi.org/10.1126/science.abb4588

Andersson, J. L. R., Skare, S., & Ashburner, J. (2003). How to correct susceptibility distortions in spin-echo echo-planar images: Application to diffusion tensor imaging. *NeuroImage*, *20*(2), 870–888. https://doi.org/10.1016/S1053-8119(03)00336-7

Arcaro, M. J., McMains, S. A., Singer, B. D., & Kastner, S. (2009). Retinotopic organization of human ventral visual cortex. *Journal of Neuroscience*, *29*(34), 10638–10652. https://doi.org/10.1523/JNEUROSCI.2807-09.2009

Auger, S. D., & Maguire, E. A. (2018). Retrosplenial cortex indexes stability beyond the spatial domain. *Journal of Neuroscience*, *38*(6), 1472–1481. https://doi.org/10.1523/JNEUROSCI.2602-17.2017

Bainbridge, W. A., Hall, E. H., & Baker, C. I. (2021). Distinct Representational Structure and Localization for Visual Encoding and Recall during Visual Imagery. *Cerebral Cortex*, *31*(4), 1898–1913. https://doi.org/10.1093/cercor/bhaa329

Balcerek, E., Włodkowska, U., & Czajkowski, R. (2021). Retrosplenial cortex in spatial memory: focus on immediate early genes mapping. *Molecular Brain*, *14*(1), 1–17. https://doi.org/10.1186/s13041-021-00880-w

Baldassano, C., Beck, D. M., & Fei-Fei, L. (2013). Differential connectivity within the Parahippocampal Place Area. *NeuroImage*, *75*, 228–237. https://doi.org/10.1016/j.neuroimage.2013.02.073

Baldassano, C., Chen, J., Zadbood, A., Pillow, J. W., Hasson, U., & Norman, K. A. (2017). Discovering Event Structure in Continuous Narrative Perception and Memory. *Neuron*, *95*(3), 709-721.e5. https://doi.org/10.1016/j.neuron.2017.06.041

Baldassano, C., Esteva, A., Fei-Fei, L., & Beck, D. M. (2016). Two distinct Scene-Processing networks connecting vision and memory. *ENeuro*, *3*(5). https://doi.org/10.1523/ENEURO.0178-16.2016

Bates, D., Mächler, M., Bolker, B. M., & Walker, S. C. (2015). Fitting linear mixed-effects models using lme4. *Journal of Statistical Software*, *67*(1). https://doi.org/10.18637/jss.v067.i01

Baumgarten, T. J., Maniscalco, B., Lee, J. L., Flounders, M. W., Abry, P., & He, B. J. (2021). Neural integration underlying naturalistic prediction flexibly adapts to varying sensory input rate. *Nature Communications*, *12*(1), 1–14. https://doi.org/10.1038/s41467-021-22632-z

Behzadi, Y., Restom, K., Liau, J., & Liu, T. T. (2007). A component based noise correction method (CompCor) for BOLD and perfusion based fMRI. *NeuroImage*, *37*(1), 90–101. https://doi.org/10.1016/j.neuroimage.2007.04.042

Benjamini, Y., & Hochberg, Y. (1995). Controlling the False Discovery Rate : A Practical and Powerful Approach to Multiple Testing Author (s): Yoav Benjamini and Yosef Hochberg Source : Journal of the Royal Statistical Society . Series B (Methodological), Vol . 57 , No . 1 (1995), Publi. *Journal of the Royal Statistical Society*, *57*(1), 289–300.

Benjamini, Y., & Yekutieli, D. (2001). The control of the false discovery rate in multiple testing under dependency. *The Annals of Statistics*, *29*(4), 1165–1188. https://doi.org/10.1214/aos/1013699998

Ben-Yakov, A., & Henson, R. N. (2018). The hippocampal film editor: Sensitivity and specificity to event boundaries in continuous experience. *Journal of Neuroscience*, *38*(47), 10057–10068. https://doi.org/10.1523/JNEUROSCI.0524-18.2018

Ben-Yakov, A., Honey, C. J., Lerner, Y., & Hasson, U. (2012). Loss of reliable temporal structure in event-related averaging of naturalistic stimuli. *NeuroImage*, *63*(1), 501–506. https://doi.org/10.1016/j.neuroimage.2012.07.008

Beyh, A., Dell'Acqua, F., Cancemi, D., De Santiago Requejo, F., ffytche, D., & Catani, M. (2022). The medial occipital longitudinal tract supports early stage encoding of visuospatial information. *Communications Biology*, *5*(1), 1–10. https://doi.org/10.1038/s42003-022-03265-4

Bilalić, M., Lindig, T., & Turella, L. (2019). Parsing rooms: the role of the PPA and RSC in perceiving object relations and spatial layout. *Brain Structure and Function*, *224*(7), 2505–2524. https://doi.org/10.1007/s00429-019-01901-0

Boccia, M., Piccardi, L., Palermo, L., Nemmi, F., Sulpizio, V., Galati, G., & Guariglia, C. (2015). A penny for your thoughts! patterns of fMRI activity reveal the content and the spatial topography of visual mental images. *Human Brain Mapping*, *36*(3), 945–958. https://doi.org/10.1002/hbm.22678

Bond, C. F., & Richardson, K. (2004). Seeing the Fisher Z-transformation. *Psychometrika*, *69*(2), 291–303. https://doi.org/10.1007/BF02295945

Bradley, M. M., & Lang, P. J. (1994). Self-Assessment Manikin (SAM). *J.Behav.Ther. & Exp. Psychiat.*, *25*(1), 49–59.

Brett, M., Anton, J.-L., Valabregue, R., & Poline, J.-B. (2002). Region of interest analysis using an SPM toolbox. *8th International Conferance on Functional Mapping of the Human Brain*, 497. https://matthew.dynevor.org/research/abstracts/marsbar/marsbar_abstract.pdf

Cavanagh, S. E., Hunt, L. T., & Kennerley, S. W. (2020). A Diversity of Intrinsic Timescales Underlie Neural Computations. *Frontiers in Neural Circuits*, *14*(December), 1–18. https://doi.org/10.3389/fncir.2020.615626

Cavanna, A. E., & Trimble, M. R. (2006). The precuneus: A review of its functional anatomy and behavioural correlates. *Brain*, *129*(3), 564–583. https://doi.org/10.1093/brain/awl004

Chakraborty, S., Thounaojam, D. M., & Sinha, N. (2021). A Shot boundary Detection Technique based on Visual Colour Information. *Multimedia Tools and Applications*, *80*(3), 4007–4022. https://doi.org/10.1007/s11042-020-09857-8

Chaudhuri, R., Knoblauch, K., Gariel, M. A., Kennedy, H., & Wang, X. J. (2015). A Large-Scale Circuit Mechanism for Hierarchical Dynamical Processing in the Primate Cortex. *Neuron*, *88*(2), 419–431. https://doi.org/10.1016/j.neuron.2015.09.008

Chen, G., Shin, Y. W., Taylor, P. A., Glen, D. R., Reynolds, R. C., Israel, R. B., & Cox, R. W. (2016). Untangling the relatedness among correlations, part I: Nonparametric approaches to inter-subject correlation analysis at the group level. *NeuroImage*, *142*, 248–259. https://doi.org/10.1016/j.neuroimage.2016.05.023

Chen, G., Taylor, P. A., Qu, X., Molfese, P. J., Bandettini, P. A., Cox, R. W., & Finn, E. S. (2020). Untangling the relatedness among correlations, part III: Inter-subject correlation analysis through Bayesian multilevel modeling for naturalistic scanning. *NeuroImage*, *216*(December 2019), 116474. https://doi.org/10.1016/j.neuroimage.2019.116474

Chen, G., Taylor, P. A., Shin, Y. W., Reynolds, R. C., & Cox, R. W. (2017). Untangling the relatedness among correlations, Part II: Inter-subject correlation group analysis through linear mixed-effects modeling. *NeuroImage*, *147*(October 2016), 825–840. https://doi.org/10.1016/j.neuroimage.2016.08.029

Chen, J., Honey, C. J., Simony, E., Arcaro, M. J., Norman, K. A., & Hasson, U. (2016). Accessing Real-Life Episodic Information from Minutes versus Hours Earlier Modulates Hippocampal and High-Order Cortical Dynamics. *Cerebral Cortex*, *26*(8), 3428–3441. https://doi.org/10.1093/cercor/bhv155

Chen, J., Leong, Y. C., Honey, C. J., Yong, C. H., Norman, K. A., & Hasson, U. (2017). Shared memories reveal shared structure in neural activity across individuals. *Nature Neuroscience*, *20*(1), 115–125. https://doi.org/10.1038/nn.4450

Cheng, Y., Xin, Y., Lu, X., Yang, T., Ma, X., Yuan, X., Liu, N., & Jiang, Y. (2025). Shared and Unique Neural Codes for Biological Motion Perception in Humans and Macaque Monkeys. *Advanced Science*, *12*(18), 1–13. https://doi.org/10.1002/advs.202411562

Cohen, D., Goddard, E., & Mullen, K. T. (2019). Reevaluating hMT+ hV4 functional specialization for motion and static contrast using fMRI-guided repetitive transcranial magnetic stimulation. *Journal of Vision*, *19*(3), 1–20. https://doi.org/10.1167/19.3.11

Cox, R. W. (1996). AFNI: Software for analysis and visualization of functional magnetic resonance neuroimages. *Computers and Biomedical Research*, *29*(3), 162–173. https://doi.org/10.1006/cbmr.1996.0014

Cutting, J. E. (2014). Event segmentation and seven types of narrative discontinuity in popular movies. *Acta Psychologica*, *149*, 69–77. https://doi.org/10.1016/j.actpsy.2014.03.003

Cutting, J. E. (2016). Narrative theory and the dynamics of popular movies. *Psychonomic Bulletin and Review*, *23*(6), 1713–1743. https://doi.org/10.3758/s13423-016-1051-4

Cutting, J. E. (2019a). Sequences in popular cinema generate inconsistent event segmentation. *Attention, Perception, and Psychophysics*, *81*(6), 2014–2025. https://doi.org/10.3758/s13414-019-01757-w

Cutting, J. E. (2019b). Simplicity, Complexity, and Narration in Popular Movies. *Narrative Complexity*, *August 2019*, 200–222. https://doi.org/10.2307/j.ctvhktjh6.14

Cutting, J. E., Brunick, K. L., & Candan, A. (2012). Perceiving event dynamics and parsing Hollywood films. *Journal of Experimental Psychology: Human Perception and Performance*, *38*(6), 1476–1490. https://doi.org/10.1037/a0027737

Cutting, J. E., Brunick, K. L., & DeLong, J. E. (2011). How Act Structure Sculpts Shot Lengths and Shot Transitions in Hollywood Film. *Projections*, *5*(1), 1–16. https://doi.org/10.3167/proj.2011.050102

Cutting, J. E., & Candan, A. (2015). Shot durations, shot classes, and the increased pace of popular movies. *Projections (New York)*, *9*(2), 40–62. https://doi.org/10.3167/proj.2015.090204

Cutting, J. E., & Iricinschi, C. (2015). Re-Presentations of Space in Hollywood Movies: An Event-Indexing Analysis. *Cognitive Science*, *39*(2), 434–456. https://doi.org/10.1111/cogs.12151

Dadario, N. B., & Sughrue, M. E. (2023). The functional role of the precuneus. *Brain*, *146*(9), 3598–3607. https://doi.org/10.1093/brain/awad181

Deng, Z. Z., Wu, J. F., Gao, J. Q., Hu, Y., Zhang, Y. W., Wang, Y. S., Dong, H. M., Yang, Z., & Zuo, X. N. (2019). Segregated precuneus network and default mode network in naturalistic imaging. *Brain Structure and Function*, *224*(9), 3133–3144. https://doi.org/10.1007/s00429-019-01953-2

Desikan, R. S., Ségonne, F., Fischl, B., Quinn, B. T., Dickerson, B. C., Blacker, D., Buckner, R. L., Dale, A. M., Maguire, R. P., Hyman, B. T., Albert, M. S., & Killiany, R. J. (2006). An automated labeling system for subdividing the human cerebral cortex on MRI scans into gyral based regions of interest. *NeuroImage*, *31*(3), 968–980. https://doi.org/10.1016/j.neuroimage.2006.01.021

Dilks, D. D., Julian, J. B., Paunov, A. M., & Kanwisher, N. (2013). The occipital place area is causally and selectively involved in scene perception. *Journal of Neuroscience*, *33*(4), 1331–1336. https://doi.org/10.1523/JNEUROSCI.4081-12.2013

Duchaine, B., & Yovel, G. (2015). A Revised Neural Framework for Face Processing. *Annual Review of Vision Science*, *1*(1), 393–416. https://doi.org/10.1146/annurev-vision-082114-035518

Dumoulin, S. O., Bittar, R. G., Kabani, N. J., Baker, C. L., Le Goualher, G., Pike, G. B., & Evans, A. C. (2000). A new anatomical landmark for reliable identification of human area V5/MT: A quantitative analysis of sulcal patterning. *Cerebral Cortex*, *10*(5), 454–463. https://doi.org/10.1093/cercor/10.5.454

Eickhoff, S. B., Milham, M., & Vanderwal, T. (2020). Towards clinical applications of movie fMRI. *NeuroImage*, *217*(April), 116860. https://doi.org/10.1016/j.neuroimage.2020.116860

Eickhoff, S. B., Stephan, K. E., Mohlberg, H., Grefkes, C., Fink, G. R., Amunts, K., & Zilles, K. (2005). A new SPM toolbox for combining probabilistic cytoarchitectonic maps and functional imaging data. *NeuroImage*, *25*(4), 1325–1335. https://doi.org/10.1016/j.neuroimage.2004.12.034

Epstein, R. A. (2008). Parahippocampal and retrosplenial contributions to human spatial navigation. *Trends in Cognitive Sciences*, *12*(10), 388–396. https://doi.org/10.1016/j.tics.2008.07.004

Epstein, R. A., & Baker, C. I. (2019). Scene Perception in the Human Brain. *Annual Review of Vision Science*, *5*, 373–397. https://doi.org/10.1146/annurev-vision-091718-014809

Epstein, R. A., Higgins, J. S., Jablonski, K., & Feiler, A. M. (2007). Visual scene processing in familiar and unfamiliar environments. *Journal of Neurophysiology*, *97*(5), 3670–3683. https://doi.org/10.1152/jn.00003.2007

Epstein, R. A., & Kanwisher, N. (1998). Acortical representation of the local visual environment. *Nature*, *392*(6676), 598–601.

Faber, M., Radvansky, G. A., & D'Mello, S. K. (2018). Driven to distraction: A lack of change gives rise to mind wandering. *Cognition*, *173*(December 2016), 133–137. https://doi.org/10.1016/j.cognition.2018.01.007

Farbood, M. M., Heeger, D. J., Marcus, G., Hasson, U., & Lerner, Y. (2015). The neural processing of hierarchical structure in music and speech at different timescales. *Frontiers in Neuroscience*, *9*(APR), 1–13. https://doi.org/10.3389/fnins.2015.00157

Field, S. (2005). *Screenplay: The Foundations of Screenwriting*. Random House Publishing Group.

FIL Methods Group. (2017). *SPM12 Manual*. *15*(3), 1–508. https://www.fil.ion.ucl.ac.uk/spm/doc/manual.pdf%0Ahttp://www.fil.ion.ucl.ac.uk/spm/

Finn, E. S., & Bandettini, P. A. (2021). Movie-watching outperforms rest for functional connectivity-based prediction of behavior. *NeuroImage*, *235*(February), 117963. https://doi.org/10.1016/j.neuroimage.2021.117963

Fitch, W. T., & Martins, M. D. (2014). Hierarchical processing in music, language, and action: Lashley revisited. *Annals of the New York Academy of Sciences*, *1316*(1), 87–104. https://doi.org/10.1111/nyas.12406

Fransson, P., & Marrelec, G. (2008). The precuneus/posterior cingulate cortex plays a pivotal role in the default mode network: Evidence from a partial correlation network analysis. *NeuroImage*, *42*(3), 1178–1184. https://doi.org/10.1016/j.neuroimage.2008.05.059

Frazier, J. A., Chiu, S., Breeze, J. L., Makris, N., Lange, N., Kennedy, D. N., Herbert, M. R., Bent, E. K., Koneru, V. K., Dieterich, M. E., Hodge, S. M., Rauch, S. L., Grant, P. E., Cohen, B. M., Seidman, L. J., Caviness, V. S., & Biederman, J. (2005). Structural brain magnetic resonance imaging of limbic and thalamic volumes in pediatric bipolar disorder. *American Journal of Psychiatry*, *162*(7), 1256–1265. https://doi.org/10.1176/appi.ajp.162.7.1256

Geerligs, L., Gözükara, D., Oetringer, D., Campbell, K. L., van Gerven, M., & Güçlü, U. (2022). A partially nested cortical hierarchy of neural states underlies event segmentation in the human brain. *ELife*, *11*, 1–36. https://doi.org/10.7554/eLife.77430

Goldstein, J. M., Seidman, L. J., Makris, N., Ahern, T., O'Brien, L. M., Caviness, V. S., Kennedy, D. N., Faraone, S. V., & Tsuang, M. T. (2007). Hypothalamic Abnormalities in Schizophrenia: Sex Effects and Genetic Vulnerability. *Biological Psychiatry*, *61*(8), 935–945. https://doi.org/10.1016/j.biopsych.2006.06.027

Golesorkhi, M., Gomez-Pilar, J., Tumati, S., Fraser, M., & Northoff, G. (2021). Temporal hierarchy of intrinsic neural timescales converges with spatial core-periphery organization. *Communications Biology*, *4*(1), 1–14. https://doi.org/10.1038/s42003-021-01785-z

Golesorkhi, M., Gomez-Pilar, J., Zilio, F., Berberian, N., Wolff, A., Yagoub, M. C. E., & Northoff, G. (2021). The brain and its time: intrinsic neural timescales are key for input processing. *Communications Biology*, *4*(1), 1–16. https://doi.org/10.1038/s42003-021-02483-6

Gollo, L. L., Zalesky, A., Matthew Hutchison, R., van den Heuvel, M. P., & Breakspear, M. (2015). Dwelling quietly in the rich club: Brain network determinants of slow cortical fluctuations. *Philosophical Transactions of the Royal Society B: Biological Sciences*, *370*(1668). https://doi.org/10.1098/rstb.2014.0165

Grafton, S. T., & Hamilton, A. F. D. C. (2007). Evidence for a distributed hierarchy of action representation in the brain. *Human Movement Science*, *26*(4), 590–616. https://doi.org/10.1016/j.humov.2007.05.009

Grill-Spector, K., & Malach, R. (2004). The human visual cortex. *Annual Review of Neuroscience*, *27*(June), 649–677. https://doi.org/10.1146/annurev.neuro.27.070203.144220

Grossman, E. D., Battelli, L., & Pascual-Leone, A. (2005). Repetitive TMS over posterior STS disrupts perception of biological motion. *Vision Research*, *45*(22), 2847–2853. https://doi.org/10.1016/j.visres.2005.05.027

Hagmann, P., Cammoun, L., Gigandet, X., Meuli, R., Honey, C. J., Van Wedeen, J., & Sporns, O. (2008). Mapping the structural core of human cerebral cortex. *PLoS Biology*, *6*(7), 1479–1493. https://doi.org/10.1371/journal.pbio.0060159

Hamilton, A. F. D. C., & Grafton, S. T. (2006). Goal representation in human anterior intraparietal sulcus. *Journal of Neuroscience*, *26*(4), 1133–1137. https://doi.org/10.1523/JNEUROSCI.4551-05.2006

Hammoud, R., & Kouam, D. G. (2000). A Mixed Classification approach of shots for constructing scene structure for movie films. *Irish Machine Vision and Image Processing Conference*, 223–230.

Han, L. T., & Epstein, R. A. (2025). Distinct mechanisms for panoramic and landmark-based view integration in human scene-selective cortex. *BioRxiv : The Preprint Server for Biology*. https://pubmed.ncbi.nlm.nih.gov/39896651/

Hanke, M., Labs, A., Reich, T., Schulenburg, H., Boennen, M., Mareike, G., Golz, M., Hartigs, B., Hoffmann, N., Keil, S., Perlow, M., Peukmann, A. K., Rabe, L. N., & von Sobbe, F. R. (2015). Portrayed emotions in the movie “Forrest Gump.” *F1000Research*, *4*. https://doi.org/10.12688/f1000research.6230.1

Haq, I. U., Muhammad, K., Hussain, T., Kwon, S., Sodanil, M., Baik, S. W., & Lee, M. Y. (2019). Movie scene segmentation using object detection and set theory. *International Journal of Distributed Sensor Networks*, *15*(6), 0–7. https://doi.org/10.1177/1550147719845277

Hasson, U., Chen, J., & Honey, C. J. (2015). Hierarchical process memory: Memory as an integral component of information processing. *Trends in Cognitive Sciences*, *19*(6), 304–313. https://doi.org/10.1016/j.tics.2015.04.006

Hasson, U., Furman, O., Clark, D., Dudai, Y., & Davachi, L. (2008). Enhanced Intersubject Correlations during Movie Viewing Correlate with Successful Episodic Encoding. *Neuron*, *57*(3), 452–462. https://doi.org/10.1016/j.neuron.2007.12.009

Hasson, U., Landesman, O., Knappmeyer, B., Vallines, I., Rubin, N., & Heeger, D. J. (2008). Neurocinematics: The Neuroscience of Film. *Projections*, *2*(1), 1–26. https://doi.org/10.3167/proj.2008.020102

Hasson, U., Nir, Y., Levy, I., Fuhrmann, G., & Malach, R. (2004). Intersubject Synchronization of Cortical Activity During Natural Vision. *Science*, *303*(5664), 1634–1640. https://doi.org/10.1126/science.1089506

Hasson, U., Nusbaum, H. C., & Small, S. L. (2006). Repetition suppression for spoken sentences and the effect of task demands. *Journal of Cognitive Neuroscience*, *18*(12), 2013–2029. https://doi.org/10.1162/jocn.2006.18.12.2013

Hasson, U., Yang, E., Vallines, I., Heeger, D. J., & Rubin, N. (2008). A hierarchy of temporal receptive windows in human cortex. *Journal of Neuroscience*, *28*(10), 2539–2550. https://doi.org/10.1523/JNEUROSCI.5487-07.2008

Häusler, C. O., Eickhoff, S. B., & Hanke, M. (2022). Processing of visual and non-visual naturalistic spatial information in the "parahippocampal place area." *Scientific Data*, *9*(1), 1–15. https://doi.org/10.1038/s41597-022-01250-4

Häusler, C. O., & Hanke, M. (2016). An annotation of cuts, depicted locations, and temporal progression in the motion picture "Forrest Gump". *F1000Research*, *5*, 1–9. https://doi.org/10.12688/F1000RESEARCH.9536.1

Häusler, C. O., Hanke, M., & Waite, A. (2021). *Annotations of low-level perceptual confounds in the research cut of the audio-visual movie "Forrest Gump" and its audio-description*. https://github.com/psychoinformatics-de/studyforrest-data-confoundsannotation

Henderson, J. M., & Hollingworth, A. (1999). HIGH-LEVEL SCENE PERCEPTION. *Annual Review of Psychology*, *50*(1), 243–271. https://doi.org/10.1146/annurev.psych.50.1.243

Herrington, J. D., Nymberg, C., & Schultz, R. T. (2011). Biological motion task performance predicts superior temporal sulcus activity. *Brain and Cognition*, *77*(3), 372–381. https://doi.org/10.1016/j.bandc.2011.09.001

Honey, C. J., Thesen, T., Donner, T. H., Silbert, L. J., Carlson, C. E., Devinsky, O., Doyle, W. K., Rubin, N., Heeger, D. J., & Hasson, U. (2012). Slow Cortical Dynamics and the Accumulation of Information over Long Timescales. *Neuron*, *76*(2), 423–434. https://doi.org/10.1016/j.neuron.2012.08.011

Ito, T., Hearne, L. J., & Cole, M. W. (2020). A cortical hierarchy of localized and distributed processes revealed via dissociation of task activations, connectivity changes, and intrinsic timescales. *NeuroImage*, *221*(February), 117141. https://doi.org/10.1016/j.neuroimage.2020.117141

Jääskeläinen, I. P., Sams, M., Glerean, E., & Ahveninen, J. (2021). Movies and narratives as naturalistic stimuli in neuroimaging. *NeuroImage*, *224*(June 2020), 117445. https://doi.org/10.1016/j.neuroimage.2020.117445

Jain, M., Katyal, N., & Alok. (2021). *Katna: Tool for automating video keyframe extraction, video compression, Image Autocrop and Smart image resize tasks*. https://github.com/keplerlab/katna

Janke, S., & Glöckner-Rist, A. (2014). Deutsche Version der Positive and Negative Affect Schedule (PANAS). *Zusammenstellung Sozialwissenschaftlicher Items Und Skalen*, 1–15.

Jeon, H. A. (2014). Hierarchical processing in the prefrontal cortex in a variety of cognitive domains. In *Frontiers in Systems Neuroscience* (Vol. 8, Issue NOV, pp. 1–8). Frontiers Research Foundation. https://doi.org/10.3389/fnsys.2014.00223

Ji, H., Hooshyar, D., Kim, K., & Lim, H. (2019). A semantic-based video scene segmentation using a deep neural network. *Journal of Information Science*, *45*(6), 833–844. https://doi.org/10.1177/0165551518819964

Julian, J. B., Keinath, A. T., Marchette, S. A., & Epstein, R. A. (2018). The Neurocognitive Basis of Spatial Reorientation. *Current Biology*, *28*(17), R1059–R1073. https://doi.org/10.1016/j.cub.2018.04.057

Kamps, F. S., Lall, V., & Dilks, D. D. (2016). The occipital place area represents first-person perspective motion information through scenes. *Cortex*, *83*, 17–26. https://doi.org/10.1016/j.cortex.2016.06.022

Kauppi, J. P., Jääskeläinen, I. P., Sams, M., & Tohka, J. (2010). Inter-subject correlation of brain hemodynamic responses during watching a movie: Localization in space and frequency. *Frontiers in Neuroinformatics*, *4*(MAR), 1–10. https://doi.org/10.3389/fninf.2010.00005

Kauppi, J. P., Pajula, J., & Tohka, J. (2014). A versatile software package for inter-subject correlation based analyses of fMRI. *Frontiers in Neuroinformatics*, *8*(JAN), 1–13. https://doi.org/10.3389/fninf.2014.00002

Knejzlíková, T., Světlák, M., Malatincová, T., Roman, R., Chládek, J., Najmanová, J., Theiner, P., Linhartová, P., & Kašpárek, T. (2021). Electrodermal Response to Mirror Exposure in Relation to Subjective Emotional Responses, Emotional Competences and Affectivity in Adolescent Girls With Restrictive Anorexia and Healthy Controls. *Frontiers in Psychology*, *12*(September). https://doi.org/10.3389/fpsyg.2021.673597

Kwok, S. C., Shallice, T., & Macaluso, E. (2012). Functional anatomy of temporal organisation and domain-specificity of episodic memory retrieval. *Neuropsychologia*, *50*(12), 2943–2955. https://doi.org/10.1016/j.neuropsychologia.2012.07.025

Lahnakoski, J. M., Jääskeläinen, I. P., Sams, M., & Nummenmaa, L. (2017). Neural mechanisms for integrating consecutive and interleaved natural events. *Human Brain Mapping*, *38*(7), 3360–3376. https://doi.org/10.1002/hbm.23591

Larsson, J., & Smith, A. T. (2012). FMRI repetition suppression: Neuronal adaptation or stimulus expectation? *Cerebral Cortex*, *22*(3), 567–576. https://doi.org/10.1093/cercor/bhr119

Lee Masson, H., & Isik, L. (2021). Functional selectivity for social interaction perception in the human superior temporal sulcus during natural viewing. *NeuroImage*, *245*(November), 118741. https://doi.org/10.1016/j.neuroimage.2021.118741

Lee, Y., & Chen, J. (2024). The Relationship between Event Boundary Strength and Pattern Shifts across the Cortical Hierarchy during Naturalistic Movie-viewing. *Journal of Cognitive Neuroscience*, *36*(11), 2317–2342. https://doi.org/10.1162/jocn_a_02213

Lerner, Y., Honey, C. J., Katkov, M., & Hasson, U. (2014). Temporal scaling of neural responses to compressed and dilated natural speech. *Journal of Neurophysiology*, *111*(12), 2433–2444. https://doi.org/10.1152/jn.00497.2013

Lerner, Y., Honey, C. J., Silbert, L. J., & Hasson, U. (2011). Topographic mapping of a hierarchy of temporal receptive windows using a narrated story. *Journal of Neuroscience*, *31*(8), 2906–2915. https://doi.org/10.1523/JNEUROSCI.3684-10.2011

Loschky, L. C., Larson, A. M., Smith, T. J., & Magliano, J. P. (2020). The Scene Perception & Event Comprehension Theory (SPECT) Applied to Visual Narratives. *Topics in Cognitive Science*, *12*(1), 311–351. https://doi.org/10.1111/tops.12455

Lu, K. H., Hung, S. C., Wen, H., Marussich, L., & Liu, Z. (2016). Influences of high-level features, gaze, and scene transitions on the reliability of BOLD responses to natural movie stimuli. *PLoS ONE*, *11*(8), 1–19. https://doi.org/10.1371/journal.pone.0161797

Ludwigs, M. (2020). Hierarchical Thinking, Grammatical Structures, and the Originary Scene. *... : The Journal of Generative Anthropology*, *2*, 1–15. https://search.ebscohost.com/login.aspx?direct=true&profile=ehost&scope=site&authtype=crawler&jrnl=10837264&AN=143353825&h=Xky38kxzpIfQlKRssQNpxCfWZA4Fq35O1ktR4GhPFwSwk3vRAPCv%2FDBAMzPOBMJRGrLQWFtxcjKRbfM%2FgsppzQ%3D%3D&crl=c

Magliano, J. P., & Zacks, J. M. (2011). The impact of continuity editing in narrative film on event segmentation. *Cognitive Science*, *35*(8), 1489–1517. https://doi.org/10.1111/j.1551-6709.2011.01202.x

Makris, N., Goldstein, J. M., Kennedy, D., Hodge, S. M., Caviness, V. S., Faraone, S. V., Tsuang, M. T., & Seidman, L. J. (2006). Decreased volume of left and total anterior insular lobule in schizophrenia. *Schizophrenia Research*, *83*(2–3), 155–171. https://doi.org/10.1016/j.schres.2005.11.020

Margulies, D. S., Ghosh, S. S., Goulas, A., Falkiewicz, M., Huntenburg, J. M., Langs, G., Bezgin, G., Eickhoff, S. B., Castellanos, F. X., Petrides, M., Jefferies, E., & Smallwood, J. (2016). Situating the default-mode network along a principal gradient of macroscale cortical organization. *Proceedings of the National Academy of Sciences of the United States of America*, *113*(44), 12574–12579. https://doi.org/10.1073/pnas.1608282113

Markhabayeva, D., & Tseng, C. I. (2024). Multimodal cohesion and viewers' comprehension of scene transitions in film: an empirical investigation. *Frontiers in Communication*, *9*. https://doi.org/10.3389/fcomm.2024.1347788

Mas, J., & Fernandez, G. (2003). VIDEO SHOT BOUNDARY DETECTION BASED ON COLOR HISTOGRAM. *TRECVID 2003: Notebook Papers*. https://www-nlpir.nist.gov/projects/tvpubs/tvpapers03/ramonlull.paper.pdf

McAleer, P., Pollick, F. E., Love, S. A., Crabbe, F., & Zacks, J. M. (2014). The role of kinematics in cortical regions for continuous human motion perception. *Cognitive, Affective and Behavioral Neuroscience*, *14*(1), 307–318. https://doi.org/10.3758/s13415-013-0192-4

Mecklenbrauck, F., Gruber, M., Siestrup, S., Zahedi, A., Grotegerd, D., Mauritz, M., Trempler, I., Dannlowski, U., & Schubotz, R. I. (2024). The significance of structural rich club hubs for the processing of hierarchical stimuli. *Human Brain Mapping*, *45*(4), 1–28. https://doi.org/10.1002/hbm.26543

Mecklenbrauck, F., Sepulcre, J., Fehring, J., & Schubotz, R. I. (2024). Decoding cortical chronotopy—Comparing the influence of different cortical organizational schemes. *NeuroImage*, *303*(October), 120914. https://doi.org/10.1016/j.neuroimage.2024.120914

Menon, V. (2023). 20 years of the default mode network: A review and synthesis. *Neuron*, *111*(16), 2469–2487. https://doi.org/10.1016/j.neuron.2023.04.023

Nasr, S., Devaney, K. J., & Tootell, R. B. H. (2013). Spatial encoding and underlying circuitry in scene-selective cortex. *NeuroImage*, *83*, 892–900. https://doi.org/10.1016/j.neuroimage.2013.07.030

Nasr, S., Echavarria, C. E., & Tootell, R. B. H. (2014). Thinking outside the box: Rectilinear shapes selectively activate scene-selective cortex. *Journal of Neuroscience*, *34*(20), 6721–6735. https://doi.org/10.1523/JNEUROSCI.4802-13.2014

Nastase, S. A., Gazzola, V., Hasson, U., & Keysers, C. (2019). Measuring shared responses across subjects using intersubject correlation. *Social Cognitive and Affective Neuroscience*, *14*(6), 669–687. https://doi.org/10.1093/scan/nsz037

Nastase, S. A., & Hasson, U. (2024). *Confound regression models for intersubject correlation analysis with naturalistic stimuli Twenty confound regression models were constructed from standard head Movie-viewing results [Poster Presentation]*. Annual Meeting of the Organization for Human Brain Mapping, Seoul, South Korea. https://github.com/snastase/isc-confounds

Nunez-Elizalde, A. O., Huth, A. G., & Gallant, J. L. (2019). Voxelwise encoding models with non-spherical multivariate normal priors. *NeuroImage*, *197*(August 2018), 482–492. https://doi.org/10.1016/j.neuroimage.2019.04.012

Oetringer, D., Gözükara, D., Güçlü, U., & Geerligs, L. (2025). The neural basis of event segmentation: Stable features in the environment are reflected by neural states. *Imaging Neuroscience*, *3*(February). https://doi.org/10.1162/imag_a_00432

Oldfield, R. C. (1971). The Assessment and Analysis of Handedness: The Edinburgh Inventory. *Neuropsychologia1*, *9*, 97–113. https://doi.org/10.1007/978-3-319-55065-7_301010

Oren, N., Shapira-Lichter, I., Lerner, Y., Tarrasch, R., Hendler, T., Giladi, N., & Ash, E. L. (2016). How attention modulates encoding of dynamic stimuli. *Frontiers in Human Neuroscience*, *10*(OCT2016), 1–11. https://doi.org/10.3389/fnhum.2016.00507

Pajula, J., Kauppi, J. P., & Tohka, J. (2012). Inter-subject correlation in fMRI: Method validation against stimulus-model based analysis. *PLoS ONE*, *7*(8). https://doi.org/10.1371/journal.pone.0041196

Pang, J. C., Aquino, K. M., Oldehinkel, M., Robinson, P. A., Fulcher, B. D., Breakspear, M., & Fornito, A. (2023). Geometric constraints on human brain function. *Nature*, *618*(7965), 566–574. https://doi.org/10.1038/s41586-023-06098-1

Patriat, R., Molloy, E. K., Meier, T. B., Kirk, G. R., Nair, V. A., Meyerand, M. E., Prabhakaran, V., & Birn, R. M. (2013). The effect of resting condition on resting-state fMRI reliability and consistency: A comparison between resting with eyes open, closed, and fixated. *NeuroImage*, *78*, 463–473. https://doi.org/10.1016/j.neuroimage.2013.04.013

Pearlman, K. (2019). On Rhythm in Film Editing. *The Palgrave Handbook of the Philosophy of Film and Motion Pictures*, 143–163. https://doi.org/10.1007/978-3-030-19601-1_7

Peer, M., Hayman, M., Tamir, B., & Arzy, S. (2021). Brain coding of social network structure. *Journal of Neuroscience*, *41*(22), 4897–4909. https://doi.org/10.1523/JNEUROSCI.2641-20.2021

Pitcher, D., & Ungerleider, L. G. (2021). Evidence for a Third Visual Pathway Specialized for Social Perception. *Trends in Cognitive Sciences*, *25*(2), 100–110. https://doi.org/10.1016/j.tics.2020.11.006

Poldrack, R. A., Mumford, J. A., & Nichols, T. E. (2011). Handbook of Functional MRI Data Analysis. In *A Practical Approach to Medical Image Processing*. Cambridge University Press. https://doi.org/10.1017/CBO9780511895029

Posit team. (2024). *RStudio: Integrated Development Environment for R*. http://www.posit.co/

Rah, Y. J., Shin, J. H., & Lee, S. A. (2025). The Visual Scene Network and Hippocampus Represent Spatial Boundary Structures for Temporal Episodic Memory Organization. *Journal of Cognitive Neuroscience*, 1–16. https://doi.org/10.1162/jocn_a_02229

Raichle, M. E. (2015). The Brain's Default Mode Network. *Annual Review of Neuroscience*, *38*, 433–447. https://doi.org/10.1146/annurev-neuro-071013-014030

Rajimehr, R., Devaney, K. J., Bilenko, N. Y., Young, J. C., & Tootell, R. B. H. (2011). The "parahippocampal place area" responds preferentially to high spatial frequencies in humans and monkeys. *PLoS Biology*, *9*(4). https://doi.org/10.1371/journal.pbio.1000608

Rajimehr, R., Xu, H., Farahani, A., Kornblith, S., Duncan, J., Desimone, R., Rajimehr, R., Xu, H., Farahani, A., Kornblith, S., Duncan, J., & Desimone, R. (2024). Functional architecture of cerebral cortex during naturalistic movie watching. *Neuron*, *112*(24), 1–17. https://doi.org/10.1016/j.neuron.2024.10.005

Raut, R. V., Snyder, A. Z., & Raichle, M. E. (2020). Hierarchical dynamics as a macroscopic organizing principle of the human brain. *Proceedings of the National Academy of Sciences*, *117*(34), 20890–20897. https://doi.org/10.1073/pnas.2003383117

Riedel, L., van den Heuvel, M. P., & Markett, S. (2022). Trajectory of rich club properties in structural brain networks. *Human Brain Mapping*, *43*(14), 4239–4253. https://doi.org/10.1002/hbm.25950

Ritchey, M., & Cooper, R. A. (2020). Deconstructing the Posterior Medial Episodic Network. *Trends in Cognitive Sciences*, *24*(6), 451–465. https://doi.org/10.1016/j.tics.2020.03.006

Rockland, K. S., & Graves, W. W. (2023). The angular gyrus: a special issue on its complex anatomy and function. *Brain Structure and Function*, *228*(1), 1–5. https://doi.org/10.1007/s00429-022-02596-6

Rubin, G. S., & Turano, K. (1992). Reading without saccadic eye movements. *Vision Research*, *32*(5), 895–902. https://doi.org/10.1016/0042-6989(92)90032-E

Rugg, M. D., & Vilberg, K. L. (2013). Brain networks underlying episodic memory retrieval. *Current Opinion in Neurobiology*, *23*(2), 255–260. https://doi.org/10.1016/j.conb.2012.11.005

Rui, Y., Huang, T. S., & Mehrotra, S. (1998). Exploring video structure beyond the shots. *Proceedings of the IEEE Conference on Protocols for Multimedia Systems and Multimedia Networking, PROMS-MmNet*, 237–240. https://doi.org/10.1109/mmcs.1998.693648

Sava-Segal, C., Richards, C., Leung, M., & Finn, E. S. (2023). Individual differences in neural event segmentation of continuous experiences. *Cerebral Cortex*, *33*(13), 8164–8178. https://doi.org/10.1093/cercor/bhad106

Schubotz, R. I., & Von Cramon, D. Y. (2002). Predicting perceptual events activates corresponding motor schemes in lateral premotor cortex: An fMRI study. *NeuroImage*, *15*(4), 787–796. https://doi.org/10.1006/nimg.2001.1043

Scrivener, C. L., Teed, J. A., & Silson, E. H. (2025). Visual imagery of familiar people and places in category selective cortex. *Neuroscience of Consciousness*, *2025*(1). https://doi.org/10.1093/nc/niaf006

Seghier, M. L. (2023). Multiple functions of the angular gyrus at high temporal resolution. *Brain Structure and Function*, *228*(1), 7–46. https://doi.org/10.1007/s00429-022-02512-y

Seidemann, E., & Geisler, W. S. (2018). Linking V1 activity to behavior. *Annual Review of Vision Science*, *4*, 287–310. https://doi.org/10.1146/annurev-vision-102016-061324

Sepulcre, J., Sabuncu, M. R., Yeo, T. B., Liu, H., & Johnson, K. A. (2012). Stepwise connectivity of the modal cortex reveals the multimodal organization of the human brain. *Journal of Neuroscience*, *32*(31), 10649–10661. https://doi.org/10.1523/JNEUROSCI.0759-12.2012

Shahdloo, M., Acar, M., & Çukur, T. (2019). *Attention During Story Listening Modulates Temporal Receptive Windows Across Human Cortex*. 168–171. https://doi.org/10.32470/ccn.2019.1039-0

Shirer, W. R., Ryali, S., Rykhlevskaia, E., Menon, V., & Greicius, M. D. (2012). Decoding subject-driven cognitive states with whole-brain connectivity patterns. *Cerebral Cortex*, *22*(1), 158–165. https://doi.org/10.1093/cercor/bhr099

Silson, E. H., Gilmore, A. W., Kalinowski, S. E., Steel, A., Kidder, A., Martin, A., & Baker, C. I. (2019). A posterior–anterior distinction between scene perception and scene construction in human medial parietal cortex. *Journal of Neuroscience*, *39*(4), 705–717. https://doi.org/10.1523/JNEUROSCI.1219-18.2018

Silson, E. H., Steel, A. D., & Baker, C. I. (2016). Scene-selectivity and retinotopy in medial parietal cortex. *Frontiers in Human Neuroscience*, *10*(August), 17. https://doi.org/10.3389/fnhum.2016.00412

Smith, S. M., Jenkinson, M., Woolrich, M. W., Beckmann, C. F., Behrens, T. E. J., Johansen-Berg, H., Bannister, P. R., de Luca, M., Drobnjak, I., Flitney, D. E., Niazy, R. K., Saunders, J., Vickers, J., Zhang, Y., de Stefano, N., Brady, J. M., & Matthews, P. M. (2004). Advances in functional and structural MR image analysis and implementation as FSL. *NeuroImage*, *23*(SUPPL. 1), 208–219. https://doi.org/10.1016/j.neuroimage.2004.07.051

Smith, T. J., Levin, D., & Cutting, J. E. (2012). A Window on Reality: Perceiving Edited Moving Images. *Current Directions in Psychological Science*, *21*(2), 107–113. https://doi.org/10.1177/0963721412437407

Soltani, A., Murray, J. D., Seo, H., & Lee, D. (2021). Timescales of cognition in the brain. *Current Opinion in Behavioral Sciences*, *41*, 30–37. https://doi.org/10.1016/j.cobeha.2021.03.003

Song, M., Shin, E. J., Seo, H., Soltani, A., Steinmetz, N. A., Lee, D., Jung, M. W., & Paik, S.-B. (2024). Hierarchical gradients of multiple timescales in the mammalian forebrain. *Proceedings of the National Academy of Sciences*, *121*(51), 2017. https://doi.org/10.1073/pnas.2415695121

Speer, N. K., Zacks, J. M., & Reynolds, J. R. (2007). Human brain activity time-locked to narrative event boundaries: Research article. *Psychological Science*, *18*(5), 449–455. https://doi.org/10.1111/j.1467-9280.2007.01920.x

Srokova, S., Hill, P. F., & Rugg, M. D. (2022). The Retrieval-Related Anterior Shift Is Moderated by Age and Correlates with Memory Performance. *Journal of Neuroscience*, *42*(9), 1765–1776. https://doi.org/10.1523/JNEUROSCI.1763-21.2021

Steel, A., Billings, M. M., Silson, E. H., & Robertson, C. E. (2021). A network linking scene perception and spatial memory systems in posterior cerebral cortex. *Nature Communications*, *12*(1). https://doi.org/10.1038/s41467-021-22848-z

Steel, A., Garcia, B. D., Goyal, K., Mynick, A., & Robertson, C. E. (2023). Scene Perception and Visuospatial Memory Converge at the Anterior Edge of Visually Responsive Cortex. *Journal of Neuroscience*, *43*(31), 5723–5737. https://doi.org/10.1523/JNEUROSCI.2043-22.2023

Steel, A., Prasad, D., Garcia, B. D., & Robertson, C. E. (2025). Relating Scene Memory and Perception Activity to Functional Properties, Networks, and Landmarks of Posterior Cerebral Cortex—A Probabilistic Atlas. *The Journal of Neuroscience*, *45*(23), e0028252025. https://doi.org/10.1523/JNEUROSCI.0028-25.2025

Steel, A., Silson, E. H., Garcia, B. D., & Robertson, C. E. (2024). A retinotopic code structures the interaction between perception and memory systems. *Nature Neuroscience*, *27*(2), 339–347. https://doi.org/10.1038/s41593-023-01512-3

Sulpizio, V., Galati, G., Fattori, P., Galletti, C., & Pitzalis, S. (2020). A common neural substrate for processing scenes and egomotion-compatible visual motion. *Brain Structure and Function*, *225*(7), 2091–2110. https://doi.org/10.1007/s00429-020-02112-8

Taylor, P. A., Reynolds, R. C., Calhoun, V., Gonzalez-Castillo, J., Handwerker, D. A., Bandettini, P. A., Mejia, A. F., & Chen, G. (2023). Highlight results, don't hide them: Enhance interpretation, reduce biases and improve reproducibility. *NeuroImage*, *274*(October 2022), 120138. https://doi.org/10.1016/j.neuroimage.2023.120138

The MathWorks Inc. (2021). *MATLAB version: 9.10.0 (R2021a)*. The MathWorks Inc. https://www.mathworks.com

Thorenz, K., Berwinkel, A., & Weigelt, M. (2023). A Validation Study for the German Versions of the Feeling Scale and the Felt Arousal Scale for a Progressive Muscle Relaxation Exercise. *Behavioral Sciences*, *13*(7). https://doi.org/10.3390/bs13070523

Tomar, S. (2006). Converting video formats with FFmpeg. *Linux Journal*, *2006*(146), 10.

Tong, F. (2003). Cognitive neuroscience: Primary visual cortex and visual awareness. *Nature Reviews Neuroscience*, *4*(3), 219–229. https://doi.org/10.1038/nrn1055

Torres-Morales, C., & Cansino, S. (2024). Brain representations of space and time in episodic memory: A systematic review and meta-analysis. *Cognitive, Affective and Behavioral Neuroscience*, *24*(1), 1–18. https://doi.org/10.3758/s13415-023-01140-1

Tylén, K., Christensen, P., Roepstorff, A., Lund, T., Østergaard, S., & Donald, M. (2015). Brains striving for coherence: Long-term cumulative plot formation in the default mode network. *NeuroImage*, *121*, 106–114. https://doi.org/10.1016/j.neuroimage.2015.07.047

Uithol, S., van Rooij, I., Bekkering, H., & Haselager, P. (2012). Hierarchies in action and motor control. *Journal of Cognitive Neuroscience*, *24*(5), 1077–1086. https://doi.org/10.1162/jocn_a_00204

Vagharchakian, L., Dehaene-Lambertz, G., Pallier, C., & Dehaene, S. (2012). A temporal bottleneck in the language comprehension network. *Journal of Neuroscience*, *32*(26), 9089–9102. https://doi.org/10.1523/JNEUROSCI.5685-11.2012

Valentine, J. W., & May, C. L. (1996). Hierarchies in biology and paleontology. *Paleobiology*, *22*(1), 23–33. https://doi.org/10.1017/S0094837300015992

Van den Stock, J., Vandenbulcke, M., Sinke, C. B. A., Goebel, R., & De Gelder, B. (2014). How affective information from faces and scenes interacts in the brain. *Social Cognitive and Affective Neuroscience*, *9*(10), 1481–1488. https://doi.org/10.1093/scan/nst138

Van Dijk, K. R. A., Hedden, T., Venkataraman, A., Evans, K. C., Lazar, S. W., & Buckner, R. L. (2010). Intrinsic functional connectivity as a tool for human connectomics: Theory, properties, and optimization. *Journal of Neurophysiology*, *103*(1), 297–321. https://doi.org/10.1152/jn.00783.2009

Vann, S. D., Aggleton, J. P., & Maguire, E. A. (2009). What does the retrosplenial cortex do? *Nature Reviews Neuroscience*, *10*(11), 792–802. https://doi.org/10.1038/nrn2733

VanRullen, R., & Koch, C. (2003). Is perception discrete or continuous? *Trends in Cognitive Sciences*, *7*(5), 207–213. https://doi.org/10.1016/S1364-6613(03)00095-0

Wade, A. R., Brewer, A. A., Rieger, J. W., & Wandell, B. A. (2002). Functional measurements of human ventral occipital cortex: Retinotopy and colour. *Philosophical Transactions of the Royal Society B: Biological Sciences*, *357*(1424), 963–973. https://doi.org/10.1098/rstb.2002.1108

Wakita, M. (2014). Broca's area processes the hierarchical organization of observed action. *Frontiers in Human Neuroscience*, *7*(JAN). https://doi.org/10.3389/fnhum.2013.00937

Wang, L., Mruczek, R. E. B., Arcaro, M. J., & Kastner, S. (2015). Probabilistic maps of visual topography in human cortex. *Cerebral Cortex*, *25*(10), 3911–3931. https://doi.org/10.1093/cercor/bhu277

Wang, X.-J. (2020). Macroscopic gradients of synaptic excitation and inhibition in the neocortex. *Nature Reviews Neuroscience*, *21*(3), 169–178. https://doi.org/10.1038/s41583-020-0262-x

Watson, D., Clark, L. A., & Tellegen, A. (1988). Development and Validation of Brief Measures of Positive and Negative Affect: The PANAS Scales. *Journal of Personality and Social Psychology*, *54*(6), 1063–1070.

Watson, D. M., & Andrews, T. J. (2024). Mapping the functional and structural connectivity of the scene network. *Human Brain Mapping*, *45*(3), 1–21. https://doi.org/10.1002/hbm.26628

Whitney, C., Huber, W., Klann, J., Weis, S., Krach, S., & Kircher, T. (2009). Neural correlates of narrative shifts during auditory story comprehension. *NeuroImage*, *47*(1), 360–366. https://doi.org/10.1016/j.neuroimage.2009.04.037

Wilcox, L. M., Allison, R. S., Helliker, J., Dunk, B., & Anthony, R. C. (2015). Evidence that viewers prefer higher frame-rate film. *ACM Transactions on Applied Perception*, *12*(4), 1–12. https://doi.org/10.1145/2810039

Winawer, J., & Witthoft, N. (2015). Human V4 and ventral occipital retinotopic maps. *Visual Neuroscience*, *32*. https://doi.org/10.1017/S0952523815000176

Wolff, A., Berberian, N., Golesorkhi, M., Gomez-Pilar, J., Zilio, F., & Northoff, G. (2022). Intrinsic neural timescales: temporal integration and segregation. *Trends in Cognitive Sciences*, *26*(2), 159–173. https://doi.org/10.1016/j.tics.2021.11.007

Wu, J. (2013). Hierarchy Theory: An Overview. In R. Rozzi, S. T. A. Pickett, C. Palmer, J. J. Armesto, & J. B. Callicott (Eds.), *Linking Ecology and Ethics for a Changing World: Values, Philosophy, and Action* (pp. 281–301). Springer Netherlands. https://doi.org/10.1007/978-94-007-7470-4_24

Xia, M., Wang, J., & He, Y. (2013). BrainNet Viewer: A Network Visualization Tool for Human Brain Connectomics. *PLoS ONE*, *8*(7). https://doi.org/10.1371/journal.pone.0068910

Yang, E., Milisav, F., Kopal, J., Holmes, A. J., Mitsis, G. D., Misic, B., Finn, E. S., & Bzdok, D. (2023). The default network dominates neural responses to evolving movie stories. *Nature Communications*, *14*(1). https://doi.org/10.1038/s41467-023-39862-y

Yang, H., Susilo, T., & Duchaine, B. (2016). The Anterior Temporal Face Area Contains Invariant Representations of Face Identity That Can Persist Despite the Loss of Right FFA and OFA. *Cerebral Cortex*, *26*(3), 1096–1107. https://doi.org/10.1093/cercor/bhu289

Yeh, M. C., Tsai, Y. W., & Hsu, H. C. (2016). A content-based approach for detecting highlights in action movies. *Multimedia Systems*, *22*(3), 287–295. https://doi.org/10.1007/s00530-015-0457-6

Yeo, B. T. T., Krienen, F. M., Sepulcre, J., Sabuncu, M. R., Lashkari, D., Hollinshead, M., Roffman, J. L., Smoller, J. W., Zöllei, L., Polimeni, J. R., Fisch, B., Liu, H., & Buckner, R. L. (2011). The organization of the human cerebral cortex estimated by intrinsic functional connectivity. *Journal of Neurophysiology*, *106*(3), 1125–1165. https://doi.org/10.1152/jn.00338.2011

Yeshurun, Y., Nguyen, M., & Hasson, U. (2021). The default mode network: where the idiosyncratic self meets the shared social world. *Nature Reviews Neuroscience*, *22*(3), 181–192. https://doi.org/10.1038/s41583-020-00420-w

Yeshurun, Y., Swanson, S., Simony, E., Chen, J., Lazaridi, C., Honey, C. J., & Hasson, U. (2017). Same Story, Different Story: The Neural Representation of Interpretive Frameworks. *Psychological Science*, *28*(3), 307–319. https://doi.org/10.1177/0956797616682029

Zacks, J. M., Braver, T. S., Sheridan, M. A., Donaldson, D. I., Snyder, A. Z., Ollinger, J. M., Buckner, R. L., & Raichle, M. E. (2001). Human brain activity time-locked. *Nature Neuroscience*, *4*(6), 651–655. http://neurosci.nature.com

Zacks, J. M., Speer, N. K., & Reynolds, J. R. (2009). Segmentation in Reading and Film Comprehension. *Journal of Experimental Psychology: General*, *138*(2), 307–327. https://doi.org/10.1037/a0015305

Zacks, J. M., Speer, N. K., Swallow, K. M., & Maley, C. J. (2010). The brain's cutting-room floor: Segmentation of narrative cinema. *Frontiers in Human Neuroscience*, *4*(October), 1–15. https://doi.org/10.3389/fnhum.2010.00168

Zadbood, A., Chen, J., Leong, Y. C., Norman, K. A., & Hasson, U. (2017). How We Transmit Memories to Other Brains: Constructing Shared Neural Representations Via Communication. *Cerebral Cortex*, *27*(10), 4988–5000. https://doi.org/10.1093/cercor/bhx202

Zemeckis, R. (1994). *Forrest Gump* [Video recording]. Paramount Pictures.

Zhen, Z., Yang, Z., Huang, L., Kong, X., Wang, X., Dang, X., Huang, Y., Song, Y., & Liu, J. (2015). Quantifying interindividual variability and asymmetry of face-selective regions: A probabilistic functional atlas. *NeuroImage*, *113*, 13–25. https://doi.org/10.1016/j.neuroimage.2015.03.010

Zhu, W., Huang, Y., Xie, X., Liu, W., Deng, J., Zhang, D., Wang, Z., & Liu, J. (2023). AutoShot: A Short Video Dataset and State-of-the-Art Shot Boundary Detection. *IEEE Computer Society Conference on Computer Vision and Pattern Recognition Workshops*, *2023-June*, 2238–2247. https://doi.org/10.1109/CVPRW59228.2023.00218

3 General Discussion

3.1 Summary of the presented studies

Environmental stimuli as well as the dynamics along the cortical hierarchy can be organized by their temporal persistency. This thesis therefore hypothesized that the different levels of the cortical chronoarchitecture make use of the stimulus' temporal structure and process the hierarchically nested natural stimuli according to their durations. Since previous models proposed the macrostructural network organization as the key feature that underlies the variation of timescales across the cortex (e.g., Gollo et al., 2015), the focus of the structural examination of cortical chronoarchitecture in this thesis was primarily on the structural rich club with its long-reaching, central connections. This network analysis stood alongside the functional investigation of the processing of hierarchically nested stimuli based on their temporal dynamics. In this context, we based the stimulus manipulation on the paradigms developed for the investigation of TRWs, which involve a hierarchically nested stimulus parcellated according to its different hierarchical levels and shuffled to break up the temporal persistency at different durations (e.g., Hasson, Yang, et al., 2008).

Study 1 (Mecklenbrauck, Gruber, et al., 2024) therefore used a hierarchically nested sequence of numbers that was made up of periodic smaller chunks. The different experimental conditions then varied in the length of these chunks, totalling either one (SINGLE), three (TRIPLET), nine (NONET) or 36 (COMPLETE) digits. During fMRI acquisition, participants were presented with each experimental condition five times in blocks of pseudorandomized order. Contrasting the blocks exposed specific activity for the three-digit sequences in the inferior frontal junction. Furthermore, the nine-digit sequence specifically activated areas including the SFG and the middle frontal gyrus (MFG), the middle temporal gyrus (MTG), the inferior temporal sulcus (ITS) as well as parietal regions, like the inferior parietal lobe (IPL) and the posterior cingulate cortex (PCC).

The same participants returned to a second scanning session where diffusion-weighted images as well as functional resting-state images were recorded that served as the basis for the graph-theoretical network analyses in **Study 1** and **Study 2** (Mecklenbrauck, Sepulcre, et al., 2024). For the structural analysis in **Study 1** we created a group-wise cortical connectome and located the rich club hub regions using a specifically developed identification method that combined multiple measures of network centrality (cf. van den Heuvel & Sporns, 2013b). Also, we explicitly tested whether the hubs connected to other hub regions more likely than expected at random, which was more in line with the original proposal of the rich club (Colizza et al., 2006). The final set of areas replicated previously indicated hub regions, validating our newly developed identification procedure.

For the subsequent rich club-focused regions of interest (ROI) analysis, we extracted the cortical activation from all areas that represented nodes in network construction and modelled the functional brain activity by the experimental conditions as well as the regions' classification as a rich club hub, feeder, or local node. The results could however not identify any effects of the node classification but reiterated significant difference of the NONET compared to the TRIPLET and SINGLE conditions. In addition, we conducted an analysis of the structural centrality of the functionally identified whole-brain clusters and showed increased network centrality for the nodes specifically activated by the nine- compared to the three-digit sequences. Moreover, descriptively, the percentage of rich club nodes was higher within the NONET-specific clusters.

An exploratory investigation of the spatial layout of brain activity in the frontal lobe revealed that the activations related to the longer nine-digit sequences were also located more anterior and medial than the three-digit associated effects. Thus, **Study 1** provided evidence for the hypothesis that stimulus sequences are processed by different cortical areas according to their temporal duration. The role of the structural rich club however remained elusive as the functional clusters in the frontal lobe better aligned with a spatially defined posterior-lateral-to-anterior-medial gradient.

To further distinguish the role of the rich club in shaping the cortical processing dynamics, **Study 2** (Mecklenbrauck, Sepulcre, et al., 2024) compared the influence of different commonly proposed cortical organizational schemes on the intrinsic timescales at rest and the temporal dynamics during a task. This was respectively calculated using the autocorrelation decay of a region's average time course as well as the ISC during the digit-sequence-task of **Study 1**. Beyond the rich club, which was identified in subject-wise connectomes while otherwise using the same method as in **Study 1**, we investigated (1) the diverse club, as a direct competitor to the rich club defined based on the participation of network nodes in the cortical module structure (Bertolero et al., 2017), (2) the uni-to-multimodal gradient, identified firstly through step-wise functional connectivity (Sepulcre et al., 2012) and secondly based on a functional atlas definition (Ji et al., 2019), and (3) the spatial gradient from posterior-lateral-to-anterior-medial indicated by the results of **Study 1**. Additionally, we explored the effect of five different structural network centrality measures and the variation of cortical thickness as an approximation of microstructural differences (Wagstyl et al., 2015).

A spin test (Alexander-Bloch et al., 2018) identified similarities between the rich club and diverse club architectures. Moreover, the two implementations of the uni-to-multimodal gradient correlated with each other as well as other typical definitions of this functional gradient (Margulies et al., 2016; Sydnor et al., 2023).

Using Bayesian model comparison **Study 2** revealed that the atlas-based uni-to-multimodal gradient (Ji et al., 2019) best explained the variations in both resting-state- and task-based dynamics. Thus, although the results indicated slower resting-state timescales within areas labelled as rich club hubs compared to local nodes, overall, **Study 2** rather suggested that the functional distinction between unimodal and multimodal areas shapes the distribution of intrinsic timescales and underlies the processing of hierarchically nested stimuli based on their temporal dynamics.

Finally, in **Study 3** (Mecklenbrauck & Schubotz, in review) we examined the specific effect of stimulus duration on its processing by disentangling it from the effect of stimulus complexity. In naturalistic stimuli, content complexity is intertwined with duration, as longer stimuli usually also depict more narrative elements. By extracting and presenting only a certain number of individual frames from shots and scenes of a movie, we were able to manipulate the level of content complexity (SHOT or SCENE) independently of the duration of the stimulus (4S, 12S, or 36S). Using pair-wise ISC, we identified cortical areas consistently engaged for specific levels of content and duration. The whole-brain findings were in line with earlier work that used naturalistic stimuli (Hasson, Yang, et al., 2008), validating the applied stimulus manipulation.

In detail, the results revealed the *scene network*, previously demonstrated in the context of visual scenery perception (cf. Steel et al., 2025). Intriguingly, movie SCENES compared to SHOTS engaged the more visually-attuned, posterior part of this network containing the occipital and posterior parahippocampal place areas. However, when comparing longer with shorter stimulus durations we found engagement in the anterior scene network, which includes the anterior parahippocampal place area, the retrosplenial cortex (RSC), and the caudal IPL and connects to memory related cortical areas. Additionally, the interaction of content level and duration indicated that especially longer, more complex stimuli engaged high-level cortical areas, including the precuneus or the anterior temporal lobe. A ROI analysis further affirmed that regions representing high levels of visual processing were more engaged by longer SCENE stimuli.

Study 3 therefore largely corroborated our hypothesis that the duration of a stimulus plays a crucial role for the higher-level processing of hierarchically nested naturalistic stimuli like movies. The effect of duration however interacts with the depicted content complexity of the stimulus.

In conclusion, the three studies contained within this thesis can be summarized in two major findings:

1. Hierarchically nested stimuli are processed according to their temporal organization (**Study 1** and **Study 3**).
2. The temporal processing hierarchy extends along the functional uni-to-multimodal gradient, with low-level, unimodal regions processing transient stimuli and the high-level association cortices being more engaged by longer, more persistent stimuli (**Study 2** and **Study 3**).

Interestingly however, the studies did not provide convincing evidence for a substantial role of the structural rich club in shaping this dynamic, functional processing hierarchy. Hence, in the following I will place the results into the larger context of cortical hierarchies and stimulus processing while exploring different possibilities for the lacking rich club results. Thereby, I will also discuss relevant methodological considerations before giving an outlook to potential next steps based on the presented findings.

3.2 The functional processing hierarchy along the uni-to-multimodal gradient

In two of the presented studies (**Study 1**: Mecklenbrauck, Gruber, et al., 2024; **Study 3**: Mecklenbrauck & Schubotz, in review), we established that hierarchically nested stimuli of higher-level persistency are processed differently from more transient stimuli. Both experiments however varied in their type of stimuli – digit sequences and movie segments – as well as in their analysis methods – classic general linear model and ISC. Consequently, the clusters revealed by the respective analyses do not overlap. Nevertheless, in the following I will demonstrate that the results arguably converge – similarly to the outcome of **Study 2** (Mecklenbrauck, Sepulcre, et al., 2024) – on the processing gradient from unimodal to multimodal cortices. For this purpose, I reassessed the results of **Study 1**, which were initially examined from the perspective of a posterior-lateral-to-anterior-medial gradient focused on the frontal cortex (e.g., Koechlin & Summerfield, 2007), to align the findings for longer digit sequences in **Study 1** with the functional uni-to-multimodal gradient and thus also with the processing of longer movie stimuli in **Study 3**.

As already discussed comprehensively in **Study 3**, we localized the effects of longer stimulus duration predominantly within the anterior scene network (e.g., Baldassano et al., 2016; Steel et al., 2021). Steel et al. (2025) used the functional connectivity gradients of Margulies et al. (2016) to concisely demonstrate that specifically these anterior portions of scene network register as more multimodal areas. This classification was further supported by results associating the posterior scene network with the early visual cortex, while the anterior scene network was linked to areas of the DMN network as well as memory related networks (Baldassano et al., 2016; Nasr et al., 2013; Silson et al., 2016). Thus, networks that comprise of high-order, multimodal cortical areas, which have slower intrinsic timescales (e.g., Raut et al., 2020) and longer TRWs (e.g., Hasson et al., 2015). Specifically, SCENE stimuli of long DURATION identified clusters in the precuneus and along the STS, which are both part of the DMN and were accordingly associated with the high-level, multimodal integration and processing of complex stimuli (cf. Yeshurun et al.,

2021). Therefore, **Study 3** clearly demonstrated a progression of the duration-based functional processing hierarchy along the uni-to-multimodal cortical gradient.

In contrast, **Study 1** focused on the structural network, but could not demonstrate a clear relationship between the rich club architecture and the functional processing of higher-order, hierarchically nested stimuli. In the discussion, we proposed that the results mapped onto the posterior-lateral-to-anterior-medial-gradient within the frontal lobe that was suggested in the context of cognitive control theories (e.g., Koechlin & Summerfield, 2007). Appropriately, we located activation specific to the temporally longer NONET digit sequences in the right MFG as well as right medial SFG (i.e., Brodmann area 8) that was previously related to processing predictable sequences of numbers (Kühn & Schubotz, 2012). Especially these findings in the dorso-medial PFC (dmPFC) thereby supported our interpretation that the processing of higher-level, more persistent, hierarchical stimuli activated higher-order cortical regions in the anterior-medial frontal lobe, which were suggested to represent the apex of the frontal, processing hierarchy (W. H. Alexander & Brown, 2011, 2018; Badre & Nee, 2018). In accordance, previous studies have consistently linked the dmPFC to high-level, integrative processes across different cognitive domains including decision making, goal-directed motor planning and social cognition (Dadario et al., 2023; Domenech & Koechlin, 2015; Ferrari et al., 2016; Jin et al., 2024; Petrides, 2015; Q. Zhang et al., 2021).

However, based on its structural and functional connectivity profile, the dmPFC crucially also classifies as a multimodal association cortex (Dadario et al., 2023), arguably aligning this finding of **Study 1** – like the results of **Studies 2 & 3** – with the uni-to-multimodal gradient as well.

Subsequently, a re-evaluation of **Study 1's** whole-brain results in the hindsight of **Studies 2 & 3** indicated that also the other clusters resulting from the block-wise comparison of the NONET > TRIPLET conditions portray the engagement of more multimodal areas in the context of longer stimulus segments. Two areas are of particular interest here: the angular gyrus (labelled IPL in **Study 1**) and the PCC.

The angular gyrus, located within the IPL, represents a parietal cross-modal association cortex collecting information from visual areas in the occipital lobe, auditory areas in the temporal lobe and somatomotor areas in the anterior parietal lobe (for a review see Seghier, 2013). As an integrative hub area, the angular gyrus was found to be involved in various cognitive domains including attention allocation, semantic processing, memory retrieval, and social cognition (Binder et al., 2009; Numssen et al., 2021; Seghier, 2013). More importantly, in the context of the hierarchical nested digit sequences in **Study 1**, the angular gyrus was also indicated to relate to numeric processing, exhibiting increased activity for ordered sequences (Zaleznik & J. Park, 2021). Furthermore, a set of studies illustrated that the angular gyrus acts as a multimodal temporal buffer region for the processing of stimulus sequences (Humphreys et al., 2020, 2022; Humphreys & Tibon, 2023). This matches the results of **Studies 2 & 3** that multimodal hub regions integrate stimuli across longer durations. Especially in **Study 3**, the angular gyrus also represented a higher-order visual processing area in the conducted ROI analysis, which further supported its role in processing longer, more complex stimuli.

Correspondingly, the PCC can also be classified as multimodal hub region, sitting at the upper end of the cortical hierarchy (Leech & Smallwood, 2019). The PCC, with its plethora of structural and functional connections, was accordingly suggested to shape the global dynamics of the cortical network (Leech & Sharp, 2014; Leech & Smallwood, 2019), similar to what **Studies 1 & 2** suspected for the dense interconnected rich club hub regions. Functionally, this area was commonly indicated to play a role in the balance between stimulus-focused and internal-thought-focused processing, being predominantly involved in more complex cognition including rule learning and multi-tasking (Leech et al., 2012; Leech & Sharp, 2014; Smallwood et al., 2016), which are essential for handling higher-order, stimulus sequences.

Therefore, finding the dmPFC alongside the angular gyrus and the PCC specifically activated for the processing of the higher levels of the hierarchically nested digit sequence highlights that the results of **Study 1** also correspond to the uni-to-multimodal gradient.

To further support this reinterpretation, I added a supplementary analysis modeling the condition-wise activity from **Study 1's** digit sequence task in each area by its position on the canonical uni-to-multimodal gradient published by Margulies et al. (2016), rather than the original classification as rich club, feeder or local node (see Appendix D). As expected, in contrast to the rich-club-based model, an increase on the uni-to-multimodal gradient not only coincided significantly with an increase in cortical activity, but more importantly, this effect was significantly larger in the NONET and COMPLETE conditions compared to the TRIPLET condition. These findings therefore underscore that multimodal areas are significantly more involved in the processing of higher levels of hierarchically nested stimuli (for more details see Appendix D).

Beyond that, the reassessment of the functional clusters in **Study 1** also outlined a possible functional network architecture that supports the processing of longer, hierarchically higher stimulus structures: The angular gyrus, the PCC as well as the dmPFC are all affiliated with the DMN (Dadario et al., 2023; P. Lin et al., 2016; Seghier, 2013), which tops the functional uni-to-multimodal hierarchy (Margulies et al., 2016). As introduced, the DMN consists of areas that are classified by slow intrinsic cortical signals (Golesorkhi, Gomez-Pilar, Tumati, et al., 2021; Ito et al., 2020; Raut et al., 2020) and respond, for instance, to high-level narrative shifts in naturalistic hierarchical stimuli (e.g., Yeshurun et al., 2021). Thus, when looking at the activation pattern associated with the longer NONET sequences as a whole, the clusters include multiple regions involved in the multimodal DMN. This is also in line with the results of **Study 3** that revealed engagement in the DMN-associated areas in the anterior scene network as well as the precuneus and anterior temporal lobe in the context of longer, more complex stimuli.

The remaining NONET-specific clusters in **Study 1**, including the MFG and the clusters in the temporal lobe (ITS and MTG), fall within the FPN. This domain-general executive control network is adaptive to the current tasks demands (Cole et al., 2013; Marek & Dosenbach, 2018) and was previously related to the integrative processes in Fuster's (2001) perception-action cycle (E. Y. Choi et al., 2018; Nee, 2021; see 1.3.1). In contrast to the DMN, which was labelled as task-

negative (i.e., active at rest), the FPN was originally associated with task-positive activity (Fox et al., 2005). However, more recent investigations have specifically identified task-induced, functional connections between the DMN and FPN during the retrieval of prior information (González-García et al., 2018; Hearne et al., 2015; Zanto & Gazzaley, 2013) as well as – intriguingly for the conducted experiments – the representation of hierarchical sequences (Rogers et al., 2010; Wen et al., 2020). In this interaction between networks, the FPN was suggested to act as a gate between external, stimulus- and internal, prediction-focused processing (Dixon et al., 2018; Spreng et al., 2013; Yin et al., 2022). Furthermore, specifically the SFG, MFG and angular gyrus were shown to act as cross-modal connector hubs between these two functional networks (Y. Xu et al., 2016).

Therefore, finding both the DMN and FPN involved in the processing of more persistent digit sequences could suggest a shift towards a more high-level, internal-focused processing that integrates across multiple functional modules prompted by longer stimuli like the NONET sequences. This shift was also indicated by the results for a higher DURATION in **Study 3**, as Steel et al. (2024) proposed that the transition from the posterior to the anterior scene network transforms the cortical representations of perception. This transformation would in turn allow for the association to memory as well as higher levels of predictive processing (see also A. S. Alexander et al., 2023). In conclusion, the presented studies thus propose that longer stimuli containing more complex content additionally engage cortical networks that are less focused on external stimuli but are more concerned with internal, integrative processes (cf. Wolff et al., 2022).

However, while this shift towards introspection was also reflected in Gollo et al.'s (2015) rich-core-periphery-axis, we did not find conclusive evidence for the structural network scaffolding of this chronoarchitecture. Furthermore, some methodological limitations must be considered when interpreting these findings. First, since the conducted experiments focused only on a specific range of environmental time scales, the full capacity of temporal integration remains unexplored (cf. Golesorkhi, Gomez-Pilar, Zilio, et al., 2021). Second, especially the most

persistent temporal conditions (COMPLETE in **Studies 1&2**, 36S in **Study 3**) deviate from the remaining results. Thus, although all studies concisely demonstrated the coherence of the temporal processing hierarchy to the functional uni-to-multimodal gradient, critical questions regarding both the temporal organization of the stimuli as well as the structural foundation of the functional hierarchy need to be discussed.

3.2.1 The timescales of integration. The first question concerns the temporal distinction between the hierarchical stimulus levels as well as the range of dynamic processing.

Summarized across all studies, the results suggest that the shorter hierarchical structures (**Studies 1 & 2**: TRIPLET = 2.1s duration, **Study 3**: SCENE 4S and SHOT 4S) were processed in more unimodal areas, while the longer stimuli (**Studies 1 & 2**: NONET = 6.3s duration, **Study 3**: SCENE 12S and SHOT 12S) engaged more multimodal regions. However, for even longer stimulus durations (**Studies 1 & 2**: COMPLETE = 25.2s, **Study 3**: SCENE 36S and SHOT 36S) we found that the processing did not vary meaningfully from the medium-to-long time ranges. Firstly, the COMPLETE condition neither showed consistent additional engagement of higher-order areas across the whole-brain and ROI analyses (**Study 1**) nor in the modelling results (**Study 2**). Secondly, in **Study 3** the contrast between the 12S and 36S conditions indicated cortical attunement to the medium 12S rather than the long 36S time range. On the other side of the spectrum, the comparisons between the SINGLE (0.7s) and TRIPLET (2.1s) conditions in **Studies 1 & 2** also did not consistently reveal the suspected increases in higher-order areas with longer duration, further highlighting the non-linearity of the stimulus duration effect on cortical processing.

Since the factor DURATION was manipulated in discrete levels instead of continuously in both experiments, the question arises, when does a stimulus classify as “long”? Accordingly, also the mechanism behind the additional, higher-level engagement remains undetermined. Does the propagation happen discretely, in a step-wise manner when a certain duration threshold is reached, or rather continuously, increasing gradually with longer stimulus duration?

The specific, temporal levels of our stimuli were based on earlier TRW analyses that also used discrete levels of duration and content complexity (e.g., Hasson, Yang, et al., 2008). These studies found engagement in multimodal cortices for longer stimuli ranging from about eight to 40 seconds or more (Farbood et al., 2015; Honey et al., 2012; Lerner et al., 2011). This temporal range was further supported in studies using continuous movie watching paradigms, as the state dwell times of higher-order functional networks (e.g., DMN) similarly demonstrated stable activity patterns for about 10 to 30 seconds (Geerligs et al., 2022; E. Yang et al., 2023). These longer persisting network states importantly aligned with high-level narrative shifts in the movie (Baldassano et al., 2017; Ben-Yakov & Henson, 2018; Geerligs et al., 2022; Y. Lee & J. Chen, 2024; E. Yang et al., 2023), which occur on average every 20 to 60 seconds (Cutting et al., 2012).

Since cortical dynamics were suggested to obey the predictive coding framework (L. P. Jiang & Rao, 2024; Kiebel et al., 2008), it could therefore be assumed that the timescales of both early sensory as well as multimodal association cortices are learned models of the environmental dynamics (cf. Soltani et al., 2021). Accordingly, TRWs were shown to adapt to the frequency of stimulus presentation (Geerligs et al., 2022; Lerner et al., 2014) as well as the attention to the stimulus (Shahdloo et al., 2019). However, as the basis of TRWs was proposed to be "hard-coded" in the structural and chemical architecture of the brain (e.g., Chaudhuri et al., 2015), the range of adaptability cannot be infinite (cf. Golesorkhi, Gomez-Pilar, Zilio, et al., 2021). Consequently, when complex stimuli were presented in a very condensed manner (i.e., twice as fast), they no longer evoked their typical higher-level cortical processing (Lerner et al., 2014; Vagharchakian et al., 2012). Yet, the dynamic transitions between functional network states flexibly aligned with the changes on different, hierarchical levels of stimulus complexity (Baldassano et al., 2017; Y. Lee & J. Chen, 2024; Oetringer et al., 2025). It was therefore suggested that cortical areas adaptively segregate or integrate stimuli not only according to their intrinsic temporal dynamics but also according to their preferred level of stimulus content (Golesorkhi, Gomez-Pilar, Zilio, et al., 2021; Lerner et al., 2014; Wolff et al., 2022). Importantly, this hypothesis is supported by the interaction

between duration and content complexity found in **Study 3**: As demonstrated, the engagement of the high levels of cortical processing along the uni-to-multimodal gradient (e.g., in the DMN) required stimuli that depicted both temporally longer and more complex content.

Based on previous studies (Geerligs et al., 2022; Lerner et al., 2014; E. Yang et al., 2023), as well as our own effective stimulus durations (**Studies 1 & 2**: NONET = 6.3s duration, **Study 3**: SCENE 12S and SHOT 12S), I would therefore infer that the TRWs of the multimodal areas can adaptively integrate their preferred hierarchically higher stimulus content of at least six seconds and likely up to about 30 seconds. Although this range allows for some flexibility, the interaction between duration and content complexity (**Study 3**) and the alignment between network state transitions and event boundaries (e.g., Baldassano et al., 2017; Oetringer et al., 2025) suggest that the processing of hierarchically nested stimuli abides by the discrete level structure of the content and consequently cannot be fully continuous.

While the lower threshold is better defined by our (**Studies 1 & 2**: TRIPLET = 2.1s duration, **Study 3**: SCENE 4S and SHOT 4S) and previous results (e.g., Lerner et al., 2014), the upper limit of the temporal spectrum is still vague (cf. Golesorkhi, Gomez-Pilar, Zilio, et al., 2021). On the one hand, particularly the DMN was suggested to integrate stimulus input at even longer durations (J. Chen et al., 2016; Hasson et al., 2015; Yeshurun et al., 2021). On the other hand, the longest stimuli (**Studies 1 & 2**: COMPLETE = 25.2s, **Study 3**: SCENE 36S and SHOT 36S) in our experiments showed comparatively sparse cortical engagement. Thus, staking out the specific margins as well as the precise mechanisms (cf. Himberger et al., 2018) of temporal integration is an intriguing topic for future studies – particularly in the everchanging, and ever-quickening environment humans are confronted with (e.g., Cutting, Brunick, DeLong, et al., 2011).

Intriguingly, since the uni-to-multimodal as well as intrinsic cortical timescale gradients also align with the developmental and evolutionary axis of the brain (Sydnor et al., 2021, 2023), the distribution of TRWs appears to be deeply intertwined with human nature. From an evolutionary perspective, it could therefore be argued that our brain was not “built” for its current,

fast-paced environment, as it was formed by the evolutionary pressures of the Pleistocene area (Cosmides & Tooby, 2013; Nairne & Pandeirada, 2010). However, especially studies on neural plasticity indicate that the human brain can adapt to its environmental and functional demands (Draganski et al., 2004; Herholz & Zatorre, 2012; Korte, 2020; Maguire et al., 2000; Moura et al., 2021). In today's digital age, this adaption is especially noticeable in changes to multitasking, self-control, memory and language networks of the "digital native" population (David & Roberts, 2025; Farkaš, 2024; Firth et al., 2019; Korte, 2020; Loh & Kanai, 2016). Since cultural changes can affect not only cognition and neural connectivity but also the selection of genetic variation (Bender, 2020), it is even imaginable that both the functional and structural foundations of TRWs are malleable as well. Future research might thus be inclined to investigate the differences and changes in TRWs, for instance influenced by the non-linear temporal structure of the contemporary short form video format (J. Lin et al., 2023), that was has already been shown to strongly affect other aspects of cognition (Barton & Smyth, 2025; Chiossi et al., 2023; David & Roberts, 2025; Q. Jiang & Ma, 2024; Nguyen et al., 2025).

3.2.2 Considerations regarding the stimulus design. As discussed above, specifically the COMPLETE, fully predictable digit sequence in **Studies 1 & 2** and the SHOT 36S condition in **Study 3** demonstrated limited findings compared to shorter stimuli. This was particularly surprising, as cortical timescales seem to be adaptable to slower stimulus dynamics (Lerner et al., 2014). Hence, the second unresolved issue concerns, why the most persistent stimuli behaved so distinctly from our expectations about the dynamic functional processing hierarchy.

In this context, it was proposed, that specifically boundaries and transitions between stimulus elements would drive cortical activity (Lu et al., 2016) as well as deeper processing of the stimulus' content (Ben-Yakov & Henson, 2018; Clewett & Davachi, 2017; Gold et al., 2017; Rah et al., 2025). More uninterrupted, temporally persistent stimuli however were less engaging (Faber et al., 2018; Sava-Segal et al., 2023). It could thus be possible that both the COMPLETE and the SHOT 36S conditions were too persistent and therefore contained too little boundaries to evoke

consistent neural activity comparable to the more transient conditions. Accordingly, in **Study 3**, the areas engaged by the SHOT 36S condition indicated that these long periods of shot-based frames were processed more like still images than a movie (e.g., Pitcher & Ungerleider, 2021). Hence, it is uncertain if the longest, most persistent stimuli across the experiments were representative enough of naturally occurring high-level hierarchical stimuli to evoke similarly complex cortical engagement (cf. Hasson, Landesman, et al., 2008; Loschky et al., 2020).

Similar methodological considerations also apply to the other experimental conditions. Since all of the conducted experiments used manipulated material for the sake of better stimulus controllability (Rust & Movshon, 2005), the engagement of the high-order association cortices areas could have been generally less reliable compared to natural stimuli (Sonkusare et al., 2019; J. Wang et al., 2017).

Boosted by methodological advancements (e.g., ISC; also see Redcay & Moraczewski, 2020), the application of naturalistic paradigms in fMRI research has surged in recent years (Grall & Finn, 2022). In particular, these approaches have enabled the investigation of complex cortical processes in quasi-real-life settings (Jääskeläinen et al., 2021; Redcay & Moraczewski, 2020; Saarimäki, 2021). Moreover, such paradigms are especially effective for identifying individuals and predicting behavior (Finn, 2021; Finn et al., 2018, 2020; Finn & Bandettini, 2021; Sonkusare et al., 2019; Vanderwal et al., 2019). The main advantage of naturalistic stimuli is their complex temporal dynamics, which were key in the discovery of TRWs and the cortical chronoarchitecture (Sonkusare et al., 2019; Vanderwal et al., 2019). Consequently, the abstract hierarchically nested digit sequence in **Studies 1 & 2** as well as the frame-wise manipulation of the movie in **Study 3** might have limited the engagement of multimodal, higher-order areas compared to more naturally occurring material.

However, also the usage of naturalistic stimuli is not without its limitations. The increased participant engagement and ecological validity is accompanied by reduced controllability and the difficulty to create appropriate models that consider all possible confounds (Grall & Finn, 2022;

Saarimäki, 2021). More critically even, naturalistic stimuli like movies are not fully representative of real life either (Grall & Finn, 2022). As most stimuli were not specifically created for the investigated scientific questions but are, for example, commercial movies, they shape the cognitive processing differently from actual real life (cf. Hasson, Landesman, et al., 2008). It is therefore recommendable to apply naturalistic paradigms alongside the classic abstract tasks, letting them mutually enhance each other's understanding of the research question at hand (Finn et al., 2018; Saarimäki, 2021).

In accordance, **Study 3** made use of naturalistic-based stimuli that replicated the engagement in high-level areas found in Hasson, Yang, et al. (2008), but also manipulated the material in a way to specifically disentangle the confounds between duration and content complexity, which would have not been possible with natural movie stimuli.

In conclusion, although limitations of stimuli and experimental paradigms have to be taken into account, the coherence of the results as well as the consistent alignment with the uni-to-multimodal gradient support our functional findings and interpretations. In reference to the posed Research Questions, I would therefore preliminarily recapitulate that the temporal persistency of the different levels plays a crucial role in the processing of hierarchically nested stimuli (Research Question 3) and that this temporal processing hierarchy extends along the functional uni-to-multimodal gradient (Research Question 2).

We could however not find convincing evidence for Research Question 1, that the structural rich club's core-periphery axis underlies this processing of environmental stimuli. Thus, the structural foundation of the additional, higher-level engagement along the uni-to-multimodal gradient still remains unsettled. Specifically, **Studies 1 & 2** failed to demonstrate a clear relationship between the rich club architecture and the processing of the temporally longer, hierarchically higher levels of stimuli in the multimodal association cortices. Possible explanations for this unexpected misalignment will be discussed in the following.

3.3 Missing link between the rich club hubs and the multimodal association cortices

Interestingly, the presented studies did not identify the consistent overlap between the functional associative cortices and the structural rich club hubs that would have been expected based on previous findings (Gollo et al., 2015; van den Heuvel & Sporns, 2013a; Zamora-López et al., 2010). As introduced, the investigation of the rich club architecture sprouted from the distribution of nodal degrees that indicated the presence of small-worldness (cf. Hagmann et al., 2008). This balance between network integration and segregation, necessary for complex cognition (Watts & Strogatz, 1998), requires a structural backbone that connects and integrates the segregated modules. Thus, early studies suggested that the rich club hubs acted as connectors and represented areas of multimodal integration (Sporns, 2013; van den Heuvel & Sporns, 2013a; Zamora-López et al., 2010). Along these lines, Gollo et al. (2015) proposed that the hubs of the rich club – similarly to the DMN (cf. Raichle, 2015) – form an integrative core of more internally focused areas, which were less concerned with sensory input which is handled in the periphery of the network.

In contrast to this account, especially **Study 2** but also the re-evaluation of the results of **Study 1** (see Appendix D) indicated that the rich club classification did not align with the uni-to-multimodal axis and therefore did not explain the variation of TRWs, intrinsic timescales or cortical activation patterns by higher-order hierarchically nested stimuli as efficiently as the functional gradient. Hence, understanding the unexpected missing link between the rich club hubs and multimodal association cortices is crucial in assessing whether the rich club organization forms the backbone of the cortical chronoarchitecture.

3.3.1 Differences in rich club identification. One possible explanation for these unexpected results could be a misclassification of rich club hubs in the here presented studies. Since the rich club phenomenon is first and foremost a mathematical property of networks, there is no ground truth for the areas that make up the rich club (Griffa & van den Heuvel, 2018). While the normalized rich club coefficient can provide an indication for the rich club architecture's

existence (Colizza et al., 2006; McAuley et al., 2007), the determined degree cut-off does not specify whether all nodes above the threshold form a consistent club-like structure, as Colizza et al. (2006) defined it.

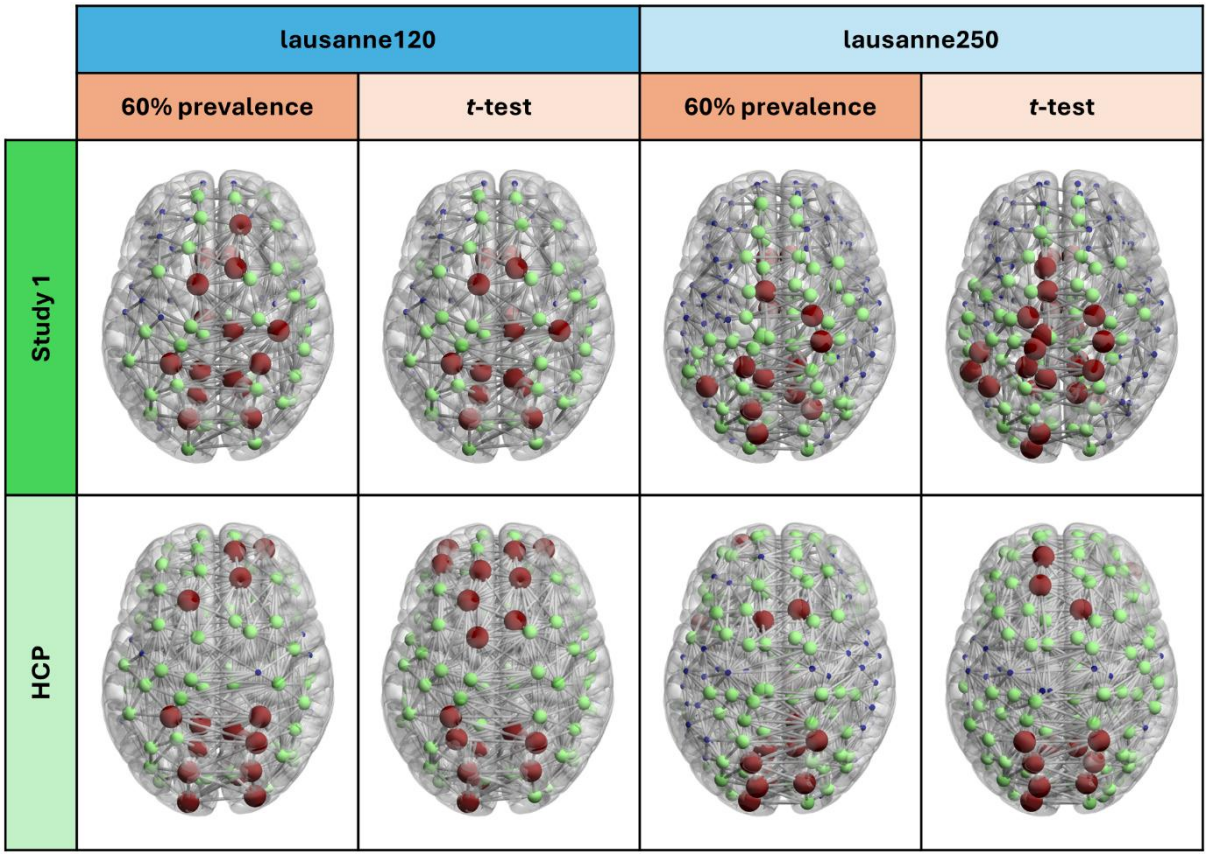
Thus, throughout the literature various strategies have been adopted to classify rich club hubs: studies used the top 10-20% nodes in the degree distribution (Ball et al., 2014; R. Cao et al., 2020; Collin, Kahn, et al., 2014; D. J. Kim & Min, 2020; K. Li et al., 2017; O'Donoghue et al., 2017; Repple et al., 2020; van den Heuvel et al., 2012, 2013; Y. Wang et al., 2019; Yan et al., 2018), various different nodal degree cut-off values (Collin, Sporns, et al., 2014; de Reus & van den Heuvel, 2013b; Grayson et al., 2014; Griffa & van den Heuvel, 2018; Ray et al., 2014; van den Heuvel & Sporns, 2011), or more intricate methods that made use of a comparison against random networks (Gómez-Gardeñes et al., 2010; Harriger et al., 2012; Keown et al., 2017; Riedel et al., 2022). Despite the lack of standardization (cf. Welton et al., 2015), the structural rich club was still consistently located in areas along the cortical midline including the precuneus, the SPL, the SFG, the anterior and posterior cingulate cortex and the insula as well as in thalamus, putamen and caudate nucleus, if the subcortex was considered (Q. Cao et al., 2013; Z. Chen et al., 2013; H. Huang et al., 2015; Riedel et al., 2022).

Within this thicket of rich club identification methods, **Study 1** (and accordingly **Study 2**) attempted to align the methodology more closely to its initial definition: Firstly, we employed more nodal measures than just degree to identify important hubs within the structural connectome (cf. van den Heuvel & Sporns, 2013b). The hub identification was also augmented with information about the rich club regime, which describes the range of nodal degrees k that depict a significantly higher rich club coefficient than the average random network (cf. Riedel et al., 2022). Secondly, the rich club was originally defined through high-degree hubs that connect to each other more than would be expected at random (Colizza et al., 2006). Thus, after localizing candidate hub regions, we – similarly to Senden et al. (2017) – verified the club-like structure by comparing the probability of inter-hub connections to random networks.

In spite of these adjustments, we were still able to demonstrate the validity of our new rich club identification method, as **Study 1** – across two datasets, two levels of cortical parcellation resolution and two different calculations for group matrix construction – consistently replicated the rich club hub locations in the SFG, SPL, precuneus, and anterior cingulate cortex (Figure 2). Due to this overlap in hubs, it is unlikely that the missing link between the structural rich club and the functional multimodal association cortices in our studies was based on a misclassification of the rich club and more probable that our results reflect a more general misalignment.

Figure 2

*Group-wise connectome rich club hub locations across parcellation schemes, group-averaging methods and data sets in **Study 1***



Note. Size and color of the nodes indicate rich club classification using the methodology established in **Study 1**. Rich club hubs are depicted as large nodes in red, feeder nodes as medium nodes in green and local nodes as small nodes in blue. Classification was conducted on two different datasets. Data collected for **Study 1** included $N_{\text{Study 1}}$ = 40 participants. Human Connectome Project (HCP) data included N_{HCP} = 100 unrelated subjects (Feinberg et al., 2010; Moeller et al., 2010; Setsompop et al., 2012; J. Xu et al., 2012). Anatomical data was parcellated according to the lausanne120 and lausanne250 parcellation schemes with 114 and 219 cortical parcels, respectively (Cammoun et al., 2012). Group-wise binary undirected connectivity matrices for graph-theoretical analyses were produced by either using a 60% group-prevalence cutoff (de Reus & van den Heuvel, 2013a) or using a false discovery rate-corrected *t*-test to evaluate the presence of each edge in the group (Ponsoda et al., 2017).

3.3.2 Structural-functional misalignment. Since the rich club is primarily a feature of the structural connectome (cf. D. J. Kim & Min, 2020) and the uni-to-multimodal gradient is functionally defined (Margulies et al., 2016; Sepulcre et al., 2012), one essential point of discussion is the overall (dis-)agreement between structural and functional cortical networks. On the one hand, early studies in this context demonstrated a significant overlap (Hagmann et al., 2008; Honey et al., 2007) and were moderately successful in predicting cortical function from the underlying structural connectome (Greicius et al., 2009; Hermundstad et al., 2013; Z. Wang et al., 2015). On the other hand, more recent investigations concluded that the relationship between structure and function varies systematically across the cortex, painting a more complex picture than a simple one-to-one mapping (Meier et al., 2016; Suárez et al., 2020; L. Zhang et al., 2022).

Specifically, it was illustrated that the close relationship between structural and functional network properties found in the unimodal cortices gradually decouples when moving up the uni-to-multimodal gradient (H.-J. Park & Friston, 2013; Preti & Van De Ville, 2019; Vázquez-Rodríguez et al., 2019; D. Wu et al., 2020). These studies hypothesized that the decoupling in higher-order areas could result from more complex intra-regional connections that allowed for their high-level functions but would not be detected by classical structural connectivity analyses (D. Wu et al., 2020). In accordance, the coupling-decoupling gradient was also reflected in the distribution of cytoarchitectural features like the patterns of myelination and laminar differentiation (Vázquez-Rodríguez et al., 2019; D. Wu et al., 2020), which common network parcellation and connections do not take into account (H.-J. Park & Friston, 2013). Importantly, this decoupling complicates finding the proposed overlap between the structurally identified rich club and the functional association cortices and might explain the missing link in **Studies 1 & 2**.

Furthermore, the coupling between structural and functional networks also differs across time. While correlating functional time courses of longer measurements can produce replicable results (Birn et al., 2013; Gonzalez-Castillo et al., 2014; Mueller et al., 2015; Shah et al., 2016),

functional networks, compared to physical connections, can and need to vary rapidly in time to allow for complex, context-sensitive cognition (H.-J. Park & Friston, 2013).

Calculating dynamic functional connectivity, which determines multiple network states based on a sliding window approach (Allen et al., 2014), can be an approach to identify functional network states that more closely resemble the underlying structural connectome and thus maybe temporarily align the locations of highly functionally and structurally connecting nodes. Along those lines, Fukushima et al. (2018) demonstrated that more integrated functional states of the network more closely echo the connections of the structural connectome than during more segregated states. Further, X. Zhang et al. (2025) recently suggested that the structural rich club may play an important role in mediating the balance between integrated and segregated states thereby supporting not only functional diversity but also high-level cognition.

However, using dynamic functional connectivity, it was also found that the functional connections of multimodal regions generally vary more than those of unimodal areas, as they are more flexible in their functional alignment (Allen et al., 2014; Gonzalez-Castillo et al., 2014; Paquola et al., 2019; Suárez et al., 2020), which further obscures a consistent overlap between the structural rich club hubs and the multimodal cortices.

3.3.3 Validity of in vivo diffusion-weighted connectomes. Another reason for the missing overlap between the structural rich club and the multimodal association cortices could be general inaccuracies in vivo connectomes when depicting the complexity of the cortical network. Mirroring Chaudhuri et al.'s (2015) model for cortical dynamics, it was suggested that especially longer, weaker, rather than dense, short-range connections were essential for the functional diversity of the cortical network (Bertagnolli & De Domenico, 2022; Hermundstad et al., 2013; R. Wang et al., 2025) as well as the overlap between structure and function (Knösche & Tittgemeyer, 2011; Liu et al., 2022). However, studies investigating the anatomical accuracy of DWI concluded that the current methods specifically still struggle with detecting these important, long-range connections (Jbabdi et al., 2015; Knösche & Tittgemeyer, 2011).

Accordingly, compared to animal tracer studies, DWI-based connectomes depicted a worse agreement between structural and functional networks (Honey et al., 2007; Straathof et al., 2019; Suárez et al., 2020; L. Zhang et al., 2022). This is especially crucial, since the results indicating the close relationship between the rich club architecture and the intrinsic cortical dynamics, examined in Research Question 1, were predominantly based on tracer studies (Chaudhuri et al., 2015; Gollo et al., 2015; Gómez-Gardeñes et al., 2010; Harriger et al., 2012; Mišić et al., 2014).

Despite increasingly sophisticated data acquisition and reconstruction methods, DWI still produces structural connectomes that are not accurate to the underlying axonal network (Aydogan et al., 2018; Maier-Hein et al., 2017; C. Thomas et al., 2014). Algorithms designed to handle crossing and kissing fibres, such as the generalized q-ball imaging applied in **Studies 1 & 2** (F. C. Yeh et al., 2010), still failed to capture the full complexity of white matter streamlines (Girard et al., 2020; Grisot et al., 2021; Maffei et al., 2022). For example, the intricate directed links between specific cortical layers, representing functionally integral top-down and bottom-up connections (cf. Felleman & Van Essen, 1991), cannot be reconstructed by diffusion-based tractography (Jbabdi et al., 2015; Knösche & Tittgemeyer, 2011; Maffei et al., 2022; Yu et al., 2025).

Also, compared to axonal tracing, even the most advanced tractographic algorithms suffer from frequent false positive connections (Maier-Hein et al., 2017) that are detrimental to the overall appearance of the structural network (Zalesky et al., 2016). Thus, although DWI offers a unique non-invasive view into the in vivo connectome, the technique still leaves room for improvement (Ferizi et al., 2017; Jones & Cercignani, 2010; Maffei et al., 2022; Rheault et al., 2020; Schilling et al., 2019, 2020; Yu et al., 2025). The anatomical accuracy and spatial resolution of the estimated structural networks might not yet be precise enough to capture the intricate microscale cortical structure or detect the weak, long-range connections between association cortices that are implicitly part of functional connectivity (Jbabdi et al., 2015).

Hence, one approach to improving the structural connectome construction is through the incorporation of microstructural data, that can inform more intricate tractography algorithms and thus enhance the overall sensitivity and anatomical accuracy of diffusion-weighted images (Daducci et al., 2016; Daducci & Schiavi, 2025; Ferizi et al., 2017; Koch et al., 2022). Moreover, most current graph theoretical analyses still assume microstructurally homogenous cortical regions as their nodes, which oversimplifies the relationship between areas (H.-J. Park & Friston, 2013; Suárez et al., 2020). Computational models in particular already showed that the inclusion of more "meta-data" for each area (i.e., the cytoarchitecture or neurotransmitter distributions) can inform connectivity analyses to improve the overlap between structure and function (Bettinardi et al., 2017; Deco et al., 2013, 2014; Sanz Leon et al., 2013). This would also align more with the proposal of Chaudhuri et al. (2015; also see X.-J. Wang, 2020), suggesting an interplay of connective and chemical architectures that shapes the cortical dynamics and functional hierarchy. In this context, **Study 2** already demonstrated that cortical thickness, as a simple approximation of cytoarchitectural differences (Wagstyl et al., 2015), correlated significantly with the uni-to-multimodal gradient and similarly explained the variation of cortical dynamics, indicating a microstructural basis of the functional hierarchy that is not captured at the macroscale level of the structural connectome.

In practice, additional microstructural and connective information could firstly be used to improve boarders of nodal divisions as it was done in various structural-based or multimodal atlases (Assaf et al., 2013; Fan et al., 2016; Glasser et al., 2016). Secondly, the microscale information can also be applied as biologically relevant weights to the network edges (Larivière et al., 2019). Adopting this method, a previous study, using the ratio of the internal and external diameter of axons as a measure of myelin density to inform structural connections, found differences in myelin concentration in the more energy-intensive rich club and feeder connections (Mancini et al., 2018). Recently, this technique was further extended to neurotransmitter concentrations to determine chemoarchitecturally-weighted structural

connectomes (Koch et al., 2025). Future endeavours should therefore explore microstructural cortical properties shown to relate to the functional hierarchy, such as genetic expression gradients (Burt et al., 2018; Hansen et al., 2021), or possibly the combination of multiple weights (cf. Hansen, Shafiei, Voigt, et al., 2022; Sydnor et al., 2023) to improve the functional and biological validity of structural connectomes.

This should however not suggest that the current diffusion-based connectomes are generally useless and not advisable. Despite their biases and shortcomings (e.g., Rheault et al., 2020), structural connectivity analyses were still able to reveal functionally and behaviourally relevant differences in healthy participants (Hong et al., 2025; D. J. Kim et al., 2016; Mansour L et al., 2021; Román et al., 2017; Yan et al., 2021) as well as across multiple different diseases (Bu et al., 2021; Imms et al., 2019; Jang et al., 2024; Pandya et al., 2017; Prescott et al., 2014; Zuo et al., 2023; for specifically rich club related reviews see Crossley et al., 2013; Griffa & van den Heuvel, 2018). I would therefore argue that, although we found only very sparse evidence for the specific functional role of the structural rich club hubs in processing higher levels of hierarchically nested stimuli, the evidence at large still supports a significant functional role of the rich club for efficient cortical function (Gollo et al., 2015; Griffa & van den Heuvel, 2018; Gu et al., 2019; Senden et al., 2014, 2018; Sporns, 2018; van den Heuvel & Sporns, 2013a). However, the question remains: If the structural rich club hubs are not substantially involved in the processing of temporally persistent, high-level stimuli, what is their exact functional purpose that makes them so fundamental to an efficient brain organization?

Yet, before delving into this outlook on potential further research on the human structural rich club architecture, I want to provide an overview of the methodological limitations of the structural MRI investigations in the presented experiments. Note that all of these shortcomings should also be considered and addressed in future investigations.

3.3.4 Limitations of the structural networks in Studies 1 & 2. As illustrated in the last section, the in vivo acquisition and reconstruction of structural connectomes and therefore also the structural-functional alignment can be limited by various technical aspects from data acquisition over tractography to network construction (for reviews see Jones & Cercignani, 2010; Rheault et al., 2020; C. H. Yeh et al., 2021). Some of these limitations that were especially relevant to **Studies 1 & 2** will be briefly highlighted in the following.

3.3.4.1 Parcellation schemes. The choice of parcellation scheme can play a substantial role in the structural-functional correspondence. Especially the resolution of parcellation influences the stability of functional connectivity patterns (Shah et al., 2016), the overall agreement between structural and functional networks (Messé, 2020) as well as the general appearance of the network (Bassett et al., 2011; Bryce et al., 2021; Seguin et al., 2020).

We specifically opted for two different Lasuanne-sub-parcellation of the Desikan-Killiany atlas (Cammoun et al., 2012; Desikan et al., 2006) with 114 (lasuanne120; **Study 1**) and 217 (lausanne250; **Studies 1 & 2**) cortical parcels, respectively. We chose the parcellation schemes because they can be precisely estimated for each individual subject (Cammoun et al., 2012; Desikan et al., 2006), represent a functionally relevant scale of cortical resolution (Amunts & Zilles, 2015) and are well-established in previous studies (e.g., Hansen et al., 2021; Hansen, Markello, et al., 2022; Hansen, Shafiei, Markello, et al., 2022; Riedel et al., 2022; van den Heuvel et al., 2019). Using the chosen Lausanne-parcellations, **Studies 1 & 2** were able to demonstrate global trends, like the significance of the uni-to-multimodal gradient for the processing of temporally more persistent stimuli, that we similarly found in **Study 3**.

However, the arbitrarily created same-sized parcels of the Lausanne parcellation scheme come at the cost of functional interpretability of individual nodes (Cammoun et al., 2012). As already discussed in the scope of **Studies 1 & 2**, since our hypotheses targeted the agreement between structural network architecture and cortical function, a parcellation scheme that follows functionally informed borders (e.g., Glasser et al., 2016; Schaefer et al., 2018) might have

benefited the agreement of rich club hubs and association cortices. Accordingly, future investigations of the structural and functional network overlap should consider the use of more sophisticated atlases that include multiple sources of information in their cortical parcellation (e.g., Glasser et al., 2016).

3.3.4.2 Acquisition parameters. Another consequential limitation of the structural data of **Studies 1 & 2** were the diffusion-weighted MRI data acquisition sequences. For diffusion-weighted MRI, the protocol included two acquisitions of 30 b = 1000 s/mm^2 weighted images, supplemented by five non-diffusion-weighted images (b = 0 s/mm^2). More modern acquisition protocols however recommend b-values of at least 2000 – 3000 s/mm^2 (Calamante, 2019; Jones et al., 2013; Yu et al., 2025). These higher b-values allow for the estimation of intra-axonal diffusion of water molecules, improving the accuracy of determined streamlines (Veraart et al., 2019; Yu et al., 2025). Moreover, 30 diffusion directions are only the minimum of gradient directions necessary to identify the orientation of streamlines, while more complex tractography algorithms benefit from the acquisition of at least 45 diffusion directions (Jones et al., 2013).

Although we replicated the overall trends of **Study 1** using the state-of-the-art DWI dataset from the Human Connectome Project (Feinberg et al., 2010; Moeller et al., 2010; Setsompop et al., 2012; Van Essen et al., 2013; J. Xu et al., 2012), the processing pipeline was still limited to the recommendations of the original DWI sequence to ensure comparability. Consequently, the structural networks investigated across **Studies 1 & 2** were based on binary connectivity matrices that excluded the subcortex from the analysis (cf. Fornito et al., 2016). Both these adjustments – binarization and subcortex exclusion – not only limited the comprehensibility of the analysis but also entailed additional drawbacks, which will be outlined below.

3.3.4.3 Binarization. The limitations of the DWI sequences firstly necessitated the binarization of the structural connectome, as connection weights estimated from non-optimal data would otherwise bias the analysis (Calamante, 2019; Jones et al., 2013; Rheault et al., 2020). Moreover, weights that are already biologically difficult to interpret, such as number of

streamlines, would not have represented meaningful variations in the connections (Daducci & Schiavi, 2025; C. H. Yeh et al., 2021). Given more modern acquisition techniques, current research recommends the use of weighted connectomes (Calamante, 2019; Daducci & Schiavi, 2025; C. H. Yeh et al., 2021), as binary structural matrices obscure information likely important for a better functional-structural network coherence (Shen et al., 2015). Thereby, weighted networks not only alleviate the need for arbitrary matrix thresholding but also allow for the inclusion of functionally important, weak, long-range connections (R. Wang et al., 2025), while also preserving global properties like rich club architecture and small-worldness (Colon-Perez et al., 2016).

Best practice would be to incorporate microstructural properties of regions and streamlines as biologically interpretable weights (Mancini et al., 2018; C. H. Yeh et al., 2021). Structural networks weighted by myelin content or axonal diameter, for example, were significantly related to functional connectivity (Nelson et al., 2023) and predicted individual cognitive abilities (Gast & Assaf, 2024). An investigation of the rich club in structural networks with physiologically relevant weights will thus offer new insights into the relationship between the structural and functional hierarchies.

3.3.3.4 Subcortical connectome. Secondly, as even state-of-the-art DWI and tractography methods struggle with the accurate depiction of the dense fibre bundles of subcortical areas (Rheault et al., 2020), the technical constraints of the data in **Studies 1 & 2** further restrict the analysis to cortex-only networks. Due to similar technical concerns, the network architecture of the subcortex is generally not thoroughly investigated (Kai et al., 2022). This is particularly unfortunate, as rich club hubs are commonly found within subcortical areas when they are included (e.g., Riedel et al., 2022) and models of cortical hierarchy also suggest that the subcortex plays an important role in gating incoming information across all levels of processing (e.g., Badre & Nee, 2018).

A recent study that investigated a high-resolution structural connectome including the cortex, subcortex and cerebellum not only replicated the presence of rich club hubs within the subcortex but, more importantly, demonstrated that specifically lesioning subcortical, compared to cortical, rich club hubs was even more detrimental to efficient global communication and integration (Schulte et al., 2025). This also aligns with research particularly emphasizing the role subcortical rich club hubs in healthy brain development and aging (Baker et al., 2015; Ball et al., 2014; Karolis et al., 2016; D. J. Kim et al., 2014, 2016; Perry et al., 2015). Therefore, given a more accurate imaging and network reconstruction methodology (e.g., Kai et al., 2022), future studies should continue to extend their investigations of the rich club architecture to the subcortex. An inclusion of subcortical regions will ultimately create a more representative connectome that will aid in specifying the structural architecture that supports the functional processing hierarchy.

3.4 Future investigation of the structural and functional hierarchy

Beyond these technical and methodological improvements, the results of the presented studies raise substantial questions about the relationship between the structural connectome and the functional processing hierarchy of the brain that warrant further investigation. As discussed, the main findings of the contained studies are twofold: Firstly, the temporal structure of hierarchically nested stimuli – as investigated in Research Question 3 – indeed plays an important role in their processing. Secondly, in response to Research Question 2, the temporal processing topography is best reflected by the functional uni-to-multimodal cortical gradient, with more persistent, higher-level stimuli additionally engaging more multimodal cortical areas. However, we could not find convincing evidence in favor of Research Question 1, namely whether the rich club architecture forms the structural network axis for the processing of hierarchically nested environmental stimuli.

It therefore remains unclear, what functional role the rich club hubs fulfil and what the structural network foundation of hierarchical processing along the predominant uni-to-multimodal gradient might be. In the following, I want to explore possible avenues for future investigations of the human connectome before proposing possible applications of the gained insights to a broader context.

3.4.1 The structural network underlying the functional processing gradient. The hypothesis that the structural rich club hubs form the basis for the processing of hierarchically higher, more persistent stimuli was primarily based on the results of Gollo et al. (2015), describing the rich club as a slow-acting, integrative core akin to proposals of the DMN or high-order cortical areas in general (also see Golesorkhi, Gomez-Pilar, Tumati, et al., 2021). This assumption was further supported by findings demonstrating that the rich club was central to the integration of information across the cortex as most of the shortest paths of the network were passing through the rich club to link different functional modules (de Reus & van den Heuvel, 2014; Gómez-Gardeñes et al., 2010; Griffa & van den Heuvel, 2018; D. J. Kim & Min, 2020; Mišić et al., 2014;

Oldham & Fornito, 2023; van den Heuvel & Sporns, 2011). The functional importance of the rich club hubs was then demonstrated in simulated lesion studies, which showed that removal of the hubs themselves or the rich-rich edges had detrimental effects on the efficiency and functional complexity of the network (Berahmand et al., 2018; Cabral et al., 2012; de Reus & van den Heuvel, 2014; Liang et al., 2019; van den Heuvel & Sporns, 2011; Zamora-López et al., 2016).

Yet, these investigations of the rich club's functional significance mainly focus on the global impact of architecture on the network and do not examine the functional properties of rich club hubs compared to other nodes, like **Studies 1 & 2** did. The role specific rich club hubs play in the task-dependent integration between different functional modules is therefore largely unexplored (cf. Griffa & van den Heuvel, 2018). Studies that do focus on the functions of individual hubs however already illustrated that the rich club might not be as functionally homogenous as **Study 1** assumed (e.g., Collin, Sporns, et al., 2014; Crossley et al., 2014; van den Heuvel & Sporns, 2013a). Accordingly, the structural rich club hubs were characterized by high functional diversity, connecting and being involved in different functional modules, thus enabling the cognitive complexity of the human mind (Bassett et al., 2013; de Pasquale et al., 2018; Senden et al., 2014; Zalesky et al., 2014). This flexibility and diversity may explain the low correlation in resting-state time courses between the structural hub regions, that for instance Collin, Sporns, et al. (2014) found, but also the inconclusiveness of the rich club's overall functional impact in **Studies 1 & 2**.

Although these results further reiterate that the rich club is essential for effective cognitive processing, the functional role of the architecture in general might be better expressed as the structural "backbone" as van den Heuvel et al. (2012) described it. Previous studies linked the connective apex motifs – that are characteristic for the rich club (Gollo et al., 2015) – to the collection and distribution of information (Harriger et al., 2012; Mišić et al., 2014; Sporns et al., 2007). Accordingly, the structural rich club might only provide the infrastructure on which integrated brain communication takes place, without being contained to a specific, common

functional task like the processing of hierarchically higher-level environmental stimuli, as was suspected in **Studies 1 & 2**.

Starting from this revised assumption, two future strands of research open up: (1) If the rich club is not homogeneously involved in higher cognition, do tasks that require cross-modal integration involve only specific parts of the rich club architecture? (2) If it is not the structural network properties of the rich club hubs that identify areas involved in processing higher-level hierarchical stimuli, is there another structural network measure that can better identify functionally relevant nodes and aligns more accurately with the association cortices?

3.4.1.1 Rich club involvement in integrative tasks. Initial support for the first hypothesis, that only specific hubs of the rich club are explicitly involved in cognitive tasks that require integrative processes, comes from the results testing the centrality of the sequence-specific clusters in **Study 1**. Although not all clusters overlapped with nodes that were highly central to the structural network, the overall trend across all datasets, parcellation schemes and group-matrix construction methods suggested that the NONET-specific clusters in the dmPFC, angular gyrus (labelled IPL) and PCC exhibited comparatively higher centrality measures and were more likely labelled as rich club hubs.

Subsequently, a first next step could be an in-depth investigation of this trend. A reasonable option for this replication could be the use of naturalistic stimuli that were shown to more consistently activate higher-order cortices compared to abstract stimuli like in **Studies 1 & 2** (Sonkusare et al., 2019). As demonstrated for instance in **Study 3,** more persistent as well as more narratively and visually complex stimuli specifically engaged areas of the anterior scene network, related to the integration between the visual and the memory system (Baldassano et al., 2016; Silson et al., 2016; Steel et al., 2021, 2025). These areas could hypothetically represent the structural connector hubs only engaged for the integration of the visual input with previous memories (cf. Steel et al., 2024). This idea is supported by a recent study that identified richly connected structural network hubs that participate in multiple functional modules

simultaneously and thus form bridges for functional integration (Bryant et al., 2025). Among others, these multi-modular hubs included the RSC, IPL and parahippocampal gyrus – which form the anterior scene network (e.g., Steel et al., 2025) – that specifically served as the structural connector hubs between the visual and limbic systems (Bryant et al., 2025).

Another possible experiment that particularly targets integrative processes could be inspired by cross-modal perception studies that showed supra-additive activation for instance in the STS during multimodal tasks that went beyond the unimodal activity (Antono & Pooresmaeili, 2023; Besle et al., 2004; I. Choi et al., 2023; Dong et al., 2022; Kayser et al., 2005; Müller et al., 2012; J. Y. Park et al., 2010; Scheliga et al., 2023).

A future investigation could therefore present participants with different tasks that explicitly require the integration of multiple functional domains, like complex narratives or multimodal stimuli, in a combined fMRI and DWI experiment. The areas that are additionally engaged by the integrative processes would hypothetically involve at least a subset of the structural rich club hubs indicating that cross-modal integration makes explicitly use of the network's infrastructure (cf. van den Heuvel et al., 2012; van den Heuvel & Sporns, 2013a).

A dataset that may allow for exactly this type of investigation was recently collected and analysed by our lab: Siestrup et al. (2026) acquired DWI as well as task-fMRI during a multi-modal masking paradigm that presented participants with point light display of hurdlers. For a brief period during the display, the stimuli either contained the full sensory information, only the auditory or visual information, or no stimulus at all. An initial analysis contrasting the full-information condition compared with a scrambled control condition revealed activations specifically in the medial parietal and medial frontal lobes, as well as the angular gyrus, all of which correspond to locations of multimodal hubs (Sepulcre et al., 2012).

In the context of the results of **Study 1**, it would be interesting to test whether areas that are supra-additively activated in the full-information condition, compared to the two unimodally masked conditions, map onto structural connector hubs that specifically link the visual and

auditory systems (cf. Bryant et al., 2025). The results could provide valuable insights towards the understanding and modelling the effective relationships between segregated functional communities (Greaves et al., 2025).

The same hurdling-study dataset (Siestrup et al., 2026) might also be especially intriguing as the participants returned for a second experimental run after completing a 6-week hurdling training, thus allowing for the investigation of plasticity-related changes to the engagement of the structural hub architecture. Bassett et al. (2013) originally demonstrated that, when learning a movement sequence, the engagement of multimodal hubs decreased with practice, which might relate to findings in the context of the neural efficiency hypothesis, describing reduced or more focused functional activity in experts compared to novices (Carius et al., 2023; M. H. Huang et al., 2023; W. Kim et al., 2014; Martins et al., 2023). Overall, this strand of research could therefore test the specific engagement of structural rich club hubs and their connections in (untrained) integrative tasks to explore the hypothesis that the rich club architecture acts as a domain-overarching backbone, enabling flexible and complex problem solving also across species and all ages (e.g., D. J. Kim & Min, 2020).

3.4.1.2 Functional importance of other structural network measures. Instead of further investigating the functionality of the structural rich club architecture, the second strand of future research into the structural connectome asks whether there are other structural network properties that better explain the functional processing gradients of the brain.

In this context, we were not the first to question the functional relevance of the rich club hubs. Another prominent graph-theoretical property, which was already proposed as an alternative to the nodal-degree-based rich club, is the diverse club, based on the participation coefficient that quantifies the diversity of modules a node is connected to (Guimerà & Nunes Amaral, 2005). In their pioneering study, Bertolero et al. (2017) directly compared the diverse club to the rich club within a human functional connectivity dataset and demonstrated that the diverse club was more integral to the functional network. This view was supported by studies recognizing

the centrality of the diverse club for functional integration (Keller et al., 2023; Lohia et al., 2024), highlighting that particularly the participation coefficient might provide important additional information beyond the degree-based rich club (Oldham et al., 2019; Xue et al., 2020).

However, in the structural connectome, the distinction between the rich and diverse clubs is more debatable, as the rich club originally was also suggested to be constructed of connector hubs, linking remote cortical modules (Sporns, 2013; Zamora-López et al., 2010). In this context, the structural participation coefficients and nodal degrees, for instance, were similarly correlated with the intrinsic cortical timescales (Lurie et al., 2024). Also, **Study 2** revealed significant agreement between the rich and diverse club classifications in the individual structural connectomes, suggesting that both might describe connector hubs within the modular network architecture. More importantly, **Study 2** also demonstrated that neither the structural rich nor diverse club explained the cortical dynamics better than the functional uni-to-modal gradient, indicating that also a hub definition by the structural participation coefficient does not identify more functional relevant hubs, compared to the rich club.

Yet, in the context of **Study 2**, we have already discussed that the applied Bayesian model comparison strategy will only identify the best-fitting model among the investigated organizations (Alston et al., 2004). Thus, although mounting evidence supports the functional importance of the uni-to-multimodal gradient (Golesorkhi, Gomez-Pilar, Zilio, et al., 2021; Huntenburg et al., 2018; Margulies et al., 2016; Wolff et al., 2022), which is also mirrored in multiple micro- and chemoarchitectural cortical features (e.g., Hansen, Shafiei, Voigt, et al., 2022; Sydnor et al., 2023), the most representative and best-fitting, structurally defined organizational scheme still remains undetermined.

In this context, Bertolero et al.'s (2017) implementation of the diverse club coefficient might be helpful nonetheless, as it can easily be extended to an "any club coefficient" that quantifies the clubness of a network based on any nodally defined measure. This allows for the examination of the structural connectivity between nodes that score particularly high on different

other network centrality measures (cf. Oldham et al., 2019) or even topological features like laminar composition or gene expression gradients (cf. Markello et al., 2022). Along these lines, Lurie et al. (2024), for example, hypothesized a structural connective club that is formed between areas with slow intrinsic timescales.

Alternatively, simulated lesion studies can offer insight into the effect that hubs, classified by different centrality measures, may have on the efficiency and integrity of the network (e.g., Alstott et al., 2009; Joyce et al., 2013). One promising network measure in this context is the recently developed *collective influence*, which quantifies not just the connectivity of a single node but also includes its role in the surrounding neighbourhood for the evaluation of centrality (Morone et al., 2017; Morone & Makse, 2015). The initial results clearly demonstrated this method's advantages in effectively localizing the most integral nodes for network connectivity (Del Ferraro et al., 2018; Morone & Makse, 2015).

Furthermore, the interdisciplinary field of network science is always evolving and sees constant development of new and improved centrality measures (Meng & Rezaeipanah, 2025; K. Shafiei et al., 2025). One of these advancements, that could be particularly applicable in the realm of neuroscience, are overlapping community structures and multi-modular hubs, which are nodes that are members of multiple network modules (Ghalmane et al., 2019; Lancichinetti et al., 2009; Palla et al., 2005). Theses hubs were already shown to be crucial for both integration between functional communities as well as the network's dynamics (Bryant et al., 2025; K. Wu et al., 2011). Especially for the identification of the structural backbone for cross-modular cortical association, overlapping community structures could be a key methodological development for the identification of structural-functional consistency.

Another methodological approach that may provide more insight into the underlying structural architecture is the incorporation of multiple network measures and sources of information in hub identification. In accordance with van den Heuvel's and Sporns's (2013b) suggestion, **Studies 1 & 2's** hub identification algorithm already included multiple structural

centrality measures and information about the rich club architecture. Along the same lines, Sydnor et al. (2023) combined different microstructural, functional as well as developmental gradients to create one unifying uni-to-multimodal axis. An intriguing option to categorize either structurally or functionally integral hubs across a range of nodal measures is offered by machine-learning based classifier algorithms (Alnuaimi & Albaldawi, 2024; Black et al., 2023). Previous studies already demonstrated the application of k-means clustering to incorporate multiple network centrality measures in the classification of hubs and non-hubs in structural and functional networks (Markett et al., 2020; Riedel et al., 2022). Future investigations can therefore apply similar data-driven methods to make use of the entire spectrum of the multi-dimensional nodal as well as hierarchical network information for hub identification instead of defaulting to arbitrary single-measure cutoff values (cf. Oldham & Fornito, 2023).

Overall, this strand of research should therefore continue to explore various centrality and topological measures to identify cortical hub areas as well as the underlying structural network architecture that supports the range of (human) cognitive functions. The gained knowledge would thereby broaden our understanding of how the brain as a structure enables cognitive processes. Furthermore, methodological advancements could also improve the validity of structural network measures as biomarkers for clinical contexts, since the current graph-theoretical measures are often still lacking the specificity for accurate diagnoses (Imms et al., 2019; Lydon-Staley & Bassett, 2018; Whiteside et al., 2023; Winter et al., 2024).

3.4.2 Looking beyond the network horizon. Last, I want to explore how the finding that complex, hierarchically nested stimuli are processed along the functional uni-to-multimodal gradient can inform research and applications beyond the realm of network neuroscience. Inspiration comes specifically from **Study 3**, that used ISC to demonstrate that persistent stimuli featuring a visually and narratively complex content – inspired by the rich, natural environment – specifically engaged multimodal areas associated with understanding and deeper levels of processing (e.g., J. Chen et al., 2017; Yeshurun, Swanson, et al., 2017).

The cortical signals during a time-locked stimulus presentation, typically correlated in ISC analyses, are made up of three components: (1) the stimulus-induced activity, (2) individual processes, and (3) a random error. High levels of ISC are predominantly driven by synchronized, stimulus-induced activity and are therefore higher in the externally focused unimodal cortices (e.g., Nastase et al., 2019; Schmälzle et al., 2017), whereas high-level, interpretive processes are less synchronized across participants (cf. Yeshurun et al., 2021). In turn, previous work has suggested that the idiosyncratic activation profiles of high-order areas are therefore particularly well-suited to identify individuals (Finn et al., 2020; Z. Yang et al., 2020). Moreover, these interpretive components can also be more in-synch between similar people, leading to increases in ISC for more alike participants (Finn et al., 2020).

Previous research in this context was thus able to link similarities in personality traits (Bacha-Trams et al., 2018; Finn et al., 2018; J. Gao et al., 2020; Matz et al., 2022; Van Baar et al., 2021) as well as in-group-membership and close inter-personal relationships to higher-levels of neural synchrony (Gruskin et al., 2024; Hyon et al., 2020; Levy et al., 2016; L. Y. Li et al., 2025; Parkinson et al., 2018). While there also might be genetic reasons (Gruskin et al., 2024), these similarities in the neural processing were mainly attributed to more agreeing interpretations of the stimulus material (Bacha-Trams et al., 2018; Van Baar et al., 2021; Yeshurun et al., 2021; Yeshurun, Nguyen, et al., 2017; Yeshurun, Swanson, et al., 2017).

In accordance with these results, ISC has many applications in social neuroscience and the investigation of interpersonal understanding (Nummenmaa et al., 2018; Ohad et al., 2025). However, even more intriguing is the possibility of using ISC to distinguish between clinical populations, as particularly in hard-to-scan groups examinations with naturalistic stimuli are generally more accepted (Vanderwal et al., 2019). First evidence for clinical variations in ISC during naturalistic stimulus viewing was already demonstrated for individuals with autism (Byrge et al., 2015; Hasson et al., 2009; Salmi et al., 2013), schizophrenia (Z. Yang et al., 2020), epilepsy (Abbas, 2021), cognitive impairments (Das & Puthankattil, 2025; Y. Zhang et al., 2017) as well as

mood disorders (Guo et al., 2015; L. Y. Li et al., 2025). A common finding across clinical populations was that, compared to healthy controls, patients demonstrated more variability in their neural processes, leading to overall reduced ISC and synchronization with other patients (Guo et al., 2015; Hasson et al., 2009; L. Y. Li et al., 2025).

In this context, Finn et al. (2020) developed the so-called inter-subject representational similarity analysis (IS-RSA) that allows prediction of neural ISC by the inter-individual similarities on behavioural variables and also provides modelling solutions for the increased inter-subject variability in clinical populations. Using this framework, previous studies could already make progress in identifying areas, associated with various behaviourally relevant measures (Jangraw et al., 2023; Klamer et al., 2024a, 2024b, 2025). Importantly however, the efficacy of IS-RSA eminently depends on the presented stimulus (Finn et al., 2020). ISC in general improves with emotionally engaging, narratively complex, well-structured stimuli (Hasson, Landesman, et al., 2008; Ye et al., 2023). Applying ISC to depressive patients, for example, it was shown that especially stimuli with a negative emotional were effective in distinguishing between patients and healthy controls (Guo et al., 2015; L. Y. Li et al., 2025; X. Li et al., 2021).

Thus, although ISC and IS-RSA have shown potential for being used as a diagnostic tool, more research is necessary to create (naturalistic) stimuli that are specifically tuned to the questions and populations of interest (Finn et al., 2020). **Study 3**, as well as other studies (Faber et al., 2018; Lu et al., 2016; Sava-Segal et al., 2023) indicated, for instance, that temporally persistent stimuli depicting complex, variable content increased the overall engagement of higher-order areas. For ISC to reach its full potential as a biomarker, future studies have to comprehensively compare the influences of different stimuli on the neural processing. This also includes investigating which types of portrayed content (e.g., social situations, emotions, surprisal) specifically drive the heterogeneity of cortical engagement between different groups of interest.

4 Conclusion

In daily life, our brains are confronted with a multitude of environmental stimuli. Crucially, both these stimuli as well as the brain itself are hierarchically organized. The present thesis examined the relationship between the stimulatory and cortical hierarchies. Specifically, it was demonstrated that the brain utilizes the increasing temporal persistency of the hierarchically nested levels of environmental stimuli such as movies in their processing. The presented studies showed that when perceiving transient, low-level stimuli only the modality-specific cortical areas were activated. However, during the processing of persistent, hierarchically higher stimuli additional multimodal association cortices were engaged. These regions included the medial prefrontal cortex, precuneus, angular gyrus and superior temporal sulcus, which interestingly were all previously associated with the integration as well as interpretation of high-level content.

Accordingly, all three presented studies concisely highlighted that the temporal-based, cortical hierarchy extends along the functional uni-to-multimodal gradient, with unimodal areas handling the transient, lower-level stimuli, while multimodal areas are characterized by temporally extended processing dynamics attuned to hierarchically higher stimuli. This finding, however, surprisingly did not align with the investigated core-periphery-axis of the structural rich club phenomenon that was proposed to orchestrate the cortical chronoarchitecture. This thesis therefore did not find conclusive evidence for the structural network architecture that underlies the functional processing gradient. In this context, multiple methodological and theoretical limitations were discussed that might explain the missing link between the structural and functional hierarchy. Subsequently, future studies should improve upon the connectome construction methodology and consider the rich club hubs more from the perspective of a network infrastructure that flexibly supports specific integrative processes without globally synchronized functional engagement.

Overall, the results provide evidence for the differentiated importance of a stimulus' temporal persistency for higher levels of cortical processing. The studies thereby contribute to

literature that highlights the significance of the functional uni-to-multimodal gradient for the cortical organization. However, more research is necessary to refine the structural scaffolding of this functional processing hierarchy. Further investigation on the relationship between the network architecture and the processing hierarchy will provide a more thorough understanding of the cortical layout, which can aid the development of structural and functional indicators for individual assessment as well as the construction of more precise models of the human cortex.

5 References

Abbas, H. H. (2021). *Inter-Subject Correlation Using Movie-Driven fMRI in Drug- Resistant Epilepsy* [Master thesis]. The University of Western Ontario.

Aberbach-Goodman, S., & Mukamel, R. (2023). Temporal hierarchy of observed goal-directed actions. *Scientific Reports*, *13*(1), 1–13. https://doi.org/10.1038/s41598-023-46917-z

Achard, S., Delon-Martin, C., Vértes, P. E., Renard, F., Schenck, M., Schneider, F., Heinrich, C., Kremer, S., & Bullmore, E. T. (2012). Hubs of brain functional networks are radically reorganized in comatose patients. *Proceedings of the National Academy of Sciences of the United States of America*, *109*(50), 20608–20613. https://doi.org/10.1073/pnas.1208933109

Achard, S., Salvador, R., Whitcher, B., Suckling, J., & Bullmore, E. (2006). A resilient, low-frequency, small-world human brain functional network with highly connected association cortical hubs. *Journal of Neuroscience*, *26*(1), 63–72. https://doi.org/10.1523/JNEUROSCI.3874-05.2006

Aerts, H., Fias, W., Caeyenberghs, K., & Marinazzo, D. (2016). Brain networks under attack: Robustness properties and the impact of lesions. *Brain*, *139*(12), 3063–3083. https://doi.org/10.1093/brain/aww194

Albert, R., & Barabási, A. L. (2002). Statistical mechanics of complex networks. *Reviews of Modern Physics*, *74*(1), 47–97. https://doi.org/10.1103/RevModPhys.74.47

Albert, R., Jeong, H., & Barabási, A. L. (2011). Error and attack tolerance of complex networks. *The Structure and Dynamics of Networks*, *9781400841*(July), 503–506. https://doi.org/10.1515/9781400841356.503

Alexander, A. S., Place, R., Starrett, M. J., Chrastil, E. R., & Nitz, D. A. (2023). Rethinking retrosplenial cortex: Perspectives and predictions. *Neuron*, *111*(2), 150–175. https://doi.org/10.1016/j.neuron.2022.11.006

Alexander, W. H., & Brown, J. W. (2011). Medial prefrontal cortex as an action-outcome predictor. *Nature Neuroscience*, *14*(10), 1338–1344. https://doi.org/10.1038/nn.2921

Alexander, W. H., & Brown, J. W. (2018). Frontal cortex function as derived from hierarchical predictive coding. *Scientific Reports*, *8*(1), 1–11. https://doi.org/10.1038/s41598-018-21407-9

Alexander-Bloch, A. F., Shou, H., Liu, S., Satterthwaite, T. D., Glahn, D. C., Shinohara, R. T., Vandekar, S. N., & Raznahan, A. (2018). On testing for spatial correspondence between maps of human brain structure and function. *NeuroImage*, *178*(February), 540–551. https://doi.org/10.1016/j.neuroimage.2018.05.070

Allen, E. A., Damaraju, E., Plis, S. M., Erhardt, E. B., Eichele, T., & Calhoun, V. D. (2014). Tracking whole-brain connectivity dynamics in the resting state. *Cerebral Cortex*, *24*(3), 663–676. https://doi.org/10.1093/cercor/bhs352

Alnuaimi, A. F. A. H., & Albaldawi, T. H. K. (2024). An overview of machine learning classification techniques. *BIO Web of Conferences*, *97*, 1–24. https://doi.org/10.1051/bioconf/20249700133

Alston, C., Kuhnert, P., Low Choy, S., Mcvinish, R., Mengersen, K., Choy, S. L., Mcvinish, R., & Mengersen, K. (2004). Bayesian Model Comparison : Review and Discussion. In *ISI 2005 : the 55th Session of the International Statistical Institute, Sydney, 2005* (Number 1995, pp. 1–4). http://iase-web.org/documents/papers/isi55/Alston-Kuhnert-Low_Choy-McVinish-Mengersen.pdf

Alstott, J., Breakspear, M., Hagmann, P., Cammoun, L., & Sporns, O. (2009). Modeling the impact of lesions in the human brain. *PLoS Computational Biology*, *5*(6). https://doi.org/10.1371/journal.pcbi.1000408

Amunts, K., & Zilles, K. (2015). Architectonic Mapping of the Human Brain beyond Brodmann. *Neuron*, *88*(6), 1086–1107. https://doi.org/10.1016/j.neuron.2015.12.001

Anderson, K. M., Krienen, F. M., Choi, E. Y., Reinen, J. M., Yeo, B. T. T., & Holmes, A. J. (2018). Gene expression links functional networks across cortex and striatum. *Nature Communications*, *9*(1). https://doi.org/10.1038/s41467-018-03811-x

Antono, J. E., & Pooresmaeili, A. (2023). Modulation of perception by visual, auditory, and audiovisual reward predicting cues. *BioRxiv*, 2023.01.29.526087. https://www.biorxiv.org/content/10.1101/2023.01.29.526087v1%0Ahttps://www.biorxiv.org/content/10.1101/2023.01.29.526087v1.abstract

Assaf, Y., Alexander, D. C., Jones, D. K., Bizzi, A., Behrens, T. E. J., Clark, C. A., Cohen, Y., Dyrby, T. B., Huppi, P. S., Knoesche, T. R., LeBihan, D., Parker, G. J. M., Poupon, C., Anaby, D., Anwander, A., Bar, L., Barazany, D., Blumenfeld-Katzir, T., De-Santis, S., … Zhou, F. L. (2013). The CONNECT project: Combining macro- and micro-structure. *NeuroImage*, *80*, 273–282. https://doi.org/10.1016/j.neuroimage.2013.05.055

Aydogan, D. B., Jacobs, R., Dulawa, S., Thompson, S. L., Francois, M. C., Toga, A. W., Dong, H., Knowles, J. A., & Shi, Y. (2018). When tractography meets tracer injections: a systematic study of trends and variation sources of diffusion-based connectivity. *Brain Structure and Function*, *223*(6), 2841–2858. https://doi.org/10.1007/s00429-018-1663-8

Bacha-Trams, M., Alexandrov, Y. I., Broman, E., Glerean, E., Kauppila, M., Kauttonen, J., Ryyppö, E., Sams, M., & Jääskeläinen, I. P. (2018). A drama movie activates brains of holistic and analytical thinkers differentially. *Social Cognitive and Affective Neuroscience*, *13*(12), 1293–1304. https://doi.org/10.1093/scan/nsy099

Badre, D., & D'Esposito, M. (2007). Functional magnetic resonance imaging evidence for a hierarchical organization of the prefrontal cortex. *Journal of Cognitive Neuroscience*, *19*(12), 2082–2099. https://doi.org/10.1162/jocn.2007.19.12.2082

Badre, D., & Frank, M. J. (2012). Mechanisms of hierarchical reinforcement learning in cortico-striatal circuits 2: Evidence from fMRI. *Cerebral Cortex*, *22*(3), 527–536. https://doi.org/10.1093/cercor/bhr117

Badre, D., & Nee, D. E. (2018). Frontal Cortex and the Hierarchical Control of Behavior. In *Trends in Cognitive Sciences* (Vol. 22, Number 2, pp. 170–188). Elsevier Ltd. https://doi.org/10.1016/j.tics.2017.11.005

Baggio, H. C., Segura, B., Junque, C., de Reus, M. A., Sala-Llonch, R., & Van den Heuvel, M. P. (2015). Rich Club Organization and Cognitive Performance in Healthy Older Participants. *Journal of Cognitive Neuroscience*, *27*(9), 1801–1810. https://doi.org/10.1162/jocn_a_00821

Baker, S. T. E., Lubman, D. I., Yücel, M., Allen, N. B., Whittle, S., Fulcher, B. D., Zalesky, A., & Fornito, A. (2015). Developmental changes in brain network hub connectivity in late adolescence. *Journal of Neuroscience*, *35*(24), 9078–9087. https://doi.org/10.1523/JNEUROSCI.5043-14.2015

Baldassano, C., Chen, J., Zadbood, A., Pillow, J. W., Hasson, U., & Norman, K. A. (2017). Discovering Event Structure in Continuous Narrative Perception and Memory. *Neuron*, *95*(3), 709-721.e5. https://doi.org/10.1016/j.neuron.2017.06.041

Baldassano, C., Esteva, A., Fei-Fei, L., & Beck, D. M. (2016). Two distinct Scene-Processing networks connecting vision and memory. *ENeuro*, *3*(5). https://doi.org/10.1523/ENEURO.0178-16.2016

Ball, G., Aljabar, P., Zebari, S., Tusor, N., Arichi, T., Merchant, N., Robinson, E. C., Ogundipe, E., Rueckert, D., Edwards, A. D., & Counsell, S. J. (2014). Rich-club organization of the newborn human brain. *Proceedings of the National Academy of Sciences of the United States of America*, *111*(20), 7456–7461. https://doi.org/10.1073/pnas.1324118111

Barabási, A.-L., & Albert, R. (1999). Emergence of Scaling in Random Networks. *Science*, *286*(5439), 509–512. https://doi.org/10.1126/science.286.5439.509

Baria, A. T., Mansour, A., Huang, L., Baliki, M. N., Cecchi, G. A., Mesulam, M. M., & Apkarian, A. V. (2013). Linking human brain local activity fluctuations to structural and functional network architectures. *NeuroImage*, *73*, 144–155. https://doi.org/10.1016/j.neuroimage.2013.01.072

Bartels, A., & Zeki, S. (2004). The chronoarchitecture of the human brain - Natural viewing conditions reveal a time-based anatomy of the brain. *NeuroImage*, *22*(1), 419–433. https://doi.org/10.1016/j.neuroimage.2004.01.007

Bartels, A., & Zeki, S. (2005). The chronoarchitecture of the cerebral cortex. *Philosophical Transactions of the Royal Society B: Biological Sciences*, *360*(1456), 733–750. https://doi.org/10.1098/rstb.2005.1627

Barton, N., & Smyth, M. (2025). Context-switching in short-form videos: What is the impact on prospective memory? *Memory*, *33*(7), 788–801. https://doi.org/10.1080/09658211.2025.2521076

Bassett, D. S., Brown, J. A., Deshpande, V., Carlson, J. M., & Grafton, S. T. (2011). Conserved and variable architecture of human white matter connectivity. *NeuroImage*, *54*(2), 1262–1279. https://doi.org/10.1016/j.neuroimage.2010.09.006

Bassett, D. S., & Bullmore, E. (2006). Small-world brain networks. *Neuroscientist*, *12*(6), 512–523. https://doi.org/10.1177/1073858406293182

Bassett, D. S., Greenfield, D. L., Meyer-Lindenberg, A., Weinberger, D. R., Moore, S. W., & Bullmore, E. T. (2010). Efficient physical embedding of topologically complex information processing networks in brains and computer circuits. *PLoS Computational Biology*, *6*(4). https://doi.org/10.1371/journal.pcbi.1000748

Bassett, D. S., Wymbs, N. F., Rombach, M. P., Porter, M. A., Mucha, P. J., & Grafton, S. T. (2013). Task-Based Core-Periphery Organization of Human Brain Dynamics. *PLoS Computational Biology*, *9*(9), 1–16. https://doi.org/10.1371/journal.pcbi.1003171

Bathelt, J., Gathercole, S. E., Butterfield, S., & Astle, D. E. (2018). Children's academic attainment is linked to the global organization of the white matter connectome. *Developmental Science*, *21*(5), 1–14. https://doi.org/10.1111/desc.12662

Baumgarten, T. J., Maniscalco, B., Lee, J. L., Flounders, M. W., Abry, P., & He, B. J. (2021). Neural integration underlying naturalistic prediction flexibly adapts to varying sensory input rate. *Nature Communications*, *12*(1), 1–14. https://doi.org/10.1038/s41467-021-22632-z

Beliveau, V., Ganz, M., Feng, L., Ozenne, B., Højgaard, L., Fisher, P. M., Svarer, C., Greve, D. N., & Knudsen, G. M. (2017). A high-resolution in vivo atlas of the human brain's serotonin system. *Journal of Neuroscience*, *37*(1), 120–128. https://doi.org/10.1523/JNEUROSCI.2830-16.2016

Bender, A. (2020). The Role of Culture and Evolution for Human Cognition. *Topics in Cognitive Science*, *12*(4), 1403–1420. https://doi.org/10.1111/tops.12449

Ben-Yakov, A., & Henson, R. N. (2018). The hippocampal film editor: Sensitivity and specificity to event boundaries in continuous experience. *Journal of Neuroscience*, *38*(47), 10057–10068. https://doi.org/10.1523/JNEUROSCI.0524-18.2018

Berahmand, K., Samadi, N., & Sheikholeslami, S. M. (2018). Effect of rich-club on diffusion in complex networks. *International Journal of Modern Physics B*, *32*(12), 1–19. https://doi.org/10.1142/S0217979218501424

Bertagnolli, G., & De Domenico, M. (2022). Functional rich clubs emerging from the diffusion geometry of complex networks. *Physical Review Research*, *4*(3). https://doi.org/10.1103/PhysRevResearch.4.033185

Bertolero, M. A., Yeo, B. T. T., & D'Esposito, M. (2017). The diverse club. *Nature Communications*, *8*(1), 1–10. https://doi.org/10.1038/s41467-017-01189-w

Besle, J., Fort, A., & Giard, M.-H. (2004). Interest and validity of the additive model in electrophysiological studies of multisensory interactions. *Cognitive Processing*, *5*(3), 189–192. https://doi.org/10.1007/s10339-004-0026-y

Bettinardi, R. G., Deco, G., Karlaftis, V. M., Van Hartevelt, T. J., Fernandes, H. M., Kourtzi, Z., Kringelbach, M. L., & Zamora-López, G. (2017). How structure sculpts function: Unveiling the contribution of anatomical connectivity to the brain's spontaneous correlation structure. *Chaos*, *27*(4). https://doi.org/10.1063/1.4980099

Betzel, R. F., & Bassett, D. S. (2017). Multi-scale brain networks. *NeuroImage*, *160*(November 2016), 73–83. https://doi.org/10.1016/j.neuroimage.2016.11.006

Binder, J. R., Desai, R. H., Graves, W. W., & Conant, L. L. (2009). Where is the semantic system? A critical review and meta-analysis of 120 functional neuroimaging studies. *Cerebral Cortex*, *19*(12), 2767–2796. https://doi.org/10.1093/cercor/bhp055

Birn, R. M., Molloy, E. K., Patriat, R., Parker, T., Meier, T. B., Kirk, G. R., Nair, V. A., Meyerand, M. E., & Prabhakaran, V. (2013). The effect of scan length on the reliability of resting-state fMRI connectivity estimates. *NeuroImage*, *83*, 550–558. https://doi.org/10.1016/j.neuroimage.2013.05.099

Black, J. E., Kueper, J. K., & Williamson, T. S. (2023). An introduction to machine learning for classification and prediction. *Family Practice*, *40*(1), 200–204. https://doi.org/10.1093/fampra/cmac104

Botvinick, M. M. (2007). Multilevel structure in behaviour and in the brain: A model of Fuster's hierarchy. *Philosophical Transactions of the Royal Society B: Biological Sciences*, *362*(1485), 1615–1626. https://doi.org/10.1098/rstb.2007.2056

Botvinick, M. M. (2008). Hierarchical models of behavior and prefrontal function. *Trends in Cognitive Sciences*, *12*(5), 201–208. https://doi.org/10.1016/j.tics.2008.02.009

Brodmann, K. (1909). *Vergleichende Lokalisationslehre der Grosshirnrinde in ihren Prinzipien dargestellt auf Grund des Zellenbaues*. Barth JA. https://archive.org/details/b28062449/page/n3/mode/2up

Bryant, A. G., Jha, A., Agarwal, S., Cahill, P., Lam, B., Oldham, S., Arnatkevičiūtė, A., Fornito, A., & Fulcher, B. D. (2025). Benchmarking overlapping community detection methods for applications in human connectomics. *Network Neuroscience*, 1–37. https://doi.org/10.1162/netn.a.39

Bryce, N. V., Flournoy, J. C., Guassi Moreira, J. F., Rosen, M. L., Sambook, K. A., Mair, P., & McLaughlin, K. A. (2021). Brain parcellation selection: An overlooked decision point with meaningful effects on individual differences in resting-state functional connectivity. *NeuroImage*, *243*(March), 118487. https://doi.org/10.1016/j.neuroimage.2021.118487

Bu, X., Cao, M., Huang, X., & He, Y. (2021). The structural connectome in ADHD. *Psychoradiology*, *1*(4), 257–271. https://doi.org/10.1093/psyrad/kkab021

Bullmore, E., & Sporns, O. (2009). Complex brain networks: Graph theoretical analysis of structural and functional systems. *Nature Reviews Neuroscience*, *10*(3), 186–198. https://doi.org/10.1038/nrn2575

Bullmore, E., & Sporns, O. (2012). The economy of brain network organization. *Nature Reviews Neuroscience*, *13*(5), 336–349. https://doi.org/10.1038/nrn3214

Burt, J. B., Demirtaş, M., Eckner, W. J., Navejar, N. M., Ji, J. L., Martin, W. J., Bernacchia, A., Anticevic, A., & Murray, J. D. (2018). Hierarchy of transcriptomic specialization across human cortex captured by structural neuroimaging topography. *Nature Neuroscience*, *21*(9), 1251–1259. https://doi.org/10.1038/s41593-018-0195-0

Byrge, L., Dubois, J., Tyszka, J. M., Adolphs, R., & Kennedy, D. P. (2015). Idiosyncratic brain activation patterns are associated with poor social comprehension in autism. *Journal of Neuroscience*, *35*(14), 5837–5850. https://doi.org/10.1523/JNEUROSCI.5182-14.2015

Cabral, J., Hugues, E., Kringelbach, M. L., & Deco, G. (2012). Modeling the outcome of structural disconnection on resting-state functional connectivity. *NeuroImage*, *62*(3), 1342–1353. https://doi.org/10.1016/j.neuroimage.2012.06.007

Calamante, F. (2019). The seven deadly sins of measuring brain structural connectivity using diffusion MRI streamlines fibre-tracking. *Diagnostics*, *9*(3). https://doi.org/10.3390/diagnostics9030115

Cammoun, L., Gigandet, X., Meskaldji, D., Thiran, J. P., Sporns, O., Do, K. Q., Maeder, P., Meuli, R., & Hagmann, P. (2012). Mapping the human connectome at multiple scales with diffusion spectrum MRI. *Journal of Neuroscience Methods*, *203*(2), 386–397. https://doi.org/10.1016/j.jneumeth.2011.09.031

Cao, M., Wang, J. H., Dai, Z. J., Cao, X. Y., Jiang, L. L., Fan, F. M., Song, X. W., Xia, M. R., Shu, N., Dong, Q., Milham, M. P., Castellanos, F. X., Zuo, X. N., & He, Y. (2014). Topological organization of the human brain functional connectome across the lifespan. *Developmental Cognitive Neuroscience*, *7*(16), 76–93. https://doi.org/10.1016/j.dcn.2013.11.004

Cao, Q., Shu, N., An, L., Wang, P., Sun, L., Xia, M. R., Wang, J. H., Gong, G. L., Zang, Y. F., Wang, Y. F., & He, Y. (2013). Probabilistic diffusion tractography and graph theory analysis reveal abnormal white matter structural connectivity networks in drug-naive boys with attention deficit/hyperactivity disorder. *Journal of Neuroscience*, *33*(26), 10676–10687. https://doi.org/10.1523/JNEUROSCI.4793-12.2013

Cao, R., Wang, X., Gao, Y., Li, T., Zhang, H., Hussain, W., Xie, Y., Wang, J., Wang, B., & Xiang, J. (2020). Abnormal Anatomical Rich-Club Organization and Structural–Functional Coupling in Mild Cognitive Impairment and Alzheimer's Disease. *Frontiers in Neurology*, *11*(February), 1–17. https://doi.org/10.3389/fneur.2020.00053

Carius, D., Herold, F., Clauß, M., Kaminski, E., Wagemann, F., Sterl, C., & Ragert, P. (2023). Increased Cortical Activity in Novices Compared to Experts During Table Tennis: A Whole-Brain fNIRS Study Using Threshold-Free Cluster Enhancement Analysis. *Brain Topography*, *36*(4), 500–516. https://doi.org/10.1007/s10548-023-00963-y

Cavanagh, S. E., Hunt, L. T., & Kennerley, S. W. (2020). A Diversity of Intrinsic Timescales Underlie Neural Computations. *Frontiers in Neural Circuits*, *14*(December), 1–18. https://doi.org/10.3389/fncir.2020.615626

Chakraborty, S., Thounaojam, D. M., & Sinha, N. (2021). A Shot boundary Detection Technique based on Visual Colour Information. *Multimedia Tools and Applications*, *80*(3), 4007–4022. https://doi.org/10.1007/s11042-020-09857-8

Chanes, L., & Feldman Barrett, L. (2016). Redefining the Role of Limbic Areas in Cortical Processing. *Trends in Cognitive Sciences*, *20*(2), 96–106. https://doi.org/10.1016/j.tics.2015.11.005

Chatham, C. H., Frank, M. J., & Badre, D. (2014). Corticostriatal output gating during selection from working memory. *Neuron*, *81*(4), 930–942. https://doi.org/10.1016/j.neuron.2014.01.002

Chaudhuri, R., Knoblauch, K., Gariel, M. A., Kennedy, H., & Wang, X. J. (2015). A Large-Scale Circuit Mechanism for Hierarchical Dynamical Processing in the Primate Cortex. *Neuron*, *88*(2), 419–431. https://doi.org/10.1016/j.neuron.2015.09.008

Chen, A., Sun, Yidi, Lei, Y., Li, Chao, Liao, S., Meng, J., Bai, Yiqin, Liu, Z., Liang, Z., Zhu, Z., Yuan, N., Yang, Hao, Wu, Z., Lin, F., Wang, K., Li, Mei, Zhang, S., Yang, M., Fei, T., … Li, C. (2023). Single-cell spatial transcriptome reveals cell-type organization in the macaque cortex. *Cell*, *186*(17), 3726-3743.e24. https://doi.org/10.1016/j.cell.2023.06.009

Chen, J., Honey, C. J., Simony, E., Arcaro, M. J., Norman, K. A., & Hasson, U. (2016). Accessing Real-Life Episodic Information from Minutes versus Hours Earlier Modulates Hippocampal and High-Order Cortical Dynamics. *Cerebral Cortex*, *26*(8), 3428–3441. https://doi.org/10.1093/cercor/bhv155

Chen, J., Leong, Y. C., Honey, C. J., Yong, C. H., Norman, K. A., & Hasson, U. (2017). Shared memories reveal shared structure in neural activity across individuals. *Nature Neuroscience*, *20*(1), 115–125. https://doi.org/10.1038/nn.4450

Chen, Z., Liu, M., Gross, D. W., & Beaulieu, C. (2013). Graph theoretical analysis of developmental patterns of the white matter network. *Frontiers in Human Neuroscience*, *7*(NOV), 1–13. https://doi.org/10.3389/fnhum.2013.00716

Chiossi, F., Haliburton, L., Ou, C., Butz, A. M., & Schmidt, A. (2023). Short-Form Videos Degrade Our Capacity to Retain Intentions: Effect of Context Switching On Prospective Memory. *Conference on Human Factors in Computing Systems - Proceedings*, (April 2023). https://doi.org/10.1145/3544548.3580778

Choi, E. Y., Drayna, G. K., & Badre, D. (2018). Evidence for a Functional Hierarchy of Association Networks. *Journal of Cognitive Neuroscience*, *30*(5), 722–736. https://doi.org/10.1162/jocn_a_01229

Choi, I., Demir, I., Oh, S., & Lee, S. H. (2023). Multisensory integration in the mammalian brain: Diversity and flexibility in health and disease. *Philosophical Transactions of the Royal Society B: Biological Sciences*, *378*(1886). https://doi.org/10.1098/rstb.2022.0338

Clewett, D., & Davachi, L. (2017). The ebb and flow of experience determines the temporal structure of memory. *Current Opinion in Behavioral Sciences*, *17*, 186–193. https://doi.org/10.1016/j.cobeha.2017.08.013

Cole, M. W., Reynolds, J. R., Power, J. D., Repovs, G., Anticevic, A., & Braver, T. S. (2013). Multi-task connectivity reveals flexible hubs for adaptive task control. *Nature Neuroscience*, *16*(9), 1348–1355. https://doi.org/10.1038/nn.3470

Colizza, V., Flammini, A., Serrano, M. A., & Vespignani, A. (2006). Detecting rich-club ordering in complex networks. *Nature Physics*, *2*(2), 110–115. https://doi.org/10.1038/nphys209

Collin, G., Kahn, R. S., De Reus, M. A., Cahn, W., & Van Den Heuvel, M. P. (2014). Impaired rich club connectivity in unaffected siblings of schizophrenia patients. *Schizophrenia Bulletin*, *40*(2), 438–448. https://doi.org/10.1093/schbul/sbt162

Collin, G., Scholtens, L. H., Kahn, R. S., Hillegers, M. H. J., & van den Heuvel, M. P. (2017). Affected Anatomical Rich Club and Structural–Functional Coupling in Young Offspring of Schizophrenia and Bipolar Disorder Patients. *Biological Psychiatry*, *82*(10), 746–755. https://doi.org/https://doi.org/10.1016/j.biopsych.2017.06.013

Collin, G., Sporns, O., Mandl, R. C. W., & Van Den Heuvel, M. P. (2014). Structural and functional aspects relating to cost and benefit of rich club organization in the human cerebral cortex. *Cerebral Cortex*, *24*(9), 2258–2267. https://doi.org/10.1093/cercor/bht064

Colon-Perez, L. M., Couret, M., Triplett, W., Price, C. C., & Mareci, T. H. (2016). Small worldness in dense and weighted connectomes. *Frontiers in Physics*, *4*(MAY), 1–15. https://doi.org/10.3389/fphy.2016.00014

Conway, M. A. (2005). Memory and the self. *Journal of Memory and Language*, *53*(4), 594–628. https://doi.org/10.1016/j.jml.2005.08.005

Cornet, R., & Chute, C. G. (2016). Health Concept and Knowledge Management: Twenty-five Years of Evolution. *Yearbook of Medical Informatics*, S32–S41. https://doi.org/10.15265/IYS-2016-s037

Cosmides, L., & Tooby, J. (2013). Evolutionary psychology: New perspectives on cognition and motivation. *Annual Review of Psychology*, *64*, 201–229. https://doi.org/10.1146/annurev.psych.121208.131628

Crossley, N. A., Mechelli, A., Scott, J., Carletti, F., Fox, P. T., Mcguire, P., & Bullmore, E. T. (2014). The hubs of the human connectome are generally implicated in the anatomy of brain disorders. *Brain*, *137*(8), 2382–2395. https://doi.org/10.1093/brain/awu132

Crossley, N. A., Mechelli, A., Vértes, P. E., Winton-Brown, T. T., Patel, A. X., Ginestet, C. E., McGuire, P., & Bullmore, E. T. (2013). Cognitive relevance of the community structure of the human brain functional coactivation network. *Proceedings of the National Academy of Sciences of the United States of America*, *110*(28), 11583–11588. https://doi.org/10.1073/pnas.1220826110

Csermely, P., London, A., Wu, L.-Y., & Uzzi, B. (2013). Structure and dynamics of core/periphery networks. *Journal of Complex Networks*, *1*(2), 93–123. https://doi.org/10.1093/comnet/cnt016

Cutting, J. E. (2014). Event segmentation and seven types of narrative discontinuity in popular movies. *Acta Psychologica*, *149*, 69–77. https://doi.org/10.1016/j.actpsy.2014.03.003

Cutting, J. E. (2016). Narrative theory and the dynamics of popular movies. *Psychonomic Bulletin and Review*, *23*(6), 1713–1743. https://doi.org/10.3758/s13423-016-1051-4

Cutting, J. E. (2019a). Sequences in popular cinema generate inconsistent event segmentation. *Attention, Perception, and Psychophysics*, *81*(6), 2014–2025. https://doi.org/10.3758/s13414-019-01757-w

Cutting, J. E. (2019b). Simplicity, Complexity, and Narration in Popular Movies. *Narrative Complexity*, (August 2019), 200–222. https://doi.org/10.2307/j.ctvhktjh6.14

Cutting, J. E., Brunick, K. L., & Candan, A. (2012). Perceiving event dynamics and parsing Hollywood films. *Journal of Experimental Psychology: Human Perception and Performance*, *38*(6), 1476–1490. https://doi.org/10.1037/a0027737

Cutting, J. E., Brunick, K. L., & DeLong, J. E. (2011). How Act Structure Sculpts Shot Lengths and Shot Transitions in Hollywood Film. *Projections*, *5*(1), 1–16. https://doi.org/10.3167/proj.2011.050102

Cutting, J. E., Brunick, K. L., DeLong, J. E., Iricinschi, C., & Candan, A. (2011). Quicker, faster, darker: Changes in hollywood film over 75 years. *I-Perception*, *2*(6), 569–576. https://doi.org/10.1068/i0441aap

Dadario, N. B., Tanglay, O., & Sughrue, M. E. (2023). Deconvoluting human Brodmann area 8 based on its unique structural and functional connectivity. *Frontiers in Neuroanatomy*, *17*(June), 1–9. https://doi.org/10.3389/fnana.2023.1127143

Daducci, A., Palú, A. D., Descoteaux, M., & Thiran, J. P. (2016). Microstructure informed tractography: Pitfalls and open challenges. *Frontiers in Neuroscience*, *10*(JUN), 1–13. https://doi.org/10.3389/fnins.2016.00247

Daducci, A., & Schiavi, S. (2025). Quantitative tractography: joys and sorrows. *Brain Structure and Function*, *230*(6), 3–6. https://doi.org/10.1007/s00429-025-02939-z

Damiani, D., Nascimento, A. M., & Pereira, L. K. (2020). Cortical Brain Functions – The Brodmann Legacy in the 21st Century. *Arquivos Brasileiros de Neurocirurgia: Brazilian Neurosurgery*, *39*(04), 261–270. https://doi.org/10.1055/s-0036-1597573

Das, S., & Puthankattil, S. D. (2025). Inter subject variability analysis in normal ageing and prodromal AD. *Brain Organoid and Systems Neuroscience Journal*, *3*(December 2024), 107–114. https://doi.org/10.1016/j.bosn.2025.04.007

David, M. E., & Roberts, J. A. (2025). TikTok Brain: An Investigation of Short-Form Video Use, Self-Control, and Phubbing. *Social Science Computer Review*, *43*(6), 1292–1305. https://doi.org/10.1177/08944393241279422

de Pasquale, F., Corbetta, M., Betti, V., & Della Penna, S. (2018). Cortical cores in network dynamics. *NeuroImage*, *180*, 370–382. https://doi.org/10.1016/j.neuroimage.2017.09.063

de Reus, M. A., & van den Heuvel, M. P. (2013a). Estimating false positives and negatives in brain networks. *NeuroImage*, *70*, 402–409. https://doi.org/10.1016/j.neuroimage.2012.12.066

de Reus, M. A., & van den Heuvel, M. P. (2013b). Rich club organization and intermodule communication in the cat connectome. *Journal of Neuroscience*, *33*(32), 12929–12939. https://doi.org/10.1523/jneurosci.1448-13.2013

de Reus, M. A., & van den Heuvel, M. P. (2014). Simulated rich club lesioning in brain networks: A scaffold for communication and integration? *Frontiers in Human Neuroscience*, *8*(AUG), 1–5. https://doi.org/10.3389/fnhum.2014.00647

Deco, G., McIntosh, A. R., Shen, K., Matthew Hutchison, R., Menon, R. S., Everling, S., Hagmann, P., & Jirsa, V. K. (2014). Identification of optimal structural connectivity using functional connectivity and neural modeling. *Journal of Neuroscience*, *34*(23), 7910–7916. https://doi.org/10.1523/JNEUROSCI.4423-13.2014

Deco, G., Ponce-Alvarez, A., Mantini, D., Romani, G. L., Hagmann, P., & Corbetta, M. (2013). Resting-state functional connectivity emerges from structurally and dynamically shaped slow linear fluctuations. *Journal of Neuroscience*, *33*(27), 11239–11252. https://doi.org/10.1523/JNEUROSCI.1091-13.2013

Del Ferraro, G., Moreno, A., Min, B., Morone, F., Pérez-Ramírez, Ú., Pérez-Cervera, L., Parra, L. C., Holodny, A., Canals, S., & Makse, H. A. (2018). Finding influential nodes for integration in brain networks using optimal percolation theory. *Nature Communications*, *9*(1). https://doi.org/10.1038/s41467-018-04718-3

Desikan, R. S., Ségonne, F., Fischl, B., Quinn, B. T., Dickerson, B. C., Blacker, D., Buckner, R. L., Dale, A. M., Maguire, R. P., Hyman, B. T., Albert, M. S., & Killiany, R. J. (2006). An automated labeling system for subdividing the human cerebral cortex on MRI scans into gyral based regions of interest. *NeuroImage*, *31*(3), 968–980. https://doi.org/10.1016/j.neuroimage.2006.01.021

Dixon, M. L., De La Vega, A., Mills, C., Andrews-Hanna, J., Spreng, R. N., Cole, M. W., & Christoff, K. (2018). Heterogeneity within the frontoparietal control network and its relationship to the default and dorsal attention networks. *Proceedings of the National Academy of Sciences of the United States of America*, *115*(7), E1598–E1607. https://doi.org/10.1073/pnas.1715766115

Domenech, P., & Koechlin, E. (2015). Executive control and decision-making in the prefrontal cortex. *Current Opinion in Behavioral Sciences*, *1*, 101–106. https://doi.org/10.1016/j.cobeha.2014.10.007

Dong, H., Li, N., Fan, L., Wei, J., & Xu, J. (2022). Integrative interaction of emotional speech in audio-visual modality. *Frontiers in Neuroscience*, *16*(November), 1–13. https://doi.org/10.3389/fnins.2022.797277

Draganski, B., Gaser, C., Busch, V., Schuierer, G., Bogdahn, U., & May, A. (2004). Changes in grey matter induced by training. *Nature*, *427*(6972), 311–312. https://doi.org/10.1038/427311a

Faber, M., Radvansky, G. A., & D'Mello, S. K. (2018). Driven to distraction: A lack of change gives rise to mind wandering. *Cognition*, *173*(December 2016), 133–137. https://doi.org/10.1016/j.cognition.2018.01.007

Fan, L., Li, H., Zhuo, J., Zhang, Y., Wang, J., Chen, L., Yang, Z., Chu, C., Xie, S., Laird, A. R., Fox, P. T., Eickhoff, S. B., Yu, C., & Jiang, T. (2016). The Human Brainnetome Atlas: A New Brain Atlas Based on Connectional Architecture. *Cerebral Cortex*, *26*(8), 3508–3526. https://doi.org/10.1093/cercor/bhw157

Farahani, F. V., Karwowski, W., & Lighthall, N. R. (2019). Application of graph theory for identifying connectivity patterns in human brain networks: A systematic review. *Frontiers in Neuroscience*, *13*(JUN), 1–27. https://doi.org/10.3389/fnins.2019.00585

Farbood, M. M., Heeger, D. J., Marcus, G., Hasson, U., & Lerner, Y. (2015). The neural processing of hierarchical structure in music and speech at different timescales. *Frontiers in Neuroscience*, *9*(APR), 1–13. https://doi.org/10.3389/fnins.2015.00157

Farkaš, I. (2024). Transforming Cognition and Human Society in the Digital Age. *Biological Theory*, (0123456789). https://doi.org/10.1007/s13752-024-00483-3

Feinberg, D. A., Moeller, S., Smith, S. M., Auerbach, E., Ramanna, S., Glasser, M. F., Miller, K. L., Ugurbil, K., & Yacoub, E. (2010). Multiplexed echo planar imaging for sub-second whole brain fmri and fast diffusion imaging. *PLoS ONE*, *5*(12). https://doi.org/10.1371/journal.pone.0015710

Felleman, D. J., & Van Essen, D. C. (1991). Distributed hierarchical processing in the primate cerebral cortex. *Cerebral Cortex*, *1*(1), 1–47. https://doi.org/10.1093/cercor/1.1.1

Ferizi, U., Scherrer, B., Schneider, T., Alipoor, M., Eufracio, O., Fick, R. H. J., Deriche, R., Nilsson, M., Loya-Olivas, A. K., Rivera, M., Poot, D. H. J., Ramirez-Manzanares, A., Marroquin, J. L., Rokem, A., Pötter, C., Dougherty, R. F., Sakaie, K., Wheeler-Kingshott, C., Warfield, S. K., … Alexander, D. C. (2017). Diffusion MRI microstructure models with in vivo human brain Connectome data: results from a multi-group comparison. *NMR in Biomedicine*, *30*(9), 1–23. https://doi.org/10.1002/nbm.3734

Ferrari, C., Lega, C., Vernice, M., Tamietto, M., Mende-Siedlecki, P., Vecchi, T., Todorov, A., & Cattaneo, Z. (2016). The Dorsomedial Prefrontal Cortex Plays a Causal Role in Integrating Social Impressions from Faces and Verbal Descriptions. *Cerebral Cortex*, *26*(1), 156–165. https://doi.org/10.1093/cercor/bhu186

Field, S. (2005). *Screenplay: The Foundations of Screenwriting*. Random House Publishing Group.

Finn, E. S. (2021). Is it time to put rest to rest? *Trends in Cognitive Sciences*, *25*(12), 1021–1032. https://doi.org/10.1016/j.tics.2021.09.005

Finn, E. S., & Bandettini, P. A. (2021). Movie-watching outperforms rest for functional connectivity-based prediction of behavior. *NeuroImage*, *235*(February), 117963. https://doi.org/10.1016/j.neuroimage.2021.117963

Finn, E. S., Corlett, P. R., Chen, G., Bandettini, P. A., & Constable, R. T. (2018). Trait paranoia shapes inter-subject synchrony in brain activity during an ambiguous social narrative. *Nature Communications*, *9*(1), 1–13. https://doi.org/10.1038/s41467-018-04387-2

Finn, E. S., Glerean, E., Khojandi, A. Y., Nielson, D., Molfese, P. J., Handwerker, D. A., & Bandettini, P. A. (2020). Idiosynchrony: From shared responses to individual differences during naturalistic neuroimaging. *NeuroImage*, *215*(October 2019), 116828. https://doi.org/10.1016/j.neuroimage.2020.116828

Firth, J., Torous, J., Stubbs, B., Firth, J. A., Steiner, G. Z., Smith, L., Alvarez-Jimenez, M., Gleeson, J., Vancampfort, D., Armitage, C. J., & Sarris, J. (2019). The “online brain”: how the Internet may be changing our cognition. *World Psychiatry*, *18*(2), 119–129. https://doi.org/10.1002/wps.20617

Fitch, W. T., & Martins, M. D. (2014). Hierarchical processing in music, language, and action: Lashley revisited. *Annals of the New York Academy of Sciences*, *1316*(1), 87–104. https://doi.org/10.1111/nyas.12406

Fornito, A., Zalesky, A., & Bullmore, E. (2016). *Fundamentals of Brain Network Analysis*. Elsevier. https://doi.org/10.1016/C2012-0-06036-X

Fox, M. D., Snyder, A. Z., Vincent, J. L., Corbetta, M., Van Essen, D. C., & Raichle, M. E. (2005). The human brain is intrinsically organized into dynamic, anticorrelated functional networks. *Proceedings of the National Academy of Sciences of the United States of America*, *102*(27), 9673–9678. https://doi.org/10.1073/pnas.0504136102

Froudist-Walsh, S., Bliss, D. P., Ding, X., Rapan, L., Niu, M., Knoblauch, K., Zilles, K., Kennedy, H., Palomero-Gallagher, N., & Wang, X. J. (2021). A dopamine gradient controls access to distributed working memory in the large-scale monkey cortex. *Neuron*, *109*(21), 3500-3520.e13. https://doi.org/10.1016/j.neuron.2021.08.024

Froudist-Walsh, S., Xu, T., Niu, M., Rapan, L., Zhao, L., Margulies, D. S., Zilles, K., Wang, X. J., & Palomero-Gallagher, N. (2023). Gradients of neurotransmitter receptor expression in the macaque cortex. *Nature Neuroscience*, *26*(7), 1281–1294. https://doi.org/10.1038/s41593-023-01351-2

Fukushima, M., Betzel, R. F., He, Y., van den Heuvel, M. P., Zuo, X. N., & Sporns, O. (2018). Structure–function relationships during segregated and integrated network states of human brain functional connectivity. *Brain Structure and Function*, *223*(3), 1091–1106. https://doi.org/10.1007/s00429-017-1539-3

Fulcher, B. D., & Fornito, A. (2016). A transcriptional signature of hub connectivity in the mouse connectome. *Proceedings of the National Academy of Sciences of the United States of America*, *113*(5), 1435–1440. https://doi.org/10.1073/pnas.1513302113

Fuster, J. M. (2001). The prefrontal cortex - An update: Time is of the essence. In *Neuron* (Vol. 30, Number 2, pp. 319–333). https://doi.org/10.1016/S0896-6273(01)00285-9

Fuster, J. M., & Bressler, S. L. (2015). Past Makes Future: Role of pFC in Prediction. *Journal of Cognitive Neuroscience*, *27*(4), 639–654. https://doi.org/10.1162/jocn_a_00746

Gao, J., Chen, G., Wu, J., Wang, Y., Hu, Y., Xu, T., Zuo, X. N., & Yang, Z. (2020). Reliability map of individual differences reflected in inter-subject correlation in naturalistic imaging. *NeuroImage*, *223*(March), 117277. https://doi.org/10.1016/j.neuroimage.2020.117277

Gao, R., van den Brink, R. L., Pfeffer, T., & Voytek, B. (2020). Neuronal timescales are functionally dynamic and shaped by cortical microarchitecture. *ELife*, *9*, 1–26. https://doi.org/10.7554/eLife.61277

Gast, H., & Assaf, Y. (2024). Weighting the structural connectome: Exploring its impact on network properties and predicting cognitive performance in the human brain. *Network Neuroscience*, *8*(1), 119–137. https://doi.org/10.1162/netn_a_00342

Geerligs, L., Gözükara, D., Oetringer, D., Campbell, K. L., van Gerven, M., & Güçlü, U. (2022). A partially nested cortical hierarchy of neural states underlies event segmentation in the human brain. *ELife*, *11*, 1–36. https://doi.org/10.7554/eLife.77430

Ghalmane, Z., Cherifi, C., Cherifi, H., & Hassouni, M. El. (2019). Centrality in Complex Networks with Overlapping Community Structure. *Scientific Reports*, *9*(1), 1–29. https://doi.org/10.1038/s41598-019-46507-y

Girard, G., Caminiti, R., Battaglia-Mayer, A., St-Onge, E., Ambrosen, K. S., Eskildsen, S. F., Krug, K., Dyrby, T. B., Descoteaux, M., Thiran, J. P., & Innocenti, G. M. (2020). On the cortical connectivity in the macaque brain: A comparison of diffusion tractography and histological tracing data. *NeuroImage*, *221*(July), 117201. https://doi.org/10.1016/j.neuroimage.2020.117201

Glasser, M. F., Coalson, T. S., Robinson, E. C., Hacker, C. D., Harwell, J., Yacoub, E., Ugurbil, K., Andersson, J., Beckmann, C. F., Jenkinson, M., Smith, S. M., & Van Essen, D. C. (2016). A multi-modal parcellation of human cerebral cortex. *Nature*, *536*(7615), 171–178. https://doi.org/10.1038/nature18933

Glasser, M. F., & van Essen, D. C. (2011). Mapping human cortical areas in vivo based on myelin content as revealed by T1- and T2-weighted MRI. *Journal of Neuroscience*, *31*(32), 11597–11616. https://doi.org/10.1523/JNEUROSCI.2180-11.2011

Gold, D. A., Zacks, J. M., & Flores, S. (2017). Effects of cues to event segmentation on subsequent memory. *Cognitive Research: Principles and Implications*, *2*(1), 1–15. https://doi.org/10.1186/s41235-016-0043-2

Golesorkhi, M., Gomez-Pilar, J., Tumati, S., Fraser, M., & Northoff, G. (2021). Temporal hierarchy of intrinsic neural timescales converges with spatial core-periphery organization. *Communications Biology*, *4*(1), 1–14. https://doi.org/10.1038/s42003-021-01785-z

Golesorkhi, M., Gomez-Pilar, J., Zilio, F., Berberian, N., Wolff, A., Yagoub, M. C. E., & Northoff, G. (2021). The brain and its time: intrinsic neural timescales are key for input processing. *Communications Biology*, *4*(1), 1–16. https://doi.org/10.1038/s42003-021-02483-6

Gollo, L. L., Zalesky, A., Matthew Hutchison, R., van den Heuvel, M. P., & Breakspear, M. (2015). Dwelling quietly in the rich club: Brain network determinants of slow cortical fluctuations. *Philosophical Transactions of the Royal Society B: Biological Sciences*, *370*(1668). https://doi.org/10.1098/rstb.2014.0165

Gómez-Gardeñes, J., Zamora-López, G., Moreno, Y., & Arenas, A. (2010). From modular to centralized organization of synchronization in functional areas of the cat cerebral cortex. *PLoS ONE*, *5*(8). https://doi.org/10.1371/journal.pone.0012313

Gonzalez-Castillo, J., Handwerker, D. A., Robinson, M. E., Hoy, C. W., Buchanan, L. C., Saad, Z. S., & Bandettini, P. A. (2014). The spatial structure of resting state connectivity stability on the scale of minutes. *Frontiers in Neuroscience*, *8*(8 JUN), 1–19. https://doi.org/10.3389/fnins.2014.00138

González-García, C., Flounders, M. W., Chang, R., Baria, A. T., & He, B. J. (2018). Content-specific activity in frontoparietal and default-mode networks during prior-guided visual perception. *ELife*, *7*, 1–25. https://doi.org/10.7554/eLife.36068

Goto, M., Abe, O., Hagiwara, A., Fujita, S., Kamagata, K., Hori, M., Aoki, S., Osada, T., Konishi, S., Masutani, Y., Sakamoto, H., Sakano, Y., Kyogoku, S., & Daida, H. (2022). Advantages of Using Both Voxel-and Surface-based Morphometry in Cortical Morphology Analysis: A Review of Various Applications. *Magnetic Resonance in Medical Sciences*, *21*(1), 41–57. https://doi.org/10.2463/mrms.rev.2021-0096

Goulas, A., Changeux, J. P., Wagstyl, K., Amunts, K., Palomero-Gallagher, N., & Hilgetag, C. C. (2021). The natural axis of transmitter receptor distribution in the human cerebral cortex. *Proceedings of the National Academy of Sciences of the United States of America*, *118*(3), 1–9. https://doi.org/10.1073/PNAS.2020574118

Goulas, A., Uylings, H. B. M., & Stiers, P. (2014). Mapping the hierarchical layout of the structural network of the macaque prefrontal cortex. *Cerebral Cortex*, *24*(5), 1178–1194. https://doi.org/10.1093/cercor/bhs399

Grafton, S. T., & Hamilton, A. F. D. C. (2007). Evidence for a distributed hierarchy of action representation in the brain. *Human Movement Science*, *26*(4), 590–616. https://doi.org/10.1016/j.humov.2007.05.009

Grall, C., & Finn, E. S. (2022). Leveraging the power of media to drive cognition: A media-informed approach to naturalistic neuroscience. *Social Cognitive and Affective Neuroscience*, *17*(6), 598–608. https://doi.org/10.1093/scan/nsac019

Grayson, D. S., Ray, S., Carpenter, S., Iyer, S., Dias, T. G. C., Stevens, C., Nigg, J. T., & Fair, D. A. (2014). Structural and functional rich club organization of the brain in children and adults. *PLoS ONE*, *9*(2), 1–13. https://doi.org/10.1371/journal.pone.0088297

Greaves, M. D., Novelli, L., Mansour L, S., Zalesky, A., & Razi, A. (2025). Structurally informed models of directed brain connectivity. *Nature Reviews Neuroscience*, *26*(1), 23–41. https://doi.org/10.1038/s41583-024-00881-3

Greicius, M. D., Supekar, K., Menon, V., & Dougherty, R. F. (2009). Resting-state functional connectivity reflects structural connectivity in the default mode network. *Cerebral Cortex*, *19*(1), 72–78. https://doi.org/10.1093/cercor/bhn059

Griffa, A., Baumann, P. S., Thiran, J. P., & Hagmann, P. (2013). Structural connectomics in brain diseases. *NeuroImage*, *80*, 515–526. https://doi.org/10.1016/j.neuroimage.2013.04.056

Griffa, A., & van den Heuvel, M. P. (2018). Rich-club neurocircuitry: Function, evolution, and vulnerability. *Dialogues in Clinical Neuroscience*, *20*(2), 121–132. https://doi.org/10.31887/dcns.2018.20.2/agriffa

Grisot, G., Haber, S. N., & Yendiki, A. (2021). Diffusion MRI and anatomic tracing in the same brain reveal common failure modes of tractography. *NeuroImage*, *239*(January), 118300. https://doi.org/10.1016/j.neuroimage.2021.118300

Gruskin, D. C., Vieira, D. J., & Lee, J. K. (2024). Heritability of movie-evoked brain activity and connectivity. *BioRxiv Neuroscience*, 1–22. https://www.biorxiv.org/cgi/content/short/2024.09.16.612469v1?rss=1&utm_source=researcher_app&utm_medium=referral&utm_campaign=RESR_MRKT_Researcher_inbound

Gu, Y., Qi, Y., & Gong, P. (2019). Rich-club connectivity, diverse population coupling, and dynamical activity patterns emerging from local cortical circuits. In *PLoS Computational Biology* (Vol. 15, Number 4). https://doi.org/10.1371/journal.pcbi.1006902

Guimerà, R., & Nunes Amaral, L. A. (2005). Functional cartography of complex metabolic networks. *Nature*, *433*(7028), 895–900. https://doi.org/10.1038/nature03288

Guo, C. C., Nguyen, V. T., Hyett, M. P., Parker, G. B., & Breakspear, M. J. (2015). Out-of-sync: Disrupted neural activity in emotional circuitry during film viewing in melancholic depression. *Scientific Reports*, *5*(June), 1–12. https://doi.org/10.1038/srep11605

Hagmann, P., Cammoun, L., Gigandet, X., Meuli, R., Honey, C. J., Van Wedeen, J., & Sporns, O. (2008). Mapping the structural core of human cerebral cortex. *PLoS Biology*, *6*(7), 1479–1493. https://doi.org/10.1371/journal.pbio.0060159

Hagmann, P., Kurant, M., Gigandet, X., Thiran, P., Wedeen, V. J., Meuli, R., & Thiran, J. P. (2007). Mapping human whole-brain structural networks with diffusion MRI. *PLoS ONE*, *2*(7). https://doi.org/10.1371/journal.pone.0000597

Hamilton, A. F. de C., & Grafton, S. T. (1993). The motor hierarchy: from kinematics to goals and intentions. In *Sensorimotor Foundations of Higher Cognition* (pp. 381–407). Oxford University Press. https://doi.org/10.1093/acprof:oso/9780199231447.003.0018

Hansen, J. Y., Markello, R. D., Tuominen, L., Nørgaard, M., Kuzmin, E., Palomero-Gallagher, N., Dagher, A., & Misic, B. (2022). Correspondence between gene expression and neurotransmitter receptor and transporter density in the human brain. *NeuroImage*, *264*(July), 119671. https://doi.org/10.1016/j.neuroimage.2022.119671

Hansen, J. Y., Markello, R. D., Vogel, J. W., Seidlitz, J., Bzdok, D., & Misic, B. (2021). Mapping gene transcription and neurocognition across human neocortex. *Nature Human Behaviour*, *5*(9), 1240–1250. https://doi.org/10.1038/s41562-021-01082-z

Hansen, J. Y., Shafiei, G., Markello, R. D., Smart, K., Cox, S. M. L., Nørgaard, M., Beliveau, V., Wu, Y., Gallezot, J. D., Aumont, É., Servaes, S., Scala, S. G., DuBois, J. M., Wainstein, G., Bezgin, G., Funck, T., Schmitz, T. W., Spreng, R. N., Galovic, M., … Misic, B. (2022). Mapping neurotransmitter systems to the structural and functional organization of the human neocortex. *Nature Neuroscience*, *25*(11), 1569–1581. https://doi.org/10.1038/s41593-022-01186-3

Hansen, J. Y., Shafiei, G., Voigt, K., Liang, E. X., Cox, S. M. L., Leyton, M., Jamadar, S. D., & Misic, B. (2022). Multimodal, multiscale connectivity blueprints of the cerebral cortex. In *bioRxiv* (p. 2022.12.02.518906). https://doi.org/10.1101/2022.12.02.518906

Haq, I. U., Muhammad, K., Hussain, T., Kwon, S., Sodanil, M., Baik, S. W., & Lee, M. Y. (2019). Movie scene segmentation using object detection and set theory. *International Journal of Distributed Sensor Networks*, *15*(6), 0–7. https://doi.org/10.1177/1550147719845277

Harriger, L., van den Heuvel, M. P., & Sporns, O. (2012). Rich Club Organization of Macaque Cerebral Cortex and Its Role in Network Communication. *PLoS ONE*, *7*(9). https://doi.org/10.1371/journal.pone.0046497

Hasson, U., Avidan, G., Gelbard, H., Vallines, I., Harel, M., Minshew, N., & Behrmann, M. (2009). Shared and idiosyncratic cortical activation patterns in autism revealed under continuous real-life viewing conditions. *Autism Research*, *2*(4), 220–231. https://doi.org/10.1002/aur.89

Hasson, U., Chen, J., & Honey, C. J. (2015). Hierarchical process memory: Memory as an integral component of information processing. *Trends in Cognitive Sciences*, *19*(6), 304–313. https://doi.org/10.1016/j.tics.2015.04.006

Hasson, U., Landesman, O., Knappmeyer, B., Vallines, I., Rubin, N., & Heeger, D. J. (2008). Neurocinematics: The Neuroscience of Film. *Projections*, *2*(1), 1–26. https://doi.org/10.3167/proj.2008.020102

Hasson, U., Yang, E., Vallines, I., Heeger, D. J., & Rubin, N. (2008). A hierarchy of temporal receptive windows in human cortex. *Journal of Neuroscience*, *28*(10), 2539–2550. https://doi.org/10.1523/JNEUROSCI.5487-07.2008

Hawrylycz, M. J., Lein, E. S., Guillozet-Bongaarts, A. L., Shen, E. H., Ng, L., Miller, J. A., Van De Lagemaat, L. N., Smith, K. A., Ebbert, A., Riley, Z. L., Abajian, C., Beckmann, C. F., Bernard, A., Bertagnolli, D., Boe, A. F., Cartagena, P. M., Mallar Chakravarty, M., Chapin, M., Chong, J., … Jones, A. R. (2012). An anatomically comprehensive atlas of the adult human brain transcriptome. *Nature*, *489*(7416), 391–399. https://doi.org/10.1038/nature11405

Hearne, L., Cocchi, L., Zalesky, A., & Mattingley, J. B. (2015). Interactions between default mode and control networks as a function of increasing cognitive reasoning complexity. *Human Brain Mapping*, *36*(7), 2719–2731. https://doi.org/10.1002/hbm.22802

Herholz, S. C., & Zatorre, R. J. (2012). Musical Training as a Framework for Brain Plasticity: Behavior, Function, and Structure. *Neuron*, *76*(3), 486–502. https://doi.org/10.1016/j.neuron.2012.10.011

Hermundstad, A. M., Bassett, D. S., Brown, K. S., Aminoff, E. M., Clewett, D., Freeman, S., Frithsen, A., Johnson, A., Tipper, C. M., Miller, M. B., Grafton, S. T., & Carlson, J. M. (2013). Structural foundations of resting-state and task-based functional connectivity in the human brain. *Proceedings of the National Academy of Sciences of the United States of America*, *110*(15), 6169–6174. https://doi.org/10.1073/pnas.1219562110

Hilgetag, C. C., & Goulas, A. (2020). 'Hierarchy' in the organization of brain networks. *Philosophical Transactions of the Royal Society B: Biological Sciences*, *375*(1796). https://doi.org/10.1098/rstb.2019.0319

Hilgetag, C. C., Goulas, A., & Changeux, J. P. (2022). A natural cortical axis connecting the outside and inside of the human brain. *Network Neuroscience*, *6*(4), 950–959. https://doi.org/10.1162/netn_a_00256

Hilgetag, C. C., Medalla, M., Beul, S. F., & Barbas, H. (2016). The primate connectome in context: Principles of connections of the cortical visual system. *NeuroImage*, *134*, 685–702. https://doi.org/10.1016/j.neuroimage.2016.04.017

Himberger, K. D., Chien, H. Y., & Honey, C. J. (2018). Principles of Temporal Processing Across the Cortical Hierarchy. *Neuroscience*, *389*, 161–174. https://doi.org/10.1016/j.neuroscience.2018.04.030

Honey, C. J., Kötter, R., Breakspear, M., & Sporns, O. (2007). Network structure of cerebral cortex shapes functional connectivity on multiple time scales. *Proceedings of the National Academy of Sciences of the United States of America*, *104*(24), 10240–10245. https://doi.org/10.1073/pnas.0701519104

Honey, C. J., & Sporns, O. (2008). Dynamical consequences of lesions in cortical networks. *Human Brain Mapping*, *29*(7), 802–809. https://doi.org/10.1002/hbm.20579

Honey, C. J., Sporns, O., Cammoun, L., Gigandet, X., Thiran, J. P., Meuli, R., & Hagmann, P. (2009). Predicting human resting-state functional connectivity from structural connectivity. *Proceedings of the National Academy of Sciences of the United States of America*, *106*(6), 2035–2040. https://doi.org/10.1073/pnas.0811168106

Honey, C. J., Thesen, T., Donner, T. H., Silbert, L. J., Carlson, C. E., Devinsky, O., Doyle, W. K., Rubin, N., Heeger, D. J., & Hasson, U. (2012). Slow Cortical Dynamics and the Accumulation of Information over Long Timescales. *Neuron*, *76*(2), 423–434. https://doi.org/10.1016/j.neuron.2012.08.011

Hong, Y., Cornea, E., Girault, J. B., Stephens, R. L., Bagonis, M., Foster, M., Kim, S. H., Prieto, J. C., Styner, M. A., & Gilmore, J. H. (2025). Structural connectome gradients and their relationship to IQ in childhood. *Frontiers in Human Neuroscience*, *19*(November), 1–12. https://doi.org/10.3389/fnhum.2025.1688296

Huang, H., Shu, N., Mishra, V., Jeon, T., Chalak, L., Wang, Z. J., Rollins, N., Gong, G., Cheng, H., Peng, Y., Dong, Q., & He, Y. (2015). Development of human brain structural networks through infancy and childhood. *Cerebral Cortex*, *25*(5), 1389–1404. https://doi.org/10.1093/cercor/bht335

Huang, M. H., Lang, J., Li, J., Qin, Z., & Cao, Y. P. (2023). Characteristics of brain activation in high-level football players at different stages of decision-making tasks off the ball: an fMRI study. *Frontiers in Human Neuroscience*, *17*(August), 1–13. https://doi.org/10.3389/fnhum.2023.1189841

Hubel, D. H., & Wiesel, T. N. (1962). Receptive fields, binocular interaction and functional architecture in the cat's visual cortex. *The Journal of Physiology*, *160*(1), 106–154. https://doi.org/10.1113/jphysiol.1962.sp006837

Humphreys, G. F., Jackson, R. L., & Lambon Ralph, M. A. (2020). Overarching Principles and Dimensions of the Functional Organization in the Inferior Parietal Cortex. *Cerebral Cortex*, *30*(11), 5639–5653. https://doi.org/10.1093/cercor/bhaa133

Humphreys, G. F., Jung, J. Y., & Lambon Ralph, M. A. (2022). The convergence and divergence of episodic and semantic functions across lateral parietal cortex. *Cerebral Cortex*, *32*(24), 5664–5681. https://doi.org/10.1093/cercor/bhac044

Humphreys, G. F., & Tibon, R. (2023). Dual-axes of functional organisation across lateral parietal cortex: the angular gyrus forms part of a multi-modal buffering system. *Brain Structure and Function*, *228*(1), 341–352. https://doi.org/10.1007/s00429-022-02510-0

Huntenburg, J. M., Bazin, P. L., Goulas, A., Tardif, C. L., Villringer, A., & Margulies, D. S. (2017). A Systematic Relationship Between Functional Connectivity and Intracortical Myelin in the Human Cerebral Cortex. *Cerebral Cortex (New York, N.Y. : 1991)*, *27*(2), 981–997. https://doi.org/10.1093/cercor/bhx030

Huntenburg, J. M., Bazin, P. L., & Margulies, D. S. (2018). Large-Scale Gradients in Human Cortical Organization. *Trends in Cognitive Sciences*, *22*(1), 21–31. https://doi.org/10.1016/j.tics.2017.11.002

Hyon, R., Kleinbaum, A. M., & Parkinson, C. (2020). Social network proximity predicts similar trajectories of psychological states: Evidence from multi-voxel spatiotemporal dynamics. *NeuroImage*, *216*(December 2019), 116492. https://doi.org/10.1016/j.neuroimage.2019.116492

Imms, P., Clemente, A., Cook, M., D'Souza, W., Wilson, P. H., Jones, D. K., & Caeyenberghs, K. (2019). The structural connectome in traumatic brain injury: A meta-analysis of graph metrics. *Neuroscience and Biobehavioral Reviews*, *99*(January), 128–137. https://doi.org/10.1016/j.neubiorev.2019.01.002

Ito, T., Hearne, L. J., & Cole, M. W. (2020). A cortical hierarchy of localized and distributed processes revealed via dissociation of task activations, connectivity changes, and intrinsic timescales. *NeuroImage*, *221*(February), 117141. https://doi.org/10.1016/j.neuroimage.2020.117141

Jääskeläinen, I. P., Sams, M., Glerean, E., & Ahveninen, J. (2021). Movies and narratives as naturalistic stimuli in neuroimaging. *NeuroImage*, *224*(June 2020), 117445. https://doi.org/10.1016/j.neuroimage.2020.117445

Jang, Y., Choi, H., Yoo, S., Park, H., & Park, B. yong. (2024). Structural connectome alterations between individuals with autism and neurotypical controls using feature representation learning. *Behavioral and Brain Functions* , *20*(1), 1–10. https://doi.org/10.1186/s12993-024-00228-z

Jangraw, D. C., Finn, E. S., Bandettini, P. A., Landi, N., Sun, H., Hoeft, F., Chen, G., Pugh, K. R., & Molfese, P. J. (2023). Inter-subject correlation during long narratives reveals widespread neural correlates of reading ability. *NeuroImage*, *282*(March), 120390. https://doi.org/10.1016/j.neuroimage.2023.120390

Jbabdi, S., Sotiropoulos, S. N., Haber, S. N., Van Essen, D. C., & Behrens, T. E. (2015). Measuring macroscopic brain connections in vivo. *Nature Neuroscience*, *18*(11), 1546–1555. https://doi.org/10.1038/nn.4134

Jeon, H. A. (2014). Hierarchical processing in the prefrontal cortex in a variety of cognitive domains. In *Frontiers in Systems Neuroscience* (Vol. 8, Number NOV, pp. 1–8). Frontiers Research Foundation. https://doi.org/10.3389/fnsys.2014.00223

Ji, J. L., Spronk, M., Kulkarni, K., Repovš, G., Anticevic, A., & Cole, M. W. (2019). Mapping the human brain's cortical-subcortical functional network organization. *NeuroImage*, *185*(October 2018), 35–57. https://doi.org/10.1016/j.neuroimage.2018.10.006

Jiang, L. P., & Rao, R. P. N. (2024). Dynamic predictive coding: A model of hierarchical sequence learning and prediction in the neocortex. *PLoS Computational Biology*, *20*(2), 1–30. https://doi.org/10.1371/journal.pcbi.1011801

Jiang, Q., & Ma, L. (2024). Swiping More, Thinking Less: Using TikTok Hinders Analytic Thinking. *Cyberpsychology*, *18*(3). https://doi.org/10.5817/CP2024-3-1

Jiao, Z., Wang, H., Cai, M., Cao, Y., Zou, L., & Wang, S. (2020). Rich club characteristics of dynamic brain functional networks in resting state. *Multimedia Tools and Applications*, *79*(21–22), 15075–15093. https://doi.org/10.1007/s11042-018-6424-4

Jin, C., Li, Y., Yin, Y., Ma, T., Hong, W., Liu, Y., Li, N., Zhang, Xinyue, Gao, J. H., Zhang, Xiaochu, & Zha, R. (2024). The dorsomedial prefrontal cortex promotes self-control by inhibiting the egocentric perspective. *NeuroImage*, *301*(July), 120879. https://doi.org/10.1016/j.neuroimage.2024.120879

Jones, D. K., & Cercignani, M. (2010). Twenty-five pitfalls in the analysis of diffusion MRI data. *NMR in Biomedicine*, *23*(7), 803–820. https://doi.org/10.1002/nbm.1543

Jones, D. K., Knösche, T. R., & Turner, R. (2013). White matter integrity, fiber count, and other fallacies: The do's and don'ts of diffusion MRI. *NeuroImage*, *73*, 239–254. https://doi.org/10.1016/j.neuroimage.2012.06.081

Joyce, K. E., Hayasaka, S., & Laurienti, P. J. (2013). The Human Functional Brain Network Demonstrates Structural and Dynamical Resilience to Targeted Attack. *PLoS Computational Biology*, *9*(1), 1–11. https://doi.org/10.1371/journal.pcbi.1002885

Kai, J., Khan, A. R., Haast, R. A., & Lau, J. C. (2022). Mapping the subcortical connectome using in vivo diffusion MRI: Feasibility and reliability. *NeuroImage*, *262*(March), 119553. https://doi.org/10.1016/j.neuroimage.2022.119553

Kaiser, M., & Hilgetag, C. C. (2006). Nonoptimal component placement, but short processing paths, due to long-distance projections in neural systems. *PLoS Computational Biology*, *2*(7), 0805–0815. https://doi.org/10.1371/journal.pcbi.0020095

Kantonen, T., Karjalainen, T., Isojärvi, J., Nuutila, P., Tuisku, J., Rinne, J., Hietala, J., Kaasinen, V., Kalliokoski, K., Scheinin, H., Hirvonen, J., Vehtari, A., & Nummenmaa, L. (2020). Interindividual variability and lateralization of μ-opioid receptors in the human brain. *NeuroImage*, *217*, 116922. https://doi.org/10.1016/j.neuroimage.2020.116922

Karolis, V. R., Froudist-Walsh, S., Brittain, P. J., Kroll, J., Ball, G., Edwards, A. D., Dell'Acqua, F., Williams, S. C., Murray, R. M., & Nosarti, C. (2016). Reinforcement of the Brain's Rich-Club Architecture Following Early Neurodevelopmental Disruption Caused by Very Preterm Birth. *Cerebral Cortex*, *26*(3), 1322–1335. https://doi.org/10.1093/cercor/bhv305

Kayser, C., Petkov, C. I., Augath, M., & Logothetis, N. K. (2005). Integration of touch and sound in auditory cortex. *Neuron*, *48*(2), 373–384. https://doi.org/10.1016/j.neuron.2005.09.018

Keller, A. S., Sydnor, V. J., Pines, A., Fair, D. A., Bassett, D. S., & Satterthwaite, T. D. (2023). Hierarchical functional system development supports executive function. *Trends in Cognitive Sciences*, *27*(2), 160–174. https://doi.org/10.1016/j.tics.2022.11.005

Keown, C. L., Datko, M. C., Chen, C. P., Maximo, J. O., Jahedi, A., & Müller, R.-A. (2017). Network Organization Is Globally Atypical in Autism: A Graph Theory Study of Intrinsic Functional Connectivity. *Biological Psychiatry: Cognitive Neuroscience and Neuroimaging*, *2*(1), 66–75. https://doi.org/10.1016/j.bpsc.2016.07.008

Khalilian, M., Kazemi, K., Fouladivanda, M., Makki, M., Helfroush, M. S., & Aarabi, A. (2021). Effect of multishell diffusion mri acquisition strategy and parcellation scale on rich-club organization of human brain structural networks. *Diagnostics*, *11*(6). https://doi.org/10.3390/diagnostics11060970

Kiebel, S. J., Daunizeau, J., & Friston, K. J. (2008). A hierarchy of time-scales and the brain. *PLoS Computational Biology*, *4*(11). https://doi.org/10.1371/journal.pcbi.1000209

Kim, D. J., Davis, E. P., Sandman, C. A., Sporns, O., O'Donnell, B. F., Buss, C., & Hetrick, W. P. (2014). Longer gestation is associated with more efficient brain networks in preadolescent children. *NeuroImage*, *100*, 619–627. https://doi.org/10.1016/j.neuroimage.2014.06.048

Kim, D. J., Davis, E. P., Sandman, C. A., Sporns, O., O'Donnell, B. F., Buss, C., & Hetrick, W. P. (2016). Children's intellectual ability is associated with structural network integrity. *NeuroImage*, *124*, 550–556. https://doi.org/10.1016/j.neuroimage.2015.09.012

Kim, D. J., & Min, B. K. (2020). Rich-club in the brain's macrostructure: Insights from graph theoretical analysis. *Computational and Structural Biotechnology Journal*, *18*, 1761–1773. https://doi.org/10.1016/j.csbj.2020.06.039

Kim, W., Chang, Y., Kim, J., Seo, J., Ryu, K., Lee, E., Woo, M., & Janelle, C. M. (2014). An fMRI study of differences in brain activity among elite, expert, and novice archers at the moment of optimal aiming. *Cognitive and Behavioral Neurology*, *27*(4), 173–182. https://doi.org/10.1097/WNN.0000000000000042

Klamer, K., Craig, J., Haines, C., Sullivan, K. A., & Ekstrand, C. (2024a). Psychological well-being modulates neural synchrony during naturalistic fMRI. *Neuropsychologia*, *204*(January), 108987. https://doi.org/10.1016/j.neuropsychologia.2024.108987

Klamer, K., Craig, J., Haines, C., Sullivan, K. A., & Ekstrand, C. (2024b). Trait-Level Somatic Anxiety Modulates Functional Magnetic Resonance Imaging (fMRI) Neural Synchrony to Naturalistic Stimuli. *Behavioral Neuroscience*, *138*(6), 409–419. https://doi.org/10.1037/bne0000615

Klamer, K., Craig, J., Haines, C., Sullivan, K. A., Seres, P., & Ekstrand, C. (2025). Differential fMRI neural synchrony associated with migraine during naturalistic stimuli with negative emotional valence. *Journal of Headache and Pain*, *26*(1). https://doi.org/10.1186/s10194-025-01993-6

Knösche, T. R., & Tittgemeyer, M. (2011). The role of long-range connectivity for the characterization of the functional-anatomical organization of the cortex. *Frontiers in Systems Neuroscience*, *5*(JULY 2011), 1–13. https://doi.org/10.3389/fnsys.2011.00058

Koch, P. J., Frey, B. M., Backhaus, W., Petersen, N., Girard, G., Wróbel, P. P., Braaß, H., Bönstrup, M., Kunkel genannt Bode, L., Cheng, B., Thomalla, G., Gerloff, C., Schacht, H., Schramm, P., Royl, G., Quandt, F., & Schulz, R. (2025). Neurotransmitter-informed connectivity maps and their application for outcome inference after stroke. *Brain*, *148*(11), 3935–3945. https://doi.org/10.1093/brain/awaf185

Koch, P. J., Girard, G., Brügger, J., Cadic-Melchior, A. G., Beanato, E., Park, C. H., Morishita, T., Wessel, M. J., Pizzolato, M., Canales-Rodríguez, E. J., Fischi-Gomez, E., Schiavi, S., Daducci, A., Piredda, G. F., Hilbert, T., Kober, T., Thiran, J. P., & Hummel, F. C. (2022). Evaluating reproducibility and subject-specificity of microstructure-informed connectivity. *NeuroImage*, *258*(May), 119356. https://doi.org/10.1016/j.neuroimage.2022.119356

Kocher, M., Gleichgerrcht, E., Nesland, T., Rorden, C., Fridriksson, J., Spampinato, M. V., & Bonilha, L. (2015). Individual variability in the anatomical distribution of nodes participating in rich club structural networks. *Frontiers in Neural Circuits*, *9*(APR), 1–7. https://doi.org/10.3389/fncir.2015.00016

Koechlin, E., Basso, G., Pietrini, P., Panzer, S., & Grafman, J. (1999). The role of the anterior prefrontal cortex in human cognition. *Nature*, *399*(6732), 148–151. https://doi.org/10.1038/20178

Koechlin, E., Ody, C., & Kouneiher, F. (2003). The Architecture of Cognitive Control in the Human Prefrontal Cortex. *Science*, *302*(5648), 1181–1185. https://doi.org/10.1126/science.1088545

Koechlin, E., & Summerfield, C. (2007). An information theoretical approach to prefrontal executive function. *Trends in Cognitive Sciences*, *11*(6), 229–235. https://doi.org/10.1016/j.tics.2007.04.005

Korte, M. (2020). The impact of the digital revolution on human brain and behavior: Where do we stand? *Dialogues in Clinical Neuroscience*, *22*(2), 101–111. https://doi.org/10.31887/DCNS.2020.22.2/mkorte

Krienen, F. M., Yeo, B. T. T., Ge, T., Buckner, R. L., & Sherwood, C. C. (2016). Transcriptional profiles of supragranular-enriched genes associate with corticocortical network architecture in the human brain. *Proceedings of the National Academy of Sciences of the United States of America*, *113*(4), E469–E478. https://doi.org/10.1073/pnas.1510903113

Kühn, A. B., & Schubotz, R. I. (2012). Temporally remote destabilization of prediction after rare breaches of expectancy. *Human Brain Mapping*, *33*(8), 1812–1820. https://doi.org/10.1002/hbm.21325

Lancichinetti, A., Fortunato, S., & Kertész, J. (2009). Detecting the overlapping and hierarchical community structure in complex networks. *New Journal of Physics*, *11*. https://doi.org/10.1088/1367-2630/11/3/033015

Larivière, S., Vos De Wael, R., Paquola, C., Hong, S. J., Mišić, B., Bernasconi, N., Bernasconi, A., Bonilha, L., & Bernhardt, B. C. (2019). Microstructure-informed connectomics: Enriching large-scale descriptions of healthy and diseased brains. *Brain Connectivity*, *9*(2), 113–127. https://doi.org/10.1089/brain.2018.0587

Latora, V., & Marchiori, M. (2001). Efficient behavior of small-world networks. *Physical Review Letters*, *87*(19), 198701-1-198701–198704. https://doi.org/10.1103/PhysRevLett.87.198701

Lawson, R. P., Mathys, C., & Rees, G. (2017). Adults with autism overestimate the volatility of the sensory environment. *Nature Neuroscience*, *20*(9), 1293–1299. https://doi.org/10.1038/nn.4615

Le Bihan, D. (2003). Looking into the functional architecture of the brain with diffusion MRI. *Nature Reviews Neuroscience*, *4*(6), 469–480. https://doi.org/10.1038/nrn1119

Le Bihan, D., Breton, E., Lallemand, D., Grenier, P., Cabanis, E., & Laval-Jeantet, M. (1986). MR imaging of intravoxel incoherent motions: application to diffusion and perfusion in neurologic disorders. *Radiology*, *161*(2), 401–407. https://doi.org/10.1148/radiology.161.2.3763909

Le Bihan, D., Mangin, J. F., Poupon, C., Clark, C. A., Pappata, S., Molko, N., & Chabriat, H. (2001). Diffusion tensor imaging: Concepts and applications. *Journal of Magnetic Resonance Imaging*, *13*(4), 534–546. https://doi.org/10.1002/jmri.1076

Lee, W. J., Han, C. E., Aganj, I., Seo, S. W., & Seong, J. K. (2018). Distinct Patterns of Rich Club Organization in Alzheimer's Disease and Subcortical Vascular Dementia: A White Matter Network Study. *Journal of Alzheimer's Disease*, *63*(3), 977–987. https://doi.org/10.3233/JAD-180027

Lee, Y., & Chen, J. (2024). The Relationship between Event Boundary Strength and Pattern Shifts across the Cortical Hierarchy during Naturalistic Movie-viewing. *Journal of Cognitive Neuroscience*, *36*(11), 2317–2342. https://doi.org/10.1162/jocn_a_02213

Leech, R., Braga, R., & Sharp, D. J. (2012). Echoes of the brain within the posterior cingulate cortex. *Journal of Neuroscience*, *32*(1), 215–222. https://doi.org/10.1523/JNEUROSCI.3689-11.2012

Leech, R., & Sharp, D. J. (2014). The role of the posterior cingulate cortex in cognition and disease. *Brain*, *137*(1), 12–32. https://doi.org/10.1093/brain/awt162

Leech, R., & Smallwood, J. (2019). The posterior cingulate cortex: Insights from structure and function. In *Handbook of Clinical Neurology* (1st ed., Vol. 166). Elsevier B.V. https://doi.org/10.1016/B978-0-444-64196-0.00005-4

Lerdahl, F., & Jackendoff, R. S. (1996). Grouping Structure. In *A Generative Theory of Tonal Music* (Number November, pp. 36–67). The MIT Press. https://doi.org/10.7551/mitpress/12513.003.0005

Lerner, Y., Honey, C. J., Katkov, M., & Hasson, U. (2014). Temporal scaling of neural responses to compressed and dilated natural speech. *Journal of Neurophysiology*, *111*(12), 2433–2444. https://doi.org/10.1152/jn.00497.2013

Lerner, Y., Honey, C. J., Silbert, L. J., & Hasson, U. (2011). Topographic mapping of a hierarchy of temporal receptive windows using a narrated story. *Journal of Neuroscience*, *31*(8), 2906–2915. https://doi.org/10.1523/JNEUROSCI.3684-10.2011

Levy, J., Goldstein, A., Influs, M., Masalha, S., Zagoory-Sharon, O., & Feldman, R. (2016). Adolescents growing up amidst intractable conflict attenuate brain response to pain of outgroup. *Proceedings of the National Academy of Sciences of the United States of America*, *113*(48), 13696–13701. https://doi.org/10.1073/pnas.1612903113

Li, F., Liu, Y., Lu, L., Shang, S., Chen, H., Haidari, N. A., Wang, P., Yin, X., & Chen, Y. C. (2022). Rich-club reorganization of functional brain networks in acute mild traumatic brain injury with cognitive impairment. *Quantitative Imaging in Medicine and Surgery*, *12*(7), 3932–3946. https://doi.org/10.21037/qims-21-915

Li, K., Liu, L., Yin, Q., Dun, W., Xu, X., Liu, J., & Zhang, M. (2017). Abnormal rich club organization and impaired correlation between structural and functional connectivity in migraine sufferers. *Brain Imaging and Behavior*, *11*(2), 526–540. https://doi.org/10.1007/s11682-016-9533-6

Li, L. Y., Grzelak, L. N., Auerbach, R. P., & Shankman, S. A. (2025). Siblings' similarity in neural responses to loss reflects mechanisms of familial transmission for depression. *Journal of Psychiatric Research*, *181*(November 2024), 286–293. https://doi.org/10.1016/j.jpsychires.2024.11.069

Li, X., Zhu, Y., Vuoriainen, E., Ye, C., & Astikainen, P. (2021). Decreased intersubject synchrony in dynamic valence ratings of sad movie contents in dysphoric individuals. *Scientific Reports*, *11*(1), 1–13. https://doi.org/10.1038/s41598-021-93825-1

Liang, X., Hsu, L. M., Lu, H., Sumiyoshi, A., He, Y., & Yang, Y. (2018). The Rich-Club Organization in Rat Functional Brain Network to Balance between Communication Cost and Efficiency. *Cerebral Cortex*, *28*(3), 924–935. https://doi.org/10.1093/cercor/bhw416

Liang, X., Yeh, C. H., Connelly, A., & Calamante, F. (2019). Robust Identification of Rich-Club Organization in Weighted and Dense Structural Connectomes. *Brain Topography*, *32*(1), 1–16. https://doi.org/10.1007/s10548-018-0661-8

Lin, J., Swart, J., & Zeng, G. (2023). Theorising TikTok cultures: Neuro-images in the era of short videos. *Media, Culture and Society*, *45*(8), 1550–1567. https://doi.org/10.1177/01634437231202167

Lin, P., Yang, Y., Jovicich, J., De Pisapia, N., Wang, X., Zuo, C. S., & Levitt, J. J. (2016). Static and dynamic posterior cingulate cortex nodal topology of default mode network predicts attention task performance. *Brain Imaging and Behavior*, *10*(1), 212–225. https://doi.org/10.1007/s11682-015-9384-6

Liu, Z. Q., Vázquez-Rodríguez, B., Spreng, R. N., Bernhardt, B. C., Betzel, R. F., & Misic, B. (2022). Time-resolved structure-function coupling in brain networks. *Communications Biology*, *5*(1), 1–10. https://doi.org/10.1038/s42003-022-03466-x

Loh, K. K., & Kanai, R. (2016). How Has the Internet Reshaped Human Cognition? *Neuroscientist*, *22*(5), 506–520. https://doi.org/10.1177/1073858415595005

Lohia, K., Soans, R. S., Saxena, R., Mahajan, K., & Gandhi, T. K. (2024). Distinct rich and diverse clubs regulate coarse and fine binocular disparity processing: Evidence from stereoscopic task-based fMRI. *IScience*, 109831. https://doi.org/10.1016/j.isci.2024.109831

Lohmann, G., Butzin, M., Eissner, N., Shi, X., & Stepanek, C. (2020). Abrupt Climate and Weather Changes Across Time Scales. *Paleoceanography and Paleoclimatology*, *35*(9), 1–38. https://doi.org/10.1029/2019PA003782

Lopes, M. A., Richardson, M. P., Abela, E., Rummel, C., Schindler, K., Goodfellow, M., & Terry, J. R. (2017). An optimal strategy for epilepsy surgery: Disruption of the rich-club? *PLoS Computational Biology*, *13*(8), e1005637. https://doi.org/10.1371/journal.pcbi.1005637

Loschky, L. C., Larson, A. M., Smith, T. J., & Magliano, J. P. (2020). The Scene Perception & Event Comprehension Theory (SPECT) Applied to Visual Narratives. *Topics in Cognitive Science*, *12*(1), 311–351. https://doi.org/10.1111/tops.12455

Lu, K. H., Hung, S. C., Wen, H., Marussich, L., & Liu, Z. (2016). Influences of high-level features, gaze, and scene transitions on the reliability of BOLD responses to natural movie stimuli. *PLoS ONE*, *11*(8), 1–19. https://doi.org/10.1371/journal.pone.0161797

Ludwigs, M. (2020). Hierarchical Thinking, Grammatical Structures, and the Originary Scene. *... : The Journal of Generative Anthropology*, (2), 1–15. https://search.ebscohost.com/login.aspx?direct=true&profile=ehost&scope=site&authtype=crawler&jrnl=10837264&AN=143353825&h=Xky38kxzpIfQlKRssQNpxCfWZA4Fq35O1ktR4GhPFwSwk3vRAPCv%2FDBAMzPOBMJRGrLQWFtxcjKRbfM%2FgsppzQ%3D%3D&crl=c

Lurie, D. J., Pappas, I., & D'Esposito, M. (2024). Cortical timescales and the modular organization of structural and functional brain networks. *Human Brain Mapping*, *45*(2). https://doi.org/10.1002/hbm.26587

Lydon-Staley, D. M., & Bassett, D. S. (2018). Network Neuroscience: A Framework for Developing Biomarkers in Psychiatry. In *Brain Imaging in Behavioral Neuroscience* (Number November 2011, pp. 79–109). https://doi.org/10.1007/7854_2018_41

Ma, J., Kang, H. J., Kim, J. Y., Jeong, H. S., Im, J. J., Namgung, E., Kim, M. J., Lee, S., Kim, T. D., Oh, J. K., Chung, Y. A., Lyoo, I. K., Lim, S. M., & Yoon, S. (2017). Network attributes underlying intellectual giftedness in the developing brain. *Scientific Reports*, *7*(1), 1–9. https://doi.org/10.1038/s41598-017-11593-3

Maffei, C., Girard, G., Schilling, K. G., Aydogan, D. B., Adluru, N., Zhylka, A., Wu, Y., Mancini, M., Hamamci, A., Sarica, A., Teillac, A., Baete, S. H., Karimi, D., Yeh, F. C., Yildiz, M. E., Gholipour, A., Bihan-Poudec, Y., Hiba, B., Quattrone, Andrea, ... Yendiki, Anastasia. (2022). Insights from the IronTract challenge: Optimal methods for mapping brain pathways from multi-shell diffusion MRI. *NeuroImage*, *257*(May). https://doi.org/10.1016/j.neuroimage.2022.119327

Magliano, J. P., & Zacks, J. M. (2011). The impact of continuity editing in narrative film on event segmentation. *Cognitive Science*, *35*(8), 1489–1517. https://doi.org/10.1111/j.1551-6709.2011.01202.x

Maguire, E. A., Gadian, D. G., Johnsrude, I. S., Good, C. D., Ashburner, J., Frackowiak, R. S. J., & Frith, C. D. (2000). Navigation-related structural change in the hippocampi of taxi drivers. *Proceedings of the National Academy of Sciences of the United States of America*, *97*(8), 4398–4403. https://doi.org/10.1073/pnas.070039597

Maier-Hein, K. H., Neher, P. F., Houde, J. C., Côté, M. A., Garyfallidis, E., Zhong, J., Chamberland, M., Yeh, F. C., Lin, Y. C., Ji, Q., Reddick, W. E., Glass, J. O., Chen, D. Q., Feng, Y., Gao, C., Wu, Y., Ma, J., Renjie, H., Li, Q., … Descoteaux, M. (2017). The challenge of mapping the human connectome based on diffusion tractography. *Nature Communications* , *8*(1). https://doi.org/10.1038/s41467-017-01285-x

Mancini, M., Giulietti, G., Dowell, N., Spanò, B., Harrison, N., Bozzali, M., & Cercignani, M. (2018). Introducing axonal myelination in connectomics: A preliminary analysis of g-ratio distribution in healthy subjects. *NeuroImage*, *182*(September 2017), 351–359. https://doi.org/10.1016/j.neuroimage.2017.09.018

Manea, A. M. G., Zilverstand, A., Ugurbil, K., Heilbronner, S. R., & Zimmermann, J. (2022). Intrinsic timescales as an organizational principle of neural processing across the whole rhesus macaque brain. *ELife*, *11*, 1–20. https://doi.org/10.7554/eLife.75540

Mansour L, S., Tian, Y., Yeo, B. T. T., Cropley, V., & Zalesky, A. (2021). High-resolution connectomic fingerprints: Mapping neural identity and behavior. *NeuroImage*, *229*(December 2020), 117695. https://doi.org/10.1016/j.neuroimage.2020.117695

Marek, S., & Dosenbach, N. U. F. (2018). The frontoparietal network: Function, electrophysiology, and importance of individual precision mapping. *Dialogues in Clinical Neuroscience*, *20*(2), 133–141. https://doi.org/10.31887/dcns.2018.20.2/smarek

Margulies, D. S., Ghosh, S. S., Goulas, A., Falkiewicz, M., Huntenburg, J. M., Langs, G., Bezgin, G., Eickhoff, S. B., Castellanos, F. X., Petrides, M., Jefferies, E., & Smallwood, J. (2016). Situating the default-mode network along a principal gradient of macroscale cortical organization. *Proceedings of the National Academy of Sciences of the United States of America*, *113*(44), 12574–12579. https://doi.org/10.1073/pnas.1608282113

Markello, R. D., Hansen, J. Y., Liu, Z. Q., Bazinet, V., Shafiei, G., Suárez, L. E., Blostein, N., Seidlitz, J., Baillet, S., Satterthwaite, T. D., Chakravarty, M. M., Raznahan, A., & Misic, B. (2022). Neuromaps: Structural and Functional Interpretation of Brain Maps. *Nature Methods*, *19*(11), 1472–1479. https://doi.org/10.1038/s41592-022-01625-w

Markett, S., Jawinski, P., Kirsch, P., & Gerchen, M. F. (2020). Specific and segregated changes to the functional connectome evoked by the processing of emotional faces: A task-based connectome study. *Scientific Reports*, *10*(1), 1–14. https://doi.org/10.1038/s41598-020-61522-0

Markov, N. T., & Kennedy, H. (2013). The importance of being hierarchical. *Current Opinion in Neurobiology*, *23*(2), 187–194. https://doi.org/10.1016/j.conb.2012.12.008

Markov, N. T., Vezoli, J., Chameau, P., Falchier, A., Quilodran, R., Huissoud, C., Lamy, C., Misery, P., Giroud, P., Ullman, S., Barone, P., Dehay, C., Knoblauch, K., & Kennedy, H. (2014). Anatomy of hierarchy: Feedforward and feedback pathways in macaque visual cortex. *Journal of Comparative Neurology*, *522*(1), 225–259. https://doi.org/10.1002/cne.23458

Martins, L. C. X., Russo, M. T., & Ribeiro, P. (2023). Neural Correlates of Shooting Sports Performance: A Systematic Review on Neural Efficiency Hypothesis. *Revista de Educação Física / Journal of Physical Education*, *91*(4), 350–374. https://doi.org/10.37310/ref.v91i4.2915

Mas, J., & Fernandez, G. (2003). VIDEO SHOT BOUNDARY DETECTION BASED ON COLOR HISTOGRAM. *TRECVID 2003: Notebook Papers*. https://www-nlpir.nist.gov/projects/tvpubs/tvpapers03/ramonlull.paper.pdf

Mattar, M. G., Kahn, D. A., Thompson-Schill, S. L., & Aguirre, G. K. (2016). Varying Timescales of Stimulus Integration Unite Neural Adaptation and Prototype Formation. *Current Biology*, *26*(13), 1669–1676. https://doi.org/10.1016/j.cub.2016.04.065

Matz, S. C., Hyon, R., Baek, E. C., Parkinson, C., & Cerf, M. (2022). Personality similarity predicts synchronous neural responses in fMRI and EEG data. *Scientific Reports*, *12*(1), 1–13. https://doi.org/10.1038/s41598-022-18237-1

McAuley, J. J., Da Fontoura Costa, L., & Caetano, T. S. (2007). Rich-club phenomenon across complex network hierarchies. *Applied Physics Letters*, *91*(8). https://doi.org/10.1063/1.2773951

Mecklenbrauck, F., Gruber, M., Siestrup, S., Zahedi, A., Grotegerd, D., Mauritz, M., Trempler, I., Dannlowski, U., & Schubotz, R. I. (2024). The significance of structural rich club hubs for the processing of hierarchical stimuli. *Human Brain Mapping*, *45*(4), 1–28. https://doi.org/10.1002/hbm.26543

Mecklenbrauck, F., & Schubotz, R. I. (2026). *Time Points or Plot Points – Are movies processed according to their temporal duration or their underlying content structure?* [Manuscript under review]. *NeuroImag*e.

Mecklenbrauck, F., Sepulcre, J., Fehring, J., & Schubotz, R. I. (2024). Decoding cortical chronotopy—Comparing the influence of different cortical organizational schemes. *NeuroImage*, *303*(October), 120914. https://doi.org/10.1016/j.neuroimage.2024.120914

Meier, J., Tewarie, P., Hillebrand, A., Douw, L., Van Dijk, B. W., Stufflebeam, S. M., & Van Mieghem, P. (2016). A Mapping between Structural and Functional Brain Networks. *Brain Connectivity*, *6*(4), 298–311. https://doi.org/10.1089/brain.2015.0408

Meng, B., & Rezaeipanah, A. (2025). Development of a multidimensional centrality metric for ranking nodes in complex networks. *Chaos, Solitons and Fractals*, *191*(November 2024), 115843. https://doi.org/10.1016/j.chaos.2024.115843

Messé, A. (2020). Parcellation influence on the connectivity-based structure–function relationship in the human brain. *Human Brain Mapping*, *41*(5), 1167–1180. https://doi.org/10.1002/hbm.24866

Mesulam, M. M. (1998). From sensation to cognition. *Brain*, *121*(6), 1013–1052. https://doi.org/10.1093/brain/121.6.1013

Meunier, D., Lambiotte, R., Fornito, A., Ersche, K. D., & Bullmore, E. T. (2009). Hierarchical modularity in human brain functional networks. *Frontiers in Neuroinformatics*, *3*(OCT), 1–12. https://doi.org/10.3389/neuro.11.037.2009

Milgram, S. (1967). The small-world problem. In *PsycEXTRA Dataset* (Vol. 55, Number 1, pp. 407–410). https://doi.org/10.1037/e400002009-005

Mišić, B., Sporns, O., & McIntosh, A. R. (2014). Communication Efficiency and Congestion of Signal Traffic in Large-Scale Brain Networks. *PLoS Computational Biology*, *10*(1). https://doi.org/10.1371/journal.pcbi.1003427

Moeller, S., Yacoub, E., Olman, C. A., Auerbach, E., Strupp, J., Harel, N., & Uğurbil, K. (2010). Multiband multislice GE-EPI at 7 tesla, with 16-fold acceleration using partial parallel imaging with application to high spatial and temporal whole-brain fMRI. *Magnetic Resonance in Medicine*, *63*(5), 1144–1153. https://doi.org/10.1002/mrm.22361

Morone, F., & Makse, H. A. (2015). Influence maximization in complex networks through optimal percolation. *Nature*, *524*(7563), 65–68. https://doi.org/10.1038/nature14604

Morone, F., Roth, K., Min, B., Stanley, H. E., & Makse, H. A. (2017). Model of brain activation predicts the neural collective influence map of the brain. *Proceedings of the National Academy of Sciences of the United States of America*, *114*(15), 3849–3854. https://doi.org/10.1073/pnas.1620808114

Moura, J. M. B., da Silva, R. H., Ferreira Júnior, W. S., da Silva, T. C., & Albuquerque, U. P. (2021). Memory for medicinal plants remains in ancient and modern environments suggesting an evolved adaptedness. *PLoS ONE*, *16*(10 October), 1–15. https://doi.org/10.1371/journal.pone.0258986

Mueller, S., Wang, D., Fox, M. D., Pan, R., Lu, J., Li, K., Sun, W., Buckner, R. L., & Liu, H. (2015). Reliability correction for functional connectivity: Theory and implementation. *Human Brain Mapping*, *36*(11), 4664–4680. https://doi.org/10.1002/hbm.22947

Müller, V. I., Cieslik, E. C., Turetsky, B. I., & Eickhoff, S. B. (2012). Crossmodal interactions in audiovisual emotion processing. *NeuroImage*, *60*(1), 553–561. https://doi.org/10.1016/j.neuroimage.2011.12.007

Murray, J. D., Bernacchia, A., Freedman, D. J., Romo, R., Wallis, J. D., Cai, X., Padoa-Schioppa, C., Pasternak, T., Seo, H., Lee, D., & Wang, X. J. (2014). A hierarchy of intrinsic timescales across primate cortex. *Nature Neuroscience*, *17*(12), 1661–1663. https://doi.org/10.1038/nn.3862

Naganawa, M., Nabulsi, N., Henry, S., Matuskey, D., Lin, S. F., Slieker, L., Schwarz, A. J., Kant, N., Jesudason, C., Ruley, K., Navarro, A., Gao, H., Ropchan, J., Labaree, D., Carson, R. E., & Huang, Y. (2021). First-in-human assessment of 11c-lsn3172176, an m1 muscarinic acetylcholine receptor pet radiotracer. *Journal of Nuclear Medicine*, *62*(4), 553–560. https://doi.org/10.2967/jnumed.120.246967

Nairne, J. S., & Pandeirada, J. N. S. (2010). Adaptive memory: Ancestral priorities and the mnemonic value of survival processing. *Cognitive Psychology*, *61*(1), 1–22. https://doi.org/10.1016/j.cogpsych.2010.01.005

Nasr, S., Devaney, K. J., & Tootell, R. B. H. (2013). Spatial encoding and underlying circuitry in scene-selective cortex. *NeuroImage*, *83*, 892–900. https://doi.org/10.1016/j.neuroimage.2013.07.030

Nastase, S. A., Gazzola, V., Hasson, U., & Keysers, C. (2019). Measuring shared responses across subjects using intersubject correlation. *Social Cognitive and Affective Neuroscience*, *14*(6), 669–687. https://doi.org/10.1093/scan/nsz037

Nee, D. E. (2021). Integrative frontal-parietal dynamics supporting cognitive control. *ELife*, *10*, 1–35. https://doi.org/10.7554/eLife.57244

Nee, D. E., & Brown, J. W. (2013). Dissociable frontal-striatal and frontal-parietal networks involved in updating hierarchical contexts in working memory. *Cerebral Cortex*, *23*(9), 2146–2158. https://doi.org/10.1093/cercor/bhs194

Nee, D. E., & D'Esposito, M. (2016). The hierarchical organization of the lateral prefrontal cortex. *ELife*, *5*(MARCH2016), 1–26. https://doi.org/10.7554/eLife.12112

Nelson, M. C., Royer, J., da Lu, W., Leppert, I. R., Campbell, J. S. W., Schiavi, S., Jin, H., Tavakol, S., Vos de Wael, R., Rodriguez-Cruces, R., Pike, G. B., Bernhardt, B. C., Daducci, A., Misic, B., & Tardif, C. L. (2023). The human brain connectome weighted by the myelin content and total intra-axonal cross-sectional area of white matter tracts. *Network Neuroscience*, *7*(4), 1363–1388. https://doi.org/10.1162/netn_a_00330

Newman, M. E. J. (2002). Assortative Mixing in Networks. *Physical Review Letters*, *89*(20), 1–4. https://doi.org/10.1103/PhysRevLett.89.208701

Newman, M. E. J. (2004). Fast algorithm for detecting community structure in networks. *Physical Review E - Statistical Physics, Plasmas, Fluids, and Related Interdisciplinary Topics*, *69*(6), 5. https://doi.org/10.1103/PhysRevE.69.066133

Nguyen, L., Walters, J., Paul, S., Monreal Ijurco, S., Rainey, G. E., Parekh, N., Blair, G., & Darrah, M. (2025). Feeds, feelings, and focus: A systematic review and meta-analysis examining the cognitive and mental health correlates of short-form video use. *Psychological Bulletin*, *151*(9), 1125–1146. https://doi.org/10.1037/bul0000498

Nigam, S., Shimono, M., Ito, S., Yeh, F. C., Timme, N., Myroshnychenko, M., Lapish, C. C., Tosi, Z., Hottowy, P., Smith, W. C., Masmanidis, S. C., Litke, A. M., Sporns, O., & Beggs, J. M. (2016). Rich-club organization in effective connectivity among cortical neurons. *Journal of Neuroscience*, *36*(3), 655–669. https://doi.org/10.1523/JNEUROSCI.2177-15.2016

Norman-Haignere, S. V., Long, L. K., Devinsky, O., Doyle, W., Irobunda, I., Merricks, E. M., Feldstein, N. A., McKhann, G. M., Schevon, C. A., Flinker, A., & Mesgarani, N. (2022). Multiscale temporal integration organizes hierarchical computation in human auditory cortex. *Nature Human Behaviour*, *6*(3), 455–469. https://doi.org/10.1038/s41562-021-01261-y

Nummenmaa, L., Lahnakoski, J. M., & Glerean, E. (2018). Sharing the social world via intersubject neural synchronisation. *Current Opinion in Psychology*, *24*, 7–14. https://doi.org/10.1016/j.copsyc.2018.02.021

Numssen, O., Bzdok, D., & Hartwigsen, G. (2021). Functional specialization within the inferior parietal lobes across cognitive domains. *ELife*, *10*, 1–25. https://doi.org/10.7554/eLife.63591

O'Donoghue, S., Kilmartin, L., O'Hora, D., Emsell, L., Langan, C., McInerney, S., Forde, N. J., Leemans, A., Jeurissen, B., Barker, G. J., McCarthy, P., Cannon, D. M., & McDonald, C. (2017). Anatomical integration and rich-club connectivity in euthymic bipolar disorder. *Psychological Medicine*, *47*(9), 1609–1623. https://doi.org/10.1017/S0033291717000058

Oetringer, D., Gözükara, D., Güçlü, U., & Geerligs, L. (2025). The neural basis of event segmentation: Stable features in the environment are reflected by neural states. *Imaging Neuroscience*, *3*(February). https://doi.org/10.1162/imag_a_00432

Ogawa, T., & Komatsu, H. (2010). Differential temporal storage capacity in the baseline activity of neurons in macaque frontal eye field and area V4. *Journal of Neurophysiology*, *103*(5), 2433–2445. https://doi.org/10.1152/jn.01066.2009

Ohad, T., Zvi, Y., & Yeshurun, Y. (2025). Default mode network synchrony reflects shared understanding. *Current Opinion in Behavioral Sciences*, *64*, 101540. https://doi.org/10.1016/j.cobeha.2025.101540

Oldham, S., & Fornito, A. (2023). Hubs and rich clubs. In *Connectome Analysis: Characterization, Methods, and Analysis*. INC. https://doi.org/10.1016/B978-0-323-85280-7.00015-4

Oldham, S., Fulcher, B., Parkes, L., Arnatkeviciūtė, A., Suo, C., & Fornito, A. (2019). Consistency and differences between centrality measures across distinct classes of networks. *PLoS ONE*, *14*(7), 1–23. https://doi.org/10.1371/journal.pone.0220061

Palla, G., Derényi, I., Farkas, I., & Vicsek, T. (2005). Uncovering the overlapping community structure of complex networks in nature and society. *Nature*, *435*(7043), 814–818. https://doi.org/10.1038/nature03607

Pandya, S., Kuceyeski, A., & Raj, A. (2017). The Brain's Structural Connectome Mediates the Relationship between Regional Neuroimaging Biomarkers in Alzheimer's Disease. *Journal of Alzheimer's Disease*, *55*(4), 1639–1657. https://doi.org/10.3233/JAD-160090

Paquola, C., Seidlitz, J., Benkarim, O., Royer, J., Klimes, P., Bethlehem, R. A. I., Larivière, S., de Wael, R. V., Rodríguez-Cruces, R., Hall, J. A., Frauscher, B., Smallwood, J., & Bernhardt, B. C. (2020). A multi-scale cortical wiring space links cellular architecture and functional dynamics in the human brain. In *PLoS Biology* (Vol. 18, Number 11). https://doi.org/10.1371/journal.pbio.3000979

Paquola, C., Vos De Wael, R., Wagstyl, K., Bethlehem, R. A. I., Hong, S. J., Seidlitz, J., Bullmore, E. T., Evans, A. C., Misic, B., Margulies, D. S., Smallwood, J., & Bernhardt, B. C. (2019). Microstructural and functional gradients are increasingly dissociated in transmodal cortices. *PLoS Biology*, *17*(5), 1–28. https://doi.org/10.1371/journal.pbio.3000284

Park, H.-J., & Friston, K. (2013). Structural and Functional Brain Networks: From Connections to Cognition. *Science*, *342*(6158). https://doi.org/10.1126/science.1238411

Park, J. Y., Gu, B. M., Kang, D. H., Shin, Y. W., Choi, C. H., Lee, J. M., & Kwon, J. S. (2010). Integration of cross-modal emotional information in the human brain: An fMRI study. *Cortex*, *46*(2), 161–169. https://doi.org/10.1016/j.cortex.2008.06.008

Parkinson, C., Kleinbaum, A. M., & Wheatley, T. (2018). Similar neural responses predict friendship. *Nature Communications*, *9*(1). https://doi.org/10.1038/s41467-017-02722-7

Peng, L., Chen, Z., & Gao, X. (2023). Altered rich-club organization of brain functional network in autism spectrum disorder. *BioFactors*, *49*(3), 612–619. https://doi.org/10.1002/biof.1933

Perry, A., Wen, W., Lord, A., Thalamuthu, A., Roberts, G., Mitchell, P. B., Sachdev, P. S., & Breakspear, M. (2015). The organisation of the elderly connectome. *NeuroImage*, *114*, 414–426. https://doi.org/10.1016/j.neuroimage.2015.04.009

Petrides, M. (2015). Lateral and Dorsomedial Prefrontal Cortex and the Control of Cognition. In *Brain Mapping: An Encyclopedic Reference* (Vol. 2). Elsevier Inc. https://doi.org/10.1016/B978-0-12-397025-1.00241-4

Pini, L., Wennberg, A. M., Salvalaggio, A., Vallesi, A., Pievani, M., & Corbetta, M. (2021). Breakdown of specific functional brain networks in clinical variants of Alzheimer's disease. *Ageing Research Reviews*, *72*(October). https://doi.org/10.1016/j.arr.2021.101482

Pitcher, D., & Ungerleider, L. G. (2021). Evidence for a Third Visual Pathway Specialized for Social Perception. *Trends in Cognitive Sciences*, *25*(2), 100–110. https://doi.org/10.1016/j.tics.2020.11.006

Poeppel, D. (2003). The analysis of speech in different temporal integration windows: Cerebral lateralization as "asymmetric sampling in time." *Speech Communication*, *41*(1), 245–255. https://doi.org/10.1016/S0167-6393(02)00107-3

Ponsoda, V., Martínez, K., Pineda-Pardo, J. A., Abad, F. J., Olea, J., Román, F. J., Barbey, A. K., & Colom, R. (2017). Structural brain connectivity and cognitive ability differences: A multivariate distance matrix regression analysis. *Human Brain Mapping*, *38*(2), 803–816. https://doi.org/10.1002/hbm.23419

Power, J. D., Cohen, A. L., Nelson, S. M., Wig, G. S., Barnes, K. A., Church, J. A., Vogel, A. C., Laumann, T. O., Miezin, F. M., Schlaggar, B. L., & Petersen, S. E. (2011). Functional Network Organization of the Human Brain. *Neuron*, *72*(4), 665–678. https://doi.org/10.1016/j.neuron.2011.09.006

Prescott, J. W., Guidon, A., Doraiswamy, P. M., Choudhury, K. R., Liu, C., & Petrella, J. R. (2014). The alzheimer structural connectome: Changes in cortical network topology with increased amyloid plaque burden. *Radiology*, *273*(1), 175–184. https://doi.org/10.1148/radiol.14132593

Preti, M. G., & Van De Ville, D. (2019). Decoupling of brain function from structure reveals regional behavioral specialization in humans. *Nature Communications*, *10*(1), 1–7. https://doi.org/10.1038/s41467-019-12765-7

Rah, Y. J., Shin, J. H., & Lee, S. A. (2025). The Visual Scene Network and Hippocampus Represent Spatial Boundary Structures for Temporal Episodic Memory Organization. *Journal of Cognitive Neuroscience*, 1–16. https://doi.org/10.1162/jocn_a_02229

Raichle, M. E. (2015). The Brain's Default Mode Network. *Annual Review of Neuroscience*, *38*, 433–447. https://doi.org/10.1146/annurev-neuro-071013-014030

Raut, R. V., Snyder, A. Z., & Raichle, M. E. (2020). Hierarchical dynamics as a macroscopic organizing principle of the human brain. *Proceedings of the National Academy of Sciences*, *117*(34), 20890–20897. https://doi.org/10.1073/pnas.2003383117

Ray, S., Miller, M., Karalunas, S., Robertson, C., Grayson, D. S., Cary, R. P., Hawkey, E., Painter, J. G., Kriz, D., Fombonne, E., Nigg, J. T., & Fair, D. A. (2014). Structural and functional connectivity of the human brain in autism spectrum disorders and attention-deficit/hyperactivity disorder: A rich club-organization study. *Human Brain Mapping*, *35*(12), 6032–6048. https://doi.org/10.1002/hbm.22603

Reavis, E. A., Lee, J., Altshuler, L. L., Cohen, M. S., Engel, S. A., Glahn, D. C., Jimenez, A. M., Narr, K. L., Nuechterlein, K. H., Riedel, P., Wynn, J. K., & Green, M. F. (2020). Structural and Functional Connectivity of Visual Cortex in Schizophrenia and Bipolar Disorder: A Graph-Theoretic Analysis. *Schizophrenia Bulletin Open*, *1*(1), 1–11. https://doi.org/10.1093/schizbullopen/sgaa056

Redcay, E., & Moraczewski, D. (2020). Social cognition in context: A naturalistic imaging approach. *NeuroImage*, *216*(October 2019), 116392. https://doi.org/10.1016/j.neuroimage.2019.116392

Reed, S. K. (2020). Hierarchies. In *Cognitive Skills You Need for the 21st Century* (pp. 69–78). Oxford University Press. https://doi.org/10.1093/oso/9780197529003.003.0007

Reid, A. T., Krumnack, A., Wanke, E., & Kötter, R. (2009). Optimization of cortical hierarchies with continuous scales and ranges. *NeuroImage*, *47*(2), 611–617. https://doi.org/10.1016/j.neuroimage.2009.04.061

Repple, J., Mauritz, M., Meinert, S., de Lange, S. C., Grotegerd, D., Opel, N., Redlich, R., Hahn, T., Förster, K., Leehr, E. J., Winter, N., Goltermann, J., Enneking, V., Fingas, S. M., Lemke, H., Waltemate, L., Nenadic, I., Krug, A., Brosch, K., … van den Heuvel, M. P. (2020). Severity of current depression and remission status are associated with structural connectome alterations in major depressive disorder. *Molecular Psychiatry*, *25*(7), 1550–1558. https://doi.org/10.1038/s41380-019-0603-1

Reynolds, J. R., O'Reilly, R. C., Cohen, J. D., & Braver, T. S. (2012). The function and organization of lateral prefrontal cortex: A test of competing hypotheses. *PLoS ONE*, *7*(2). https://doi.org/10.1371/journal.pone.0030284

Rheault, F., Poulin, P., Valcourt Caron, A., St-Onge, E., & Descoteaux, M. (2020). Common misconceptions, hidden biases and modern challenges of dMRI tractography. *Journal of Neural Engineering*, *17*(1), 011001. https://doi.org/10.1088/1741-2552/ab6aad

Richiardi, J., Altmann, A., Milazzo, A. C., Chang, C., Chakravarty, M. M., Banaschewski, T., Barker, G. J., Bokde, A. L. W., Bromberg, U., Büchel, C., Conrod, P., Fauth-Bühler, M., Flor, H., Frouin, V., Gallinat, J., Garavan, H., Gowland, P., Heinz, A., Lemaître, H., … Greicius, M. D. (2015). Correlated gene expression supports synchronous activity in brain networks. *Science*, *348*(6240), 1241–1244. https://doi.org/10.1126/science.1255905

Riedel, L., van den Heuvel, M. P., & Markett, S. (2022). Trajectory of rich club properties in structural brain networks. *Human Brain Mapping*, *43*(14), 4239–4253. https://doi.org/10.1002/hbm.25950

Rogers, B. P., Avery, S. N., & Heckers, S. (2010). Internal representation of hierarchical sequences involves the default network. *BMC Neuroscience*, *11*. https://doi.org/10.1186/1471-2202-11-54

Román, F. J., Iturria-Medina, Y., Martínez, K., Karama, S., Burgaleta, M., Evans, A. C., Jaeggi, S. M., & Colom, R. (2017). Enhanced structural connectivity within a brain sub-network supporting working memory and engagement processes after cognitive training. *Neurobiology of Learning and Memory*, *141*, 33–43. https://doi.org/10.1016/j.nlm.2017.03.010

Rossi-Pool, R., Zainos, A., Alvarez, M., Parra, S., Zizumbo, J., & Romo, R. (2021). Invariant timescale hierarchy across the cortical somatosensory network. *Proceedings of the National Academy of Sciences of the United States of America*, *118*(3). https://doi.org/10.1073/pnas.2021843118

Rowley, C. D., Bazin, P. L., Tardif, C. L., Sehmbi, M., Hashim, E., Zaharieva, N., Minuzzi, L., Frey, B. N., & Bock, N. A. (2015). Assessing intracortical myelin in the living human brain using myelinated cortical thickness. *Frontiers in Neuroscience*, *9*(OCT), 1–14. https://doi.org/10.3389/fnins.2015.00396

Rubinov, M., & Sporns, O. (2010). Complex network measures of brain connectivity: Uses and interpretations. *NeuroImage*, *52*(3), 1059–1069. https://doi.org/10.1016/j.neuroimage.2009.10.003

Rubinov, M., Ypma, R. J. F., Watson, C., Bullmore, E. T., & Raichle, M. E. (2015). Wiring cost and topological participation of the mouse brain connectome. *Proceedings of the National Academy of Sciences of the United States of America*, *112*(32), 10032–10037. https://doi.org/10.1073/pnas.1420315112

Rui, Y., Huang, T. S., & Mehrotra, S. (1998). Exploring video structure beyond the shots. *Proceedings of the IEEE Conference on Protocols for Multimedia Systems and Multimedia Networking, PROMS-MmNet*, 237–240. https://doi.org/10.1109/mmcs.1998.693648

Runyan, C. A., Piasini, E., Panzeri, S., & Harvey, C. D. (2017). Distinct timescales of population coding across cortex. *Nature*, *548*(7665), 92–96. https://doi.org/10.1038/nature23020

Rust, N. C., & Movshon, J. A. (2005). In praise of artifice. *Nature Neuroscience*, *8*(12), 1647–1650. https://doi.org/10.1038/nn1606

Saarimäki, H. (2021). Naturalistic Stimuli in Affective Neuroimaging: A Review. *Frontiers in Human Neuroscience*, *15*(June). https://doi.org/10.3389/fnhum.2021.675068

Saberi, A., Paquola, C., Wagstyl, K., Hettwer, M. D., Bernhardt, B. C., Eickhoff, S. B., & Valk, S. L. (2023). The regional variation of laminar thickness in the human isocortex is related to cortical hierarchy and interregional connectivity. *PLoS Biology*, *21*(11 November), 1–29. https://doi.org/10.1371/journal.pbio.3002365

Salmi, J., Roine, U., Glerean, E., Lahnakoski, J., Nieminen-Von Wendt, T., Tani, P., Leppämäki, S., Nummenmaa, L., Jääskeläinen, I. P., Carlson, S., Rintahaka, P., & Sams, M. (2013). The brains of high functioning autistic individuals do not synchronize with those of others. *NeuroImage: Clinical*, *3*, 489–497. https://doi.org/10.1016/j.nicl.2013.10.011

Salthe, S. N. (2012). Hierarchical Structures. *Axiomathes*, *22*(3), 355–383. https://doi.org/10.1007/s10516-012-9185-0

Salvador, R., Suckling, J., Coleman, M. R., Pickard, J. D., Menon, D., & Bullmore, E. (2005). Neurophysiological architecture of functional magnetic resonance images of human brain. *Cerebral Cortex*, *15*(9), 1332–2342. https://doi.org/10.1093/cercor/bhi016

Sanz Leon, P., Knock, S. A., Woodman, M. M., Domide, L., Mersmann, J., Mcintosh, A. R., & Jirsa, V. (2013). The virtual brain: A simulator of primate brain network dynamics. *Frontiers in Neuroinformatics*, *7*(MAY). https://doi.org/10.3389/fninf.2013.00010

Sava-Segal, C., Richards, C., Leung, M., & Finn, E. S. (2023). Individual differences in neural event segmentation of continuous experiences. *Cerebral Cortex*, *33*(13), 8164–8178. https://doi.org/10.1093/cercor/bhad106

Savli, M., Bauer, A., Mitterhauser, M., Ding, Y. S., Hahn, A., Kroll, T., Neumeister, A., Haeusler, D., Ungersboeck, J., Henry, S., Isfahani, S. A., Rattay, F., Wadsak, W., Kasper, S., & Lanzenberger, R. (2012). Normative database of the serotonergic system in healthy subjects using multi-tracer PET. *NeuroImage*, *63*(1), 447–459. https://doi.org/10.1016/j.neuroimage.2012.07.001

Schaefer, A., Kong, R., Gordon, E. M., Laumann, T. O., Zuo, X.-N., Holmes, A. J., Eickhoff, S. B., & Yeo, B. T. T. (2018). Local-Global Parcellation of the Human Cerebral Cortex from Intrinsic Functional Connectivity MRI. *Cerebral Cortex*, *28*(9), 3095–3114. https://doi.org/10.1093/cercor/bhx179

Scheliga, S., Kellermann, T., Lampert, A., Rolke, R., Spehr, M., & Habel, U. (2023). Neural correlates of multisensory integration in the human brain: An ALE meta-analysis. *Reviews in the Neurosciences*, *34*(2), 223–245. https://doi.org/10.1515/revneuro-2022-0065

Schilling, K. G., Nath, V., Hansen, C., Parvathaneni, P., Blaber, J., Gao, Y., Neher, P., Aydogan, D. B., Shi, Y., Ocampo-Pineda, M., Schiavi, S., Daducci, A., Girard, G., Barakovic, M., Rafael-Patino, J., Romascano, D., Rensonnet, G., Pizzolato, M., Bates, A., … Landman, B. A. (2019). Limits to anatomical accuracy of diffusion tractography using modern approaches. *NeuroImage*, *185*(October 2018), 1–11. https://doi.org/10.1016/j.neuroimage.2018.10.029

Schilling, K. G., Petit, L., Rheault, F., Remedios, S., Pierpaoli, C., Anderson, A. W., Landman, B. A., & Descoteaux, M. (2020). Brain connections derived from diffusion MRI tractography can be highly anatomically accurate—if we know where white matter pathways start, where they end, and where they do not go. *Brain Structure and Function*, *225*(8), 2387–2402. https://doi.org/10.1007/s00429-020-02129-z

Schmälzle, R., Imhof, M. A., Grall, C., Flaisch, T., Schupp, H. T., Schmälzle, R., Imhof, M. A., Grall, C., Flaisch, T., & Schupp, H. T. (2017). Reliability of fMRI time series: Similarity of neural processing during movie viewing. *BioRxiv*, 158188. https://doi.org/10.1101/158188

Schmidt, R., LaFleur, K. J. R., de Reus, M. A., van den Berg, L. H., & van den Heuvel, M. P. (2015). Kuramoto model simulation of neural hubs and dynamic synchrony in the human cerebral connectome. *BMC Neuroscience*, *16*(1), 1–13. https://doi.org/10.1186/s12868-015-0193-z

Scholtens, L. H., Schmidt, R., de Reus, M. A., & van den Heuvel, M. P. (2014). Linking macroscale graph analytical organization to microscale neuroarchitectonics in the macaque connectome. *Journal of Neuroscience*, *34*(36), 12192–12205. https://doi.org/10.1523/JNEUROSCI.0752-14.2014

Schroeter, M. S., Charlesworth, P., Kitzbichler, M. G., Paulsen, O., & Bullmore, E. T. (2015). Emergence of rich-club topology and coordinated dynamics in development of hippocampal functional networks In vitro. *Journal of Neuroscience*, *35*(14), 5459–5470. https://doi.org/10.1523/JNEUROSCI.4259-14.2015

Schulte, J., Senden, M., Deco, G., Kobeleva, X., & Zamora-López, G. (2025). The global communication pathways of the human brain transcend the cortical-subcortical-cerebellar division. *BioRxiv*, 2023.07.07.548139. https://doi.org/https://doi.org/10.48550/arXiv.2505.22893

Seghier, M. L. (2013). The angular gyrus: Multiple functions and multiple subdivisions. *Neuroscientist*, *19*(1), 43–61. https://doi.org/10.1177/1073858412440596

Seguin, C., Tian, Y., & Zalesky, A. (2020). Network communication models improve the behavioral and functional predictive utility of the human structural connectome. *Network Neuroscience*, *4*(4), 980–1006. https://doi.org/10.1162/netn_a_00161

Senden, M., Deco, G., De Reus, M. A., Goebel, R., & van den Heuvel, M. P. (2014). Rich club organization supports a diverse set of functional network configurations. *NeuroImage*, *96*, 174–182. https://doi.org/10.1016/j.neuroimage.2014.03.066

Senden, M., Reuter, N., van den Heuvel, M. P., Goebel, R., & Deco, G. (2017). Cortical rich club regions can organize state-dependent functional network formation by engaging in oscillatory behavior. *NeuroImage*, *146*, 561–574. https://doi.org/10.1016/j.neuroimage.2016.10.044

Senden, M., Reuter, N., van den Heuvel, M. P., Goebel, R., Deco, G., & Gilson, M. (2018). Task-related effective connectivity reveals that the cortical rich club gates cortex-wide communication. *Human Brain Mapping*, *39*(3), 1246–1262. https://doi.org/10.1002/hbm.23913

Sepulcre, J., Sabuncu, M. R., Yeo, T. B., Liu, H., & Johnson, K. A. (2012). Stepwise connectivity of the modal cortex reveals the multimodal organization of the human brain. *Journal of Neuroscience*, *32*(31), 10649–10661. https://doi.org/10.1523/JNEUROSCI.0759-12.2012

Setsompop, K., Gagoski, B. A., Polimeni, J. R., Witzel, T., Wedeen, V. J., & Wald, L. L. (2012). Blipped-controlled aliasing in parallel imaging for simultaneous multislice echo planar imaging with reduced g -factor penalty. *Magnetic Resonance in Medicine*, *67*(5), 1210–1224. https://doi.org/10.1002/mrm.23097

Shafiei, G., Markello, R. D., De Wael, R. V., Bernhardt, B. C., Fulcher, B. D., & Misic, B. (2020). Topographic gradients of intrinsic dynamics across neocortex. *ELife*, *9*, 1–24. https://doi.org/10.7554/eLife.62116

Shafiei, K., Zadeh, S. G., & Hagh, M. T. (2025). Robustness and resilience of energy systems to extreme events: A review of assessment methods and strategies. *Energy Strategy Reviews*, *58*(January), 101660. https://doi.org/10.1016/j.esr.2025.101660

Shah, L. M., Cramer, J. A., Ferguson, M. A., Birn, R. M., & Anderson, J. S. (2016). Reliability and reproducibility of individual differences in functional connectivity acquired during task and resting state. *Brain and Behavior*, *6*(5), 1–15. https://doi.org/10.1002/brb3.456

Shahdloo, M., Acar, M., & Çukur, T. (2019). Attention During Story Listening Modulates Temporal Receptive Windows Across Human Cortex. *2019 Conference on Cognitive Computational Neuroscience*, 168–171. https://doi.org/10.32470/CCN.2019.1039-0

Shen, K., Hutchison, R. M., Bezgin, G., Everling, S., & McIntosh, A. R. (2015). Network structure shapes spontaneous functional connectivity dynamics. *Journal of Neuroscience*, *35*(14), 5579–5588. https://doi.org/10.1523/JNEUROSCI.4903-14.2015

Siestrup, S., Dührkop, M., Villafañe Barraza, V., Redlich, D., Pizzera, A., Mecklenbrauck, F., Bauer, J., Raab, M., & Schubotz, R. I. (2026). Jumping to predictions: Auditory and visual prediction in hurdling. *NeuroImage*, *325*(September 2025). https://doi.org/10.1016/j.neuroimage.2025.121673

Silson, E. H., Steel, A. D., & Baker, C. I. (2016). Scene-selectivity and retinotopy in medial parietal cortex. *Frontiers in Human Neuroscience*, *10*(August), 17. https://doi.org/10.3389/fnhum.2016.00412

Simon, H. A. (1977). *The Organization of Complex Systems* (pp. 245–261). https://doi.org/10.1007/978-94-010-9521-1_14

Smallwood, J., Karapanagiotidis, T., Ruby, F., Medea, B., Caso, I. De, Konishi, M., Wang, H. T., Hallam, G., Margulies, D. S., & Jefferies, E. (2016). Representing representation: Integration between the temporal lobe and the posterior cingulate influences the content and form of spontaneous thought. *PLoS ONE*, *11*(4), 1–19. https://doi.org/10.1371/journal.pone.0152272

Smith, T. J., Levin, D., & Cutting, J. E. (2012). A Window on Reality: Perceiving Edited Moving Images. *Current Directions in Psychological Science*, *21*(2), 107–113. https://doi.org/10.1177/0963721412437407

Solé-Casals, J., Serra-Grabulosa, J. M., Romero-Garcia, R., Vilaseca, G., Adan, A., Vilaró, N., Bargalló, N., & Bullmore, E. T. (2019). Structural brain network of gifted children has a more integrated and versatile topology. *Brain Structure and Function*, *224*(7), 2373–2383. https://doi.org/10.1007/s00429-019-01914-9

Soltani, A., Murray, J. D., Seo, H., & Lee, D. (2021). Timescales of cognition in the brain. *Current Opinion in Behavioral Sciences*, *41*, 30–37. https://doi.org/10.1016/j.cobeha.2021.03.003

Song, M., Shin, E. J., Seo, H., Soltani, A., Steinmetz, N. A., Lee, D., Jung, M. W., & Paik, S.-B. (2024). Hierarchical gradients of multiple timescales in the mammalian forebrain. *Proceedings of the National Academy of Sciences*, *121*(51), 2017. https://doi.org/10.1073/pnas.2415695121

Sonkusare, S., Breakspear, M., & Guo, C. (2019). Naturalistic Stimuli in Neuroscience: Critically Acclaimed. *Trends in Cognitive Sciences*, *23*(8), 699–714. https://doi.org/10.1016/j.tics.2019.05.004

Sporns, O. (2011). The human connectome: A complex network. *Annals of the New York Academy of Sciences*, *1224*(1), 109–125. https://doi.org/10.1111/j.1749-6632.2010.05888.x

Sporns, O. (2013). Structure and function of complex brain networks. *Dialogues in Clinical Neuroscience*, *15*(3), 247–262. https://doi.org/10.31887/dcns.2013.15.3/osporns

Sporns, O. (2018). Graph theory methods: Applications in brain networks. *Dialogues in Clinical Neuroscience*, *20*(2), 111–120. https://doi.org/10.31887/DCNS.2018.20.2/OSPORNS

Sporns, O., Chialvo, D. R., Kaiser, M., & Hilgetag, C. C. (2004). Organization, development and function of complex brain networks. *Trends in Cognitive Sciences*, *8*(9), 418–425. https://doi.org/10.1016/j.tics.2004.07.008

Sporns, O., Honey, C. J., & Kötter, R. (2007). Identification and Classification of Hubs in Brain Networks. *PLoS ONE*, *2*(10), e1049. https://doi.org/10.1371/journal.pone.0001049

Sporns, O., Tononi, G., & Kötter, R. (2005). The human connectome: A structural description of the human brain. *PLoS Computational Biology*, *1*(4), 0245–0251. https://doi.org/10.1371/journal.pcbi.0010042

Sporns, O., & Zwi, J. D. (2004). The Small World of the Cerebral Cortex. *Neuroinformatics*, *2*(2), 145–162. https://doi.org/10.1385/NI:2:2:145

Spreng, R. N., Sepulcre, J., Turner, G. R., Stevens, W. D., & Schacter, D. L. (2013). Intrinsic architecture underlying the relations among the default, dorsal attention, and frontoparietal control networks of the human brain. *Journal of Cognitive Neuroscience*, *25*(1), 74–86. https://doi.org/10.1162/jocn_a_00281

Steel, A., Billings, M. M., Silson, E. H., & Robertson, C. E. (2021). A network linking scene perception and spatial memory systems in posterior cerebral cortex. *Nature Communications*, *12*(1). https://doi.org/10.1038/s41467-021-22848-z

Steel, A., Prasad, D., Garcia, B. D., & Robertson, C. E. (2025). Relating Scene Memory and Perception Activity to Functional Properties, Networks, and Landmarks of Posterior Cerebral Cortex—A Probabilistic Atlas. *The Journal of Neuroscience*, *45*(23), e0028252025. https://doi.org/10.1523/JNEUROSCI.0028-25.2025

Steel, A., Silson, E. H., Garcia, B. D., & Robertson, C. E. (2024). A retinotopic code structures the interaction between perception and memory systems. *Nature Neuroscience*, *27*(2), 339–347. https://doi.org/10.1038/s41593-023-01512-3

Stephan, K. E., Kamper, L., Bozkurt, A., Burns, G. A. P. C., Young, M. P., & Kötter, R. (2001). Advanced database methodology for the Collation of Connectivity data on the Macaque brain (CoCoMac). *Philosophical Transactions of the Royal Society B: Biological Sciences*, *356*(1412), 1159–1186. https://doi.org/10.1098/rstb.2001.0908

Stephens, G. J., Honey, C. J., & Hasson, U. (2013). A place for time: The spatiotemporal structure of neural dynamics during natural audition. *Journal of Neurophysiology*, *110*(9), 2019–2026. https://doi.org/10.1152/jn.00268.2013

Straathof, M., Sinke, M. R. T., Dijkhuizen, R. M., & Otte, W. M. (2019). A systematic review on the quantitative relationship between structural and functional network connectivity strength in mammalian brains. *Journal of Cerebral Blood Flow and Metabolism*, *39*(2), 189–209. https://doi.org/10.1177/0271678X18809547

Suárez, L. E., Markello, R. D., Betzel, R. F., & Misic, B. (2020). Linking Structure and Function in Macroscale Brain Networks. *Trends in Cognitive Sciences*, *24*(4), 302–315. https://doi.org/10.1016/j.tics.2020.01.008

Sydnor, V. J., Larsen, B., Bassett, D. S., Alexander-Bloch, A., Fair, D. A., Liston, C., Mackey, A. P., Milham, M. P., Pines, A., Roalf, D. R., Seidlitz, J., Xu, T., Raznahan, A., & Satterthwaite, T. D. (2021). Neurodevelopment of the association cortices: Patterns, mechanisms, and implications for psychopathology. *Neuron*, *109*(18), 2820–2846. https://doi.org/10.1016/j.neuron.2021.06.016

Sydnor, V. J., Larsen, B., Seidlitz, J., Adebimpe, A., Alexander-Bloch, A. F., Bassett, D. S., Bertolero, M. A., Cieslak, M., Covitz, S., Fan, Y., Gur, R. E., Gur, R. C., Mackey, A. P., Moore, T. M., Roalf, D. R., Shinohara, R. T., & Satterthwaite, T. D. (2023). Intrinsic activity development unfolds along a sensorimotor–association cortical axis in youth. *Nature Neuroscience*, *26*(4), 638–649. https://doi.org/10.1038/s41593-023-01282-y

Tang, X., Guo, Z., Chen, G., Sun, S., Xiao, S., Chen, P., Tang, G., Huang, L., & Wang, Y. (2024). A Multimodal Meta-Analytical Evidence of Functional and Structural Brain Abnormalities Across Alzheimer's Disease Spectrum. *Ageing Research Reviews*, *95*(February), 102240. https://doi.org/10.1016/j.arr.2024.102240

Thomas, C., Ye, F. Q., Irfanoglu, M. O., Modi, P., Saleem, K. S., Leopold, D. A., & Pierpaoli, C. (2014). Anatomical accuracy of brain connections derived from diffusion MRI tractography is inherently limited. *Proceedings of the National Academy of Sciences of the United States of America*, *111*(46), 16574–16579. https://doi.org/10.1073/pnas.1405672111

Thomas, J. H. (1986). The structure of the nervous system of the nematode Caenorhabditis elegans. *Philosophical Transactions of the Royal Society of London. B, Biological Sciences*, *314*(1165), 1–340. https://doi.org/10.1098/rstb.1986.0056

Thomas, R. M., De Sanctis, T., Gazzola, V., & Keysers, C. (2018). Where and how our brain represents the temporal structure of observed action. *NeuroImage*, *183*(November 2017), 677–697. https://doi.org/10.1016/j.neuroimage.2018.08.056

Tian, Y., & Sun, P. (2022). Percolation may explain efficiency, robustness, and economy of the brain. *Network Neuroscience*, *6*(3), 765–790. https://doi.org/10.1162/netn_a_00246

Tononi, G., Sporns, O., & Edelman, G. M. (1994). A measure for brain complexity: Relating functional segregation and integration in the nervous system. *Proceedings of the National Academy of Sciences of the United States of America*, *91*(11), 5033–5037. https://doi.org/10.1073/pnas.91.11.5033

Turk, E., Scholtens, L. H., & van den Heuvel, M. P. (2016). Cortical chemoarchitecture shapes macroscale effective functional connectivity patterns in macaque cerebral cortex. *Human Brain Mapping*, *37*(5), 1856–1865. https://doi.org/10.1002/hbm.23141

Uithol, S., van Rooij, I., Bekkering, H., & Haselager, P. (2012). Hierarchies in action and motor control. *Journal of Cognitive Neuroscience*, *24*(5), 1077–1086. https://doi.org/10.1162/jocn_a_00204

Vagharchakian, L., Dehaene-Lambertz, G., Pallier, C., & Dehaene, S. (2012). A temporal bottleneck in the language comprehension network. *Journal of Neuroscience*, *32*(26), 9089–9102. https://doi.org/10.1523/JNEUROSCI.5685-11.2012

Valentine, J. W., & May, C. L. (1996). Hierarchies in biology and paleontology. *Paleobiology*, *22*(1), 23–33. https://doi.org/10.1017/S0094837300015992

Van Baar, J. M., Halpern, D. J., & FeldmanHall, O. (2021). Intolerance of uncertainty modulates brain-to-brain synchrony during politically polarized perception. *Proceedings of the National Academy of Sciences of the United States of America*, *118*(20), 1–9. https://doi.org/10.1073/pnas.2022491118

van den Heuvel, M. P., & Hulshoff Pol, H. E. (2010). Exploring the brain network: A review on resting-state fMRI functional connectivity. *European Neuropsychopharmacology*, *20*(8), 519–534. https://doi.org/10.1016/j.euroneuro.2010.03.008

van den Heuvel, M. P., Kahn, R. S., Goñi, J., & Sporns, O. (2012). High-cost, high-capacity backbone for global brain communication. *Proceedings of the National Academy of Sciences*, *109*(28), 11372–11377. https://doi.org/10.1073/pnas.1203593109

van den Heuvel, M. P., Mandl, R. C. W., Stam, C. J., Kahn, R. S., & Hulshoff Pol, H. E. (2010). Aberrant Frontal and Temporal Complex Network Structure in Schizophrenia: A Graph Theoretical Analysis. *The Journal of Neuroscience*, *30*(47), 15915–15926. https://doi.org/10.1523/JNEUROSCI.2874-10.2010

van den Heuvel, M. P., Scholtens, L. H., van der Burgh, H. K., Agosta, F., Alloza, C., Arango, C., Auyeung, B., Baron-Cohen, S., Basaia, S., Benders, M. J. N. L., Beyer, F., Booij, L., Braun, K. P. J., Filho, G. B., Cahn, W., Cannon, D. M., Chaim-Avancini, T. M., Chan, S. S. M., Chen, E. Y. H., … de Lange, S. C. (2019). 10kin1day: A bottom-up neuroimaging initiative. *Frontiers in Neurology*, *10*(MAY). https://doi.org/10.3389/fneur.2019.00425

van den Heuvel, M. P., & Sporns, O. (2011). Rich-club organization of the human connectome. *Journal of Neuroscience*, *31*(44), 15775–15786. https://doi.org/10.1523/JNEUROSCI.3539-11.2011

van den Heuvel, M. P., & Sporns, O. (2013a). An anatomical substrate for integration among functional networks in human cortex. *Journal of Neuroscience*, *33*(36), 14489–14500. https://doi.org/10.1523/JNEUROSCI.2128-13.2013

van den Heuvel, M. P., & Sporns, O. (2013b). Network hubs in the human brain. *Trends in Cognitive Sciences*, *17*(12), 683–696. https://doi.org/10.1016/j.tics.2013.09.012

van den Heuvel, M. P., Sporns, O., Collin, G., Scheewe, T., Mandl, R. C. W., Cahn, W., Goni, J., Pol, H. E. H., & Kahn, R. S. (2013). Abnormal rich club organization and functional brain dynamics in schizophrenia. *JAMA Psychiatry*, *70*(8), 783–792. https://doi.org/10.1001/jamapsychiatry.2013.1328

van den Heuvel, M. P., Stam, C. J., Boersma, M., & Hulshoff Pol, H. E. (2008). Small-world and scale-free organization of voxel-based resting-state functional connectivity in the human brain. *NeuroImage*, *43*(3), 528–539. https://doi.org/10.1016/j.neuroimage.2008.08.010

van der Meer, J. N., Breakspear, M., Chang, L. J., Sonkusare, S., & Cocchi, L. (2020). Movie viewing elicits rich and reliable brain state dynamics. *Nature Communications*, *11*(1), 1–14. https://doi.org/10.1038/s41467-020-18717-w

Van Essen, D. C., Smith, S. M., Barch, D. M., Behrens, T. E. J., Yacoub, E., & Ugurbil, K. (2013). The WU-Minn Human Connectome Project: An overview. *NeuroImage*, *80*, 62–79. https://doi.org/10.1016/j.neuroimage.2013.05.041

Vanderwal, T., Eilbott, J., & Castellanos, F. X. (2019). Movies in the magnet: Naturalistic paradigms in developmental functional neuroimaging. *Developmental Cognitive Neuroscience*, *36*(May 2018), 100600. https://doi.org/10.1016/j.dcn.2018.10.004

Váša, F., Shanahan, M., Hellyer, P. J., Scott, G., Cabral, J., & Leech, R. (2015). Effects of lesions on synchrony and metastability in cortical networks. *NeuroImage*, *118*, 456–467. https://doi.org/10.1016/j.neuroimage.2015.05.042

Vázquez-Rodríguez, B., Suárez, L. E., Markello, R. D., Shafiei, G., Paquola, C., Hagmann, P., Van Den Heuvel, M. P., Bernhardt, B. C., Spreng, R. N., & Misic, B. (2019). Gradients of structure–function tethering across neocortex. *Proceedings of the National Academy of Sciences of the United States of America*, *116*(42), 21219–21227. https://doi.org/10.1073/pnas.1903403116

Veraart, J., Fieremans, E., & Novikov, D. S. (2019). On the scaling behavior of water diffusion in human brain white matter. *NeuroImage*, *185*(October 2018), 379–387. https://doi.org/10.1016/j.neuroimage.2018.09.075

Vértes, P. E., Rittman, T., Whitaker, K. J., Romero-Garcia, R., Váša, F., Kitzbichler, M. G., Wagstyl, K., Fonagy, P., Dolan, R. J., Jones, P. B., Goodyer, I. M., & Bullmore, E. T. (2016). Gene transcription profiles associated with inter-modular hubs and connection distance in human functional magnetic resonance imaging networks. *Philosophical Transactions of the Royal Society B: Biological Sciences*, *371*(1705). https://doi.org/10.1098/rstb.2015.0362

Vezoli, J., Magrou, L., Goebel, R., Wang, X. J., Knoblauch, K., Vinck, M., & Kennedy, H. (2021). Cortical hierarchy, dual counterstream architecture and the importance of top-down generative networks. *NeuroImage*, *225*. https://doi.org/10.1016/j.neuroimage.2020.117479

Vogt, C., & Vogt, O. (1928). Die Grundlagen und die Teildisziplinen der mikroskopischen Anatomie des Zentralnervensystems. In M. Bielschowsky, S. T. Bok, R. Greving, A. Jakob, G. Mingazzini, Ph. Stöhr, C. Vogt, & O. Vogt (Eds.), *Nervensystem: Erster Teil Nervengewebe das Peripherische Nervensystem das Zentralnervensystem* (pp. 448–477). Springer Berlin Heidelberg. https://doi.org/10.1007/978-3-642-66443-4_8

von Economo, C., & Koskinas, G. N. (1926). Die Cytoarchitektonik der Hirnrinde des erwachsenen Menschen. (The Cyto-Architectonics of the Cerebral Cortex of Adult Man.). *Archives of Neurology And Psychiatry*, *16*(6), 816. https://doi.org/10.1001/archneurpsyc.1926.02200300136013

Wagstyl, K., Larocque, S., Cucurull, G., Lepage, C., Cohen, J. P., Bludau, S., Palomero-Gallagher, N., Lewis, L. B., Funck, T., Spitzer, H., Dickscheid, T., Fletcher, P. C., Romero, A., Zilles, K., Amunts, K., Bengio, Y., & Evans, A. C. (2020). BigBrain 3D atlas of cortical layers: Cortical and laminar thickness gradients diverge in sensory and motor cortices. *PLoS Biology*, *18*(4), 1–21. https://doi.org/10.1371/journal.pbio.3000678

Wagstyl, K., Ronan, L., Goodyer, I. M., & Fletcher, P. C. (2015). Cortical thickness gradients in structural hierarchies. *NeuroImage*, *111*, 241–250. https://doi.org/10.1016/j.neuroimage.2015.02.036

Wang, J., Ren, Y., Hu, X., Nguyen, V. T., Guo, L., Han, J., & Guo, C. C. (2017). Test–retest reliability of functional connectivity networks during naturalistic fMRI paradigms. *Human Brain Mapping*, *38*(4), 2226–2241. https://doi.org/10.1002/hbm.23517

Wang, M., Yang, Y., Wang, C. J., Gamo, N. J., Jin, L. E., Mazer, J. A., Morrison, J. H., Wang, X. J., & Arnsten, A. F. T. (2013). NMDA Receptors Subserve Persistent Neuronal Firing during Working Memory in Dorsolateral Prefrontal Cortex. *Neuron*, *77*(4), 736–749. https://doi.org/10.1016/j.neuron.2012.12.032

Wang, R., Chang, Z., Liu, Xuechun, Kristanto, D., Gartner, É. G. G., Liu, Xinyang, Liu, M., Wu, Y., Lui, M., & Zhou, C. (2025). *Weak but influential Nonlinear contributions of structural connectivity to human cognitive abilities and brain functions*. httpsarxiv.orgabs2505.24125

Wang, X.-J. (2020). Macroscopic gradients of synaptic excitation and inhibition in the neocortex. *Nature Reviews Neuroscience*, *21*(3), 169–178. https://doi.org/10.1038/s41583-020-0262-x

Wang, X.-J., & Kennedy, H. (2016). Brain structure and dynamics across scales: In search of rules. *Current Opinion in Neurobiology*, *37*, 92–98. https://doi.org/10.1016/j.conb.2015.12.010

Wang, Y., Deng, F., Jia, Y., Wang, J., Zhong, S., Huang, H., Chen, L., Chen, G., Hu, H., Huang, L., & Huang, R. (2019). Disrupted rich club organization and structural brain connectome in unmedicated bipolar disorder. *Psychological Medicine*, *49*(3), 510–518. https://doi.org/10.1017/S0033291718001150

Wang, Z., Dai, Z., Gong, G., Zhou, C., & He, Y. (2015). Understanding structural-functional relationships in the human brain: A large-scale network perspective. *Neuroscientist*, *21*(3), 290–305. https://doi.org/10.1177/1073858414537560

Watanabe, T. (2013). Rich-club network topology to minimize synchronization cost due to phase difference among frequency-synchronized oscillators. *Physica A: Statistical Mechanics and Its Applications*, *392*(5), 1246–1255. https://doi.org/10.1016/j.physa.2012.11.041

Watts, D. J., & Strogatz, S. H. (1998). Collective dinamycs of "small world" networks. *Nature*, *393*(4), 440–442.

Welton, T., Kent, D. A., Auer, D. P., & Dineen, R. A. (2015). Reproducibility of Graph-Theoretic Brain Network Metrics: A Systematic Review. *Brain Connectivity*, *5*(4), 193–202. https://doi.org/10.1089/brain.2014.0313

Wen, T., Duncan, J., & Mitchell, D. J. (2020). Hierarchical representation of multistep tasks in multiple-demand and default mode networks. *Journal of Neuroscience*, *40*(40), 7724–7738. https://doi.org/10.1523/JNEUROSCI.0594-20.2020

Whiteside, D. J., Street, D., Murley, A. G., Jones, P. S., Malpetti, M., Ghosh, B. C. P., Coyle-Gilchrist, I., Gerhard, A., Hu, M. T., Klein, J. C., Leigh, P. N., Church, A., Burn, D. J., Morris, H. R., Rowe, J. B., & Rittman, T. (2023). Network connectivity and structural correlates of survival in progressive supranuclear palsy and corticobasal syndrome. *Human Brain Mapping*, *44*(11), 4239–4255. https://doi.org/10.1002/hbm.26342

Winter, N. R., Blanke, J., Leenings, R., Ernsting, J., Fisch, L., Sarink, K., Barkhau, C., Emden, D., Thiel, K., Flinkenflügel, K., Winter, A., Goltermann, J., Meinert, S., Dohm, K., Repple, J., Gruber, M., Leehr, E. J., Opel, N., Grotegerd, D., … Hahn, T. (2024). A Systematic Evaluation of Machine Learning–Based Biomarkers for Major Depressive Disorder. *JAMA Psychiatry*, *81*(4), 386. https://doi.org/10.1001/jamapsychiatry.2023.5083

Wolff, A., Berberian, N., Golesorkhi, M., Gomez-Pilar, J., Zilio, F., & Northoff, G. (2022). Intrinsic neural timescales: temporal integration and segregation. *Trends in Cognitive Sciences*, *26*(2), 159–173. https://doi.org/10.1016/j.tics.2021.11.007

Wu, D., Fan, L., Song, M., Wang, H., Chu, C., Yu, S., & Jiang, T. (2020). Hierarchy of Connectivity-Function Relationship of the Human Cortex Revealed through Predicting Activity across Functional Domains. *Cerebral Cortex*, *30*(8), 4607–4616. https://doi.org/10.1093/cercor/bhaa063

Wu, J. (2013). Hierarchy Theory: An Overview. In R. Rozzi, S. T. A. Pickett, C. Palmer, J. J. Armesto, & J. B. Callicott (Eds.), *Linking Ecology and Ethics for a Changing World* (Number January, pp. 281–301). Springer Netherlands. https://doi.org/10.1007/978-94-007-7470-4_24

Wu, K., Taki, Y., Sato, K., Sassa, Y., Inoue, K., Goto, R., Okada, K., Kawashima, R., He, Y., Evans, A. C., & Fukuda, H. (2011). The overlapping community structure of structural brain network in young healthy individuals. *PLoS ONE*, *6*(5). https://doi.org/10.1371/journal.pone.0019608

Xu, J., Moeller, S., Strupp, J., Auerbach, E., Chen, L., Feinberg, D. a, & Uğurbil, K. (2012). Highly Accelerated Whole Brain Imaging Using Aligned-Blipped-Controlled-aliasing Multiband EPI. *Proceedings of the 20th Annual Meeting of ISMRM, Melbourne*, *5*(12), 91657.

Xu, Y., Lin, Q., Han, Z., He, Y., & Bi, Y. (2016). Intrinsic functional network architecture of human semantic processing: Modules and hubs. *NeuroImage*, *132*, 542–555. https://doi.org/10.1016/j.neuroimage.2016.03.004

Xue, C., Sun, H., Hu, G., Qi, W., Yue, Y., Rao, J., Yang, W., Xiao, C., & Chen, J. (2020). Disrupted Patterns of Rich-Club and Diverse-Club Organizations in Subjective Cognitive Decline and Amnestic Mild Cognitive Impairment. *Frontiers in Neuroscience*, *14*(October), 1–14. https://doi.org/10.3389/fnins.2020.575652

Yan, T., Liu, T., Ai, J., Shi, Z., Zhang, J., Pei, G., & Wu, J. (2021). Task-induced activation transmitted by structural connectivity is associated with behavioral performance. *Brain Structure and Function*, *226*(5), 1437–1452. https://doi.org/10.1007/s00429-021-02249-0

Yan, T., Wang, W., Yang, L., Chen, K., Chen, R., & Han, Y. (2018). Rich club disturbances of the human connectome from subjective cognitive decline to Alzheimer's disease. *Theranostics*, *8*(12), 3237–3255. https://doi.org/10.7150/thno.23772

Yang, E., Milisav, F., Kopal, J., Holmes, A. J., Mitsis, G. D., Misic, B., Finn, E. S., & Bzdok, D. (2023). The default network dominates neural responses to evolving movie stories. *Nature Communications*, *14*(1). https://doi.org/10.1038/s41467-023-39862-y

Yang, Z., Wu, J., Xu, L., Deng, Z., Tang, Y., Gao, J., Hu, Y., Zhang, Y., Qin, S., Li, C., & Wang, J. (2020). Individualized psychiatric imaging based on inter-subject neural synchronization in movie watching. *NeuroImage*, *216*(September 2019), 116227. https://doi.org/10.1016/j.neuroimage.2019.116227

Yao, Z., Hu, B., Xie, Y., Moore, P., & Zheng, J. (2015). A review of structural and functional brain networks: small world and atlas. *Brain Informatics*, *2*(1), 45–52. https://doi.org/10.1007/s40708-015-0009-z

Ye, M., Liu, J., Guan, Y., Ma, H., & Tian, L. (2023). Are inter-subject functional correlations consistent across different movies? *Brain Imaging and Behavior*, *17*(1), 44–53. https://doi.org/10.1007/s11682-022-00740-8

Yeh, C. H., Jones, D. K., Liang, X., Descoteaux, M., & Connelly, A. (2021). Mapping Structural Connectivity Using Diffusion MRI: Challenges and Opportunities. *Journal of Magnetic Resonance Imaging*, *53*(6), 1666–1682. https://doi.org/10.1002/jmri.27188

Yeh, F. C., Wedeen, V. J., & Tseng, W. Y. I. (2010). Generalized q-sampling imaging. *IEEE Transactions on Medical Imaging*, *29*(9), 1626–1635. https://doi.org/10.1109/TMI.2010.2045126

Yeo, B. T. T., Krienen, F. M., Sepulcre, J., Sabuncu, M. R., Lashkari, D., Hollinshead, M., Roffman, J. L., Smoller, J. W., Zöllei, L., Polimeni, J. R., Fisch, B., Liu, H., & Buckner, R. L. (2011). The organization of the human cerebral cortex estimated by intrinsic functional connectivity. *Journal of Neurophysiology*, *106*(3), 1125–1165. https://doi.org/10.1152/jn.00338.2011

Yeshurun, Y., Nguyen, M., & Hasson, U. (2017). Amplification of local changes along the timescale processing hierarchy. *Proceedings of the National Academy of Sciences of the United States of America*, *114*(35), 9475–9480. https://doi.org/10.1073/pnas.1701652114

Yeshurun, Y., Nguyen, M., & Hasson, U. (2021). The default mode network: where the idiosyncratic self meets the shared social world. *Nature Reviews Neuroscience*, *22*(3), 181–192. https://doi.org/10.1038/s41583-020-00420-w

Yeshurun, Y., Swanson, S., Simony, E., Chen, J., Lazaridi, C., Honey, C. J., & Hasson, U. (2017). Same Story, Different Story: The Neural Representation of Interpretive Frameworks. *Psychological Science*, *28*(3), 307–319. https://doi.org/10.1177/0956797616682029

Yin, S., Li, Y., & Chen, A. (2022). Functional coupling between frontoparietal control subnetworks bridges the default and dorsal attention networks. *Brain Structure and Function*, *227*(7), 2243–2260. https://doi.org/10.1007/s00429-022-02517-7

Yu, L., Flinker, A., & Veraart, J. (2025). Enhanced structural brain connectivity analyses using high diffusion-weighting strengths. *Brain Structure and Function*, *230*(5), 1–10. https://doi.org/10.1007/s00429-025-02916-6

Zacks, J. M., Speer, N. K., Swallow, K. M., & Maley, C. J. (2010). The brain's cutting-room floor: Segmentation of narrative cinema. *Frontiers in Human Neuroscience*, *4*(October), 1–15. https://doi.org/10.3389/fnhum.2010.00168

Zadbood, A., Chen, J., Leong, Y. C., Norman, K. A., & Hasson, U. (2017). How We Transmit Memories to Other Brains: Constructing Shared Neural Representations Via Communication. *Cerebral Cortex*, *27*(10), 4988–5000. https://doi.org/10.1093/cercor/bhx202

Zalesky, A., Fornito, A., Cocchi, L., Gollo, L. L., & Breakspear, M. (2014). Time-resolved resting-state brain networks. *Proceedings of the National Academy of Sciences of the United States of America*, *111*(28), 10341–10346. https://doi.org/10.1073/pnas.1400181111

Zalesky, A., Fornito, A., Cocchi, L., Gollo, L. L., van den Heuvel, M. P., & Breakspear, M. (2016). Connectome sensitivity or specificity: which is more important? *NeuroImage*, *142*, 407–420. https://doi.org/10.1016/j.neuroimage.2016.06.035

Zaleznik, E., & Park, J. (2021). The neural basis of counting sequences. *NeuroImage*, *237*(May), 118146. https://doi.org/10.1016/j.neuroimage.2021.118146

Zamora-López, G., Chen, Y., Deco, G., Kringelbach, M. L., & Zhou, C. (2016). Functional complexity emerging from anatomical constraints in the brain: The significance of network modularity and rich-clubs. *Scientific Reports*, *6*(November), 1–18. https://doi.org/10.1038/srep38424

Zamora-López, G., Zhou, C., & Kurths, J. (2009). Graph analysis of cortical networks reveals complex anatomical communication substrate. *Chaos*, *19*(1). https://doi.org/10.1063/1.3089559

Zamora-López, G., Zhou, C., & Kurths, J. (2010). Cortical hubs form a module for multisensory integration on top of the hierarchy of cortical networks. *Frontiers in Neuroinformatics*, *4*(MAR), 1–13. https://doi.org/10.3389/neuro.11.001.2010

Zanto, T. P., & Gazzaley, A. (2013). Fronto-parietal network: Flexible hub of cognitive control. *Trends in Cognitive Sciences*, *17*(12), 602–603. https://doi.org/10.1016/j.tics.2013.10.001

Zhang, H., Zhao, R., Hu, X., Guan, S., Margulies, D. S., Meng, C., & Biswal, B. B. (2022). Cortical connectivity gradients and local timescales during cognitive states are modulated by cognitive loads. *Brain Structure and Function*, *227*(8), 2701–2712. https://doi.org/10.1007/s00429-022-02564-0

Zhang, J., Abiose, O., Katsumi, Y., Touroutoglou, A., Dickerson, B. C., & Barrett, L. F. (2019). Intrinsic Functional Connectivity is Organized as Three Interdependent Gradients. *Scientific Reports*, *9*(1), 1–14. https://doi.org/10.1038/s41598-019-51793-7

Zhang, L., Wang, L., & Zhu, D. (2022). Predicting brain structural network using functional connectivity. *Medical Image Analysis*, *79*, 102463. https://doi.org/10.1016/j.media.2022.102463

Zhang, Q., Weber, M. A., & Narayanan, N. S. (2021). Medial prefrontal cortex and the temporal control of action. *International Review of Neurobiology*, *158*, 421–441. https://doi.org/10.1016/bs.irn.2020.11.004

Zhang, X., Song, M., Jiang, W., Lu, Y., Chu, C., Li, W., Wang, H., Shi, W., Lan, Y., & Jiang, T. (2025). Evolution of the Rich Club Properties in Mouse, Macaque, and Human Brain Networks: A Study of Functional Integration, Segregation, and Balance. *Neuroscience Bulletin*, *41*(9), 1630–1644. https://doi.org/10.1007/s12264-025-01393-5

Zhang, Y., Zhang, H., Chen, X., Liu, M., Zhu, X., & Shen, D. (2017). *Inter-subject Similarity Guided Brain Network Modeling for MCI Diagnosis* (Vol. 10541, Number November, pp. 168–175). https://doi.org/10.1007/978-3-319-67389-9_20

Zhou, S., & Mondragón, R. J. (2004). The rich-club phenomenon in the internet topology. *IEEE Communications Letters*, *8*(3), 180–182. https://doi.org/10.1109/LCOMM.2004.823426

Zhu, W., Huang, Y., Xie, X., Liu, W., Deng, J., Zhang, D., Wang, Z., & Liu, J. (2023). AutoShot: A Short Video Dataset and State-of-the-Art Shot Boundary Detection. *IEEE Computer Society Conference on Computer Vision and Pattern Recognition Workshops*, *2023-June*, 2238–2247. https://doi.org/10.1109/CVPRW59228.2023.00218

Zilles, K., & Amunts, K. (2010). Centenary of Brodmann's map conception and fate. *Nature Reviews Neuroscience*, *11*(2), 139–145. https://doi.org/10.1038/nrn2776

Zuo, C., Suo, X., Lan, H., Pan, N., Wang, S., Kemp, G. J., & Gong, Q. (2023). Global Alterations of Whole Brain Structural Connectome in Parkinson's Disease: A Meta-analysis. *Neuropsychology Review*, *33*(4), 783–802. https://doi.org/10.1007/s11065-022-09559-y

Appendix A – Selected Supplemental Material for Study 1

The full extend of the of the supplemental martial for **Study 1** (Mecklenbrauck, Gruber, et al., 2024) can be found in the OSF project associated with this dissertation.

AA.1 Supplemental Material 1: The calculation of Shannon surprise

The Shannon surprise of a stimulus was calculated using the formula derived from the infinite time scale model (Harrison et al., 2006). In the first step, the model counts the number of a certain event *m* in the sequence of presented stimuli (adapted from Harrison et al. (2011) and Trempler et al. (2020))

$$\alpha_m(N) = \sum_{i=1}^{N} \delta(x_i = m) \quad \text{(S1.1)},$$

where $\delta(x_i = m)$ is 1 if the *i*-th element in the sequence equals the event *m*. Then the model calculates the posterior probability of the event *m* occurring at trial *N* (Bernardo & Smith, 2001)

$$\rho_k(N) = \frac{\alpha_m(N)+\alpha_m(0)}{\sum_{j=1}^{M} \alpha_j(N)+\alpha_j(0)} \quad \text{(S1.2)},$$

with $\alpha_j(0)$ being the prior probability. We set the prior probability of all elements of $M = \{0,4,5,6,7,8,9\}$ to 1/7 as an uninformative, flat prior (Jeffreys, 1946). The surprise of trial *N* is then given by

$$I_k(N) = -\log \rho_m(N) \quad \text{(S1.3)}.$$

AA.2 Supplemental Material 2: The analysis using the lausanne250 parcellation

Employing the lausanne250 parcellation scheme and not including the subcortical regions resulted in the construction of 219 x 219 connectivity matrices for each participant. The same quality control measures like for the lausanne120 parcellated matrices were applied to test the matrices for outliers (van den Heuvel et al., 2019). None of the subjects had to be excluded.

To create a group matrix, we also used the same two methods described for the lasuanne120 parcellation schema (see section 2.7). That resulted in 838 edges in the case of 60% prevalence in the group and 738 edges using the FDR-corrected *t* test method based on Ponsoda et al. (2017) (Figure S5.1).

We continued the analysis as described in the section 2.7 for the group matrices which concluded with the final set of rich club (RC) hubs seen in Table S6.3-S6.4 and Figure S5.4C-D. We again used the *Multi-Scale Brain Parcellator* (Tourbier et al., 2019) to parcellate the MNI-152 template, now in accordance with the lausanne250 parcellation scheme. That enabled us to transform each of the 219 parcels to a binary region of interest (ROI) map that was extracted and dilated by one voxel size using the WFU pick atlas toolbox (Maldjian et al., 2003). Finally, we classified all nodes as *Rich Club* (RC), *Feeder*, or *Local* as we did for the lausanne120 which resulted in the classifications in Table S6.7-S6.8 and were later used in the ROI and centrality analyses (see sections 2.8.3 & 2.8.4).

Centrality Analysis for the lausanne250 parcellation. The extraction of the individual centrality measures we done as described for the lausanne120 parcellation in the section 2.8.4. On a descriptive level we looked at the regions that are covered by the clusters identified from the whole brain analysis with the determined threshold of 47 voxel in regard to their network-based classification as RC hub, Feeder or Local node (Figure S5.6B-D).

On the model side, we used a MANOVA-like approach within the brms (Bürkner, 2017) framework to compare the centrality measures calculated for each subject between the identified clusters. No model had any divergent transitions, all *Rhat* < 1.05, and all variables had

bulk- and tail-effective samples ≥ 1478 and ≥ 3973, respectively. Posterior checks showed that the cumulative count model simulations reasonably capture the means and distributions of the observed data (Figure S6.8).

Firstly, we compared the model (Eq. 5) including the factor HIERARCHY CONTRAST with a null model to see if the factor explained any variance of the centrality measures (Table S2.1). The leave-one-out-cross-validation (loo) comparison revealed an increase in the expected log pointwise predictive density (elpd) with inclusion of the factor HIERARCHY CONTRAST.

Table S2.1

Fit indices of the HIERARCHY *CONTRAST Model (Eq. 5) compared to the null model for lausanne120 parcellation scheme*

Model	$\widehat{elpd}_{diff}$	$se(\widehat{elpd}_{diff})$	$\widehat{elpd}_{loo}$	$se(\widehat{elpd}_{loo})$
Hierarchy Contrast + (1|Subject)	0.0	0.0	-1757.27	49.44
1 + (1|Subject)	-5.2	2.6	-1762.51	49.43

Note. Models are considered to be better if the absolute difference is larger than the standard error (Mohor et al., 2021); $\widehat{elpd}_{loo}$ = expected log pointwise predictive density for a new dataset using Pareto smoothed importance sampling (PSIS) leave-one-out-cross-validation (loo) criterion. The closer to zero the better the model; $\widehat{elpd}_{diff}$ = difference between the $\widehat{elpd}_{loo}$ of two compared models; se = standard error of the variable.

To specifically test the one-sided hypothesis that the centrality measures of the areas derived from the NONET > TRIPLET contrast were higher than those for the TRIPLET > SINGLE contrast, we again used the hypothesis function from the brms library (Bürkner, 2017) (Table S2.2). The expected effect was revealed for the centrality measures degree centrality, betweenness centrality and participation coefficient. Only closeness centrality and within-module degree *z*-score failed to show the predicted effect (Figure S2.1). Therefore, the results are very similar to what has been found for the lausanne120 parcellation scheme (see section 3.5).

Table S2.2

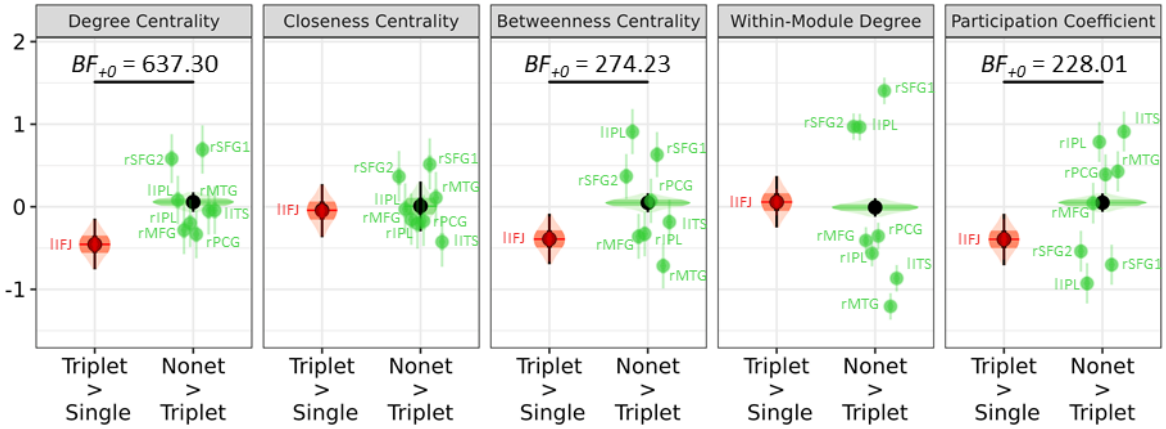
Results of testing (NONET > TRIPLET) > (TRIPLET > SINGLE) for model Eq. 5 for all five centrality measures extracted from individual connectivity matrices following lasuanne250 parcellation scheme

Centrality measure	*M*	*SD*	CI lower	CI upper	Evidence Ratio	Posterior probability
Degree Centrality	**0.51**	**0.16**	**0.24**	**0.78**	**637.30**	**1**
Closeness Centrality	0.05	0.07	-0.06	0.16	3.59	0.78
Betweenness Centrality	**0.44**	**0.16**	**0.17**	**0.71**	**274.23**	**1**
Within-Module Degree z-Score	-0.07	0.17	-0.34	0.21	0.54	0.35
Participation Coefficient	**0.44**	**0.17**	**0.17**	**0.72**	**228.01**	**1**

Note. CI = Credible Interval. Rich Club = Rich Club. Evidence ratio of one-sided hypothesis test is equal to the Bayes factor.

Figure S2.1

Results of the centrality analysis for lausanne250 parcellation scheme



Note. Density distributions with mean point estimate, 50 and 95% highest probability density areas marked. Centrality measures are controlled for cluster size and *z*-standardized for comparability. Eye plots describe distribution of contrast on average, colorful point-interval plots describe each individual cluster. l = left; r = right; IFJ = Inferior frontal junction; MFG = Middle frontal gyrus; SFG = Superior frontal gyrus; IPL = Inferior parietal lobule; PCG = Posterior cingulate gyrus; MTG = Middle temporal sulcus; ITS = Inferior temporal sulcus; rSFG1 = rSFG (22,60,14); rSFG2 = rSFG (22,18,58); BF = Bayes factor.

AA.3 Supplemental Material 3: FDR-cluster corrected whole-brain fMRI Analysis

To analyze the effect of the hierarchical stimulus structure on the brain activity, we contrasted the estimated BOLD activation of the four conditions. Results were corrected for multiple comparisons using cluster-wise FDR. Clusters were thresholded at a corrected $p < .05$. We found significant clusters in three contrasts NONET > SINGLE, COMPLETE > SINGLE and NONET > TRIPLET (Table S3.1 and Figure S3.1). The contrast NONET > SINGLE revealed significant clusters in the right middle frontal gyrus (MFG) extending into the superior frontal sulcus, the left inferior frontal junction including the inferior precentral sulcus, and the bilateral intraparietal sulcus (IPS). Similarly, the contrast COMPLETE > SINGLE also identified a significant cluster in the left inferior frontal junction which included Local maxima in the inferior frontal sulcus (IFS), inferior frontal gyrus (IFG) and the inferior precentral sulcus. Also, clusters in the bilateral IPS were found with a second cluster in the left IPS which contained more posterior areas of the IPS. Additionally, this contrast found a cluster in the right MFG but closer to the right inferior precentral sulcus. Finally, the contrast NONET > TRIPLET found one significant cluster in in the right superior frontal gyrus (SFG) which extended to more anterior as well as medial portions of the SFG corresponding to Brodmann Area (BA) 8.

Table S3.1

Significant activation clusters from second-level whole-brain block contrasts

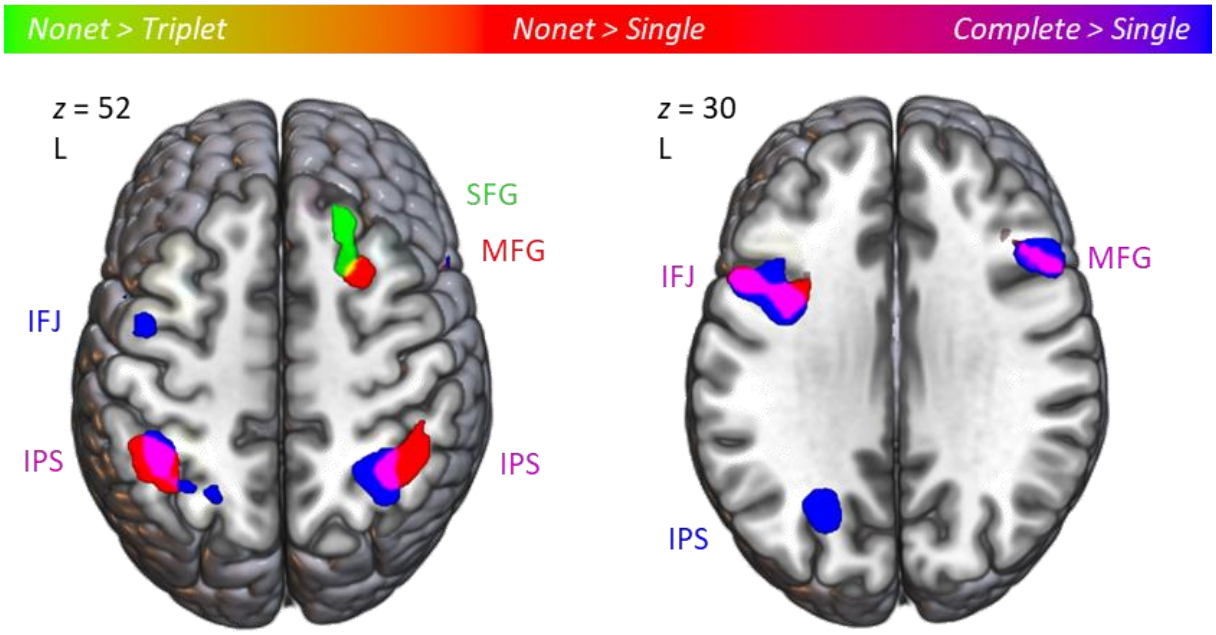
Localization	H	Cluster extent (in voxel)	MNI coordinates x	y	z	*t* value	*p*-value (FDR cluster corrected)
NONET > SINGLE							
Middle frontal gyrus	R	510	38	24	40	5.17	.005
Superior frontal sulcus	R	l.m.	26	16	52	3.75	
Inferior frontal junction	L	380	-32	6	30	4.17	.011
Inferior precentral sulcus	L	l.m.	-50	12	30	3.90	
Intraparietal sulcus	R	457	44	-48	54	4.45	.006
	L	611	-42	-52	52	4.34	.004
COMPLETE > SINGLE							
Middle frontal gyrus	R	248	48	20	30	4.50	.004
Inferior frontal junction	L	1160	-38	2	26	5.79	< .001
Intraparietal sulcus	R	515	28	-50	46	5.15	< .001
	L	507	-26	-48	38	4.39	< .001

Intraparietal sulcus	L	266	-24	-68	30	4.53	.003
Posterior intraparietal sulcus	L	l.m.	-22	-64	38	3.87	
NONET > TRIPLET							
Superior frontal gyrus	R	401	22	18	58	4.32	.030
Medial superior frontal gyrus	R	l.m.	12	36	42	4.01	
Superior frontal gyrus	R	l.m.	22	32	56	3.96	

Note. H = Hemisphere; L = left; R = right; MNI = *Montreal Neurological Institute; l.m. = local maximum*.

Figure S3.1

BOLD activation clusters for the contrasts NONET > SINGLE, COMPLETE > SINGLE, and NONET > TRIPLET



Note. Significant clusters FDR cluster corrected at $p < .05$, depicted on MNI template. L = left; *z* = z coordinate; IFJ = Inferior frontal junction; IPS = Intraparietal sulcus; SFG = Superior frontal gyrus; MFG = Middle frontal gyrus; MNI = Montreal Neurological Institute.

AA.4 Supplemental Material 4: ROI analysis results tabled for the remaining three combinations of parcellation scheme and group matrix construction method

Table S4.1

Results of the hypothesis test of model Eq. 4 for the data from parcellation scheme lausanne120 and t-test-based group matrix

Hypothesis	*M*	*SD*	CI lower	CI upper	Evidence Ratio	Posterior probability
Increase of beta values with level of Hierarchy separated by Node Classification						
Local						
TRIPLET > SINGLE	-0.09	0.12	-0.29	0.11	0.30	0.23
NONET > TRIPLET	**0.39**	**0.20**	**0.06**	**0.71**	**37.91**	**0.97**
COMPLETE > NONET	-0.07	0.16	-0.33	0.19	0.50	0.33
Feeder						
TRIPLET > SINGLE	-0.03	0.12	-0.23	0.18	0.69	0.41
NONET > TRIPLET	**0.46**	**0.20**	**0.13**	**0.78**	**87.50**	**0.99**
COMPLETE > NONET	-0.11	0.16	-0.37	0.15	0.32	0.24
RC						
TRIPLET > SINGLE	0.02	0.14	-0.21	0.26	1.30	0.57
NONET > TRIPLET	**0.41**	**0.21**	**0.07**	**0.76**	**38.53**	**0.97**
COMPLETE > NONET	-0.13	0.17	-0.42	0.15	0.28	0.22
Increase of beta values with level of Hierarchy compared between Node Classifications						
TRIPLET > SINGLE						
Feeder > Local	0.06	0.06	-0.05	0.16	4.55	0.82
RC > Local	0.11	0.09	-0.05	0.26	7.05	0.88
RC > Feeder	0.05	0.10	-0.11	0.21	2.34	0.70
NONET > TRIPLET						
Feeder > Local	0.07	0.06	-0.03	0.18	6.42	0.87
RC > Local	0.03	0.09	-0.13	0.19	1.62	0.62
RC > Feeder	-0.04	0.10	-0.20	0.12	0.50	0.33
COMPLETE > NONET						
Feeder > Local	-0.04	0.07	-0.15	0.06	0.34	0.25
RC > Local	-0.07	0.10	-0.23	0.09	0.31	0.24
RC > Feeder	-0.07	0.10	-0.23	0.09	0.31	0.24
No difference of beta values between Node Classification						
Local = Feeder	**-0.96**	**0.28**	**-1.50**	**-0.41**	**0.05**	**0.04**
Local = RC	**-1.41**	**0.41**	**-2.21**	**-0.60**	**0.04**	**0.04**
Feeder = RC	-0.45	0.42	-1.27	0.37	9.92	0.91

Note. CI = Credible Interval. RC = Rich Club. The evidence ratio of one-sided hypothesis tests is equal to the Bayes factor. All Rhat = 1.00, Bulk_ESS $\geq$ 2775 Tail_ESS $\geq$ 4726, N = 17905.

Table S4.2

Results of the hypothesis test of model Eq. 4 for the data from parcellation scheme lausanne250 and 60% prevalence-based group matrix

Hypothesis	*M*	*SD*	CI lower	CI upper	Evidence Ratio	Posterior probability
Increase of beta values with level of Hierarchy separated by Node Classification						
Local						
TRIPLET > SINGLE	-0.03	0.12	-0.23	0.16	0.62	0.38
NONET > TRIPLET	**0.38**	**0.19**	**0.06**	**0.70**	**39.54**	**0.98**
COMPLETE > NONET	-0.08	0.16	-0.34	0.17	0.41	0.29
Feeder						
TRIPLET > SINGLE	0.00	0.12	-0.20	0.20	0.95	0.49
NONET > TRIPLET	**0.43**	**0.19**	**0.11**	**0.75**	**73.63**	**0.99**
COMPLETE > NONET	-0.09	0.16	-0.35	0.17	0.38	0.28
RC						
TRIPLET > SINGLE	-0.01	0.14	-0.25	0.22	0.88	0.47
NONET > TRIPLET	**0.51**	**0.21**	**0.17**	**0.85**	**130.58**	**0.99**
COMPLETE > NONET	-0.16	0.18	-0.45	0.12	0.21	0.17
Increase of beta values with level of Hierarchy compared between Node Classifications						
TRIPLET > SINGLE						
Feeder > Local	0.03	0.05	-0.05	0.12	2.68	0.73
RC > Local	0.02	0.09	-0.13	0.17	1.48	0.60
RC > Feeder	-0.01	0.10	-0.17	0.15	0.86	0.46
NONET > TRIPLET						
Feeder > Local	0.05	0.05	-0.03	0.14	5.25	0.84
RC > Local	0.13	0.09	-0.02	0.28	11.41	0.92
RC > Feeder	0.08	0.10	-0.08	0.24	3.70	0.79
COMPLETE > NONET						
Feeder > Local	-0.01	0.05	-0.09	0.08	0.81	0.45
RC > Local	-0.08	0.09	-0.23	0.07	0.24	0.19
RC > Feeder	-0.07	0.10	-0.23	0.09	0.29	0.22
No difference of beta values between Node Classifications						
Local = Feeder	**-0.63**	**0.22**	**-1.06**	**-0.20**	**0.43**	**0.30**
Local = RC	**-1.21**	**0.38**	**-1.96**	**-0.46**	**0.08**	**0.07**
Feeder = RC	-0.58	0.40	-1.36	0.19	6.31	0.86

Note. CI = Credible Interval. RC = Rich Club. The evidence ratio of one-sided hypothesis tests is equal to the Bayes factor. All Rhat < 1.05, Bulk_ESS ≥ 480, Tail_ESS ≥ 1226, N = 34677.

Table S4.3

Results of the hypothesis test of model Eq. 4 for the data from parcellation scheme lausanne250 and t-test-based group matrix

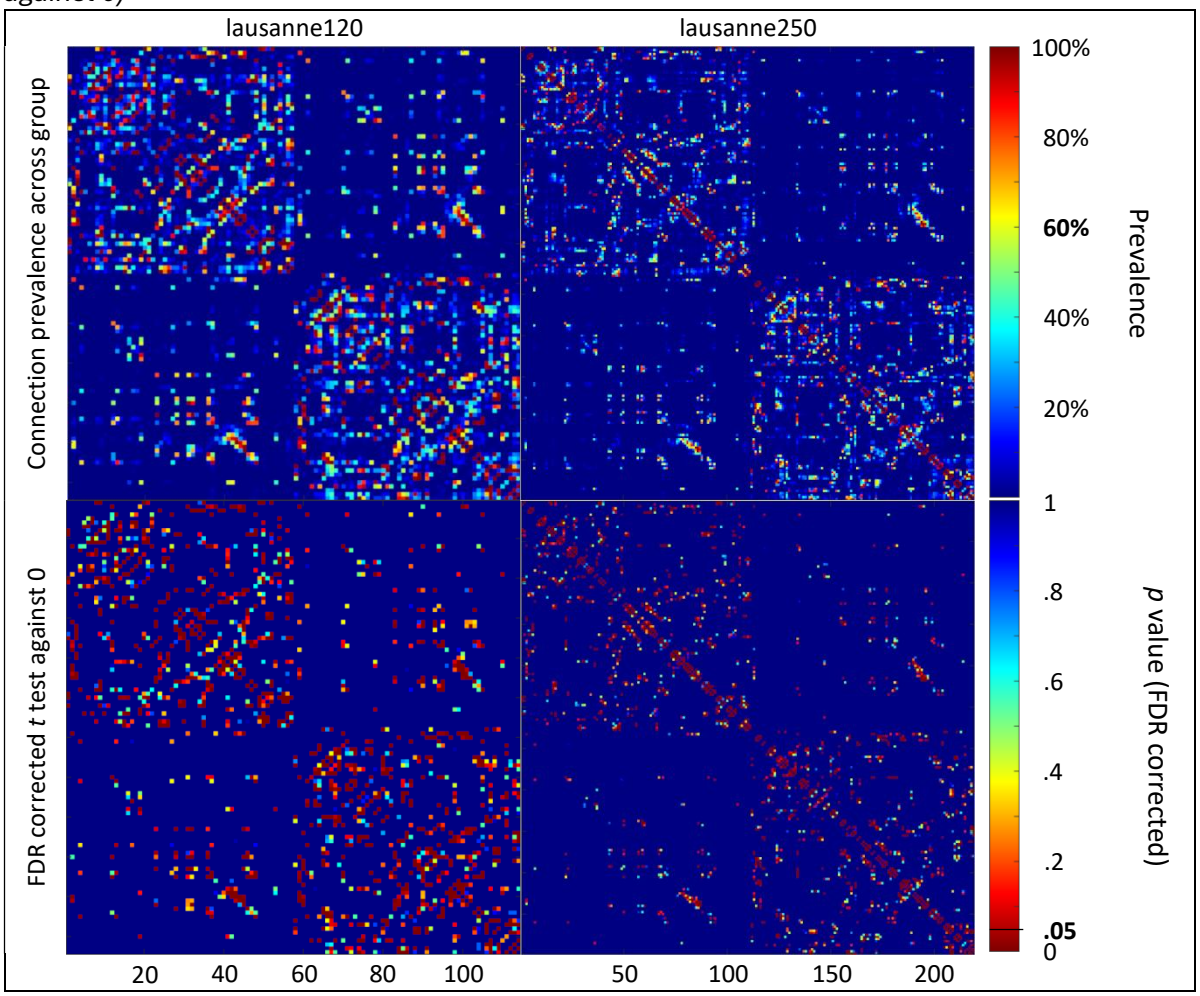
Hypothesis	*M*	*SD*	CI lower	CI upper	Evidence Ratio	Posterior probability
Increase of beta values with level of Hierarchy separated by Node Classification						
Local						
TRIPLET > SINGLE	-0.06	0.12	-0.26	0.14	0.45	0.31
NONET > TRIPLET	**0.40**	**0.19**	**0.08**	**0.71**	**48.42**	**0.98**
COMPLETE > NONET	-0.08	0.15	-0.33	0.17	0.41	0.29
Feeder						
TRIPLET > SINGLE	0.03	0.12	-0.18	0.23	1.39	0.58
NONET > TRIPLET	**0.41**	**0.19**	**0.09**	**0.73**	**50.81**	**0.98**
COMPLETE > NONET	-0.09	0.15	-0.34	0.17	0.38	0.28
RC						
TRIPLET > SINGLE	-0.02	0.14	-0.24	0.21	0.82	0.45
NONET > TRIPLET	**0.43**	**0.20**	**0.09**	**0.75**	**51.26**	**0.98**
COMPLETE > NONET	-0.14	0.16	-0.40	0.13	0.24	0.20
Increase of beta values with level of Hierarchy compared between Node Classifications						
TRIPLET > SINGLE						
Feeder > Local	0.08	0.05	0.00	0.17	16.56	0.94
RC > Local	0.04	0.08	-0.08	0.17	2.52	0.72
RC > Feeder	-0.04	0.08	-0.17	0.09	0.44	0.30
NONET > TRIPLET						
Feeder > Local	0.01	0.05	-0.08	0.10	1.40	0.58
RC > Local	0.03	0.08	-0.10	0.15	1.73	0.63
RC > Feeder	0.01	0.08	-0.12	0.15	1.31	0.57
COMPLETE > NONET						
Feeder > Local	-0.01	0.05	-0.09	0.08	0.78	0.44
RC > Local	-0.06	0.08	-0.18	0.07	0.28	0.22
RC > Feeder	-0.05	0.08	-0.18	0.08	0.37	0.27
No difference of beta values between Node Classifications						
Local = Feeder	**-0.70**	**0.22**	**-1.15**	**-0.27**	**0.18**	**0.15**
Local = RC	**-0.82**	**0.32**	**-1.44**	**-0.18**	**0.66**	**0.40**
Feeder = RC	-0.12	0.34	-0.77	0.55	19.78	0.95

Note. CI = Credible Interval. RC = Rich Club. The evidence ratio of one-sided hypothesis tests is equal to the Bayes factor. All Rhat < 1.05, Bulk_ESS $\geq$ 673, Bulk_ESS $\geq$ 1284, N = 34677.

AA.5 Supplemental Material 5: Additional results figures

Figure S5.1

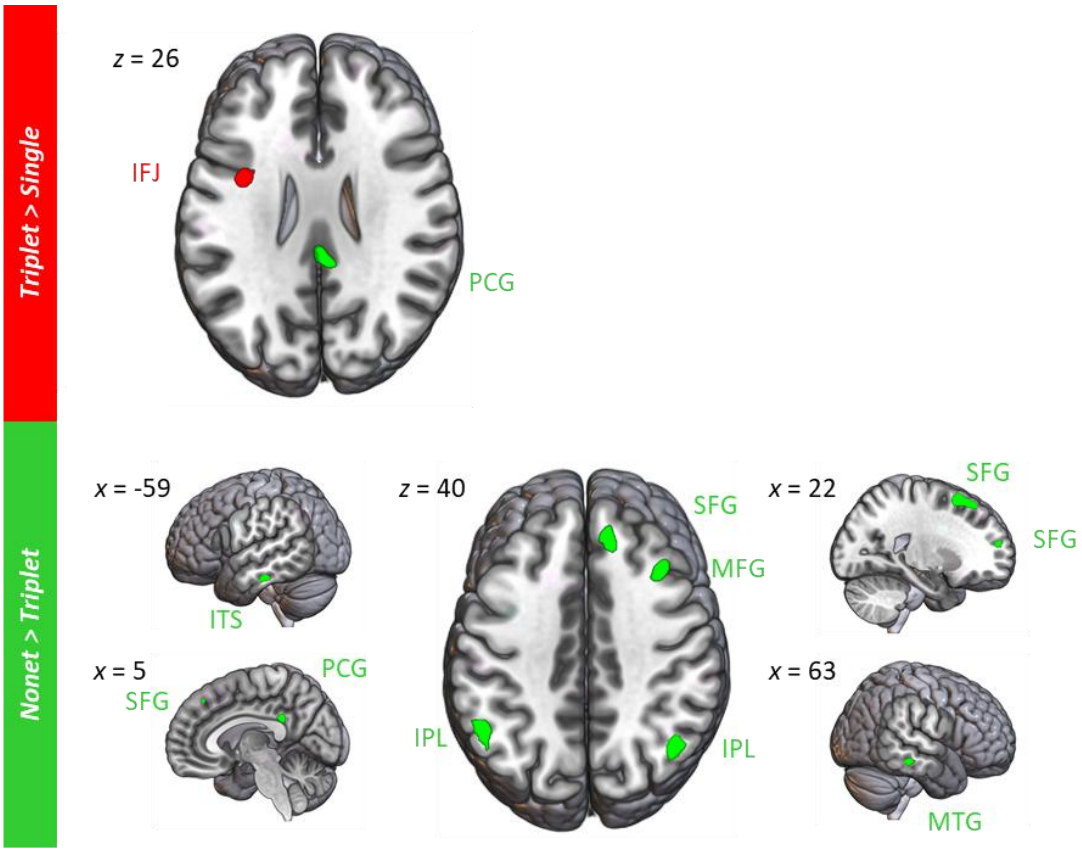
Group connectivity matrices for the four combinations of parcellation scheme (lausanne120 or lausanne250) and methods of group matrix construction (prevalence or FDR-corrected t-test against 0)



Note. To get binary matrices prevalence-based matrices were thresholded at ≥ 60% and FDR corrected *t*-tests-based matrices at $p < .05$.

Figure S5.2

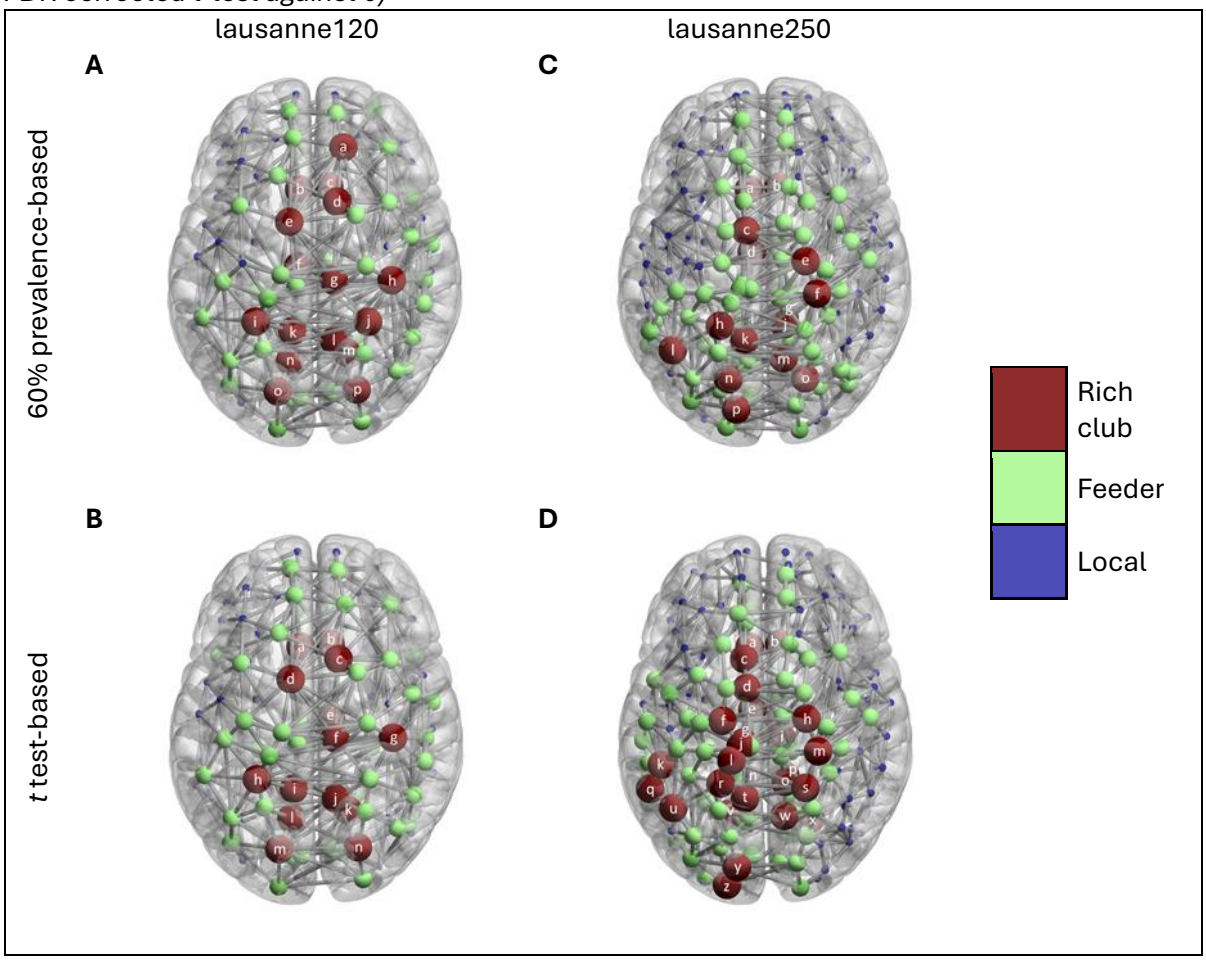
BOLD activation clusters for the contrasts TRIPLET > SINGLE and NONET > TRIPLET



Note. Significant clusters at the cluster threshold of 47 voxels, depicted on MNI template. *x* = x coordinate; *z* = z coordinate; IFJ= Inferior frontal junction; PCG = Posterior cingulate gyrus; ITS = Inferior temporal sulcus; MTG = Middle temporal sulcus; SFG = Superior frontal gyrus; IPL = Inferior parietal lobule; MNI = Montreal Neurological Institute.

Figure S5.3

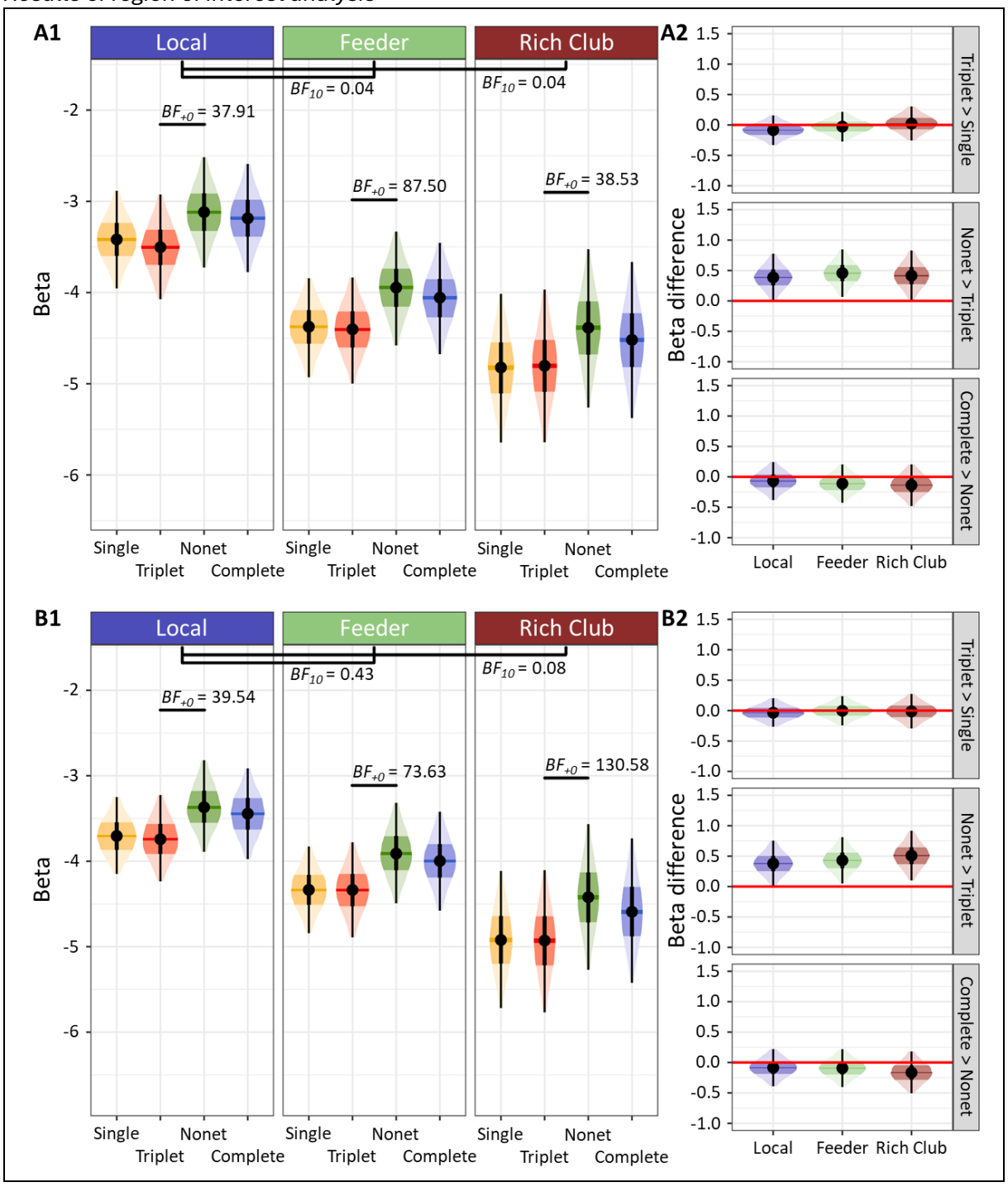
Node classification and identified rich club network for the four combinations of parcellation scheme (lausanne120 or lausanne250) and methods of group matrix construction (prevalence or FDR corrected t-test against 0)

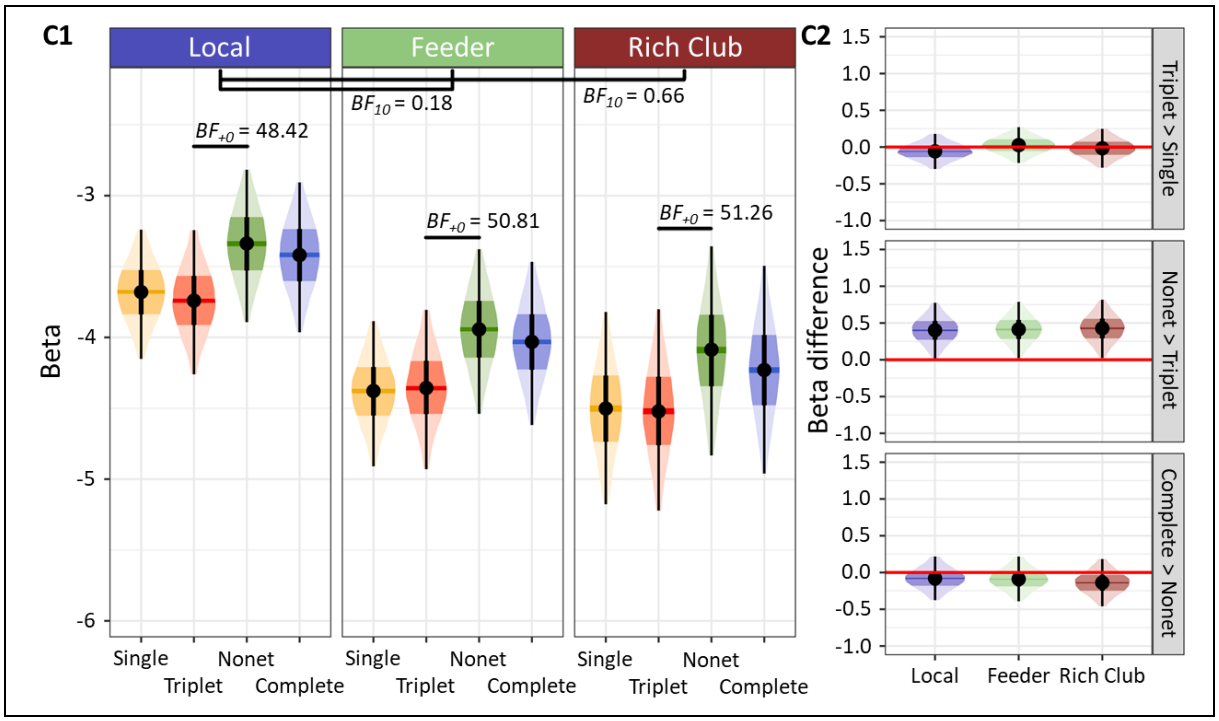


Note. (A) Rich club hubs of lausanne120 and 60% prevalence-based group matrix: (a) right superiorfrontal_2, (b) left caudalanteriorcingulate_1, (c) right caudalanteriorcingulate_1, (d) right superiorfrontal_3, (e) left superiorfrontal_4, (f) left posteriorcingulate_1, (g) right paracentral_1, (h) right postcentral_2, (i) left superiorparietal_1, (j) right superiorparietal_1, (k) left precuneus_1, (l) right precuneus_2, (m) right precuneus_1, (n) left precuneus_2, (o) left superiorparietal_3, (p) right superiorparietal_3. (B) Rich club hubs of lausanne120 and *t* test-based group matrix: (a) left caudalanteriorcingulate_1, (b) right caudalanteriorcingulate_1, (c) right superiorfrontal_3, (d) left superiorfrontal_4, (e) right posteriorcingulate_1, (f) right paracentral_1, (g) right postcentral_2, (h) left superiorparietal_1, (i) left precuneus_1, (j) right precuneus_2, (k) right precuneus_1, (l) left precuneus_2, (m) left superiorparietal_3, (n) right superiorparietal_3. (C) Rich club hubs of lausanne250 and 60% prevalence-based group matrix: (a) left caudalanteriorcingulate_1, (b) right caudalanteriorcingulate_1, (c) left superiorfrontal_8, (d) left posteriorcingulate_1, (e) right precentral_6, (f) right postcentral_5, (g) right isthmuscingulate_1, (h) left superiorparietal_1, (i) left isthmuscingulate_1, (j) right precuneus_5, (k) left precuneus_1, (l) left inferiorparietal_5, (m) right precuneus_4, (n) left superiorparietal_5, (o) right superiorparietal_5, (p) left superiorparietal_7. (D) Rich club hubs of lausanne250 and *t* test-based group matrix: (a) left caudalanteriorcingulate_1, (b) right caudalanteriorcingulate_1, (c) left superiorfrontal_7, (d) left superiorfrontal_8, (e) left posteriorcingulate_1, (f) left precentral_2, (g) left paracentral_2, (h) right precentral_6, (i) right posteriorcingulate_2, (j) left precentral_1, (k) left supramarginal_5, (l) left postcentral_1, (m) right postcentral_5, (n) left isthmuscingulate_1, (o) right precuneus_5, (p) right isthmuscingulate_1, (q) left supramarginal_4, (r) left superiorparietal_1, (s) right superiorparietal_2, (t) left precuneus_1, (u) left inferiorparietal_5, (v) left precuneus_5, (w) right precuneus_4, (x) right precuneus_1, (y) left superiorparietal_7, (z) left lateraloccipital_1.

Figure S5.4

Results of region of interest analysis

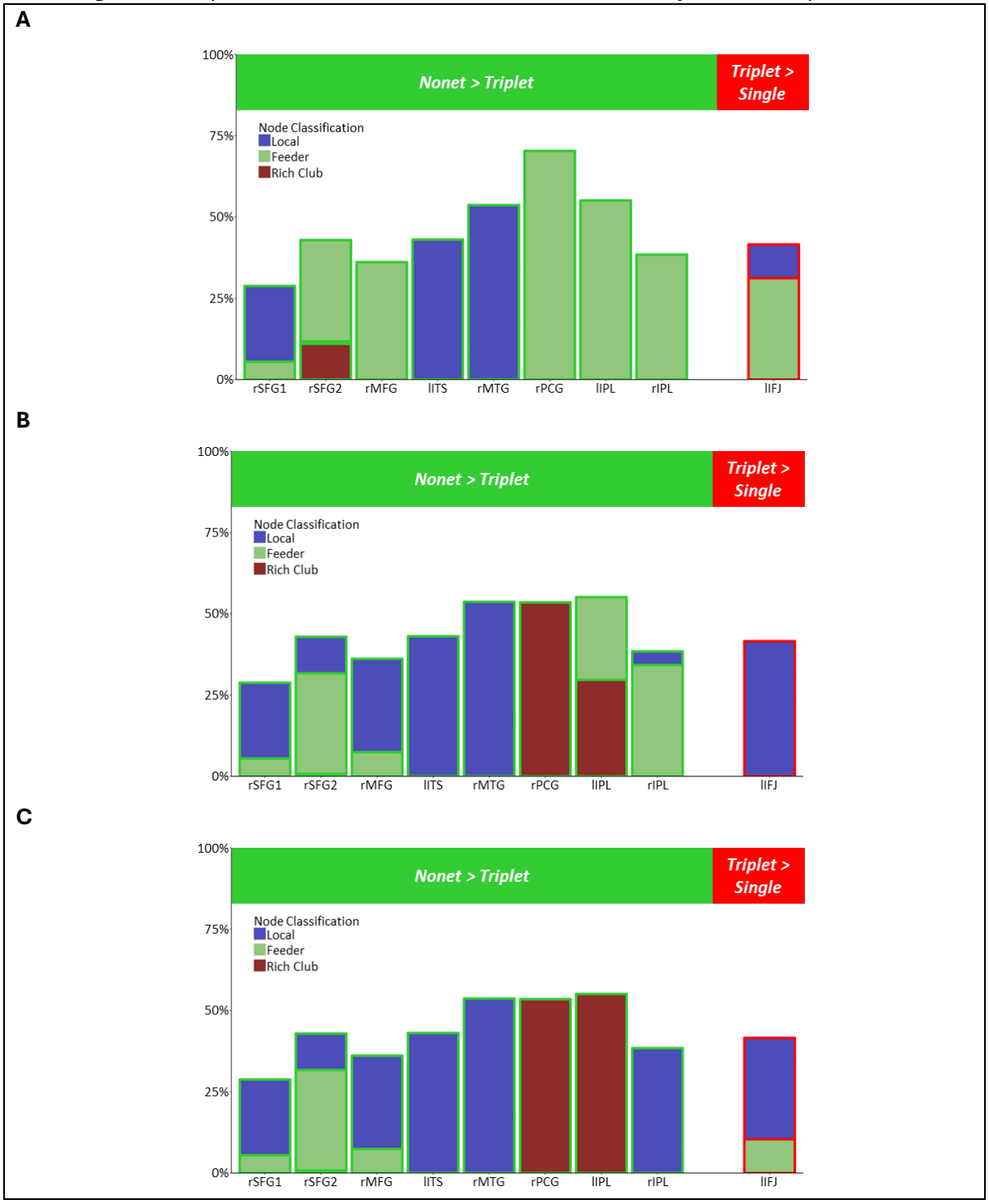




Note. Beta values represent mean activations per condition compared to the implicit baseline. Density plots of posterior distributions with mean point estimate, 50% and 95% highest probability density areas marked. Local = no connection rich club; Feeder = connection to rich club; Rich Club = rich club hubs. Yellow = SINGLE; Red = TRIPLET; Green = NONET; Blue = COMPLETE; Dark blue = Local; Light green = Feeder, Dark red = Rich Club. (A) Based on the combination lausanne120 and *t* test. (B) Based on the combination lausanne250 and 60% prevalence. (C) Based on the combination lausanne250 and *t* test. (1) Level of HIERARCHY estimates in different levels of NODE CLASSIFICATION. (2) HIERARCHY differences in different levels of NODE CLASSIFICATION. Red line marks no difference.

Figure S5.5

Percentage of overlap of activation clusters of the whole brain analysis with the parcellation



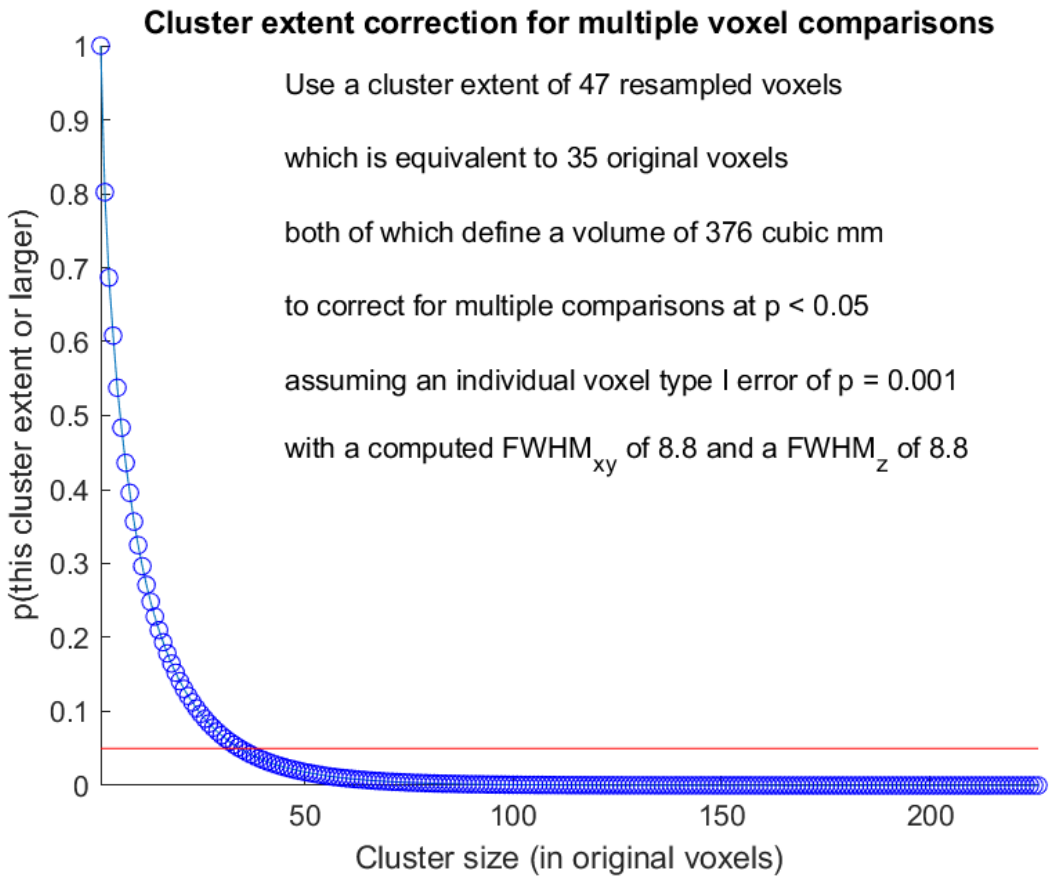
Note. (A) Colored according to lausanne120 and *t* test-based NODE CLASSIFICATION. (B) Colored according to lausanne250 and 60% prevalence-based NODE CLASSIFICATION. (C) Colored according to lausanne250 and *t* test-based NODE CLASSIFICATION. l = left; r = right; SFG = Superior frontal gyrus; MFG = Middle frontal gyrus; ITS = Inferior temporal sulcus; MTG = Middle temporal sulcus; PCG = Posterior cingulate gyrus; IPL = Inferior parietal lobule; IFJ = Inferior frontal junction; rSFG1 = rSFG (22, 60, 14); rSFG2 = rSFG (22, 18, 58).

AA.6 Supplemental Material 8: Results of cluster threshold simulation

In accordance with Slotnick et al. (2003, 2017) we simulated a cluster size threshold using cluster_threshold_beta.m for our fMRI results that corresponds to a voxel-wise *p* value of .001 and cluster size $p < .05$ corrected for multiple comparisons. We applied the specific acquisition and preprocessing parameters representative for our data: acquisition matrix 94 x 94 x 66 voxels, voxel size 2.2 x 2.2 x 2.2 mm^3 and normalized voxel size 2 x 2 x 2 mm^3. To estimate the actual spatial smoothness of the data we used img_xcorr.m which is also developed by Slotnick (Slotnick, 2020). Therefore, we had to determine a mostly noise contrast as the basis for the spatial autocorrelation calculation. To accomplish this, we calculated a second level contrast in SPM12 using different stepwise contrasts for different subjects. In detail, we took the first level contrast images of the contrasts TRIPLET > SINGLE, NONET > TRIPLET, COMPLETE > NONET, and SINGLE > COMPLETE ten times each across our forty participants to create a 'nonsensical' noise contrast image necessary for the correct calculation. This resulted in a computed spatial autocorrelation of 8.5707 mm. Using all the specified parameter we ran the Markov-Chain-Monte-Carlo simulation 10,000 times to obtain the cluster threshold for our data specifications. This resulted in a cluster threshold of 47 voxels which corresponds to 376 mm^3.

Figure S8.1

Results of the cluster threshold simulation



Note. Full-width half-maximum (FWHM) spatial autocorrelation gets calculated in simulation based on the determined autocorrelation in noise contrast. 10,000 iterations.

AA.7 Supplemental Material 9: Rich club analysis using the Human Connectome Project dataset

The Human Connectome Project (HCP) collected structural and functional MRI as well as behavioral, electroencephalography and magnetoencephalography, and genetic data of 1200 healthy individuals (Van Essen et al., 2013). This data is publicly available for download. For the purpose of validating our node classification and the subsequent analyses on an external dataset, we downloaded structural and DW-MRI data from a subset of 100 unrelated subjects from the HCP dataset. The sample included 53 female subjects and was between 22 and 35 years old. The structural T1 weighted data was collected using a 3D-MPRAGE sequence with a TR = 2400 ms, a TE = 2.14 ms and a flip angle of 8°. The matrix spanned an area of 224 x 224 mm and was sampled using an isotropic voxel size of 0.7 mm. The DWI was accomplished using a spin-echo EPI sequence with a TR = 5520 ms, a TE = 89.5 ms and a flip angle of 78°. The field of view was 210 x 180 mm and was sampled using 111 slices with an isotropic voxel size of 1.25 mm. The sequence used multislice acquisition and collected three slices simultaneously. In total, three different diffusion gradients b = 1000 s/mm^2, b = 2000 s/mm^2 and b = 3000 s/mm^2 were applied, each gradient table including approximately 90 diffusion weighting directions (Feinberg et al., 2010; Moeller et al., 2010; Setsompop et al., 2012; Xu et al., 2012).

The DWI data downloaded was already minimally preprocessed which included the correction of intensity differences across runs, EPI distortion correction using topup, eddy current and motion correction as well as gradient nonlinearity correction and the registration of the mean b0 image to the structural volume (Glasser et al., 2013).

We applied the CATO Toolbox (de Lange et al., 2023) to extract the structural connectivity matrices using the same combined DTI-GQI algorithm that we applied to our own data (see section 2.6). Subsequently, we also created four binarized group matrices using the same thresholds and methods as described in section 2.7 for the two parcellation schemes and prevalence- and *t* test-based group matrices, respectively. Finally, the same pipeline was used to

define RC hubs, Feeder nodes and Local nodes in the group-wise structural connectivity matrices from the HCP dataset.

S9.1 Rich club analysis results. We compared the hub classification based on the HCP dataset (Table S9.8) with the one determined using the data collected in the present study by calculating Cohen's κ as a measure of inter-rater reliability. The two raters in this case are the classification based on our own data and the classification based on the HCP data, respectively. According to the conventions by Landis and Koch (1977), we find a slight agreement between the node classifications and a fair to moderate agreement when just considering the binary classification of a RC hub and a non-RC node (Table S9.1).

Table S9.1

Cohen's κ for the comparison of RC classification using our own or Human Connectome Project connectivity data

Parcellation scheme		lausanne120		lausanne250	
Group matrix method		prevalence	*t* test	prevalence	*t* test
Cohen's κ	Node classification	.18	.09	.18	.02
	Binary RC classification	.45	.39	.21	.23

Note. Prevalence is 60% prevalence, *t* test is FDR corrected. RC = Rich Club.

S9.2 ROI analysis. We repeated the ROI analysis using our own functional data but the NODE CLASSIFICATION was based on the HCP dataset. Again, we ran the models for all four combinations of parcellation scheme and group matrix creation method. None of the models using the HCP classification had any divergent transitions, all *Rhat* < 1.05 and the bulk- and tail-effective sample sizes are given in Table S9.2 - S9.5. Posterior checks showed that the cumulative count model simulations reasonably capture the means and distributions of the observed data.

Table S9.2

Results of the hypothesis test of model Eq. 4 for the data from parcellation scheme lausanne120 and 60% prevalence-based group matrix using the HCP dataset

Hypothesis	*M*	*SD*	CI lower	CI upper	Evidence Ratio	Posterior probability
Increase of beta values with level of Hierarchy separated by Node Classification						
Local						
TRIPLET > SINGLE	-0.02	0.14	-0.25	0.22	0.84	0.46
NONET > TRIPLET	**0.35**	**0.21**	**0.01**	**0.70**	**20.51**	**0.95**
COMPLETE > NONET	-0.03	0.17	-0.31	0.25	0.76	0.43
Feeder						
TRIPLET > SINGLE	-0.07	0.12	-0.27	0.13	0.39	0.28
NONET > TRIPLET	**0.41**	**0.20**	**0.09**	**0.73**	**52.57**	**0.98**
COMPLETE > NONET	-0.10	0.16	-0.36	0.15	0.33	0.25
RC						
TRIPLET > SINGLE	-0.01	0.14	-0.24	0.21	0.85	0.46
NONET > TRIPLET	**0.51**	**0.21**	**0.17**	**0.85**	**134.75**	**0.99**
COMPLETE > NONET	-0.11	0.17	-0.39	0.17	0.34	0.26
Increase of beta values with level of Hierarchy compared between Node Classifications						
TRIPLET > SINGLE						
Feeder > Local	-0.05	0.09	-0.20	0.10	0.39	0.28
RC > Local	0.00	0.11	-0.18	0.19	1.02	0.51
RC > Feeder	0.05	0.08	-0.08	0.19	2.93	0.75
NONET > TRIPLET						
Feeder > Local	0.06	0.09	-0.09	0.21	2.99	0.75
RC > Local	0.16	0.11	-0.03	0.34	11.73	0.92
RC > Feeder	0.10	0.08	-0.04	0.24	7.23	0.88
COMPLETE > NONET						
Feeder > Local	-0.07	0.09	-0.22	0.07	0.25	0.20
RC > Local	-0.08	0.11	-0.26	0.10	0.30	0.23
RC > Feeder	-0.01	0.08	-0.14	0.13	0.89	0.47
No difference of beta values between Node Classification						
Local = Feeder	**-0.75**	**0.38**	**-1.49**	**-0.01**	**1.97**	**0.66**
Local = RC	**-2.25**	**0.47**	**-3.16**	**-1.33**	**0**	**0**
Feeder = RC	**-1.50**	**0.35**	**-2.18**	**-0.81**	**0**	**0**

Note. HCP = Human Connectome Project. CI = Credible Interval. RC = Rich Club. The evidence ratio of one-sided hypothesis tests is equal to the Bayes factor. All Rhat = 1.00, Bulk_ESS $\geq$ 4719 Tail_ESS $\geq$ 6669, N = 17905.

Table S9.3

Results of the hypothesis test of model Eq. 4 for the data from parcellation scheme lausanne120 and t test-based group matrix using the HCP dataset

Hypothesis	*M*	*SD*	CI lower	CI upper	Evidence Ratio	Posterior probability
Increase of beta values with level of Hierarchy separated by Node Classification						
Local						
TRIPLET > SINGLE	-0.07	0.25	-0.49	0.34	0.64	0.39
NONET > TRIPLET	0.40	0.29	-0.08	0.88	10.62	0.91
COMPLETE > NONET	0.05	0.27	-0.40	0.50	1.33	0.57
Feeder						
TRIPLET > SINGLE	-0.05	0.12	-0.25	0.14	0.47	0.32
NONET > TRIPLET	**0.39**	**0.19**	**0.07**	**0.71**	**47.47**	**0.98**
COMPLETE > NONET	-0.09	0.16	-0.34	0.17	0.39	0.28
RC						
TRIPLET > SINGLE	-0.03	0.13	-0.25	0.19	0.74	0.42
NONET > TRIPLET	**0.54**	**0.20**	**0.21**	**0.87**	**231.56**	**1**
COMPLETE > NONET	-0.14	0.17	-0.41	0.13	0.24	0.19
Increase of beta values with level of Hierarchy compared between Node Classifications						
TRIPLET > SINGLE						
Feeder > Local	0.02	0.22	-0.35	0.39	1.12	0.53
RC > Local	0.05	0.23	-0.34	0.43	1.37	0.58
RC > Feeder	0.03	0.08	-0.10	0.15	1.86	0.65
NONET > TRIPLET						
Feeder > Local	-0.01	0.23	-0.38	0.36	0.96	0.49
RC > Local	0.14	0.23	-0.24	0.53	2.69	0.73
RC > Feeder	**0.15**	**0.08**	**0.02**	**0.27**	**41.80**	**0.98**
COMPLETE > NONET						
Feeder > Local	-0.14	0.23	-0.51	0.24	0.37	0.27
RC > Local	-0.19	0.23	-0.58	0.19	0.26	0.21
RC > Feeder	-0.05	0.08	-0.18	0.07	0.33	0.25
No difference of beta values between Node Classification						
Local = Feeder	-1.23	0.95	-3.09	0.64	2.38	0.70
Local = RC	**-2.58**	**0.98**	**-4.49**	**-0.64**	**0.16**	**0.14**
Feeder = RC	**-1.35**	**0.33**	**-1.99**	**-0.70**	**0**	**0**

Note. HCP = Human Connectome Project. CI = Credible Interval. RC = Rich Club. The evidence ratio of one-sided hypothesis tests is equal to the Bayes factor. All Rhat = 1.00, Bulk_ESS $\geq$ 3011 Tail_ESS $\geq$ 5722, *N* = 17905.

Table S9.4

Results of the hypothesis test of model Eq. 4 for the data from parcellation scheme lausanne250 and 60% prevalence-based group matrix using the HCP dataset

Hypothesis	*M*	*SD*	CI lower	CI upper	Evidence Ratio	Posterior probability
Increase of beta values with level of Hierarchy separated by Node Classification						
Local						
TRIPLET > SINGLE	-0.05	0.12	-0.25	0.15	0.54	0.35
NONET > TRIPLET	**0.39**	**0.20**	**0.07**	**0.71**	**39.11**	**0.98**
COMPLETE > NONET	-0.10	0.16	-0.35	0.16	0.36	0.27
Feeder						
TRIPLET > SINGLE	-0.01	0.12	-0.22	0.18	0.85	0.46
NONET > TRIPLET	**0.40**	**0.19**	**0.09**	**0.72**	**52.86**	**0.98**
COMPLETE > NONET	-0.09	0.15	-0.34	0.16	0.38	0.28
RC						
TRIPLET > SINGLE	-0.02	0.14	-0.26	0.21	0.80	0.44
NONET > TRIPLET	**0.51**	**0.21**	**0.18**	**0.85**	**147.51**	**0.99**
COMPLETE > NONET	-0.11	0.17	-0.38	0.17	0.35	0.26
Increase of beta values with level of Hierarchy compared between Node Classifications						
TRIPLET > SINGLE						
Feeder > Local	0.03	0.05	-0.05	0.12	2.86	0.74
RC > Local	0.03	0.09	-0.12	0.17	1.60	0.61
RC > Feeder	-0.01	0.08	-0.15	0.13	0.86	0.46
NONET > TRIPLET						
Feeder > Local	0.02	0.05	-0.07	0.11	1.79	0.64
RC > Local	0.13	0.09	-0.02	0.28	11.86	0.92
RC > Feeder	0.11	0.08	-0.03	0.25	9.11	0.90
COMPLETE > NONET						
Feeder > Local	0.01	0.05	-0.08	0.09	1.27	0.56
RC > Local	-0.01	0.09	-0.16	0.13	0.80	0.44
RC > Feeder	-0.02	0.09	-0.16	0.12	0.69	0.41
No difference of beta values between Node Classifications						
Local = Feeder	**-1.24**	**0.20**	**-1.63**	**-0.84**	**0**	**0**
Local = RC	**-2.46**	**0.34**	**-3.12**	**-1.78**	**0**	**0**
Feeder = RC	**-1.22**	**0.32**	**-1.86**	**-0.60**	**0.04**	**0.04**

Note. HCP = Human Connectome Project. CI = Credible Interval. RC = Rich Club. The evidence ratio of one-sided hypothesis tests is equal to the Bayes factor. All Rhat < 1.05, Bulk_ESS ≥ 693, Tail_ESS ≥ 1276, N = 34677.

Table S9.5

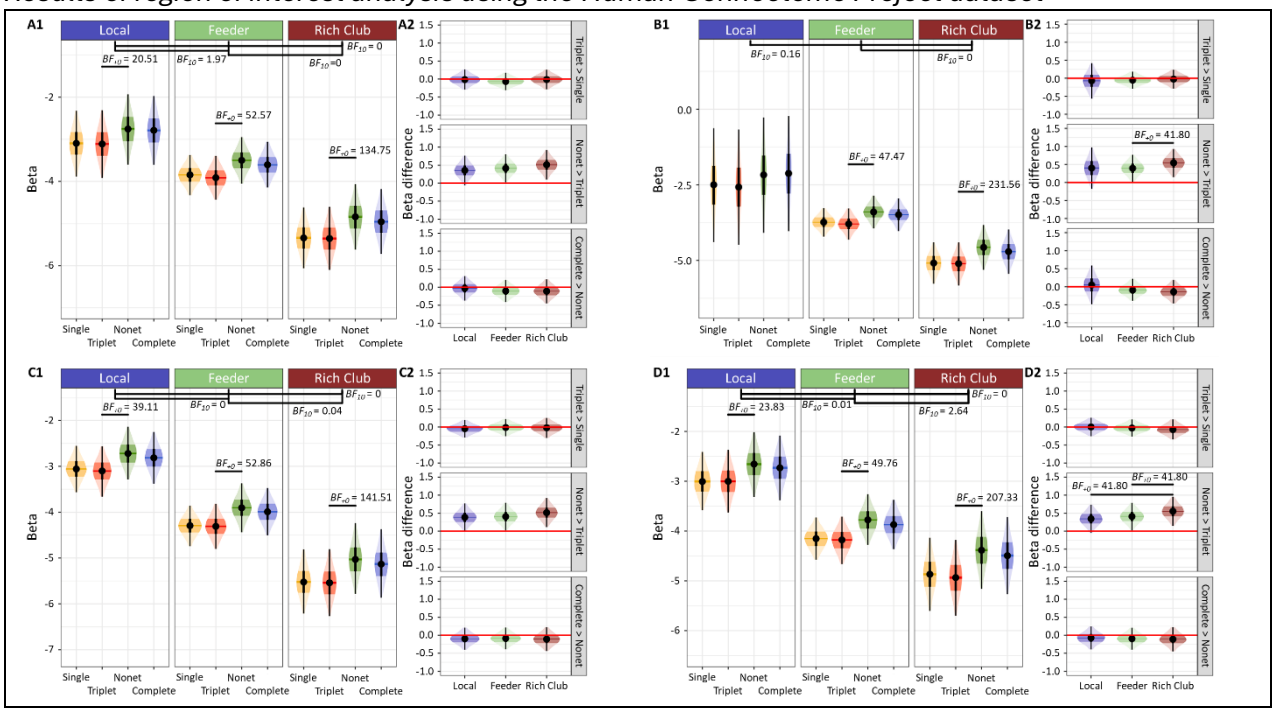
Results of the hypothesis test of model Eq. 4 for the data from parcellation scheme lausanne250 and t test-based group matrix using the HCP dataset

Hypothesis	*M*	*SD*	CI lower	CI upper	Evidence Ratio	Posterior probability
Increase of beta values with level of Hierarchy separated by Node Classification						
Local						
TRIPLET > SINGLE	0.00	0.13	-0.21	0.22	1.03	0.51
NONET > TRIPLET	**0.34**	**0.20**	**0.02**	**0.67**	**23.83**	**0.96**
COMPLETE > NONET	-0.07	0.16	-0.34	0.19	0.48	0.32
Feeder						
TRIPLET > SINGLE	-0.03	0.12	-0.22	0.17	0.69	0.41
NONET > TRIPLET	**0.41**	**0.19**	**0.09**	**0.72**	**49.76**	**0.98**
COMPLETE > NONET	-0.09	0.15	-0.35	0.16	0.36	0.26
RC						
TRIPLET > SINGLE	-0.07	0.14	-0.30	0.17	0.45	0.31
NONET > TRIPLET	**0.55**	**0.21**	**0.21**	**0.89**	**207.33**	**1**
COMPLETE > NONET	-0.11	0.17	-0.39	0.17	0.35	0.26
Increase of beta values with level of Hierarchy compared between Node Classifications						
TRIPLET > SINGLE						
Feeder > Local	-0.03	0.06	-0.13	0.07	0.47	0.32
RC > Local	-0.07	0.10	-0.23	0.09	0.31	0.24
RC > Feeder	-0.04	0.08	-0.18	0.10	0.46	0.31
NONET > TRIPLET						
Feeder > Local	0.06	0.06	-0.04	0.17	5.41	0.84
RC > Local	**0.21**	**0.10**	**0.05**	**0.37**	**60.60**	**0.98**
RC > Feeder	**0.15**	**0.08**	**0.01**	**0.29**	**22.08**	**0.96**
COMPLETE > NONET						
Feeder > Local	-0.02	0.06	-0.12	0.08	0.57	0.36
RC > Local	-0.04	0.10	-0.20	0.13	0.54	0.35
RC > Feeder	-0.01	0.08	-0.15	0.13	0.76	0.43
No difference of beta values between Node Classifications						
Local = Feeder	**-1.15**	**0.26**	**-1.65**	**-0.65**	**0.01**	**0.01**
Local = RC	**-1.87**	**0.40**	**-2.65**	**-1.08**	**0**	**0**
Feeder = RC	**-0.71**	**0.34**	**-1.37**	**-0.04**	**2.64**	**0.72**

Note. HCP = Human Connectome Project. CI = Credible Interval. RC = Rich Club. The evidence ratio of one-sided hypothesis tests is equal to the Bayes factor. All Rhat < 1.05, Bulk_ESS $\geq$ 750, Bulk_ESS $\geq$ 2003, N = 34677.

Figure S9.1

Results of region of interest analysis using the Human Connectome Project dataset



Note. Beta values represent mean activations per condition compared to the implicit baseline. Density plots of posterior distributions with mean point estimate, 50% and 95% highest probability density areas marked. Local = no connection rich club; Feeder = connection to rich club; Rich Club = rich club hubs. Yellow = SINGLE; Red = TRIPLET; Green = NONET; Blue = COMPLETE; Dark blue = Local; Light green = Feeder, Dark red = Rich Club. (A) Based on the combination lausanne120 and 60% prevalence. (B) Based on the combination lausanne120 and *t* test. (C) Based on the combination lausanne250 and 60% prevalence. (D) Based on the combination lausanne250 and *t* test. (1) Level of HIERARCHY estimates in different levels of NODE CLASSIFICATION. (2) HIERARCHY differences in different levels of NODE CLASSIFICATION. Red line marks no difference.

In general, applying the same model (Eq. 4) based on the HCP dataset replicated the results from our own data. We again found a significant increase in beta values between the TRIPLET and NONET conditions across the levels of NODE CLASSIFICATION for all but one comparison. Also, we once more observed a decrease of beta values in RC hubs in comparison to Local nodes (Table S9.2-S9.5 and Figure S9.1). However, using the HCP based classification the beta values of RC hubs were even lower than for Feeder nodes, while the Feeder nodes' beta values were only significantly lower for three of the four matrix methods (Table S9.2-S9.5 and Figure S9.1). Interestingly, using the FDR-corrected *t*-test method in group matrix creation, we could identify a significant larger difference between the NONET and TRIPLET condition in the RC hubs compared to Feeder node for the lausanne120 parcellation (Table 9.3 and Figure 9.1B) and Feeder and Local nodes in the lausanne250 parcellation (Table 9.5 and Figure 9.1D). This effect was only seen as a non-significant tendency when classifying nodes based on our own data.

To summarize, despite differences in the classification of individual nodes, the effects of the ROI analysis could in large parts be replicated when applying a classification that uses the same identification pipeline but an external dataset.

S9.3 Centrality analysis. Firstly, we descriptively examined the overlap between the significant functional clusters at a cluster threshold of 47 voxels, that were found using our own data, with the areas of the lausanne120 and lausanne250 scheme classified by the RC analysis using the HCP dataset (Figure S9.2). Thereafter, replicating the MANOVA-like approach with the HCP dataset for both the lausanne120 and lausanne250 parcellation schemes resulted in models that had no divergent transitions, all *Rhat* < 1.05, and all variables had bulk- and tail-effective samples ≥ 1486 and ≥ 3395, respectively. Posterior checks showed that the cumulative count model simulations reasonably capture the means and distributions of the observed data.

Firstly, we compared the model (Eq. 5) including the factor HIERARCHY CONTRAST with a null model to see if the factor explained any variance of the centrality measures (Table S9.6). The leave-one-out-cross-validation (loo) comparison revealed an increase in the expected log pointwise predictive density (elpd) with inclusion of the factor HIERARCHY CONTRAST.

To specifically test the one-sided hypothesis that the centrality measures of the areas derived from the NONET > TRIPLET contrast were higher than those for the TRIPLET > SINGLE contrast, we again used the hypothesis function from the brms library (Bürkner, 2017) (Table S9.7). Using the lausanne120 parcellation, the expected effect was revealed for the centrality measures degree centrality, betweenness centrality and participation coefficient. For the lausanne250 parcellation, only degree centrality and participation coefficient revealed significant differences for the comparison between NONET- and TRIPLET specific clusters (Figure S9.3). Overall, despite differences in the classification of nodes, we see comparable results when using our own or the HCP dataset (see section 3.5).

Table S9.6

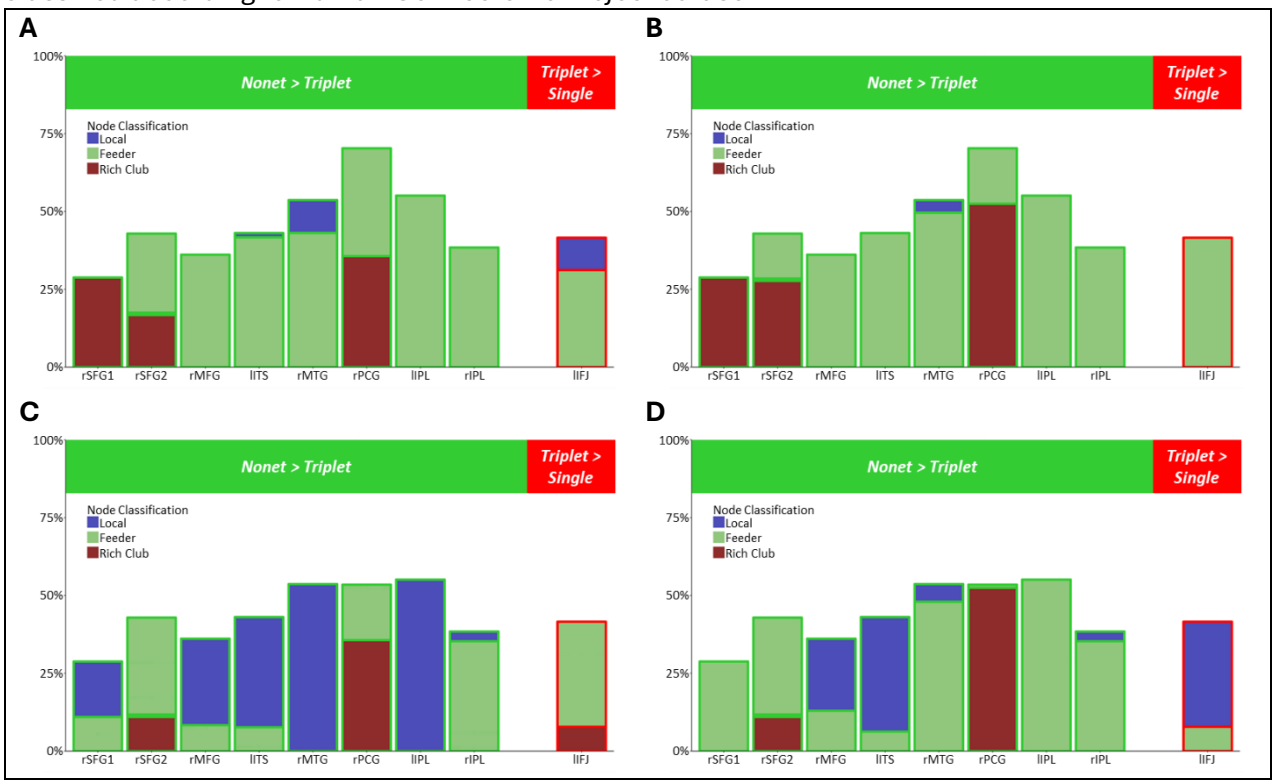
Fit indices of the HIERARCHY *CONTRAST Model (Eq. 5) compared to the null model for both parcellation schemes using the Human Connectome Project data*

Model	$\widehat{elpd}_{diff}$	$se(\widehat{elpd}_{diff})$	$\widehat{elpd}_{loo}$	$se(\widehat{elpd}_{loo})$
lausanne120				
Hierarchy Contrast + (1|Subject)	0.0	0.0	-3998.85	59.31
1 + (1|Subject)	-131.7	15.2	-4130.50	54.80
lausanne250				
Hierarchy Contrast + (1|Subject)	0.0	0.0	-3833.89	78.60
1 + (1|Subject)	-41.5	7.6	-3875.41	77.49

Note. Models are considered to be better if the absolute difference is larger than the standard error (Mohor et al., 2021); $\widehat{elpd}_{loo}$ = expected log pointwise predictive density for a new dataset using Pareto smoothed importance sampling (PSIS) leave-one-out-cross-validation (loo) criterion. The closer to zero the better the model; $\widehat{elpd}_{diff}$ = difference between the $\widehat{elpd}_{loo}$ of two compared models; se = standard error of the variable.

Figure S9.2

Percentage of overlap of activation clusters of the whole brain analysis with the parcellation classified according to Human Connectome Project dataset



Note. (A) Colored according to lausanne120 and 60% prevalence-based NODE CLASSIFICATION. (B) Colored according to lausanne120 and *t* test-based NODE CLASSIFICATION. (C) Colored according to lausanne250 and 60% prevalence-based NODE CLASSIFICATION. (D) Colored according to lausanne250 and *t* test-based NODE CLASSIFICATION. l = left; r = right; SFG = Superior frontal gyrus; MFG = Middle frontal gyrus; ITS = Inferior temporal sulcus; MTG = Middle temporal sulcus; PCG = Posterior cingulate gyrus; IPL = Inferior parietal lobule; IFJ = Inferior frontal junction; rSFG1 = rSFG (22, 60, 14); rSFG2 = rSFG (22, 18, 58).

Table S9.7

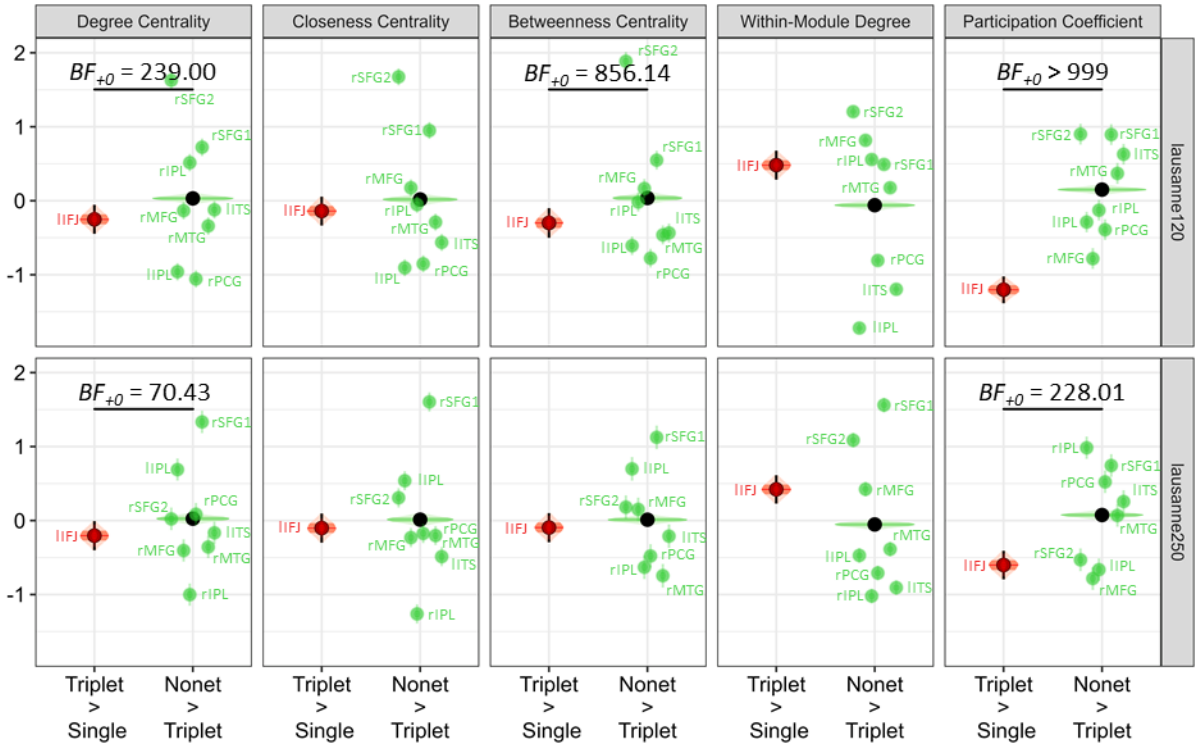
Results of testing (NONET > TRIPLET) > (TRIPLET > SINGLE) for model Eq. 5 for all five centrality measures extracted from individual connectivity matrices following both parcellation schemes and using the Human Connectome Project data

Centrality measure	*M*	*SD*	CI lower	CI upper	Evidence Ratio	Posterior probability
lausanne120						
Degree Centrality	**0.28**	**0.11**	**0.11**	**0.46**	**239.00**	**1**
Closeness Centrality	0.16	0.10	-0.01	0.33	14.41	0.94
Betweenness Centrality	**0.34**	**0.11**	**0.16**	**0.51**	**856.14**	**1**
Within-Module Degree z-Score	-0.54	0.11	-0.71	-0.37	0.00	0
Participation Coefficient	**1.35**	**0.10**	**1.19**	**1.51**	**> 999**	**1**
lausanne250						
Degree Centrality	**0.23**	**0.11**	**0.06**	**0.40**	**70.43**	**0.99**
Closeness Centrality	0.11	0.10	-0.06	0.28	6.48	0.87
Betweenness Centrality	0.11	0.11	-0.07	0.28	5.26	0.84
Within-Module Degree z-Score	-0.47	0.10	-0.65	-0.30	0.00	0
Participation Coefficient	**0.68**	**0.10**	**0.51**	**0.85**	**> 999**	**1**

Note. CI = Credible Interval. Rich Club = Rich Club. Evidence ratio of one-sided hypothesis test is equal to the Bayes factor.

Figure S9.3

Results of the centrality analysis for both parcellation schemes using the centrality measures from the Human Connectome Project data



Note. Density distributions with mean point estimate, 50 and 95% highest probability density areas marked. Centrality measures are controlled for cluster size and *z*-standardized for comparability. Eye plots describe distribution of contrast on average, colorful point-interval plots describe each individual cluster. l = left; r = right; IFJ = Inferior frontal junction; MFG = Middle frontal gyrus; SFG = Superior frontal gyrus; IPL = Inferior parietal lobule; PCG = Posterior cingulate gyrus; MTG = Middle temporal sulcus; ITS = Inferior temporal sulcus; rSFG1 = rSFG (22,60,14); rSFG2 = rSFG (22,18,58); BF = Bayes factor.

Table S9.8

Identified rich club hubs for all parcellation schemes and group-matrix creation methods using the Human Connectome Project validation dataset

ROI	Degree	Number of Hub Connections
lausanne120 & prevalence-based group matrix		
right superiorparietal_3	34	14
left superiorparietal_3	32	14
left precuneus_2	29	12
right rostralmiddlefrontal_2	27	11
right precuneus_2	26	13
right lingual_1	24	9
right precuneus_1	23	12
right superiorparietal_2	23	10
left lateraloccipital_1	22	10
right pericalcarine_1	22	12
left precuneus_1	21	10
left superiorfrontal_3	21	8
right isthmuscingulate_1	21	11
right superiorfrontal_2	21	9
left superiorparietal_1	20	9
right lateraloccipital_1	20	8
right superiorfrontal_1	20	8
right superiorparietal_1	19	8
lausanne120 & t test-based group matrix		
left superiorparietal_3	49	22
right rostralmiddlefrontal_2	48	16
left precuneus_2	45	19
right precuneus_2	42	20
right superiorparietal_3	40	13
left superiorfrontal_4	37	15
left rostralmiddlefrontal_3	37	15
left superiorfrontal_3	36	18
left insula_1	36	13
right superiorfrontal_2	35	15
right precuneus_1	35	15
left superiorparietal_1	35	15
left superiorfrontal_2	33	17
right superiorparietal_2	32	11
right superiorfrontal_1	32	14
right superiorfrontal_3	31	12
right isthmuscingulate_1	31	11
left lateraloccipital_1	30	13
left rostralmiddlefrontal_2	29	14
left pericalcarine_1	29	10
left isthmuscingulate_1	29	12
left superiorparietal_2	28	15

lausanne250 & prevalence-based group matrix		
left insula_2	32	9
right superiorparietal_7	32	11
right precuneus_4	29	12
left superiorparietal_7	28	11
left insula_3	28	6
right posteriorcingulate_2	27	6
right precuneus_5	27	7
right superiorfrontal_5	27	7
left precuneus_3	26	9
right isthmuscingulate_1	25	7
right superiorparietal_3	25	5
left parsopercularis_2	24	5
right precuneus_3	24	10
left cuneus_1	23	7
left pericalcarine_1	23	6
left precuneus_4	23	8
left rostralmiddlefrontal_6	23	5
left lateraloccipital_1	22	7
left superiorfrontal_7	22	6
left superiorparietal_5	22	11
lausanne250 & t test-based group matrix		
right superiorparietal_7	50	15
left insula_2	48	12
right superiorparietal_3	45	10
right precuneus_4	42	16
left superiorparietal_7	41	10
left superiorfrontal_5	38	11
left superiorparietal_5	38	15
right isthmuscingulate_1	37	11
left precuneus_3	36	15
right superiorparietal_5	36	16
right superiortemporal_5	36	8
left lateraloccipital_1	35	8
right parsorbitalis_1	35	9
right superiorfrontal_5	35	8
right temporalpole_1	35	8
left isthmuscingulate_1	33	8
left precuneus_5	33	12
left superiorfrontal_3	33	10
left superiorparietal_4	33	10

AA.8 Supplemental Material 10: Control analysis to show anterior-medial shift for hierarchically higher stimulus structures

To specifically test our assumption that hierarchically higher structures of the stimulus are processed more anterior and more medial portions of the frontal lobe we extracted beta values from the TRIPLET- and NONET-specific contrasts that revealed significant clusters in the whole brain fMRI analysis. As the frontal lobe mask for extraction, we used all Desikan-Killiany atlas (Desikan et al., 2006) parcels that belong to the frontal lobe dilated by one voxel size as it was done for the ROI analysis (see section 2.7). We controlled the beta values for the effect of the subjects and averaged them across the z-dimension as the anterior-medial trend just regards the x-y-plane. Within that plane we calculated the Euclidian distance *d* of each voxel to the reference point X_{MNI} = 0, Y_{MNI} = 72 (Figure 10.1) using the formula:

$$d(x,y) = \sqrt{(X_{MNI} - x)^2 + (Y_{MNI} - y)^2} \qquad \text{(S.10.1).}$$

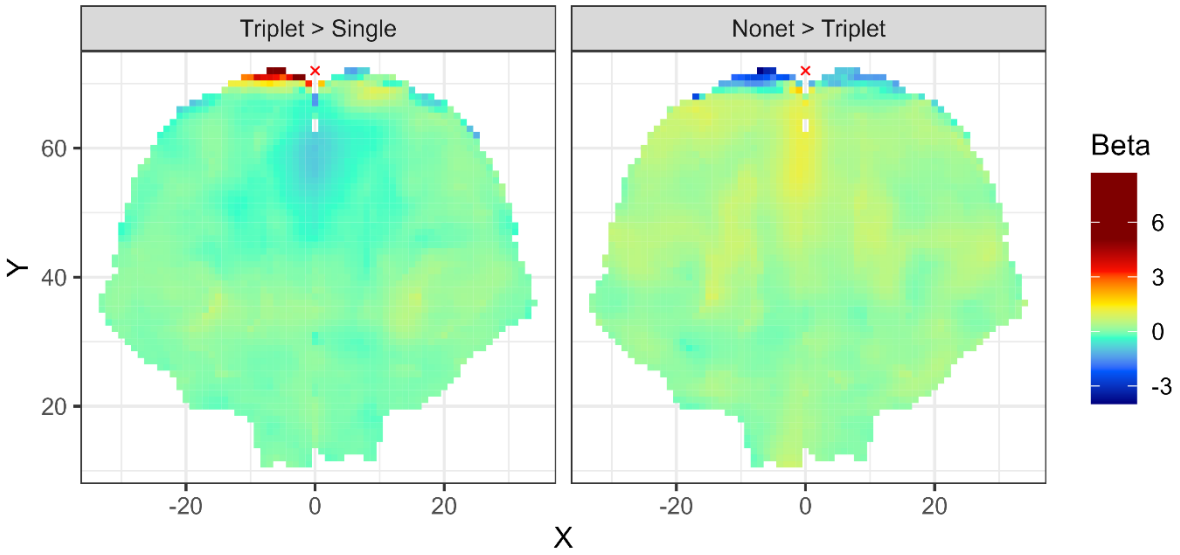
This reference point was chosen as it marks the most anterior and medial point within the area of the brain mask. Thus, a large Euclidian distance *d* indicates coordinates that are highly lateral and more posterior in the frontal lobe.

We correlated the Euclidian distance *d* with the TRIPLET-, r_{EdT} = .09, $t(2020557) = 122.88$, $p < .001$, and NONET-specific beta values, r_{EdN} = -.07, $t(2020557) = -97.81$, $p < .001$, respectively. To compare these two correlations, we applied the Hittner et al. (2003) modification of the *z* test by Dunn and Clark (1969) within the cocor framework (Diedenhofen & Musch, 2015). This test demonstrated that the correlation r_{EdN} = -.07 was significantly smaller than r_{EdT} = .09, $z = -126.60$, $p < .001$. That shows that the NONET-specific beta values increase less with the distance from the anterior-medial reference point than the TRIPLET-specific values. Looking at the sign of correlation coefficients and significance difference to zero it can be assumed that larger NONET-specific beta values were found closer to the anterior-medial reference, while larger beta values in the TRIPLET > SINGLE contrast were found more towards the posterior periphery. Thus, these results provide evidence for the hypothesis, that hierarchically higher stimulus structures are processed closer

to anterior-medial regions of the frontal lobe, while activations related to hierarchically lower stimulus structures can be found in more posterior and lateral regions.

Figure 10.1

Contrast-specific beta values of the frontal lobe averaged and plotted by x and y coordinates



Note. Red 'X' marks the reference point for Euclidian distance *d* calculation at $X_{MNI} = 0$, $Y_{MNI} = 72$.

AA.9 Supplemental References

Bernardo, J. M., & Smith, A. F. M. (2001). Bayesian Theory. *Measurement Science and Technology*, *12*(2), 221–222. https://doi.org/10.1088/0957-0233/12/2/702

Bürkner, P. C. (2017). brms: An R package for Bayesian multilevel models using Stan. *Journal of Statistical Software*, *80*(1). https://doi.org/10.18637/jss.v080.i01

de Lange, S. C., Helwegen, K., & van den Heuvel, M. P. (2023). Structural and functional connectivity reconstruction with CATO - A Connectivity Analysis TOolbox. *NeuroImage*, *273*(April), 120108. https://doi.org/10.1016/j.neuroimage.2023.120108

Desikan, R. S., Ségonne, F., Fischl, B., Quinn, B. T., Dickerson, B. C., Blacker, D., Buckner, R. L., Dale, A. M., Maguire, R. P., Hyman, B. T., Albert, M. S., & Killiany, R. J. (2006). An automated labeling system for subdividing the human cerebral cortex on MRI scans into gyral based regions of interest. *NeuroImage*, *31*(3), 968–980. https://doi.org/10.1016/j.neuroimage.2006.01.021

Diedenhofen, B., & Musch, J. (2015). Cocor: A comprehensive solution for the statistical comparison of correlations. *PLoS ONE*, *10*(4), 1–12. https://doi.org/10.1371/journal.pone.0121945

Dunn, O. J., & Clark, V. (1969). Correlation Coefficients Measured on the Same Individuals. *Journal of the American Statistical Association*, *64*(325), 366–377. https://doi.org/10.1080/01621459.1969.10500981

Feinberg, D. A., Moeller, S., Smith, S. M., Auerbach, E., Ramanna, S., Glasser, M. F., Miller, K. L., Ugurbil, K., & Yacoub, E. (2010). Multiplexed echo planar imaging for sub-second whole brain fmri and fast diffusion imaging. *PLoS ONE*, *5*(12). https://doi.org/10.1371/journal.pone.0015710

Glasser, M. F., Sotiropoulos, S. N., Wilson, J. A., Coalson, T. S., Fischl, B., Andersson, J. L., Xu, J., Jbabdi, S., Webster, M., Polimeni, J. R., Van Essen, D. C., & Jenkinson, M. (2013). The minimal preprocessing pipelines for the Human Connectome Project. *NeuroImage*, *80*, 105–124. https://doi.org/10.1016/j.neuroimage.2013.04.127

Harrison, L. M., Bestmann, S., Rosa, M. J., Penny, W., & Green, G. G. R. (2011). Time scales of representation in the human brain: Weighing past information to predict future events. *Frontiers in Human Neuroscience*, *5*(APRIL), 1–8. https://doi.org/10.3389/fnhum.2011.00037

Harrison, L. M., Duggins, A., & Friston, K. J. (2006). Encoding uncertainty in the hippocampus. *Neural Networks*, *19*(5), 535–546. https://doi.org/10.1016/j.neunet.2005.11.002

Hittner, J. B., May, K., & Silver, N. C. (2003). A monte carlo evaluation of tests for comparing dependent correlations. *Journal of General Psychology*, *130*(2), 149–168. https://doi.org/10.1080/00221300309601282

Jeffreys, H. (1946). An invariant form for the prior probability in estimation problems. *Proceedings of the Royal Society of London. Series A, Mathematical and Physical Sciences*, *186*(1007), 453–461. https://doi.org/10.1098/rspa.1946.0056

Landis, J. R., & Koch, G. G. (1977). The Measurement of Observer Agreement for Categorical Data. *Biometrics*, *33*(1), 159. https://doi.org/10.2307/2529310

Maldjian, J. A., Laurienti, P. J., Kraft, R. A., & Burdette, J. H. (2003). An automated method for neuroanatomic and cytoarchitectonic atlas-based interrogation of fMRI data sets. *NeuroImage*, *19*(3), 1233–1239. https://doi.org/10.1016/S1053-8119(03)00169-1

Moeller, S., Yacoub, E., Olman, C. A., Auerbach, E., Strupp, J., Harel, N., & Uğurbil, K. (2010). Multiband multislice GE-EPI at 7 tesla, with 16-fold acceleration using partial parallel imaging with application to high spatial and temporal whole-brain fMRI. *Magnetic Resonance in Medicine*, *63*(5), 1144–1153. https://doi.org/10.1002/mrm.22361

Mohor, G. S., Thieken, A. H., & Korup, O. (2021). Residential flood loss estimated from Bayesian multilevel models. *Natural Hazards and Earth System Sciences*, *21*(5), 1599–1614. https://doi.org/10.5194/nhess-21-1599-2021

Ponsoda, V., Martínez, K., Pineda-Pardo, J. A., Abad, F. J., Olea, J., Román, F. J., Barbey, A. K., & Colom, R. (2017). Structural brain connectivity and cognitive ability differences: A multivariate distance matrix regression analysis. *Human Brain Mapping*, *38*(2), 803–816. https://doi.org/10.1002/hbm.23419

Setsompop, K., Gagoski, B. A., Polimeni, J. R., Witzel, T., Wedeen, V. J., & Wald, L. L. (2012). Blipped-controlled aliasing in parallel imaging for simultaneous multislice echo planar imaging with reduced g -factor penalty. *Magnetic Resonance in Medicine*, *67*(5), 1210–1224. https://doi.org/10.1002/mrm.23097

Slotnick, S. D. (2017). Cluster success: fMRI inferences for spatial extent have acceptable false-positive rates. *Cognitive Neuroscience*, *8*(3), 150–155. https://doi.org/10.1080/17588928.2017.1319350

Slotnick, S. D. (2020). *img_xcorr.m* (12/26/20). https://drive.google.com/file/d/1aC3o7E6z9CxyOqp0givEkeR6iJahLbVU/view?usp=sharing

Slotnick, S. D., Moo, L. R., Segal, J. B., & Hart, J. (2003). Distinct prefrontal cortex activity associated with item memory and source memory for visual shapes. *Cognitive Brain Research*, *17*(1), 75–82. https://doi.org/10.1016/S0926-6410(03)00082-X

Tourbier, S., Aleman-Gomez, Y., Griffa, A., Bach Cuadra, M., & Hagmann, P. (2019). *sebastientourbier/multiscalebrainparcellator: Multi-Scale Brain Parcellator v1.1.1*. https://doi.org/10.5281/ZENODO.3627097

Trempler, I., Bürkner, P. C., El-Sourani, N., Binder, E., Reker, P., Fink, G. R., & Schubotz, R. I. (2020). Impaired context-sensitive adjustment of behaviour in Parkinson's disease patients tested on and off medication: An fMRI study. *NeuroImage*, *212*(February), 116674. https://doi.org/10.1016/j.neuroimage.2020.116674

van den Heuvel, M. P., Scholtens, L. H., van der Burgh, H. K., Agosta, F., Alloza, C., Arango, C., Auyeung, B., Baron-Cohen, S., Basaia, S., Benders, M. J. N. L., Beyer, F., Booij, L., Braun, K. P. J., Filho, G. B., Cahn, W., Cannon, D. M., Chaim-Avancini, T. M., Chan, S. S. M., Chen, E. Y. H., … De Lange, S. C. (2019). 10kin1day: A bottom-up neuroimaging initiative. *Frontiers in Neurology*, *10*(MAY). https://doi.org/10.3389/fneur.2019.00425

Van Essen, D. C., Smith, S. M., Barch, D. M., Behrens, T. E. J., Yacoub, E., & Ugurbil, K. (2013). The WU-Minn Human Connectome Project: An overview. *NeuroImage*, *80*, 62–79. https://doi.org/10.1016/j.neuroimage.2013.05.041

Xu, J., Moeller, S., Strupp, J., Auerbach, E., Chen, L., Feinberg, D. a, & Uğurbil, K. (2012). Highly Accelerated Whole Brain Imaging Using Aligned-Blipped-Controlled-aliasing Multiband EPI. *Proceedings of the 20th Annual Meeting of ISMRM, Melbourne*, *5*(12), 91657.

Appendix B – Selected Supplemental Material for Study 2

The full extend of the of the supplemental martial for **Study 2** (Mecklenbrauck, Sepulcre, et al., 2024) can be found in the OSF project associated with this dissertation.

AB.1 Supplemental Material 1: Spin test comparing stepwise functional connectivity and Ji atlas maps with the uni-to-multimodal maps from Margulies et al. (2016) and Sydnor et al. (2021).

We applied two approaches to estimate the uni-to-multimodal gradient. First, we took the data-driven route and used stepwise functional connectivity (SFC) to identify the unimodal and multimodal areas from the SFC values at link-step one and seven, respectively (Sepulcre et al., 2012). The individual uni-to-multimodal topography was then determined by subtracting the SFC map at link-step one from the SFC map at step seven, to capture full extend of the uni-to-multimodal gradient in a single map (see 2.4.3.1). We are the first to adopt this method for estimating the uni-to-multimodal gradient using. Secondly, we made use of the atlas of functional networks introduced in Ji et al. (2019) (see 2.4.3.2). A classification of unimodal and multimodal cortices according to this atlas was previously shown to successfully predict the chronotopy of the cortex (Golesorkhi et al., 2021; Ito et al., 2020). The Ji atlas however uses the parcellation according to the Glasser atlas (Glasser et al., 2016) while we parcellated the cortex according to the lausanne250 parcellation scheme (Cammoun et al., 2012). So, translating this supported classification (Golesorkhi et al., 2021; Ito et al., 2020) to another parcellation scheme has also never been done before. To validate our chosen methods, we tested whether the uni-to-multimodal maps we estimated correlate with previously established uni-to-multimodal gradients found in Margulies et al. (2016) and Sydnor et al. (2021). Margulies and colleagues (2016) used a principal component analysis approach to identify gradients that explain the variance in functional connectivity patterns. They found that the first two components that explain the most variance, describe a uni-to-multimodal gradient and a distinction between different unimodal sensory modalities, respectively. Sydnor et al. (2021) on the other hand combined, inter

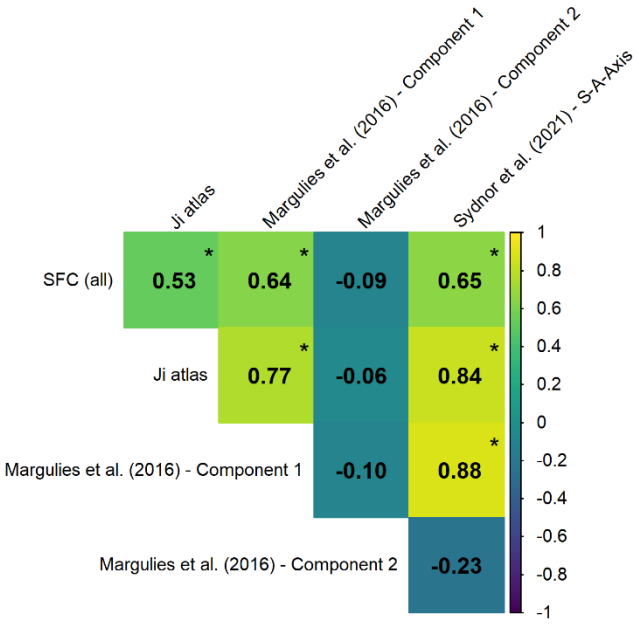
alia, anatomical, functional, genetic and neurometabolic maps and identified a coherent axis from sensorimotor to association cortices. Both these established uni-to-multimodal gradient maps are included in the neuromaps toolbox (Markello et al., 2022) thus the correlation between these maps and our uni-to-multimodal gradients could be tested using the same spin test approach we used to later explore the relationships between the independent and dependent variables (see 3.1; Alexander-Bloch et al., 2018).

Methods. Firstly, we extracted the average SFC values across all participants. Secondly, as each subject hast the same Ji atlas map, describing the overlap between a parcel in the Lausanne parcellation scheme and a multimodal area according to the classification based on the Ji atlas (Golesorkhi et al., 2021; Ito et al., 2020) only this single map was extracted. For the previously established maps we used the first and second components from Margulies et al. (2016) and the sensorimotor-association-axis from Sydnor et al. (2021) and re-parceled them in the neuromaps toolbox (parcellate.Parcellater.fit_transform; Markello et al., 2022) to match the lausanne250 parcellation scheme, that was used throughout the main analyses. We then calculated the Pearson correlation between the uni-to-multimodal maps used in our models and the maps from literature. The significance of the correlation coefficients was tested via 100,000 spin test permutation (Alexander-Bloch et al., 2018). All *p*-values were corrected for multiple testing using false discovery rate correction (Benjamini & Hochberg, 1995).

Results. We found a significant relationship between the average SFC maps and the Ji atlas map, $r = .53$, $p_{spin} < .001$. Furthermore, the SFC map correlated significantly with both the first component from Margulies et al. (2016), $r = .64$, $p_{spin} < .001$, and the sensorimotor-association axis from the Sydnor et al. (2021), $r = .65$, $p_{spin} < .001$. The the Ji atlas map also correlated significantly with both the first component of Margulies et al. (2016), $r = .77$, $p_{spin} < .001$, and the sensorimotor-association axis from the Sydnor et al. (2021), $r = .84$, $p_{spin} < .001$. Additionally, the first component and the sensory-association axis also correlated highly with each other, $r = .88$, $p_{spin} < .001$, (see Figure S1.1).

Figure S1.1

Results of the spin tests investigating the validity of the uni-to-multimodal gradient methodology



Note. SFC = Stepwise functional connectivity, S-A-Axis = sensorimotor-association axis, * $p_{FDR} < .05$.

Discussion. These results indicate that both approaches, the estimation of the uni-to-multimodal gradient, using SFC and via the Ji atlas, capture the uni-to-multimodal gradients that were established by Margulies et al. (2016) and Sydnor et al. (2021). This underlines the validity of our implemented methods for uni-to-multimodal gradient estimation. The established gradients were previously found to relate to cytoarchitectural and electrophysiological features as well as the functional hierarchy of the brain (Huntenburg et al., 2018; Markello et al., 2022) and were shown to be important axes for cortical development (Sydnor et al., 2023), which further demonstrates the significance of the uni-to-multimodal gradient as a cortical organizational scheme.

AB.2 Supplemental Material 2: Hypothesis test for the intrinsic resting-state timescale and inter-subject correlation analyses

Table S2.1

Results of hypothesis tests of model Eq. 3 for all organizational schemes in the intrinsic resting-state timescale analysis

Hypothesis	Estimate	SE	CI lower	CI upper	Evidence Ratio	Posterior probability
Rich Club architecture						
Feeder > Local	**0.04**	**0.02**	**0.01**	**0.08**	**66.72**	**0.99**
RC > Local	**0.05**	**0.03**	**0.00**	**0.10**	**17.18**	**0.95**
RC > Feeder	0.00	0.03	-0.04	0.05	1.17	0.54
Diverse Club architecture						
Feeder > Local	0.02	0.02	-0.01	0.05	4.95	0.83
DC > Local	**0.05**	**0.03**	**0.01**	**0.10**	**38.22**	**0.97**
DC > Feeder	**0.03**	**0.03**	**-0.01**	**0.08**	**10.26**	**0.91**
Uni-to-multimodal gradient (2 separate models)						
$\beta_{SFC} > 0$	**0.09**	**0.01**	**0.07**	**0.11**	**> 999**	**1**
$\beta_{Ji\ atlas} > 0$	**0.11**	**0.01**	**0.10**	**0.12**	**> 999**	**1**
Posterior/lateral-to-anterior/medial gradient						
$\beta_{\lvert x\rvert} < 0$	0.01	0.01	0.00	0.03	0.10	0.09
$\beta_{y} > 0$	**0.06**	**0.01**	**0.05**	**0.08**	**> 999**	**1**
$\beta_{\lvert x\rvert * y} < 0$	**-0.05**	**0.01**	**-0.07**	**-0.03**	**> 999**	**1**
Graph measures of centrality						
$\beta_{Degree\ centrality} > 0$	-0.01	0.02	-0.05	0.02	0.42	0.29
$\beta_{Closeness\ centrality} > 0$	**0.03**	**0.01**	**0.01**	**0.05**	**40.44**	**0.98**
$\beta_{Betweenness\ centrality} > 0$	**0.03**	**0.01**	**0.01**	**0.05**	**70.43**	**0.99**
$\beta_{Participation\ coefficient} > 0$	0.02	0.01	-0.01	0.04	6.06	0.86
$\beta_{Within\text{-}module\ degree\ z\text{-}score} > 0$	0.00	0.02	-0.03	0.03	0.89	0.47
Cytoarchitecture						
$\beta_{Cortical\ thickness} > 0$	**0.05**	**0.01**	**0.03**	**0.06**	**> 999**	**1**

Note. SE = Standard error, CI = Credible Interval, RC = Rich Club, SFC = Stepwise functional connectivity, Ji atlas = Multimodality percentage according to Ji atlas (Ji et al., 2019), DC = Diverse Club. Evidence ratio of one-sided hypothesis test is equal to the Bayes factor. All $\widehat{R} \leq 1.05$, Bulk_ESS $\geq$ 1444, Tail_ESS $\geq$ 2792, N = 9495. Estimating the model parameters entails running multiple Markov chain Monte Carlo chains in parallel. The convergence diagnostic $\widehat{R}$ evaluates how well the estimations converge within and between the chains. Generally, values below 1.05 indicate a successful convergence.

Table S2.2

Results of hypothesis test of model Eq. 4 for all organizational schemes in the inter-subject correlation analysis

Hypothesis	Estimate	SE	CI lower	CI upper	Evidence Ratio	Posterior probability
Rich Club architecture						
Comparison of ISC values between Rich Club classification within the conditions						
SINGLE						
Feeder = Local	0.0002	0.0003	-0.0004	0.0009	> 999	1
RC = Local	0.0011	0.0005	0.0001	0.0020	> 999	1
RC = Feeder	0.0008	0.0005	-0.0001	0.0017	> 999	1
TRIPLET						
Feeder = Local	-0.0006	0.0003	-0.0013	0.0000	> 999	1
RC = Local	0.0000	0.0005	-0.0009	0.0010	> 999	1
RC = Feeder	0.0007	0.0005	-0.0002	0.0016	> 999	1
NONET						
Feeder = Local	-0.0010	0.0003	-0.0017	-0.0004	172.55	0.99
RC = Local	-0.0002	0.0005	-0.0012	0.0007	> 999	1
RC = Feeder	0.0008	0.0005	-0.0001	0.0017	> 999	1
COMPLETE						
Feeder = Local	-0.0011	0.0003	-0.0017	-0.0004	106.45	0.99
RC = Local	-0.0013	0.0005	-0.0022	-0.0004	416.37	1
RC = Feeder	-0.0002	0.0005	-0.0011	0.0007	> 999	1
Comparison of ISC values between different conditions within Rich Club classification						
Local nodes						
TRIPLET = SINGLE	**0.0008**	**0.0003**	**0.0001**	**0.0014**	**>999**	**1**
NONET = TRIPLET	**0.0002**	**0.0003**	**-0.0005**	**0.0009**	**> 999**	**1**
COMPLETE = NONET	**-0.0009**	**0.0003**	**-0.0016**	**-0.0003**	**589.87**	**1**
Feeder nodes						
TRIPLET > SINGLE	-0.0001	0.0003	-0.0006	0.0004	0.61	0.38
NONET = TRIPLET	**-0.0002**	**0.0003**	**-0.0008**	**0.0004**	**> 999**	**1**
COMPLETE = NONET	**-0.0010**	**0.0003**	**-0.0016**	**-0.0004**	**211.36**	**1**
Rich Club hubs						
TRIPLET = SINGLE	**-0.0003**	**0.0006**	**-0.0014**	**0.0009**	**> 999**	**1**
NONET > TRIPLET	0.0000	0.0006	-0.0010	0.0009	0.91	0.48
COMPLETE > NONET	-0.0020	0.0006	-0.0030	-0.0011	0	0
Diverse Club architecture						
Comparison of ISC values between Diverse Club classification within the conditions						
SINGLE						
Feeder = Local	0.0007	0.0003	0.0001	0.0014	> 999	1
DC = Local	0.0007	0.0005	-0.0002	0.0016	> 999	1
DC = Feeder	0.0000	0.0004	-0.0009	0.0009	> 999	1
TRIPLET						
Feeder = Local	-0.0003	0.0003	-0.0009	0.0004	> 999	1
DC = Local	0.0005	0.0005	-0.0004	0.0014	> 999	1
DC = Feeder	0.0008	0.0004	-0.0001	0.0017	> 999	1
NONET						
Feeder = Local	-0.0001	0.0003	-0.0008	0.0005	> 999	1
RC = Local	-0.0002	0.0005	-0.0011	0.0007	> 999	1
RC = Feeder	-0.0001	0.0004	-0.0009	0.0008	> 999	1

COMPLETE						
Feeder = Local	-0.0003	0.0003	-0.0009	0.0004	> 999	1
RC = Local	-0.0011	0.0005	-0.0021	-0.0003	634.01	1
RC = Feeder	-0.0009	0.0004	-0.0017	0.0000	> 999	1
Comparison of ISC values between different conditions within Diverse Club classification						
Local nodes						
TRIPLET = SINGLE	**0.0007**	**0.0004**	**0.0000**	**0.0014**	**> 999**	**1**
NONET = TRIPLET	**0.0000**	**0.0004**	**-0.0007**	**0.0007**	**> 999**	**1**
COMPLETE = NONET	**-0.0009**	**0.0004**	**-0.0016**	**-0.0002**	**844.70**	**1**
Feeder nodes						
TRIPLET > SINGLE	-0.0003	0.0003	-0.0008	0.0002	0.23	0.19
NONET = TRIPLET	**0.0002**	**0.0003**	**-0.0004**	**0.0008**	**> 999**	**1**
COMPLETE = NONET	**-0.0010**	**0.0003**	**-0.0016**	**-0.0004**	**113.89**	**0.99**
Diverse Club hubs						
TRIPLET = SINGLE	**0.0005**	**0.0005**	**-0.0005**	**0.0016**	**> 999**	**1**
NONET > TRIPLET	-0.0007	0.0005	-0.0016	0.0002	0.11	0.10
COMPLETE > NONET	-0.0018	0.0005	-0.0027	-0.0010	0	0
Uni-to-multimodal gradient: Stepwise functional connectivity						
Testing influence of SFC on ISC values within each condition						
SINGLE: $\beta_{SFC} = 0$	**-0.0014**	**0.0002**	**-0.0017**	**-0.0010**	**0**	**0**
TRIPLET: $\beta_{SFC} = 0$	**-0.0010**	**0.0002**	**-0.0013**	**-0.0007**	**0**	**0**
NONET: $\beta_{SFC} = 0$	0.0000	0.0002	-0.0004	0.0003	> 999	1
COMPLETE: $\beta_{SFC} = 0$	**-0.0010**	**0.0002**	**-0.0013**	**-0.0006**	**0**	**0**
Comparing the influence of SFC on the ISC values between the conditions						
TRIPLET > SINGLE	**0.0004**	**0.0002**	**0.0000**	**0.0007**	**23.59**	**0.96**
NONET > TRIPLET	**0.0010**	**0.0002**	**0.0006**	**0.0013**	**> 999**	**1**
COMPLETE > NONET	-0.0009	0.0002	-0.0013	-0.0006	0	0
Uni-to-multimodal gradient: Ji atlas						
Testing influence of the Ji atlas classification on ISC values within each condition						
SINGLE: $\beta_{Ji\ atlas} = 0$	**-0.0026**	**0.0002**	**-0.0029**	**-0.0023**	**0**	**0**
TRIPLET: $\beta_{Ji\ atlas} = 0$	**-0.0011**	**0.0001**	**-0.0014**	**-0.0009**	**0**	**0**
NONET: $\beta_{Ji\ atlas} = 0$	**-0.0021**	**0.0001**	**-0.0024**	**-0.0018**	**0**	**0**
COMPLETE: $\beta_{Ji\ atlas} = 0$	**-0.0028**	**0.0001**	**-0.0031**	**-0.0025**	**0**	**0**
Comparing the influence of the Ji atlas on the ISC values between the conditions						
TRIPLET > SINGLE	**0.0015**	**0.0002**	**0.0011**	**0.0018**	**> 999**	**1.00**
NONET > TRIPLET	-0.0010	0.0002	-0.0013	-0.0006	0	0
COMPLETE > NONET	-0.0007	0.0002	-0.0010	-0.0003	0	0
Posterior/lateral-to-anterior/medial gradient						
Testing influence of the Coordinates on ISC values within each condition						
SINGLE						
$\beta_{\|x\|} = 0$	**-0.0018**	**0.0001**	**-0.0021**	**-0.0015**	**0**	**0**
$\beta_{y} = 0$	**-0.0015**	**0.0002**	**-0.0018**	**-0.0012**	**0**	**0**
$\beta_{\|x\|*y} = 0$	**-0.0030**	**0.0003**	**-0.0036**	**-0.0023**	**0**	**0**
TRIPLET						
$\beta_{\|x\|} = 0$	-0.0005	0.0001	-0.0008	-0.0002	317.62	1
$\beta_{y} = 0$	0.0004	0.0002	0.0000	0.0007	> 999	1
$\beta_{\|x\|*y} = 0$	0.0008	0.0003	0.0001	0.0014	> 999	1
NONET						
$\beta_{\|x\|} = 0$	**-0.0009**	**0.0001**	**-0.0012**	**-0.0007**	**0**	**0**
$\beta_{y} = 0$	**-0.0009**	**0.0002**	**-0.0013**	**-0.0006**	**0**	**0**
$\beta_{\|x\|*y} = 0$	-0.0012	0.0003	-0.0018	-0.0006	73.32	0.99

COMPLETE						
$\beta_{\|x\|} = 0$	**-0.0010**	**0.0001**	**-0.0013**	**-0.0007**	**0**	**0**
$\beta_{y} = 0$	**-0.0014**	**0.0002**	**-0.0018**	**-0.0011**	**0**	**0**
$\beta_{\|x\|*y} = 0$	**-0.0016**	**0.0003**	**-0.0022**	**-0.0010**	**0**	**0**
Comparing the influence of the coordinates on the ISC values between the conditions						
$\beta_{\|x\|}$						
TRIPLET < SINGLE	0.0013	0.0002	0.0010	0.0017	0	0
NONET < TRIPLET	**-0.0005**	**0.0002**	**-0.0008**	**-0.0001**	**81.42**	**0.99**
COMPLETE < NONET	-0.0001	0.0002	-0.0004	0.0003	1.51	0.60
β_{y}						
TRIPLET > SINGLE	**0.0019**	**0.0002**	**0.0015**	**0.0022**	**> 999**	**1**
NONET > TRIPLET	-0.0013	0.0002	-0.0017	-0.0009	0	0
COMPLETE > NONET	-0.0005	0.0002	-0.0009	-0.0001	0.02	0.01
$\beta_{\|x\|*y}$						
TRIPLET < SINGLE	0.0037	0.0005	0.0030	0.0045	0	0
NONET < TRIPLET	**-0.0020**	**0.0005**	**-0.0027**	**-0.0012**	**> 999**	**1**
COMPLETE < NONET	-0.0004	0.0005	-0.0012	0.0003	4.15	0.81
Graph measures of centrality						
Testing influence of the measures of centrality on ISC values within each condition						
SINGLE						
$\beta_{\text{Degree centrality}} = 0$	-0.0005	0.0004	-0.0012	0.0002	> 999	1
$\beta_{\text{Closeness centrality}} = 0$	0.0000	0.0002	-0.0005	0.0004	> 999	1
$\beta_{\text{Betweenness centrality}} = 0$	0.0001	0.0002	-0.0004	0.0005	> 999	1
$\beta_{\text{Participation coefficient}} = 0$	0.0004	0.0002	-0.0001	0.0008	> 999	1
$\beta_{\text{Within-module degree } z\text{-score}} = 0$	0.0003	0.0003	-0.0003	0.0009	> 999	1
TRIPLET						
$\beta_{\text{Degree centrality}} = 0$	0.0005	0.0004	-0.0002	0.0012	> 999	1
$\beta_{\text{Closeness centrality}} = 0$	-0.0002	0.0002	-0.0007	0.0003	> 999	1
$\beta_{\text{Betweenness centrality}} = 0$	0.0004	0.0002	-0.0001	0.0008	> 999	1
$\beta_{\text{Participation coefficient}} = 0$	-0.0004	0.0002	-0.0009	0.0000	> 999	1
$\beta_{\text{Within-module degree } z\text{-score}} = 0$	-0.0006	0.0003	-0.0012	0.0000	> 999	1
NONET						
$\beta_{\text{Degree centrality}} = 0$	-0.0003	0.0004	-0.0010	0.0004	> 999	1
$\beta_{\text{Closeness centrality}} = 0$	0.0001	0.0002	-0.0004	0.0005	> 999	1
$\beta_{\text{Betweenness centrality}} = 0$	0.0002	0.0002	-0.0003	0.0006	> 999	1
$\beta_{\text{Participation coefficient}} = 0$	-0.0001	0.0002	-0.0005	0.0004	> 999	1
$\beta_{\text{Within-module degree } z\text{-score}} = 0$	-0.0001	0.0003	-0.0007	0.0005	> 999	1
COMPLETE						
$\beta_{\text{Degree centrality}} = 0$	-0.0005	0.0004	-0.0012	0.0002	> 999	1
$\beta_{\text{Closeness centrality}} = 0$	0.0004	0.0002	0.0000	0.0009	> 999	1
$\beta_{\text{Betweenness centrality}} = 0$	-0.0002	0.0002	-0.0006	0.0003	> 999	1
$\beta_{\text{Participation coefficient}} = 0$	0.0004	0.0002	0.0000	0.0009	> 999	1
$\beta_{\text{Within-module degree } z\text{-score}} = 0$	0.0003	0.0003	-0.0003	0.0009	> 999	1
Comparing the influence of the Measures of Centrality on the ISC values between the conditions						
$\beta_{\text{Degree centrality}}$						
TRIPLET > SINGLE	**0.0010**	**0.0005**	**0.0002**	**0.0018**	**39.21**	**0.98**
NONET > TRIPLET	-0.0008	0.0005	-0.0017	0.0000	0.05	0.05
COMPLETE > NONET	-0.0002	0.0005	-0.0010	0.0007	0.58	0.37
$\beta_{\text{Closeness centrality}}$						
TRIPLET > SINGLE	-0.0002	0.0003	-0.0007	0.0004	0.45	0.31
NONET > TRIPLET	0.0003	0.0003	-0.0003	0.0008	3.90	0.80
COMPLETE > NONET	0.0004	0.0003	-0.0002	0.0009	7.18	0.88

$\beta_{\text{Betweenness centrality}}$						
TRIPLET > SINGLE	0.0003	0.0003	-0.0002	0.0008	4.51	0.82
NONET > TRIPLET	-0.0002	0.0003	-0.0007	0.0003	0.37	0.27
COMPLETE > NONET	-0.0004	0.0003	-0.0009	0.0002	0.15	0.13
$\beta_{\text{Participation coefficient}}$						
TRIPLET > SINGLE	-0.0008	0.0003	-0.0014	-0.0002	0.01	0.01
NONET > TRIPLET	0.0004	0.0003	-0.0002	0.0009	5.93	0.86
COMPLETE > NONET	**0.0005**	**0.0003**	**-0.0001**	**0.0010**	**13.21**	**0.93**
$\beta_{\text{Within-module degree } z\text{-score}}$						
TRIPLET > SINGLE	-0.0009	0.0004	-0.0016	-0.0002	0.01	0.01
NONET > TRIPLET	0.0005	0.0004	-0.0002	0.0012	8.51	0.89
COMPLETE > NONET	0.0004	0.0004	-0.0003	0.0011	4.03	0.80
Cytoarchitecture (Cortical thickness)						
Testing influence of the cortical thickness on ISC values within each condition						
SINGLE: $\beta_{\text{Cortical thickness}} = 0$	**-0.0015**	**0.0002**	**-0.0018**	**-0.0011**	**0**	**0**
TRIPLET: $\beta_{\text{Cortical thickness}} = 0$	**-0.0014**	**0.0002**	**-0.0017**	**-0.0011**	**0**	**0**
NONET: $\beta_{\text{Cortical thickness}} = 0$	**-0.0019**	**0.0002**	**-0.0023**	**-0.0016**	**0**	**0**
COMPLETE: $\beta_{\text{Cortical thickness}} = 0$	**-0.0016**	**0.0002**	**-0.0019**	**-0.0013**	**0**	**0**
Comparing the influence of the cortical thickness on the ISC values between the conditions						
TRIPLET > SINGLE	0.0001	0.0002	-0.0003	0.0004	1.75	0.64
NONET > TRIPLET	-0.0006	0.0002	-0.0009	-0.0002	0	0
COMPLETE > NONET	0.0003	0.0002	0.0000	0.0007	17.06	0.94

Note. SE = Standard error, CI = Credible Interval, ISC = Inter-subject correlation, RC = Rich Club, SFC = Stepwise functional connectivity, Ji atlas = Multimodality percentage according to Ji atlas (Ji et al., 2019), DC = Diverse Club. Evidence ratio of one-sided hypothesis test is equal to the Bayes factor. All $\widehat{R} \leq 1.05$, Bulk_ESS $\geq$ 1612, Tail_ESS $\geq$ 3112, N = 31156. Estimating the model parameters entails running multiple Markov chain Monte Carlo chains in parallel. The convergence diagnostic $\widehat{R}$ evaluates how well the estimations converge within and between the chains. Generally, values below 1.05 indicate a successful convergence.

AB.3 Supplementary References

Alexander-Bloch, A. F., Shou, H., Liu, S., Satterthwaite, T. D., Glahn, D. C., Shinohara, R. T., Vandekar, S. N., & Raznahan, A. (2018). On testing for spatial correspondence between maps of human brain structure and function. *NeuroImage*, *178*(February), 540–551. https://doi.org/10.1016/j.neuroimage.2018.05.070

Benjamini, Y., & Hochberg, Y. (1995). Controlling the False Discovery Rate : A Practical and Powerful Approach to Multiple Testing Author (s): Yoav Benjamini and Yosef Hochberg Source : Journal of the Royal Statistical Society . Series B (Methodological), Vol . 57 , No . 1 (1995), Publi. *Journal of the Royal Statistical Society*, *57*(1), 289–300.

Cammoun, L., Gigandet, X., Meskaldji, D., Thiran, J. P., Sporns, O., Do, K. Q., Maeder, P., Meuli, R., & Hagmann, P. (2012). Mapping the human connectome at multiple scales with diffusion spectrum MRI. *Journal of Neuroscience Methods*, *203*(2), 386–397. https://doi.org/10.1016/j.jneumeth.2011.09.031

Golesorkhi, M., Gomez-Pilar, J., Tumati, S., Fraser, M., & Northoff, G. (2021). Temporal hierarchy of intrinsic neural timescales converges with spatial core-periphery organization. *Communications Biology*, *4*(1), 1–14. https://doi.org/10.1038/s42003-021-01785-z

Huntenburg, J. M., Bazin, P. L., & Margulies, D. S. (2018). Large-Scale Gradients in Human Cortical Organization. *Trends in Cognitive Sciences*, *22*(1), 21–31. https://doi.org/10.1016/j.tics.2017.11.002

Ito, T., Hearne, L. J., & Cole, M. W. (2020). A cortical hierarchy of localized and distributed processes revealed via dissociation of task activations, connectivity changes, and intrinsic timescales. *NeuroImage*, *221*(February), 117141. https://doi.org/10.1016/j.neuroimage.2020.117141

Ji, J. L., Spronk, M., Kulkarni, K., Repovš, G., Anticevic, A., & Cole, M. W. (2019). Mapping the human brain's cortical-subcortical functional network organization. *NeuroImage*, *185*(October 2018), 35–57. https://doi.org/10.1016/j.neuroimage.2018.10.006

Margulies, D. S., Ghosh, S. S., Goulas, A., Falkiewicz, M., Huntenburg, J. M., Langs, G., Bezgin, G., Eickhoff, S. B., Castellanos, F. X., Petrides, M., Jefferies, E., & Smallwood, J. (2016). Situating the default-mode network along a principal gradient of macroscale cortical organization. *Proceedings of the National Academy of Sciences of the United States of America*, *113*(44), 12574–12579. https://doi.org/10.1073/pnas.1608282113

Markello, R. D., Hansen, J. Y., Liu, Z. Q., Bazinet, V., Shafiei, G., Suárez, L. E., Blostein, N., Seidlitz, J., Baillet, S., Satterthwaite, T. D., Chakravarty, M. M., Raznahan, A., & Misic, B. (2022). Neuromaps: Structural and Functional Interpretation of Brain Maps. *Nature Methods*, *19*(11), 1472–1479. https://doi.org/10.1038/s41592-022-01625-w

Sepulcre, J., Sabuncu, M. R., Yeo, T. B., Liu, H., & Johnson, K. A. (2012). Stepwise connectivity of the modal cortex reveals the multimodal organization of the human brain. *Journal of Neuroscience*, *32*(31), 10649–10661. https://doi.org/10.1523/JNEUROSCI.0759-12.2012

Sydnor, V. J., Larsen, B., Bassett, D. S., Alexander-Bloch, A., Fair, D. A., Liston, C., Mackey, A. P., Milham, M. P., Pines, A., Roalf, D. R., Seidlitz, J., Xu, T., Raznahan, A., & Satterthwaite, T. D. (2021). Neurodevelopment of the association cortices: Patterns, mechanisms, and implications for psychopathology. *Neuron*, *109*(18), 2820–2846. https://doi.org/10.1016/j.neuron.2021.06.016

Sydnor, V. J., Larsen, B., Seidlitz, J., Adebimpe, A., Alexander-Bloch, A. F., Bassett, D. S., Bertolero, M. A., Cieslak, M., Covitz, S., Fan, Y., Gur, R. E., Gur, R. C., Mackey, A. P., Moore, T. M., Roalf, D. R., Shinohara, R. T., & Satterthwaite, T. D. (2023). Intrinsic activity development unfolds along a sensorimotor–association cortical axis in youth. *Nature Neuroscience*, *26*(4), 638–649. https://doi.org/10.1038/s41593-023-01282-y

Appendix C – Supplemental Material for Study 3

AC.1 Supplemental Material 1: Comparing low-level visual features between the conditions

After we have extracted all the frames used in all conditions, we compared the final stimulus set in regards to several low-level visual features, to control for visual cofounds that could bias the results across the experiment, as it was shown that differences in low-level visual features were specifically associated with neural state boundaries in the early visual cortex (Oetringer et al., 2025). We specifically were interested in luminance, color contrast, saturation and overall image complexity. The luminance of each frame was calculated by the average gray scale intensity and then averaged for each movie scene or shot. Similarly, the contrast was calculated as the root means square of the gray scale intensity of each frame (Peli, 1990) averaged for every movie segment. The saturation can be extracted by transforming the red-green-blue color values from each frame into their hue-saturation-value representations (Smith, 1978) and averaging the saturation. Finally, for calculating overall image complexity we applied the image processing algorithm introduced by (Durmus, 2020) to receive a single complexity value for each frame, which were again averaged per movie segment. Additionally, we considered two measures that quantify the visual difference between two consecutive, extracted frames of each scene or shot. The first measure was the motion energy as defined by the average change of the gray scale value from one frame to the next (Ramseyer, 2020). Secondly, we applied code from the StudyForrest project (process_movie_frames.py; Häusler et al., 2021) to receive the normalized perceptual difference between frames, which is based on the perceptual hash, i.e. the fingerprint of each frame, that describes a simplification of the image to a string of letters and number that is firstly more similar if the images are similar, secondly it is insensitive to cropping or resolution changes and most crucially for movies it is thirdly not effected by smooth changes like movement (Farid, 2021; Oetringer et al., 2025).

To compare the average visual features between conditions, we conducted a non-parametric ANOVA (ARTool; 0.11.2; Elkin et al., 2021) investigating the effects of CONTENT LEVEL,

DURATION as well as their interactions on the extracted features. The results were corrected across features for multiple comparison using controlling the false discovery rate (FDR; Benjamini & Yekutieli, 2001) at α = 5%. As outlined in Table S1.1, none of the low-level frame-specific features differed between the conditions. However, looking at the two features that considered the change between frames, i.e., motion energy and normalized perceptional difference, we identified a significant difference between significantly between SCENES and SHOTS, with more visual variation in the SCENE conditions. Also, the effect of DURATION was significant for both of these features, demonstrating more visual changes for shorter DURATIONS.

Table S1.1.
Results of the non-parametric analysis of variance comparing the visual features of frames between conditions of CONTENT LEVEL x DURATION design

Feature	Effect	*F*	df_1	df_2	p_{FDR}	η_p^2
Luminance	CONTENT LEVEL	4.81	1	150	.060	0.03
	DURATION	0.13	2	150	.876	0
	CONTENT LEVEL x DURATION	0.85	2	150	.740	0.01
Color Contrast	CONTENT LEVEL	1.87	1	150	.261	0.01
	DURATION	1.49	2	150	.428	0.02
	CONTENT LEVEL x DURATION	1.76	2	150	.740	0.02
Saturation	CONTENT LEVEL	0.09	1	150	.761	0
	DURATION	0.84	2	150	.521	0.01
	CONTENT LEVEL x DURATION	0.74	2	150	.740	0.01
Overall Complexity	CONTENT LEVEL	0.34	1	150	.674	0
	DURATION	1.26	2	150	.428	0.02
	CONTENT LEVEL x DURATION	0.26	2	150	.768	0
Normalized Perceptual Difference	**CONTENT LEVEL**	**7.15**	**1**	**150**	**.025**	**0.05**
	DURATION	**14.67**	**2**	**150**	**<.001**	**0.16**
	CONTENT LEVEL x DURATION	0.71	2	150	.740	0.01
Motion Energy	**CONTENT LEVEL**	**19.8**	**1**	**150**	**<.001**	**0.12**
	DURATION	**8.83**	**2**	**150**	**.001**	**0.11**
	CONTENT LEVEL x DURATION	0.34	2	150	.768	0

Notes. Non-parametric variance analysis was conducted using ARTool (0.11.2; Elkin et al., 2021).

While these differences between the conditions have to be considered when interpreting and discussion the results of this study, a larger variation of visual features in SCENES as well as between frames of shorter DURATION are innate components of the naturalistic material. Per definition movie SCENES incorporate multiple camera perspectives (Cutting, 2014) thus a larger visual variation is to be expected. The visual differences between frames are even a common

indicator to automatically annotate boundaries of movie shots (Chakraborty et al., 2021; Mas & Fernandez, 2003; Rui et al., 1998; Zhu et al., 2023), highlighting that natural movie scenes will always be more visually complex than shots. As we established in the introduction, we include the visual and narrative differences between movie SCENES and SHOTS as part of the CONTENT LEVEL differences.

Also, condensing longer movie segments down to a selection of only twelve frames in the case of the 4S DURATION conditions will naturally induce longer temporal gaps and therefore more visual differences between adjacent frames. As described in the method section (see main manuscript 2.2.), we tried to mitigate this effect by controlling the condensing ratio between condition, which was, however, only possible to a certain extent. We considered this thusly introduced visual variation between stimuli of longer and shorter DURATION in more detail in the discussion.

AC.2 Supplemental Material 2: Results table for visual cortical hierarchy ROI analysis

Table S2.1.
Results of the post-hoc comparisons of the region of interest analysis for the five regions along the visual processing hierarchy (Baldassano et al., 2017)

ROI	Contrast		Estimate (*b*)	95% CI lower	95% CI upper	$p_{FDR\text{-}boot}$
Left V1						
	Shot 4s	Scene 4s	.0011	-.0015	.0038	1
	Shot 4s	**Shot 12s**	**.0103**	**.0078**	**.0127**	**< .001**
	Scene 4s	**Scene 12s**	**.0083**	**.0061**	**.0108**	**< .001**
	Shot 12s	Scene 12s	-.0008	-.0033	.0017	1
	Shot 12s	**Shot 36s**	**.0203**	**.0180**	**.0227**	**< .001**
	Scene 12s	**Scene 36s**	**.0159**	**.0135**	**.0182**	**< .001**
	Shot 36s	**Scene 36s**	**-.0051**	**-.0074**	**-.0027**	**< .001**
Right V1						
	Shot 4s	Scene 4s	.0008	-.0015	.0031	1
	Shot 4s	**Shot 12s**	**.0073**	**.0049**	**.0096**	**< .001**
	Scene 4s	**Scene 12s**	**.0066**	**.0042**	**.0089**	**< .001**
	Shot 12s	Scene 12s	.0001	-.0021	.0024	1
	Shot 12s	**Shot 36s**	**.0234**	**.0210**	**.0257**	**< .001**
	Scene 12s	**Scene 36s**	**.0121**	**.0096**	**.0144**	**< .001**
	Shot 36s	**Scene 36s**	**-.0113**	**-.0135**	**-.0090**	**< .001**
Left A1						
	Shot 4s	Scene 4s	-.0004	-.0024	.0015	1
	Shot 4s	Shot 12s	.0001	-.0018	.0019	1
	Scene 4s	Scene 12s	.0004	-.0014	.0023	1
	Shot 12s	Scene 12s	-.0002	-.0021	.0018	1
	Shot 12s	Shot 36s	-.0002	-.0022	.0016	1
	Scene 12s	Scene 36s	-.0014	-.0033	.0005	1
	Shot 36s	Scene 36s	-.0013	-.0033	.0005	1
Right A1						
	Shot 4s	Scene 4s	.0001	-.0018	.0021	1
	Shot 4s	Shot 12s	-.0002	-.0021	.0020	1
	Scene 4s	Scene 12s	-.0016	-.0039	.0002	1
	Shot 12s	Scene 12s	-.0013	-.0033	.0004	1
	Shot 12s	Shot 36s	.0009	-.0011	.0027	1
	Scene 12s	**Scene 36s**	**.0033**	**.0015**	**.0052**	**< .001**
	Shot 36s	Scene 36s	.0012	-.0010	.0030	1
Left hV4						
	Shot 4s	Scene 4s	.0009	-.0020	.0041	1
	Shot 4s	**Shot 12s**	**.0478**	**.0451**	**.0508**	**< .001**
	Scene 4s	**Scene 12s**	**.0071**	**.0041**	**.0098**	**< .001**
	Shot 12s	**Scene 12s**	**-.0398**	**-.0427**	**-.0370**	**< .001**
	Shot 12s	Shot 36s	.0015	-.0016	.0046	1
	Scene 12s	**Scene 36s**	**.0258**	**.0228**	**.0289**	**< .001**
	Shot 36s	**Scene 36s**	**-.0156**	**-.0185**	**-.0123**	**< .001**

Right hV4						
	SHOT 4S	SCENE 4S	.0002	-.0029	.0036	1
	SHOT 4S	**SHOT 12S**	**.0239**	**.0205**	**.0272**	**< .001**
	SCENE 4S	**SCENE 12S**	**.0102**	**.0070**	**.0131**	**< .001**
	SHOT 12S	**SCENE 12S**	**-.0136**	**-.0172**	**-.0101**	**< .001**
	SHOT 12S	**SHOT 36S**	**.0252**	**.0222**	**.0282**	**< .001**
	SCENE 12S	SCENE 36S	.0050	.0015	.0082	.1539
	SHOT 36S	**SCENE 36S**	**-.0338**	**-.0373**	**-.0302**	**< .001**
Left AG						
	SHOT 4S	SCENE 4S	.0002	-.0026	.0030	1
	SHOT 4S	SHOT 12S	.0031	.0005	.0058	.3770
	SCENE 4S	SCENE 12S	-.0022	-.0049	.0007	1
	SHOT 12S	**SCENE 12S**	**-.0050**	**-.0079**	**-.0023**	**< .001**
	SHOT 12S	**SHOT 36S**	**.0049**	**.0022**	**.0077**	**< .001**
	SCENE 12S	SCENE 36S	.0042	.0015	.0068	.0554
	SHOT 36S	**SCENE 36S**	**-.0058**	**-.0085**	**-.0032**	**< .001**
Right AG						
	SHOT 4S	SCENE 4S	-.0024	-.0049	.0003	1
	SHOT 4S	**SHOT 12S**	**.0069**	**.0041**	**.0095**	**< .001**
	SCENE 4S	SCENE 12S	-.0010	-.0037	.0017	1
	SHOT 12S	**SCENE 12S**	**-.0103**	**-.0129**	**-.0076**	**< .001**
	SHOT 12S	SHOT 36S	-.0015	-.0043	.0012	1
	SCENE 12S	**SCENE 36S**	**.0097**	**.0073**	**.0121**	**< .001**
	SHOT 36S	SCENE 36S	.0009	-.0018	.0034	1
Left pmDMN						
	SHOT 4S	SCENE 4S	.0049	.0018	.0077	.0554
	SHOT 4S	SHOT 12S	.0018	-.0013	.0048	1
	SCENE 4S	SCENE 12S	-.0038	-.0066	-.0009	.1539
	SHOT 12S	SCENE 12S	-.0007	-.0034	.0022	1
	SHOT 12S	**SHOT 36S**	**.0088**	**.0060**	**.0115**	**< .001**
	SCENE 12S	SCENE 36S	.0015	-.0013	.0041	1
	SHOT 36S	**SCENE 36S**	**-.0081**	**-.0111**	**-.0050**	**< .001**
Right pmDMN						
	SHOT 4S	**SCENE 4S**	**.0046**	**.0020**	**.0075**	**< .001**
	SHOT 4S	SHOT 12S	.0042	.0013	.0071	.1047
	SCENE 4S	SCENE 12S	-.0026	-.0054	.0001	.6652
	SHOT 12S	SCENE 12S	-.0022	-.0048	.0008	1
	SHOT 12S	**SHOT 36S**	**.0101**	**.0072**	**.0129**	**< .001**
	SCENE 12S	SCENE 36S	.0038	.0010	.0071	.0554
	SHOT 36S	**SCENE 36S**	**-.0084**	**-.0111**	**-.0057**	**< .001**

Notes. Post-hoc comparison of the region of interest (ROI) analysis modelling the inter-subject correlation values by the CONTENT LEVEL x DURATION. Confidence intervals (CI) and *p*-values were determined using parametric bootstrapping via lme4's bootMer (N_{boot} = 500). Significant comparisons are printed in bold. V1 = *primary visual cortex*, A1 = *primary auditory cortex*, hV4 = *extrastriate visual cortex*, AG = *angular gyrus*, pmDMN = *posterior medial cluster of the default mode network*.

AC.3 Supplemental Material 3: Supplementary discussion of clusters outside the scene network

Beyond the scene network (Epstein & Baker, 2019) the contrasts of CONTENT LEVEL and DURATION and their interaction revealed more clusters which mainly related to domains of visual scene processing and therefore supported the main finding of the scene network even further.

The effect of CONTENT LEVEL. Additionally to the occipital place area (OPA) and posterior parahippocampal place areas (PPA), contrasting SCENES and SHOTS also yielded clusters in the bilateral areas V3A/B, the bilateral superior parietal lobe (SPL), left supramarginal gyrus (SMG) and right anterior middle temporal gyrus (MTG), which all play different roles in supporting the visual perspective taking and the functionality of the posterior scene network (Baldassano et al., 2016).

Firstly, the large, bilateral middle occipital gyrus clusters did not only contain OPA but also extended inferiorly to the areas V3A/B, which represent motion selective visual areas (Barton & Brewer, 2017; Press et al., 2001; Tootell et al., 1997) that specifically handle egocentric motion perception in three-dimensional space (Anzai et al., 2011; McKeefry et al., 2010; Ng et al., 2021; Rosenberg et al., 2023; Sulpizio et al., 2020). While not directly a part of the posterior scene network, this finding not only corresponds to the idea that movie SCENE perception requires additional visual processing to integrate across the multiple perspectives that viewer takes through the different SHOTS within a SCENE, but also supports that the OPA might be more closely connected to the visual areas and the actual sensory input (Baldassano et al., 2016).

Secondly, along a similar vein, we bilaterally identified large SPL clusters covering multiple functionally distinct subregions, namely the more posterior Brodmann area (BA) 7 and the more anterior BA 5 (Alahmadi, 2021). In general, the SPL is predominantly connected to the OPA (Yoon et al., 2025) and is commonly found for visual shifts in movies (Kwok et al., 2012; Zacks et al., 2010). Thereby, this area further supports the egocentric perspective taking which was introduced as a main function of OPA (Julian et al., 2018). On the one hand, the posterior SPL, representing

BA 7, focuses on egocentric motion to aid visually guided navigation (Baumann & Mattingley, 2021; Yoon et al., 2025). The anterior SPL, i.e., BA 5 on the other hand, which includes the cluster we found in the left cingulate sulcus, supports a body-centred coordinate system guiding the localization in three-dimensional space (Lacquaniti et al., 1995; Sakata et al., 1973; Scheperjans et al., 2008) and the integration of visual and motor imagery to solve object rotation tasks (Stephan et al., 1995; Wolbers et al., 2003). Taken together, the clusters in the SPL detected by the differences between SCENES and SHOTS all are in line with the continuous representation of a three-dimensional environment and spatial navigation within that environment from an egocentric point of view, which is necessary for the integration of multiple SHOTS within one SCENE.

Next, we found a cluster in the left SMG. While this area is also not a part of the scene network, the multifaceted SMG (Oberhuber et al., 2016) was found to be engaged during movie watching, specifically at the boundaries of events (Zacks et al., 2001, 2010). Beyond that, the anterior portion of the SMG, that we found more engaged for SCENES, was related to motor planning and information integration for tool-use (Orban & Caruana, 2014; Potok et al., 2019), executive functioning (Oberhuber et al., 2016) as well as perspective taking (Arora et al., 2015). Even though not directly linked to scene processing, the functional domains of the SMG are evidently related to spatial processing which is also the main focus of the posterior subnetwork of the scene network.

Finally, we found a cluster of more engagement in the right anterior MTG, i.e., the temporal pole. Reviews on the function of the temporal pole suggests that this area functions as a cross-modal integration hub especially utilized in semantic knowledge (Herlin et al., 2021; Olson et al., 2007; Ralph et al., 2016). The right temporal pole was thereby indicated to focus on complex visual task, social cognition tasks and connecting faces to names (Herlin et al., 2021; Ralph et al., 2016). In the context of the study, this resulting cluster could therefore firstly indicate that the processing of SCENES is more complex and requires the integration of semantic knowledge more than SHOTS. Secondly, especially the right anterior temporal lobe was identified for the recognition of famous

faces (H. Yang et al., 2016). Thus, this result could also hint at the processing of more faces and perspectives of the well-known actors in the SCENES than in the SHOTS.

Overall, the areas beyond the posterior scene network that were additionally engaged by SCENES compared to SHOTS, included regions like V3A/B or the SPL that are commonly related to spatial processing from an egocentric reference frame (e.g., Yoon et al., 2025). Therefore, these results further support the interpretation, that movie scene processing requires the integration of multiple egocentric viewpoints, i.e., camera perspectives, across different shots.

The effect of DURATION. In comparison to the CONTENT LEVEL, contrasts the DURATION effects were predominantly found in the anterior scene network which might indicate a higher level of processing and memory integration enabled by longer stimuli (Baldassano et al., 2016). Outside of this subnetwork we found clusters in the bilateral SPL and superior frontal gyrus (SFG) in the 12S > 4S contrast as well as a cluster in the right inferior frontal junction (IFJ) for the 36S > 4S contrast.

Longer compared to shorter DURATIONS. The cluster in the right SPL might represent the so-called posterior intraparietal gyrus scene-selective site (Kennedy et al., 2024), an area related to the processing of egocentric motion. Additionally, the left SPL cluster of the 12s > 4s contrast falls into the BA 7 subarea in the posterior SPL which, as mentioned before, is involved in egocentric motion as well (Baumann & Mattingley, 2021; Yoon et al., 2025). Taken together, these SPL areas indicate that also for the DURATION effect we see areas related to the egocentric orientation and navigation which were also found for SCENES > SHOTS. Accordingly, when looking at the interaction effects (see main manuscript 4.2.3.), we saw, that the cluster in the left SPL also appeared for the specific engagement of SCENES of 12S DURATION. This could suggest that the SPL mainly is involved in spatial orientation necessary when processing SCENES with multiple perspectives. But, due to its position in the cortical hierarchy, the SPL might work on a slower timescale (Ito et al., 2020; Margulies et al., 2016; Mecklenbrauck et al., 2024; Raut et al., 2020) and thus is more reliably engaged especially by longer SCENES.

Furthermore, finding these bilateral clusters in the SPL might be related to the clusters in the bilateral SFG. These frontal lobe clusters, that were revealed by the 12S > 4S contrast, are located in the dorsal premotor cortex, which is commonly believed to form a network with the SPL in the context of visuospatial motor imagery tasks (Bencivenga et al., 2021; De Lange et al., 2005; Hétu et al., 2013; Sack et al., 2008; Spagna et al., 2021). This would correspond to the function of the anterior subset of the scene network which is less concerned with the visual input and consists of areas related to spatial imagery (Boccia et al., 2015; Häusler et al., 2022). Moreover, the dorsal premotor cortex in collaboration with the posterior parietal cortex is generally involved in the conscious planning of motor action (Desmurget & Sirigu, 2009; Nakayama et al., 2022; Pilacinski et al., 2018). In conjunction with its function in motor imagery involvement, it was suggested that the dorsal premotor cortex integrates internal and external data for targeted motor planning, possibly also including semantic information about present objects (Bencivenga et al., 2021; Hoshi & Tanji, 2000). In the context of the presented SCENES and SHOTS of longer durations, the result of a reliable engagement of the dorsal premotor cortex in unison with the SPL could indicate that higher level of action understanding and integration of information from memory is only enabled at longer presentation of the content.

Finally, we discovered one more reliably engaged cluster in the right IFJ for SCENES and SHOTS of 36S in comparison to 4S stimuli. The IFJ is involved in the top-down attentional control, with specifically the right IFJ related to the attention to salient features of a stimulus rather that its spatial orientation (Meyyappan et al., 2021; Sebastian et al., 2016; Siestrup & Schubotz, 2023; Zanto et al., 2010). This is a surprising finding, since the clusters and networks discussed so far focused mainly of the spatial processing of visual scenery. However, especially in the rather visually persistent 36S condition compared to the very transient 4S condition the attention of participants might have been more focused on the processing of features and details in the depicted frames. Additionally, the right IFJ was previously related to the inhibition motor activity as well as task-switching and cognitive control (Brass et al., 2005; O'Connor et al., 2015;

Sebastian et al., 2016; Sundermann & Pfleiderer, 2012). Thus, the finding of a cluster in the right IFJ could suggest a possible change in processing, which could explain the unexpected reduction in reliable ISC values for this level of DURATION. As participants paid more attention to features in the frames, they might have explored the stimulus more, leading to less synchronization and limiting ISC (Hasson, Landesman, et al., 2008; Loschky et al., 2020).

Shorter compared to longer DURATIONS. This interpretation is supported by findings of the opposed DURATION comparisons. Firstly, contrasting, 4S > 36S as well as 12S > 36S uncovered clusters like the precuneus, retrosplenial cortex, or SMG, so areas usually associated with higher levels of visual processing (e.g., Baldassano et al., 2017). As the ISC is reduced in higher level areas in general as the processed become less stimulus-driven (Schmälzle et al., 2017; Yeshurun, Nguyen, et al., 2017), less engaging, more constant stimuli in the 36s condition could have further limited the necessary synchronization (Hasson, Landesman, et al., 2008). Secondly and more importantly, the change to a more feature focused, static perception of 36S stimuli is especially supported by finding clusters in the posterior STS as well as area MT+ for the 4S > 36S and 12S > 36S contrasts, respectively. These areas are commonly linked to the perception of biological motion (Allison et al., 2000; Cheng et al., 2025; Grossman et al., 2005; Herrington et al., 2011; McAleer et al., 2014), further indicating that the 36S stimuli were less processed as motion, which might have led to a desynchronization in processing, as participants explore a static stimulus more freely (Loschky et al., 2020). Adding eye-tracking to the experiment as a control measure could offer new insight in the synchronization of watching the stimuli.

The majority of significant clusters when contrasting conditions of shorter DURATION with those of longer DURATION however were located in the early visual cortex, including areas like the lingual gyrus, fusiform gyrus, cuneus, and inferior occipital gyrus, that are primarily concerned with low-level visual functions like orientation, color, depth and motion perception or visual awareness (Grill-Spector & Malach, 2004; Knight et al., 2024; Koivisto et al., 2010; Palejwala et al., 2021; Roelfsema & de Lange, 2016; Tong, 2003). These findings align with earlier temporal

receptive window (TRW) results showing that temporally shorter stimuli consistently engaged the primary sensory areas (Farbood et al., 2015; Hasson, Yang, et al., 2008; Lerner et al., 2011).

Yet, the differences between shorter and longer DURATIONS could also have been affected by low-level visual differences identified between these conditions. As the supplementary analysis of visual features revealed (see Supplemental Material 1), the average motion energy as well as the normalized perceptual difference were significantly higher for the shorter DURATION conditions. In previous studies, these two visual features – both indicating a greater visual variability – were related to variance in early and motion-related visual areas during movie watching (Huth et al., 2012; Nunez-Elizalde et al., 2019; Oetringer et al., 2025). Specifically, Oetringer et al. (2025) showed that shifts in low-level perceptual features significantly coincided with transitions in neural states in the early visual cortex.

Relatedly, the effects in the early visual cortex might also be attributed to differences in the number of visual boundaries between segments included in each experimental condition, as presenting stimuli on a shorter temporal naturally increases the number of transitions between distinct SHOTS or SCENES. Previous studies showed that both activity and inter-subject similarity in early sensory cortices can be driven by event-related activity at stimulus segment transitions (Lee & Chen, 2024; Lu et al., 2016).

Beyond the early visual cortex, our analysis revealed additional clusters in the bilateral PPA when comparing the 12S against the 36S condition. Similarly, (Oetringer et al., 2025) found an effect of low-level visual features shifts in the PPA as well, suggesting despite convincing evidence that the PPA is part of the scene network (e.g., Epstein & Baker, 2019), it might also be affected by more low-level visual processing.

To summarize, the DURATION effects beyond the anterior scene network on the one hand revealed areas that further supported the integration of visual scenery like the SPL and SFG for longer DURATIONS. Especially these two regions were shown to form a network that functionally

relates to visual imagery complementing the anterior scene network which is less involved with the actual sensory input.

For shorter DURATIONS on the other hand, we found increased engagement in the early visual cortex which was expected in the context of TRW. These clusters might however also trace back to an increased visual variability and higher number of stimulus transitions in shorter DURATION conditions. Future studies should therefore consider further controlling their stimuli for the effects of visual transition (Lu et al., 2016), although these perceptual differences are natural consequences of the stimulus manipulation. Additionally, the results for the shorter conditions compared to the 36S condition yielded clusters indicating that the 36S stimuli could have been seen less as a motion picture but rather as a static image, which could be investigated more thoroughly with the addition of eye tracking during the experiment.

AC.4 Supplemental Material 4: Supplementary region of interest analysis

Methods. Beyond the five regions of interest (ROIs) representing the visual processing hierarchy (Baldassano et al., 2017), we were also interested in additional areas that were previously related to the processing of audio-visual narratives (for a review see Jääskeläinen et al., 2021). These included the parahippocampal gyrus (PHG) and the hippocampus, which were engaged in processing and recollection of the movie's plot (Ben-Yakov & Henson, 2018; Chen et al., 2016; Hasson, Furman, et al., 2008; Jääskeläinen et al., 2021; E. Yang et al., 2023; Zadbood et al., 2017). Both these areas were defined using the anatomical Desikan-Killiany atlas (Desikan et al., 2006), while the hippocampus was further split into the anterior (aHC) and posterior (pHC) sections at y = -21 with a 2 mm gap to both sides to avoid signal contamination (Guo et al., 2020; Poppenk et al., 2013). We also investigated the ISC in the temporo-parietal junction (TPJ), which, as a part of the default mode network (DMN; Wang et al., 2020), was previously detected in the context of remembering the movie's content (Jääskeläinen et al., 2021; Zadbood et al., 2017). In accordance with Lee Masson et al. (2024), we defined the TPJ using a unilateral connectivity based parcellation atlas (Mars et al., 2012; Sallet et al., 2013) and mirrored the cluster into the left hemisphere. Lastly, we were additionally interested in the medial prefrontal cortex (mPFC), which, as another cluster of the DMN (Shirer et al., 2012), was frequently found in the context of higher levels of processing naturalistic stimuli (Chen et al., 2017; Lee Masson et al., 2024; Lee & Chen, 2024; Zadbood et al., 2017). We used a sub-parcellation (Cammoun et al., 2012) of the Desikan-Killiany atlas (Desikan et al., 2006) consisting of 219 cortical parcels to be able to specifically select the anterior mPFC section. In the left hemisphere we selected the areas labelled superiorfrontal_2, _3, and _4 and in the right hemisphere the areas superiorfrontal_3, _4, and _5. To limit the analysis to only the medial portions, we additionally removed any parts of the extracted binary mask that exceeded a coordinate of $x_{MNI} = \pm 15$ (Córcoles-Parada et al., 2017).

As for the visual hierarchy ROIs, we used MarsBaR (Brett et al., 2002) functions to extract the average Fisher *z*-transformed pairwise inter-subject correlations (ISCs) for each condition

from both hemispheres of all five supplementary ROIs. Also, we used the lme4 framework (Bates et al., 2015) once more to model the effects of CONTENT LEVEL, DURATION and their interaction while adding crossed random effects for the two respective subjects to address the complex covariance structure of ISC data:

$$\overline{z_{AB_{ROI}}} = 1 + \text{CONTENT LEVEL} * \text{DURATION} + (1|\text{Subj}_A) + (1|\text{Subj}_B) \qquad \text{(S1)}.$$

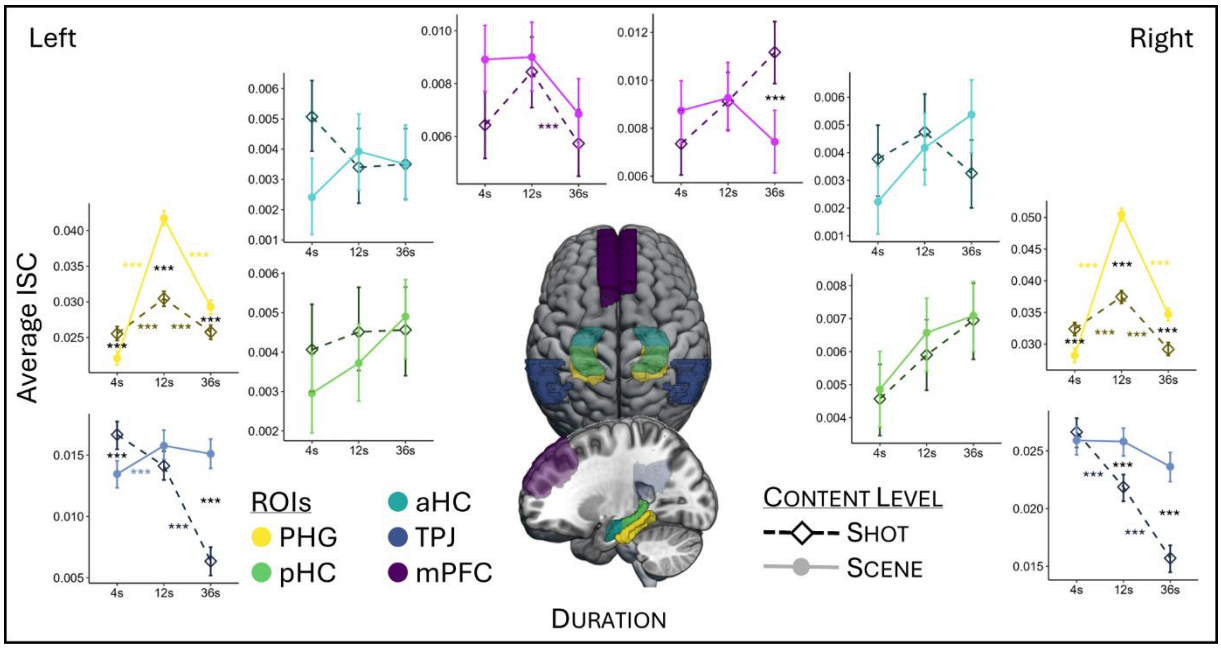
Parametric bootstrapping (N_{boot} = 500) was applied to determine estimates, confidence intervals and *p*-values for all fixed effects. *P*-values were adjusted for multiple comparisons using false discovery rate (FDR) correction at α =.05 (Benjamini & Hochberg, 1995; Benjamini & Yekutieli, 2001).

Results. As the results were very similar for the left and right equivalents of the five additional ROIs, we will jointly outline the trends across both hemispheres.

Looking at the results for these ROIs (Figure S3.1, Table S3.1), the ISC spiked in PHG for 12S DURATION stimuli of both CONTENT LEVELS. This is demonstrated by the significant increase from 4S to 12S and significant decrease from 12S to 36S for both SHOTS and SCENES. Additionally, the two CONTENT LEVELS significantly differ at each DURATION with higher values for the SHOT 4S, while SCENES produced higher ISC in both the 12S and 36S DURATIONS. We could not find any significant differences between any of the conditions in both the pHC and aHC. Also, the mPFC demonstrated rather spurious results, with only a significant decrease between SHOTS of 12S and 36S DURATION in the left mPFC and significantly higher ISC for SHOTS of 36s than SCENES of 36S DURATION in the right mPFC. Lastly, the pattern in TPJ was more in line with the trend along the visual processing hierarchy with a significant decrease in the CONTENT LEVEL SHOT with higher DURATIONS, while the ISC in the CONTENT LEVEL SCENE stayed constant, even increasing between 4S and 12S in the left TPJ. Thus, we also found a significantly higher ISC in SCENES of 36S than SHOTS of 36S in both hemispheres, while the ISC for SCENES of 12S was only higher in the right TPJ and even significantly lower for SCENES of 4S DURATION than SHOTS in the left TPJ.

Figure S4.1

Post-hoc test results of supplementary region of interest analysis



Note. Results from the additionally selected regions of interest (ROIs). CONTENT LEVEL SHOT in darker shade and dashed line, CONTENT LEVEL SCENE in lighter shade and solid line. PHG = *parahippocampal gyrus*, pHC = *posterior hippocampus*, aHC = *anterior hippocampus*, TPJ = *temporo-parietal junction*, mPFC = *medial prefrontal cortex*. * $p_{FDR\text{-}boot} < .05$, ** $p_{FDR\text{-}boot} < .01$, *** $p_{FDR\text{-}boot} < .001$, $N_{boot} = 500$. ROI masks are depicted on the MNI152 standard template. For a depiction of the ROIs on the pial fsaverage surface space see Figure S6.5b.

Table S4.1

Results of the post-hoc comparisons of the region of interest analysis for the five regions additionally movie-processing related areas (e.g., Jääskeläinen et al., 2021).

ROI	Contrast		Estimate (*b*)	95% CI lower	95% CI upper	$p_{FDR\text{-}boot}$
Left PHG						
	SHOT 4S	**SCENE 4S**	**.0034**	**.0021**	**.0047**	**< .001**
	SHOT 4S	**SHOT 12S**	**-.0049**	**-.0063**	**-.0034**	**< .001**
	SCENE 4S	**SCENE 12S**	**-.0196**	**-.0210**	**-.0182**	**< .001**
	SHOT 12S	**SCENE 12S**	**-.0112**	**-.0128**	**-.0098**	**< .001**
	SHOT 12S	**SHOT 36S**	**.0047**	**.0031**	**.0062**	**< .001**
	SCENE 12S	**SCENE 36S**	**.0124**	**.0110**	**.0138**	**< .001**
	SHOT 36S	**SCENE 36S**	**-.0035**	**-.0050**	**-.0022**	**< .001**
Right PHG						
	SHOT 4S	**SCENE 4S**	**.0042**	**.0026**	**.0056**	**< .001**
	SHOT 4S	**SHOT 12S**	**-.0051**	**-.0064**	**-.0036**	**< .001**
	SCENE 4S	**SCENE 12S**	**-.0223**	**-.0238**	**-.0207**	**< .001**
	SHOT 12S	**SCENE 12S**	**-.0130**	**-.0144**	**-.0116**	**< .001**
	SHOT 12S	**SHOT 36S**	**.0083**	**.0070**	**.0098**	**< .001**
	SCENE 12S	**SCENE 36S**	**.0158**	**.0143**	**.0172**	**< .001**
	SHOT 36S	**SCENE 36S**	**-.0055**	**-.0069**	**-.0041**	**< .001**

Left pHC						
	Shot 4s	Scene 4s	.0011	-.0003	.0027	1
	Shot 4s	Shot 12s	-.0004	-.0020	.0012	1
	Scene 4s	Scene 12s	-.0008	-.0021	.0006	1
	Shot 12s	Scene 12s	.0008	-.0007	.0023	1
	Shot 12s	Shot 36s	-.0001	-.0014	.0014	1
	Scene 12s	Scene 36s	-.0012	-.0026	.0003	1
	Shot 36s	Scene 36s	-.0003	-.0017	.0011	1
Right pHC						
	Shot 4s	Scene 4s	-.0003	-.0019	.0012	1
	Shot 4s	Shot 12s	-.0013	-.0029	.0004	1
	Scene 4s	Scene 12s	-.0017	-.0032	.0000	.6652
	Shot 12s	Scene 12s	-.0007	-.0023	.0008	1
	Shot 12s	Shot 36s	-.0011	-.0025	.0006	1
	Scene 12s	Scene 36s	-.0005	-.0021	.0011	1
	Shot 36s	Scene 36s	-.0001	-.0018	.0014	1
Left aHC						
	Shot 4s	Scene 4s	.0027	.0010	.0045	.1047
	Shot 4s	Shot 12s	.0017	.0000	.0034	.5417
	Scene 4s	Scene 12s	-.0015	-.0032	.0001	.8699
	Shot 12s	Scene 12s	-.0005	-.0023	.0010	1
	Shot 12s	Shot 36s	-.0001	-.0018	.0016	1
	Scene 12s	Scene 36s	.0004	-.0013	.0019	1
	Shot 36s	Scene 36s	.0000	-.0017	.0017	1
Right aHC						
	Shot 4s	Scene 4s	.0015	-.0001	.0033	.8093
	Shot 4s	Shot 12s	-.0010	-.0028	.0010	1
	Scene 4s	Scene 12s	-.0019	-.0036	-.0001	.4163
	Shot 12s	Scene 12s	.0006	-.0013	.0023	1
	Shot 12s	Shot 36s	.0015	-.0003	.0033	1
	Scene 12s	Scene 36s	-.0012	-.0031	.0008	1
	Shot 36s	Scene 36s	-.0021	-.0039	-.0002	.3770
Left TPJ						
	Shot 4s	**Scene 4s**	**.0032**	**.0016**	**.0048**	**< .001**
	Shot 4s	Shot 12s	.0026	.0010	.0042	.0554
	Scene 4s	**Scene 12s**	**-.0023**	**-.0040**	**-.0008**	**< .001**
	Shot 12s	Scene 12s	-.0016	-.0032	-.0002	.3405
	Shot 12s	**Shot 36s**	**.0078**	**.0062**	**.0093**	**< .001**
	Scene 12s	Scene 36s	.0007	-.0008	.0023	1
	Shot 36s	**Scene 36s**	**-.0088**	**-.0105**	**-.0071**	**< .001**
Right TPJ						
	Shot 4s	Scene 4s	.0007	-.0010	.0024	1
	Shot 4s	**Shot 12s**	**.0048**	**.0031**	**.0067**	**< .001**
	Scene 4s	Scene 12s	.0001	-.0014	.0019	1
	Shot 12s	**Scene 12s**	**-.0039**	**-.0056**	**-.0022**	**< .001**
	Shot 12s	**Shot 36s**	**.0062**	**.0044**	**.0078**	**< .001**
	Scene 12s	Scene 36s	.0022	.0003	.0038	.2957
	Shot 36s	**Scene 36s**	**-.0079**	**-.0098**	**-.0062**	**< .001**

Left mPFC						
	SHOT 4S	SCENE 4S	-.0025	-.0043	-.0007	.1047
	SHOT 4S	SHOT 12S	-.0020	-.0038	-.0002	.2957
	SCENE 4S	SCENE 12S	-.0001	-.0020	.0016	1
	SHOT 12S	SCENE 12S	-.0006	-.0024	.0013	1
	SHOT 12S	**SHOT 36S**	**.0027**	**.0011**	**.0044**	**< .001**
	SCENE 12S	SCENE 36S	-.0011	-.0029	.0007	1
	SHOT 36S	SCENE 36S	-.0014	-.0032	.0005	1
Right mPFC						
	SHOT 4S	SCENE 4S	-.0014	-.0032	.0005	1
	SHOT 4S	SHOT 12S	-.0018	-.0036	.0002	.8699
	SCENE 4S	SCENE 12S	-.0005	-.0025	.0014	1
	SHOT 12S	SCENE 12S	-.0001	-.0021	.0018	1
	SHOT 12S	SHOT 36S	-.0020	-.0038	-.0002	.4163
	SCENE 12S	SCENE 36S	.0018	-.0001	.0037	.6973
	SHOT 36S	**SCENE 36S**	**.0037**	**.0020**	**.0055**	**< .001**

Notes. Post-hoc comparison of the supplementary region of interest (ROI) analysis modelling the inter-subject correlation values by the CONTENT LEVEL x DURATION. Confidence intervals (CI) and *p*-values were determined using parametric bootstrapping via lme4's bootMer (N_{boot} = 500). Significant comparisons are printed in bold. PHG = *parahippocampal gyrus*, pHC = *posterior hippocampus*, aHC = *anterior hippocampus*, TPJ = *temporo-parietal junction*, mPFC = *medial prefrontal cortex*.

Discussion. The results of the supplement ROI revealed two interesting, significant findings: First, the ISC pattern we found in the TPJ ROI (Mars et al., 2012; Sallet et al., 2013) very much resembled the patterns found in the findings for the angular gyrus (AG) and the posterior medial DMN ROI; having unchanging ISC for all SCENE conditions, but exhibiting a gradual decrease of ISC with DURATION for the SHOT conditions. The TPJ circumscribes a functionally and structurally heterogenous (Doricchi, 2022), high-level area (Patel et al., 2019), whose posterior parts overlap with the AG and are connected to the DMN (Lattanzio et al., 2021; Wang et al., 2020). In the context of movies, it was related to the memory of the content and processing social cues (Jääskeläinen et al., 2021). Additionally, theories on the function of the TPJ converge on a role in prediction and updating of internal and external perspectives, integrating information from stimulus and memory (Bzdok et al., 2013; Doricchi, 2022; Lo Presti et al., 2025). Thus, the TPJ results join the ranks of findings in this study suggesting an increased engagement of areas that process information from different viewpoints when watching SCENES especially of longer DURATION.

The second interesting finding is the very prevalent attunement of the parahippocampal gyrus (PHG) with stimuli of 12s DURATION. While much more pronounced for SCENES, both CONTENT LEVELS demonstrate a peak in ISC for the respective 12s conditions. Previous studies indicated the PHG in the context of spatial (Zacks et al., 2010) as well as temporal transitions between events (Ezzyat & Davachi, 2011) and the higher-level understanding of the narrative (AbdulSabur et al., 2014). In this context, it was also related to the encoding of events to memory (Hasson, Furman, et al., 2008). Fittingly, the Desikan-Killiany atlas-based ROI of the PHG (Desikan et al., 2006) mainly overlaps with the memory-related (Steel et al., 2025) and DMN-connected (Baldassano et al., 2013) anterior PPA, that the whole-brain analysis also revealed specifically for the contrasts 12s > 4s and 12s > 36s as well as the interaction SCENE x 12s. As mentioned in the context of the whole-brain contrasts of DURATION (see main manuscript 4.2.2.), the signal in this part of the PPA peaks between four to twelve seconds after cue onset in a recall task (Steel et al., 2023), indicating that especially this time range is more relevant for semantic or memory processes. This is also supported by recent studies that identified dwell times of cortical network states during naturalistic movie watching (Geerligs et al., 2022; E. Yang et al., 2023). Specifically for networks containing the anterior PPA, they found median dwell times between ten and 16 seconds (E. Yang et al., 2023), which might explain this specific attunement to the 12s condition within this area. Further, based on natural coherencies of SCENES and SHOTS, the 12s time window might also be more essential to the event structure of the movie (Cutting et al., 2011, 2012; Cutting & Candan, 2015; Pearlman, 2019; Zacks et al., 2009, 2010) and thus more relevant for the PHG, which was previously related to the memorizing the movie's plot (Hasson, Furman, et al., 2008; Zadbood et al., 2017).

AC.5 Supplemental Material 5: Post-hoc region of interest analysis of the superior temporal sulcus

As the visual inspection of the condition-wise results as well as the contrasts specifically for SCENES of 36S DURATION revealed an extension of engagement along the superior temporal sulcus (STS) we wanted to further investigate the effects of CONTENT LEVEL and DURATION using a region of interest (ROI) analysis within this functionally distinct region (Pitcher & Ungerleider, 2021; Zhen et al., 2015).

As discussed in the main manuscript (see 4.2.3.), the STS is generally often related to the dynamical processing of social and especially facial information (Duchaine & Yovel, 2015; Pitcher & Ungerleider, 2021). In the context of movie perception specifically, this was demonstrated by studies localizing the processing of social interactions and intentions in the STS (Lahnakoski et al., 2012; Lee Masson et al., 2024; Lee Masson & Isik, 2021). Beyond this social aspect alone, the posterior STS in particular has been identified as containing longer temporal receptive windows (TRW), being engaged specifically by more temporally persistent stimuli across different stimulus modalities (Farbood et al., 2015; Hasson, Yang, et al., 2008; Lerner et al., 2014). Furthermore, the STS has also been shown to be engaged by a shared understanding of the plot (Chen et al., 2017; Zadbood et al., 2017) as well as a more abstract interpretation of the content (Akimoto et al., 2014; Yeshurun, Swanson, et al., 2017) which suggests its involvement in high-level processing of naturalistic stimuli in general. The initial analysis presented in the main manuscript demonstrated strong engagement of the STS, especially for the interaction between SCENE and 36S DURATION. However, we discussed that the contrast might be driven by the differences between the content-rich SCENE 36S condition compared to the rather static SHOT 36S condition, as the processing pathway along the STS can also reflect biological motion (Pitcher & Ungerleider, 2021). It is therefore highly intriguing to investigate the different subregions along the STS in more detail to explore the evoked ISC across conditions. Since the STS was not part of the initial set of ROIs, this post-hoc analysis is exploratory and aims to better characterize the effects already observed.

Methods. As previous TRW studies used face recognition localizer to identify their STS ROIs (e.g., Hasson et al., 2008), we also looked for established definitions from face processing literature. Ultimately, we created the STS ROIs using the face specific functional atlas published by Zhen et al. (2015). Importantly, this atlas distinguishes the STS into three separate regions in each hemisphere based on the data of 202 subject performing a dynamic face localizer task: anterior (aSTS), posterior (pSTS) and posterior continuation of the STS (pcSTS; Figure S4.1 and Figure S6.5c for ROIs on fsaverage surface). All ROI masks were available as part of the FreeROI toolbox (0.2.2; Huang et al., 2014 https://freeroi.brainactivityatlas.org/). A distinction between these functionally distinct regions (e.g. Pitcher & Ungerleider, 2021) allows for a more in-depth insight, as previous movie studies identified various areas along the STS all supposedly involved with a high-level understanding of the content and plot-structure (Chen et al., 2017; Lahnakoski et al., 2017; Yeshurun, Swanson, et al., 2017).

Like previous iterations of the ROI analyses, MarsBaR (Brett et al., 2002) was used to extract all data for each of the in total six STS ROIs across both hemispheres. Then, we once more modelled the average Fisher *z*-transformed pairwise inter-subject correlations (ISCs) in the lme4 framework (Bates et al., 2015), estimating the effects of CONTENT LEVEL, DURATION and their interaction while controlling for the convoluted covariance structure of ISC data by adding crossed random effects for the respective subject pair:

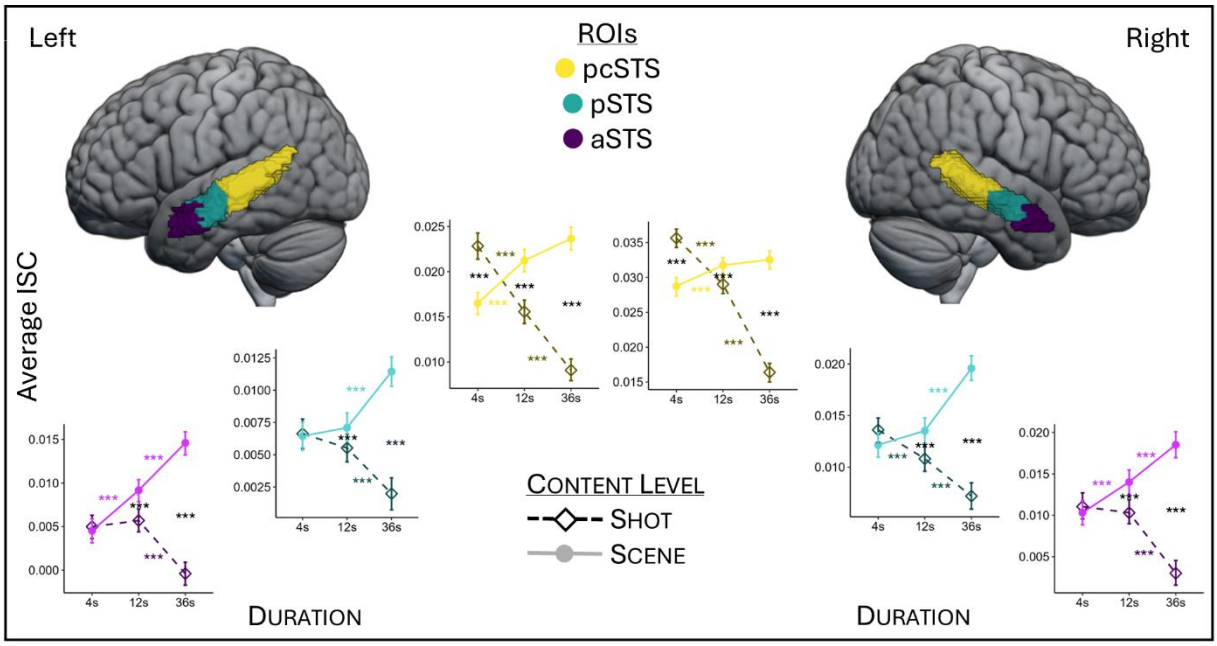
$$\overline{z_{AB_{ROI}}} = 1 + \text{CONTENT LEVEL} * \text{DURATION} + (1|\text{Subj}_A) + (1|\text{Subj}_B) \qquad \text{(S2)}.$$

Following the modelling, estimates, confidence intervals and *p*-values were determined in a parametric bootstrapping procedure (N_{boot} = 500) for all fixed effects. Finally, the *p*-values were corrected for multiple comparisons by controlling the FDR at α =.05 (Benjamini & Hochberg, 1995; Benjamini & Yekutieli, 2001).

Results. Since the results (Figure S5.1, Table S5.1) are again very similar across hemispheres, we summarize the depicted effects and trends in a combined manner. In the most posterior subregion, the pcSTS, which circumscribes the tail end of the STS transitioning into the

occipital lobe, a trend similar to the higher-level regions in visual processing hierarchy emerged. In both hemispheres we found a significant increase for the SCENE condition between the 4S and 12S DURATION, while the 12S and 36S DURATIONS did not differ significantly.

Figure S5.1
Results of post-hoc region of interest analysis along the superior temporal sulcus



Note. Regions of interest (ROIs) were based on face-selective functional regions (Zhang et al., 2015, Huang et al., 2014). CONTENT LEVEL SHOT in darker shade and dashed line, CONTENT LEVEL SCENE in lighter shade and solid line. pcSTS = *posterior continuation of the superior temporal sulcus*, pSTS = *posterior superior temporal sulcus*, aSTS = *anterior superior temporal sulcus*. * $p_{FDR\text{-}boot} < .05$, ** $p_{FDR\text{-}boot} < .01$, *** $p_{FDR\text{-}boot} < .001$, $N_{boot} = 500$. ROI masks are depicted on the MNI152 standard template. For a depiction of the ROIs on the pial fsaverage surface space see Figure S6.5c.

This is accompanied by a significant decrease of the average ISC with DURATION in the SHOT conditions, resulting in a higher ISC for SHOTS than SCENES of 4S DURATION, but higher ISC in the SCENE condition 12S and 36S conditions. Moving anteriorly to the pSTS the ISC was still significantly higher in the Scene condition for 12S and 36S DURATION, but no longer different for the 4S DURATION. Moreover, the pSTS showed an increase in ISC between the SCENE 12S and SCENE 36S conditions, while the SHOT condition ISC still largely decreased with DURATION. This shift in trend continued in the aSTS as the results demonstrated a steady increase of ISC with duration in the SCENE conditions, while the SHOT condition showed a significant ISC reduction between the 12S and 36S conditions.

Table S5.1

Results of the post-hoc region of interest analysis in the superior temporal sulcus.

ROI	Contrast		Estimate (*b*)	95% CI lower	95% CI upper	$p_{FDR\text{-}boot}$
Left pcSTS						
	Shot 4s	**Scene 4s**	**.0063**	**.0043**	**.0083**	**< .001**
	Shot 4s	**Shot 12s**	**.0073**	**.0054**	**.0090**	**< .001**
	Scene 4s	**Scene 12s**	**-.0047**	**-.0065**	**-.0029**	**< .001**
	Shot 12s	**Scene 12s**	**-.0057**	**-.0076**	**-.0038**	**< .001**
	Shot 12s	**Shot 36s**	**.0065**	**.0048**	**.0083**	**< .001**
	Scene 12s	Scene 36s	-.0024	-.0043	-.0007	.0796
	Shot 36s	**Scene 36s**	**-.0146**	**-.0162**	**-.0128**	**< .001**
Right pcSTS						
	Shot 4s	**Scene 4s**	**.0069**	**.0051**	**.0088**	**< .001**
	Shot 4s	**Shot 12s**	**.0066**	**.0046**	**.0085**	**< .001**
	Scene 4s	**Scene 12s**	**-.0030**	**-.0049**	**-.0011**	**.0273**
	Shot 12s	**Scene 12s**	**-.0027**	**-.0045**	**-.0008**	**< .001**
	Shot 12s	**Shot 36s**	**.0126**	**.0107**	**.0145**	**< .001**
	Scene 12s	**Scene 36s**	**-.0008**	**-.0025**	**.0009**	**< .001**
	Shot 36s	**Scene 36s**	**-.0162**	**-.0181**	**-.0144**	**< .001**
Left pSTS						
	Shot 4s	Scene 4s	.0002	-.0015	.0018	1
	Shot 4s	Shot 12s	.0011	-.0005	.0026	1
	Scene 4s	Scene 12s	-.0006	-.0022	.0010	1
	Shot 12s	Scene 12s	-.0016	-.0032	.0001	.4182
	Shot 12s	**Shot 36s**	**.0035**	**.0019**	**.0051**	**< .001**
	Scene 12s	**Scene 36s**	**-.0043**	**-.0059**	**-.0028**	**< .001**
	Shot 36s	**Scene 36s**	**-.0095**	**-.0111**	**-.0079**	**< .001**
Right pSTS						
	Shot 4s	Scene 4s	.0014	-.0002	.0032	.6099
	Shot 4s	**Shot 12s**	**.0028**	**.0012**	**.0045**	**< .001**
	Scene 4s	Scene 12s	-.0014	-.0030	.0002	.6266
	Shot 12s	**Scene 12s**	**-.0027**	**-.0044**	**-.0011**	**< .001**
	Shot 12s	**Shot 36s**	**.0036**	**.0018**	**.0054**	**< .001**
	Scene 12s	**Scene 36s**	**-.0061**	**-.0077**	**-.0043**	**< .001**
	Shot 36s	**Scene 36s**	**-.0124**	**-.0141**	**-.0105**	**< .001**
Left aSTS						
	Shot 4s	Scene 4s	.0005	-.0014	.0023	1
	Shot 4s	Shot 12s	-.0007	-.0024	.0011	1
	Scene 4s	**Scene 12s**	**-.0046**	**-.0065**	**-.0027**	**< .001**
	Shot 12s	**Scene 12s**	**-.0035**	**-.0053**	**-.0016**	**< .001**
	Shot 12s	**Shot 36s**	**.0061**	**.0043**	**.0079**	**< .001**
	Scene 12s	**Scene 36s**	**-.0054**	**-.0072**	**-.0037**	**< .001**
	Shot 36s	**Scene 36s**	**-.0150**	**-.0168**	**-.0133**	**< .001**
Right aSTS						
	Shot 4s	Scene 4s	.0007	-.0016	.0027	1
	Shot 4s	Shot 12s	.0007	-.0016	.0029	1
	Scene 4s	**Scene 12s**	**-.0037**	**-.0058**	**-.0015**	**< .001**
	Shot 12s	**Scene 12s**	**-.0037**	**-.0057**	**-.0016**	**< .001**
	Shot 12s	**Shot 36s**	**.0073**	**.0052**	**.0093**	**< .001**
	Scene 12s	**Scene 36s**	**-.0045**	**-.0066**	**-.0025**	**< .001**
	Shot 36s	**Scene 36s**	**-.0155**	**-.0178**	**-.0133**	**< .001**

Notes. Post-hoc comparison of the supplementary region of interest (ROI) analysis modelling the inter-subject correlation values by the CONTENT LEVEL x DURATION. Confidence intervals (CI) and *p*-values were determined using parametric bootstrapping via lme4's bootMer (N_{boot} = 500). Significant comparisons are printed in bold. pcSTS = *posterior continuation of the superior temporal sulcus*, pSTS = *posterior superior temporal sulcus*, aSTS = *anterior superior temporal sulcus*.

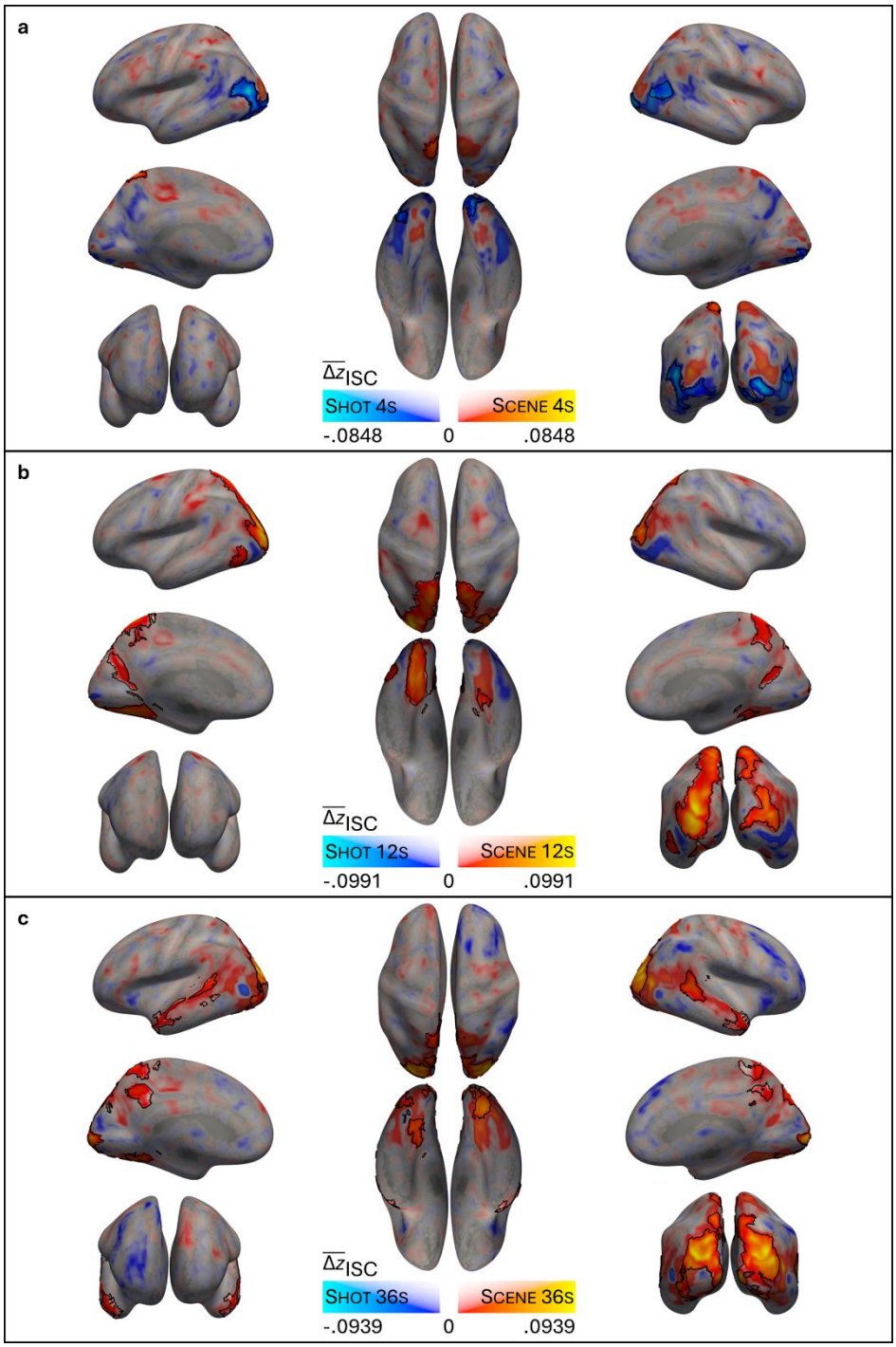
Discussion. The results depict a trend similar to that observed for the higher-order ROIs in the main analysis, i.e., a significant difference between the SCENE and SHOT conditions for longer DURATIONS. However, especially the pSTS and aSTS ROIs differ from the previous trend in one crucial detail: The average ISC increases with duration in the SCENE condition and does not remain constant like in the temporo-parietal junction or posterior medial default mode network. This post-hoc ROI analysis therefore suggests that the results found specifically for SCENES of longer DURATION do not stem only from a relative difference between the rather static SHOT 36S and content-rich SCENE 36S condition, but that the more anterior regions show significantly more engagement with more complex content of longer DURATIONS. These exploratory results thus support our claims in the main discussion (see 4.2.3.) attributing the identified engagement of the anterior temporal lobe to the higher-level processing and memory of complex, longer-lasting components of the stimulus, which previous studies already located in this area (Akimoto et al., 2014; Chen et al., 2017; Hasson, Furman, et al., 2008; Yeshurun, Swanson, et al., 2017). Nevertheless, the reduced engagement of the entire STS with an increase in DURATION in the SHOT condition cannot be dismissed. In the context of the clusters identified in areas associated with the perception of biological motion (e.g., area MT+, McAleer et al., 2014), we would trace this reduction to a more static and therefore less engaging and synchronized perception of the longer shot stimuli (Hasson et al., 2010; Loschky et al., 2020). Importantly, this might also be related to the differences in movie scene/shot condensation or stretching across scenes, respectively (see main manuscript 2.2.). Since movie shots are in general shorter than movie scenes, with most shots lasting less than ten seconds (Cutting & Candan, 2015), the longer DURATION conditions might have caused the stimuli to appear unnaturally slow and elongated, creating this

misalignment in the engagement of the STS between more naturalistic and our manipulated stimulus presentation.

ACD.6 Supplemental Material 6: Additional whole-brain result figures

Figure S6.1

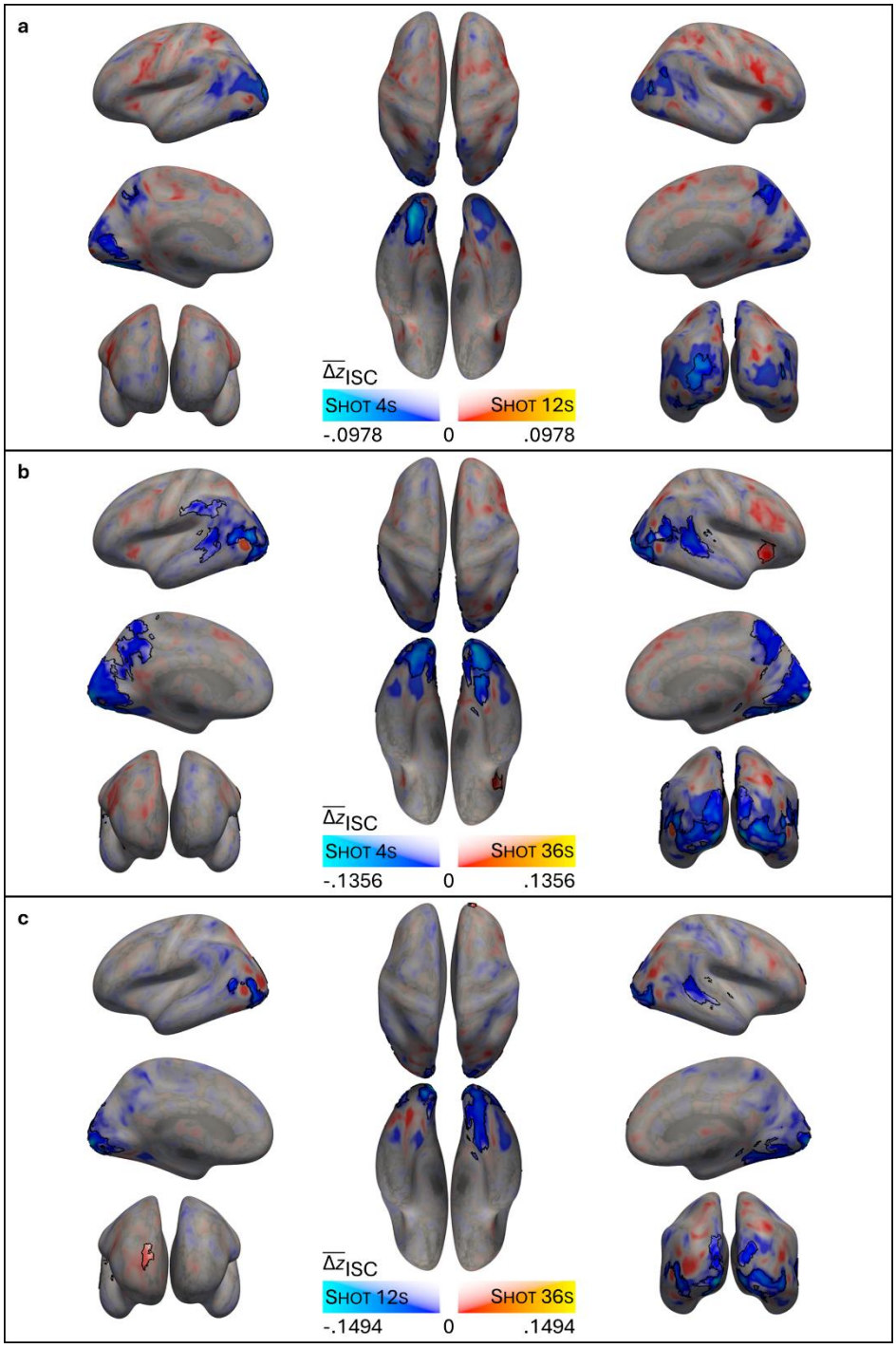
Whole-brain results of the differences in Fisher z-transformed inter-subject correlations between the levels of CONTENT LEVELS separate for the levels of DURATION



Note. (a) Results of contrasting SCENE and SHOT for the 4S DURATION. (b) Results of contrasting SCENE and SHOT for the 12S DURATION. (c) Results of contrasting SCENE and SHOT for the 36S DURATION. SCENE > SHOT contrasts in warm colors, SHOT > SCENE contrasts cold colors. Results are FWE-cluster corrected at $\alpha = .05$ with a cluster forming threshold of $p < .001$, Monte Carlo simulated cluster extend thresholds were 35 (a), 35 (b) and 36 (c) voxels, respectively. Significant clusters are depicted with a black border. Results figures applies the "Highlight, don't Hide" principle (Taylor et al., 2023). Thus, clusters with non-significant *p*-values are not omitted but displayed at lower opacity. Whole-brain results are projected on inflated fsaverage pial surface.

Figure S6.2

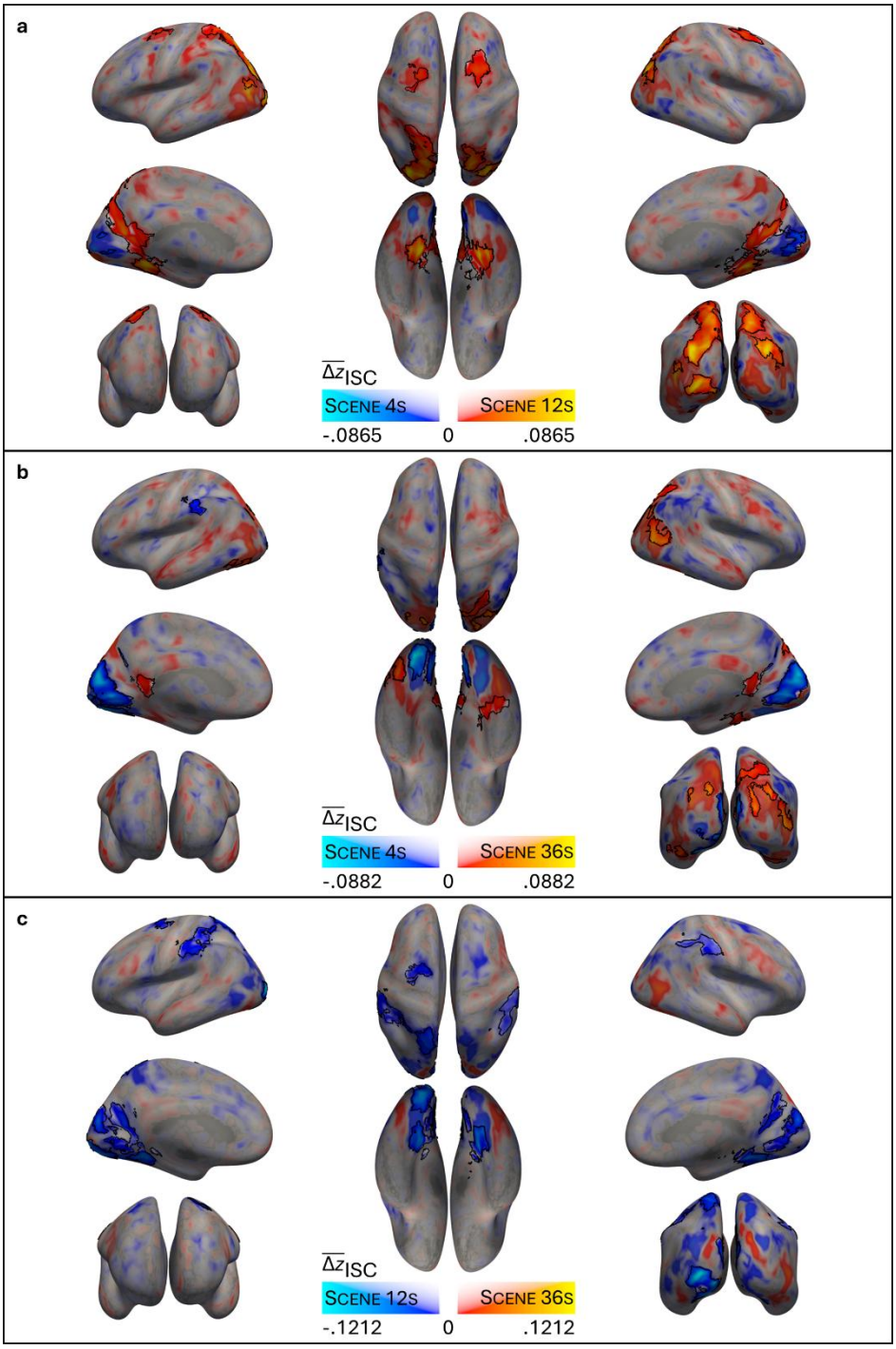
Whole-brain results of the differences in Fisher z-transformed inter-subject correlations between the levels of DURATION separate in the SHOT condition



Note. (a) Results of contrasting 4s and 12s DURATION for SHOTS. (b) Results of contrasting 4s and 36s DURATION for SHOTS. (c) Results of contrasting 12s and 36s DURATION for SHOTS. Longer DURATION > shorter DURATION contrasts in warm colors, shorter DURATION > longer DURATION contrasts cold colors. Results are FWE-cluster corrected at $\alpha = .05$ with a cluster forming threshold of $p < .001$, Monte Carlo simulated cluster extend thresholds were 36 (a), 34 (b) and 35 (c) voxels, respectively. Significant clusters are depicted with a black border. Results figures applies the "Highlight, don't Hide" principle (Taylor et al., 2023). Thus, clusters with non-significant *p*-values are not omitted but displayed at lower opacity. Whole-brain results are projected on inflated fsaverage pial surface.

Figure S6.3

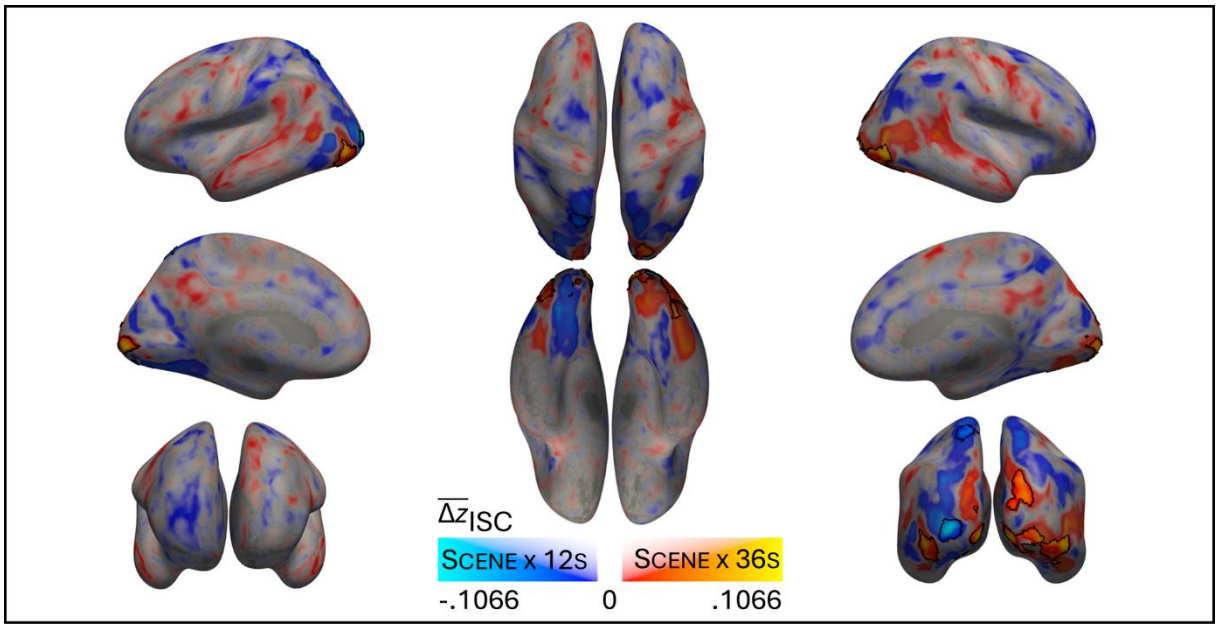
Whole-brain results of the differences in Fisher z-transformed inter-subject correlations between the levels of DURATION *separate in the* SCENE *condition*



Note. (a) Results of contrasting 4s and 12s DURATION for SCENES. (b) Results of contrasting 4s and 36s DURATION for SCENES. (c) Results of contrasting 12s and 36s DURATION for SCENES. Longer DURATION > shorter DURATION contrasts in warm colors, shorter DURATION > longer DURATION contrasts cold colors. Results are FWE-cluster corrected at α = .05 with a cluster forming threshold of $p < .001$, Monte Carlo simulated cluster extend thresholds were 34 (a), 35 (b) and 34 (c) voxels, respectively. Significant clusters are depicted with a black border. Results figures applies the "Highlight, don't Hide" principle (Taylor et al., 2023). Thus, clusters with non-significant *p*-values are not omitted but displayed at lower opacity. Whole-brain results are projected on inflated fsaverage pial surface.

Figure S6.4

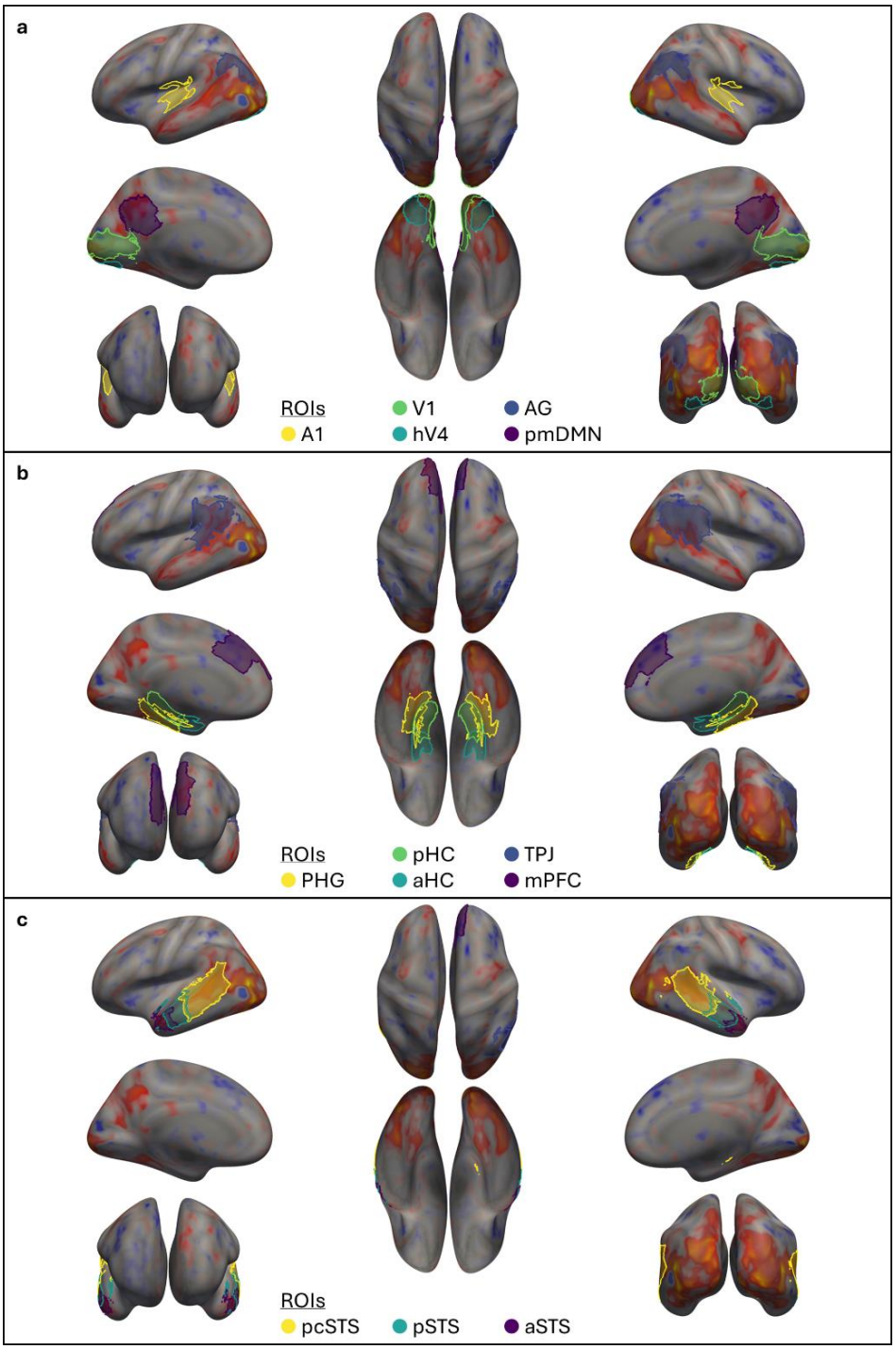
Whole-brain results of the differences in Fisher z-transformed correlations from comparing the specific interaction effects for SCENES x 12S and SCENES x 36S DURATIONS



Note. SCENES x 36S > SCENES x 12S contrasts in warm colors, SCENES x 12S > SCENES x 36S contrasts cold colors. Results are FWE-cluster corrected at α = .05 with a cluster forming threshold of $p < .001$, Monte Carlo simulated cluster extend threshold was 34 voxels. Significant clusters are depicted with a black border. Results figures applies the "Highlight, don't Hide" principle (Taylor et al., 2023). Thus, clusters with non-significant *p*-values are not omitted but displayed at lower opacity. Whole-brain results are projected on inflated fsaverage pial surface.

Figure **S6.5**

Regions of interest depicted on SCENE x 36S interaction contrast projected on the pial surface



Note. (a) ROIs based on Baldassano et al. (2017). Results are reported in Figure 8 and Table S2.1. (b) Additionally considers movie-relevant ROIs (e.g., Jääskeläinen et al., 2021). Results are reported in Figure S4.1 and Table S4.1. (c) Exploratory ROI analysis in three subregions of the superior temporal sulcus (STS; Huang et al., 2014; Zhen et al., 2015). Results are reported in Figure S5.1 and Table S5.1. ROI masks are overlayed on results of the interaction contrast SCENE x 36s. SCENE x 36s > 0 contrast in warm colors, SCENE x 36s < 0 contrast cold colors. Contrast results apply the "Highlight, don't Hide" principle (Taylor et al., 2023). Thus, clusters with non-significant *p*-values are not omitted but displayed at lower opacity. ROIs and whole-brain results are projected on inflated fsaverage pial surface. ROI = region of interest, A1 = primary auditory cortex, V1 = primary visual cortex, hV4 = extrastriate visual cortex, AG = angular gyrus, pmDMN = posterior medial cluster of the default mode network, PHG = *parahippocampal gyrus*, pHC = *posterior hippocampus*, aHC = *anterior hippocampus*, TPJ = *temporo-parietal junction*, mPFC = *medial prefrontal cortex,* pcSTS = *posterior continuation of the superior temporal sulcus*, pSTS = *posterior superior temporal sulcus*, aSTS = *anterior superior temporal sulcus.*

AC.7 Supplemental References

AbdulSabur, N. Y., Xu, Y., Liu, S., Chow, H. M., Baxter, M., Carson, J., & Braun, A. R. (2014). Neural correlates and network connectivity underlying narrative production and comprehension: A combined fMRI and PET study. *Cortex*, *57*, 107–127. https://doi.org/10.1016/j.cortex.2014.01.017

Akimoto, Y., Sugiura, M., Yomogida, Y., Miyauchi, C. M., Miyazawa, S., & Kawashima, R. (2014). Irony comprehension: Social conceptual knowledge and emotional response. *Human Brain Mapping*, *35*(4), 1167–1178. https://doi.org/10.1002/hbm.22242

Alahmadi, A. A. S. (2021). Investigating the sub-regions of the superior parietal cortex using functional magnetic resonance imaging connectivity. *Insights into Imaging*, *12*(1). https://doi.org/10.1186/s13244-021-00993-9

Allison, T., Puce, A., & McCarthy, G. (2000). Social perception from visual cues: role of the STS region. *Trends in Cognitive Sciences*, *4*(7), 267–278. https://doi.org/10.1016/S1364-6613(00)01501-1

Anzai, A., Chowdhury, S. A., & DeAngelis, G. C. (2011). Coding of stereoscopic depth information in visual areas V3 and V3A. *Journal of Neuroscience*, *31*(28), 10270–10282. https://doi.org/10.1523/JNEUROSCI.5956-10.2011

Arora, A., Weiss, B., Schurz, M., Aichhorn, M., Wieshofer, R. C., & Perner, J. (2015). Left inferior-parietal lobe activity in perspective tasks: Identity statements. *Frontiers in Human Neuroscience*, *9*(JUNE), 1–17. https://doi.org/10.3389/fnhum.2015.00360

Baldassano, C., Beck, D. M., & Fei-Fei, L. (2013). Differential connectivity within the Parahippocampal Place Area. *NeuroImage*, *75*, 228–237. https://doi.org/10.1016/j.neuroimage.2013.02.073

Baldassano, C., Chen, J., Zadbood, A., Pillow, J. W., Hasson, U., & Norman, K. A. (2017). Discovering Event Structure in Continuous Narrative Perception and Memory. *Neuron*, *95*(3), 709-721.e5. https://doi.org/10.1016/j.neuron.2017.06.041

Baldassano, C., Esteva, A., Fei-Fei, L., & Beck, D. M. (2016). Two distinct Scene-Processing networks connecting vision and memory. *ENeuro*, *3*(5). https://doi.org/10.1523/ENEURO.0178-16.2016

Barton, B., & Brewer, A. A. (2017). Visual field map clusters in high-order visual processing: Organization of V3a/V3B and a new cloverleaf cluster in the posterior superior temporal sulcus. *Frontiers in Integrative Neuroscience*, *11*(February), 1–18. https://doi.org/10.3389/fnint.2017.00004

Bates, D., Mächler, M., Bolker, B. M., & Walker, S. C. (2015). Fitting linear mixed-effects models using lme4. *Journal of Statistical Software*, *67*(1). https://doi.org/10.18637/jss.v067.i01

Baumann, O., & Mattingley, J. B. (2021). Extrahippocampal contributions to spatial navigation in humans: A review of the neuroimaging evidence. *Hippocampus*, *31*(7), 640–657. https://doi.org/10.1002/hipo.23313

Bencivenga, F., Sulpizio, V., Tullo, M. G., & Galati, G. (2021). Assessing the effective connectivity of premotor areas during real vs imagined grasping: a DCM-PEB approach. *NeuroImage*, *230*(January), 117806. https://doi.org/10.1016/j.neuroimage.2021.117806

Benjamini, Y., & Hochberg, Y. (1995). Controlling the False Discovery Rate : A Practical and Powerful Approach to Multiple Testing Author (s): Yoav Benjamini and Yosef Hochberg Source : Journal of the Royal Statistical Society . Series B (Methodological), Vol . 57 , No . 1 (1995), Publi. *Journal of the Royal Statistical Society*, *57*(1), 289–300.

Benjamini, Y., & Yekutieli, D. (2001). The control of the false discovery rate in multiple testing under dependency. *The Annals of Statistics*, *29*(4), 1165–1188. https://doi.org/10.1214/aos/1013699998

Ben-Yakov, A., & Henson, R. N. (2018). The hippocampal film editor: Sensitivity and specificity to event boundaries in continuous experience. *Journal of Neuroscience*, *38*(47), 10057–10068. https://doi.org/10.1523/JNEUROSCI.0524-18.2018

Boccia, M., Piccardi, L., Palermo, L., Nemmi, F., Sulpizio, V., Galati, G., & Guariglia, C. (2015). A penny for your thoughts! patterns of fMRI activity reveal the content and the spatial topography of visual mental images. *Human Brain Mapping*, *36*(3), 945–958. https://doi.org/10.1002/hbm.22678

Brass, M., Ullsperger, M., Knoesche, T. R., Von Cramon, D. Y., & Phillips, N. A. (2005). Who comes first? The role of the prefrontal and parietal cortex in cognitive control. *Journal of Cognitive Neuroscience*, *17*(9), 1367–1375. https://doi.org/10.1162/0898929054985400

Brett, M., Anton, J.-L., Valabregue, R., & Poline, J.-B. (2002). Region of interest analysis using an SPM toolbox. *8th International Conferance on Functional Mapping of the Human Brain*, 497. https://matthew.dynevor.org/research/abstracts/marsbar/marsbar_abstract.pdf

Bzdok, D., Langner, R., Schilbach, L., Jakobs, O., Roski, C., Caspers, S., Laird, A. R., Fox, P. T., Zilles, K., & Eickhoff, S. B. (2013). Characterization of the temporo-parietal junction by combining data-driven parcellation, complementary connectivity analyses, and functional decoding. *NeuroImage*, *81*(1), 381–392. https://doi.org/10.1016/j.neuroimage.2013.05.046

Cammoun, L., Gigandet, X., Meskaldji, D., Thiran, J. P., Sporns, O., Do, K. Q., Maeder, P., Meuli, R., & Hagmann, P. (2012). Mapping the human connectome at multiple scales with diffusion spectrum MRI. *Journal of Neuroscience Methods*, *203*(2), 386–397. https://doi.org/10.1016/j.jneumeth.2011.09.031

Chakraborty, S., Thounaojam, D. M., & Sinha, N. (2021). A Shot boundary Detection Technique based on Visual Colour Information. *Multimedia Tools and Applications*, *80*(3), 4007–4022. https://doi.org/10.1007/s11042-020-09857-8

Chen, J., Honey, C. J., Simony, E., Arcaro, M. J., Norman, K. A., & Hasson, U. (2016). Accessing Real-Life Episodic Information from Minutes versus Hours Earlier Modulates Hippocampal and High-Order Cortical Dynamics. *Cerebral Cortex*, *26*(8), 3428–3441. https://doi.org/10.1093/cercor/bhv155

Chen, J., Leong, Y. C., Honey, C. J., Yong, C. H., Norman, K. A., & Hasson, U. (2017). Shared memories reveal shared structure in neural activity across individuals. *Nature Neuroscience*, *20*(1), 115–125. https://doi.org/10.1038/nn.4450

Cheng, Y., Xin, Y., Lu, X., Yang, T., Ma, X., Yuan, X., Liu, N., & Jiang, Y. (2025). Shared and Unique Neural Codes for Biological Motion Perception in Humans and Macaque Monkeys. *Advanced Science*, *12*(18), 1–13. https://doi.org/10.1002/advs.202411562

Córcoles-Parada, M., Müller, N. C. J., Ubero, M., Serrano-del-Pueblo, V. M., Mansilla, F., Marcos-Rabal, P., Artacho-Pérula, E., Dresler, M., Insausti, R., Fernández, G., & Muñoz-López, M. (2017). Anatomical segmentation of the human medial prefrontal cortex. *Journal of Comparative Neurology*, *525*(10), 2376–2393. https://doi.org/10.1002/cne.24212

Cutting, J. E. (2014). Event segmentation and seven types of narrative discontinuity in popular movies. *Acta Psychologica*, *149*, 69–77. https://doi.org/10.1016/j.actpsy.2014.03.003

Cutting, J. E., Brunick, K. L., & Candan, A. (2012). Perceiving event dynamics and parsing Hollywood films. *Journal of Experimental Psychology: Human Perception and Performance*, *38*(6), 1476–1490. https://doi.org/10.1037/a0027737

Cutting, J. E., Brunick, K. L., & DeLong, J. E. (2011). How Act Structure Sculpts Shot Lengths and Shot Transitions in Hollywood Film. *Projections*, *5*(1), 1–16. https://doi.org/10.3167/proj.2011.050102

Cutting, J. E., & Candan, A. (2015). Shot durations, shot classes, and the increased pace of popular movies. *Projections (New York)*, *9*(2), 40–62. https://doi.org/10.3167/proj.2015.090204

De Lange, F. P., Hagoort, P., & Toni, I. (2005). Neural topography and content of movement representations. *Journal of Cognitive Neuroscience*, *17*(1), 97–112. https://doi.org/10.1162/0898929052880039

Desikan, R. S., Ségonne, F., Fischl, B., Quinn, B. T., Dickerson, B. C., Blacker, D., Buckner, R. L., Dale, A. M., Maguire, R. P., Hyman, B. T., Albert, M. S., & Killiany, R. J. (2006). An automated labeling system for subdividing the human cerebral cortex on MRI scans into gyral based regions of interest. *NeuroImage*, *31*(3), 968–980. https://doi.org/10.1016/j.neuroimage.2006.01.021

Desmurget, M., & Sirigu, A. (2009). A parietal-premotor network for movement intention and motor awareness. *Trends in Cognitive Sciences*, *13*(10), 411–419. https://doi.org/10.1016/j.tics.2009.08.001

Doricchi, F. (2022). The functions of the temporal–parietal junction. In *Handbook of Clinical Neurology* (1st ed., Vol. 187). Elsevier B.V. https://doi.org/10.1016/B978-0-12-823493-8.00020-1

Duchaine, B., & Yovel, G. (2015). A Revised Neural Framework for Face Processing. *Annual Review of Vision Science*, *1*(1), 393–416. https://doi.org/10.1146/annurev-vision-082114-035518

Durmus, D. (2020). Spatial Frequency and the Performance of Image-Based Visual Complexity Metrics. *IEEE Access*, *8*, 100111–100119. https://doi.org/10.1109/ACCESS.2020.2998292

Elkin, L. A., Kay, M., Higgins, J. J., & Wobbrock, J. O. (2021). An Aligned Rank Transform Procedure for Multifactor Contrast Tests. *The 34th Annual ACM Symposium on User Interface Software and Technology*, 754–768. https://doi.org/10.1145/3472749.3474784

Epstein, R. A., & Baker, C. I. (2019). Scene Perception in the Human Brain. *Annual Review of Vision Science*, *5*, 373–397. https://doi.org/10.1146/annurev-vision-091718-014809

Ezzyat, Y., & Davachi, L. (2011). What constitutes an episode in episodic memory? *Psychological Science*, *22*(2), 243–252. https://doi.org/10.1177/0956797610393742

Farbood, M. M., Heeger, D. J., Marcus, G., Hasson, U., & Lerner, Y. (2015). The neural processing of hierarchical structure in music and speech at different timescales. *Frontiers in Neuroscience*, *9*(APR), 1–13. https://doi.org/10.3389/fnins.2015.00157

Farid, H. (2021). An Overview of Perceptual Hashing. *Journal of Online Trust and Safety*, *1*(1). https://doi.org/10.54501/jots.v1i1.24

Geerligs, L., Gözükara, D., Oetringer, D., Campbell, K. L., van Gerven, M., & Güçlü, U. (2022). A partially nested cortical hierarchy of neural states underlies event segmentation in the human brain. *ELife*, *11*, 1–36. https://doi.org/10.7554/eLife.77430

Grill-Spector, K., & Malach, R. (2004). The human visual cortex. *Annual Review of Neuroscience*, *27*(June), 649–677. https://doi.org/10.1146/annurev.neuro.27.070203.144220

Grossman, E. D., Battelli, L., & Pascual-Leone, A. (2005). Repetitive TMS over posterior STS disrupts perception of biological motion. *Vision Research*, *45*(22), 2847–2853. https://doi.org/10.1016/j.visres.2005.05.027

Guo, P., Li, Q., Wang, X., Li, X., Wang, S., Xie, Y., Xie, Y., Fu, Z., Zhang, X., & Li, S. (2020). Structural Covariance Changes of Anterior and Posterior Hippocampus During Musical Training in Young Adults. *Frontiers in Neuroanatomy*, *14*(May), 1–10. https://doi.org/10.3389/fnana.2020.00020

Hasson, U., Furman, O., Clark, D., Dudai, Y., & Davachi, L. (2008). Enhanced Intersubject Correlations during Movie Viewing Correlate with Successful Episodic Encoding. *Neuron*, *57*(3), 452–462. https://doi.org/10.1016/j.neuron.2007.12.009

Hasson, U., Landesman, O., Knappmeyer, B., Vallines, I., Rubin, N., & Heeger, D. J. (2008). Neurocinematics: The Neuroscience of Film. *Projections*, *2*(1), 1–26. https://doi.org/10.3167/proj.2008.020102

Hasson, U., Malach, R., & Heeger, D. J. (2010). Reliability of cortical activity during natural stimulation. *Trends in Cognitive Sciences*, *14*(1), 40–48. https://doi.org/10.1016/j.tics.2009.10.011

Hasson, U., Yang, E., Vallines, I., Heeger, D. J., & Rubin, N. (2008). A hierarchy of temporal receptive windows in human cortex. *Journal of Neuroscience*, *28*(10), 2539–2550. https://doi.org/10.1523/JNEUROSCI.5487-07.2008

Häusler, C. O., Eickhoff, S. B., & Hanke, M. (2022). Processing of visual and non-visual naturalistic spatial information in the "parahippocampal place area." *Scientific Data*, *9*(1), 1–15. https://doi.org/10.1038/s41597-022-01250-4

Häusler, C. O., Hanke, M., & Waite, A. (2021). *studyforrest-data-confoundsannotation: Frame-wise annotation of low-level auditory and visual confounds in the "Forrest Gump" movie stimulus*. GitHub. https://github.com/psychoinformatics-de/studyforrest-data-confoundsannotatio

Herlin, B., Navarro, V., & Dupont, S. (2021). The temporal pole: From anatomy to function—A literature appraisal. *Journal of Chemical Neuroanatomy*, *113*. https://doi.org/10.1016/j.jchemneu.2021.101925

Herrington, J. D., Nymberg, C., & Schultz, R. T. (2011). Biological motion task performance predicts superior temporal sulcus activity. *Brain and Cognition*, *77*(3), 372–381. https://doi.org/10.1016/j.bandc.2011.09.001

Hétu, S., Grégoire, M., Saimpont, A., Coll, M. P., Eugène, F., Michon, P. E., & Jackson, P. L. (2013). The neural network of motor imagery: An ALE meta-analysis. *Neuroscience and Biobehavioral Reviews*, *37*(5), 930–949. https://doi.org/10.1016/j.neubiorev.2013.03.017

Hoshi, E., & Tanji, J. (2000). Integration of target and body-part information in the premotor cortex when planning action. *Nature*, *408*(6811), 466–470. https://doi.org/10.1038/35044075

Huang, L., Yang, Z., Zhou, G., Liu, Z., Dang, X., Kong, X., Wang, X., Zhen, Z., & Liu, J. (2014). *FreeROI : an integrated toolbox for region of interest definition and visualization*. The 17th National Academic Congress of Psychology. https://d1wqtxts1xzle7.cloudfront.net/35152544/poster_flatten_v2-libre.pdf?1413435137=&response-content-disposition=inline%3B+filename%3DFreeROI_an_integrated_toolbox_for_region.pdf&Expires=1761925566&Signature=Oisna~h8KMP9DfzwPE1zDDQRMIyeCJ8SNCTWuC~WQSIL

Huth, A. G., Nishimoto, S., Vu, A. T., & Gallant, J. L. (2012). A Continuous Semantic Space Describes the Representation of Thousands of Object and Action Categories across the Human Brain. *Neuron*, *76*(6), 1210–1224. https://doi.org/10.1016/j.neuron.2012.10.014

Ito, T., Hearne, L. J., & Cole, M. W. (2020). A cortical hierarchy of localized and distributed processes revealed via dissociation of task activations, connectivity changes, and intrinsic timescales. *NeuroImage*, *221*(February), 117141. https://doi.org/10.1016/j.neuroimage.2020.117141

Jääskeläinen, I. P., Sams, M., Glerean, E., & Ahveninen, J. (2021). Movies and narratives as naturalistic stimuli in neuroimaging. *NeuroImage*, *224*(June 2020), 117445. https://doi.org/10.1016/j.neuroimage.2020.117445

Julian, J. B., Keinath, A. T., Marchette, S. A., & Epstein, R. A. (2018). The Neurocognitive Basis of Spatial Reorientation. *Current Biology*, *28*(17), R1059–R1073. https://doi.org/10.1016/j.cub.2018.04.057

Kennedy, B., Malladi, S. N., Tootell, R. B., & Nasr, S. (2024). A previously undescribed scene-selective site is the key to encoding ego-motion in naturalistic environments. *ELife*, *13*, 1–25. https://doi.org/10.7554/elife.91601.3

Knight, R. S., Chen, T., Center, E. G., Gratton, G., Fabiani, M., Savazzi, S., Mazzi, C., & Beck, D. M. (2024). Bypassing input to V1 in visual awareness: A TMS-EROS investigation. *Neuropsychologia*, *198*(March 2024), 108864. https://doi.org/10.1016/j.neuropsychologia.2024.108864

Koivisto, M., Mäntylä, T., & Silvanto, J. (2010). The role of early visual cortex (V1/V2) in conscious and unconscious visual perception. *NeuroImage*, *51*(2), 828–834. https://doi.org/10.1016/j.neuroimage.2010.02.042

Kwok, S. C., Shallice, T., & Macaluso, E. (2012). Functional anatomy of temporal organisation and domain-specificity of episodic memory retrieval. *Neuropsychologia*, *50*(12), 2943–2955. https://doi.org/10.1016/j.neuropsychologia.2012.07.025

Lacquaniti, F., Guigon, E., Bianchi, L., Ferraina, S., & Caminiti, R. (1995). Representing spatial information for limb movement: Role of area 5 in the monkey. *Cerebral Cortex*, *5*(5), 391–409. https://doi.org/10.1093/cercor/5.5.391

Lahnakoski, J. M., Glerean, E., Salmi, J., Jääskeläinen, I. P., Sams, M., Hari, R., & Nummenmaa, L. (2012). Naturalistic fMRI mapping reveals superior temporal sulcus as the hub for the distributed brain network for social perception. *Frontiers in Human Neuroscience*, *6*(AUGUST), 1–14. https://doi.org/10.3389/fnhum.2012.00233

Lahnakoski, J. M., Jääskeläinen, I. P., Sams, M., & Nummenmaa, L. (2017). Neural mechanisms for integrating consecutive and interleaved natural events. *Human Brain Mapping*, *38*(7), 3360–3376. https://doi.org/10.1002/hbm.23591

Lattanzio, L., Seames, A., Holden, S. K., & Buard, I. (2021). The emergent relationship between temporoparietal junction and anosognosia in Alzheimer's disease. *Journal of Neuroscience Research*, *99*(9), 2091–2096. https://doi.org/10.1002/jnr.24904

Lee Masson, H., Chang, L., & Isik, L. (2024). Multidimensional neural representations of social features during movie viewing. *Social Cognitive and Affective Neuroscience*, *19*(1). https://doi.org/10.1093/scan/nsae030

Lee Masson, H., & Isik, L. (2021). Functional selectivity for social interaction perception in the human superior temporal sulcus during natural viewing. *NeuroImage*, *245*(November), 118741. https://doi.org/10.1016/j.neuroimage.2021.118741

Lee, Y., & Chen, J. (2024). The Relationship between Event Boundary Strength and Pattern Shifts across the Cortical Hierarchy during Naturalistic Movie-viewing. *Journal of Cognitive Neuroscience*, *36*(11), 2317–2342. https://doi.org/10.1162/jocn_a_02213

Lerner, Y., Honey, C. J., Katkov, M., & Hasson, U. (2014). Temporal scaling of neural responses to compressed and dilated natural speech. *Journal of Neurophysiology*, *111*(12), 2433–2444. https://doi.org/10.1152/jn.00497.2013

Lerner, Y., Honey, C. J., Silbert, L. J., & Hasson, U. (2011). Topographic mapping of a hierarchy of temporal receptive windows using a narrated story. *Journal of Neuroscience*, *31*(8), 2906–2915. https://doi.org/10.1523/JNEUROSCI.3684-10.2011

Lo Presti, S., Bonavita, M., Piga, V., Lozito, S., Doricchi, F., & Lasaponara, S. (2025). "Don't stop believing" - Decoding belief dynamics in the brain: An ALE meta-analysis of neural correlates in belief formation and updating. *Neuroscience and Biobehavioral Reviews*, *173*(December 2024), 106153. https://doi.org/10.1016/j.neubiorev.2025.106153

Loschky, L. C., Larson, A. M., Smith, T. J., & Magliano, J. P. (2020). The Scene Perception & Event Comprehension Theory (SPECT) Applied to Visual Narratives. *Topics in Cognitive Science*, *12*(1), 311–351. https://doi.org/10.1111/tops.12455

Lu, K. H., Hung, S. C., Wen, H., Marussich, L., & Liu, Z. (2016). Influences of high-level features, gaze, and scene transitions on the reliability of BOLD responses to natural movie stimuli. *PLoS ONE*, *11*(8), 1–19. https://doi.org/10.1371/journal.pone.0161797

Margulies, D. S., Ghosh, S. S., Goulas, A., Falkiewicz, M., Huntenburg, J. M., Langs, G., Bezgin, G., Eickhoff, S. B., Castellanos, F. X., Petrides, M., Jefferies, E., & Smallwood, J. (2016). Situating the default-mode network along a principal gradient of macroscale cortical organization. *Proceedings of the National Academy of Sciences of the United States of America*, *113*(44), 12574–12579. https://doi.org/10.1073/pnas.1608282113

Mars, R. B., Sallet, J., Schüffelgen, U., Jbabdi, S., Toni, I., & Rushworth, M. F. S. (2012). Connectivity-based subdivisions of the human right "temporoparietal junction area": Evidence for different areas participating in different cortical networks. *Cerebral Cortex*, *22*(8), 1894–1903. https://doi.org/10.1093/cercor/bhr268

Mas, J., & Fernandez, G. (2003). VIDEO SHOT BOUNDARY DETECTION BASED ON COLOR HISTOGRAM. *TRECVID 2003: Notebook Papers*. https://www-nlpir.nist.gov/projects/tvpubs/tvpapers03/ramonlull.paper.pdf

McAleer, P., Pollick, F. E., Love, S. A., Crabbe, F., & Zacks, J. M. (2014). The role of kinematics in cortical regions for continuous human motion perception. *Cognitive, Affective and Behavioral Neuroscience*, *14*(1), 307–318. https://doi.org/10.3758/s13415-013-0192-4

McKeefry, D. J., Burton, M. P., & Morland, A. B. (2010). The contribution of human cortical area V3A to the perception of chromatic motion: A transcranial magnetic stimulation study. *European Journal of Neuroscience*, *31*(3), 575–584. https://doi.org/10.1111/j.1460-9568.2010.07095.x

Mecklenbrauck, F., Sepulcre, J., Fehring, J., & Schubotz, R. I. (2024). Decoding cortical chronotopy—Comparing the influence of different cortical organizational schemes. *NeuroImage*, *303*(October), 120914. https://doi.org/10.1016/j.neuroimage.2024.120914

Meyyappan, S., Rajan, A., Mangun, G. R., & Ding, M. (2021). Role of inferior frontal junction (ifj) in the control of feature versus spatial attention. *Journal of Neuroscience*, *41*(38), 8065–8074. https://doi.org/10.1523/JNEUROSCI.2883-20.2021

Nakayama, Y., Sugawara, S. K., Fukunaga, M., Hamano, Y. H., Sadato, N., & Nishimura, Y. (2022). The dorsal premotor cortex encodes the step-by-step planning processes for goal-directed motor behavior in humans. *NeuroImage*, *256*(April). https://doi.org/10.1016/j.neuroimage.2022.119221

Ng, A. K. T., Jia, K., Goncalves, N. R., Zamboni, E., Kemper, V. G., Goebel, R., Welchman, A. E., & Kourtzi, Z. (2021). Ultra-high-field neuroimaging reveals fine-scale processing for 3d perception. *Journal of Neuroscience*, *41*(41), 8362–8374. https://doi.org/10.1523/JNEUROSCI.0065-21.2021

Nunez-Elizalde, A. O., Huth, A. G., & Gallant, J. L. (2019). Voxelwise encoding models with non-spherical multivariate normal priors. *NeuroImage*, *197*(August 2018), 482–492. https://doi.org/10.1016/j.neuroimage.2019.04.012

Oberhuber, M., Hope, T. M. H., Seghier, M. L., Parker Jones, O., Prejawa, S., Green, D. W., & Price, C. J. (2016). Four Functionally Distinct Regions in the Left Supramarginal Gyrus Support Word Processing. *Cerebral Cortex*, *26*(11), 4212–4226. https://doi.org/10.1093/cercor/bhw251

O'Connor, D. A., Upton, D. J., Moore, J., & Hester, R. (2015). Motivationally Significant Self-control: Enhanced Action Withholding Involves the Right Inferior Frontal Junction. *Journal of Cognitive Neuroscience*, *27*(1), 112–123. https://doi.org/10.1162/jocn_a_00695

Oetringer, D., Gözükara, D., Güçlü, U., & Geerligs, L. (2025). The neural basis of event segmentation: Stable features in the environment are reflected by neural states. *Imaging Neuroscience*, *3*(February). https://doi.org/10.1162/imag_a_00432

Olson, I. R., Plotzker, A., & Ezzyat, Y. (2007). The Enigmatic temporal pole: A review of findings on social and emotional processing. *Brain*, *130*(7), 1718–1731. https://doi.org/10.1093/brain/awm052

Orban, G. A., & Caruana, F. (2014). The neural basis of human tool use. *Frontiers in Psychology*, *5*(APR), 1–12. https://doi.org/10.3389/fpsyg.2014.00310

Palejwala, A. H., Dadario, N. B., Young, I. M., O'Connor, K., Briggs, R. G., Conner, A. K., O'Donoghue, D. L., & Sughrue, M. E. (2021). Anatomy and White Matter Connections of the Lingual Gyrus and Cuneus. *World Neurosurgery*, *151*, e426–e437. https://doi.org/10.1016/j.wneu.2021.04.050

Patel, G. H., Sestieri, C., & Corbetta, M. (2019). The evolution of the temporoparietal junction and posterior superior temporal sulcus. *Cortex*, *118*, 38–50. https://doi.org/10.1016/j.cortex.2019.01.026

Pearlman, K. (2019). On Rhythm in Film Editing. *The Palgrave Handbook of the Philosophy of Film and Motion Pictures*, 143–163. https://doi.org/10.1007/978-3-030-19601-1_7

Peli, E. (1990). Contrast in complex images. *Journal of the Optical Society of America A*, *7*(10), 2032. https://doi.org/10.1364/JOSAA.7.002032

Pilacinski, A., Wallscheid, M., & Lindner, A. (2018). Human posterior parietal and dorsal premotor cortex encode the visual properties of an upcoming action. *PLoS ONE*, *13*(10), 1–20. https://doi.org/10.1371/journal.pone.0198051

Pitcher, D., & Ungerleider, L. G. (2021). Evidence for a Third Visual Pathway Specialized for Social Perception. *Trends in Cognitive Sciences*, *25*(2), 100–110. https://doi.org/10.1016/j.tics.2020.11.006

Poppenk, J., Evensmoen, H. R., Moscovitch, M., & Nadel, L. (2013). Long-axis specialization of the human hippocampus. *Trends in Cognitive Sciences*, *17*(5), 230–240. https://doi.org/10.1016/j.tics.2013.03.005

Potok, W., Maskiewicz, A., Króliczak, G., & Marangon, M. (2019). The temporal involvement of the left supramarginal gyrus in planning functional grasps: A neuronavigated TMS study. *Cortex*, *111*, 16–34. https://doi.org/10.1016/j.cortex.2018.10.010

Press, W. A., Brewer, A. A., Dougherty, R. F., Wade, A. R., & Wandell, B. A. (2001). Visual areas and spatial summation in human visual cortex. *Vision Research*, *41*(10–11), 1321–1332. https://doi.org/10.1016/S0042-6989(01)00074-8

Ralph, M. A. L., Jefferies, E., Patterson, K., & Rogers, T. T. (2016). The neural and computational bases of semantic cognition. *Nature Reviews Neuroscience*, *18*(1), 42–55. https://doi.org/10.1038/nrn.2016.150

Ramseyer, F. T. (2020). Motion energy analysis (MEA): A primer on the assessment of motion from video. *Journal of Counseling Psychology*, *67*(4), 536–549. https://doi.org/10.1037/cou0000407

Raut, R. V., Snyder, A. Z., & Raichle, M. E. (2020). Hierarchical dynamics as a macroscopic organizing principle of the human brain. *Proceedings of the National Academy of Sciences*, *117*(34), 20890–20897. https://doi.org/10.1073/pnas.2003383117

Roelfsema, P. R., & de Lange, F. P. (2016). Early Visual Cortex as a Multiscale Cognitive Blackboard. *Annual Review of Vision Science*, *2*, 131–151. https://doi.org/10.1146/annurev-vision-111815-114443

Rosenberg, A., Thompson, L. W., Doudlah, R., & Chang, T. Y. (2023). Neuronal Representations Supporting Three-Dimensional Vision in Nonhuman Primates. *Annual Review of Vision Science*, *9*, 337–359. https://doi.org/10.1146/annurev-vision-111022-123857

Rui, Y., Huang, T. S., & Mehrotra, S. (1998). Exploring video structure beyond the shots. *Proceedings of the IEEE Conference on Protocols for Multimedia Systems and Multimedia Networking, PROMS-MmNet*, 237–240. https://doi.org/10.1109/mmcs.1998.693648

Sack, A. T., Jacobs, C., De Martino, F., Staeren, N., Goebel, R., & Formisano, E. (2008). Dynamic premotor-to-parietal interactions during spatial imagery. *Journal of Neuroscience*, *28*(34), 8417–8429. https://doi.org/10.1523/JNEUROSCI.2656-08.2008

Sakata, H., Takaoka, Y., Kawarasaki, A., & Shibutani, H. (1973). Somatosensory properties of neurons in the superior parietal cortex (area 5) of the rhesus monkey. *Brain Research*, *64*(August), 85–102. https://doi.org/10.1016/0006-8993(73)90172-8

Sallet, J., Mars, R. B., Noonan, M. P., Neubert, F. X., Jbabdi, S., O'Reilly, J. X., Filippini, N., Thomas, A. G., & Rushworth, M. F. (2013). The organization of dorsal frontal cortex in humans and macaques. *Journal of Neuroscience*, *33*(30), 12255–12274. https://doi.org/10.1523/JNEUROSCI.5108-12.2013

Scheperjans, F., Hermann, K., Eickhoff, S. B., Amunts, K., Schleicher, A., & Zilles, K. (2008). Observer-independent cytoarchitectonic mapping of the human superior parietal cortex. *Cerebral Cortex*, *18*(4), 846–867. https://doi.org/10.1093/cercor/bhm116

Schmälzle, R., Imhof, M. A., Grall, C., Flaisch, T., Schupp, H. T., Schmälzle, R., Imhof, M. A., Grall, C., Flaisch, T., & Schupp, H. T. (2017). Reliability of fMRI time series: Similarity of neural processing during movie viewing. *BioRxiv*, 158188. https://doi.org/10.1101/158188

Sebastian, A., Jung, P., Neuhoff, J., Wibral, M., Fox, P. T., Lieb, K., Fries, P., Eickhoff, S. B., Tüscher, O., & Mobascher, A. (2016). Dissociable attentional and inhibitory networks of dorsal and ventral areas of the right inferior frontal cortex: a combined task-specific and coordinate-based meta-analytic fMRI study. *Brain Structure and Function*, *221*(3), 1635–1651. https://doi.org/10.1007/s00429-015-0994-y

Shirer, W. R., Ryali, S., Rykhlevskaia, E., Menon, V., & Greicius, M. D. (2012). Decoding subject-driven cognitive states with whole-brain connectivity patterns. *Cerebral Cortex*, *22*(1), 158–165. https://doi.org/10.1093/cercor/bhr099

Siestrup, S., & Schubotz, R. I. (2023). Minor Changes Change Memories: Functional Magnetic Resonance Imaging and Behavioral Reflections of Episodic Prediction Errors. *Journal of Cognitive Neuroscience*, *35*(11), 1823–1845. https://doi.org/10.1162/jocn_a_02047

Smith, A. R. (1978). Color gamut transform pairs. *ACM SIGGRAPH Computer Graphics*, *12*(3), 12–19. https://doi.org/10.1145/965139.807361

Spagna, A., Hajhajate, D., Liu, J., & Bartolomeo, P. (2021). Visual mental imagery engages the left fusiform gyrus, but not the early visual cortex: A meta-analysis of neuroimaging evidence. *Neuroscience and Biobehavioral Reviews*, *122*(April 2020), 201–217. https://doi.org/10.1016/j.neubiorev.2020.12.029

Steel, A., Garcia, B. D., Goyal, K., Mynick, A., & Robertson, C. E. (2023). Scene Perception and Visuospatial Memory Converge at the Anterior Edge of Visually Responsive Cortex. *Journal of Neuroscience*, *43*(31), 5723–5737. https://doi.org/10.1523/JNEUROSCI.2043-22.2023

Steel, A., Prasad, D., Garcia, B. D., & Robertson, C. E. (2025). Relating Scene Memory and Perception Activity to Functional Properties, Networks, and Landmarks of Posterior Cerebral Cortex—A Probabilistic Atlas. *The Journal of Neuroscience*, *45*(23), e0028252025. https://doi.org/10.1523/JNEUROSCI.0028-25.2025

Stephan, K. M., Fink, G. R., Passingham, R. E., Silbersweig, D., Ceballos-Baumann, A. O., Frith, C. D., & Frackowiak, R. S. J. (1995). Functional anatomy of the mental representation of upper extremity movements in healthy subjects. *Journal of Neurophysiology*, *73*(1), 373–386. https://doi.org/10.1152/jn.1995.73.1.373

Sulpizio, V., Galati, G., Fattori, P., Galletti, C., & Pitzalis, S. (2020). A common neural substrate for processing scenes and egomotion-compatible visual motion. *Brain Structure and Function*, *225*(7), 2091–2110. https://doi.org/10.1007/s00429-020-02112-8

Sundermann, B., & Pfleiderer, B. (2012). Functional connectivity profile of the human inferior frontal junction: Involvement in a cognitive control network. *BMC Neuroscience*, *13*(1). https://doi.org/10.1186/1471-2202-13-119

Taylor, P. A., Reynolds, R. C., Calhoun, V., Gonzalez-Castillo, J., Handwerker, D. A., Bandettini, P. A., Mejia, A. F., & Chen, G. (2023). Highlight results, don't hide them: Enhance interpretation, reduce biases and improve reproducibility. *NeuroImage*, *274*(October 2022), 120138. https://doi.org/10.1016/j.neuroimage.2023.120138

Tong, F. (2003). Cognitive neuroscience: Primary visual cortex and visual awareness. *Nature Reviews Neuroscience*, *4*(3), 219–229. https://doi.org/10.1038/nrn1055

Tootell, R. B. H., Mendola, J. D., Hadjikhani, N. K., Ledden, P. J., Liu, Arthur. K., Reppas, J. B., Sereno, M. I., & Dale, A. M. (1997). Functional Analysis of V3A and Related Areas in Human Visual Cortex. *The Journal of Neuroscience*, *17*(18), 7060–7078. https://doi.org/10.1523/JNEUROSCI.17-18-07060.1997

Wang, S., Tepfer, L. J., Taren, A. A., & Smith, D. V. (2020). Functional parcellation of the default mode network: a large-scale meta-analysis. *Scientific Reports*, *10*(1). https://doi.org/10.1038/s41598-020-72317-8

Wolbers, T., Weiller, C., & Büchel, C. (2003). Contralateral coding of imagined body parts in the superior parietal lobe. *Cerebral Cortex*, *13*(4), 392–399. https://doi.org/10.1093/cercor/13.4.392

Yang, E., Milisav, F., Kopal, J., Holmes, A. J., Mitsis, G. D., Misic, B., Finn, E. S., & Bzdok, D. (2023). The default network dominates neural responses to evolving movie stories. *Nature Communications*, *14*(1). https://doi.org/10.1038/s41467-023-39862-y

Yang, H., Susilo, T., & Duchaine, B. (2016). The Anterior Temporal Face Area Contains Invariant Representations of Face Identity That Can Persist Despite the Loss of Right FFA and OFA. *Cerebral Cortex*, *26*(3), 1096–1107. https://doi.org/10.1093/cercor/bhu289

Yeshurun, Y., Nguyen, M., & Hasson, U. (2017). Amplification of local changes along the timescale processing hierarchy. *Proceedings of the National Academy of Sciences of the United States of America*, *114*(35), 9475–9480. https://doi.org/10.1073/pnas.1701652114

Yeshurun, Y., Swanson, S., Simony, E., Chen, J., Lazaridi, C., Honey, C. J., & Hasson, U. (2017). Same Story, Different Story: The Neural Representation of Interpretive Frameworks. *Psychological Science*, *28*(3), 307–319. https://doi.org/10.1177/0956797616682029

Yoon, H. K., Jung, Y., Persichetti, A. S., & Dilks, D. D. (2025). A scene-selective region in the superior parietal lobule for visually guided navigation. *Cerebral Cortex*, *35*(4). https://doi.org/10.1093/cercor/bhaf082

Zacks, J. M., Braver, T. S., Sheridan, M. A., Donaldson, D. I., Snyder, A. Z., Ollinger, J. M., Buckner, R. L., & Raichle, M. E. (2001). Human brain activity time-locked. *Nature Neuroscience*, *4*(6), 651–655. http://neurosci.nature.com

Zacks, J. M., Speer, N. K., & Reynolds, J. R. (2009). Segmentation in Reading and Film Comprehension. *Journal of Experimental Psychology: General*, *138*(2), 307–327. https://doi.org/10.1037/a0015305

Zacks, J. M., Speer, N. K., Swallow, K. M., & Maley, C. J. (2010). The brain's cutting-room floor: Segmentation of narrative cinema. *Frontiers in Human Neuroscience*, *4*(October), 1–15. https://doi.org/10.3389/fnhum.2010.00168

Zadbood, A., Chen, J., Leong, Y. C., Norman, K. A., & Hasson, U. (2017). How We Transmit Memories to Other Brains: Constructing Shared Neural Representations Via Communication. *Cerebral Cortex*, *27*(10), 4988–5000. https://doi.org/10.1093/cercor/bhx202

Zanto, T. P., Rubens, M. T., Bollinger, J., & Gazzaley, A. (2010). Inferior Frontal Junction. *NeuroImage*, *53*(2), 736–745. https://doi.org/10.1016/j.neuroimage.2010.06.012.Top-down

Zhen, Z., Yang, Z., Huang, L., Kong, X., Wang, X., Dang, X., Huang, Y., Song, Y., & Liu, J. (2015). Quantifying interindividual variability and asymmetry of face-selective regions: A probabilistic functional atlas. *NeuroImage*, *113*, 13–25. https://doi.org/10.1016/j.neuroimage.2015.03.010

Zhu, W., Huang, Y., Xie, X., Liu, W., Deng, J., Zhang, D., Wang, Z., & Liu, J. (2023). AutoShot: A Short Video Dataset and State-of-the-Art Shot Boundary Detection. *IEEE Computer Society Conference on Computer Vision and Pattern Recognition Workshops*, *2023-June*, 2238–2247. https://doi.org/10.1109/CVPRW59228.2023.00218

Appendix D – Supplemental Analysis: Testing the uni-to-multimodal gradient in Study 1

AD.1 Methods

In the scope of the re-evaluation of the results of **Study 1** in the hindsight of all the combined studies, I tested whether the task effects seen for the contrast between the SINGLE, TRIPLET, NONET and COMPLETE conditions can be between explained by the uni-to-multimodal gradient as was revealed for the resting-state timescales and inter-subject correlation (ISC) results in **Study 2** as well as suggested by the distinction between the anterior and posterior scene network (cf. Steel et al., 2025) in **Study 3**. For this purpose, I extracted the first principal component of Margulies' et al. (2016) gradient of functional connectivity that represents the transition from unimodal cortices to multimodal association areas. This gradient is provided as part of the *neuromaps* toolbox (Markello et al., 2022). The gradient was mapped onto the lausanne120 and lausanne250 parcellation scheme (Cammoun et al., 2012), matching the parcellations applied in **Study 1**. Equivalent to **Study 1**, I modelled the unthresholded beta values ($\bar{\beta}_{\text{exp}}$) averaged per area included in the two Lausanne-parcellations by each of the four experimental conditions (HIERARCHY), the value on the Margulies gradient (GRADIENT) as well as the interaction between the two and further including a random intercept per ROI and Subject and a random slope for the HIERARCHY effect per Subject (Eq. D1):

$$\bar{\beta}_{\text{exp}} \sim \text{HIERARCHY} + \text{GRADIENT} + \text{HIERARCHY} \times \text{GRADIENT} + (1 + \text{HIERARCHY}|\text{Subject}) + (1|\text{ROI}) \quad \text{(D1)}.$$

Modelling was performed in the Bayesian hierarchical generalized linear model framework (Bürkner, 2017). As recommended from multilevel modelling (Bürkner, 2017), I applied uninformative priors: β coefficients were informed using normal $N(0, 5)$ distribution, for the standard deviation a Student's $t(3, 0, 5)$ distribution was used and finally for the interaction a Lewandowski-Kurowicka-Joe (LKJ(2)) distribution as applied. Models were estimated with 10 chains, each containing 4000 iterations with the first 1000 iterations as warmup.

AD.2 Results & Discussion

The results were largely equivalent for both parcellation schemes (Table AD.1, Figure AD.1), importantly showing a significantly positive main effect of Margulies' et al. (2016) uni-to-multimodal gradient within and across conditions, indicating increasing cortical activity along the gradient in all experimental conditions. Similarly to the results of **Study 1**, the model demonstrated a significant increase in average beta values $\bar{\beta}_{exp}$ between the TRIPLET and NONET conditions. Intriguingly, the results also revealed a significantly larger effect of the uni-to-multimodal gradient in the NONET and COMPLETE conditions compared to the TRIPLET condition for both parcellations schemes. Further, only in the lausanne250 parcellation scheme the analysis indicated a slightly larger effect of the Margulies-gradient for the NONET compared to the SINGLE condition. Overall, the results suggest that especially temporally more persistent stimuli induce more activity in the high-order, multi-modal association cortices.

Table AD.1
Results of the hypothesis test of model Eq. D1 for both the lausanne120 and lasuanne250 parcellation schemes.

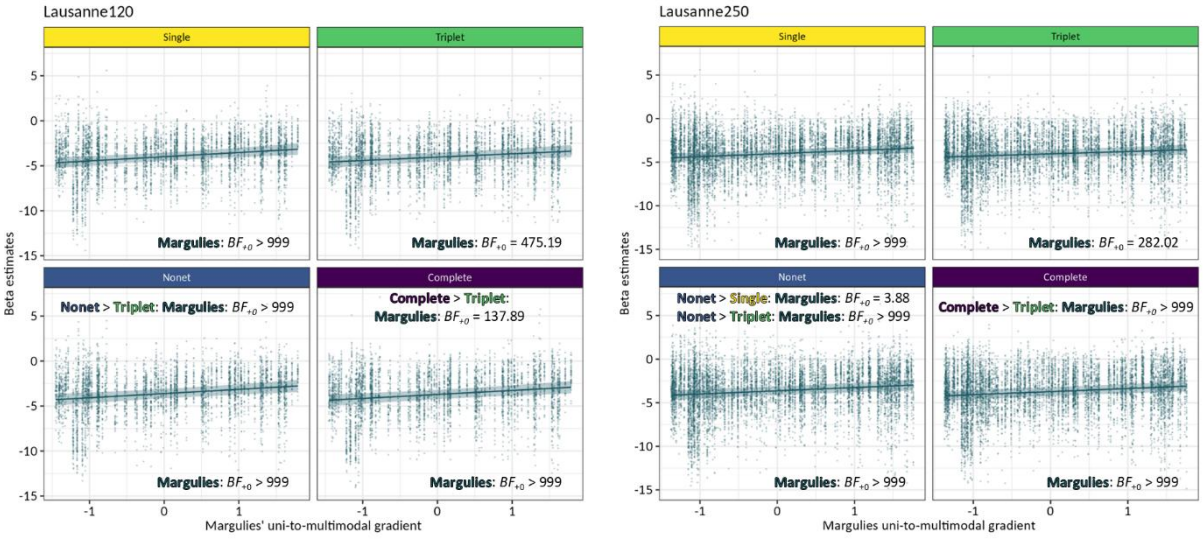
	Estimate	SE	CI lower	CI upper	Evidence Ratio	Posterior probability
			lausanne120			
Testing the main contrasts between experimental conditions						
TRIPLET > SINGLE	-0.05	0.12	-0.25	0.15	0.51	0.34
NONET > TRIPLET	**0.43**	**0.19**	**0.11**	**0.75**	**74.19**	**0.99**
COMPLETE > NONET	-0.10	0.16	-0.35	0.16	0.35	0.26
Testing the main effect of the Margulies gradient across experimental conditions						
Margulies > 0	**0.46**	**0.13**	**0.25**	**0.69**	**> 999**	**1**
Testing the effect of the Margulies gradient within each experimental condition						
SINGLE: Margulies > 0	**0.46**	**0.13**	**0.25**	**0.69**	**> 999**	**1**
TRIPLET: Margulies > 0	**0.37**	**0.13**	**0.16**	**0.59**	**475.19**	**1**
NONET: Margulies > 0	**0.47**	**0.13**	**0.26**	**0.69**	**> 999**	**1**
COMPLETE: Margulies > 0	**0.44**	**0.13**	**0.23**	**0.66**	**> 999**	**1**
Comparing the influence of the Margulies gradient between experimental conditions						
TRIPLET > SINGLE	-0.09	0.03	-0.14	-0.04	0	0
NONET > SINGLE	0.00	0.03	-0.05	0.05	1.25	0.56
NONET > TRIPLET	**0.10**	**0.03**	**0.05**	**0.15**	**> 999**	**1**
COMPLETE > SINGLE	-0.02	0.03	-0.07	0.03	0.32	0.25
COMPLETE > TRIPLET	**0.07**	**0.03**	**0.02**	**0.12**	**137.89**	**0.99**
COMPLETE > NONET	-0.02	0.03	-0.07	0.03	0.27	0.21

			lausanne250			
Testing the main contrasts between experimental conditions						
TRIPLET > SINGLE	-0.03	0.12	-0.22	0.16	0.69	0.41
NONET > TRIPLET	**0.41**	**0.19**	**0.09**	**0.73**	**58.52**	**0.98**
COMPLETE > NONET	-0.10	0.15	-0.35	0.15	0.36	0.26
Testing the main effect of the Margulies gradient across experimental conditions						
Margulies > 0	**0.35**	**0.10**	**0.18**	**0.52**	**> 999**	**1**
Testing the effect of the Margulies gradient within each experimental condition						
SINGLE: Margulies > 0	**0.35**	**0.10**	**0.18**	**0.52**	**> 999**	**1**
TRIPLET: Margulies > 0	**0.27**	**0.10**	**0.10**	**0.43**	**282.02**	**1**
NONET: Margulies > 0	**0.37**	**0.10**	**0.20**	**0.54**	**> 999**	**1**
COMPLETE: Margulies > 0	**0.35**	**0.10**	**0.18**	**0.52**	**> 999**	**1**
Comparing the influence of the Margulies gradient between experimental conditions						
TRIPLET > SINGLE	-0.09	0.02	-0.13	-0.05	0	0
NONET > SINGLE	0.02	0.02	-0.02	0.06	3.88[a]	0.80
NONET > TRIPLET	**0.11**	**0.02**	**0.07**	**0.15**	**> 999**	**1**
COMPLETE > SINGLE	0.00	0.02	-0.04	0.04	1.04	0.51
COMPLETE > TRIPLET	**0.09**	**0.02**	**0.05**	**0.13**	**> 999**	**1**
COMPLETE > NONET	-0.02	0.02	-0.06	0.02	0.27	0.21

Notes. Significant hypothesis test results are printed in bold. SE = Standard error, CI = Credible Interval. Evidence ratio of one-sided hypothesis test is equal to the Bayes factor. All $\widehat{R} \leq 1.01$, Bulk_ESS $\geq$ 844, Tail_ESS $\geq$ 1890, N_{L120} = 17905, N_{L250} = 34677. Estimating the model parameters entails running multiple Markov chain Monte Carlo chains in parallel. The convergence diagnostic $\widehat{R}$ evaluates how well the estimations converge within and between the chains. Generally, values below 1.05 indicate a successful convergence. [a] Bayes factors > 3 are considered as moderate evidence, while Bayes factors > 10 are considered as strong evidence (van Doorn et al., 2021).

Figure AD.1

Results for the uni-to-multimodal gradient effect within the regions of interest of the lausanne120 and lausanne250 parcellation schemes



Notes. Beta values represent mean activations per experimental condition compared to the implicit baseline. Plots are arranged according to experimental conditions. Depicting fixed effect predictions of the Margulies et al. (2016)-based uni-to-multimodal gradient with 95 % credibility interval marked.

To further examine whether the uni-to-multimodal gradient based on Margulies et al. (2016) explained the condition-wise beta value estimates $\bar{\beta}_{exp}$ of **Study 1** better than the rich club

classification, I additionally conducted a model comparison between the models contained in **Study 1** and these supplemental models. Therefore, I applied the Bayesian model comparison framework, based on leave-one-out-cross-validations (LOO-CV), to estimate the expected log pointwise predictive density ($elpd_{loo}$) of all models. The $elpd_{loo}$ can be interpreted as each model's accuracy when predicting new data not contained in the original sample, while controlling for effects of overfitting (Gelman et al., 2014). Due to the high computation load of cross-validation, the LOO-CV was estimated using Pareto smoothed importance sampling (Vehtari et al., 2017). Higher values of $elpd_{loo}$ (i.e., closer to zero) can be interpreted as a better model fit (Table AD.2)

Table AD.2

Comparison of Bayesian fit indices for the uni-to-multimodal gradient model compared with original 60%-prevalence- and t-test-based rich club classification models of Study 1

Model	$\widehat{elpd}_{loo}$	$se(\widehat{elpd}_{loo})$	$\widehat{elpd}_{diff}$	$se(\widehat{elpd}_{diff})$
		lausanne120		
Uni-to-multimodal gradient (Margulies)	-32045.72	126.58	0.00	0.00
Study 1: Rich club classification (FDR-corrected group *t*-test)	-32052.02	126.57	-6.30	4.55
Study 1: Rich club classification (60% group prevalence)	-32052.54	126.57	-6.82	4.70
		lausanne250		
Uni-to-multimodal gradient (Margulies)	-65565.11	178.48	0.00	0.00
Study 1: Rich club classification (60% group prevalence)	-65577.60	178.53	-12.49	5.78
Study 1: Rich club classification (FDR-corrected group *t*-test)	-65577.91	178.54	-12.80	5.55

Note. Models are considered to be better if the absolute $elpd_{loo}$ difference is larger than one standard error (Mohor et al., 2021); $\widehat{elpd}_{loo}$ = expected log pointwise predictive density for a new dataset using Pareto smoothed importance sampling (PSIS) leave-one-out-cross-validation (loo) criterion. $\widehat{elpd}_{diff}$ = difference between the $\widehat{elpd}_{loo}$ of the two compared models; *se* = standard error of the variable.

Unexpectedly, the Bayesian model comparisons did not clearly support the hypothesis test results. Specifically, the uni-to-multimodal gradient explained the variation of the beta value estimates $\bar{\beta}_{exp}$ only marginally better than the node classifications (i.e., rich club, feeder, local) that were originally investigated in **Study 1**. This difference however did not result in a significantly improved model fit.

To summarize, this supplemental analysis still demonstrates that – similarly to the results of **Study 2 & 3** – temporally longer stimuli engaged the multimodal association areas more compared to transient stimuli. This further supports the overall interpretation that the functional uni-to-multimodal gradient shapes the dynamic processing hierarchy of the cortex.

AD.3 Supplemental References

Bürkner, P. C. (2017). brms: An R package for Bayesian multilevel models using Stan. *Journal of Statistical Software*, *80*(1). https://doi.org/10.18637/jss.v080.i01

Cammoun, L., Gigandet, X., Meskaldji, D., Thiran, J. P., Sporns, O., Do, K. Q., Maeder, P., Meuli, R., & Hagmann, P. (2012). Mapping the human connectome at multiple scales with diffusion spectrum MRI. *Journal of Neuroscience Methods*, *203*(2), 386–397. https://doi.org/10.1016/j.jneumeth.2011.09.031

Gelman, A., Hwang, J., & Vehtari, A. (2014). Understanding predictive information criteria for Bayesian models. *Statistics and Computing*, *24*(6), 997–1016. https://doi.org/10.1007/s11222-013-9416-2

Margulies, D. S., Ghosh, S. S., Goulas, A., Falkiewicz, M., Huntenburg, J. M., Langs, G., Bezgin, G., Eickhoff, S. B., Castellanos, F. X., Petrides, M., Jefferies, E., & Smallwood, J. (2016). Situating the default-mode network along a principal gradient of macroscale cortical organization. *Proceedings of the National Academy of Sciences of the United States of America*, *113*(44), 12574–12579. https://doi.org/10.1073/pnas.1608282113

Markello, R. D., Hansen, J. Y., Liu, Z. Q., Bazinet, V., Shafiei, G., Suárez, L. E., Blostein, N., Seidlitz, J., Baillet, S., Satterthwaite, T. D., Chakravarty, M. M., Raznahan, A., & Misic, B. (2022). Neuromaps: Structural and Functional Interpretation of Brain Maps. *Nature Methods*, *19*(11), 1472–1479. https://doi.org/10.1038/s41592-022-01625-w

Mohor, G. S., Thieken, A. H., & Korup, O. (2021). Residential flood loss estimated from Bayesian multilevel models. *Natural Hazards and Earth System Sciences*, *21*(5), 1599–1614. https://doi.org/10.5194/nhess-21-1599-2021

Steel, A., Prasad, D., Garcia, B. D., & Robertson, C. E. (2025). Relating Scene Memory and Perception Activity to Functional Properties, Networks, and Landmarks of Posterior Cerebral Cortex—A Probabilistic Atlas. *The Journal of Neuroscience*, *45*(23), e0028252025. https://doi.org/10.1523/JNEUROSCI.0028-25.2025

van Doorn, J., van den Bergh, D., Böhm, U., Dablander, F., Derks, K., Draws, T., Etz, A., Evans, N. J., Gronau, Q. F., Haaf, J. M., Hinne, M., Kucharský, Š., Ly, A., Marsman, M., Matzke, D., Gupta, A. R. K. N., Sarafoglou, A., Stefan, A., Voelkel, J. G., & Wagenmakers, E. J. (2021). The JASP guidelines for conducting and reporting a Bayesian analysis. *Psychonomic Bulletin and Review*, *28*(3), 813–826. https://doi.org/10.3758/s13423-020-01798-5

Vehtari, A., Gelman, A., & Gabry, J. (2017). Practical Bayesian model evaluation using leave-one-out cross-validation and WAIC. *Statistics and Computing*, *27*(5), 1413–1432. https://doi.org/10.1007/s11222-016-9696-4

Abbreviations

DMN	default mode network
DWI	diffusion-weighted imaging
FPN	fronto-parietal control network
(c)IPL	(caudal) inferior parietal lobe
ISC	inter-subject correlation
IS-RSA	inter-subject representational similarity analysis
ITS	inferior temporal sulcus
MFG	middle frontal gyrus
(f)MRI	(functional) magnetic resonance imaging
MTG	middle temporal gyrus
NMDA	N-methyl-D-aspartate
PCC	posterior cingulate cortex
(dm)PFC	(dorso-medial) prefrontal cortex
RSC	retrosplenial cortex
ROI(s)	Region(s) of interest
SFG	superior frontal gyrus
SPL	superior parietal lobe
STS	superior temporal sulcus
TPJ	temporo-parietal junction
TRW(s)	temporal receptive window(s)

List of Figures

Figure 1 The definition of hierarchically nested stimuli using the example of a movie 7

Figure 2 Group-wise connectome rich club hub locations across parcellation schemes, group-averaging methods and data sets in **Study 1** 180

Curriculum Vitae

A curriculum vitae is not included in this public version of the dissertation.

Enquiries regarding the author may be directed to the following contact email:

bipsy@uni-muenster.de

Declarations

Erklärung des Promovenden / der Promovendin
zur Dokumentation von **Open Science-Aktivitäten** und der Erklärung zur **Beschäftigung mit ethischen Aspekten** im Rahmen der Promotion und zum **eigenen Anteil** an den vorgelegten wissenschaftlichen Abhandlungen mit zwei oder mehr Autor(inn)en
(kumulative Dissertation)

Promovend/Promoventin: **Falko Mecklenbrauck**

Titel der Dissertation: **Still Dwelling in the Rich Club? –
The Role of Structural Hubs and Cortical Chronoarchitecture
in the Processing of Hierarchically Nested Stimuli**

1. Dokumentation von **Open Science Aktivitäten**

Wissenschaftliche Abhandlung 1

	ja	nein	Wenn ja, unter welcher Quelle verfügbar
Präregistrierung	◯	⊗	
Veröffentlichung der Daten	◯	⊗	
Veröffentlichung von Auswertungsskripten	◯	⊗	
Open Access Publikation	⊗	◯	https://doi.org/10.1002/hbm.26543
Preprint	◯	⊗	

Wissenschaftliche Abhandlung 2

	ja	nein	Wenn ja, unter welcher Quelle verfügbar
Präregistrierung	◯	⊗	
Veröffentlichung der Daten	◯	⊗	
Veröffentlichung von Auswertungsskripten	⊗	◯	https://github.com/FalkMeck/Decoding_Cortical_Chronotopy
Open Access Publikation	⊗	◯	https://doi.org/10.1016/j.neuroimage.2024.120914
Preprint	◯	⊗	

Wissenschaftliche Abhandlung 3

	ja	nein	Wenn ja, unter welcher Quelle verfügbar
Präregistrierung	◯	⊗	
Veröffentlichung der Daten	⊗	◯	https://osf.io/xk6cv/overview?view_only=036a15ee8620401a9b1db5fd6fc25086
Veröffentlichung von Auswertungsskripten	⊗	◯	https://github.com/FalkMeck/Time_Points_or_Plot_Points
Open Access Publikation	◯	⊗	*noch nicht veröffentlicht, in Begutachtung bei NeuroImage (Gold Open Access Journal)*
Preprint	◯	⊗	

2. Erklärung zur **Beschäftigung mit ethischen Aspekten**

Studien-nummer	Quellenangabe (Manuskript / Kapitel der Promotion):	Begutachtung der Studie durch eine Ethikkommission	
		ja	nein
1 & 2	Manuskript 1: 2.1 The significance of structural rich club hubs Manuskript 2: 2.2 Decoding cortical chronotopy	⊗	◯
3	Manuskript 3: 2.3 Time Points or Plot Points	⊗	◯

3. Erklärung zum **eigenen Anteil** an den vorgelegten wissenschaftlichen Abhandlungen mit zwei oder mehr Autor(inn)en

Wissenschaftliche Abhandlung 1

Titel	The significance of structural rich club hubs for the processing of hierarchical stimuli		
Autor(en)	Falko Mecklenbrauck, Marius Gruber, Sophie Siestrup, Anoushiravan Zahedi, Dominik Grotegerd, Marco Mauritz, Ima Trempler, Udo Dannlowski, & Ricarda I. Schubotz		
Publikationsstatus:	nicht eingereicht	◯	(bitte ankreuzen)
	eingereicht	◯	
	in Begutachtung	◯	
	in Revision	◯	
	angenommen	◯	
	publiziert	⊗	
Journal	Human Brain Mapping		
Publikationsjahr	2024		

Beschreibung des eigenen Anteils, wenn keine Alleinautorenschaft vorliegt:

- geteilt-verantwortlich für Konzeption und Design der Studie
- hauptverantwortlich für Erhebung der Daten
- hauptverantwortlich für Analyse der Daten
- geteilt-verantwortlich für Interpretation der Daten
- hauptverantwortlich für die Formulierung und Überarbeitung des Manuskripts
- korrespondierender Autor

Wissenschaftliche Abhandlung 2

Titel	Decoding cortical chronotopy – Comparing the influence of different cortical organizational schemes		
Autor(en)	Falko Mecklenbrauck, Jorge Sepulcre, Jana Fehring, & Ricarda I. Schubotz		
Publikationsstatus:	nicht eingereicht	◯	(bitte ankreuzen)
	eingereicht	◯	
	in Begutachtung	◯	
	in Revision	◯	
	angenommen	◯	
	publiziert	⊗	
Journal	NeuroImage		
Publikationsjahr	2024		

Beschreibung des eigenen Anteils, wenn keine Alleinautorenschaft vorliegt:

- geteilt-verantwortlich für Konzeption und Design der Studie
- hauptverantwortlich für Erhebung der Daten (gleiche Daten wie Abhandlung 1)
- hauptverantwortlich für Analyse der Daten
- geteilt-verantwortlich für Interpretation der Daten
- hauptverantwortlich für die Formulierung und Überarbeitung des Manuskripts
- korrespondierender Autor

Wissenschaftliche Abhandlung 3

Titel	Time Points or Plot Points – Are movies processed according to their temporal duration or their underlying content structure?		
Autor(en)	Falko Mecklenbrauck & Ricarda I. Schubotz		
Publikationsstatus:	nicht eingereicht	◯	(bitte ankreuzen)
	eingereicht	◯	
	in Begutachtung	⊗	
	in Revision	◯	
	angenommen	◯	
	publiziert	◯	
Journal	*in Begutachtung bei NeuroImage*		
Publikationsjahr	*voraussichtlich 2026*		

Beschreibung des eigenen Anteils, wenn keine Alleinautorenschaft vorliegt:

- geteilt-verantwortlich für Konzeption und Design der Studie
- hauptverantwortlich für Erhebung der Daten
- allein-verantwortlich für Analyse der Daten
- geteilt-verantwortlich für Interpretation der Daten
- hauptverantwortlich für die Formulierung und Überarbeitung des Manuskripts
- korrespondierender Autor

_____ _____

Ort, Datum Unterschrift Promovend/in